Organische Salze Sulfid- und Selenid-basierter Anionen: Bausteine für die Materialsynthese bi- und multinärer Metallchalkogenide

Kumulative Dissertation

zur Erlangung des Doktorgrades der Naturwissenschaften

(Dr. rer. nat.)

Dem Fachbereich Chemie

der Philipps-Universität Marburg

vorgelegt von

Jannick Guschlbauer

(M. Sc. Chemie)

aus Bietigheim-Bissingen

Marburg 2019

Erklärung

Ich erkläre, dass eine Promotion noch an keiner anderen Hochschule als der Philipps-Universität Marburg, Fachbereich Chemie, versucht wurde.

Ich versichere, dass ich die vorgelegte Dissertation „Organische Salze Sulfid- und Selenid-basierter Anionen: Bausteine für die Materialsynthese bi- und multinärer Metallchalkogenide“ selbst und ohne fremde Hilfe verfasst, nicht andere als die in ihr angegebenen Quellen oder Hilfsmittel benutzt, alle vollständig oder sinngemäß übernommenen Zitate als solche gekennzeichnet, sowie die Dissertation in der vorliegenden oder einer ähnlichen Form noch bei keiner anderen in- oder ausländischen Hochschule anlässlich eines Promotionsgesuchs oder zu anderen Prüfungszwecken eingereicht habe.

Die vorliegende Arbeit wurde in der Zeit vom April 2016 bis Juli 2019 unter Leitung von Herrn Prof. Dr. Jörg Sundermeyer am Fachbereich Chemie der Philipps-Universität Marburg angefertigt.

Vom Fachbereich Chemie der Philipps-Universität (Hochschulkennziffer 1180) angenommen am: 11.12.2019

Erstgutachter: Prof. Dr. Jörg Sundermeyer

Zweitgutachterin: Prof. Dr. Stefanie Dehnen

Tag der Mündlichen Prüfung: 11.12.2019

Publikationsliste

Artikel in Fachzeitschriften

L. H. Finger, J. Guschlbauer, K. Harms, J. Sundermeyer; „N-Heterocyclic Olefin – Carbon Dioxides and Sulfur Dioxide Adducts: Structures and Interesting Reactivity Patterns“, *Chem. Eur. J.*, **2016**, 22 (45), 16292-16303.

J. Guschlbauer, T. Vollgraff, J. Sundermeyer**;** „Systematic study on anion–cation interactions via doubly ionic H-bonds in 1,3-dimethylimidazolium salts comprising chalcogenolate anions MMIm[ER] (E = S, Se; R = H, *t*Bu, $SiMe_3$)“, *Dalton Trans.*, **2019**, 48, 10971-10978.

J. Guschlbauer, T. Vollgraff, J. Sundermeyer; „Homoleptic Group 13 Metalates $[M(ESiMe_3)_4]^-$ (M = Ga, In; E = S, Se): Metastable Precursors for Low Temperature Syntheses of Chalcogenide Based Materials“, *Inorg. Chem., accepted 22.10.2019,* DOI: 10.1021/acs.inorgchem.9b02453.

M. Loor, S. Salloum, P. Kawoluk, S. Izadi, G. Bendt, J. Guschlbauer, J. Sundermeyer, N. Pérez, K. Nielsch, G. Schierning, S. Schulz; „Ionic liquid-based low-temperature synthesis of phase-pure tetradymite-type materials and their thermoelectric properties”, *manuscript submitted (18.10.2019).*

J. Guschlbauer, T. Vollgraff, J. Sundermeyer; „Homoleptic Trimethylsilylchalcogenolato Zinkates $[Zn(ESiMe_3)_3]^-$ and Stannanides $[Sn(ESiMe_3)_3]^-$ (E = S, Se): Precursors in Solution Based Low-Temperature Cu_2ZnSnS_4 (CZTS) Synthesis“, *manuscript submitted (24.10.2019).*

J. Guschlbauer, T. Vollgraff, X. Xie, F. Weigend, J. Sundermeyer; „A Series of Homoleptic Linear Coinage Metal Trimethylsilylchalcogenolate Complexes $Cat[Me_3E\text{-}M\text{-}ESiMe_3]$ (M = Cu, Ag, Au; E = S, Se), *manuscript submitted (14.11.2019).*

J. Guschlbauer, L. H. Finger, T. Vollgraff, K. Harms, J. Sundermeyer; „Dimethylpyrrolidinium Chalcogenido-Dimethylgallates and -indates $DMPyr_2[Me_2M(\mu_2\text{-}E)]_2$ (M = Ga, In; E = S, Se): Their use in the Synthesis of Higher or Lower Order Chalcogenidoindates“*, in preparation.*

J. Guschlbauer, T. Vollgraff, A. Fetoh, J. Sundermeyer; „Organic Methylcarbonate Salts comprising Non-methylated Onium Cations $Cat[OCO_2Me]$ (Cat = Ph_4P^+, PPN^+, TBA^+) via Fluoride-Induced Demethylation of Dimethylcarbonate”, *in preparation.*

Tagungsbeiträge

Poster: J. Guschlbauer, L. H. Finger, J. Sundermeyer; „Chalcogenide-based Anions in Synthesis for the Preparation of Metalates“, Materialforschungstag Mittelhessen, Gießen, 28.06.2017.

Vortrag: J. Guschlbauer, M. Hoffmann, J. Sundermeyer; „Chalcogen-based Ionic Liquids for the Preparation of Metal Chalcogenide Meaterials near Room Temperature“, SPP 1708 „Materialsynthese nahe Raumtemperatur“, Kick-Off-Meeting, Würzburg, 20.09.2017.

Vortrag: J. Guschlbauer, M. Hoffmann, L. H. Finger, J. Sundermeyer; „Synthesis and Purification of Water- and Halide free Chalcogen-based Ionic Liquids“, SPP 1708 „Materialsynthese nahe Raumtemperatur“, Workshop: Synthesis Strategies in Ionic Liquids, Nürnberg, 08.11.2017 bis 10.11.2017.

Vortrag: J. Guschlbauer, T. Vollgraff, J. Sundermeyer; „Copper-Indium-Gallium-Sulfide/Selenide (CIGS) Synthesis with Chalcogen-based Ionic Liquids Cat[E-$SiMe_3$] (E = S, Se)“, Materialforschungstag Mittelhessen, Marburg, 16.05.2018.

Vortrag: J. Guschlbauer, T. Vollgraff, J. Sundermeyer; „Homoleptic Trimethylsilylchalcogenolato Metalate Anions Cat[M(E-$SiMe_3$)$_{n+1}$] for Material Syntheses“, SPP 1708 „Materialsynthese nahe Raumtemperatur“, Mid-term Report Colloquium, Dresden, 17.09.2018 bis 18.09.2018.

Vortrag: J. Guschlbauer; Chalkogenolatbasierte Ionische Flüssigkeiten und Silylierte Chalkogenolato-Metallate – Ionische Bausteine für die Niedrigtemperatur-Materialsynthese“, Anorganisch-chemisches Doktorandenkolloquium, Marburg, 26.11.2018.

Poster: J. Guschlbauer, T. Vollgraff, L. H. Finger, J. Sundermeyer; Chalcogenide-based Organic Salts Cat E-R (E = S, Se; R H, *t*Bu, $SiMe_3$)“, Materialforschungstag Mittelhessen, Gießen, 05.06.2019.

Vortrag: J. Guschlbauer, T. Vollgraff, J. Sundermeyer; „Metalate Complexes with Unsubstituted Chalcogenide and Silylated Chalcogenolate Moieties“, 23rd European Conference on Organometallic Chemistry, Helsinki, 16.06.2019 bis 20.06.2019.

Inhaltsverzeichnis

1 Einleitung

Die Frage nach der Energieversorgung der Zukunft ist nicht zuletzt aufgrund der aktuellen Klimadiskussion im Hinblick auf die Limitierung und die Nachwirkungen fossiler und nuklearer Brennstoffe von übergeordnetem Interesse.[1] Ein Großteil der Energie für Mobilität, Heizung und Maschinenbetrieb wird durch die Verbrennung fossiler Brennstoffe wie Benzin, Diesel, Kerosin, Erdgas oder Stein- bzw. Braunkohle unter Freisetzung immenser Mengen an CO_2 und den ökologisch deutlich schädlicheren Stick- und Schwefeloxiden bereitgestellt.[2] Neben den fatalen ökologischen Konsequenzen[3] dieser Energiegewinnungsart sind es auch global ausgelegte wirtschaftliche Abhängigkeitsverhältnisse mit öl-/kohlereichen Staaten, die seit dem vergangenen Jahrhundert immer wieder Anlass zu politischen Spannungen und kriegerischen Auseinandersetzungen gaben.[4] Um die rohstofflichen Konfliktpotentiale und dem verschwenderischen Umgang mit endlichen Ressourcen entgegenzuwirken, sind nachhaltige Ansätze als Ersatz zu Mineralölerzeugnissen – insbesondere denen zur Energiegewinnung – gefragter denn je.[5]

Neben Wind- und Wasserkraft sind vor allem Erdwärme und Photovoltaik vielversprechende nachthaltige Alternativen zur herkömmlichen Energiegewinnung.[6] Die Photovoltaik gilt nach wie vor als eine der vielversprechendsten und damit zukunftsträchtigsten Technologien zur Energiegewinnung, da die auf der Erde zur Verfügung stehende Sonnenenergie überall zugänglich und mit einer Leistung von durchschnittlich $1.8 \cdot 10^{14}$ kW auf der bestrahlten Fläche auch betragsmäßig attraktiv ist.[7] Zur Veranschaulichung: in weniger als 50 Minuten wird von der Sonne eine Strahlungsenergiemenge auf die Erde abgegeben, die dem weltweiten Jahresenergieverbrauch von 2008 entspricht (142300 TWh). Allein 2017 konnten in Deutschland durch den photovoltaisch generierten Strom 19 Mio. t CO_2 eingespart werden.[7]

Der schematische Aufbau einer einfachen, kristallinen siliziumbasierten Solarzelle soll im Folgenden vereinfacht veranschaulicht werden.[8] Grundlage ist das Si-Gerüst einkristallinen Siliziums. Durch gezielten Ersatz einzelner Siliziumatome durch Atome der 13. Gruppe (Triele, *Tr*) oder 15. Gruppe (Pnictogene, *Pn*) ähnlicher Größe resultiert eine p- bzw. n-Dotierung des siliziumbasierten Halbleiterbauteils. Diese ist auf die von Silizium verschiedenen Valenzelektronenzahlen der Fremdatome zurückzuführen, die entweder zusätzliche Elektronen (n-Dotierung) oder Lochstellen (p-Dotierung) in das Kristallgitter integrieren. Verbindet man ein p-dotiertes- mit einem n-dotiertem Siliziumgitter, so diffundieren die mobilen Elektronen der n-Typ Schicht in die Elektronenlöcher der p-Typ Schicht und umgekehrt, bis sich ein Gleichgewicht zwischen der Diffusion und einem entgegengesetzten elektrischen Feld einstellt

(*Abbildung 1.1*). Die Potentialdifferenz dieses elektrischen Feldes wird als Driftspannung bezeichnet, die einen p-n Übergang kennzeichnet. Sie entsteht durch die Anreicherung von negativer bzw. positiver Ladung in die zuvor zuvor ungeladenen Siliziumgitter des n- und p-Halbleiterteils. In *Abbildung 1.1* ist der schematische Aufbau eines wichtigen Bauelements elektrischer Schaltkreise gezeigt: der Halbleiterdiode.

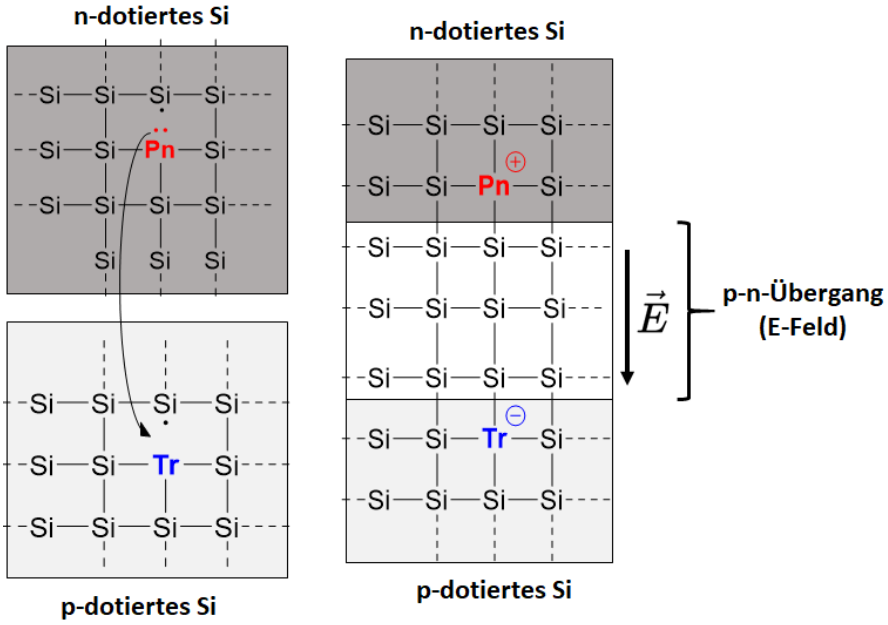

Abbildung 1.1: An der Grenzfläche zwischen p- (links) und n-dotierten (mittig) Siliziumgittern entsteht ein elektrisches Feld (p-n Übergang, rechts). Tr: Trielatom, Pn: Pnictogenatom. In Anlehnung an [8].

Erfolgt durch Absorption eines Photons geeigneter Energie an diesem p-n Übergang eine photolytische Anregung eines Elektrons vom Valenz- in das Leitungsband, entsteht ein Elektron-Loch-Paar, das als Exziton bezeichnet wird. Das Elektron wandert dann in Richtung positiv geladenem, n-dotierten Halbleiterbauteil, während das verbleibende Defektelektron hin zum negativ geladenen, p-dotierten Halbleiter wandert. Durch das im p-n Übergang herrschende elektrische Feld ist eine Rekombination weniger günstig als der Stromfluss über einen Verbraucher. Die Elektronen fließen dabei vom n-Halbleiter über den Verbraucher hin zum p-Halbleiter, wo die Rekombination der Elektron-Loch-Paare stattfinden kann (*Abbildung 1.2*).[8]

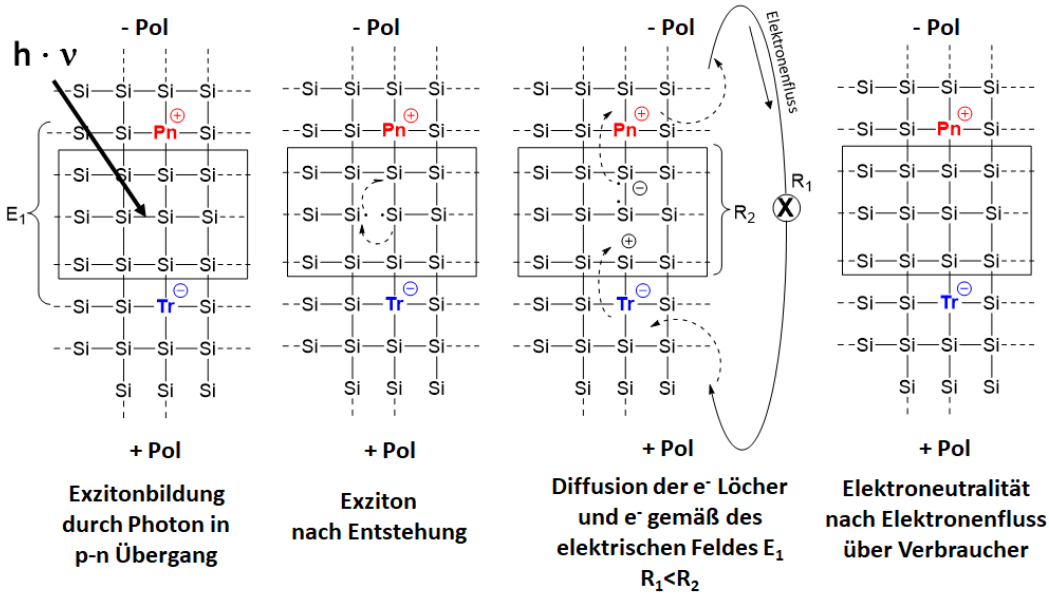

Abbildung 1.2: Stark vereinfachte funktionsweise einer Si-Solarzelle. Tr: Trielatom, Pn: Pnictogenatom. In Anlehnung an [8].

Die kommerziell etablierten, auf dotiertem, einkristallinem Silizium basierenden Solarzellen sind hinsichtlich ihres mit 26.7%[7] sehr guten Wirkungsgrades und der hohen natürlichen Häufigkeit von Silizium vorteilhaft, was ihre marktbeherrschende Position erklärt (95% der Produktionskapazität für Solarzellen sind auf Si-Waferbasis ausgerichtet).[7] Allerdings sorgen die teure Herstellung und das aufwändige Handling für hohe Kosten und Einschränkungen in der Anwendbarkeit. Diese Probleme werden durch Einsatz von Dünnschichtsolarzellen elegant umgangen.[7,9,10] Der schematische Aufbau und ein Beispiel einer flexiblen Dünnschichtsolarzelle sind exemplarisch für CIGS-basierte Solarzellen in *Abbildung 1.3* gezeigt. Unter CIGS versteht man alle Vertreter des Phasensystems $CuGa_xIn_{1-x}S_ySe_{2-y}$. Diese und vergleichbare Materialien werden im nächsten Unterkapitel näher vorgestell.

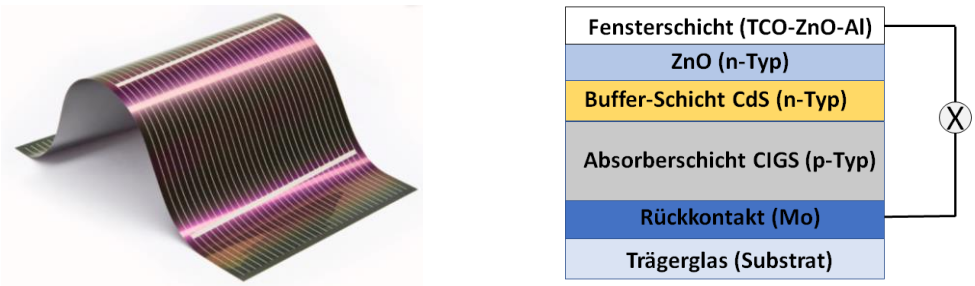

Abbildung 1.3: Flexible CIGS-Solarzelle (links)[11] und vereinfachter Aufbau einer CIGS-Solazelle (rechts).[12]

Die oberste Schicht einer Dünnschichtsolarzelle besteht aus einem transparenten, leitfähigen Oxidmaterial (TCO für *transparent conductive oxide*, hier Al-dotiertes ZnO). Anschließend kommt eine Schicht von n-dotiertem ZnO, welches die Diffusion der Aluminiumatome der TCO in die Absorberschicht unterbindet. Es folgt die n-CdS Buffer-Schicht, die weitgehend transparent für die zu absorbierende Strahlung sein sollte. Zusammen bilden diese beiden Schichten das n-Typ Halbleiterkompartiment aus, das an eine p-dotierte CIGS Absorberschicht grenzt. Zwischen n-ZnO/n-CdS und p-CIGS bildet sich ein n-p Übergang aus. Unter der Absorberschicht befindet sich die Rückkontaktschicht, in diesem Fall Molybdän. Der ganze Aufbau ist auf einem geeigneten Substrat, im Regelfall ein Glas oder Polymer, aufgebracht. Nachdem ein Photon die TCO und n-ZnO-Schicht passiert, wird es in der Absorberschicht unter Ausbildung eines Exzitons absorbiert. Dabei werden von der Buffer-Schicht die Photonen durchgelassen, die unter der Bandlücke von CdS (E_g (CdS) = 2.4 eV) liegen, während die energiereicheren Photonen bereits hier absorbiert werden. Bildet sich ein Exziton, bewegt sich das freie Elektron in Richtung des positiv geladenen n-Typ Halbleiterkompartiments, während das Elektronenloch im positiv geladenen n-Typ Halbleiterkompartiment bleibt. Über das TCO fließt das Elektron in Form eines elektrischen Stroms über einen Verbraucher zu dem Rückkontakt, wobei die Elektroneutralität wiederhergestellt wird.[9,12]

Ein großer Vorteil von CIGS-Dünnschichtsolarzellen ist die verhältnismäßig einfache Synthese des Absorbermaterials, die mit Standardlaborequiment durchführbar ist. Dies qualifiziert Dünnschichtsolarzellen als kostengünstigere und mittlerweile auch hinsichtlich ihres Wirkungsgrads von bis zu 23.35%[13] vergleichbare Alternativen zu konventionellen Solarzellen. Die wichtigsten Absorbermaterialien etablierter Dünnschichtsolarzellen sind CIGS ($CuIn_{1-x}Ga_xS_ySe_{2-y}$), CdTe, GaAs und amorphes Silizium (a-Si), während an Alternativmaterialien wie CZTS ($Cu_2ZnSnS_ySe_{4-y}$), organischen Halbleitern, sowie Farbstoffsolarzellen aktiv geforscht wird.[10] Im Folgenden werden die chalkogenbasierten Vertreter CIGS und CZTS näher vorgestellt, da sich die vorliegende Arbeit zu einem Großteil mit potentiellen Präkursoren für diese Materialien befasst. Erwähnt seien der Vollständigkeit halber die in dieser Arbeit nicht weiter behandelten, aber für die Zukunft äußerst vielversprechenden Perowskit-basierten Photovoltaikmaterialien, für deren erschöpfende Vorstellung auf die Literatur verwiesen sei.[14] Perowskit-basierte Silizium-Tandem Solarzellen erreichen Wirkungsgrade von bis zu 28% und sind damit bisherige Rekordhalter für Single-Junction Solarzellen.[15] Auch reine Perowskit Dünnschichtsolarzellen können mittlerweile Wirkungsgrade von über 24% aufweisen, womit die CIGS-Technologie als Rekordhalter für nicht-Si-basierte Photovoltaik abgelöst wurde.[14]

1.1 Chalkogenbasierte Photovoltaikmaterialien

Wichtige und prominente Dünnschicht-Photovoltaikmaterialien sind Vertreter der CIGS-Familie ($CuIn_{1-x}Ga_xS_ySe_{2-y}$), die sich bereits kommerziell durchsetzen konnten[9] und Vertreter der CZTS ($Cu_2SnZnS_ySe_{4-y}$) Familie, die durch ihre geringe Kosten und die hohe Verfügbarkeit der verwendeten Elemente als besonderes nachhaltige Materialien gelten.[16]

Während CIGS-Dünnschichtsolarzellen einen Wirkungsgrad von bis zu 23.35%[17] aufweisen, liegt der bisher höchst Wirkungsgrad für CZTS bei 12.6%[18] bzw. knapp bei 11%[19] für Se-freie CZTS Materialien. Vorteilhaft ist, dass CZTS keine übermäßig toxischen, oder rohstoffversorgungskritischen Elemente enthält, und somit okönomisch wie ökologisch im Vergleich zu anderen Dünnschichtsolarzellenabsorbermaterialien – auch CIGS – deutlich überlegen ist. Dennoch wurde dieses Material noch nicht in größerem Maßstab kommerzialisiert, was in dem noch zu optimierenden Wirkungsgrad begründet liegt.[20]

CIGS Materialien $CuIn_{1-x}Ga_xS_ySe_{2-y}$ (bzw. auch die Aluminium-Vertreter $Cu(Al_xIn_{1-x})(S_ySe_{2-y})$) sind direkte Halbleiter, deren Bandlücken in Abhängigkeit von x bzw. y zwischen 1.55 eV bis 3.45 eV gezielt eingestellt werden können. Sie zeichnen sich durch einen vorteilhaft hohen Absorptionskoeffizienten von $10^5\ cm^{-1}$ aus.[9] CZTS Cu_2ZnSnS_4 ist ebenso ein direkter Halbleiter mit Bandlücken von 1.4-1.5 eV und einem hohen Absorptionskoeffizienten ($>10^4\ cm^{-1}$).[16]

Die Festkörperstrukturen der wichtigsten Modifikationen von CIGS und CZTS lassen sich aus der kubischen Zinkblendestruktur zahlreicher II-VI-Materialien (z. B. ZnSe) entwickeln. CIGS Materialien kristallisieren in unterschiedlichen Modifikationen, von denen dem tetragonalen Chalkopyristrukturtyp ($CuFeS_2$-Typ) die größte Bedeutung zukommt. Ausgehend vom Zinkblendestrukturtyp werden hier zwei zweiwertige Metallatome durch ein einwertiges Kupfer- und ein dreiwertiges Trielatom ausgetauscht (*Abbildung 1.1.4, links*).[9,21] Auch CZTS hat mehrere Modifikationen von denen der Késteritstrukturtyp ($Cu_2Zn_xFe_{1-x}SnS_4$-Typ) der wichtigste ist. Diese Struktur geht aus der Chalkopyritstruktur hervor, wenn zwei Trielatome durch ein vierwertiges Zinn- und ein zweiwertiges Zinkatom ersetzt werden (*Abbildung 1.1.4, rechts*).[16,22]

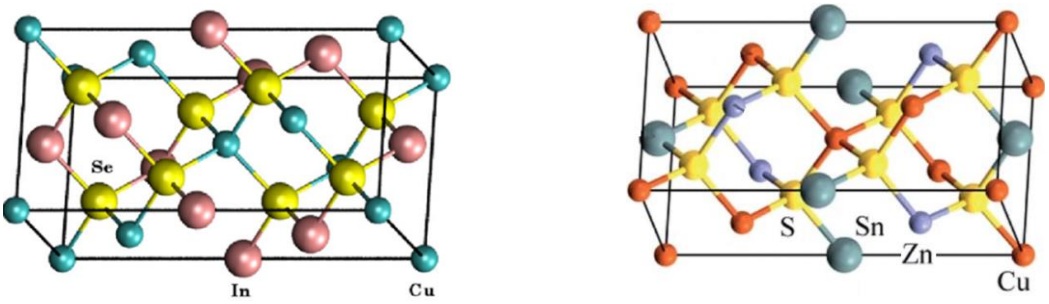

$CuInSe_2$[21] **Cu_2ZnSnS_4[22]**

Abbildung 1.1.4: Chalkopyritstruktur am Beispiel von $CuInSe_2$ (links)[21] und die Késteritstruktur am Beispiel von Cu_2ZnSnS_4 (rechts).[22]

Die Herstellung der Absorptionsschichten von CIGS-basierten Solarzellen erfolgt hauptsächlich durch teure und technologisch aufwändige Technologien, wie der Co-Verdampfung der elementaren Metalle mit anschließender Selenierung/Sulfurierung des Precursor-Metallfilms mit H_2Se/H_2S.[9] Diese Methoden sind trotz ihrer verbreiteten Anwendung sowohl im Laboratoriums- als auch im Industriemaßstab sehr teuer mit diversen praktischen Nachteilen behaftet: bei Co-Verdampfungsverfahren ist die Menge der jeweiligen Elementquellen der aufzusublimieren Schicht schwierig zu kontrollieren was sich in lokalen Schwankungen der Zusammensetzung innerhalb einer Schicht äußert, während bei Selenierung/Sulfurierungsprozessen große Mengen der hochgiftigen Gase H_2Se und H_2S verwendet werden müssen.[9] Alternativ finden atom- und energieökonomischere Nichtvakuumtechniken Anwendung. Bei diesen lösungsmittelbasierten Prozessen werden geeignete Präkursorlösungen oder Nanopartikeldispersionen auf ein Target gedruckt und anschließend thermisch zu einer Dünnschicht des gewünschten Materials prozessiert. Die erreichten Effizienzen von Zellen mit derartig hergestellten Halbleiterschichten sind im Vergleich zu den vakuumprozessierten Zellen allerdings unterlegen.[9] Dies begründet ein Interesse an neuen Präkursoren, mit deren Hilfe Materialien mit verbesserten elektronischen Kenngrößen ressourcenschonend hergestellt werden können. Im Folgenden sollen ein paar Präkursoren näher beschrieben werden: Die ersten *Single-Source* Präkursoren für CIGS Materialien sind die von *Hirpo et al.* erstmals beschriebenen[23] und von *Corrigan et al.* ausführlich untersuchten[24] Verbindungen $[R_nCuIn(ER')_4]$ (E = S, Se; R = Et, Ph). Diese weisen zweikernige Grundgerüste auf, die jeweils aus über verbrückende Liganden verknüpfte Trielat, und phosphingeschützte Kupfer(I)-Zentren aufgebaut sind *(Abbildung 1.1.5, oben links)*. Die von *Krautscheit et al.* beschriebenen Clustermoleküle $[(R_3PCu)_4(MeM)_4E_6]$, $[(R_3PCu)_6(MeM)_4M_4S_{13}]$ und $[(^iPr_3PCuEPh)_3(MeGaE)_4]$ (*Abbildung 1.1.5 oben rechts bis unten rechts*) liefern ebenfalls CIGS nach Thermolyse.[25] Eine ausführliche Gegenüberstellung

diverser CIGS Single Source Präkursoren findet sich in einem Übersichtsartikel von *Friedrich et al*.[26]

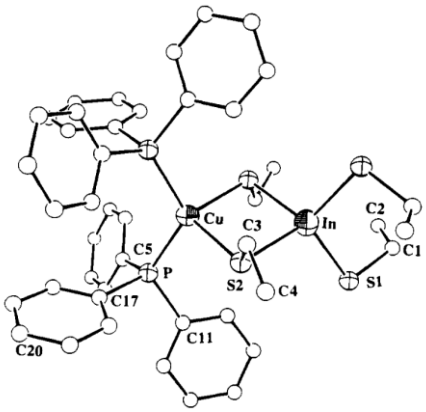

$[R_nCuM(ER')_4]$[23]

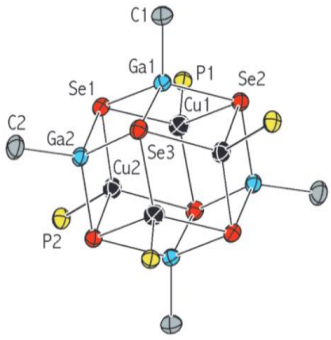

$[(R_3PCu)_4(MeM)_4E_6]$[25]

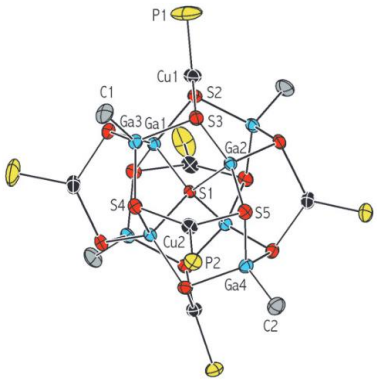

$[(R_3PCu)_6(MeM)_4M_4S_{13}]$[25]

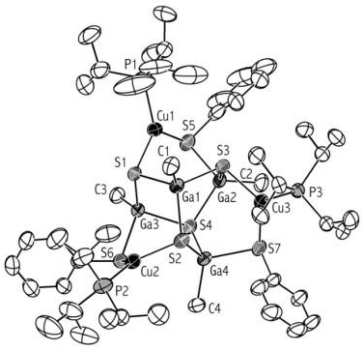

$[(^iPr_3PCuEPh)_3(MeGaE)_4]$[25]

Abbildung 1.1.5: Auswahl kristallographisch charakterisierter Molekülstrukturen von Single-Source Präkursoren für $CuME_2$ Materialien (M = Ga, In; E = S, Se).[23,25]

Die Herstellung von CZTS ist vergleichbar mit den Methoden für die CIGS Herstellung. Verbreitet sind auch hier die technologisch anspruchsvollen Vakuumtechniken, insbesondere Elektronenstrahlverdampfung und Sputtering der Metalle, für die jedoch eine anschließende Sulfurierung mit immensen Mengen hochtoxischen H_2S notwendig ist, um das gewünschte Material zu erhalten.[16] Auch für CZTS sind lösungsmittelbasierte Nichtvakummethoden bekannt, wie das Spincoaten von Nanopartikeldispersionen[16] oder ethanolischen Lösungen von *in situ* generierten Dithiocarbamaten (dtc) von Kupfer, Zinn und Zink $[M(dtc)_n]$ (n = 1 für M = Cu; n = 2 für M = Sn, Zn) auf ein festes Substrat mit anschließender thermischer Nachbehandlung.[27] Zudem gibt es die elektrochemische Zersetzung, Sol-Gel-Routen oder Nanopartikeltintendruck-verfahren die an anderer Stelle ausführlich diskutiert sind.[16]

Es gibt nur sehr wenige Moleküle, die mehr als zwei der in CZTS beteiligten Atome enthalten. Zu erwähnen sind hier die ternären Ethandithiolat (edt) basierten Cu / S / Zn Verbindungen[28] $[i\text{Pr}_3\text{PCu})_2(\text{ZnEt}_2)(\text{edt})]_2$ (*Abbildung 1.1.6 oben links*), $[(i\text{Pr}_3\text{PCu})_2(\text{Zn}(i\text{Pr})_2)(\text{edt})]_2$, $[(i\text{Pr}_3\text{PCu})_4(\text{edt})_2(\text{ZnMe}_2)]_2$, $[(i\text{Pr}_3\text{PCu})_3(\text{ZnPh}_2)(\text{ZnPh})(\text{edt})_2]_2$, $[(i\text{Pr}_3\text{PCu})_2\text{Zn}_2(\text{edt})_3]_6$ sowie die Zn / E / Sn (E = S, Se) Verbindungen $[(\text{tmeda})\text{Zn}(\text{SnR}_2)_2\text{E}_3]$ (*Abbildung 1.1.6 oben links*).[29] Alle genannten Präkursormoleküle wurden von *Krautscheid et al.* hinsichtlich ihrer Eigenschaft, in Anwesenheit zugesetzter Präkursoren der jeweils fehlenden Metallkationen zu CZTS(Se) zu zerfallen eingehend untersucht.[28,29] Des Weiteren gibt es einige Clustermoleküle von *Dehnen et al.*, die sich von der binären Sn / S - Heteroadamantanstruktur $[(\mu_2\text{-S})_6(\text{SnR})_4]$ ableiten und als potentielle CZTS-Präkursoren diskutiert wurden, wie etwa der Cu / S / Sn Cluster $[(\text{CuPPh}_3)_4(\text{PhSn})_{18}\text{Cu}_6\text{S}_{31}\text{Cl}_2]$ *Abbildung 1.1.6 unten*.[30] Geeignete *Single-Source* Präkursoren, die alle Elemente Cu, Sn, Zn und S bzw. Se der quartären Verbindung CZTS(Se) enthalten, gibt es bisher nicht. Eine Single-Source-Strategie mag wahrscheinlich auch nicht die nützlichste Synthese für CZTS darstellen.

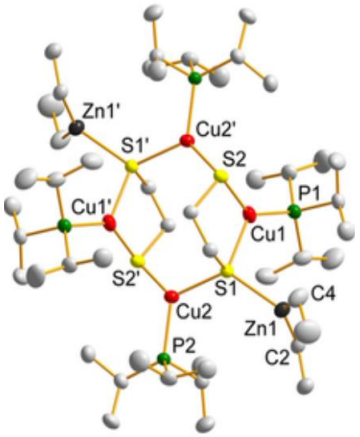

$[i\text{Pr}_3\text{PCu})_2(\text{ZnEt}_2)(\text{edt})]_2$[28]

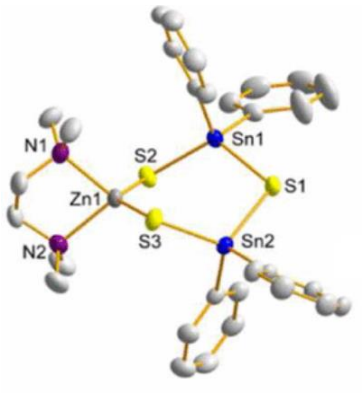

$[(\text{tmeda})\text{Zn}(\text{SnR}_2)_2\text{S}_3]$[29]

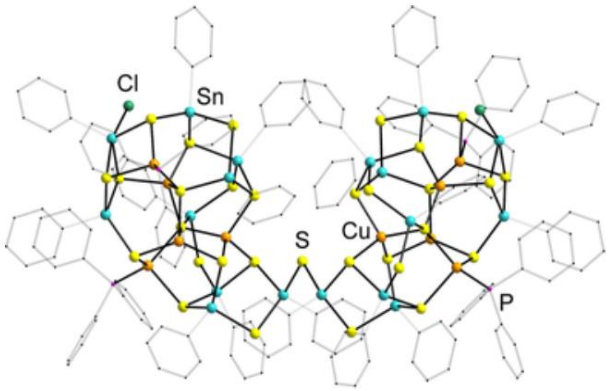

$[(\text{CuPPh}_3)_4(\text{PhSn})_{18}\text{Cu}_6\text{S}_{31}\text{Cl}_2]$[30]

Abbildung 1.1.6: Auswahl kristallographisch charakterisierter Molekülstrukturen unterschiedlicher ternärer Präkursoren für Cu_2ZnSnS_4 Materialien.[28–30]

1.2 Ionische Flüssigkeiten bzw. Organische Salze

Ionische Flüssigkeiten (ILs) sind ionische Verbindungen, deren Schmelztemperaturen definitionsgemäß unterhalb von 100 °C zu liegen haben.[31] Um die Gitterenergie zu senken, enthalten ILs oft ein organisches, asymmetrisches gebautes Kation und ein anorganisches Anion. Auch inverse Varianten oder rein organische Salze sind bekannt. Im Laufe der vergangenen Jahrzehnte hat sich die Anzahl an Publikationen um dieses Themengebiet rasant entwickelt, was die zunehmende Forschungsrelevanz dieser Substanzklasse unterstreicht.[31] Dabei wurde das Potential der vor gut 100 Jahren erstmals beiläufig in elektrochemischen Studien angewendeten, aber lange Zeit nicht weiter beachteten Substanzklasse zunächst nicht erkannt.[31] Mittlerweile sind ILs Gegenstand zahlreicher anwendungsnaher Forschungsgebiete: IL-basierte Elektrolyte gelten aufgrund ihres großen Spannungsfensters und vernachlässigbaren Dampfdrucks nach wie vor als sichere Alternativen zu herkömmlichen Elektrolytlösungen für Superkondensatoren und Akkumulatoren[32] und es gibt einige organische Reaktionen bzw. industrielle Verfahren, die durch Anwendung IL-basierter Technologien einfacher und nachhaltiger durchgeführt werden können.[33] Darunter fallen die Auflösung und Prozessierung von Biomasse[34,35] und Polymeren[36] sowie die Anwendung als nichtflüchtiges Lösungsmittel in organischen Synthesen, die mit ILs deutlich bessere Ausbeuten und Selektivitäten liefern können.[37] Seit einiger Zeit werden ILs zudem ausgiebig in ihrer Funktion als Templatmedium zur Herstellung von Nanopartikeln und anderen Materialien erforscht, was Anlass zur Gründung des DFG-Schwerpunktprogramms „SPP 1708 - Materialsynthese nahe Raumtemperatur“ gab.[38] Dieses Schwerpunktprogramm hat die vorliegende Arbeit maßgeblich mitfinanziert.[39]

Die Ionen von ILs sind durch eine ausgeprägte Ladungsdelokalisation und eine einfache sterische Modifizierbarkeit gekennzeichnet. Prominente Kationen ionischer Flüssigkeiten leiten sich von alkylierten Heterozyklen (z. B. *N,N‘*-Dialkylimidazolium- oder *N,N*-Dialkylpyrrolidinium-kationen) und alkylierten Aminen bzw. Phosphinen (Ammonium- bzw. Phosphoniumkationen) ab (*Abbildung 1.2.1, links*).[31] Als Anionen dienen typische Vertretern schwach koordinierender Anionen z. B. Tetrafluoridoborat $[BF_4]^-$, Hexafluoridophosphat $[PF_6]^-$ oder Bistriflimid $[TFSI]^-$.[31] Auch den durch Addition organischer Chloridsalze an Metallchloride zugänglichen Chlorometallat-Anionen $[MCl_{n+x}]^{x-}$ kommt Relevanz als Ausgangspunkt für die Synthesen der vorliegenden Arbeit zu (*Abbildung 1.2.1, rechts*).

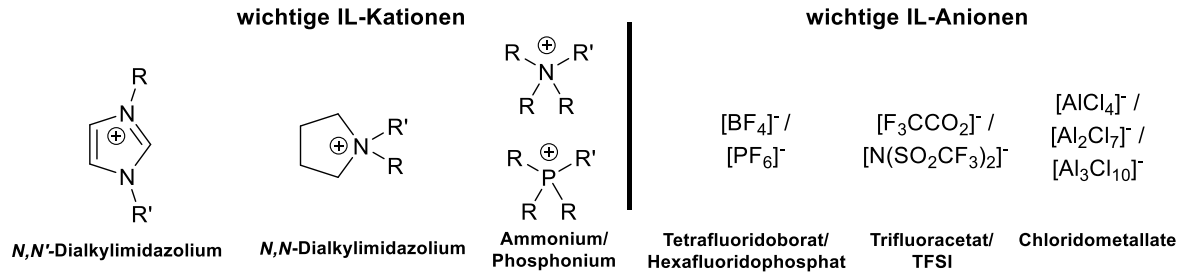

Abbildung 1.2.1: Auswahl üblicher IL-Kationen (links) und Anionen (rechts) (R = Alkyl, Aryl; R‘ = Alkyl).[31]

Der chemische Aufbau einer IL kann der entsprechenden Anwendung angepasst werden. Durch eine wohlgewählte Substitution des Heteroatoms kann die Symmetrie der Kationen auf eine Art und Weise beeinflusst werden, die der Kristallisation des entsprechenden Salzes (bzw. der IL) zuträglich oder hinderlich ist. Dadurch kann z. B. dessen Schmelzpunkt oder Viskosität erniedrigt oder erhöht werden, wobei ein niedriger Schmelzpunkt für die Anwendung- und ein hoher Schmelzpunkt für die strukturelle Charakterisierung des Salzes von Interesse sein kann. Auch Fragen der chemischen Inertheit hinsichtlich der thermischen und elektrochemischen Stabilität der IL können bei der Wahl geeigneter Anionen und Kationen berücksichtigt werden.[31,33] Durch die mannigfaltig substituierbaren Grundkörper für Kationen und Anionen steht eine nahezu beliebige Vielfalt an Ionen zur Verfügung, mit denen eine anwendungsspezifische IL designt werden kann. Dies führte zum Begriff der „*Task Specific Ionic Liquids*“, welcher der eigenschaftsbestimmenden Modifizierbarkeit von ILs Rechnung trägt.[31] Gegenstand der vorliegenden Arbeit ist die Darstellung chalkogenbasierter Materialien unter Verwendung metastabiler Metallat-Anionen, die in IL-ähnlichen, organischen Salzen vorliegen. Dabei geht es auch um die Fragestellung, wie aus den von *Dr. Lars Finger* systematisch erschlossenen Salzen Cat[ESiMe$_3$][40] über definierte Zwischenstufen Materialien wie CIGS oder CZTS hergestellt werden können.

Ein etabliertes Syntheseprotokoll zur Herstellung von ILs verläuft i. d. r. über die Alkylierung eines nucleophilen Heteroatoms, etwa in *N*-Methylpyrrolidin, durch ein elektrophiles Alkylierungsmittel wie z. B. 1-Chlorobutan unter Ausbildung des *N,N*-Dialkylpyrrolidinium-chlorid Salzes BMPyr[Cl] (BMPyr$^+$ = *N*-Butyl-*N*-methylpyrrolidinium). Dieses kann anschließend entweder mit geeigneten Metallsalzen, z. B. Ag[TFSI], unter Eliminierung von AgCl zur gewünschten IL BMPyr[TFSI], oder unter Addition einer Lewis-aciden Verbindung MX’$_n$ zu einem Addukt BMPyr[ClMR‘$_n$] umgesetzt werden (*Schema 1.2.1*). Alternativ gibt es IL-Synthesen über Anionenaustauschharze oder Brønsted-Säuren, die je nach Art des einzuführenden Kations mehr oder weniger gut zugänglich sind (*Schema 1.2.1*).[31]

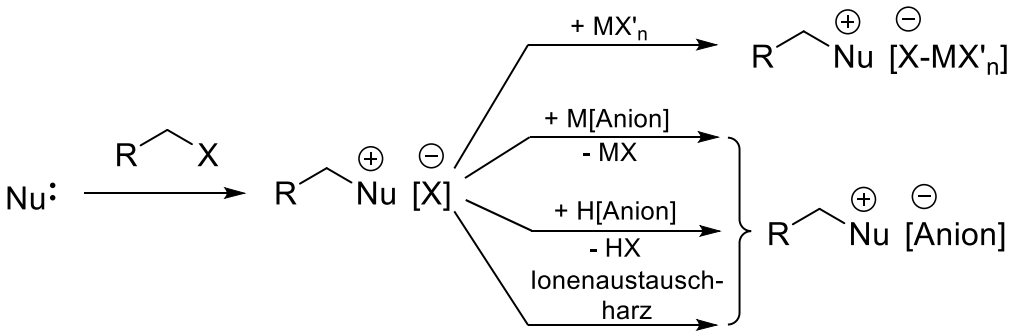

Schema 1.2.1: Allgemein übliche Synthesestrategien zur Herstellung von ILs.[31]

Werden hochreine ILs benötigt, so sind die Salzeliminierungsstrategien im Regelfall unbrauchbar, da die eliminierten Salze oft nicht zufriedenstellend von der nicht flüchtigen IL getrennt werden können. Dabei sind es insbesondere die Metall- und Halogenidionen, die eine nachteilige Auswirkung auf die elektrochemischen Eigenschaften einer derart verunreinigten IL haben. Ebenso störend können sich Spuren von Wasser auswirken, z. B. auf das realisierbare Spannungsfenster der IL. Aus diesem Grund sind IL-Synthesestrategien gefragt, bei denen von vornherein keine salzartigen Nebenprodukte anfallen und im Idealfall kein Wasser in die IL-Phase gelangt.[31] Daher ist die Methylcarbonat-Route eine weitverbreitete Methode zur Herstellung hochreiner ILs, die sich sowohl hinsichtlich ihrer Umweltverträglichkeit als auch ihrer Zuverlässigkeit bewähren konnte.[41–43] Die geforderte Salz- und Wasserfreiheit wird bereits durch die Methodik gewährleistet. Auch zur Herstellung der im Zuge dieser Arbeit bedeutsamen chalkogenbasierten organischen Salzen ist die Methylcarbonat-Route von übergeordneter Relevanz,[40,44,45] weshalb sie im Folgenden näher vorgestellt werden soll.

1.2.1 Chalkogenanionen-basierte organische Salze

Organische Methylcarbonatsalze (Nu-Me[OCO_2Me]) lassen sich sehr einfach über die Methylierung geeigneter Nukleophile (Nu:) mit Dimethylcarboant (Me_2CO_3) unter Solvothermalbedingungen, z. B. in Methanol bei 130°C für 18 h,[40] herstellen (*Schema 1.2.1.1*, *links*). Das Methylcarbonatanion kann genügend starke Brønsted-Säuren deprotonieren und geeignete Präkursoren mit elektrophilen Trimethylsilylgruppen desilylieren.[40,45] Der gebildete protonierte bzw. silylierte Kohlensäureester $ROCO_2Me$ (R = H bzw. $SiMe_3$) zerfällt direkt, irreversibel und selektiv unter Ausbildung von CO_2 und MeOH bzw. $MeOSiMe_3$ (*Abbildung 1.2.1.1, rechts*). Diese Nebenprodukte lassen sich sehr einfach unter vermindertem

Druck entfernen. Da der zugrundeliegende Quaternisierungsschritt eine Methylierung ist und andere analoge Alkylierungen gar nicht oder nicht quantitativ verlaufen, beschränkt sich diese Methode auf mindestens einfach methylierte Oniumionen. Ein Teil der vorliegenden Arbeit ist der Umgehung dieser Limitierung gewidmet.

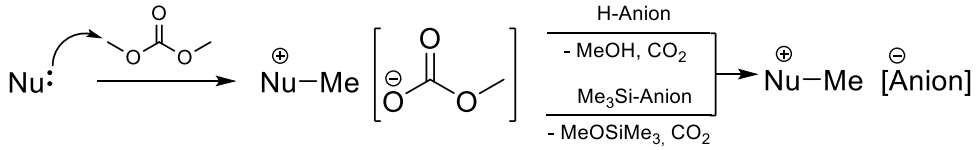

Schema 1.2.1.1: Herstellung organischer Methylcarbonatsalze und deren auf Deprotonierung und Desilylierung beruhende Folgechemie.

Diese für tertiäre und zyklische Amine und Phosphine ohne weitere Komplikationen durchführbare Reaktionsführung ist für Methylcarbonat Salze mit CH-aziden Kationen, wie den *N,N'*-Dialkylimidazoliumkationen $RRIm^+$ komplexer: zunächst liegt direkt nach der Methylierung des Alkylimidazolvorläufers RIm mit Me_2CO_3 das entsprechende Methylcarbonatsalz $MRIm[OCO_2Me]$ in verdünnter methanolischer Lösung vor. Bei Entfernen des Lösungsmittels unter vermindertem Druck wird die Basizität des Methylcarbonatanions durch Verringerung der Solvatation derart gesteigert, dass das C2-gebundene Proton abstrahiert wird und ein intermediäres NHC entsteht. Dieses reagiert unmittelbar mit dem durch den Zerfall des protonierten Methylcarbonats generierten CO_2 unter Ausbildung der Carboxylatverbindung $NHC\text{-}CO_2$ (*Schema 1.2.1.2*).[46]

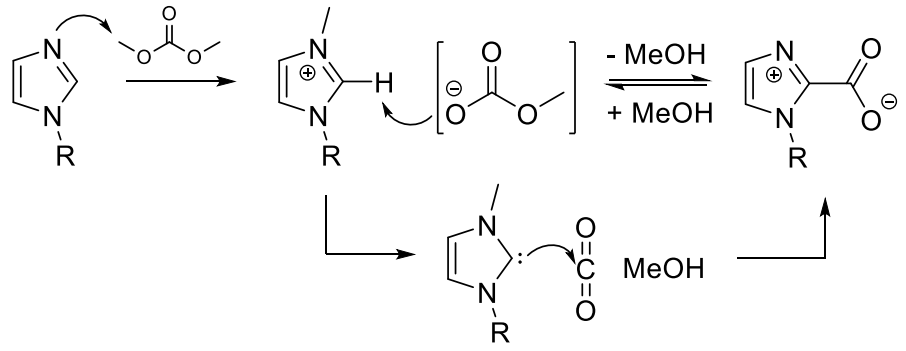

Schema 1.2.1.2: Mechanismus der Entstehung von NHC-CO_2 aus solvothermal dargestellten Dialkylimidazolium-Methylcarbonatsalzen.

Die reversible Addition/Eliminierung von Methanol impliziert, dass das Methylcarbonatsalz nur in verdünnter methanolischer Lösung zur Deprotonierung/Desilylierung zur Verfügung

steht. Somit ist diese Route ungeeignet für Synthesen, in denen methanolempfindliche Edukte und Produkte involviert sind, wie z. B. $E(SiMe_3)_2$ oder *t*BuE($SiMe_3$), die in Methanol zu H_2E bzw. *t*BuEH und $MeOSiMe_3$ solvolysiert werden (E = S, Se, Te). Die etablierte Desilylierungsroute[40] zur Darstellung chalkogen-basierter organischer Salze über entsprechende Methylcarboantsalze war bislang somit nur für Ammonium- und Phosphonium-, nicht jedoch für Dialkylimidazoliumkationen anwendbar. Die organischen Hydrogenchalkogenidsalze sind hingegen ohne weiteres auch für Dialkylimidazoliumsalze zugänglich, da diese über Deprotonierungsreaktionen in Methanol zugänglich sind und nicht methanolysiert werden können (*Schema 1.2.1.3*).[45]

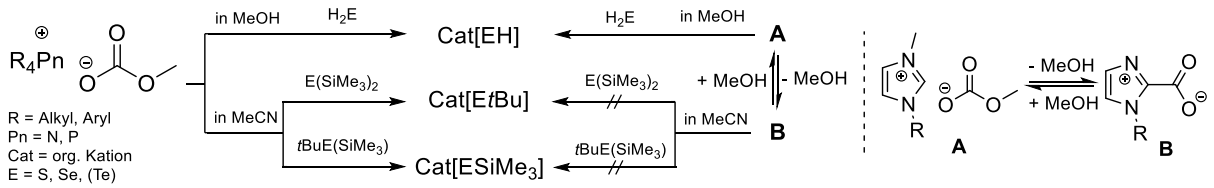

Schema 1.2.1.3: Etablierte Synthesewege zu E = S, Se, Te basierten ILs.[40,45]

Um diese Beschränkungen zu umgehen, wurden von *Finger* 1,2,3-Trialkylimidazolium-Methylcarbonatsalze untersucht.[47] Da das CH azide, C2-gebundene Proton dort durch eine Methylgruppe ausgetauscht wurde, ist die Carboxylatbildung unterbunden. Allerdings lässt sich das Methylcarbonatsalz EMMIm[OCO_2Me] auf diese Weise nicht rein isolieren, da dieses immer zu 5-10% Verunreinigung durch das CO_2-Addukt des *N*-heterozyklischen Olefins (NHOs) NHO-CO_2 enthält. Trotzdem gelang mit diesem verunreinigten Produkt die Darstellung von EMMIm[$SSiMe_3$], einer Verbindung, die gemäß *Schema 1.2.1.3* für Alkylimidazoliumkationen zuvor unzugänglich war. Interessanterweise stellte es sich dennoch als unmöglich heraus, das entsprechende Tertbutylthiolat EMMIm[S*t*Bu] über eine Deprotonierung von HS*t*Bu oder eine Desilylierung von Me_3SiStBu mit EMMIm[OCO_2Me] durchzuführen.[47] Die Gründe dafür sind die zu geringe Brönstedbasizität des Methylcarbonatanions und die hohe Basizität des $[St\text{Bu}]^-$ Anions. Letzteres deprotoniert das $EMMIm^+$ Kation partiell zum NHO, das in Anwesenheit von CO_2 irreversibel zum zwitterionischen NHO-CO_2 Addukt abreagiert und das NHO damit aus dem Gleichgewicht entfernt (*Schema 1.2.1.4*).[47]

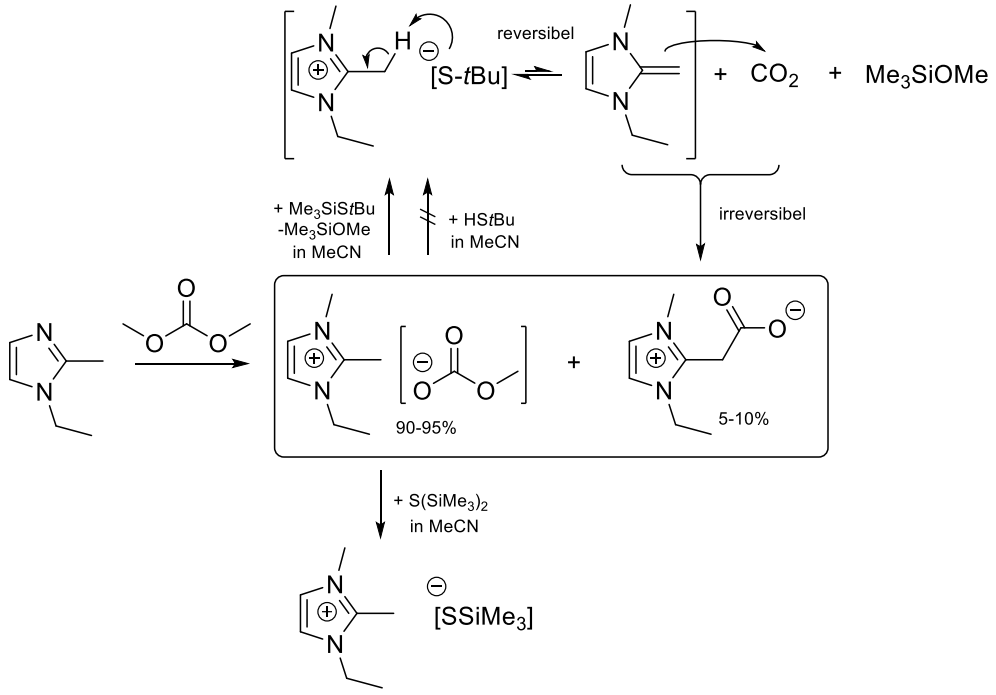

Schema 1.2.1.4: Darstellung bisher unzugänglicher, chalkogenbasierter organischer Salze mit Imidazoliumkationen.[47]

Eine im Zuge dieser Untersuchungen ausgearbeitete, elegante Methode, die diese Beschränkung der Einsetzbarkeit von Dialkylimidazolium Methylcarbonatsalzen umgeht, ist über die Addition von *N*-Heterozyklischen Olefinen an Brønsted-Säuren gegeben.[47] Durch die Addition des EMMIm-NHOs an HS*t*Bu wurde aus Tetrahydrofuran das *Tert*buthylthiolat EMMIm[StBu] ausgefällt, das nach Filtration und Trocknung im Feinvakuum hochrein vorliegt (*Schema 1.2.1.5, links*).[47] Die Addition von NHOs an Brønsted-Säuren zur Herstellung organischer Salze/ILs wurde von *Linder* und *Sundermeyer* veröffentlicht (*Schema 1.2.1.5, mittig*).[48,49] Die homologe Variante mit *N*-Heterozyklischen Carbenen (NHC) wurde zuvor von *Earle* und *Seddon* in einem Patent veröffentlicht (*Schema 1.2.1.5, rechts*).[50] Die diesen Patenten zugrundeliegende Strategie ist ein Ausgangspunkt der vorliegenden Arbeit.

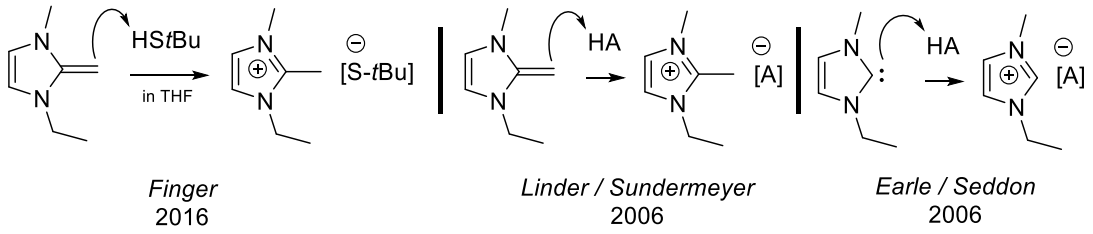

Schema 1.2.1.5: Selektive Darstellung von EMMIm[StBu] über Addition/Deprotonierung von HStBu mit NHO (links), nach Vorbild der patentierten Addition von Brønsted-Säuren an NHOs (mittig) und NHCs (rechts).[47,48,50]

Das synthetische Anwendungspotential chalkogenbasierter organischer Salze wurde bereits eingehend durch die Synthesen organischer Salze mit diversen Polychalkogenidanionen belegt.[40,45] So können Cat[HS] Salze mit unterschiedlichen Mengen elementaren Schwefels (S_8) zu den Polysulfidsalzen $Cat_2[S_n]$ (n = 2, 4, 6, 8) umgesetzt werden. Dabei wird davon ausgegangen, dass elementarer Schwefel „(n/8) S_8“ in Anwesenheit von 2 $[HS]^-$ Anionen unter Eliminierung von H_2S zu „$[S_{n+1}]^{-2}$“ reduziert wird.[45] Dies konnte analog für Cat[$ESiMe_3$]-Salze durchgeführt werden, womit Polysulfide wie $Cat_2[S_6]$ und Polyselenide wie $Cat_2[Se_3]$ hergestellt wurden (*Abbildung 1.1.1.1*, links bzw. mittig).[40] Zudem wurde die Bildung von Polychalkogeniden, etwa des tetraanionischen Dodekatellurids $Cat_4[Te_{12}]$ (*Abbildung 1.1.1.1*, *links*), beobachtet. Dieses wurde als Zerfallsprodukt von DMPyr[$TeSiMe_3$][40] aber auch von BMPyr [TeH] erhalten.[45]

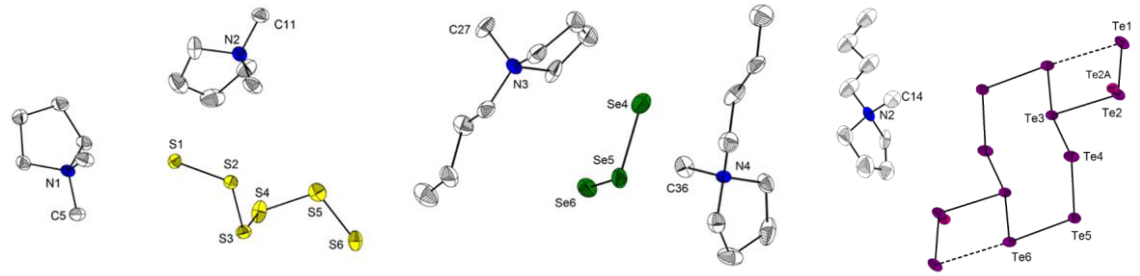

DMPyr$_2$[S$_6$]^{40} **BMPyr$_2$[Se$_3$]^{40}** **BMPyr$_4$[Te$_{12}$]^{45}**

Abbildung 1.1.1.1: Kristallographisch charakterisierte organische Polychalkogenidsalze, die über chalkogenbasierte organische Salze erhalten wurden.[40,45]

Eine weitere Anwendung wurde durch den *Pseudoflux-Approach* ausgearbeitet. Dabei werden Selenomerkurate wie z. B. Na_2HgSe_2 in eine Schmelze aus EMIm[SH] gegeben. Hierbei wird ein partieller Austausch von Selenatomen durch Schwefelatome bei vergleichsweise sehr niedrigen Temperaturen beobachtet.[51]

Im Zuge der vorliegenden Arbeit wird die Integration von Metallkationen in Systeme der organischen Salze mit chalkogenbasierten Anionen Cat[ER] (Cat = organisches Kation; E = S, Se, (Te); R = H, *t*Bu, $SiMe_3$) beschrieben. Die dadurch erhaltenen Metallate Cat[L_nM-ER] (M = Metall, L = weitere, anionische Liganden) und deren Folgeprodukte können als binäre M/E Bausteine zur Materialsynthese angesehen werden. Damit ist eine Schnittmenge zwischen Metallkomplexen und reaktiven Chalkogenliganen definiert: Je nach Chalkogensubstituent korrekterweise als Chalkogenid (E^{2-}), Chalkogenolat ($[ESiMe_3]^-$ / [E*t*Bu]$^-$) und Chalkogenol (EH) bezeichnet. Bislang bekannte Metallkomplexe mit reaktiven $[ESiMe_3]^-$ Liganden sollen im Folgendem ausführlicher beschrieben werden.

1.3 Komplexe mit Trimethylsilylchalkogenolatliganden

Metallkomplexe $[L_nM(ESiR_3)_n]$, die neben stabilisierenden Hilfsliganden L silylierte Chalkogenolatliganden $[ESiR_3]^-$ enthalten, sind potenzielle Synthone für $\{ME_n\}^{n-}$ Einheiten, etwa in heterometallischen Clustermolekülen.[52] In den Arbeiten von *J. F. Corrigan et al.* werden zahlreiche entsprechende Verbindungen eingehender hinsichtlich ihres Potenzials bei der Synthese mehrkerniger Komplexe und niedermolekularer heterometallischer Cluster und Halbleitermaterialien untersucht.[52–61] Grundlage der Reaktivität von Silylchalkogenolato-liganden ist die ausgeprägte Schwäche der E-Si (E = S, Se, Te) Bindung. Diese kann leicht durch geeignete Desilylierungsmittel wie z. B. organische Fluorid- oder Chloridsalze, Metallacetate oder auch thermisch heterolytisch gebrochen werden kann (*Schema 1.3.1*).[52] Dadurch sind Komplexe mit $[ESiR_3]^-$ Liganden eine nützliche Erweiterung zu den weitverbreiteten Organochalkogenolato-Liganden, deren E-C Bindungen deutlich schwerer zu brechen sind.

Illustrative Beispiele für das synthetische Potenzial von $[L_nM(ESiMe_3)_n]$ Verbindungen sind unter anderem die Darstellung hochempfindlicher heterometallischer Cluster wie $[(NHC\text{-}Ag)_2Hg]$ aus $Hg(OAc)_2$ und NHC-AgSSiMe$_3$ (*Abbildung 1.3.1*, mittig),[53] oder die Synthese der kleinsten bekannten molekularen Einheit von Cu_2S, $[(NHC\text{-}Cu)_2S]$ (*Abbildung 1.3.2*, rechts), die ausgehend von NHC-CuSiMe$_3$ über eine fluoridvermittelte Desilylierung von NHC-CuSSiMe mit NHC-CuF sehr einfach durchführbar ist *(Schema 1.3.1)*.[62]

Allgemein:

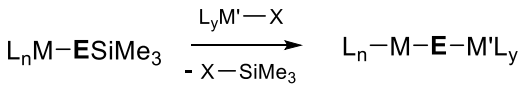

Beispiel 1:

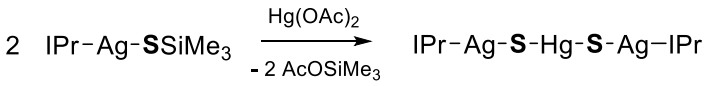

Beispiel 2:

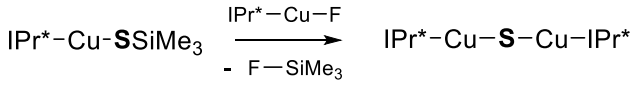

Schema 1.3.1: Kondensationen unter Eliminierung von Me_3SiX (oben). Beispiel 1: Herstellung von $[(IPrAgS)_2Hg]$. Beispiel 2: $[IPr^*Cu)_2S]$ (unten) (IPr: 1,3-bis(2,6-diisopropylphenyl)imidazolin-2-yli-dene; IPr = 1,3-bis(2,6-(diphenylmethyl)-4-methylphenyl)imidazol-2-ylidene).*

Hier sei darauf verwiesen, dass in den Zielverbindungen die verbrückenden Chalkogenatome als „$[\mu_2\text{-E}]^{2-}$“ vorliegen und damit als kleine Untereinheiten der entsprechenden Metallchalkogenidmaterialien angesehen werden können. Ein weiteres Wachstum zum Festkörper wird durch die stabilisierenden Hilfsliganden am Metall unterbunden. Durch Thermolyse von $[L_nM(ESiMe_3)_n]$ werden nach Eliminierung von $E(SiMe_3)_2$ und n L (L = z. B. TMEDA, Phosphine, etc.) die sauberen Metallchalkogenid-Volumenphasen erhalten. Dies wurde für $[Cd(ESiMe_3)_2]$[63] und $[L_nZn(ESiMe_3)_2]$[54,56] ausführlich untersucht. Eine weitere erwähnenswerte Anwendung ist die Herstellung mehrkerniger Münzmetallchalkogenid-Cluster $[Au_4M_4(\mu_3\text{-E})_4(IPr)_4]$ (M = Au, Ag; E = S, Se, Te) mit einstellbaren optischen Eigenschaften. Deren Synthese geht von $[IPrAuESiMe_3]$ aus,[59] und konnte vergleichbar auf kupferbasierte Cluster $[Cu_4M_4(\mu_3\text{-E})_4(CAAC^{Cy})_4]$ (M = Cu, Ag, Au; E = S, Se) übertragen werden. Hierbei wurde allerdings ein deutlich stärker stabilisierender zyklischer Alkyl-amincarben ($CAAC^{Cy}$) Hilfsligand für das Edukt $[(CAAC^{Cy})CuESiMe_3]$ (E = S, Se) benötigt.[60]

Bei Verwendung der stabileren Organochalkogenolatliganden können die organischen Reste erst bei vergleichsweise hohen Temperaturen entfernt werden. Entsprechend ungeeignet sind sie für die Darstellung besonders metastabiler heterometallischer Komplexe. Als Beispiel sei hier dennoch die Clusterverbindung $Ph_4P[Cu_6In_3(SEt)_{16}]$ genannt,[64] deren heteroadamantanartige Struktur als niedermolekulare Untereinheit der Chalkopyritstruktur von CIGS Materialien angesehen werden kann (*Abbildung 1.3.1, links*). Auch Präkursoren für sowohl Volumenphasen als auch Nanopartikel wurden mit derartigen Liganden stabilisiert, etwa die bereits vorgestellten CIGS-*Single Source* Präkursoren.[23]

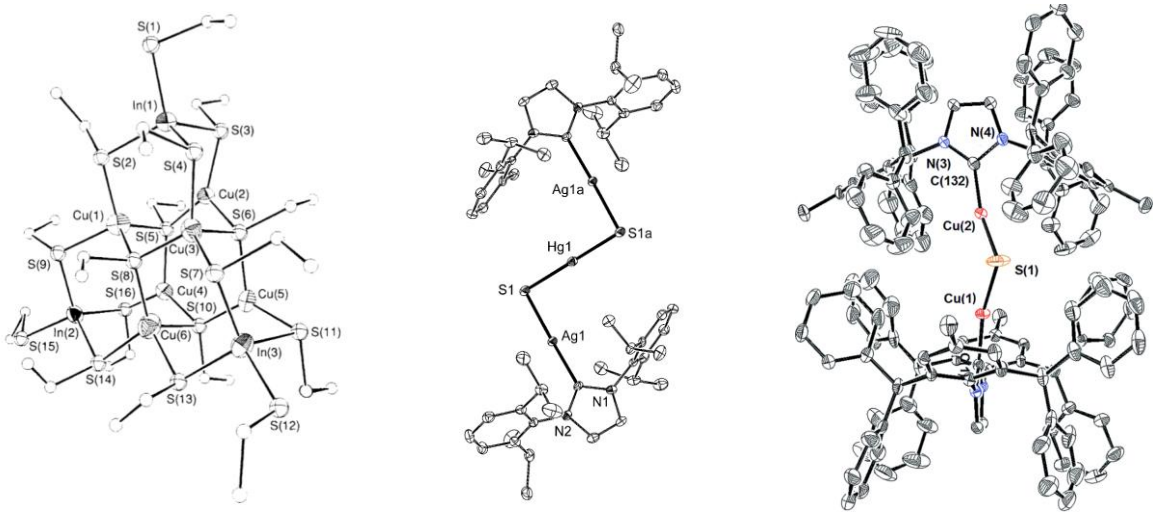

$Ph_4P[Cu_6In_3(SEt)_{16}]$[64] **$[(NHC\text{-}AgS)_2Hg]$[53]** **$[(NHC\text{-}Cu)_2S]$[62]**

Abbildung 1.3.1: Gezielter Aufbau chalkogenbasierter heterometallischer Verbindungen. Links: Alkylchalkogenolat-Cluster, mittig/rechts: mehrkernige Komplexe mit „$[\mu_2\text{-S}]^{2-}$“ Einheiten aus entsprechenden $[SSiMe_3]^-$-Vorläufern.

Im Folgenden soll auf die wichtigsten bisher bekannten und eingehend charakterisierten Vertreter von $[L_nM(ESiMe_3)_n]$ Verbindungen eingegangen werden. Für eine weitergehende Diskussion der bisher erschlossenen Folgechemie von sei an dieser Stelle auf die Literatur verwiesen.[52,53,55–59]

Die Darstellung von $[L_nM(ESiMe_3)_n]$ erfolgt im Regelfall entweder direkt über die Desilylierung von $E(SiMe_3)_2$[52] oder über eine Salzeliminierung ausgehend von $NaESiMe_3$[65] bzw. $LiESiMe_3$[66] mit Acetato- oder chloridokomplexen geeigneter Hilfsliganden L_n: L_nMX_y (X = OAc, Cl) (*Schema 1.3.2*).[52,66]

Schema 1.3.2: Synthesestrategien für $[L_nM(ESiMe_3)_n]$ Verbindungen.[52]

In *Tabelle 1.3.1* ist ein Überblick über die wichtigsten bisher bekannten und untersuchten Neutralverbindungen mit $[ESiMe_3]^-$ Liganden gezeigt. Obwohl Trialkylphosphinkomplexe $[(R_3P)_nCuESiMe_3]$[67] im Vergleich zu den einfach handhabbaren NHC-Vertretern deutlich instabiler sind,[53,57] bilden sie die Grundlage für eine der äußerst wenigen Verbindungen, in denen eine an ein Gruppe 13 Metall gebundene $ESiMe_3$-Gruppe vorliegt. Diese beschränken sich auf das Addukt von $[(i\text{Pr}_3P)_2CuESiMe_3]$ mit $InMe_3$, $[(i\text{Pr}_3P)_2Cu(\mu_3\text{-E-SiMe}_3)(InMe_3)]$ (E = S, Se) (*Abbildung 1.3.2, links*),[68] und die über partielle Methanolyse in Anwesenheit von MMe_3 und $ESiMe_3$ gewonnenen spirocyclischen Verbindungen $[(Me_2M)_6E(ESiMe_3)_4]$ (E = S (M = In), Se (M = Ga)) *(Abbildung 1.3.2, mittig*).[69] Die Vierringverbindungen $[t\text{Bu}_2M(\mu_2\text{-SeSiMe}_3)]_2$ (M = Ga, In) konnten durch Umsetzung von Me_2MCl und $Se(SiMe_3)_2$ hergestellt werden.[70] Ausdrücklich erwähnt sei hier auch der einzig bisher strukturell charakterisierte homoleptische Metallatkomplex $[(TMEDA)Li]_2[Mn(SSiMe_3)_4]$ (*Abbildung 1.3.2, rechts*).[58]

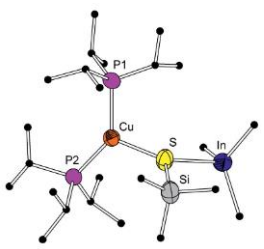

$[(i\text{Pr}_3P)_2Cu(\mu_3\text{-E-SiMe}_3)(InMe_3)]$
(E = S, Se)[68]

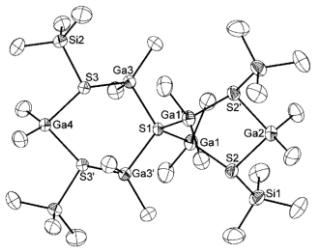

$\{[(Me_2M)_3(\mu_3\text{-ESiMe}_3)_2]_2(\mu_4\text{-E})\}$
(E = S (M = In), Se (M = Ga))[69]

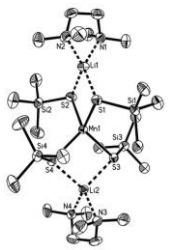

$[(TMEDA)Li]_2[Mn(SSiMe_3)_4]$ [58]

Abbildung1.3.2: Gruppe 13-Komplexe (links, mittig) und einziger strukturell belegter homoleptischer Metallatkomplex (rechts) mit $[ESiMe_3]^-$ Liganden.

Tabelle 1.3.1: Übersicht der bekannten Metallkomplexe mit $ESiMe_3$-Liganden; es ist jeweils nur ein kristallographisch charakterisierter Vertreter homologer Verbindungen gezeigt.

Gruppe 1: $LiESiMe_3$,[61,66] $NaESiMe_3$.[65]

Gruppe 11: IPr-Cu($ESiMe_3$) (E = S, Se, Te),[57] [($CAAC^{Cy}$)Cu$ESiMe_3$] (E = S, Se),[60] IPr-Ag($ESiMe_3$) (E = S, Se),[53] IPr-Ag($ESiMe_3$) (E = S, Se, Te).[59]

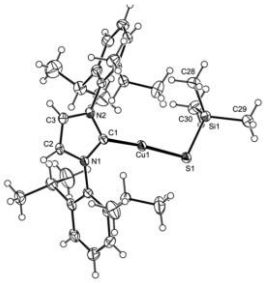

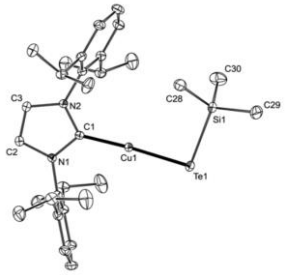

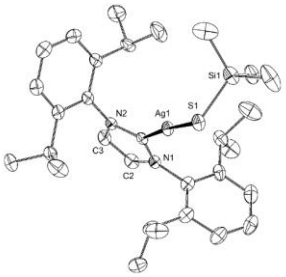

Gruppe 4: $Cp_2Ti(SSiMe_3)_2$[71]

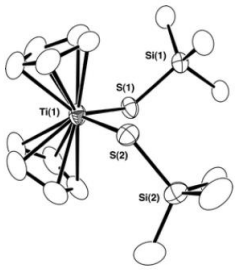

Gruppe 9: [(TMEDA)Co($ESiMe_3$)$_2$] (E = S, Se),[58] [(3,5-$Me_2C_5H_3N$)$_2$Co($ESiMe_3$)$_2$] (E = S, Se).[58]

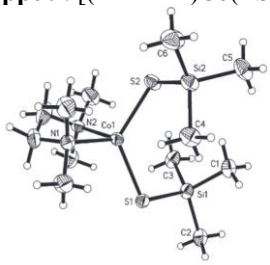

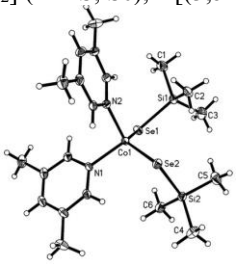

Gruppe 10: [(dppe)M($SSiMe_3$)$_2$] (M = Ni, Pt, Pd).[65]

Gruppe 12: [(3,5-$Me_2C_5H_3N$)$_2$Zn($ESiMe_3$)$_2$] (E = S, Se, Te),[55] [(TMEDA)Cd($ESiMe_3$)$_2$] (E = S, Se),[54] [(TMEDA)Zn($ESiMe_3$)$_2$] (E = S, Se, Te).[55]

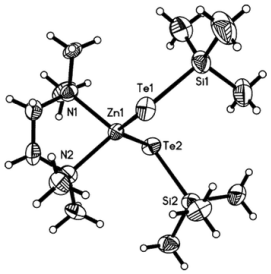

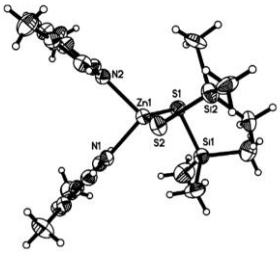

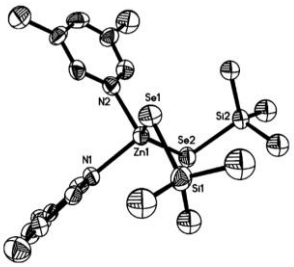

Dies ist der Kenntnisstand zu Beginn der vorliegenden Arbeit. Aus diesem ergab sich die folgende Aufgabenstellung.

1.4 Literaturverzeichnis

(1) https://www.bmu.de/themen/klima-energie/klimaschutz/nationale-klimapolitik/klimaschutzplan-2050/#c8418 (Status 18:00 Uhr, 20.08.2019).

(2) https://ourworldindata.org/fossil-fuels (Status 17:30 Uhr, 20.08.2019).

(3) https://www.nrcan.gc.ca/energy/publications/efficiency/industrial/cipec/6695 (Status 17:00 Uhr, 20.08.2019).

(4) https://energypost.eu/twenty-first-century-energy-wars-oil-gas-fuelling-global-conflicts/ (Status 18:20 Uhr, 20.08.2019).

(5) Dincer, I. Renewable energy and sustainable development: a crucial review. *Renewable and Sustainable Energy Reviews* **2000**, *4*, 157–175.

(6) http://www.collector-ag.com/erneuerbare-energien/arten-von-erneuerbaren-energien.html (Status 8:30 Uhr; 21.08.2019).

(7) Fraunhofer Institute for Solar Energy Systems, ISE. Photovoltaic Report: https://www.ise.fraunhofer.de/content/dam/ise/de/documents/publications/studies/Photovoltaics-Report.pdf (Status (8:40 Uhr, 21.08.2019).

(8) Hersch, P.; Zweibel, K. *Basic Photovoltaic Principles and Methods*, U. S. Government Printing Office, Washington D. C., **1982**, 9ff.

(9) Ramanujam, J.; Singh, U. P. Copper indium gallium selenide based solar cells – a review. *Energy Environ. Sci.* **2017**, *10*, 1306–1319.

(10) Green, M. A. Third generation photovoltaics: solar cells for 2020 and beyond. *Physica E* **2002**, *14*, 65–70.

(11) Kessler, F.; Rudmann, D. Technological aspects of flexible CIGS solar cells and modules. *Solar Energy* **2004**, *77*, 685–695.

(12) Parisi, A.; Pernice, R.; Rocca, V.; Curcio, L.; Stivala, S.; Cino, A. C.; Cipriani, G.; Di Dio, V.; Ricco Galluzzo, G.; Miceli, R.; Busacca A. C. Graded Carrier Concentration Absorber Profile for High Efficiency CIGS Solar Cells. *Int. J. Photoenerg.* **2015**, *2015*, 1–9.

(13) http://www.solar-frontier.com/eng/news/2019/ 0117_press.html (Stand 28.08.2019). http://www.solar-frontier.com/eng/news/2019/ 0117_press.html (Status 15:00 Uhr, 28.08.2019).

(14) Tai, Q.; Tang, K.-C.; Yan, F. Recent progress of inorganic perovskite solar cells. *Energ. Environ. Sci.* **2019**, *12*, 2375–2405.

(15) Qian, J.; Ernst, M.; Wu, N.; Blakers, A. Impact of perovskite solar cell degradation on the lifetime energy yield and economic viability of perovskite/silicon tandem modules. *Sust. Energ. Fuels* **2019**, *3*, 1439–1447.

(16) Ravindiran, M.; Praveenkumar, C. Status review and the future prospects of CZTS based solar cell – A novel approach on the device structure and material modeling for CZTS based photovoltaic device. *Renew. and Sust. Energ. Rev.* **2018**, *94*, 317–329.

(17) http://www.solar-frontier.com/eng/news/2019/ 0117_press.html (Status 12:00 Uhr, 21.08.2019).

(18) https://www.pv-magazine.com/2013/12/11/solar-frontier-breaks-czts-cell-efficiency-record_100013707/ (Status 11:00 Uhr, 21.08.2019).

(19) Yan, C.; Huang, J.; Sun, K.; Johnston, S.; Zhang, Y.; Sun, H.; Pu, A.; He, M.; Liu, F.; Eder, K.; Yang, L.; Cairney, J. M.; Ekins-Daukes, N. J.; Hameiri, Z.; Stride, J. A.; Chen, S; Green, M. A.; Hao, X. Cu_2ZnSnS_4 solar cells with over 10% power conversion efficiency enabled by heterojunction heat treatment. *Nat. Energ.* **2018**, *3*, 764–772.

(20) Wallace, S. K.; Frost, J. M.; Walsh, A. Atomistic insights into the order–disorder transition in Cu_2ZnSnS_4 solar cells from Monte Carlo simulations. *J. Mater. Chem. A* **2019**, *7*, 312–321.

(21) Ghorbani, E.; Kiss, J.; Mirhosseini, H.; Roma, G.; Schmidt, M.; Windeln, J.; Kühne, T. D.; Felser, C. Hybrid-Functional Calculations on the Incorporation of Na and K Impurities into the $CuInSe_2$ and $CuIn_5Se_8$ Solar-Cell Materials. *J. Phys. Chem. C* **2015**, *119*, 25197–25203.

(22) Bosson, C. J.; Birch, M. T.; Halliday, D. P.; Knight, K. S.; Gibbs, A. S.; Hatton, P. D. Cation disorder and phase transitions in the structurally complex solar cell material Cu_2ZnSnS_4. *J. Mater. Chem. A* **2017**, *5*, 16672–16680.

(23) Hirpo, W.; Dhingra, S.; Sutorik, A. C.; Kanatzidis, M. G. Synthesis of mixed copper-indium chalcogenolates. Single-source precursors for the photovoltaic materials $CuInQ_2$ (Q = S, Se). *J. Am. Chem. Soc.* **1993**, *115*, 1597–1599.

(24) Zhao, X.; Huang, Y.; Corrigan, J. F. Facile Preparation of Wurtzite $CuInE_2$ (E = S, Se) Nanoparticles Under Solvothermal Conditions. *Inorg. Chem.* **2016**, *55*, 10810–10817.

(25) Kluge, O.; Biedermann, R.; Holldorf, J.; Krautscheid, H. Organo-gallium/indium chalcogenide complexes of copper(I): molecular structures and thermal decomposition to ternary semiconductors. *Chem. Eur. J.* **2014**, *20*, 1318–1331.

(26) Kluge, O.; Krautscheid, H. Single-Source Precursors for I–III–VI2 Semiconductor Materials. *Reference Module in Chemistry, Molecular Sciences and Chemical Engineering*; Elsevier, **2016** (DOI: 10.1016/B978-0-12-409547-2.11684-1).

(27) Wang, G.; Zhao, W.; Cui, Y.; Tian, Q.; Gao, S.; Huang, L.; Pan, D. Fabrication of a $Cu_2ZnSn(S,Se)_4$ photovoltaic device by a low-toxicity ethanol solution process. *ACS Appl. Mater. Interfaces* **2013**, *5*, 10042–10047.

(28) Fuhrmann, D.; Dietrich, S.; Krautscheid, H. Copper Zinc Thiolate Complexes as Potential Molecular Precursors for Copper Zinc Tin Sulfide (CZTS). *Chem. Eur. J.* **2017**, *23*, 3338–3346.

(29) Fuhrmann, D.; Dietrich, S.; Krautscheid, H. Zinc Tin Chalcogenide Complexes and Their Evaluation as Molecular Precursors for Cu_2ZnSnS_4 (CZTS) and $Cu_2ZnSnSe_4$ (CZTSe). *Inorg. Chem.* **2017**, *56*, 13123–13131.

(30) Dornsiepen, E.; Weigend, F.; Dehnen, S. Transition-Metal-Induced Rearrangement of $(PhSn)_4S_6$ Towards Ternary CuI/Sn/S or CuII/Sn/S Clusters. *Chem. Eur. J.* **2019**, *25*, 2486–2490.

(31) Wasserscheid, P.; Welton, T. *Ionic Liquids in Synthesis*; Wiley, **2007**.

(32) Yu, L.; Chen, G. Z. Ionic Liquid-Based Electrolytes for Supercapacitor and Supercapattery. *Front. Chem.* **2019**, *7* (272), 1–15.

(33) https://iolitec.de/index.php/en/technology/synthesis-catalysis (Status 13:00 Uhr, 22.08.2019).

(34) Swatloski, R. P.; Spear, S. K.; Holbrey, J. D.; Rogers, R. D. Dissolution of cellulose correction of cellose with ionic liquids. *J. Am. Chem. Soc.* **2002**, *124*, 4974–4975.

(35) Nguyen, N. A.; Kim, K.; Bowland, C. C.; Keum, J. K.; Kearney, L. T.; André, N.; Labbé, N.; Naskar, A. K. A fundamental understanding of whole biomass dissolution in ionic liquid for regeneration of fiber by solution-spinning. *Green Chem.* **2019**, *21*, 4354–4367.

(36) Winterton, N. Solubilization of polymers by ionic liquids. *J. Mater. Chem.* **2006**, *16*, 4281-4293.

(37) Sowmiah, S.; I. Cheng, C.; Chu, Y.-H. Ionic Liquids for Green Organic Synthesis. *Curr. Org. Syn.* **2012**, *9*, 74–95.

(38) Feldmann, C.; Ruck, M. Ionic Liquids - Designer Solvents for the Synthesis of New Compounds and Functional Materials. *Z. Anorg. Allg. Chem.* **2017**, *643*, 2.

(39) http://www.low-temperature-synthesis.de/pdf/Sundermeyer_english.pdf (Status 13:30 Uhr, 22.08.2019).

(40) Finger, L. H.; Scheibe, B.; Sundermeyer, J. Synthesis of organic (trimethylsilyl)chalcogenolate salts CatTMS-E (E = S, Se, Te): the methylcarbonate anion as a desilylating agent. *Inorg. Chem.* **2015**, *54*, 9568–9575.

(41) R. Kalb, WO2008052861A2, Verfahren zur Herstellung von 1,3-hetero-aromatischen Carbonaten. **2007**.

(42) R. Kalb, WO2008052860A1, Verfahren zur Herstellung quarternärer Carbonate. **2007**.

(43) Oelkers, B.; Sundermeyer, J. Pentaalkylmethylguanidinium methylcarbonates – versatile precursors for the preparation of halide-free and metal-free guanidinium-based ILs. *Green Chem.* **2011**, *13*, 608.

(44) Finger, L. H.; Wohde, F.; Grigoryev, E. I.; Hansmann, A.-K.; Berger, R.; Roling, B.; Sundermeyer, J. Access to pure and highly volatile hydrochalcogenide ionic liquids. *Chem. Commun.* **2015**, *51*, 16169–16172.

(45) Finger, L. H.; Sundermeyer, J. Halide-Free Synthesis of Hydrochalcogenide Ionic Liquids of the Type [Cation][HE] (E=S, Se, Te). *Chem. Eur. J.* **2016**, *22*, 4218–4230.

(46) Holbrey, J. D.; Reichert, W. M.; Tkatchenko, I.; Bouajila, E.; Walter, O.; Tommasi, I.; Rogers, R. D. 1,3-Dimethylimidazolium-2-carboxylate: the unexpected synthesis of an ionic liquid precursor and carbene-CO_2 adduct. *Chem. Commun.* **2003**, 28–29.

(47) Finger, L. H.; Guschlbauer, J.; Harms, K.; Sundermeyer, J. N-Heterocyclic Olefin-Carbon Dioxide and -Sulfur Dioxide Adducts: Structures and Interesting Reactivity Patterns. *Chem. Eur. J.* **2016**, *22*, 16292–16303.

(48) Linder, T.; Sundermeyer, J., DE102006023649A1, Hydrophobe ionische Flüssigkeiten. **2006**.

(49) Linder, T.; Sundermeyer, J. Three novel anions based on pentafluorophenyl amine combined with two new synthetic strategies for the synthesis of highly lipophilic ionic liquids. *Chem. Commun.* **2009**, 2914–2916.

(50) Earle, M. J.; Seddon, K. R., WO2001077081A1, Imidazole carbenes. **2000**.

(51) Donsbach, C.; Thiele, G.; Finger, L. H.; Sundermeyer, J.; Dehnen, S. Mercurates from a Revised Ionothermal Synthesis Route: The Pseudo-Flux Approach. *Inorg. Chem.* **2016**, *55*, 6725–6730.

(52) DeGroot, M. W.; Corrigan, J. F. Metal-Chalcogenolate Complexes with Silyl Functionalities: Synthesis and Reaction Chemistry. *Z. Anorg. Allg. Chem.* **2006**, *632*, 19–29.

(53) Azizpoor Fard, M.; Levchenko, T. I.; Cadogan, C.; Humenny, W. J.; Corrigan, J. F. Stable -ESiMe$_3$ Complexes of Cu(I) and Ag(I) (E=S, Se) with NHCs: Synthons in Ternary Nanocluster Assembly. *Chem. Eur. J.* **2016**, *22*, 4543–4550.

(54) DeGroot, M. W.; Atkins, K. M.; Borecki, A.; Rösner, H.; Corrigan, J. F. A molecular precursor approach for the synthesis of composition-controlled $Zn_xCd_{1-x}S$ and $Zn_xCd_{1-x}Se$ nanoparticles. *J. Mater. Chem.* **2008**, *18*, 1123.

(55) DeGroot, M. W.; Corrigan, J. F. Coordination Complexes of Zinc with Reactive ESiMe 3 (E = S, Se, Te) Ligands. *Organometallics* **2005**, *24*, 3378–3385.

(56) DeGroot, M. W.; Khadka, C.; Rösner, H.; Corrigan, J. F. ZnS and ZnSe Nanoparticles via Solid-State and Solution Thermolysis of Zinc Silylchalcogenolate Complexes. *J. Clust. Sci.* **2006**, *17*, 97–110.

(57) Fard, M. A.; Weigend, F.; Corrigan, J. F. Simple but effective: thermally stable Cu-ESiMe$_3$ via NHC ligation. *Chem. Commun.* **2015**, *51*, 8361–8364.

(58) Khadka, C. B.; Macdonald, D. G.; Lan, Y.; Powell, A. K.; Fenske, D.; Corrigan, J. F. Trimethylsilylchalcogenolates of Co(II) and Mn(II): from mononuclear coordination complexes to clusters containing -ESiMe$_3$ moieties (E = S, Se). *Inorg. Chem.* **2010**, *49*, 7289–7297.

(59) Polgar, A. M.; Weigend, F.; Zhang, A.; Stillman, M. J.; Corrigan, J. F. A N-Heterocyclic Carbene-Stabilized Coinage Metal-Chalcogenide Framework with Tunable Optical Properties. *J. Am. Chem. Soc.* **2017**, *139*, 14045–14048.

(60) Polgar, A. M.; Zhang, A.; Mack, F.; Weigend, F.; Lebedkin, S.; Stillman, M. J.; Corrigan, J. F. Tuning the Metal/Chalcogen Composition in Copper(I)-Chalcogenide Clusters with Cyclic (Alkyl)(amino)carbene Ligands. *Inorg. Chem.* **2019**, *58*, 3338–3348.

(61) Taher, D.; Wallbank, A. I.; Turner, E. A.; Cuthbert, H. L.; Corrigan, J. F. Alk-2-ynyl Trimethylsilyl Chalcogenoethers by Nucleophilic Substitution of Propargyl Bromides. *Eur. J. Inorg. Chem.* **2006**, *2006*, 4616–4620.

(62) Zhai, J.; Filatov, A. S.; Hillhouse, G. L.; Hopkins, M. D. Synthesis, structure, and reactions of a copper-sulfido cluster comprised of the parent Cu_2S unit: {(NHC)Cu}$_2$(μ-S). *Chem. Sci.* **2016**, *7*, 589–595.

(63) Babcock, J. R.; Zehner, R. W.; Sita, L. R. A Heterocumulene Metathesis Route to Cd[ESiMe$_3$]$_2$ and Passivated CdE (E = S and Se) Nanocrystals. *Chem. Mater.* **1998**, *10*, 2027–2029.

(64) Hirpo, W.; Dhingra, S.; Kanatzidis, M. G. Synthesis and structure of the first indium–copper cluster, $[Cu_6In_3(SEt)_{16}]$ – and its possible relevance to $CuInS_2$. *J. Chem. Soc., Chem. Commun.* **1992**, *27*, 557–559.

(65) Shapley, P. A.; Liang, H.-C.; Dopke, N. C. Synthesis of (dppe)Pt(μ_3-S)$_2${Ru(N)Me_2}$_2$, (dppe)Pt(μ_3-S)$_2$ {Os(N)(CH_2SiMe_3)$_2$}$_2$, and Related Heterometallic Complexes. *Organometallics* **2001**, *20*, 4700–4704.

(66) Kraus, G. A.; Andersh, B. A versatile synthesis of functionalized thiols. *Tetrahedron Letters* **1991**, *32*, 2189–2192.

(67) Tran, D. T. T.; Taylor, N. J.; Corrigan, J. F. Copper Chalcogenolate Complexes as Precursors to Ternary Nanoclusters: Synthesis and Characterization of $[Hg_{15}Cu_{20}S_{25}(n Pr_3P)_{18}]$. *Angew. Chem. Int. Ed.* **2000**, *39*, 935–937.

(68) Biedermann, R.; Kluge, O.; Fuhrmann, D.; Krautscheid, H. Synthesis and Crystal Structures of $[(i Pr_3P)_2Cu(\mu\text{-}ESiMe_3)(InMe_3)]$ (E = S, Se): Lewis Acid-Base Adducts with Chalcogen Atoms in Planar Coordination. *Eur. J. Inorg. Chem.* **2013**, *2013*, 4727–4731.

(69) Kluge, O.; Puidokait, M.; Biedermann, R.; Krautscheid, H. Synthese und Kristallstruktur der spirocyclischen Gallium- und Indium-Chalkogen-Heterocyclen $[(Me_2Ga)_6S(SSiMe_3)_4]$, $[(Me_2Ga)_6Se(SeSiMe_3)_4]$ und $[(Me_2In)_6S(SSiMe_3)_4]$. *Z. Anorg. Allg. Chem.* **2007**, *633*, 2138–2140.

(70) Stoll, S. L.; Bott, S. G.; Barron, A. R. Selenide and selenolate compounds of indium: a comparative study of In–Se bond-forming reactions. *J. Chem. Soc., Dalton Trans.* **1997**, 1315–1322.

(71) Komuro, T.; Matsuo, T.; Kawaguchi, H.; Tatsumi, K. Synthesis and structural characterization of silanethiolato complexes having tert-butyldimethylsilyl and trimethylsilyl groups. *Dalton Trans.***2004**, *10*, 1618–1625.

2 Aufgabenstellung

Im Arbeitskreis *Sundermeyer* wurde von *Dr. Lars H. Finger* ein Zugang zu hochreinen, salz- und wasserfreien organischen Salzen mit chalkogenbasierten Anionen über organische Methylcarbonatsalze ausgearbeitet. Diese erlauben erstmals auch Umsetzungen mit hochreaktiven Edukten und Produkten und bilden den Ausgangspunkt der vorliegenden Arbeit.

Organische Methylcarbonatsalze Cat[OCO_2Me] sind im Zuge ihrer vielseitigen Anwendbarkeit speziell zur Synthese ionischer Flüssigkeiten von übergeordnetem Interesse. Der bisher vorteilhafteste Zugang zu diesen Salzen erfolgt über eine Methylierung tertiärer Amine, Phosphine oder geeigneter Heterozyklen mit Dimethylcarbonat Me_2CO_3 unter solvothermalen Bedingungen. Diese Methode führt zu einer entscheidenden Beschränkung: Es sind nur Methylcarbonatsalze mit mindestens einfach methylierten Kationen zugänglich, was Untersuchungen zur Folgechemie erschweren kann, insbesondere hinsichtlich der Kristallisierbarkeit oder der Löslichkeit etwaiger Produkte. Eine weitere Problematik ergibt sich für Methylcarbonatsalze mit *N,N'*-Dialkylimidazoliumkationen, die nur in verdünnten methanolischen Lösungen als Cat[OCO_2Me] – und in Abwesenheit von Methanol als NHC-CO_2 Addukt vorliegen. Dies unterbindet Umsetzungen, die methanolempfindliche Verbindungen involvieren, z. B. die silylierten Chalkogenvorläufer *t*BuESiMe_3 und E($SiMe_3$)$_2$ (E = S, Se, Te) sowie [$ESiMe_3$]$^-$ Anionen. Ein Ziel dieser Arbeit ist die Synthese von organischen Salzen mit bisher unzugänglicher Kation-Anion Kombinationen. Dazu sollen neue, selektive Zugänge zu Methylcarbonatsalzen mit nichtmethylierten Kationen, sowie zu methanolempfindlichen Trimethylsilylchalkogenolatsalzen mit *N,N'*-Dialkylimidazolium Kationen ausgearbeitet werden (*Abbildung 2.1*).

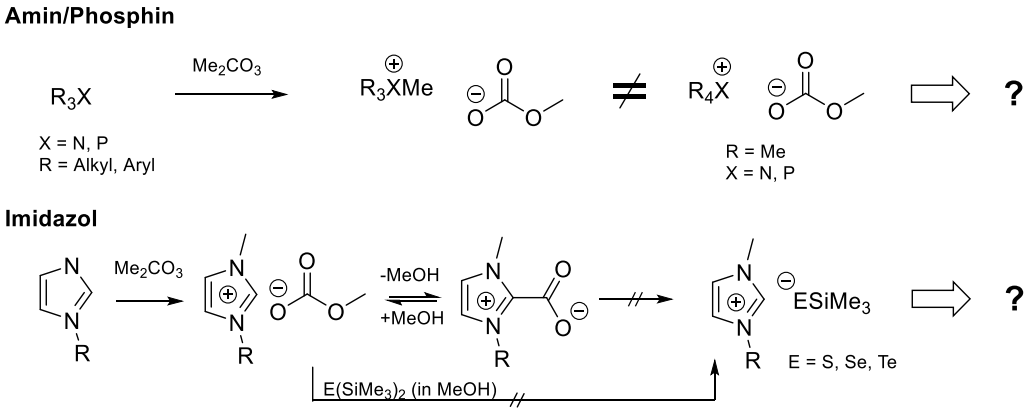

Abbildung 2.1: Quaternisierung von tertiären Aminen/Phosphinen mit Me_2CO_3 zu Methylcarbonatsalzen mit Ammonium/Phosphoniumkation (oben). Die entsprechende Quaternisierung von Alkylimidazolen erfolgt unter Ausbildung des Methylcarbonatsalzes, das in ein NHC-CO_2-Addukt zerfällt, sobald das Methanol entfernt wird.

Durch die organischen Salze mit Trimethylsilylchalkogenolatanionen $[ESiMe_3]^-$ (E = S, Se, Te) sind die freien Anionenliganden einiger bekannter Metallkomplexe $[L_nM(ESiMe_3)_m]$ verfügbar, die als metastabile molekulare Vorstufen zur Herstellung von Metall-Chalkogen Halbleitern oder heterometallischen Clustern Verwendung finden. Einschlägige Vorarbeiten der Arbeitsgruppe *Corrigan* (University of Western Ontario) konnten zeigen, dass entsprechende Neutralkomplexe $[L_nM(ESiMe_3)_m]$ unter Abspaltung von n L und 0.5 m $E(SiMe_3)_2$ die entsprechenden binären Metallchalkogenide $ME_{0.5n}$ ausbilden.

Einen definierten synthetischen Zugang zu multinären Halbleitern wie $CuGa_xIn_{1-x}S_ySe_{2-y}$ könnten homoleptische Metallate $[M(ESiMe_3)_{n+1}]^-$ (M = Ga, In) eröffnen, die sich theoretisch zu den geladenen binären Chalkogenidometallaten $[ME_{(n+1)/2}]^-$ zersetzen könnten. Diese sollten durch Kopräzipitation mit einer geeigneten Kupferquelle die gewünschten CIGS-Materialien ausbilden, was von Interesse für denkbare Niedrigtemperatur-Materialsynthesen ist.

Homoleptische Metallatanionen $[M(ESiMe_3)_{n+1}]^-$ mit organischen Kationen Cat^+ vereinen Aspekte der IL- und Materialpräkursorenchemie. Während man durch Variation des Kations den Schmelzpunkt anpassen kann, stünde durch die Variation der Metall- und Chalkogenatome ein ganzes Portfolio neuartiger Präkursoren $Cat[M(ESiMe_3)_{n+1}]$ zur Verfügung, die als $\{Cat[ME_{n+1}]^{(n+1)-}\}$-Synthone eingesetzt werden könnten. Damit wären diese Verbindungen eine wertvolle Erweiterung zu den bekannten $\{ME_n\}^{n-}$ Synthonen, die bereits durch die neutralen Verbindungen $[L_nM(ESiMe_3)_n]$ bereitgestellt werden können.

Zunächst soll eine selektiver Zugang zu diesen homoleptischen Metallatsalzen ausgearbeitet werden – idealerweise mit Hilfe der $Cat[ESiMe_3]$-Salze. Die erhaltenen Metallatsalze sollen dann definierten zu chalkogenbasierten Festkörpermaterialien $CuM\mathit{E}_2$ umgesetzt werden. Anschließend soll diese Strategie auf andere Metalle übertragen werden, um die Allgemeine Nutzbarkeit dieses Ansatzes durch die Darstellung anderer sulfidischer und selenidischer Halbleiter zu unterstreichen (*Abbildung 2.2*).

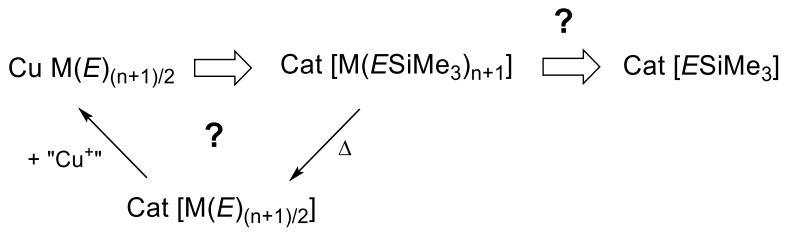

Abbildung 2.2: Durch Darstellung von organischen Salzen mit homoleptischen Metallatanionen $[M(ESiMe_3)_{n+1}]^-$ mit den $Cat[ESiMe_3]$ wird ein definierter Zugang zu chalkogenbasierten Materialien eröffnet.

Eine weitere aus eigenen Vorarbeiten bekannte Möglichkeit, organischen Salze mit chalkogenbasierten Anionen Cat[ER] (E = S, Se, Te; R = H, *t*Bu, $SiMe_3$) synthetisch zu nutzen, ist die Addition an Metallorganyle MR'_n unter Ausbildung von Addukten $Cat[R'_nM\text{-}ER]$ und deren Kondensationsprodukte. Die Additionen und Kondensationsmechanismen sollten für unterschiedliche Metallorganyle und chalkogenolatbasierte Anionen näher untersucht werden (*Abbildung 2.3*).

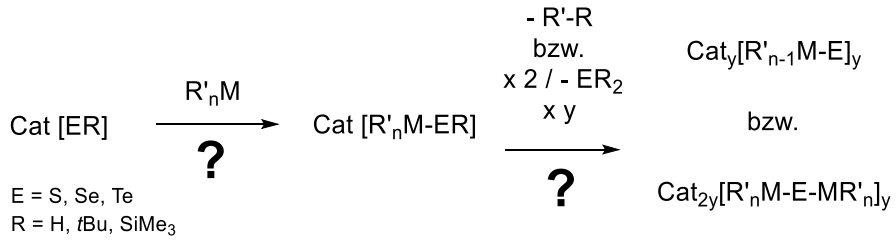

Abbildung 2.3: Reaktionen von organischen Salzen mit chalkogenbasierten Anionen Cat[ER] (1. Addition, 2. Kondensation) mit Metallorganylen R'$_n$M.

Die Umsetzungen von Hydrogenchalkogenidsalzen Cat[EH] (E = S, Se) mit Trimethyltrielverbindungen Me_3M (M = Ga, In) zu zweikernigen, dianionischen Komplexen $Cat_2[Me_2M(\mu_2\text{-}E)]_2$ wurden einschlägig in eigenen Vorarbeiten untersucht. Neben der Vervollständigung dieser Arbeiten sollte das synthetische Potential dieser Dianionen untersucht werden. Dies soll Untersuchungen zur Bildung des bisher ausschließlich kristallographisch nachgewiesenen, inversen Heteroadamantandianions $Cat_2[(Me_2In)_6(\mu_3\text{-}S)_4]$ und alternative Zugänge zu $Cat[Me_2M(ESiMe_3)_2]$ Verbindungen umfassen. Letztere konnten bisher nur durch Salzeliminierungen mit zweifelhafter Reinheit hergestellt werden.

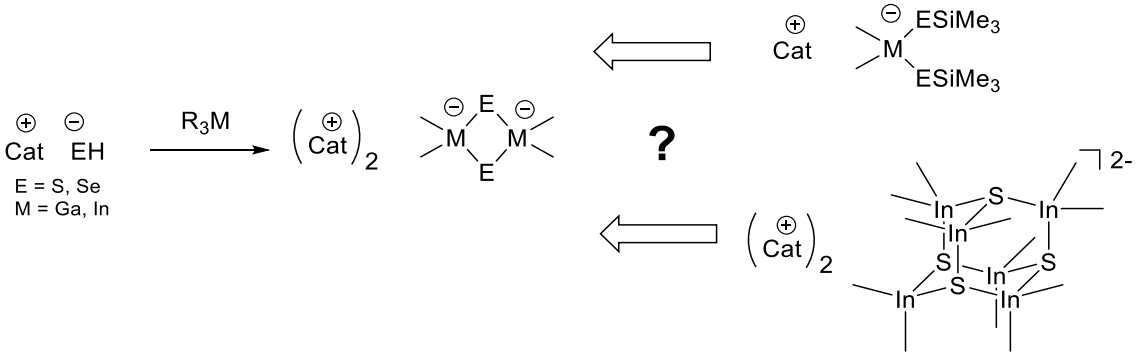

Abbildung 2.4: Die Umsetzung organischer Hydrochalkogenidsalze mit Trimethyltrielen liefert das zweikernige Dianions $Cat_2[(Me_2M)(\mu_2\text{-}E)]_2$, dessen Reaktivität hinsichtlich der Synthesen von $Cat[Me_2M(ESiMe_3)_2]$ und $Cat_2[(Me_2In)_6(\mu_3\text{-}S)_4]$ untersucht werden soll.

3 Kumulativer Teil

3.1 Systematische Studie der Anion-Kation Wechselwirkungen über doppelt ionische Wasserstoffbrückenbindungen in 1,3-Dimethylimidazolium Salzen mit unterschiedlich substituierten Chalkogenolat Anionen MMIm[E-R] (E = S, Se; R = H, *t*Bu, $SiMe_3$)

Dalton Trans., **2019**, 48, 10971-10978.

Systematic study on anion–cation interactions *via* doubly ionic H-bonds in 1,3-dimethylimidazolium salts comprising chalcogenolate anions MMIm[ER] (E = S, Se; R = H, *t*Bu, $SiMe_3$)

Jannick Guschlbauer, Tobias Vollgraff, Jörg Sundermeyer

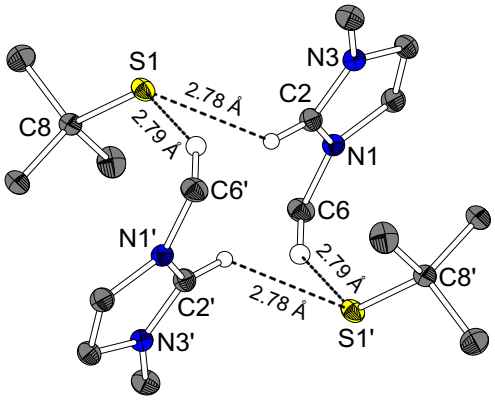

Ausgehend von der NHC-Verbindung 1,3-Dimethylimidazol-2-yliden wurde durch Deprotonierung von *tert*-Butylthiol in Tetrahydrofuran die Ausgangsverbindung 1,3-Dimethylimidazolium-tertbutylthiolat MMIm[S*t*Bu] ausgefällt und isoliert. Das damit verfügbare, außergewöhnlich nukleophile $[S\textit{t}Bu]^-$ Anion wurde als Ausgangspunkt für die Synthesen organischer Salze mit weniger nukleophilen Anionen verwendet, die über Desilylierung entsprechender Vorstufen – und der damit einhergehenden Eliminierung von *t*Bu-S-$SiMe_3$ zugänglich sind. Ausgehend von MMIm[S*t*Bu] und $E(SiMe_3)_2$ können auf diese Weise die bisher nicht in dieser Kationen-Anionen Kombination zugänglichen Trimethylsilylchalkogenolat Salze MMIm[E-$SiMe_3$] (E = S, Se) sauber und zuverlässig hergestellt werden. Diese Salze können über einfache Methanolysen in die entsprechenden Hydrogenchalkogenid Salze MMIm[EH] (E = S, Se) überführt werden. Zudem gelang es, durch Umsetzung von MMIm[S*t*Bu] mit *t*Bu-Se-$SiMe_3$, das organische Salz MMIm[Se*t*Bu] herzustellen. Von MMIm[SH], MMIm[SeH], MMIm[S-*t*Bu], MMIm[Se-*t*Bu], MMIm[S-$SiMe_3$] und MMIm[Se-$SiMe_3$] konnten die Festkörperstrukturen kristallographisch bestimmt

werden. Die Nahordnungen innerhalb der Ionenpaare geben Aufschlüsse über nichtkovalente Wechselwirkungen, insbesondere über die durch die komplementäre Ladung der Teilchen verstärkten, doppelt ionischen Wasserstoffbrückenbindungen. Durch die Anzahl und Ausprägung der identifizierten Wasserstoffbrückenbindungen konnten qualitative Trends in Bezug auf das Chalkogenatom und dessen Substituent identifiziert werden. Überraschenderweise korreliert die Anzahl der Wasserstoffbrücken-bindungen zwischen Chalkogenatom und 1,3-Dimethylimidazoliumkation nicht mit der über die ^{1}H NMR-Verschiebungen des C2-gebundenen Protons quantifizierbaren Basizität des Anions ([S-*t*Bu]$^{-}$ > [Se-*t*Bu]$^{-}$ > [S-H]$^{-}$ > [Se-H]$^{-}$ > [S-SiMe$_3$]$^{-}$ > [Se-SiMe$_3$]$^{-}$). Vielmehr ist die Bindungslänge zwischen Chalkogenatom und dessen Substituenten maßgebend ([S-H]$^{-}$ ≈ [Se-H]$^{-}$ ≈ [Se-SiMe$_3$]$^{-}$ > [S-SiMe$_3$]$^{-}$ ≈ [Se-*t*Bu]$^{-}$ > [S-*t*Bu]$^{-}$), was die Bedeutung sterischer Aspekte und damit einhergehender Kristallpackungseffekte unterstreicht. Alle Titelverbindungen sind im Feinvakuum ($1 \cdot 10^{-3}$ mbar) bei 50 °C sublimierbar, was die allgemeine Gültigkeit der von *Dr. Lars Finger* entdeckten Flüchtigkeit von 1,3-Ethyl-methylimidazolium Hydrogensulfid Salzen auf entsprechende Salze mit andersartig substituierten Chalkogenolatanionen erweitert.

Erklärung der Eigenleistung

Der größte Teil der synthetischen und analytischen Arbeiten, sowie die Konzeption der Thematik wurden von mir im Rahmen meiner Doktorarbeit durchgeführt. Ausgenommen hiervon sind Lösung sowie Verfeinerung aller Kristalldaten, die durch *Tobias Vollgraff* vorgenommen wurden. Einzelne Spektren, Elementaranalysen, sowie die Sammlung von Kristalldaten erfolgte durch die Serviceabteilungen des Fachbereichs Chemie der Philipps-Universität Marburg. Die TGA-DSC Messungen wurden von mir persönlich aufgenommen und ausgewertet. Die Darstellung von MMIm[S*t*Bu] und MMIm[SSiMe$_3$] erfolgte erstmals durch *Haowen Wang* im Zuge eines von mir angeleiteten Forschungsprojektes. Die Darstellung von MMIm[Se*t*Bu] erfolgte erstmals durch *Maria Gutschke* im Zuge eines von mir angeleiteten Forschungsprojekts. Das Manuskript und die Supporting Information wurden von mir geschrieben. Die wissenschaftliche Fragestellung und Ausrichtung dieses Projektes wurden intensiv mit *Prof. Dr. Jörg Sundermeyer* formuliert und diskutiert.

3.2 Homoleptische Gruppe 13 Metallate mit Trimethylsilylchalkogenolat Liganden [M(ESiMe$_3$)$_4$] (M = Ga, In; E = S, Se): Präkursoren für die Synthese chalkogenbasierter Materialien bei niedrigen Temperaturen

Inorg. Chem., accepted 22.10.2019, DOI: 10.1021/acs.inorgchem.9b02453.

Homoleptic Group 13 Metalates [M(ESiMe$_3$)$_4$]$^-$ (M = Ga, In; E = S, Se): Metastable Precursors for Low Temperature Syntheses of Chalcogenide Based Materials

Jannick Guschlbauer, Tobis Vollgraff, Jörg Sundermeyer

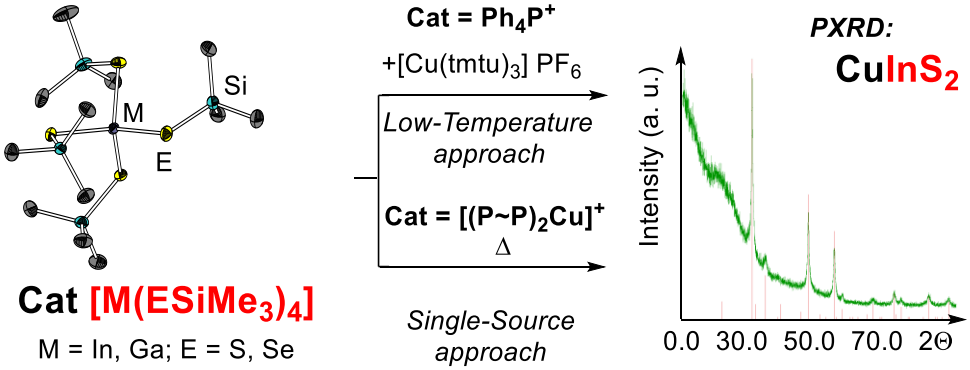

Komplexe mit funktionellen ESiMe$_3$ (E = S, Se, Te) Liganden sind überwiegend als mit Hilfsliganden (L) stabilisierte, heteroleptische Neutralkomplexe [L$_n$M(ESiMe$_3$)$_x$] bekannt. Durch die leichte Spaltbarkeit der E-Si Bindung sind derartige Komplexe geeignete molekulare Vorstufen für die Darstellung von Metallchalkogenid Materialien ME$_{0.5x}$ und Chalkogenid-Clustermoleküle L$_n$M-E-M‘-L’$_{n‘}$, womit sie ein vielfältiges Anwendungsspektrum abdecken. In dieser Arbeit wurde im Vergleich zu den bekannten Neutralkomplexen [L$_n$M(ESiMe$_3$)$_x$] anstelle der Hilfsliganden L eine anionische [ESiMe$_3$]$^-$ Einheit, beispielsweise über die von *Lars H. Finger* entwickelten organischen Salze Cat[ESiMe$_3$], als zusätzlich stabilisierende Liganden eingeführt. Mit den daraus hervorgehenden homoleptischen Trimethylsilyltrielaten [M(ESiMe$_3$)$_4$]$^-$ (M = Ga, In) wird eine neue Substanzklasse monoanionischer Metallatverbindungen vorgestellt. Diese zeichnen sich durch eine im Vergleich zu den Neutralkomplexen deutlich ausgeprägtere thermischen Stabilität aus, die auf der elektrostatischen Repulsion der Anionen, und der damit einhergehenden Kondensationsinhibierung beruht. Zudem werden neue Anwendungsperspektiven in der Materialsynthese eröffnet und der Einsatz von Hilfsliganden umgangen. Es wurden zwei Wege ausgearbeitet, die photovoltaischen Absorbermaterialien der CIGS Familie (Cu(Ga, In)(S, Se)$_2$) herzustellen: Zum einen wurde über eine Kopräzipitationsstrategie, bei der die Titelverbindung Ph$_4$P[In(SSiMe$_3$)$_4$] mit der externen Kupfer(I)-Quelle [Cu(tmtu)$_3$]PF$_6$ (tmtut = *N,N,N‘,N‘*-

Tetramethylthiourea) $CuInS_2$ hergestellt, wobei der Fällungsschritt bei –20°C vollzogen wurde. Nach thermischer Nachbehandlung konnte das Material röntgenpulverdiffraktometrisch nachgewiesen werden. Zum anderen konnten $CuInS_2$ und $CuGaS_2$ über die Pyrolyse der im Zuge dieser Arbeiten dargestellten und strukturell charakterisierten Single-Source Präkursoren $[Cu(R_2PCH_2CH_2PR_2)_2]$ $[M(ESiMe_3)_4]$ (r = Me, Ph) dargestellt werden. Der Nachweis der Materialien erfolgte durch röntgenpulverdiffraktometrische Messungen der Rückstände der entsprechenden TGA-DSC Proben. Diese Arbeit dient als Ausgangspunkt für die Erforschung der in weiteren Manuskripten beschriebenen organischen Salzen mit homoleptischen Monoanionen mit $ESiMe_3$-Liganden. Indirekt wird hier ein definierter Weg beschrieben, wie die nukleophilen $Cat[E\text{-}SiMe_3]$ Salze aus Vorarbeiten des Arbeitskreises als Chalkogenquelle für die Herstellung chalkogenbasierter Materialien verwendet werden können.

Erklärung der Eigenleistung

Der größte Teil der synthetischen und analytischen Arbeiten, sowie die Konzeption der Thematik wurden von mir im Rahmen meiner Doktorarbeit durchgeführt. Ausgenommen hiervon sind Lösung sowie Verfeinerung aller Kristalldaten, die durch *Tobias Vollgraff* vorgenommen wurden. Einzelne Spektren, Elementaranalysen, sowie die Sammlung von Kristalldaten erfolgte durch die Serviceabteilungen des Fachbereichs Chemie der Philipps-Universität Marburg. Die TGA-DSC Messungen, sowie die PXRD-Messungen wurden von mir persönlich aufgenommen und ausgewertet. Die Herstellung der in der *Supporting Information* diskutierten Verbindung $Li[In(SSiMe_3)_4]$ erfolgte durch *Nima Heidary* im Zuge eines von mir angeleiteten Forschungsprojektes. Das Manuskript und die Supporting Information wurden von mir geschrieben. Die wissenschaftliche Fragestellung und Ausrichtung dieses Projektes wurden intensiv mit *Prof. Dr. Jörg Sundermeyer* formuliert und diskutiert.

3.3 Homoleptische Trimethylsilylchalkogenolatzinkate $[Zn(ESiMe_3)_3]^-$ und -stannanide $[Sn(ESiMe_3)_3]^-$ (E = S, Se) als Präkursoren für lösungsbasierte Niedrigtemperatursynthesen von Cu_2ZnSnS_4 (CZTS)

Manuscript submitted (24.10.2019)

Homoleptic Trimethylsilylchalcogenolato Zinkates $[Zn(ESiMe_3)_3]^-$ and Stannanides $[Sn(ESiMe_3)_3]^-$ (E = S, Se): Precursors in Solution Based Low-Temperature Cu_2ZnSnS_4 (CZTS) Synthesis

Jannick Guschlbauer, Tobias Vollgraff, Jörg Sundermeyer

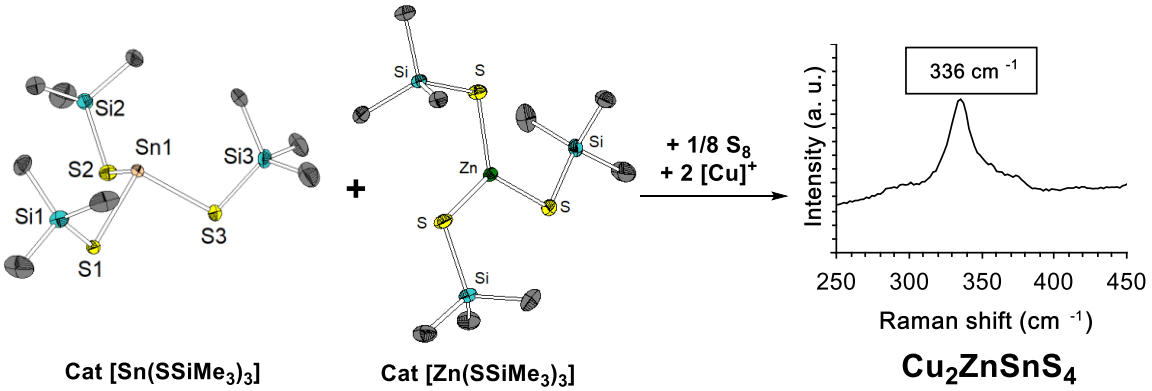

Aufbauend auf den Arbeiten zu homoleptischen Trimethylsilylchalkogenolatotrielaten zur Herstellung von CIGS-Materialien wurde ein vergleichbarer Niedrigtemperatur-Ansatz ausgearbeitet, um das zukunftsträchtige Dünnschichtsolarzellenabsorbermaterial Cu_2ZnSnS_4 (CZTS) herzustellen. Dazu wurden die Stannanide $Ph_4P[Sn(ESiMe_3)_3]$ und die Zinkate $Ph_4P[Zn(ESiMe_3)_3]$ (E = S, Se) hergestellt, und – mit Außnahme von $Ph_4P[Sn(SeSiMe_3)_3]$ – strukturell charakterisiert. Die Molekülstruktur von $Ph_4P[Sn(SSiMe_3)_3]$ ist eines der wenigen Beispiele für eine niedermolekulare Sn(II) Verbindung mit anionischen Schwefelliganden, und das erste strukturell belegte Beispiel einer zinngebundenen Trimethylsilylthiolatgruppe. Während die Trimethylsilylthiolatverbindungen $Ph_4P[M(SSiMe_3)_3]$ (M = Zn, Sn) im Festkörper in Form mononuklearer Monoanionen in Erscheinung treten, bildet die Trimethylsilylselenolatverbindung $(Ph_4P)_2[Zn(SeSiMe_3)_3]_2$ im Festkörper ein dinukleares Dianion aus. Dieses tritt in Form eines viergliedrigen Rings in Erscheinung, der aus zwei „$Zn(SeSiMe_3)_2$“ Einheiten aufgebaut ist, die über verbrückende „(μ_3-$SeSiMe_3$)“ Einheiten verbunden sind. Obwohl es bekannt ist, dass das allgemeine Aggregierungsbestreben innerhalb der Chalkogene mit steigender Ordnungszahl zunimmt, ist dies das bisher einzige Beispiel für ein homoleptisches Trimethylsilylchalkogenolatometallat, in dem das Selenhomologe ein anderes Strukturmotiv im Vergleich zum Schwefelhomologen ausbildet. Die TGA-Messungen der Titelverbindungen zeigen einen mehrstufigen Zerfall bei Temperaturen zwischen 100 °C

und 450 °C, der in einem Rückstand mündet, welcher röntgenpulverdiffraktometrisch den entsprechenden binären Metallchalkogeniden ME (M = Zn, Sn; E = S, Se) zugeordnet werden konnte. Oxidiert man das Stannanid Cat[Sn($SeSiMe_3$)$_3$] mit einem Äquivalen elementarem Schwefel und versetzt das Produkt mit einem Äquivalenten Cat[Zn($SSiMe_3$)$_3$], so kann nach Zugabe zweier Äquivalente der Kupfer(I)-Quelle [Cu(tmtu)$_3$] PF_6 (tmtu = *N, N, N', N'*-Tetramethylthiourea) das nachhaltige photovoltaische Absorbermaterial CZTS (Cu_2SnZnS_4) ausgefällt werden. Dieses konnte nach thermischer Nachbehandlung durch zwei komplementäre Methoden nachgewiesen werden: einerseits über Röntgenpulver-diffraktometrie, andererseits über Ramanspektroskopie. Diese Arbeit unterstreicht die allgemeine Möglichkeit, organische Salze mit Silylchalkogenolatometallatanionen als Bausteine für Niedrigtemperatursynthesen multinärer chalkogenbasierter Materialien zu verwenden. Im Zuge dieser Arbeit werden auch die Synthesen und die Charakterisierungen der neutralen Zinnverbindungen Sn($ESiMe_3$)$_4$ (E = S, Se) vorgestellt, sowie deren thermischer Zerfall zu verschiedenen Zinnsulfiden und $SnSe_2$ eingehend beschrieben.

Erklärung der Eigenleistung

Der größte Teil der synthetischen und analytischen Arbeiten, sowie die Konzeption der Thematik wurden von mir im Rahmen meiner Doktorarbeit durchgeführt. Ausgenommen hiervon sind Lösung sowie Verfeinerung der röntgendiffraktometrischen Strukturbestimmungen, die durch *Tobias Vollgraff* vorgenommen wurden. Einzelne Spektren, Elementaranalysen, sowie die Sammlung von Kristalldaten erfolgte durch die Serviceabteilungen des Fachbereichs Chemie der Philipps-Universität Marburg. Die Aufnahme von Raman-Spektren erfolgte durch Melanie Förster (Arbeitskreis Roling). Die TGA-DSC und PXRD Messungen wurden von mir persönlich aufgenommen und ausgewertet. Das Manuskript und die Supporting Information wurden von mir geschrieben. Die wissenschaftliche Fragestellung und Ausrichtung dieses Projektes wurden intensiv mit *Prof. Dr. Jörg Sundermeyer* formuliert und diskutiert.

3.4 Eine Serie Linear koordinierter homoleptischer Münzmetallatkomplexe Cat[M(ESiMe$_3$)$_2$] (M = Cu, Ag, Au; E = S, Se)

Manuscript submitted (14.11.2019)

A Series of Homoleptic Linear Coinage Metal Trimethylsilylchalcogenolate Complexes Cat[Me$_3$E-M-ESiMe$_3$] (M = Cu, Ag, Au; E = S, Se)

Jannick Guschlbauer, Tobias Vollgraff, Xiulan Xie, Florian Weigend, Jörg Sundemeyer

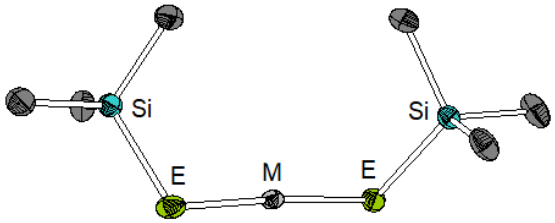

Cat[M(ESiMe$_3$)$_2$]
M = Cu^{I}, Ag^{I}, Au^{I}; E = S, Se
Cat = Ph$_4$P$^+$ or PPN$^+$

Homoleptic linear [ESiMe$_3$]$^-$ coinage metallates

Gauche-like conformation (XRD, DFT)

Selenolates: ^{1}H/^{77}Se HMQC NMR Spectra

Die organischen Salze der homoleptischen Triemthylsilylchalkogenolatomünzmetallate Cat[M(ESiMe$_3$)$_2$] (M = Cu, Ag, Au; E = S, Se; Cat = Ph$_4$P, PPN) wurden hergestellt und kristallographisch charakterisiert. Im Festkörper der entsprechenden organischen Salze liegen die Anionen allesamt in Form mononuklearer, linear koordinierter Monoanionen vor. Anders als sterische Überlegungen nahelegen, sind die Trimethylsilylgruppen innerhalb eines Metallatanions in einer ungewöhnlichen *Gauche*-Konformation zueinander ausgerichtet. Dabei wurden Si-E-M-E-Si Diederwinkel zwischen 27.8° und 77.5° gefunden. Literaturbekannte Metallatanionen vergleichbaren sterischen Anspruchs zeigen eine ähnliche Konformation, was allerdings nie belastbar begründet wurde. Im Zuge dieser Arbeit wurden von *Priv.-Doz. Dr. Florian Weigend* quantenchemische Berechnungen an den Titelverbindungen durchgeführt. Diese belegen, dass die *Gauche*-Konformation um den geringfügigen Energiebetrag von 2-6 kJ/mol stabiler im Vergleich zu einer idealen *anti*-Ausrichtung der Trimethylsilylgruppen ist. Der elektronische Hintergrund wird auf eine Reduktion des antibindenden Charakters von M-Si Wechselwirkungen und auf Elektronenkorrelationeffekte zurückgeführt. Des Weiteren wurde zur NMR-spektroskopischen Charakterisierung der ^{77}Se-Kerne von *Dr. Xiulan Xie* eine neue, zweidimensionale ^{1}H/^{77}Se-HMQC Methode entwickelt, durch welche die in vielen Fällen schwierige bis unmögliche Aufnahme eines aussagekräftigen ^{77}Se NMR Spektrums ermöglicht wurde. Zudem wurde eine bereits bekannte vergleichbare ^{1}H/^{29}Si-HMQC Methode verwendet, welche die Messzeit zur Aufnahme adäquater ^{29}Si-NMR

Spektren drastisch reduziert. Dadurch ist eine vollständige NMR-Charakterisierung der ^{1}H-, ^{13}C-, ^{29}Si- und ^{77}Se-Kerne der Titelanionen möglich. Zudem wurde exemplarisch der thermische Zerfall der Kupratspezies $Ph_4P[Cu(SSiMe_3)_2]$ näher untersucht. Die TGA-DSC Messung (30°C bis 600°C, 10 K min^{-1}) zeigt einen Schmelzpunkt bei 91 °C und einen Zersetzungsprozess ab 179 °C. Der Rückstand der Messung wurde über PXRD als $Cu_{1.81}S$ identifiziert. Durch eine definierte Zersetzung der Verbindung bei 180°C für zwei Minuten im Feinvakuum und Züchtung geeigneter Einkristalle aus seiner DMF-Lösung des Rückstandes wurde über eine Einkristallstrukturanalyse die bekannte Verbindung $(Ph_4P)_4[Cu_{12}S_8]$ identifiziert. Dies impliziert einen partiellen Zerfall der Ausgangsverbindung (12 Äq.) zu $Ph_4P[SSiMe_3]$ (8 Äq.), $S(SiMe_3)_2$ (8 Äq.) und $(Ph_4P)_4[Cu_{12}S_8]$ (1 Äq.). Durch eine bei der Thermolyse anfallende Mischung aus $(Ph_4P)_4[Cu_{12}S_8]$ und $Ph_4P[SSiMe_3]$ entstehen vermutlich Addukte der Art $(Ph_4P)_{4+n}[Cu_{12}S_8(SSiMe_3)_n]$, die bei vollständiger Thermolyse $[S_2]^{2-}$ Anionen ausbilden könnten. Kommt es zur partiellen Substitution der vorliegenden S^{2-}Anionen, könnte nach vollständiger Thermolyse $Cu_{1.81}S$ ausgebildet werden.

Erklärung der Eigenleistung

Der größte Teil der synthetischen und analytischen Arbeiten, sowie die Konzeption der Thematik wurden von mir im Rahmen meiner Doktorarbeit durchgeführt. Ausgenommen hiervon sind Lösung sowie Verfeinerung der Kristalldaten, die durch *Tobias Vollgraff* vorgenommen wurde. Die quantenchemischen Berechnungen und Interpretationen wurden durch *Priv.-Doz. Dr. Florian Weigend* durchgeführt. Die Entwicklung der zweidimensionalen NMR Methoden, und die Aufnahme der entsprechenden Spektren erfolgte durch *Dr. Xiulan Xie*. Weitere, einzelne Spektren, Elementaranalysen, sowie die Sammlung von Kristalldaten erfolgte durch die Serviceabteilungen des Fachbereichs Chemie der Philipps-Universität Marburg. Die TGA-DSC und PXRD Messungen wurden von mir persönlich aufgenommen und ausgewertet. Das Manuskript und die Supporting Information wurden größtenteils von mir geschrieben, mit Außnahme der theoretisch chemischen Analysen und Interpretationen von *Priv.-Doz. Dr. Florian Weigend*, sowie den für die ^{29}Si/^{77}Se-^{1}H-HMQC-NMR-relevanten Erläuterungen durch *Dr. Xiulan Xie*. Durch *Bertram Peters* erfolgten einzelne PXRD-Messungen. Die wissenschaftliche Fragestellung und Ausrichtung dieses Projektes wurden intensiv mit *Prof. Dr. Jörg Sundermeyer* formuliert und diskutiert.

3.5 Dimethylpyrrolidinium Chalkogenido-Dimethylgallate und -indate $DMPyr_2[Me_2M(\mu_2\text{-}E)]_2$ (M = Ga, In; E = S, Se): Ihre Anwendung in der Synthese höher- und niedermolekularer Chalcogenidoindate)

In preparation

Dimethylpyrrolidinium Chalcogenido-Dimethylgallates and -indates $DMPyr_2[Me_2M(\mu_2\text{-}E)]_2$ (M = Ga, In; E = S, Se): Their use in the Synthesis of Higher or Lower Order Chalcogenidoindates

Jannick Guschlbauer, Lars H. Finger, Tobias Vollgraff, Klaus Harms, Jörg Sundermeyer

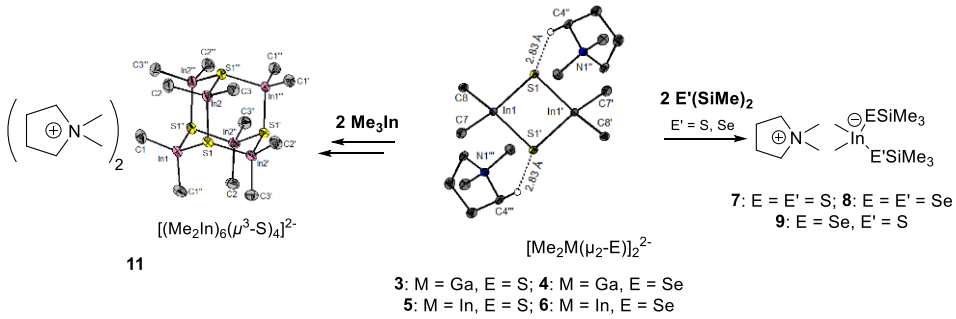

Durch die von *Lars Finger et al.* ausgearbeiteten Synthesen hochreiner organischer Hydrogenchalkogenid Salze wurde die Umsetzung dieser Verbindungen mit den extrem luft- und feuchtigkeitsempfindlichen Trialkyltrielen Me_3In und Me_3Ga möglich. Eine äquimolare Umsetzung der *N,N'*-Dimetylpyrrolidinium Hydrogenchalkogenide DMPyr[EH] (E = S, Se) mit den Trimethyltrielen Me_3M (M = Ga, In) in Tetrahydrofuran führt nach einmaliger Methaneliminierung zur Bildung von $DMPyr_2[Me_2M(\mu_2\text{-}E)]_2)]_2$. Die röntgenographische Strukturbestimmung dieser Salze zeigt, dass die Anionen in allen vier Vertretern M = Ga, In und E = S, Se als zweikernige Dianionen $[Me_2M(\mu_2\text{-}E)]_2)]_2^{2-}$ vorliegen, die durch eine viergliedrige, aus zwei über „μ_2-E“ Brücken verknüpfte „Me_2M“ Einheiten aufgebaute Ringstruktur ausgezeichnet sind. Die ausgeprägte Nukleophilie der Chalkogenatome in den Indat-Dianionen kann synthetisch genutzt werden, um silylierte- oder höhermolekulare Organoindate auf sehr einfachem um selektivem Weg herzustellen. Versetzt man $DMPyr_2[Me_2In(\mu_2\text{-}S)]_2)]_2$ mit zwei Äquivalenten $S(SiMe_3)_2$, erhält man zwei Äquivalente $DMPyr[Me_2In(S\text{-}SiMe_3)_2]$ was ebenso mit den Selenhomologen funktioniert. Auch die gemischt substituierte Verbindung $DMPyr[Me_2In(S\text{-}SiMe_3)(Se\text{-}SiMe_3)]$ kann durch Umsetzung von $DMPyr_2[Me_2In(\mu_2\text{-}Se)]_2)]_2$ mit zwei Äquivalenten $S(SiMe_3)_2$ erhalten werden. Setzt man $DMPyr_2[Me_2In(\mu_2\text{-}S)]_2)]_2$ mit zwei weiteren Äquivalenten Me_3In um, entsteht ein organisches Salz mit hexanuklearem, sechsgliedrigem Ring-Trianion $DMPyr_3[(Me_2In)(\mu_3\text{-}SInMe_3)]_3$. Dieses kann durch vorsichtige thermische Zersetzung zu einem organischen Salz

des hexanuklearen inversen Heteroadamantandianions $DMPyr_2[(Me_2In)_6(\mu_3\text{-}S)_4]$ umgewandelt werden. Dieses konnte nur kristallographisch identifiziert werden, und könnte über eine Dismutation der Ausgangsverbindung zusätzlich zu $DMPyr[InMe_4]$ entstanden sein. Auch die nichtkovalenten Wechselwirkungen zwischen den Ionen der kristallographisch charakterisierten Hydrochalkogenidsalze DMPyr[SH] und DMPyr[SeH], sowie der Chalkogenidodimethyltrielat Salze $DMPyr_2[Me_2Ga(\mu_2\text{-}Se)]_2)]_2$, $DMPyr_2[Me_2In(\mu_2\text{-}S)]_2)]_2$ und $DMPyr_2[Me_2In(\mu_2\text{-}Se)]_2)]_2$ wurden untersucht, die den nukleophilen Charakter der Chalkogenatome unterstreichen. Auffällig ist hierbei die ausgeprägte Neigung zur Ausbildung von Wasserstoff-brückenbindungen (H-Brücken) von $DMPyr_2[Me_2In(\mu_2\text{-}Se)]_2)]_2$ (sechs H-Brücken pro Dianion mit drei H-Brücken pro Chalkogenatom), die auf die sterische Zugänglichkeit, und die leichte Polarisierbarkeit der Selenatome zurückzuführen ist. Diese Arbeit zeigt erstmals einen definierten Zugang zu neuartigen Verbindungen durch die Umsetzung chalkogenbasierter organischer Salze mit hochreaktiven Metallorganylen. Zudem wird die Reaktivität der bisher unbekannten Chalkogenidoorganotrielat Dianionen erläutert, die in erster Linie auf der Nukleophilie der ausschließlich Trielgebundenen „μ_2-E" Chalkogenbrücken basiert.

Erklärung der Eigenleistung

Den Grundstein der behandelten Thematik wurde von mir unter Anleitung von *Lars H. Finger* in einem Forschungsprojekt im Arbeitskreis *Sundermeyer* gelegt, aus dem die Struktur des Salzes $DMPyr_2[Me_2In(\mu_2\text{-}Se)]_2$ hervorging. Diese ist Bestandteil der Doktorarbeit von *Lars H. Finger*. Im Zuge meiner Masterarbeit folgten die Synthesen und Kristallstrukturen (*) der Salze *DMPyr[SH], $^*DMPyr_2[Me_2Ga(\mu_2\text{-}S)]_2$, $DMPyr_2[Me_2Ga(\mu_2\text{-}Se)]_2$, $^*DMPyr_2[Me_2In(\mu_2\text{-}S)]_2$, $DMPyr_2[Me_2In(\mu_2\text{-}Se)]_2$, sowie die Struktur von $DMPyr_2[(Me_2In)_6(\mu_3\text{-}S)_4]$. Die Lösung und Verfeinerung der Kristalldaten erfolgte durch *Lars H. Finger*. Die verbleibenden Homologen $DMPyr_2[Me_2Ga(\mu_2\text{-}Se)]_2$, sowie DMPyr[SeH] wurden von mir im Zuge meiner Doktorarbeit charakterisiert und kristallisiert. Die Lösung und Verfeinerung dieser Kristallstrukturen erfolgte durch *Tobias Vollgraff*. Die Darstellung und analytische Charakterisierung von $DMPyr_3[(Me_2In)(\mu_3\text{-}SInMe_3)]_3$ erfolgte von mir. Die unvollständige Lösung und Verfeinerung der qualitativ minderwertigen Kristalldaten wurde von *Dr. Klaus Harms* übernommen. Einzelne Spektren, Elementaranalysen, sowie die Sammlung von Kristalldaten erfolgte durch die Serviceabteilungen des Fachbereichs Chemie der Philipps-Universität Marburg. Das Manuskript und die Supporting Information wurden von mir geschrieben. Die wissenschaftliche Fragestellung und Ausrichtung dieses Projektes wurden intensiv mit *Prof. Dr. Jörg Sundermeyer* formuliert und diskutiert.

3.6 Organische Methylcarbonat-Salze mit nicht-methylierten Kationen Cat[OCO_2Me] (Cat = Ph_4P^+, PPN^+, TBA^+) über Fluorid-induzierte Demethylierung von Dimethylcarbonat

In preparation

Organic Methylcarbonate Salts Comprising Non-methylated Onium Cations Cat[OCO_2Me] (Cat = Ph_4P^+, PPN^+, TBA^+) via Fluoride-Induced Demethylation of Dimethylcarbonate

Jannick Guschlbauer, Tobis Vollgraff, Ahmed Fetoh, Jörg Sundermeyer

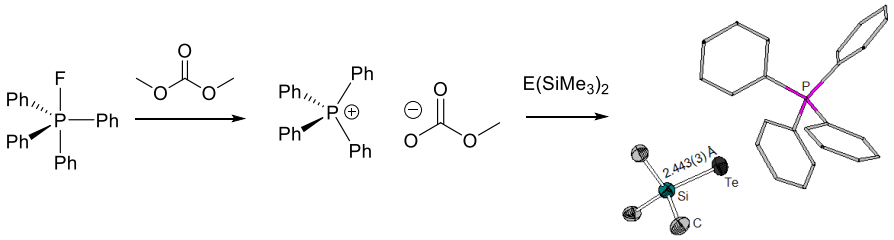

Organische Salze mit großen, symmetrisch substituierten Phosphoniumkationen, wie Ph_4P^+ oder $[Ph_3P{=}N{-}PPh_3]^+$ (PPN), zeichnen sich durch eine im Vergleich zu unsymmetrisch substituierten Kationen deutlich ausgeprägtere Kristallisationstendenz aus. Organische Methylcarbonatsalze werden durch solvothermale Quaternisierung tertiärer Amine NR_3 oder Phosphine PR_3 mit Dimethylcarbonat Me_2CO_3 unter Ausbildung von $MeNR_3$ [OCO_2Me]] hergestellt. Weitere Methoden umfassen die Addition von CO_2 an NR_4 [OMe] unter Ausbildung von NR_4 [OCO_2Me] und die Kondensation von NR_4 [OH] mit Me_2CO_3 unter Eliminierung von MeOH zu NR_4 [OCO_2Me]. Diese Methoden haben entweder zwangsläufig eine mindestens einmalige Methylierung der Kationen zur Folge, oder sind auf symmetrisch substituierte Ammoniumkationen beschränkt, da Phosphoniumkationen im Regelfall in Anwesenheit anionischer *O*-Basen nicht stabil sind. Alternative Salzeliminierungsstrategien sind ebenfalls nicht möglich, da die entsprechenden Edukte schwerlöslich sind, oder eine vergleichbare Löslichkeit der Produkte und des zu eliminierenden Salzes eine Isolierung unmöglich machen. Um diese Einschränkungen zu überwinden wurden organischen Fluoride Cat[F] als nukleophile Demethylierungsmittel verwendet, die durch solvothermale Kondensation mit Me_2CO_3 unter Eliminierung von flüchtigem MeF zu den entsprechenden Methylcarbonatsalzen Cat[OCO_2Me] umgesetzt werden. Maßgeblich für diese Strategie ist die inhärente Stabilität von Phosphoniumfluoriden, die auf der Ausbildung einer P-F Bindung und der Aufweitung der Koordinationszahl des Phosphoratoms von vier auf fünf beruht. Während im literaturbekannten PPN[F] das Fluoratom im Festkörper gleichmäßig an beiden Phosphoratomen gebunden vorliegt, liegt das Phosphoratom im hier beschriebenen Ph_4P-F im

Festkörper als fünffach koordiniertes Zentralatom vor, wodurch die starke Basizität des Fluoridanions reduziert wird. Unter solvothermalen Bedingungen steht dieses Fluoratom zur Verfügung, um eine Methylgruppe von Me_2CO_3 abzuspalten. Auf diese Weise wurden aus den organischen Fluoriden PPN[F], Ph_4P[F] und dem kommerziell erhältlichen $Bu_4N[F] \cdot 3\ H_2O$ (Bu_4N^+ = TBA) die organischen Methylcarbonatsalze PPN[OCO_2Me], $Ph_4P[OCO_2Me]$ und das bisher nur unzureichend charakterisierte, literaturbekannte $Bu_4N[OCO_2Me]$ hergestellt. Eine kristallographische Strukturbestimmung konnte für PPN[OCO_2Me] und TBA[OCO_2Me] erfolgen. Zudem kann durch die Hydratwasseräuqivalente in $TBA[F] \cdot 3\ H_2O$ der Schluss gezogen werden, dass Methylcarbonate gegenüber geringfügigen aber hyperstöchiometrischen Mengen Wasser stabil sind. Mit $Ph_4P[OCO_2Me]$ wurde eine komplette Homologenreihe $Ph_4P[ESiMe_3]$ für E = S, Se, Te dargestellt, sowie deren Strukturen kristallographisch bestimmt und verglichen. Dabei erfolgte nicht nur die erste strukturelle Charakterisierung eines $[TeSiMe_3]^-$ Anions, sondern auch die Beobachtung des erwartungskonformen Trends, dass die Wasserstoffbrückenbindungsbildungstendenz mit zunehmender Ordnungszahl des Chalkogens abnimmt. Dieser Trend ist einerseits auf den steigenden Atomradius, andererseits die immer weniger ausgeprägte Donorfähigkeit der Anionen mit steigender Ordnungszahl des Chalkogenatoms zurückzuführen. Diese Arbeit legt den Grundstein für verlässlich kristallisierbare Salze der über die Methylcarbonatroute zugänglichen Anionen und deren Folgechemie. So wurden bereits erfolgreiche erste Versuche zur strukturellen Charakterisierung von Lanthanatkomplexen angestellt, die durch einfache Addition von Cp_3La an $Ph_4P[ESiMe_3]$ zugänglich sind.

Erklärung der Eigenleistung

Der größte Teil der synthetischen und analytischen Arbeiten, sowie die Konzeption der Thematik wurden von mir im Rahmen meiner Doktorarbeit durchgeführt. Ausgenommen hiervon sind Lösung sowie Verfeinerung der Kristalldaten, die durch *Tobias Vollgraff* vorgenommen wurde, ebenso wie die Darstellung und Charakterisierung von Ph_4P-F. Desweiteren erfolgte die Darstellung und Charakterisierung von PPN[OCO_2Me] durch *Hui Qu* im Zuge eines von mir betreuten Forschungsprojektes und von $Ph_4P[SeSiMe_3]$ unter meiner Anleitung durch *Ahmed Fetoh* im Zuge seiner Einarbeitung als Postdoktorand in der Arbeitsgruppe *Sundermeyer*. Einzelne Spektren, Elementaranalysen, sowie die Sammlung von Kristalldaten erfolgte durch die Serviceabteilungen des Fachbereichs Chemie der Philipps-Universität Marburg. Das Manuskript und die Supporting Information wurden von mir geschrieben. Die wissenschaftliche Fragestellung und Ausrichtung dieses Projektes wurden intensiv mit *Prof. Dr. Jörg Sundermeyer* formuliert und diskutiert.

3.7 Weitere Arbeiten

3.7.1 Erste Versuche zur Charakterisierung von $CuInS_2$-Partikeln aus Cat[$In(SSiMe_3)_4$]-Verbindungen

In Kooperation mit dem Arbeitskreis *Dr. Wedel* (Fraunhofer Institut Potsdam IAP) wurden erste Versuche angestellt, über Cat[$In(SSiMe_3)_4$] hergestellte Partikel zu charakterisieren. Zusammen mit *Yohan Kim* und der Unterstützung von *Hyung Seok Choi* sowie *Benjamin Heyne* wurden die Partikel synthetisiert und untersucht. Über SEM- und TEM-Aufnahmen wurde das Vorhandensein von Nanopartikeln nachgewiesen, die einerseits über eine thermische Zersetzung von [$Cu(dmpe)_2$][$In(SSiMe_3)_4$] (3 Tage bei 160°C im Feinvakuum), andererseits über die Kopräzipitation durch Zusammengabe von MeCN Lösungen von Ph_4P[$In(SSiMe_3)_4$] und [$Cu(tmtu)_3$]PF_6 bei –20°C, und anschließender thermischer Nachbehandlung (200 °C, 18h), erhalten wurden (*Abbildung 3.7.1.1*).

[$Cu(dmpe)_2$] [$In(SSiMe_3)_4$] (3 Tage, 160°C, Feinvakuum):

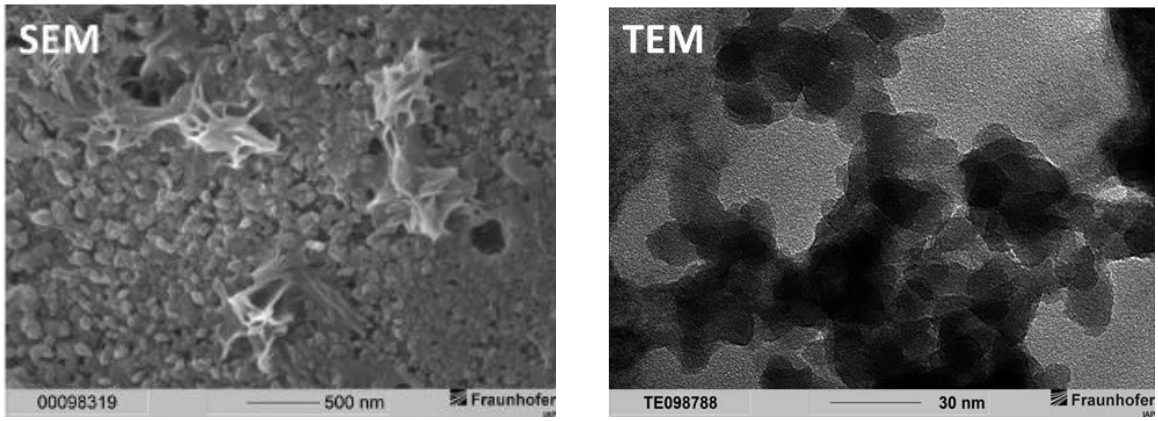

Ph_4P[$In(SSiMe_3)_4$] und [$Cu(tmtu)_3$]PF_6 in MeCN bei –20°C, dann 18 h bei 200°C:

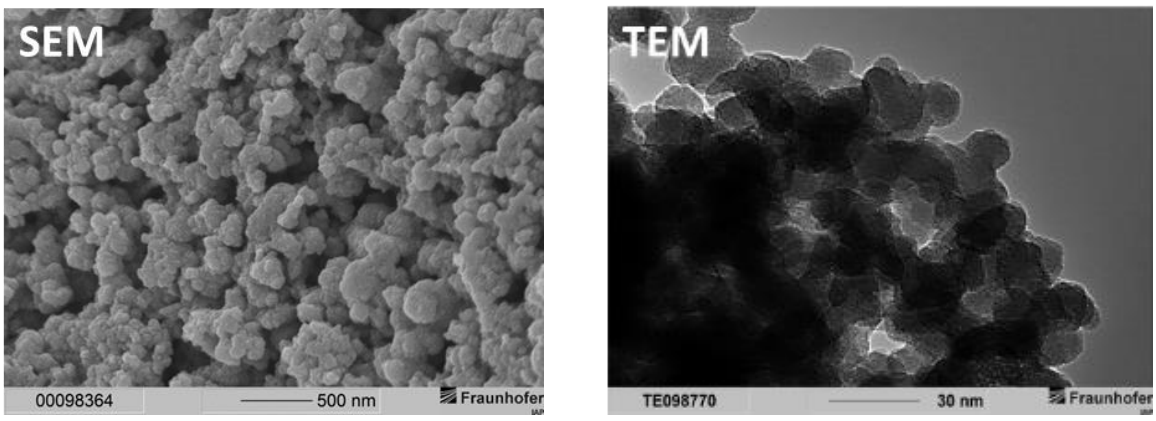

Abbildung 3.7.1.1: SEM und TEM Aufnahmen von $CuInS_2$-Partikeln, die über Verbindungen mit $[In(SSiMe_3)_4]^-$ Anionen hergestellt wurden.

Darstellung der $CuInS_2$ Partikel über Kopräzipitationsverfahren: Eine Lösung von $Ph_4P[In(SSiMe_3)_4]$ (100 mg, 0.1 mol, 1.0 Äq.) wird bei –20 °C in MeCN (10 mL) vorgelegt und mit einer Lösung von $[Cu(tmtu)_3]$ $[PF_6]$ (70 mg, 0.1 mol, 1.0 Äq.) in MeCN (10 mL) versetzt. Das Gemisch wird zunächst für 30 min. bei –20 °C, dann für 60 min. bei Raumtemperatur gerührt. Die Suspension wurde zentrifugiert und der rot-braune Niederschlag mit MeCN (2 x 5 mL) und thf (1 x 5 mL) gewaschen. Der Rückstand wurde unter vermindertem Druck für 18 h bei 200 °C gelagert.

Darstellung der $CuInS_2$ Partikel über Single-source Precursor: $[Cu(dmpe)_2][In(SSiMe_3)_4]$ (50 mg, 0.1 mmol, 1.0 Äq.) wurde im Feinvakuum für 72 h bei 160 °C gelagert. Der schwarze Rückstand wurde untersucht.

3.7.2 Umsetzung von DMPyr[SH] mit CuPh

Die im Zuge dieser Arbeit versuchten Umsetzungen zwischen Kupferorganylen CuR mit chalkogenbasierten organischen Salzen Cat[ER] (E = S, Se, Te; R = H, tBu, SiMe3) beschränkten sich auf nur unzureichend charakterisierbare Addukte Cat[RCu-ER]. Lediglich die Umsetzung zwischen DMPyr[SH] mit CuPh resultierte in der nur kristallographisch charakterisierten Organothiocupratspezies $DMPyr_2[S(CuPh)_2]$ (*Schema 3.7.2.1*).

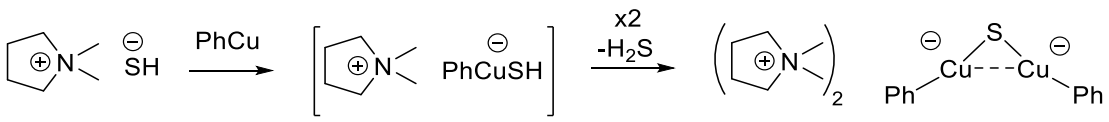

Schema 3.7.2.1: Postulierter Mechanismus der Entstehung von $DMPyr_2[S(CuPh)_2]$.

Diese weist nicht nur die seltene Cu-S-Cu Bindungseinheit auf, sondern auch die bisher kleinste molekulare „Cu_2S"-Einheit in einem Anion (*Abbildung 3.7.2.1, kristallographischer Anhang 6.7.2*). Offenbar ist die Bindung zwischen Kupferatomen und carbanionischem Arylliganden in Kombination mit der elektrostatischen Repulsion stark genug, um die Festkörperbildung zu unterbinden. Die einzig bekannte Struktur mit vergleichbarem Strukturmotiv ist die Neutralverbindung $[(IPr^*Cu)_2S]$ (IPr* = 1,3-bis(2,6-(diphenylmethyl)-4-methylphenyl)imidazol-2-ylidene),[3.1] die auch aus zwei nahezu linear koordinierten Kupferatomen aufgebaut ist, die mit einer μ_2-S-Brücke verbunden sind (ausgewählte Bindungslängen (in Å) und -winkel (in°) von $[(IPr^*Cu)_2S]$ zum Vergleich: C-Cu 1.869(5) & 1.873(5); Cu-S 2.079(2) & 2.085(2); Cu-Cu 3.6085(9); Cu-S-Cu 120.15(9), C-Cu-S 158.8(2) & 162.9(2)).

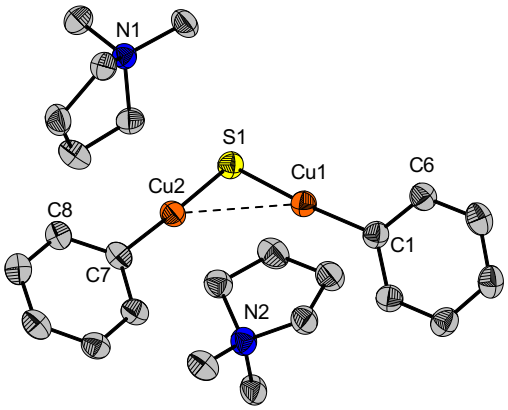

Abbildung 3.7.2.1: Kristallographisch bestimmte Molekülstruktur von DMPyr$_2$[S(CuPh)$_2$] (orthorhombisch, $P2_12_12_1$, vier Formeleinheiten pro Elementarzelle). Die Wasserstoffatome wurde der Übersicht halber nicht abgebildet. Ausgewählte Bindungslängen (in Å) und -winkel (in °): S1-Cu1 2.136(1), S1-Cu2 2.134(1), Cu1-Cu2 2.8693(9), Cu1-C1 1.905(5), Cu2-C7 1.912(5), C1-C6 1.419(7), C7-C8 1.419(6), Cu1-S1-Cu2 84.45(5), S1-Cu1-C1 172.3(2), S1-Cu2-C7 178.2(2), Cu1-C1-C6 123.5(4), Cu2-C7-C8 123.7(3), C6-C1-Cu1-S1 68(1), C8-C7-Cu2-S1 -12(5).

Allerdings konnte DMPyr$_2$[S(CuPh)$_2$] in THF weder selektiv hergestellt noch sauber isoliert werden. Versuche zur Reproduktion scheiterten und zeigten im ^{1}H-NMR in d^6-dmso lediglich das Vorhandensein des Eduktes DMPyr[SH] zusammen mit einer geringen Menge an CuPh (*Abbildung 3.7.2.2*, unten). Das ^{1}H-NMR in d^8-thf der gemessenen Einkristalle (*Abbildung 3.7.2.1*, oben) zeigt diverse Schlifffettverunreinigungen und – neben Benzol, das durch die Protonierung von CuPh entsteht – weitere Verunreinigungen im aromatischen Bereich. Vermutlich kristallisiert DMPyr$_2$[S(CuPh)$_2$] aus der mit Et$_2$O überschichtet DMF-Lösung des Rohproduktes über einen Zeitraum von Wochen durch eine Gleichgewichtsverschiebung in der Diffusionszone.

Herstellungsversuch von DMPyr$_2$[S(CuPh)$_2$]: Ein Gemisch aus DMPyr[SH] (104 mg, 0.8 mmol, 2.0 Äq.) und CuPh (110 mg, 0.8 mmol, 2.0 Äq.) wird bei –78°C in thf (10 mL) aufgenommen und bei ständigem Rühren langsam über einen Zeitraum von 18 h auf Raumtemperatur gebracht. Das Reaktionsgemisch wird weitere 72 h bei Raumtemperatur gerührt. Am Feinvakuum werden alle flüchtigen Bestandteile entfernt. Der farblose Rückstand wurde über ein ^{1}H-NMR untersucht (*Abbildung 3.7.2.2*. unten). Der Rückstand wurde in DMF (5 mL) aufgenommen und über einen Spritzenfilter unter 10 mL Et$_2$O geschichtet und bei Raumtemperatur für einige Wochen gelagert. Es wurden Einkristalle erhalten, die röntgenographisch als DMPyr$_2$[S(CuPh)$_2$] identifiziert werden konnten (XRD: *Abbildung 3.7.2.1*., ^{1}H-NMR *Abbildung 3.7.2.2*. oben). Das ^{1}H-NMR Spektrum zeigt nicht zuordenbare Verunreinigungen im aromatischen Bereich.

NMR Spektren von DMPyr$_2$[(PhCu)$_2$S]:

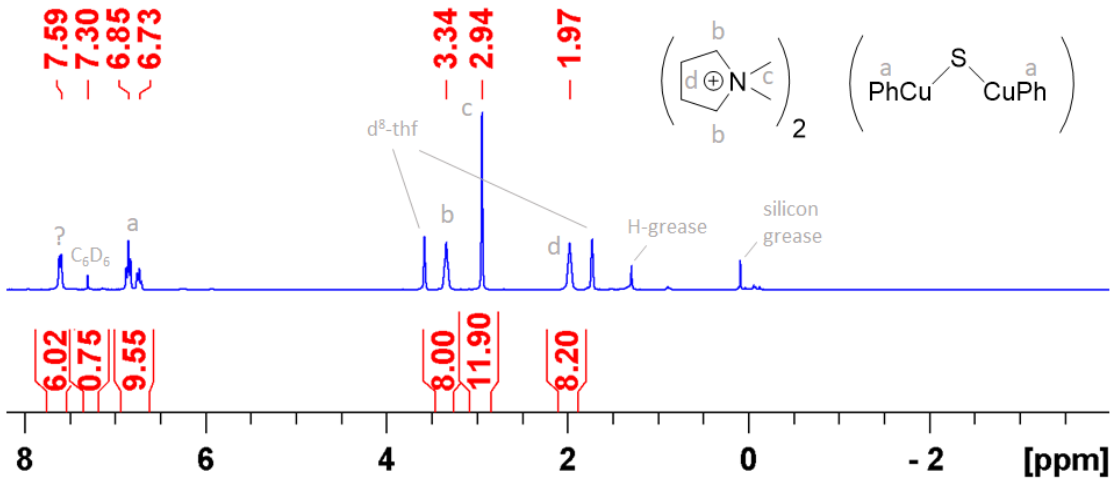

^{1}H-NMR *(300.2 MHz, d^8-thf): Probe mit den gemessenen Einkristallen von DMPyr$_2$[S(CuPh)$_2$].*

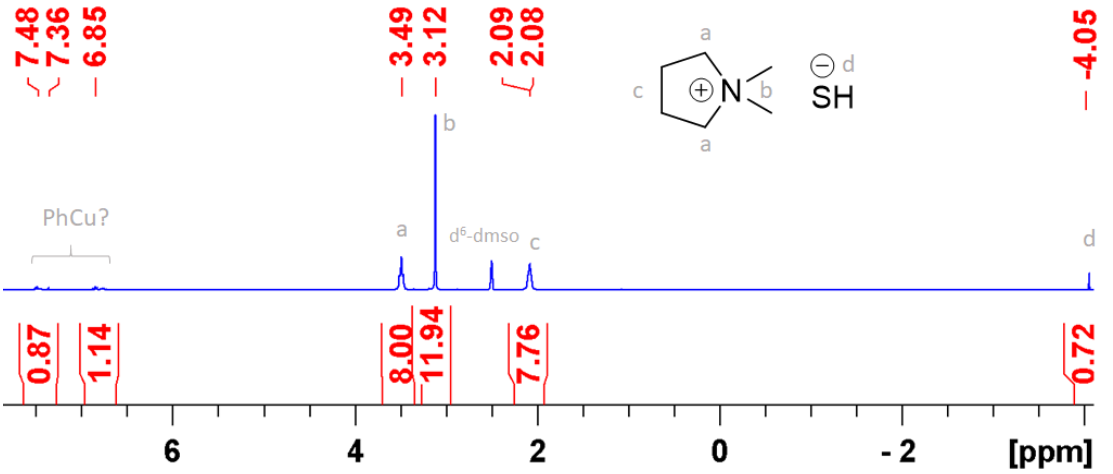

^{1}H-NMR *(300.2 MHz, d^6-dmso): Rohproduktes bei Reproduktionsversuch.*

3.7.3 Umsetzung von DMPyr[SH] mit doppelt NHC-geschütztem CuCl

Bei dem Versuch, Ph$_4$P[Cu(SSiMe$_3$)$_2$] mit zwei Äquivalenten IMes-AgOAc (IMes = = 1,3-bis(2,4,6-trimethylphenyl)imidazol-2-yliden) unter doppelter Desilylierung zu Ph$_4$P[Cu(SAgIMes)$_2$] umzusetzen (*Schema 3.7.3.1*), wurden überraschender-weise Einkristalle von [(IMes)$_2$CuSH] erhalten (*Abbildung 3.7.3.1, Kristallographischer Anhang 6.7.5*). Vergleichbare Strukturen [L$_n$CuSH] mit terminalen kupfergebundenen, unverbrückenden [SH]$^-$ Liganden gibt es nur für n = 1, L = IPr* (Cu-C 1.843(5) Å, Cu-S 2.080(2) Å) und IPr‘ (Cu-C

1.890(4) Å, Cu-S 2.127(1) Å) (IPr‘ = 1,3-bis(2,6-di-isopropylphenyl)imidazol-2-yliden),[3.1] oder n = 3, L = 2 x Ph_3P und 1 x py (Cu-S 2.322(1) Å).[3.2] Die Cu-S Bindungslänge in [$(IMes)_2$CuSH] ist mit 2.303(1) Å kürzer als die in [$(Ph_3P)_2$(py)CuSH], aber länger als die in in [IPr*CuSH] und [IPr‘CuSH].

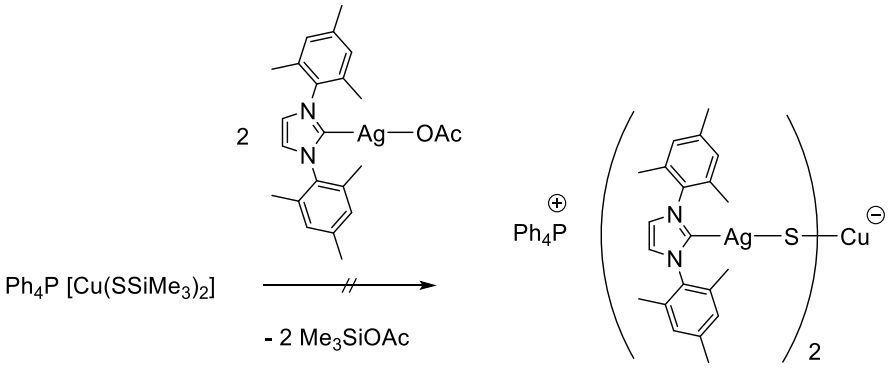

Schema 3.7.3.1: Darstellungsversuch von $Ph_4P[Cu(SAgIMes)_2]$.

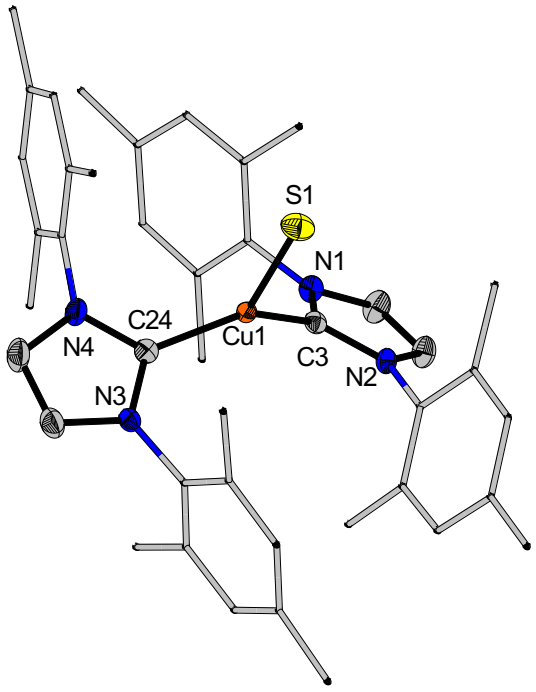

Abbildung 3.7.3.1: Kristallographisch bestimmte Molekülstruktur von $[(IMes)_2CuSH]$ (orthorhombisch Pccn, acht Formeleinheiten pro Elementarzelle). Wasserstoffatome und ein Diethylethermolekül sind der Übersicht halber nicht abgebildet. Ellipsoide in 50% Level, die Mesitylsubstituenten sind ebenso der Übersicht halber als Stäbchenmodell abgebildet. Wichtige Bindungslängen (in Å) und -winkel (in °): Cu1-S1 2.303(1), Cu1-C3 1.939(2), Cu1-C24 1.941(3), C3-N1 1.368(3), C3-N2 1.368(3), C24-N3 1.367(3), C24-N4 1.365(3), C3-Cu1-S1 111.55(7), C24-Cu1-S1 107.96(7), C3-Cu1-C24 140.5(1), N1-C2-N2 102.0(2), N4-C24-N3 102.3(2), N1-C3-Cu1-S1 -101.5(2), N2-C3-Cu1-S1 72.3(2), N3-C24-Cu1-S1 -97.2(2), N4-C24-Cu1-S1 74.9(2).

Zunächst konnte nicht eindeutig geklärt werden, ob es sich bei der kristallographisch bestimmten Struktur um die durch Ag^+ oxidierte Kupfer(II)spezies $[(IMes)_2Cu^{II}S]$, oder um die durch Spuren von Feuchtigkeit protonierte Kupfer(I) Verbindung $[(IMes)_2CuSH]$ handelt, da sich diese Strukturen nur um ein kristallographisch schwer identifizierbares, schwefelgebundenes Proton unterschieden. Diese Problematik wurde auch bei dem verlgeichbaren $[(Ph_3P)_2(py)CuSH]$ System diskutiert.[3.2] Allerdings konnte $[(IMes)_2CuSH]$ durch APCI Massenspektren der in Toluol gelösten, gemessenen Einkristalle nachgewiesen werden. Ebenso erfolgte dieser massenspektroskopische Nachweis durch eine definierte Synthese, bei der zwei Äquivalente IMes mit einem Äuqivalent CuCl und einem Äquivalenten DMPyr[SH] in thf umgesetzt und die Zielverbindung anschließend durch Extraktion mit Toluol isoliert wurde (*Schema 3.7.3.2*). Für letztgenannte Umsetzung konnten auch ^1H und ^{13}C-NMR Spektren erhalten werden.

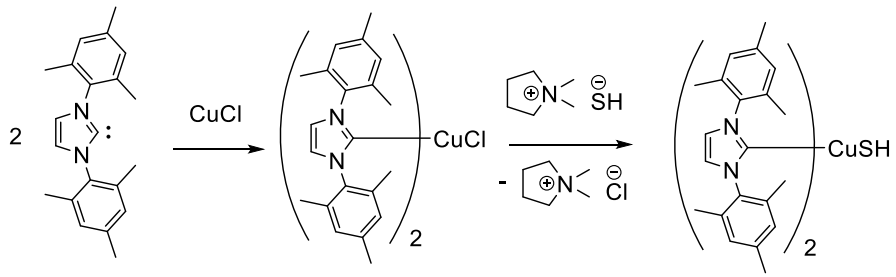

Schema 3.7.3.2: Darstellung von $[(IMes)_2CuSH]$.

Herstellungsversuch von $Ph_4P[Cu(SAgIMes)_2]$: Zu einer Lösung von $Ph_4P[Cu(SSiMe_3)_2]$ (95 mg, 0.2 mmol, 1.0 Äq.) in thf (10 mL) wird bei –78°C tropfenweise eine Lösung von [IMesAgOAc] (146 mg, 0.3 mmol, 2.0 Äq.) in thf (5 mL) gegeben und das Reaktionsgemisch über einen Zeitraum von 18 h auf etwa 0°C erwärmt. Das Reaktionsgemisch wird am Feinvakuum von allen flüchtigen Bestandteilen getrennt und der Rückstand in Diethylether (10 mL) suspendiert. Diese Suspension wird über einen Spritzenfilter filtriert, und das Filtrat unter Pentan (10 mL) geschichtet. Nach einigen Tagen konnten bei –30 °C Einkristalle erhalten werden, die als $[(IMes)_2CuSH]$ identifiziert wurden. Über ein APCI Massenspektrum konnte dies bestätigt werden (HRMS(APCI): m/z gefunden 703.2887 ($C_{42}H_{48}CuN_4S$ soll 703.2890).

Darstellung von $[(IMes)_2CuSH]$: IMes (173 mg, 0.6 mmol, 2.0 Äq.) und CuCl (28 mg, 0.3 mmol, 1.0 Äq.) werden gemeinsam eingewogen und für 18 h in thf (10 mL) bei Raumtemperatur gerührt. Alle flüchtigen Bestandteile werden am Feinvakuum entfernt. Der farblose Rückstand wird mit DMPyr[SH] (38 mg, 0.3 mmol, 1.0 Äq.) versetzt. Das Gemisch

wird bei –78 °C mit thf (10 mL) versetzt und innerhalb von 18 h auf Raumtemperatur gebracht. Am Feinvakuum werden alle flüchtigen Bestandteile entfernt und der Rückstand in Toluol (10 mL) aufgenommen. Nach Filtration und Entfernen aller flüchtigen Bestandteile wird [(IMes)$_2$CuSH] (127 mg, 0.2 mmol, 64%) als farbloses Pulver erhalten.

^{1}H-NMR (500.1 MHz, d^6-dmso): δ = 7.34 (s, 4H, $H_{Ar(Imidazol)}$), 6.91 (s, 8H, $H_{Ar(mes)}$), 2.39 (s, 12H, $H_{Alip(para)}$), 1.68 (s, 12H, $H_{Alip(ortho)}$), –3.55 (s, 1H, [(IMes)$_2$CuSH]) ppm. **^{13}C-NMR** (125.8 MHz, d^6-dmso): δ = 137.8 (s, $C_{Ar(mes,para)}$), 135.3 (s, $C_{Ar(mes,ipso)}$), 134.2 (s, $C_{Ar(mes,meta)}$), 128.6 (s, $C_{Ar(mes,ortho)}$), 122.4 (s, $C_{Ar(Imidazol)}$), 20.7 (s, $C_{Alip(para)}$), 16.9 (s, $C_{alip(ortho)}$) ppm. Das Signal für das kupfergebundene C-Atom konnte aufgrund der geringen Konzentration nicht detektiert werden**. HRMS(APCI)**: m/z gefunden 703.2893 ($C_{42}H_{48}CuN_4S$ soll 703.2890).

NMR Spektren von [(IMes)$_2$CuSH]:

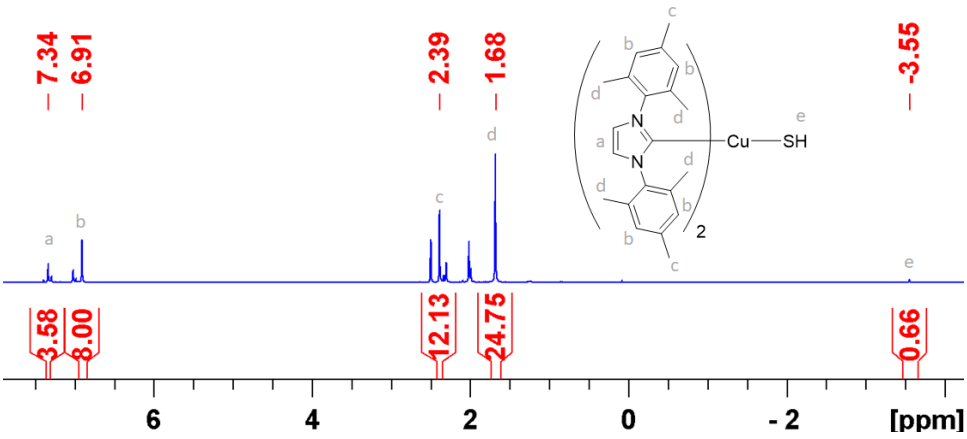

^{1}H-NMR (500.1 MHz, d^6-dmso).

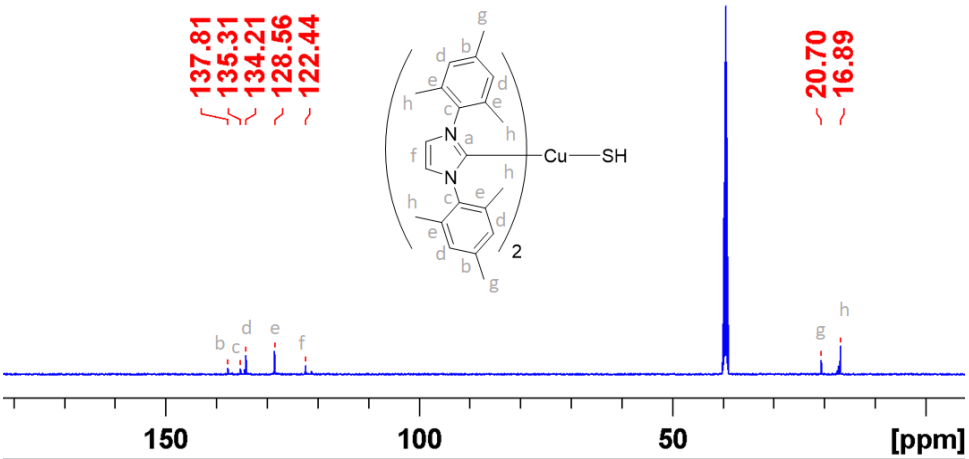

^{13}C-NMR (125.8 MHz, d^6-dmso). Das Signal für das kupfergebundene C-Atom konnte aufgrund der geringen Konzentration nicht detektiert werden.

3.7.4 NHC-stabilisierte Sn(II) Komplexe mit Trimethylsilylchalkogenolat Liganden

In ergänzenden Arbeiten wurde das NHC-Stannylen Addukt [IMesSn($SSiMe_3$)$_2$] dargestellt und strukturell charakterisiert (*Abbildung 3.7.3.1, Kristallographischer Anhang 6.7.3*). Der Winkel der C-Sn Bindung von annähernd 90° spricht für eine Wechselwirkung des NHC-Liganden mit einem p-Orbital am Zinnatom, während das freie Elektronenpaar am Zinnatom eine verzerrt pseudotetraedrische Koordination am Zinnatom verursacht. Vergleichbare Strukturmerkmale wurden auch bei dem NHC-Addukt von $SnCl_2$ [IPr$SnCl_2$] (IPr = 1,3-bis(isopropyl)imidazol-2-yliden) beobachtet (C-Sn 2.290(5) Å, Cl-Sn-C 93.6(1)° & 95.9(1)°.[3.3] Vergleichbare NHC-Addukte des Zinns mit Thiolatliganden gibt es nicht.

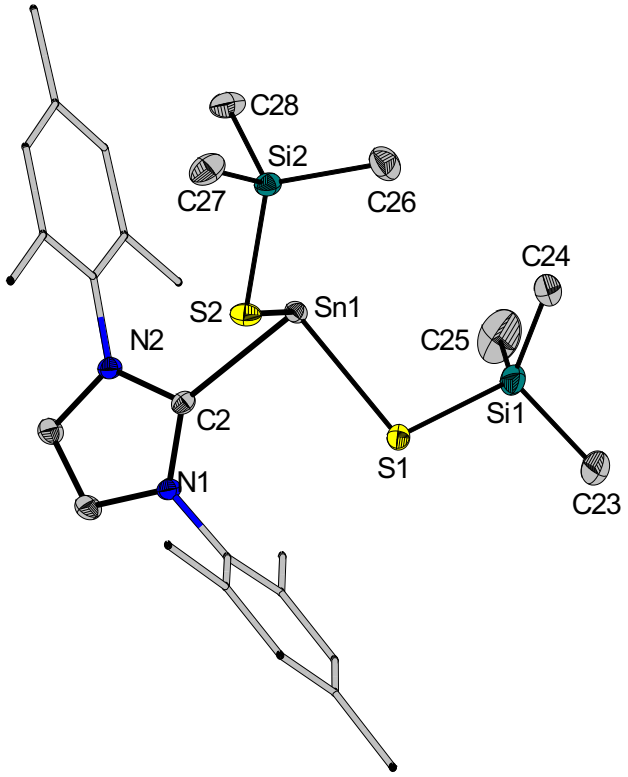

Abbildung 3.7.3.1: Kristallographisch bestimmte Molekülstruktur von [IMes-Sn($SSiMe_3$)$_2$] (monoklin, P21/n, vier Formeleinheiten pro Elementarzelle). Die Wasserstoffatome wurde der Übersicht halber nicht abgebildet. Ausgewählte Bindungslängen (in Å) und -winkel (in °): Sn1-C2 2.311(2), Sn1-S1 2.5146(7), Sn1-S2 2.5324(6), S1-Si1 2.1200(7), S2-Si2 2.1328(7), Si1-C23 1.872(2), Si1-C24 1.877(3), Si1-C25 1.863(3), Si2-C26 1.870(2), Si2-C27 1.875(2), Si2-C28 1.871(2), C2-N1 1.363(2), C2-N2 1.357(2), S1-Sn1-S2 97.09(2), S2-Sn1-C2 89.07(5), C2-Sn1-S1 91.52(4), Sn1-S1-Si1 100.67(2), Sn1-S2-Si2 101.70(3), C23-Si1-C24 110.0(1), C24-Si1-C25 108.9(1), C25-Si1-C23 109.7(1), C26-Si2-C27 109.40(9), C27-Si2-C28 109.11(9), C28-Si2-C26 108.71(9), Sn1-C2-N1 136.9(1), Sn1-C2-N2 119.0(1), C2-Sn1-S1-Si1 -144.47(5), C2-Sn1-S2-Si2 141.56(5), Sn1-S1-Si1-C23 177.85(7), Sn1-S1-Si1-C24 -63.51(9), Sn1-S1-Si1-C25 58.11(9), Sn1-S2-Si2-C26 75.76(7), Sn1-S2-Si2-C27 -165.34(7), N1-S2-Si2-C28 -46.32(7), S1-Sn1-C2-N1 -9.4(2), S1-Sn1-C2-N2 165.8(1).

Da die analog hergestellte homologe Selenolatspezies bei Raumtemperatur rapide zerfällt, ist eine Blockierung der Stabilisierung am p-Orbitals durch den NHC-Liganden am Zinnatom durch pi-Wechselwirkungen mit den Selenatomen anzunehmen. Der dabei angefallene Rückstand konnte nach thermischer Nachbehandlung röntgenpulverdiffraktometrisch als SnSe identifiziert werden (*Abbildung 3.7.3.2*).

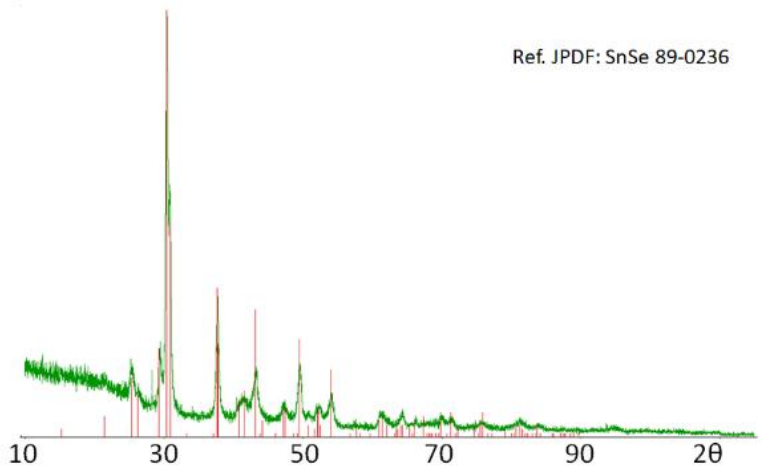

Abbildung 3.7.3.2: Röntgenpulverdiffraktogramm des therimsch nachbehandelten Rückstandes (3 Tage bei 160°C unter Vakuum), der bei der versuchten Darstellung von IMes-Sn(SeSiMe$_3$)$_2$ entstanden ist. Bei dem schwarzen Feststoff handelt es sich um SnSe.

Herstellung von [IMes-Sn(SSiMe$_3$)$_2$]: $SnCl_2$ (60 mg, 0.32 mmol, 1.0 Äq.) werden mit 1,3-Dimesitylimidazol-2-yliden (IMes, 96 mg, 0.32 mmol, 1.0 Äq.) zusammen eingewogen und mit thf (10 mL) versetzt. Das Gemisch wird für 18h bei Raumtemperatur gerührt. Zu einer Lösung aus $S(SiMe_3)_2$ (118 mg, 0.66 mmol, 2.1 Äq.) in thf (5 mL) wird bei 0 °C tropfenweise BuLi (0.26 mL einer 2.43M Lösung in Hexan, 0.63 mmol, 2.0 Äq.) hinzugegeben. Das Gemisch wird für 30 min. bei 0°C, dann für 30 min bei Raumtemperatur gerührt, dann am Feinvakuum von allen flüchtigen Bestandteilen getrennt, bis $LiSSiMe_3$ als wachsartiger Rückstand zurückbleibt. Dieser wird in thf (5 mL) gelöst. Die vorbereitete IMes-$SnCl_2$ Lösung wird bei –78 °C vorgelegt und tropfenweise mit der $LiSSiMe_3$-Lösung versetzt. Das reaktionsgemisch wird über einen Zeitraum von 18 h auf Raumtemperatur gebracht und am Feinvakuum von allen flüchtigen Bestanteilen getrennt. Die Zielverbindung wird mit 2 x 20 mL Et_2O extrahiert und am Feinvakuum von allen flüchtigen Bestanteilen getrennt und getrocknet. [IMes-Sn(SSiMe$_3$)$_2$] (157 mg, 0.25mmol, 78%) wird als farbloses Pulver erhalten. Aus in einer gesättigten Et_2O/Pentan-Lösung konnten bei –30 °C Einkristalle zur kristallographischen Charakterisierung gezüchtet werden.

^{1}H-NMR (300.3 Mhz, d^{8}-THF): δ = 7.43 (s, 2H, $H_{Ar(Imidazol)}$), 6.98 (s, 4H, $H_{Ar(mes)}$), 2.33 (s, 6H, $H_{Alip(para)}$), 2.18 (s, 12H, $H_{Alip(ortho)}$), 0.06 (s, 18H, Sn(S(Si(CH_3)$_3$)$_2$) ppm. **^{13}C-NMR** (75.5 MHz, d^{8}-THF): δ = 177.4 (s, *C*2), 140.0 (s, $C_{Ar(mes,para)}$), 136.0 (s, $C_{Ar(mes,meta)}$), 135.4 (s, $C_{Ar(mes,ipos)}$), 129.7 (s, $C_{Ar(mes,ortho)}$), 125.0 (s, $C_{Ar(Imidazol)}$), 21.0 (s, $C_{Alip(para)}$), 18.5 (s, $C_{alip(ortho)}$), 5.2 (s, 2 x SSi(CH_3)$_3$) ppm. **^{29}Si-NMR** (59.7 MHz, d^{8}-THF): δ = 10.1 (t, $^{2}J_{Sn\text{-}Si}$ = 27.7 Hz, 2 x S*Si*Me$_3$) ppm. **^{119}Sn-NMR** (112.0 MHz, d^{8}-THF): d = 44.0 (t, $^{2}J_{Sn\text{-}Si}$ = 28.2 Hz, IMes-*Sn*(SSiMe$_3$)$_2$) ppm. **Elementaranalyse $C_{27}H_{42}N_2S_2Si_2Sn$ gef. (theor.):** C 50.9 (51.2), H 6.5 (6.7), N 4.7 (4.4), S 9.7 (10.1).

Versuch der Herstellung von [IMes-Sn(SeSiMe$_3$)$_2$]: SnCl$_2$ (39 mg, 0.21 mmol, 1.0 Äq.) werden mit 1,3-Dimesitylimidazol-2-yliden (IMes, 63 mg, 0.21 mmol, 1.0 Äq.) zusammen eingewogen und mit thf (10 mL) versetzt. Das Gemisch wird für 18h bei Raumtemperatur gerührt. Zu einer Lösung aus Se(SiMe$_3$)$_2$ (98 mg, 0.43 mmol, 2.1 Äq.) in thf (5 mL) wird bei 0 °C tropfenweise BuLi (0.17 mL einer 2.43M Lösung in Hexan, 0.41 mmol, 2.0 Äq.) hinzugegeben. Das Gemisch wird für 30 min. bei 0°C, dann für 30 min bei Raumtemperatur gerührt, dann am Feinvakuum von allen flüchtigen Bestandteilen getrennt, bis LiSeSiMe$_3$ als wachsartiger Rückstand zurückbleibt. Dieser wird in thf (5 mL) gelöst. Die vorbereitete IMes-SnCl$_2$ Lösung wird bei –78 °C vorgelegt und tropfenweise mit der LiSeSiMe$_3$-Lösung versetzt. Das Reaktionsgemisch wird über einen Zeitraum von 18 h auf Raumtemperatur gebracht. Bei Raumtemperatur fällt innerhalb weniger Minuten ein schwarzer Feststoff aus. Dieser wurde durch Dekantieren der überstehenden Lösung und thermischer Nachbehandlung für 72 h bei 160 °C röntgenpulverdiffraktometrisch als SnSe identifiziert.

NMR Spektren von [IMes-Sn(SSiMe$_3$)$_2$]:

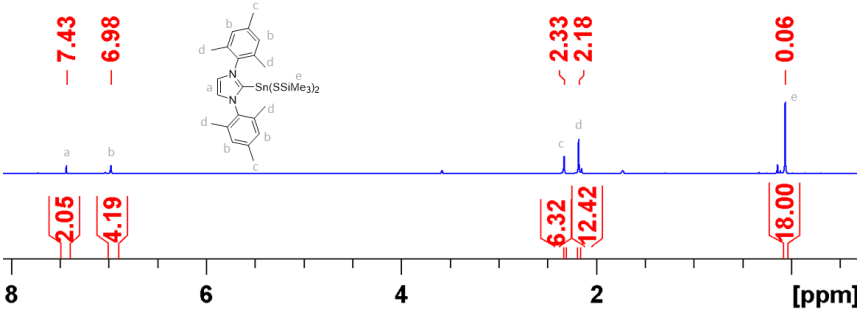

^{1}H-NMR (300.3 Mhz, d^{8}-THF).

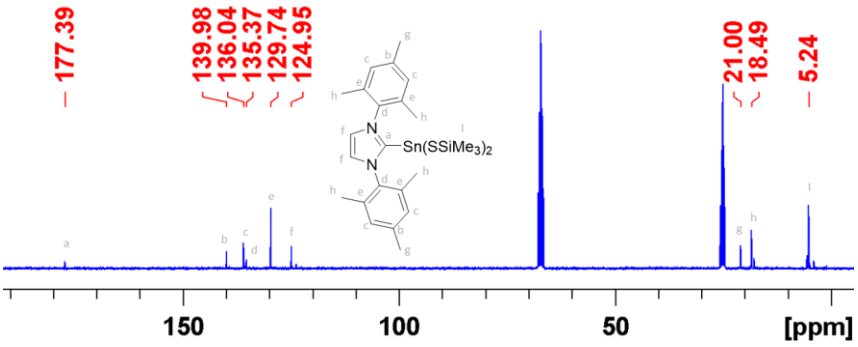

^{13}C-NMR (75.5 MHz, d^8-THF).

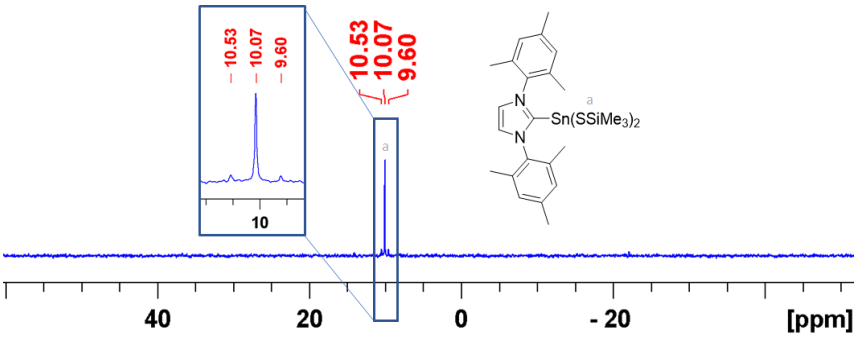

^{29}Si-NMR (59.7 MHz, d^8-THF).

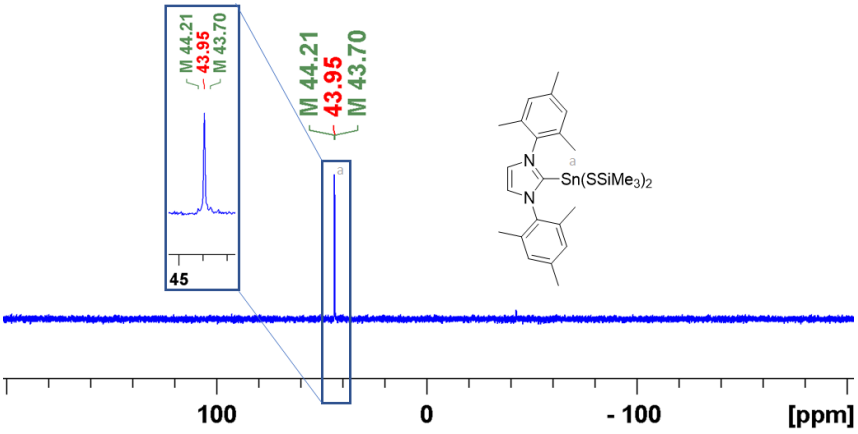

^{119}Sn-NMR (112.0 MHz, d^8-THF).

3.7.5 Lanthantricyclopentadienid Addukte mit $Ph_4P[ESiMe_3]$ (E = S, Se, Te)

Noch nicht abgeschlossene Arbeiten behandeln die Addukte der Trimethylsilylchalkogenolatsalze $Ph_4P[ESiMe_3]$ mit der Lewis-Säure Cp_3La. Es bilden sich mononukleare Lanthanatkomplexe der Form $Ph_4P[Cp_3LaESiMe_3]$ (E = S (*Abbildung 3.7.2.1)*, Se (*Abbildung 3.7.2.2*), Te (*Abbildung 3.7.2.3*)). Diese wurden kristallographisch nachgewiesen (*Kristallographischer Anhang 6.7.1*). Einige anionische $[Cp_3LaX]^-$ Addukte sind zwar bekannt,[3.4–3.7] allerdings nicht für X = $[ER]^-$ (E = S, Se, Te; R = beliebiger Substituent).

Vergleicht man die E-Si Bindungslänge der homologen $Ph_4P[ESiMe_3]$ Salze mit denen der entsprechenden Lanthanat-Addukte $Ph_4P[Cp_3LaESiMe_3]$ fällt auf, dass die Metallierung eine Verlängerung dieser Bindung provoziert. Diese Expansion ist relativ betrachtet von vergleichbarem Ausmaß für E = Se und Te (je +1.2%), aber deutlich ausgeprägter für E = S (+1.6%) (*Abbildung 3.7.2.4*). Dies überrascht, da die Ähnlichkeiten zwischen Se und Te erfahrungsgemäß weniger ausgeprägt sind als zwischen S und Se. Quantenchemische Rechnungen sollten die elektronischen Ursachen dieser Beobachtung erklären können.

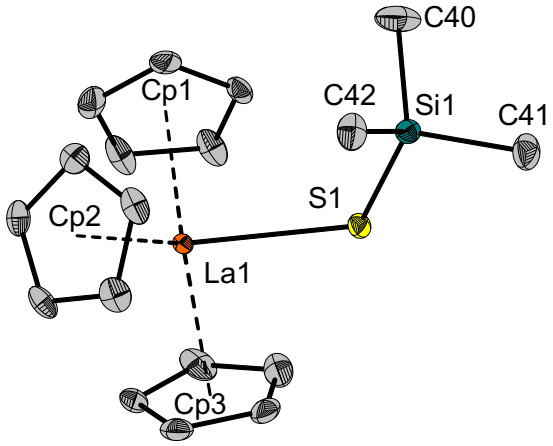

Abbildung 3.7.2.1: Kristallographisch bestimmte Molekülstruktur des Anions von $Ph_4P[Cp_3LaSSiMe_3]$ (monoklin, P21/c, vier Ionenpaare pro Elementarzelle). Das Kation und die Wasserstoffatome wurde der Übersicht halber nicht abgebildet. Ausgewählte Bindungslängen (in Å) und -winkel (in °): La1-S1 2.922(1), S1-Si1 2.0978(9), Si1-C40 1.867(3), Si1-C41 1.878(3), Si1-C42 1.877(3), La1-Cp1 2.6250(7), La1-Cp2 2.6023(8), La1-Cp3 2.5887(9), La1-S1-Si1 128.33(3), S1-Si1-C40 112.50(9), S1-Si1-C41 110.23(8), S1-Si1-C42 112.98(7), C40-Si1-C41 107.4(1), C41-Si1-C42 106.5(1), C42-Si1-C40 106.9(1), S1-La1-Cp1 104.05(2), S1-La1-Cp2 107.29(2), S1-La1-Cp3 94.45(2), Cp1-La1-Cp2 112.93(2), Cp2-La1-Cp3 117.52(1), Cp3-La1-Cp1 117.18(2), La1-S1-Si1-C40 -60.6(1), La1-S1-Si1-C41 179.64(9), La1-S1-Si1-C42 60.6(1), Si1-S1-La1-Cp1 70.15(4), Si1-S1-La1-Cp2 -49.75(4), Si1-S1-La1-Cp3 -170.39(4).

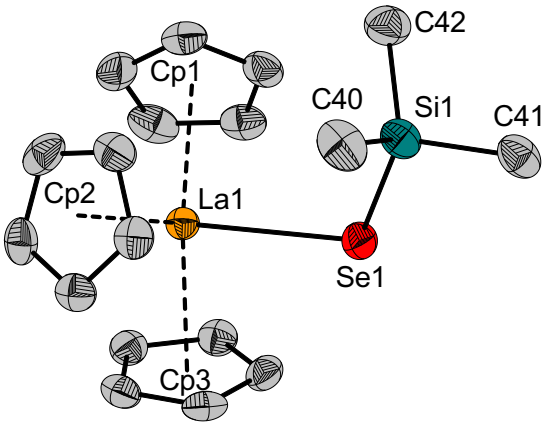

Abbildung 3.7.2.2: Kristallographisch bestimmte Molekülstruktur des Anions von $Ph_4P[Cp_3LaSeSiMe_3]$ (monoklin, P21/n, vier Ionenpaare pro Elementarzelle). Das Kation und die Wasserstoffatome wurde der Übersicht halber nicht abgebildet. Ausgewählte Bindungslängen (in Å) und -winkel (in °): La1-Se1 2.9981(6), Se1-Si1 2.236(1), Si1-C40 1.871(5), Si1-C41 1.878(5), Si1-C42 1.876(4), La1-Cp1 2.6093(3), La1-Cp2 2.5972(3), La1-Cp3 2.6161(4), La1-Se1-Si1 117.34(4), Se1-Si1-C40 113.1(2), Se1-Si1-C41 107.1(2), Se1-Si1-C42 113.4(2), Se1-Si1-Cp1 104.60(1), Se1-Si1-Cp2 104.74(1), Se1-Si1-Cp3 95.53(1), La1-Se1-Si1-C40 71.1(2), La1-Se1-Si1-C41 -170.7(2), La1-Se1-Si1-C42 -51.8(2), Si1-Se1-La1-Cp1 67.00(4), Si1-Se1-La1-Cp2 -55.79(4), Si1-Se1-La1-Cp3 -174.87(4).

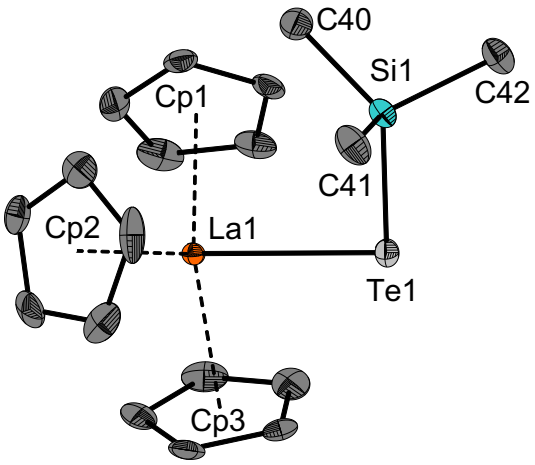

Abbildung 3.7.2.3: Kristallographisch bestimmte Molekülstruktur des Anions von $Ph_4P[Cp_3LaTeSiMe_3]$ (monoklin, P21, ein Ionenpaar pro Elementarzelle). Das Kation und die Wasserstoffatome wurde der Übersicht halber nicht abgebildet. Ausgewählte Bindungslängen (in Å) und -winkel (in °): La1-Te1 3.2833(8), Te1-Si1 2.476(1), Si1-C40 1.877(5), Si1-C41 1.875(4), Si1-C42 1.873(4), La1-Cp1 2.5950(6), La1-Cp2 2.5949(8), La1-Cp3 2.5977(6), La1-Te1-Si1 106.27(3), Te1-Si1-C40 115.0(1), Te1-Si1-C41 110.2(1), Te1-Si1-C42 109.5(1), C40-Si1-C41 106.1(2), C41-Si1-C42 109.2(2), C42-Si1-C40 106.7(2), Te1-La1-Cp1 106.86(1), Te1-La1-Cp2 101.46(1), Te1-La1-Cp3 95.96(1), Cp1-La1-Cp2 115.82(1), Cp2-La1-Cp3 116.59(1), Cp3-La1-Cp1 116.08(1), La1-Te1-Si1-C40 -17.5(2), La1-Te1-Si1-C41 102.3(1), La1-Te1-Si1-C42 -137.6(1), Si1-Se1-La1-Cp1 64.55(3), Si1-Se1-La1-Cp2 -57.17(2), Si1-Se1-La1-Cp3 -175.88(3).

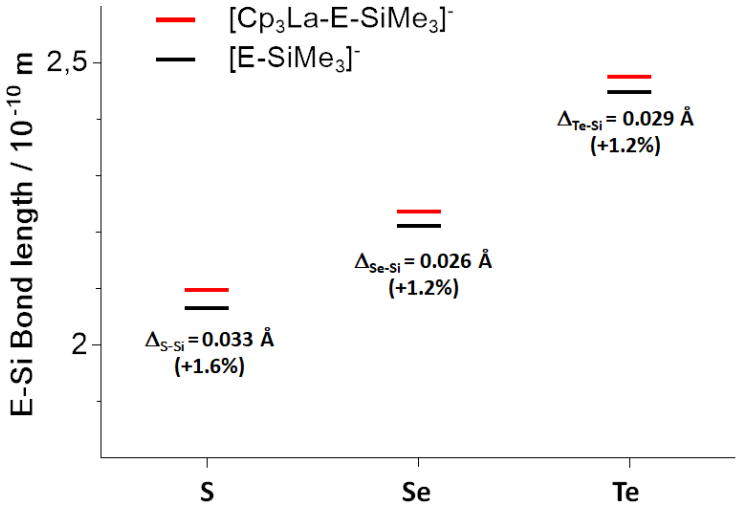

Abbildung 3.7.2.4: Vergleich der kristallographisch bestimmten E-Si Bindungslängen von $Ph_4P[ESiMe_3]$ (schwarz) und der Lanthanocen Addukte $Ph_4P[Cp_3LaESiMe_3]$ (rot). E = S (links), Se (mittig), Te (rechts). E-Si Bindungslänge $[E\text{-}SiMe_3]^-$ / $[Cp_3LaE\text{-}SiMe_3]^-$ (in Å) E = S: 2.0647(8) / 2.0978(9); E = Se: 2.2102(9) / 2.236(1); E = Te: 2.447(2) / 2.476(1).

Herstellung von $Ph_4P[Cp_3LaESiMe_3]$: Ein Gemisch aus $Ph_4P[ESiMe_3]$ (m1, n1, Äq.1) und Cp_3La (m1, n1, Äq.1) wird bei – 20 °C mit thf (10 mL) versetzt und über einen Zeitraum von 18 h auf Raumtemperatur gebracht. Die Reaktionslösung wird mit Pentan überschichtet und bei –30 °C für einige Tage gelagert. Die Zielverbindung wird in Form farbloser Einkristalle erhalten. Für E = Te wurde die Reaktion unter Lichtausschluss durchgeführt.

Tabelle 3.7.2.1: Menge der verwendeten Edukte.

$Ph_4P[Cp_3La\ ESiMe_3]$	**m1, n1, Äq.1**	**m1, n1, Äq.1**
$Ph_4P[Cp_3La\ SSiMe_3]$	114 mg, 0.26 mmol, 1.0 Äq	85 mg, 0.26 mmol, 1.0 Äq.
$Ph_4P[Cp_3La\ SeSiMe_3]$	119 mg, 0.24 mmol, 1.0 Äq.	81 mg, 0.24 mmol, 1.0 Äq.
$Ph_4P[Cp_3La\ TeSiMe_3]$	124 mg, 0.23 mmol, 1.0 Äq.	76 mg, 0.23 mmol, 1.0 Äq.

3.7.6 Systematische Studie zum Zugang zu organischen Trithiocarbonat-Salzen

Metallkomplexe mit Tertbutyltrithiocarbonat-Liganden, wie z. B. $Mo(SCS_2tBu)_4$ sind als molekulare Vorstufen für sulfidische Halbleiter wie MoS_2. Tertbutyltrithiocarbonat Anionen $[SCS_2tBu]^-$ sind zwar mit zahlreichen metallischen Kationen bekannt, allerdings wurde noch kein systematischer Zugang zu organischen Salzen von ihnen ausgearbeitet. Vergleichbare Ausnahmen bildet hierbei das von *Henkel et al.* ausschließlich strukturell charakterisierte adamantylhomologe $PPN[SCS_2Ad]$[3.8] und das von *Heyl et al*. beschriebene $Me_4N[SCS_2Me]$.[79]

In den von mir betreuten Vertiefungspraktika von *Haowen Wang* und *Nima Heidary* wurden systematische Untersuchungen zu Darstellung, Charkaterisierung und Struktur diverser $Cat[SCS_2tBu]$ Salze durchgeführt und abgeschlossen. Zunächst wurde die Herstellung von $Cat[SCS_2tBu]$ Salzen durch Addition von CS_2 an isolierte oder intermediär gebildete Salze $Cat[StBu]$ untersucht. Anschließend wurde gezeigt, dass eine Deprotonierung des protonierten Tertbutyltrithiocarbonats $HSCS_2tBu$ mit einem Methylcarbonatanion $[OCO_2Me]^-$ ohne weiteres möglich ist. Dies reduziert im Vergleich zur erstgenannten Methode die Anzahl notwendiger Reaktionsschritte, da die Deprotonierung von $HStBu$ mit Methylcarbonat-Anionen nicht direkt erfolgen kann, sondern über eine Desilylierung der silylierten Vorstufe $Me_3SiStBu$ verlaufen müsste.

Wird $MMIm[StBu]$ in thf suspendiert und mit einem Äquivalent CS_2 versetzt, erfolgt eine Klärung der Suspension hin zu einer transparenten Lösung. Bei Entfernen des Lösungsmittels wird die Zielverbindung $MMIm[SCS_2tBu]$ als farbloser Feststoff erhalten (*Schema 3.7.6.1*).

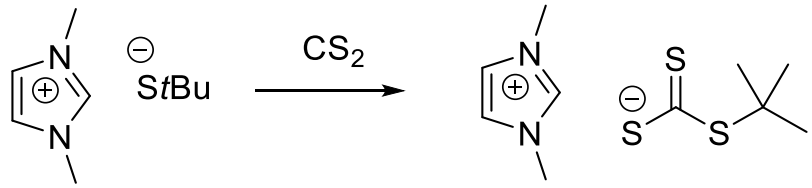

Schema 3.7.6.1: Addition von CS_2 an $MMIm[StBu]$ zur Darstellung von $MMIm[SCS_2tBu]$.

Die kristallographisch bestimmte Molekülstruktur von $MMIm[SCS_2tBu]$ zeigt die erwartete Struktur (*Abbildung 3.7.6.1*).

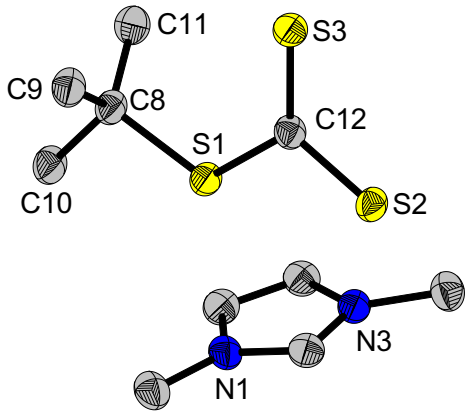

Abbildung 3.7.6.1: Kristallographisch bestimmte Molekülstruktur von MMIm[SCS₂tBu] (triklin, P-1, zwei Ionenpaare pro Elementarzelle). Das die Wasserstoffatome wurde der Übersicht halber nicht abgebildet. Ausgewählte Bindungslängen (in Å) und -winkel (in °) des Anions: C12-S1 1.757(3), C12-S2 1.699(3), C12-S3 1.682(2), S1-C8 1.852(3), C8-C9 1.524(4), C8-C10 1.534(4), C8-C11 1.529(3), S2-C12-S3 125.3(2), S3-C12-S1 124.9(2), S1-C12-S2 109.8(1), C12-S1-C8 113.7(1), S1-C8-C9 110.8(2), S1-C8-C10 101.7(2), S1-C8-C11 112.9(2), C9-C8-C10 108.7(2), C10-C8-C11 109.8(2), C11-C8-C9 112.3(2), S2-C12-S1-C8 177.9(1), S3-C12-S1-C8 -3.2(2), C12-S1-C8-C9 -64.1(2), C12-S1-C8-C10 -179.6(2), C12-S1-C8-C11 62.8(2).

Über das ^{1}H-NMR-Spektrum und eine Elementaranalyse kann eine zufriedenstellende Reinheit der Zielverbindung bestätigt werden. Der Nachweis über eine erfolgreiche CS_2-Addition kann über das Signal des quartären Kohlenstoffatoms des „SCS_2“ Fragments erfolgen, das im ^{13}C-NMR-Spektrum in d^{6}-DMSO bei etwa 240 ppm erscheint.

Eine Möglichkeit, phosphoniumbasierte Salze mit dem [SCS_2tBu]$^-$ Anion herzustellen wurde durch die Addition von CS_2 an *in situ* generiertem Ph_3PMe [S*t*Bu] zur Zielverbindung Ph_3PMe [SCS_2tBu] realisiert, das durch Deprotonierung von HS*t*Bu durch das P-Ylid Ph_3PCH_2 entsteht (*Schema 3.7.6.2*).

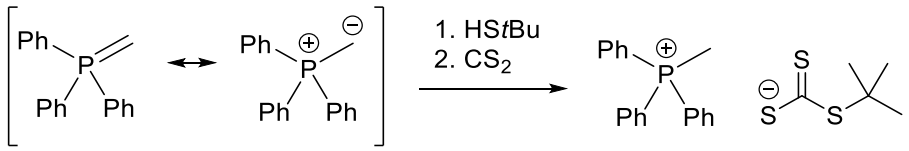

Schema 3.7.6.2: Darstellung von Ph_3PMe [SCS_2tBu] ausgehend vom P-Ylid Ph_3PCH_2.

Die Identität und Struktur von Ph_3PMe [SCS_2tBu] wurden kristallographisch und ^{13}C-NMR spektroskopisch bestimmt und die Reinheit ^{1}H-NMR-spektroskopisch und elementaranalytisch bestätigt. Die Kristallstruktur von Ph_3PMe [SCS_2tBu] wurde als Inversionszwilling gelöst. Die kristallographisch bestimmt Molekülstruktur ist in *Abbildung 3.7.6.2* gezeigt.

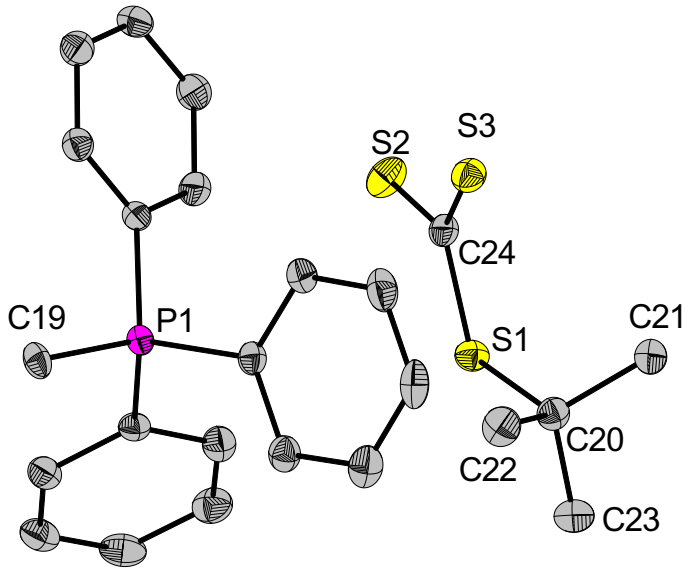

Abbildung 3.7.6.2: Kristallographisch bestimmte Molekülstruktur von Ph_3PMe [SCS_2tBu] (monoklin, $P2_1$, zwei Ionenpaare pro Elementarzelle). Das die Wasserstoffatome wurde der Übersicht halber nicht abgebildet. Ausgewählte Bindungslängen (in Å) und -winkel (in °) des Anions: C24-S11.773(3), C24-S2 1.687(3), C24-S3 1.680(3), C20-S1 1.853(3), C20-C21 1.529(3), C20-C22 1.525(4), C20-C23 1.534(5), P1-C19 1.795(2), C24-S1-C20 112.9(1), S1-C24-S2 110.1(2), S2-C24-S3 125.8(2), S3-C24-S1 124.1(2), S1-C20-C21 110.5(2), S1-C20-C22 112.5(2), S1-C20-C23 102.7(2), C21-C20-C22 112.5(2), C22-C20-C23 109.2(2), C23-C20-C21 109.1(2), S2-C24-S1-C20 170.5(1), S3-C24-S1-C20 -10.9(2), C24-S1-C20-C21 -58.8(2), C24-S1-C20-C22 67.8(2), C24-S1-C20-C23 -175.0(2).

Eine direkte Umsetzung eines Methylcarbonatsalzes zum entsprechenden Tertbutyltrithiocarbonat kann über die Tertbutyltrithiocarbonsäure erfolgen. Dies wurde zur Herstellung von $Ph_4P[SCS_2tBu]$ ausgehend von $Ph_4P[OCO_2Me]$ realisiert. Dazu wurde eine Suspension von $Ph_4P[OCO_2Me]$ in thf unter Kühlung zunächst mit einem Äquivalent HS*t*Bu, dann mit einem Äquivalent CS_2 versetzt. Während das Methylcarbonat-Anion nicht in der Lage ist, HS*t*Bu zu deprotonieren, gelingt dies ohne weiteres an der durch Addition von HS*t*Bu und CS_2 intermediär gebildete Tertbutyltrithiocarbonsäure $HSCS_2tBu$ (*Schema 3.7.6.3*).

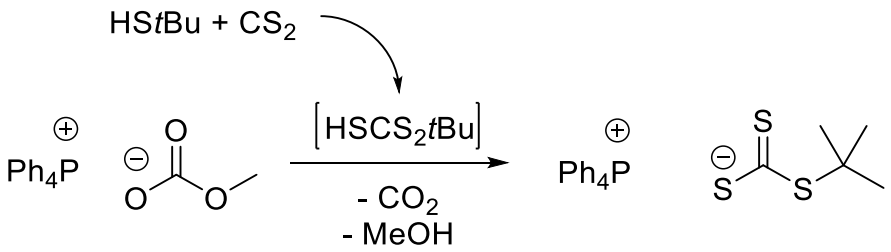

Schema 3.7.6.3 Darstellung von $Ph_4P[SCS_2tBu]$ ausgehend vom P-Ylid $Ph_4P[OCO_2Me]$.

Die Identität und Struktur von $Ph_4P[SCS_2tBu]$ wurden kristallographisch und ^{13}C-NMR spektroskopisch bestimmt und die Reinheit ^{1}H-NMR-spektroskopisch und elementaranalytisch bestätigt. Die kristallographisch bestimmt Molekülstruktur ist in *Abbildung 3.7.6.3* gezeigt.

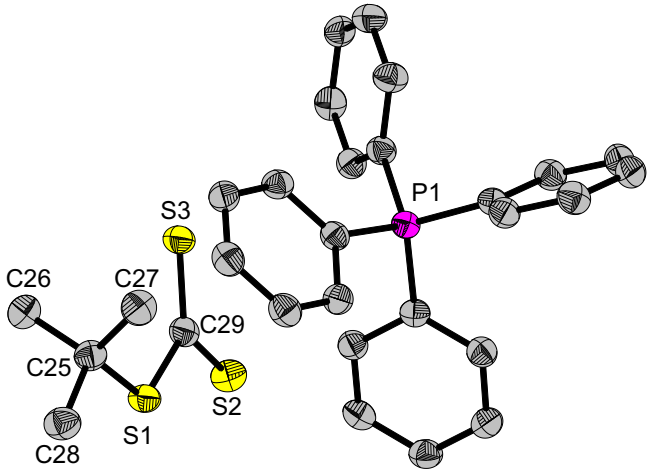

Abbildung 3.7.6.3: Kristallographisch bestimmte Molekülstruktur von $Ph_4P[SCS_2tBu]$ (monoklin, P21/c, vier Ionenpaare pro Elementarzelle). Das die Wasserstoffatome wurde der Übersicht halber nicht abgebildet. Ausgewählte Bindungslängen (in Å) und -winkel (in °) des Anions: S1-C29 1.775(2), S2-C29 1.695(2), S3-C29 1.674(2), S1-C25 1.858(2), C25-C26 1.529(3), C25-C27 1.523(3), C25-C28 1.535(3), S1-C29-S2 109.9(1), S2-C29-S3 125.9(1), S3-C29-S1 124.2(1), C29-S1-C25 112.99(9), S1-C25-C26 110.7(1), S1-C25-C27 112.3(1), S1-C25-C28 102.6(1), C26-C25-C27 111.8(2), C27-C25-C28 109.5(2), C28-C25-C26 109.5(2), S2-C29-S1-C25 -177.17(9), S3-C29-S1-C25 3.9(2), C29-S1-C25-C26 62.9(2), C29-S1-C25-C27 -62.8(2), C29-S1-C25-C28 179.7(1).

Herstellung von MMIm[SCS$_2$*t*Bu]: Zu einer Suspension von MMIm[S*t*Bu] (355 mg, 1.9 mmol, 1.0 Äq.) in thf (20 mL) wird bei 0 °C tropfenweise CS_2 (160 g, 2.1 mmol, 1.1 Äq.) zugegeben. Das Reaktionsgemisch wird für 30 min. bei 0°C gerührt, und dann auf Raumtemperatur gebracht. Die klare Lösung wird für weitere 30 min. bei Raumtemperatur gerührt und am Feinvakuum von allen flüchtigen Bestandteilen getrennt. Die Zielverbindung wird als farbloser Feststoff erhalten. Durch Überschichten einer verdünnten Lösung in thf mit Pentan können durch Lagerung bei 0°C für einige Tage Einkristalle zur strukturellen Charakterisierung gezüchtet werden.

^{1}H-NMR (500.2 MHz, d^6-dmso): δ = 9.05 (s, 1H, C2-*H*), 7.68 (d, 2H, $^{3}J_{HH}$ = 1.5 Hz, C4/5-*H*), 3.84 (s, 6H, 2 x N-C*H*$_3$), 1.44 (s, 9H, [SCSC(C*H*$_3$)$_3$]$^-$) ppm. **^{13}C-NMR** (125.8 MHz, d^6-dmso): δ = 241.4 (s, S*C*S$_2$C(CH$_3$)$_3$), 137.0 (s, C2), 123.4 (C4/5), 50.2 (s, SCS$_2$C(C*H*$_3$)$_3$), 35.7 (s, 2x N-*C*H$_3$), 28.7 (s. SCS$_2$C(*C*H$_3$)$_3$) ppm. **Elementaranalyse $C_{10}H_{18}N_2S_3$ gef. (theor.):** C

44.7 (45.7), H 6.7 (6.9), N 10.2 (10.7), S 37.7 (36.7). Die Abweichungen sind dadurch erklärbar, dass das Rohprodukt untersucht wurde.

Herstellung von Ph_3PMe [SCS_2*t*Bu]: Zu einer Lösung von Ph_3PCH_2 (62 mg, 0.2 mmol, 1.0 Äq.) in thf (10 mL) wurde bei 0°C tropfenweise HS*t*Bu (20 mg, 0,2 mmol, 1.0 Äq.) hinzugegeben. Das Reaktionsgemisch wurde für 30 min. bei 0°C gerührt, dann wurde tropfenweise CS_2 (17 mg, 0.2 mmol, 1.0 Äq.) bei 0°C hinzugetropft. Das Reaktionsgemisch wurde für 30 min. bei 0°C, dann für weitere 30 min. bei Raumtemperatur gerührt. Die klare Lösung wird am Feinvakuum von allen flüchtigen Bestandteilen getrennt. Die Zielverbindung wird als wachsartiger Feststoff erhalten. Durch Überschichten einer thf-Lösung der Zielverbindung mit Pentan und lagern bei 0°C für einige Tage kann das Produkt als kristalliner Feststoff erhalten werden. So gelang auch die Züchtung der Einkristalle, die zur kristallographischen Strukturbestimmung herangezogen wurden.

^{1}H-NMR (300.3 MHz, d^6-dmso): δ = 7.89-7.74 (m, 15H, $[(H_5C_6)_3PCH_3]^+$), 3.15 (d, $^2J_{PH}$ = 14.7 Hz, 3H, $[(H_5C_6)_3PCH_3]^+$), 1.43 (s, 9H, $[SCS_2C(CH_3)_3]^-$) ppm. **^{13}C-NMR (75.5 MHz, d^6-dmso)**: δ = 241.3 (s, $[SCS_2C(CH_3)_3]^-$), 134.8 (d, $^4J_{PC}$ = 3.0 Hz) & 133.2 (d, $^3J_{PC}$ = 10.9 Hz) & 130.1 (d, $^2J_{PC}$ = 12.8 Hz) & 119.9 (d, $^1J_{PC}$ = 87.6 Hz) ($[(H_5C_6)_3PCH_3]^+$), 50.1 (s, $[SCS_2C(CH_3)_3]^-$), 28.7 (s, $[SCS_2C(CH_3)_3]^-$), 6.3 (d, $^1J_{PC}$ = 55.7 Hz, $[(H_5C_6)_3PCH_3]^+$) ppm. **Elementaranalyse $C_{24}H_{27}P_1S_3$ gef. (theor.):** C 65.0 (65.1), H 6.1 (6.2), S 20.5 (21.7).

Herstellung von Ph_4P[SCS_2*t*Bu]: Einer Suspension aus $Ph_4P[OCO_2Me]$ (82 mg, 0.2 mmol, 1.0Äq.) in thf (10 mL) wird bei 0°C mit HS*t*Bu (18 mg, 0.2 mmol, 1.0 Äq.) versetzt und für 5 min. bei 0°C gerührt. Dem Gemisch wird bei 0 °C tropfenweise CS_2 (15 mg, 0.2 mmol, 1.0Äq.) hinzugetropft und für 30 min. bei 0°C, dann für 30 min. bei Raumtemperatur gerührt. Die klare Lösung wird am Feinvakuum von allen flüchtigen Bestandteilen getrennt. Die Zielverbindung wird als farbloser Feststoff erhalten. Durch Überschichten einer thf-Lösung der Zielverbindung mit Pentan und lagern bei 0°C für einige Tage kann das Produkt als kristalliner Feststoff erhalten werden. So gelang auch die Züchtung der Einkristalle, die zur kristallographischen Strukturbestimmung herangezogen wurden.

^{1}H-NMR (300.3 MHz, d^6-dmso): δ = 7.97-7.78 (m, 20H, $[(H_5C_6)_4P]^+$), 1.43 (s, 9H, $[SCS_2C(CH_3)_3]^-$) ppm. **^{13}C-NMR (75.5 MHz, d^6-dmso)**: δ = 241.3 (s, $SCS_2C(CH_3)_3$), 135.3 (d, $^4J_{PC}$ = 2.8 Hz) & 134.5 (d, $^3J_{PC}$ = 10.4 Hz) & 130.4 (d, $^2J_{PC}$ = 13.0 Hz), 117.8 (d,

$^{1}J_{PC}$ = 90.1 Hz) ($[(H_5C_6)_4P]^+$), 50.1 (s, $SCS_2C(CH_3)_3$), 28.7 (s, $SCS_2C(CH_3)_3$) ppm. **Elementaranalyse $C_{29}H_{29}P_1S_3$ gef. (theor.):** C 68.4 (69.0), H 5.6 (5.8), S 18.2 (19.1). Die Abweichungen sind dadurch erklärbar, dass das Rohprodukt untersucht wurde.

NMR Spektren von MMIm[SCS$_2$*t*Bu]

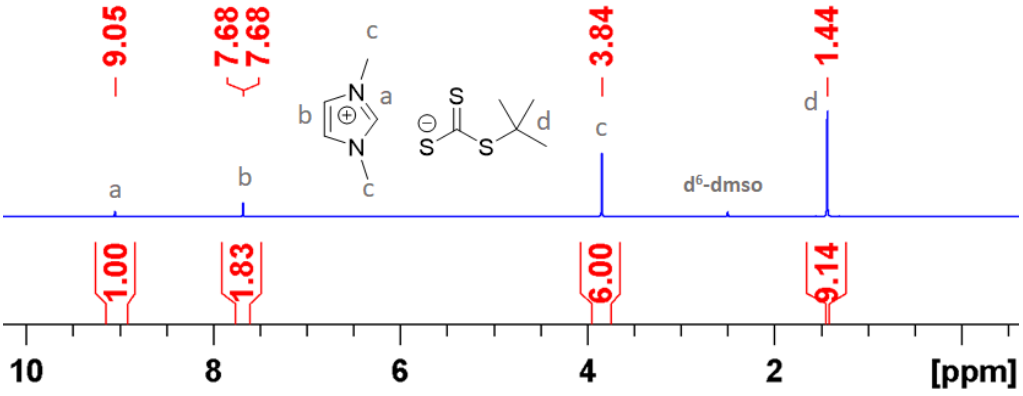

^{1}H-NMR (500.2 MHz, d^6-dmso).

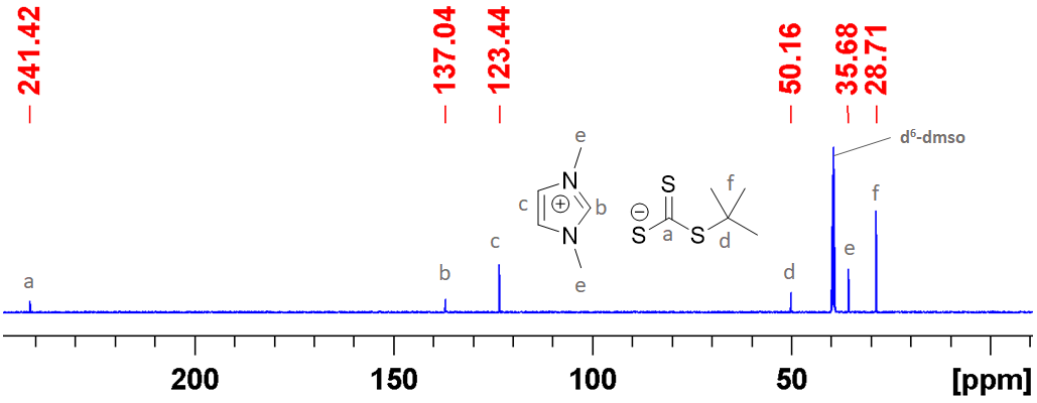

^{13}C-NMR (125.8 MHz, d^6-dmso)

NMR-Spektren von Ph$_3$PMe [SCS$_2$*t*Bu]

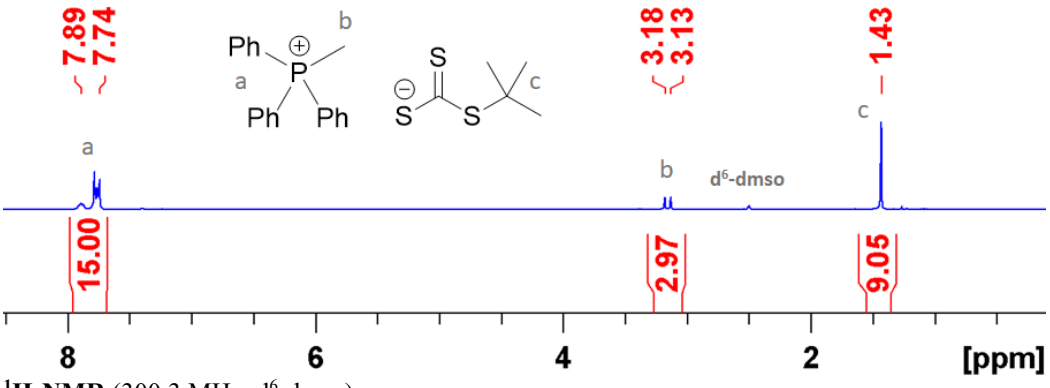

^{1}H-NMR (300.3 MHz, d^6-dmso).

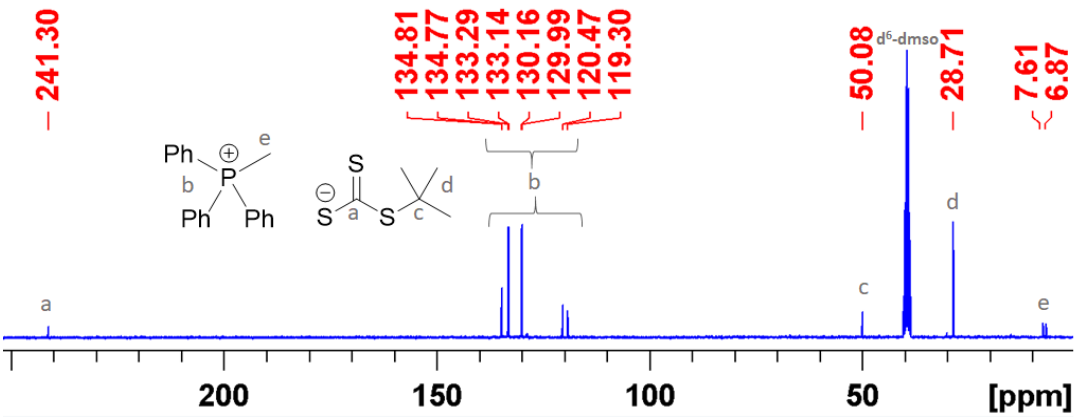

^{13}C-NMR (75.5 MHz, d^6-dmso).

NMR-Spektren von Ph_3PMe [SCS_2tBu]

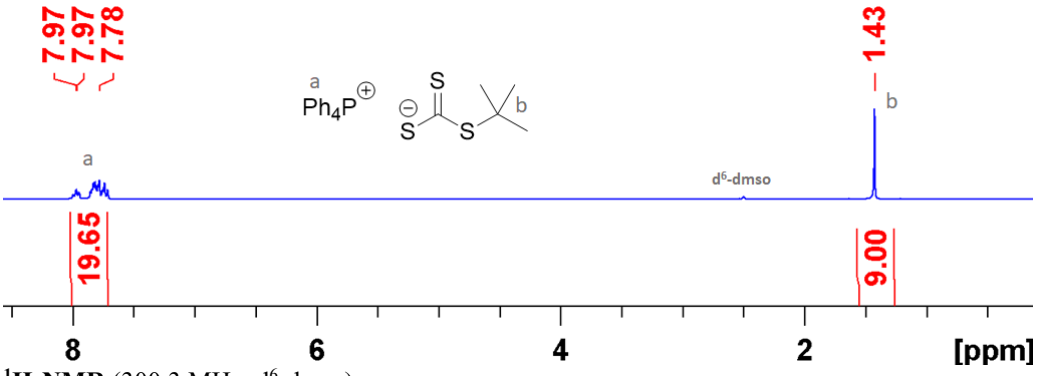

^{1}H-NMR (300.3 MHz, d^6-dmso).

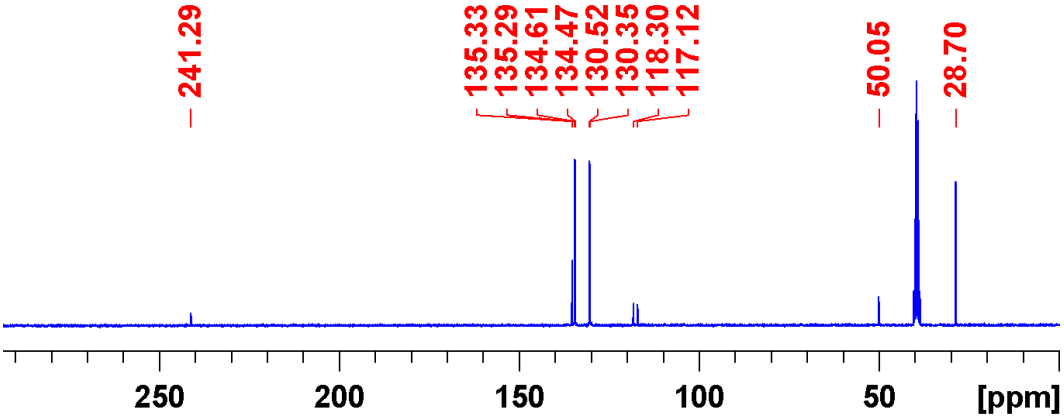

^{13}C-NMR (75.5 MHz, d^6-dmso).

3.7.7 Literaturverzeichnis

(3.1) Zhai, J.; Filatov, A. S.; Hillhouse, G. L.; Hopkins, M. D. Synthesis, structure, and reactions of a copper-sulfido cluster comprised of the parent Cu_2S unit: $\{(NHC)Cu\}_2(\mu\text{-}S)$. *Chem. Sci.* **2016**, *7*, 589–595.

(3.2) Strauch, P.; Dietzsch, W.; Goli, L. Photolysereaktionen an Thiooxalat-Zweikernkomplexen - Kristall- und Molekülstruktur von Hydrogensulfidopyridinbis(triphenylphosphan)kupfer(I). *Z. Anorg. Allg. Chem.* **1997**, *623*, 129–134.

(3.3) Kuhn, N.; Kratz, T.; Bläser, D.; Boese, R. Derivate des Imidazols, XIII. Carben-Komplexe des Siliciums und Zinns. *Eur. J. Inorg. Chem.* **1995**, *128*, 245–250.

(3.4) Jacob, K.; Glanz, M.; Tittes, K.; Thiele, K.-H.; Pavlik, I.; Lyčka, A. Beitrge zur Organolanthanoidchemie. I. Synthese und Charakterisierung von Organolanthanoid-Komplexen des Typs $Na[Ln(C_5H_5)_4]$ x n THF. *Z. Anorg. Allg. Chem.* **1989**, *577*, 145–154.

(3.5) Qian, C.; Wang, B.; Xin, Y.; Lin, Y. Studies on organolanthanide complexes. Part 56. Formation of ion-pair complexes [Na·3 phen] + $[Ln(C_5H_5)_3Cl]^-$ ·phen (Ln = La, Pr or Nd; phen = 1,10-phenanthroline) and crystal structure for Ln = Pr. *J. Chem. Soc., Dalton Trans.* **1994**, *2*, 2109–2112.

(3.6) Eggers, S. H.; Adam, M.; Haupt, E. T.K.; Dieter Fischer, R. Lanthanum-139 NMR spectroscopy of triscyclopentadienyllanthanum(III) derivatives: a promising new tool for solution studies. *Inorg. Chim. Acta* **1987**, *139*, 315–318.

(3.7) Beletskaya, I. P.; Voskoboynikov, A. Z.; Chuklanova, E. B.; Kirillova, N. I.; Shestakova, A. K.; Parshina, I. N.; Gusev, A. I.; Magomedov, G. K. I. Bimetallic lanthanide complexes with lanthanide-transition metal bonds. Molecular structure of $(C_4H_8O)(C_5H_5)_2LuRu(CO)_2(C_5H_5)$. The use of ^{139}La NMR spectroscopy. *J. Am. Chem. Soc.* **1993**, *115*, 3156–3166.

(3.8) Flörke, U.; Ayaz, M.; Henkel, G. *CCDC 1521483,* **2016** *(Experimental Crystal Structure Determination)*.

(3.9) Dean, W. K.; Heyl, B. L. Synthesis and reactions of xanthate and thioxanthate carbonyl complexes of molybdenum and tungsten. *J. Organomet. Chem.* **1978**, *159*, 171–178.

4 Zusammenfassung

Organische Salze Sulfid- und Selenid-basierter Anionen: Bausteine für die Materialsynthese bi- und multinärer Metallchalkogenide

4.1 Organische Salze mit bisher unzugänglichen Kation-Anion Kombinationen

Obwohl sich die Methylcarbonatroute zur Herstellung organischer Salze über Desilylierungs- und Deprotonierungsreaktionen etabliert hat, sind viele Anion-Kation Kombinationen bisher unzugänglich. Dies trifft insbesondere für entsprechende Salze mit 1,3-Dialkylimidazolium Kationen ($RRIm^+$) zu. Zwar sind entsprechende Methylcarbonatsalz-Lösungen bekannt und sogar kommerziell erhältlich, allerdings nur in verdünnter methanolischer Lösung, da durch die Azidität der aromatischen Protonen am Imidazoliumring das Methylcarbonatanion selbiges unter Ausbildung eines NHC-CO_2-Adduktes deprotoniert, sobald das Lösungsmittel entfernt wird. Dadurch sind Folgeprodukte mit methanolempfindlichen Anionen (z. B. Trimethylsilylchalkogenolate) nicht herstellbar. Zudem genügt die Basizität des Methylcarbonat Anions nicht, um schwache Säuren wie das *Tert*butylmercaptan (HS*t*Bu) zu deprotonieren. Um diese Beschränkungen zu umgehen, wurde in dieser Arbeit die Deprotonierung von HStBu mit der NHC-Verbindung 1,3-Dimethylimidazol-2-yliden und unter Ausbildung des äußerst nukleophilen Salzes MMIm[S*t*Bu] realisiert. Dieses wurde als Ausgangsverbindung für methanolfreie Desilylierungsreaktionen verwendet, durch welche die bisher unzugänglichen Verbindungen MMIm[Se*t*Bu], MMIm[$SSiMe_3$] und MMIm[$SeSiMe_3$] hergestellt wurden. Durch Methanolyse der Trimethylsilylthiolatsalze wurden zudem die Hydrogenchalkogenidsalze MMIm[SH] und MMIm[SeH] synthetisiert (*Schema 4.1.1*).

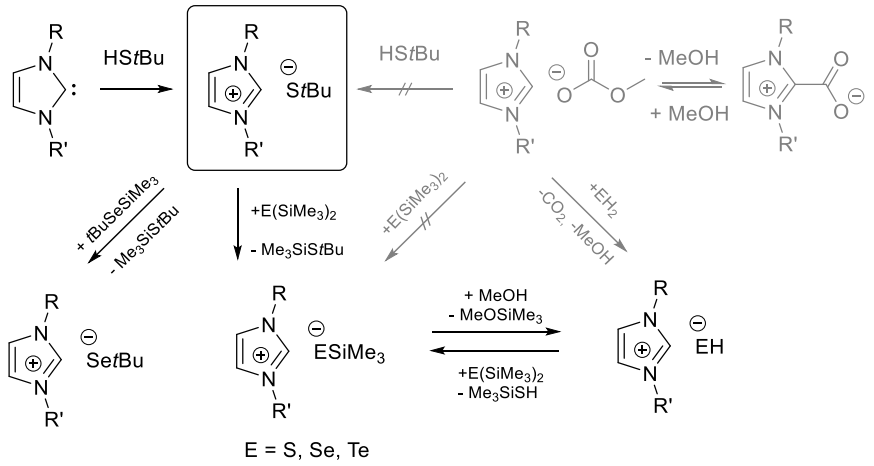

Schema 4.1.1: Herstellung von organischen Salzen mit 1,3-Dialkylimidazolium Kation ausgehend von RR'Im[StBu]. Mit Ausnahme der Hydrogenchalkogenidsalze sind diese über die konventionelle Methylcarbonatroute (grau) unzugänglich.

In den ^{1}H-NMR Spektren der dargestellten Verbindungen kann ein Trend in der Verschiebung des azidesten Protons an der C2-Position des Imidazoliumkations beobachten werden: mit zunehmender Basizität des chalkogenbasierten Anions ist eine zunehmend ausgeprägtere Tieffeldverschiebung des Signals zu beobachen, die maximal für MMIm[S*t*Bu] (10.14 ppm) und minimal für die Silylthiolatsalze MMIm[ESiMe$_3$] (9.17 ppm) ist (*Abbildung 4.1.1.*).

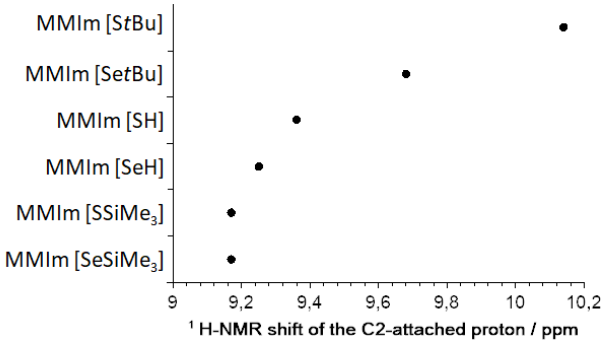

Abbildung 4.1.1.: ^{1}H-NMR-Verschiebungen (300.1 MHz, d^6-dmso) der C2-gebundenen Protonen chalkogenbasierter organischer Salze mit 1,3-Dimethylimidaziolium Kationen. Je basischer das Anion, desto tieffeldverschobener das Signal (Konzentration: 30 mg in 0.6 mL d^6-dmso).

Die Festkörperstrukturen aller dargestellten MMIm[ER]-Salze konnten kristallographisch bestimmt werden. Die aus den Strukturen zugänglichen nichtkovalenten Wechselwirkungen wurden identifiziert und die doppelt ionischen Wasserstoffbrückenbindungen zwischen den Chalkogenatomen der Anionen und den Protonen der Imidazoliumkationen ausführlich untersucht. Es wurde eine Korrelation zwischen der Anzahl von einem Anion ausgehenden Wasserstoffbrückenbindungen und der Bindungslänge zwischen Chalkogenatom und dessen Substituent festgestellt. Je kürzer diese Bindung ist, desto weniger nichtkovalente Bindungen gehen vom Anion aus, wobei die Hydrogenchalkogenid-Anionen durch ihre sterische Zugänglichkeit die meisten Wechselwirkungen ausbilden (Abbildung 4.1.2).

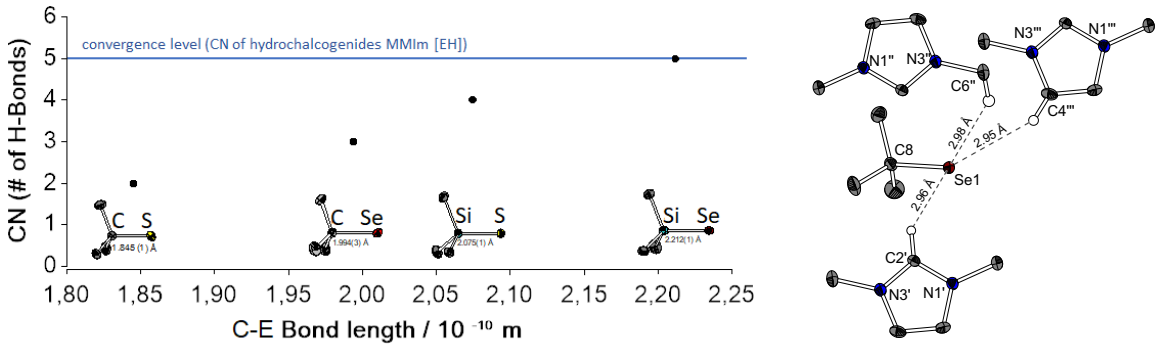

Abbildung 4.1.2: Die Anzahl der von einem Anion ausgehenden nichtkovalenten Wechselwirkungen in Abhängigkeit der Bindungslänge Chalkogen-Substituent (links). Beispielhaft: die in MMIm[SetBu] identifizierten, vom Anion ausgehenden Wasserstoffbrückenbindungen (rechts).

Organische Methylcarbonatsalze sind in erster Linie für nicht-symmetrisch substituierte Kationen bekannt. Grund dafür ist, dass der Quaternisierung tertiärer Amine, Phosphine oder Heterozyklen durch Dimethylcarbonat eine Methylierung zugrunde liegt. Diese Reaktion lässt sich nicht auf Alkylierungen mit anderen Alkylgruppen aus Dialkylcarbonaten übertragen. Die durch diese Asymmetrie reduzierte Kristallisationstendenz der Methyl-Onium Methylcarbonate ist für viele Anwendungen ionischer Flüssigkeiten von Vorteil, erschwert aber die Bildung von Einkristallen zur Strukturbestimmung interessierender Ionenpaare. Obwohl es Synthesemethoden für symmetrisch substituierte Ammoniumkationen gibt, wurde noch nie ein symmetrisch, nicht-methyliertes Phosphoniumkation in Kombination mit einem Methylcarbonatanion synthetisiert. Dies konnte nun durch die Anwendung einer neuen Demethylierungsstrategie in dieser Arbeit erzielt werden, bei der organische Fluoridsalze oder Fluoridphosphorane Cat[F] unter Solvothermalbedingungen mit Me_2CO_3 unter Eliminierung von flüchtigem MeF zu Cat[OCO_2Me] (Cat = Ph_4P^+, PPN^+, TBA^+) umgesetzt werden (*Schema 4.1.2*).

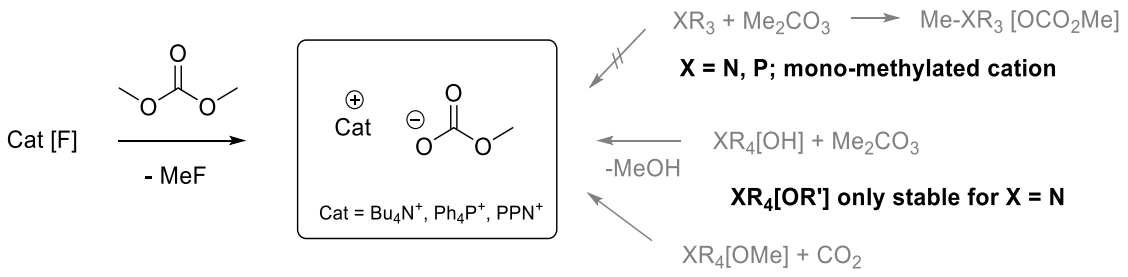

Schema 4.1.2: Zugang zu mit bekannten Methoden (grau) unzugänglichen Methylcarbonatsalzen mit nichtmethylierten, symmetrisch substituierten Phosphoniumkationen durch fluoridvermittelte Demethylierung.

Mithilfe von $Ph_4P[OCO_2Me]$ wurde durch Desilylierung von $E(SiMe_3)_2$ ein vollständige Homologenreihe an $Ph_4P[ESiMe_3]$ (E = S, Se, Te) Salzen hergestellt und strukturell charakterisiert, wobei die erste strukturelle Charakterisierung eines $[TeSiMe_3]^-$ Anions erfolgte. Noch nicht abgeschlossene Arbeiten behandeln die Cp_3La-Addukte $Ph_4P[Cp_3LaESiMe_3]$ (E = S, Se, Te) dieser Salze, die bereits kristallographisch nachgewiesen wurden (*Abbildung 4.1.3*).

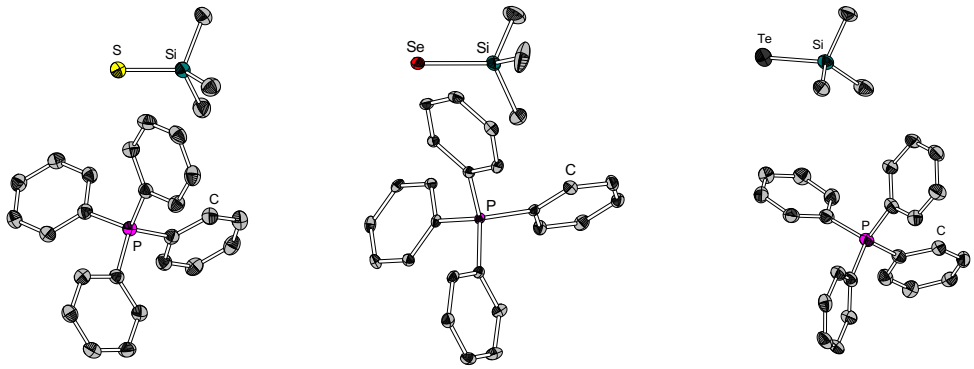

Abbildung 4.1.3: Kristallographisch bestimmte Molekülstrukturen von $Ph_4P[ESiMe_3]$ für E = S (links), Se (mittig), Te (rechts).

4.2 Organische Salze mit homoleptischen Trimethylsilylchalkogenolatometallat Anionen

Organische Salze mit homoleptischen Trimethylsilylchalkogenolatometallat Monoanionen $[M(ESiMe_3)_{n+1}]^-$ wurden erstmals als dezidiert neue Substanzklasse für verschiedene Metalle (M = Ga, In, Zn, Sn^{II}, Cu^{I}, Ag^{I}, Au^{I}) dargestellt und charakterisiert. Zudem wurde das Potenzial dieser Verbindungen zur Darstellung chalkogenbasierter Materialien eruiert.

Für die Darstellung der Trielverbindungen $Cat[M(ESiMe_3)_4]$ (E = S, Se; M = Ga, In) wurden drei Strategien ausgearbeitet: 1. Addition von $DMPyr[ESiMe_3]$ (DMPyr = *N,N*-Dimethylpyrrolidinium) an $GaCl_3$ und anschließende Chloridsubstitution mit drei Äquivalenten $LiESiMe_3$ (E = S, Se), 2. Addition von $Ph_4P[Cl]$ an $InCl_3$ und anschließende Chloridsubstitution mit vier Äquivalenten $LiESiMe_3$ (E = S, Se) und 3. Addition von $[Cu(L_2)_2Cl]$ (L_2 = dppe, dmpe) an $InCl_3$ bzw. $GaCl_3$ und anschließende Chloridsubstitution mit vier Äquivalenten $LiESiMe_3$ (E = S, Se) (*Schema 4.2.1.*).

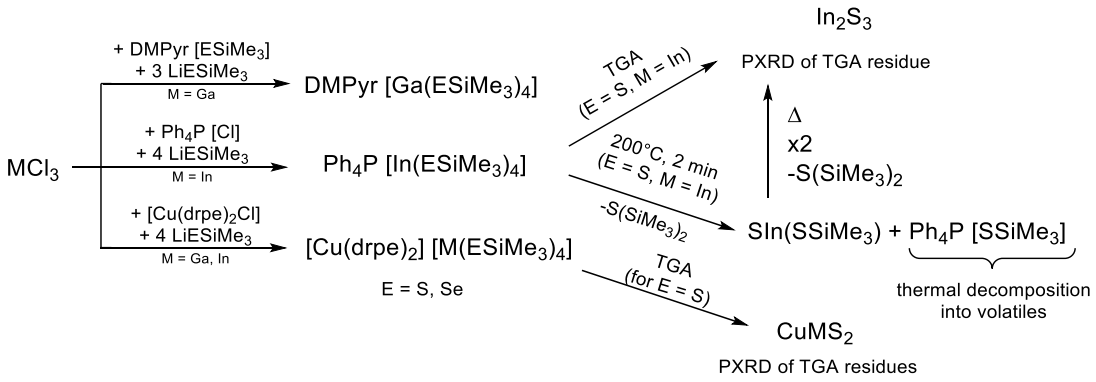

Schema 4.2.1: Darstellung organischer Salze $Cat[M(ESiMe_3)_4]$ (M = Ga, In; E = S, Se) ausgehend von MCl_3. Oben: Addition von $Cat[ESiMe_3]$ und Chloridsubstitution mit $LiESiMe_3$, mittig und unten: über Chloridsubstitution mit $LiESiMe_3$ an Chloridometallatsalzen $Cat[MCl_4]$. Links: thermischer Zerfall.

Die ersten zwei Methoden machen die binären M:E Grundbausteine Cat[M(ESiMe$_3$)$_4$] (E = S, Se; Cat = DMPyr$^+$ (M = Ga), Ph$_4$P$^+$ (M = In)) zugänglich, die bei Temperaturen über 450 °C in die binären Sesquichalkogene M_2E_3 und Nebenprodukte zerfallen, was über Röntgenpulverdiffraktogramme der Rückstände der TGA Messungen ermittelt wurde. Genauere Studien zum Zerfallsmechanismus von Ph$_4$P[In(SSiMe$_3$)$_4$] konnten zeigen, dass zunächst ein formaler Zerfall in Ph$_4$P[SSiMe$_3$] und [In(SSiMe$_3$)$_3$] erfolgt, wobei letzteres nach zwei Minuten bei 200 °C partiell desilyliert als „[SIn(SSiMe$_3$)]$_n$“ vorliegt. Während Ph$_4$P[SSiMe$_3$] bei höheren Temperaturen rückstandslos zerfällt, liefert „[SIn(SSiMe$_3$)]$_n$“ nach vollständiger Desilylierung In_2S_3. Dies erklärt im Prinzip das thermische Zerfallsverhalten der meisten im Zuge dieser Arbeit dargestellten Cat[M(ESiMe$_3$)$_{n+1}$] Verbindungen. Die über die dritte Methode zugänglichen Single-Source Präkursoren [Cu(L$_2$)$_2$][M(ESiMe$_3$)$_4$] (L$_2$ = dppe, dmpe); M = Ga, In; E = S, Se) zerfallen dagegen thermisch direkt zu $CuME_2$. Eine Auswahl der hergestellten organischen Trimethylsilylchalkogenolatotrielat-Salze ist in *Abbildung 4.2.1* zu sehen.

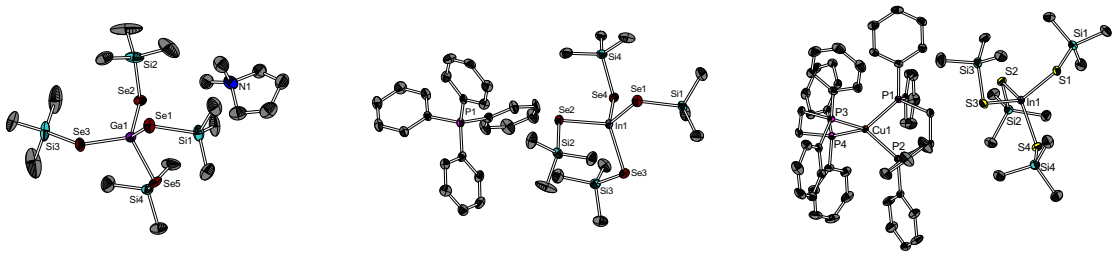

Abbildung 4.2.1: Beispiele kristallographisch bestimmter Molekülstrukturen organischer Salze und ionischer Single Source Präkursoren mit Trimethylsilychalkogenolatotrielat Anion. Links: DMPyr[Ga(SeSiMe$_3$)$_4$], mittig: Ph$_4$P[In(SeSiMe$_3$)$_4$], rechts: [Cu(dppe)$_2$][In(SSiMe$_3$)$_4$].

An Ph$_4$P[In(SSiMe$_3$)$_4$] wurde exemplarisch gezeigt, dass diese Verbindung als binärer In/S Vorläufer für die lösungsbasierte Kopräzipitation von $CuInS_2$ bei niedrigen Temperaturen fungieren kann. Dazu wird Ph$_4$P[In(SSiMe$_3$)$_4$] zunächst durch definiertes Erhitzen zu einem Gemisch aus Ph$_4$P[SSiMe$_3$] und „[SInSSiMe$_3$]$_n$“ umgesetzt, das in MeCN gelöst bei –20 °C vorgelegt wird und mit einem in MeCN gelösten Äquivalen [Cu(tmtu)$_3$][PF$_6$] (tmtu = *N,N,N‘,N‘*-Tetramethylthioharnstoff) versetzt wird. Nach Filtration, Waschen und thermischer Nachbehandlung des ausgefallenen Feststoffes konnte $CuInS_2$ röntgenpulverdiffraktometrisch nachgewiesen werden (*Abbildung 4.2.2*). Dies ist ein neuer möglicher Ansatz zur Darstellung von CIGS Materialien aus Lösung bei niedrigen Temperaturen.

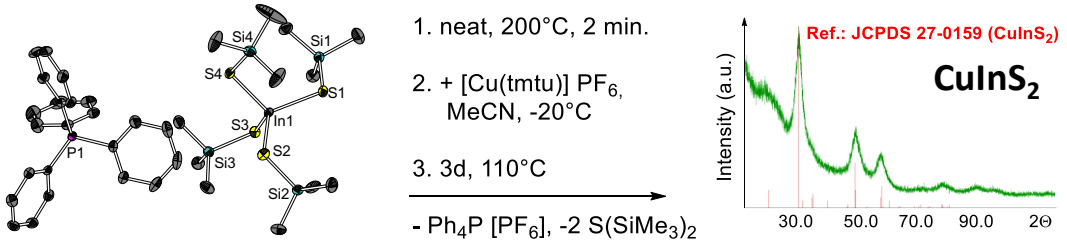

Abbildung 4.2.2: Darstellung von $CuInS_2$ über eine Kopräzipitation bei –20 °C ausgehend von $Ph_4P[In(SSiMe_3)_4]$ mit $[Cu(tmtu)_3][PF_6]$.

Der Kopräzipitationsansatz wurde auf die Synthese des quaternären Materials Cu_2ZnSnS_4 übertragen. Dafür wurden die entsprechenden Salze $Cat[M(ESiMe_3)_3]$ (Cat = Ph_4P^+, PPN^+; M = Zn, Sn^{II}, E = S; Se) hergestellt, die bei vollständiger thermischer Zersetzung die binären Chalkogenide ME ausbilden und mit Ausnahme von $[Sn(SeSiMe_3)_3]^-$ kristallographisch charakterisiert wurden (*Abbildung 4.2.4*). Für die Zinkate liegt das Thiolat als einkerniger Komplex $[Zn(SSiMe)_3]^-$ mit trigonal planar koordiniertem Zinkatom vor, während das Selenolat als zweikerniger Komplex $[(Me_3SiSe)_2Zn(\mu_2\text{-}SeSiMe)_2]_2^{2-}$ mit tetraedrisch koordinierten Zinkatomen auftritt.

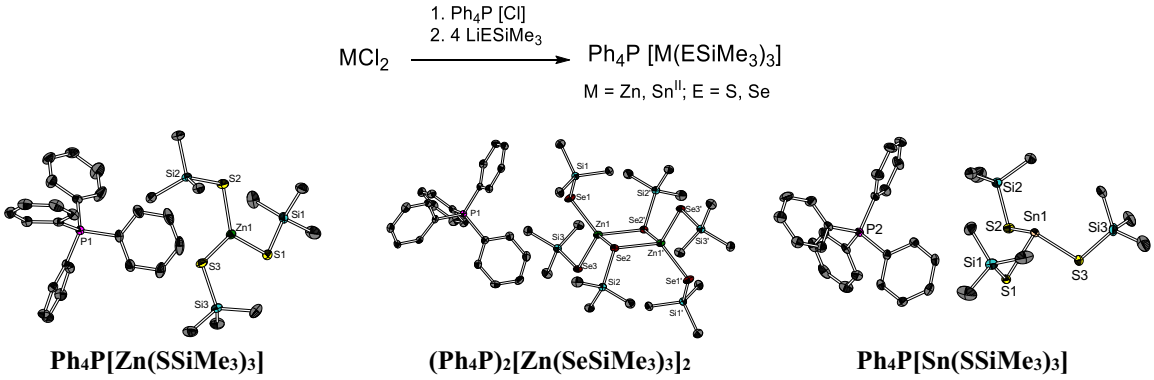

Abbildung 4.2.4: Synthese der Zinkate und Stannanide $Ph_4P[M(ESiMe_3)_3]$ (M = Zn, Sn^{II}; E = S, Se) und die kristallographisch bestimmten Molekülstrukturen von $Ph_4P[Zn(ESiMe_3)_3]$ (E = S (links), Se (mittig) und $Ph_4P[Sn(SSiMe_3)_3]$ (rechts).

Oxidiert man $Cat[Sn^{II}(SSiMe_3)_3]$ mit einem Äquivalenten elementaren Schwefels zu „$Cat[SSn^{IV}(SSiMe_3)_3]$“ und versetzt dies mit einem Äquivalenten $Cat[Zn(SSiMe_3)_3]$, kann nach definierter partieller Desilylierung bei 200°C für 2 min., Suspendierung in MeCN und anschließender Kopräzipitation mit zwei Äquivalenten $[Cu(tmtu)_3][PF_6]$ ein schwarzer Feststoff erhalten werden. Dieser wurde nach Isolierung und thermischer Nachbehandlung

röntgenpulverdiffraktometrisch und Raman-spektroskopisch als Cu_2ZnSnS_4 identifiziert (*Abbildung 4.2.5*).

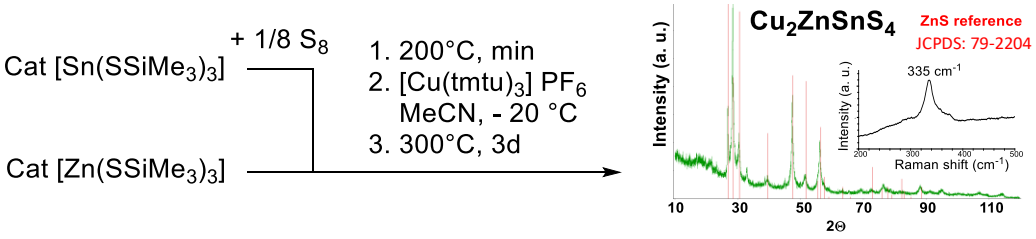

Abbildung 4.2.5: Darstellung von Cu_2ZnSnS_4 über eine Kopräzipitation bei –20 °C ausgehend von Cat[M(SSiMe$_3$)$_3$] (M = Zn und Sn) mit [Cu(tmtu)$_3$] [PF$_6$]. Das PXRD von Cu_2ZnSnS_4 ist identisch mit dem von ZnS (Wurtzit). Das Ramanspektrum zeigt, dass Cu_2ZnSnS_4 vorliegt (335cm^{-1}), und nicht ZnS (351 cm^{-1}).

Die Synthese der entsprechenden organischen Münzmetallatsalze Cat[M(ESiMe$_3$)$_2$] (Cat = PPN^+, Ph_4P^+; M = Cu^I, Ag^I, Au^I; E = S, Se) gelang vergleichbar überraschend durch Umsetzung von Cat[MCl$_2$] mit zwei Äquivalenten LiESiMe$_3$. Die Strukturen aller Münzmetallatanionen konnten kristallographisch aufgeklärt werden, die allesamt als mononukleare Monoanionen mit linear koordiniertem Münzmetallatom in Erscheinung treten. Die SiMe$_3$-Substituenten nehmen dabei immer eine sterisch nicht nachvollziebare *gauche*-Konformation ein (*Abbildung 4.2.6*).

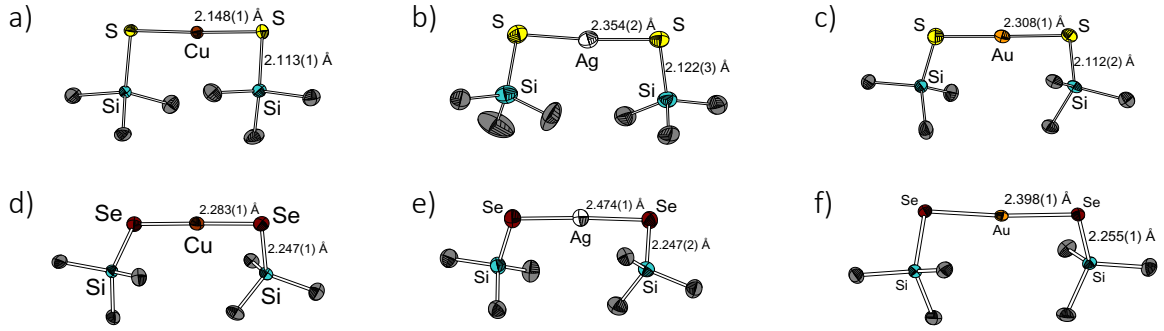

Abbildung 4.2.6: Kristallographisch bestimmte Molekülstrukturen der Anionen in den Müntzmetallatsatzen a) Ph_4P[Cu(SSiMe$_3$)$_2$], b) Ph_4P[Ag(SSiMe$_3$)$_2$], c) PPN[Au(SSiMe$_3$)$_2$], d) PPN[Cu(SeSiMe$_3$)$_2$], e) PPN[Ag(SeSiMe$_3$)$_2$] und f) PPN[Au(SeSiMe$_3$)$_2$].

In Kooperation mit *Priv. Doz. Dr. Florian Weigend* (Karlsruher Institut für Technologie) konnte dieses offenbar elektronisch begründbare Phänomen über dichtefunktionaltheoretische Berechnungen auf eine Verringerung des antibindenden Charakters der E-Si Bindung durch die *gauche*-Konformation zurückgeführt werden. Die Selenolate Ph_4P[M(SeSiMe$_3$)$_2$] (M = Cu, Ag, Au) sind wahrscheinlich die ersten Verbindungen, deren ^{77}Se-Kerne über ^{1}H/^{77}Se-HMQC-

NMR Spektren detektiert wurden. Die entsprechende Methode wurde von *Dr. Xiulan Xie* entwickelt.

4.3 Organische Salze mit Chalkogenidoorganometallat Anionen

Ausgehend von eigenen Vorarbeiten in Zusammenarbeit mit *Dr. Lars H. Finger* wurden ergänzende und abschließende Arbeiten zur Umsetzung hochreaktiver Alkyltrielverbindungen mit organischen Hydrogenchalkogenid Salzen durchgeführt. Die aus den entsprechenden Vorarbeiten bekannten Umsetzungen von DMPyr[EH] (E = S, Se) mit Me_3M (M = In, Ga) zu den zweikernigen Chalkogenidodimethylmetallatsalzen $DMPyr_2[Me_2M(\mu_2\text{-}E)]_2$ wurden optimiert und die kristallographische Charakterisierung für alle Homologen vervollständigt. Dadurch konnten interessante Einblicke in doppelt ionische Wasserstoffbrückenbindungen zwischen den Ionen identifiziert werden, die den nukleophilen Charakter der verbrückenden Chalkogenatome dieser Verbindungsklasse unterstreicht (*Abbildung 4.3.1*).

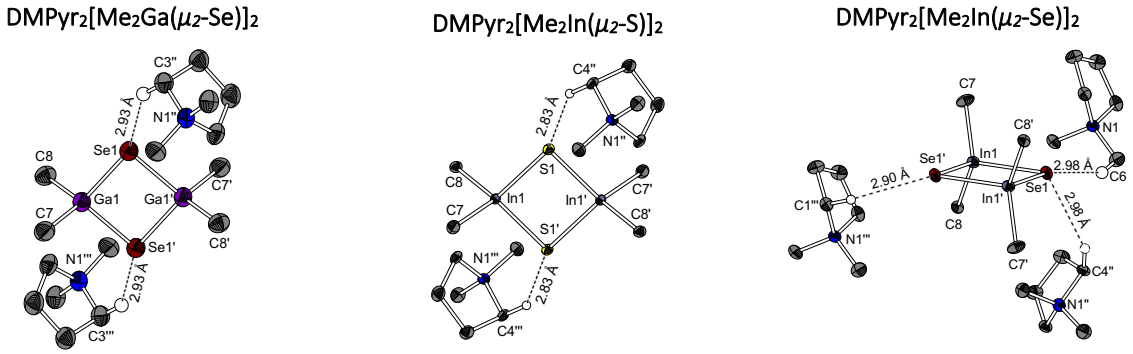

Abbildung 4.3.1: Kristallographisch bestimmte Molekülstrukturen ausgewählter $DMPyr_2[Me_2M(\mu_2\text{-}SE)]_2$ Verbindungen. Die Ga/Se (links) und In/S (mittig) Homologen haben vergleichbare H-Bindungsmodi (zwei H-Brücken pro Anion). Entsprechende Wechselwirkungen im In/Se Homologen (rechts) unterscheiden sich stark (sechs H-Brücken pro Anion. Hier sind nur kristallographisch einmalige H-Brücken gezeigt).

Die nukleophile Natur der Schwefelatome in $DMPyr_2[Me_2In(\mu_2\text{-}S)]_2$ wurde durch Umsetzung mit weiteren Äquivalenten Me_3In bereits für die Herstellung der hexanuklearen Komplexe $DMPyr_3[(Me_2In)(\mu_3\text{-}SInMe_3)]_3$ und $DMPyr_2[(Me_2In)_6(\mu_3\text{-}S)_4]$ synthetisch genutzt. Weiterführende Arbeiten konnten zeigen, dass es auch möglich ist, die Chalkogenatome in $DMPyr_2[Me_2In(\mu_2\text{-}E)]_2$ mit den Silylchalkogen-Präkursoren $E'(SiMe_3)_2$ (E‘ = S, Se) zu silylieren. Dies macht die Indatsalze $DMPyr[Me_2In(ESiMe_3)_2]$ (E = E‘ = S, Se) und

DMPyr[$Me_2In(ESiMe_3)(E'SiMe_3)$] (E = Se, E‘ = S) ohne Nebenprodukte zugänglich (*Schema 4.3.1*).

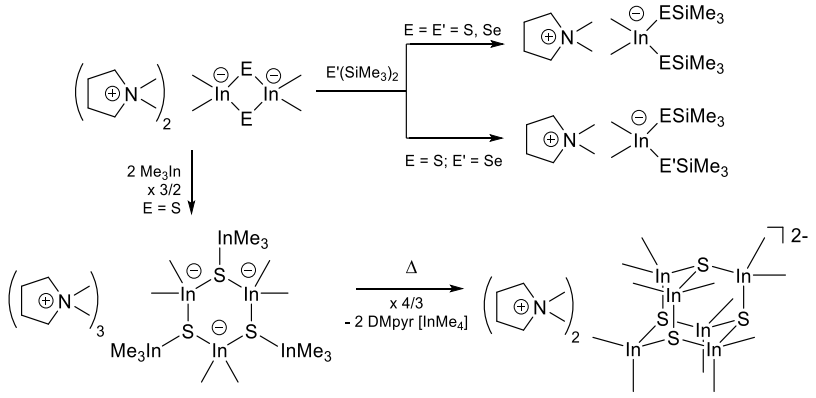

Schema 4.3.1: Reaktivität von $DMPyr_2[Me_2In(\mu_2\text{-}E)]_2$. Durch Silylierung mit $E'(SiMe_3)_2$ entstehen die Salze $DMPyr[Me_2In(ESiMe_3)(E'SiMe_3)]$ (oben). Durch doppelte Indierung von $DMPyr_2[Me_2In(\mu_2\text{-}S)]_2$ können die hexanuklearen Komplexe $DMPyr_3[(Me_2In)(\mu_3\text{-}SInMe_3)]_3$ und $DMPyr_2[(Me_2In)_6(\mu_3\text{-}S)_4]$ erhalten werden.

Alles zusammenfassend beschreibt diese Dissertation eine Reihe neuer Strategien und neuer Trimethylsilylchalkogenolat-Intermediate sowie molekularer Bausteine auf dem Weg ihrer Transformation zu bedeutenden di- oder multinären Metallchalkogenid-Halbleitermaterialien.

5 Summary

Organic Salts of Sulfide- and Selenide-based Anions: Building Blocks for Bi- and Multinary Metal Chalcogenide Materials Synthesis

5.1 Organic salts with yet inaccessible anion-cation combinations

Though the methylcarbonate route is an established method for the preparation of organic salts by deprotonation and desilylation reactions, many anion-cation combinations were synthetically inaccessible. This is especially true for salts with 1,3-dialkylimidazolium cation ($RRIm^+$), for which the corresponding methylcarbonate salts are only stable in diluted methanolic solution due to the NHC-CO_2 adduct formation that takes place as soon as the methanol is removed. This prevents syntheses that involve methanol sensitive educts or products like trimethylsilylchalcogenolates. Further, the methylcarbonate anion is not sufficiently basic to deprotonate *tert*butylthiol (HS*t*Bu). To overcome this, HS*t*Bu was deprotonated using the NHC compound 1,3-dimethylimidazol-2-ylidene to get MMIm[S*t*Bu]. This highly nucleophilic salt was used as a starting point for several desilylation reactions to prepare the yet inaccessible compounds MMIm[Se*t*Bu], MMIm[$SSiMe_3$] and MMIm[$SeSiMe_3$]. By methanolysis of the trimethylsilylchalcogenolate salts the corresponding hydrochalcogenide salts MMIm[SH] and MMIm[SeH] could be prepared (*Scheme 5.1.1*).

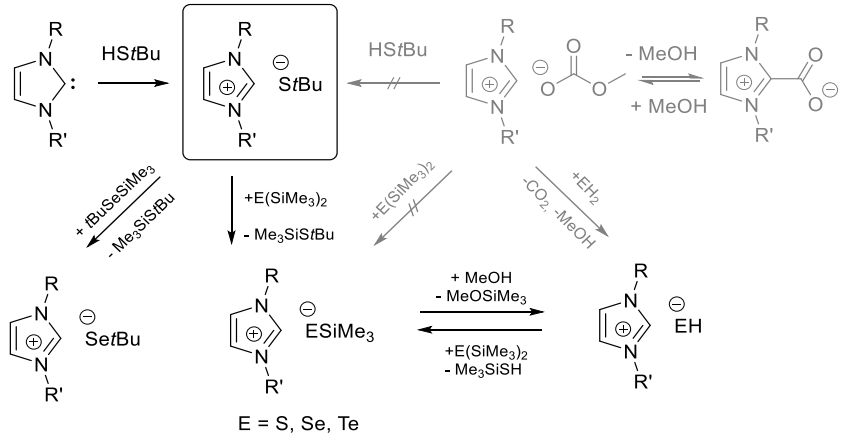

Scheme 5.1.1: Preparation of organic salts with 1,3-dialkylimidazolium cations starting from RR'Im[StBu]. With exception of the $[HE]^-$ salts these compounds are inaccessbile by estblished methylcarbonate routes (grey).

By comparing the ^{1}H-NMR shifts of the C2-attached protons – the most acidic protons in the observed system – a trend can be identified that is connected with the anions‘ basicities: with increasing basicity of the anion an increasing low-field shift can be observed for the

corresponding signal, which is highest for MMIm[S*t*Bu] (10.14 ppm) and lowest for the silylthiolate salts MMIm[ESiMe$_3$] (9.17 ppm) (*Figure 5.1.1*).

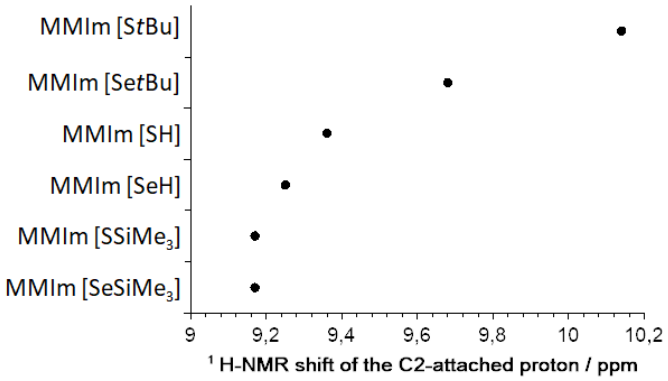

Figure 5.1.1.: ^{1}H-NMR-Shifts (300.1 MHz, d^6-dmso) of the C2-attached protons of chalcogenolate-based organic salts with 1,3-dimethylimidaziolium cations. With increasing basicity of the anion, a more and more pronounced low field shift is observed (concentration: 30 mg in 0.6 mL d^6-dmso).

The solid-state structures of all prepared MMIm[ER] salts could be determined crystallographically. The interactions between the ions have been investigated with a distinct focus on the doubly ionic hydrogen bonds (H-bonds) between the chalcogen atoms and the imidazolium cations' aromatic protons. Thereby a correlation between the number of H-bonds involving one anion and the bond length between the chalcogen atom and its substituent was observed. With decreasing length of this bond, a decreasing amount of non-covalent interactions can be detected. Thereby, the hydrochalcogenide anions have the highest number of interactions as these have the most pronounced steric accessibility of the chalcogen atoms (*Figure 5.1.2*).

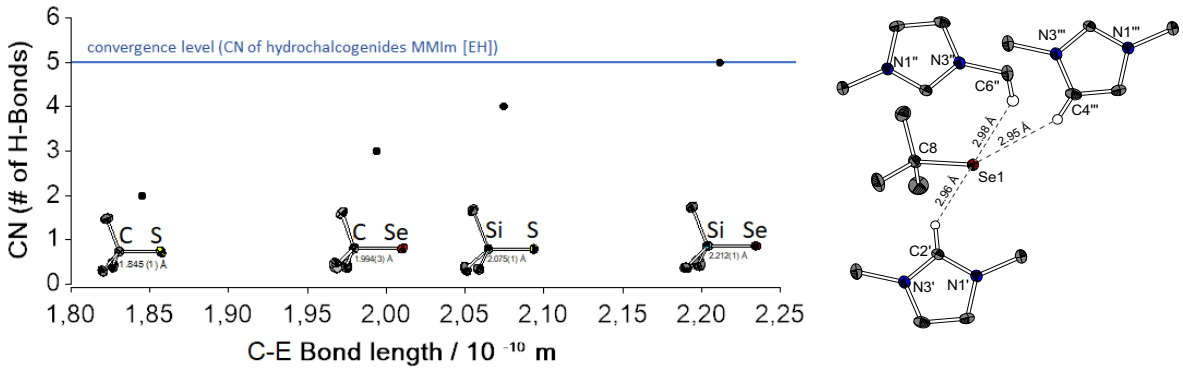

Figure 5.1.2: Left: The dependency of the amount of H-bonds involving one anion and the bond length between the chalcogen atom and its substituent. Right: Exemplarily the H-bonds involving one [SetBu]$^-$ anion in MMIm[SetBu].

Organic methylcarbonate salts are mainly known with cations that are at least mono-methylated, as the quaternization step of tertiary amines, phosphines, or heterocycles with dimethylcarbonate Me_2CO_3 is connected with a methylation. The trend of reduced crystallization tendency by this asymmetric substitution of the cation is desirable for the design of ionic liquids. Yet, it often hinders the formation of X-ray suitable single crystals for the structural characterization of interesting ion pairs. Even though there are methods known that involve symmetrically substituted non-methylated ammonium cations, the synthesis of a symmetrically substituted, non-methylated phosphonium cations has never been described yet. In this work this could be realized by utilizing a novel demethylation strategy, for which organic fluoride salts or fluoridophosphoranes Cat[F] are used to demethylate Me_2CO_3 under elimination of MeF to get Cat[OCO_2Me] (Cat = Ph_4P^+, PPN^+, TBA^+) (*Scheme 5.1.2*).

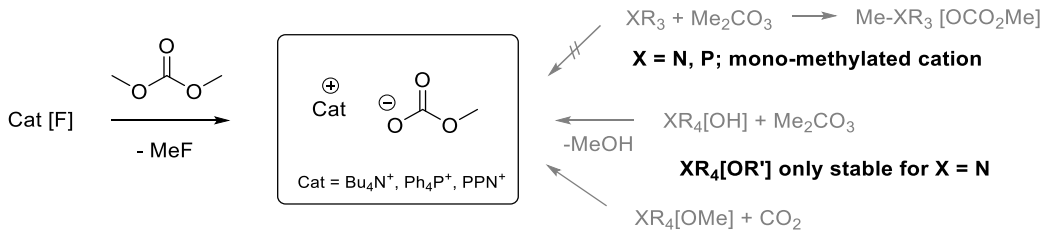

Scheme 5.1.2: Access to organic methylcarbonate salts that are inaccessible via known methods (grey) with symmetrically substituted, non-methylated phosphonium cations by demethylation of Me_2CO_3 with fluorides.

By using $Ph_4P[OCO_2Me]$, a complete set of homologues $Ph_4P[ESiMe_3]$ (E = S, Se, Te) could be prepared by desilylation of $E(SiMe_3)_2$ and structurally characterized by X-ray diffraction (*Figure 5.1.3*). Thereby, for the first time a $[TeSiMe_3]^-$ anion could be structurally characterized. Not yet finished work deals with the addition of these salts to Cp_3La to form the lanthanate salts $Ph_4P[Cp_3La\text{-}ESiMe_3]$ (E = S, Se, Te). Yet, these are only characterized crystallographically.

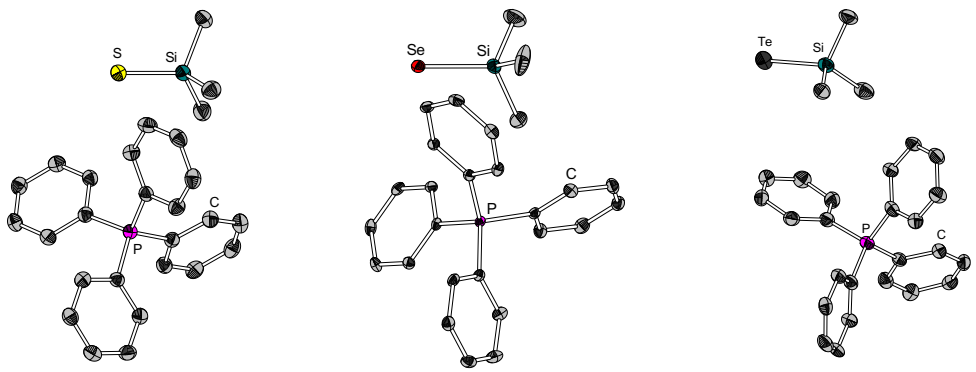

Figure 5.1.3: Crystallographically determined molecular structures of Ph_4P [$ESiMe_3$] for E = S (left), Se (middle), Te (right).

5.2 Organic salts with homoleptic trimethylsilylchalcogenolatometalate anions

Previously unknown organic salts with the homoleptic trimethylsilylchalcogenolate monoanions $[M(ESiMe_3)_{n+1}]^-$ have been introduced, prepared and characterised for different metals (M = Ga, In, Zn, Sn^{II}, Cu^{I}, Ag^{I}, Au^{I}). Furthermore, the potential of these compounds to act as precursors for the preparation of chalcogenide-based materials has been evaluated.

For the preparation of the trielate complexes $Cat[M(ESiMe_3)_4]$ (E = S, Se, M = Ga, In), three strategies have been developed: 1. Addition of $DMPyr[ESiMe_3]$ ($DMPyr^+$ = *N,N*-dimethylpyrrolidinium) and $GaCl_3$ during substitution of the chlorido ligands by adding three equivalents of $LiESiMe_3$, 2. Addition of $Ph_4P[Cl]$ and subsequent substitution of chloride by adding four equivalents of $LiESiMe_3$, and 3. Addition of $[Cu(L_2)_2Cl]$ (L_2 = dppe, dmpe) and $InCl_3$ or $GaCl_3$ and substitution of the chlorides by four equivalents of $LiESiMe_3$ (*Scheme 5.2.1*).

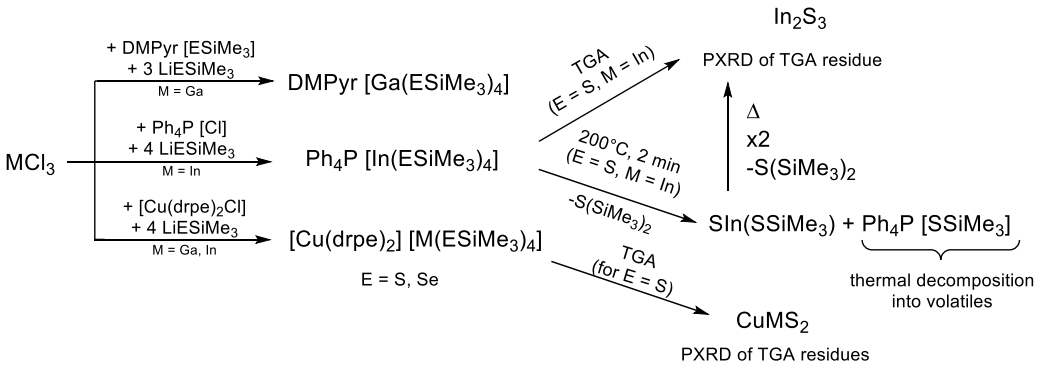

Scheme 5.2.1: Preparation of organic metalate salts $Cat[M(ESiMe_3)_4]$ (M = Ga, In; E = S, Se) starting from MCl_3. Top row: Addition of $Cat[ESiMe_3]$ and chloride substitution with $LiESiMe_3$. Middle and bottom row: chloride substitution of organic chlorometalate salts $Cat[MCl_4]$ with $LiESiMe_3$. Left: thermal decay.

Methods 1 and 2 yield the binary M:E anions with purely organic cations $Cat[M(ESiMe_3)_4]$ (E = S, Se; Cat = $DMPyr^+$ (M = Ga), Ph_4P^+ (M = In)). These decompose at temperatures beyond 450°C into the binary triel sesquichalcogenides M_2E_3 and non-crystalline side products, which was proven by PXRD measurements of the residues obtained by the TGA measurements. More detailed studies of the decay mechanism of $Ph_4P[In(SSiMe_3)_4]$ indicate a formal decomposition into $Ph_4P[SSiMe_3]$ and $[In(SSiMe_3)_3]$, which is present as partially desilylated species „$[SInSSiMe_3]_n$“ after defined thermolysis at 200°C for two minutes. While $Ph_4P[SSiMe_3]$

decomposes without residue, „[SInSSiMe$_3$]$_n$“ yields In_2S_3 after complete desilylation. This explains the thermal decomposition behaviour of almost every Cat[M(ESiMe$_3$)$_{n+1}$] compound within this work. The single-source precursors accessible by the third method [Cu(L$_2$)$_2$][M(ESiMe$_3$)$_4$] (L$_2$ = dppe, dmpe; M = Ga, In; E = S, Se) decompose directly to ternary $CuME_2$ materials. A small set of representative crystallographically determined molecular structures of trimethylsilylchalcogenolato trielate salts are shown in *Figure 5.2.1*.

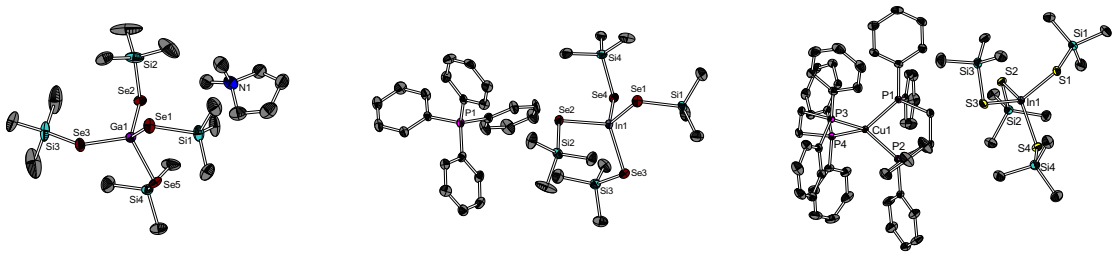

Figure 5.2.1: Examples of crystallographically determined molecular structures of organic salts and ionic single source precursors comprising trimethylsilylchalcogenolato metalate anions. Left: DMPyr[Ga(SeSiMe$_3$)$_4$], middle: Ph$_4$P[In(SeSiMe$_3$)$_4$], right: [Cu(dppe)$_2$][In(SSiMe$_3$)$_4$].

For Ph$_4$P[In(SSiMe$_3$)$_4$] it was shown that this compound can act as a binary In/S precursor for the solution-based co-precipitation of $CuInS_2$ at low temperature. Therefore, Ph$_4$P[In(SSiMe$_3$)$_4$] is decomposed by defined thermolysis at 200 °C for 2 min into a mixture of Ph$_4$P[SSiMe$_3$] and “[SInSSiMe]$_n$” which is dissolved in acetonitrile. During stirring of this solution at –20 °C a solution of [Cu(tmtu)$_3$][PF$_6$] (tmtu = *N,N,N‘,N‘*-tetramethylthiourea) in MeCN is slowly added. After filtration, washing and thermal post-treatment of the black precipitate, $CuInS_2$ could be identified via PXRD (*Figure 5.2.2*). This method is a new approach to prepare CIGS materials at low temperatures.

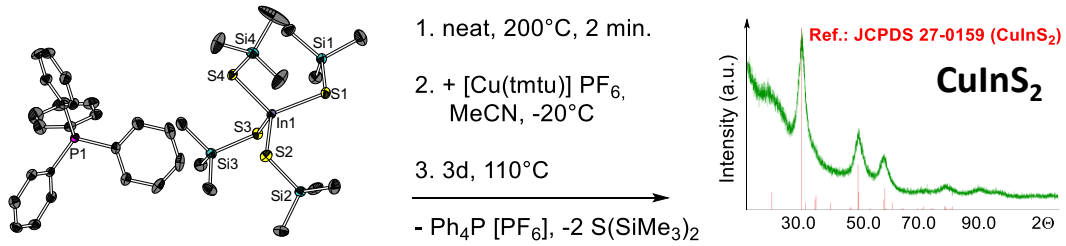

Figure 5.2.2: $CuInS_2$ preparation by coprecipitation at –20 °C using Ph$_4$P[In(SSiMe$_3$)$_4$] and [Cu(tmtu)$_3$] [PF$_6$].

The co-precipitation strategy was transferred on the quaternary chalcogenide material Cu_2ZnSnS_4. Therefore, the corresponding salts Cat[M(ESiMe$_3$)$_3$] (Cat = Ph$_4$P$^+$, PPN$^+$; M = Zn, Sn^{II}; E = S, Se) were prepared. These yield the binary metal chalcogenides ME by complete

thermolysis. They were characterized crystallographically (*Figure 5.2.4*). For the zincates the thiolato species is a mononuclear complex $[Zn(SSiMe_3)_3]^-$ while for the selenolate, the formation of a dinuclear complex $[(Me_3SiSe)_2Zn(\mu_2\text{-}SeSiMe)_2]_2^{2-}$ with tetrahedrally coordinated zinc atoms is observed in the solid state.

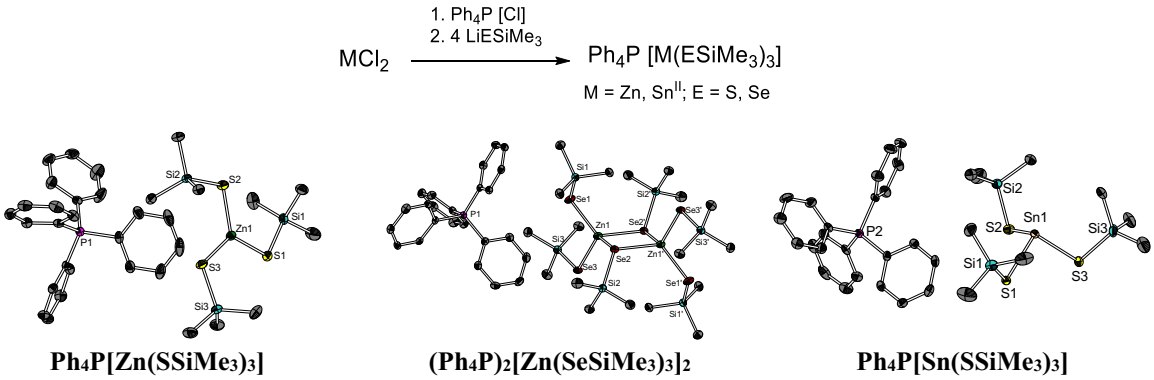

Figure 5.2.4: Synthesis of the zincates and stannanides $Ph_4P[M(ESiMe_3)_3]$ (M = Zn, Sn^{II}; E = S, Se) and crystallographically determined molecular structures of $Ph_4P[Zn(ESiMe_3)_3]$ (E = S (left), Se (middle) and $Ph_4P[Sn(SSiMe_3)_3]$ (right).

For the preparation of Cu_2ZnSnS_4 an oxidation of $Cat[Sn^{II}(SSiMe_3)_3]$ with one equivalent elemental sulfur to „$Cat[SSn^{IV}(SSiMe_3)_3]$“ was performed first. Then, one equivalent of $Cat[Zn(SSiMe_3)_3]$ was added and the mixture is thermolyzed at 200 °C for 2 min. The thermolyzed mixture is suspended in acetonitrile and an acetonitrile solution of two equivalents of $[Cu(tmtu)_3][PF_6]$ was added. The precipitation of a black solid was observed, which could be identified as Cu_2ZnSnS_4 after isolation and thermal annealing (*Figure 5.2.5*). This supports the generality of this coprecipitation procedure using $Cat[M(ESiMe_3)_{n+1}]$ salts.

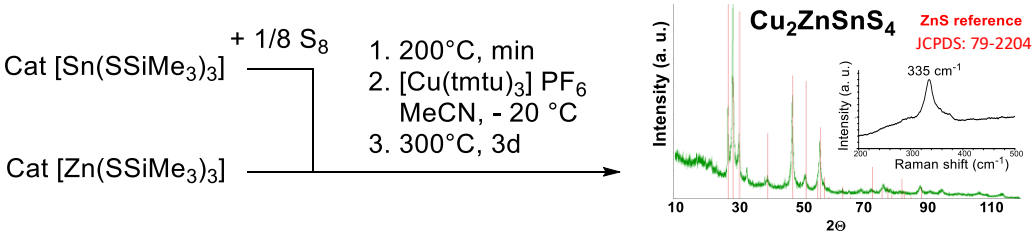

Abbildung 5.2.5: Preparation of Cu_2ZnSnS_4 by co-precipitation at –20°C using $Cat[M(SSiMe_3)_3]$ (M = Zn and Sn) and $[Cu(tmtu)_3]$ $[PF_6]$. The PXRD pattern of the target material is indistinguishable from the one of ZnS (wurtzite). The Raman spectrum proves the presence of Cu_2ZnSnS_4 (335cm^{-1}) and the absence of ZnS (351 cm^{-1}).

The syntheses of organic coinage metalate salts $Cat[M(ESiMe_3)_2]$ (Cat = PPN^+, Ph_4P^+; M = Cu^I, Ag^I, Au^I; E = S, Se) was realized by chloride substitution of $Cat[CuCl_2]$ with $LiESiMe_3$.

All representatives could crystallographically be characterised, all showing the presence of mononuclear monoanions with a linearly coordinated coinage metal atom. An interesting structural aspect of all structures is the unexpected *gauche* conformation, which is in contrast to steric repulsion arguments (*Figure 5.2.6*).

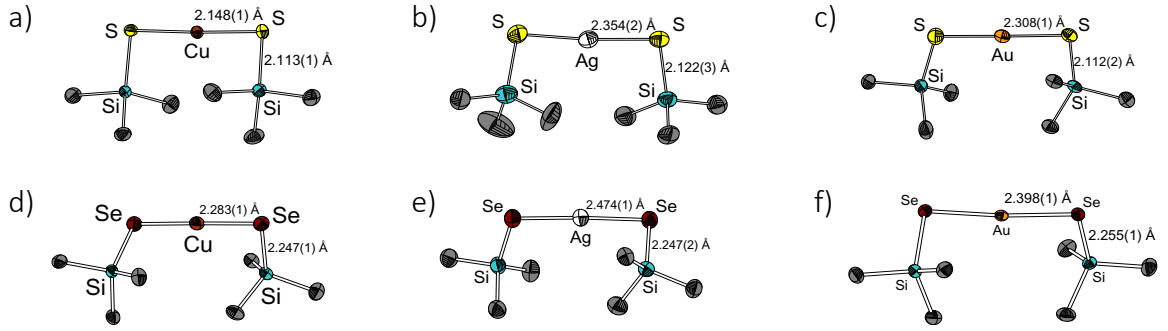

Figure 5.2.6: Crystallographically determined molecular structures of the anions in the coinage metalate salts a) $Ph_4P[Cu(SSiMe_3)_2]$, b) $Ph_4P[Ag(SSiMe_3)_2]$, c) $PPN[Au(SSiMe_3)_2]$, d) $PPN[Cu(SeSiMe_3)_2]$, e) $PPN[Ag(SeSiMe_3)_2]$ and f) $PPN[Au(SeSiMe_3)_2]$.

Together with *PD Dr. Florian Weigend* (Karlsruhe Institute of Technology) this electronic phenomenon was investigated by density functional theory calculations. These trace back this conformation on a reduction of the antibonding character of the E-Si bonding interactions. Furthermore, the selenolato complexes $Ph_4P[M(SeSiMe_3)_2]$ (M = Cu, Ag, Au) are probably the first compounds, for which the ^{77}Se-nuclei have been investigated by ^{1}H/^{77}Se-NMR HMQC. The corresponding method was developed by *Dr. Xiulan Xie*.

5.3 Organic Salts with Chalcogenidoorganometalate Anions

Starting from own previous work under the supervision of *Dr. Lars H. Finger,* additional and finalising work was performed regarding studies on the conversions of the highly reactive trimethyl gallium and indium Me_3M (M = Ga, In) and organic hydrochalcogenide salts DMPyr[EH] (E = S, Se) yielding salts with dinuclear chalcogenidoorganotrielate anions $DMPyr_2[Me_2(\mu_2\text{-}E)]_2$. The reaction conditions have been optimized, and the stuctural characterization have been completed for all homologues comprising M = Ga, In and E = S, Se. Thereby, interesting doubly ionic H-bonding modes could be observed that are connected with the pronounced nucleophilicity of the chalcogen atoms (*Figure 5.3.1*).

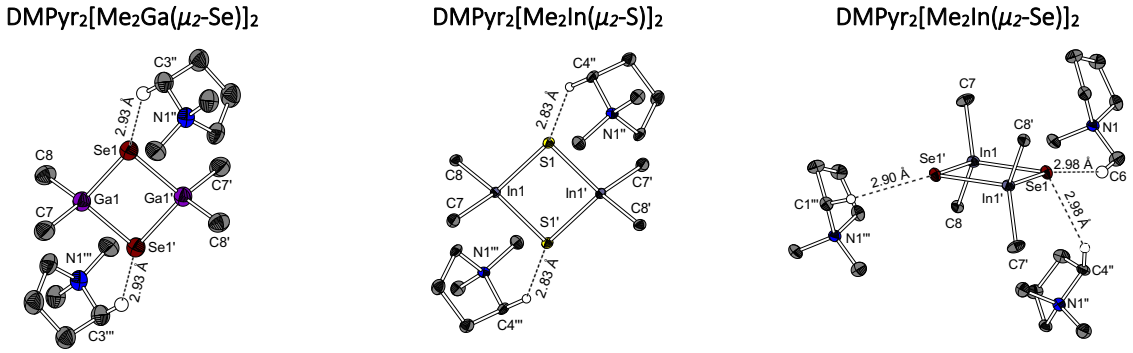

Figure 5.3.1: Crystallographically determined molecular structures of DMPyr$_2$[Me$_2$M(μ_2-SE)]$_2$ salts. The Ga/Se (left) and In/S (middle) homologues have comparable H-bonding modes. The H-bonding interactions for the In/Se homologue (right) differ strongly (six H-bonds per anion. Here only crystallographically unique H-bonds are shown, while all H-bond interactions are shown for the Ga/Se and In/S homologue).

The nucleophilic reactivity of the DMPyr$_2$[Me$_2$In(μ$_2$-E)]$_2$ salts has been investigated by conversion with further equivalents of Me$_3$In to yield the hexanuclear compounds DMPyr$_3$[(Me$_2$In)(μ_3-SInMe$_3$)]$_3$ und DMPyr$_2$[(Me$_2$In)$_6$(μ_3-S)$_4$]. More detailed studies have shown, that even a selective silylation of the DMPyr$_2$[Me$_2$In(μ$_2$-E)]$_2$ salts by E'(SiMe$_3$)$_2$ (E' = S, Se) can be performed. This gives a new, convenient access to novel indate salts DMPyr[Me$_2$In(ESiMe$_3$)$_2$] (E = E' = S, Se) and DMPyr[Me$_2$In(ESiMe$_3$)(E'SiMe$_3$)] (E = Se, E' = S) without any by-products (*Scheme 5.3.1*).

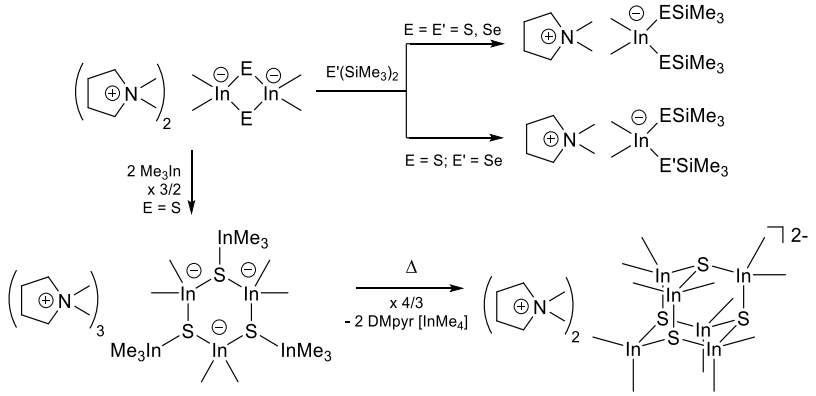

Scheme 5.3.1: Reactivity of DMPyr$_2$[Me$_2$In(μ_2-E)]$_2$. By silylation with E'(SiMe$_3$)$_2$ the indates DMPyr[Me$_2$In(ESiMe$_3$)(E'SiMe$_3$)] (top row) are obtained. Reaction with two equivalents of Me$_3$In yields hexanuclear complexes DMPyr$_3$[(Me$_2$In)(μ_3-SInMe$_3$)]$_3$ and DMPyr$_2$[(Me$_2$In)$_6$(μ_3-S)$_4$].

In summary, this thesis describes several new strategies and new trimethylsilylchalcogenido metalate intermediates and molecular building blocks on their way to be transformed into valuable bi- and multinary metal chalcogenide semiconductor materials.

6 Kristallographischer Teil

Alle Strukturen der hier aufgeführten von mir hergestellten und charakterisierten Verbindungen wurden von *Tobias Vollgraff* gelöst und verfeinert (mit wenigen, an entsprechender Stelle angegeben Ausnahmen). Die Lösung und Verfeinerung sind ausdrücklich Teil seiner wissenschaftlichen Arbeit. Die Kristalldaten wurden durch *Radostan Riedel* oder *Michael Marsch* der Service-Abteilung für Kristallographie des Fachbereiches Chemie (Universität Marburg) durchgeführt. Ein Großteil der CIF-Daten wurde in die CCDC-Datenbank hochgeladen und damit der Allgemeinheit zur Verfügung gestellt. Im Folgenden sind die Strukturen mit 50%-Ellipsoiden abgebildet, und – falls vorhanden – der CCDC-Code angegeben. Im Folgenden sind die Molekülstrukturen der kristallographisch charakterisierten Verbindungen abgebildet und die wichtigsten Bindungslängen und -winkel aufgeführt. Die Strukturdatentabellen sind hier nur bei „Weitere Kristallstrukturen“ aufgeführt, und finden sich ansonsten in den Supporting Information zu den jeweiligen Manuskripten.

6.1 Systematische Studie der Anion-Kation Wechselwirkungen über doppelt ionische Wasserstoffbrückenbindungen in 1,3-Dimethylimidazolium Salzen mit unterschiedlich substituierten Chalkogenolat Anionen MMIm[E-R] (E = S, Se; R = H, *t*Bu, $SiMe_3$)

6.1.1 MMIm[ER] (E = S, Se; R = H, tBu, $SSiMe_3$)

MMIm[SH]
CCDC: 1908996

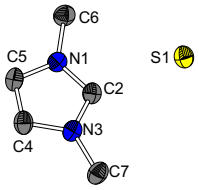

Kristallographisch bestimmte Molekülstruktur von MMIm[SH] (**1**). Protonen wurden der Übersicht halber nicht abgebildet. Ausgewählte Bindungslängen (in Å) und -winkel (in °): N1-C2 1.332(4), C2-N3 1.333(4), N3-C4 1.377(4), C4-C5 1.354(4), C5-N1 1.368(4), N1-C6 1.459(4), N3-C7 1.474(4), C2-S1 3.572(4), N1-C2-S1 101.0(2), C5-N1-C2-S1 161.4(2).

MMIm[S*t*Bu]
CCDC: 1908997

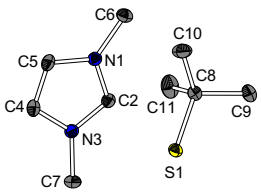

Kristallographisch bestimmte Molekülstruktur von MMIm[S*t*Bu] (**2**). Protonen wurden der Übersicht halber nicht abgebildet. Ausgewählte Bindungslängen (in Å) und -winkel (in °): N1-C2 1.329(2), C2-N3 1.3301(1), N3-C4 1.378(2), C4-C5 1.352(2), C5-N1 1.376(2), N1-C6 1.463(1), N3-C7 1.465(2), S1-C8 1.845(1), C8-C9 1.527(2), C8-C10 1.526(2), C8-C11 1.531(2), S1-C8-C9 110.38(8), S1-C8-C10 109.78(8), S1-C8-C11 110.17(8), C9-C8-C10 108.4(1), C10-C8-C11 109.3(1), C9-S1-C11 108.7(1), N1-C2-S1 141.76(8), C2-S1 3.541(1), C5-N1-C2-S1 141.1(1), C2-S1-C8 98.10(4), N1-C2-S1-C8 0.9(1).

MMIm[SSiMe$_3$]
CCDC: 1908998

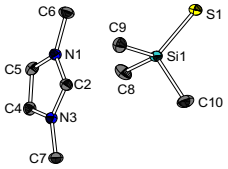

Kristallographisch bestimmte Molekülstruktur von MMIm[SSiMe$_3$] (**3**). Protonen wurden der Übersicht halber nicht abgebildet. Ausgewählte Bindungslängen (in Å) und -winkel (in °): N1-C2: 1.330(2), C2-N3 1.334(2), N3-C4 1.389(2), C4-C5 1.352(2), C5-N1 1.377(2), N1-C6 1.466(2), 1.462(2), S1-Si1 2.075(8), Si1-C8 1.882(2), Si1-C9 1.884(2), Si1-C10 1.879(2), S1-Si1-C8 112.07(6), S1-Si1-C9 114.28(6), S1-Si1-C10 111.79(6), C8-Si1-C9 106.78(7), C9-Si1-C10 104.40(7), C10-Si1-C8 106.96(8), C2-S1 7.544(2), N1-C2-S1 56.58(8), C5-N1-C2-S1 90.9(1). C2-S1-Si1 39.45(2), N1-C2-S1-Si1 –103.5(1).

MMIm[SeH]
CCDC: 1908993

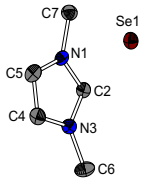

Kristallographisch bestimmte Molekülstruktur von MMIm[SeH] (**4**). Protons are not shown. Protonen wurden der Übersicht halber nicht abgebildet. Ausgewählte Bindungslängen (in Å) und -winkel (in °): N1-C2 1.335(5), C2-N3 1.339(6), N3-C4 1.381(5), C4-C5 1.351(7), C5-N1- 1.369(6), N1-C7 1.468(6), N3-C6 1.458(6), C2-Se1 3.690(5), N1-C2-Se1 102.3(3), C5-N1-C2-Se1 162.7(3).

MMIm[Se*t*Bu]
CCDC: 1908994

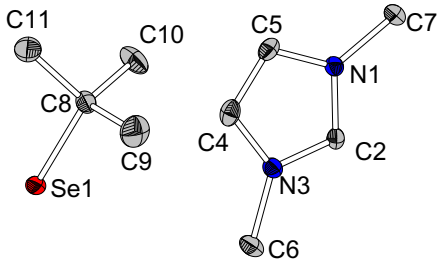

Kristallographisch bestimmte Molekülstruktur von MMIm[SetBu] (**5**). Protonen wurden der Übersicht halber nicht abgebildet. Ausgewählte Bindungslängen (in Å) und -winkel (in °): N1-C2 1.333(5), C2-N3 1.331(5), N3-C4 1.383(5), C4-C5 1.349(6), C5-N1 1.380(5), N1-C7 1.464(5), N3-C6 1.467(6), Se1-C8 1.994(4), C8-C9 1.525(4), C8-C10 1.529(5), C8-C11 1.530(6), Se1-C8-C9 110.4(3), Se1-C8-C10 109.1(3), 109.5(3), C2-Se1 6.889(4), N1-C2-Se1 102.7(2), C5-N1-C2-Se1 61.6(2), N1-C2-Se1-C8 1.5(2).

MMIm[SeSiMe$_3$]
CCDC: 1908995

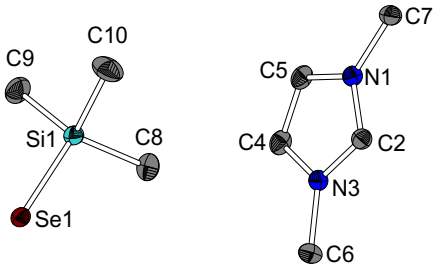

Kristallographisch bestimmte Molekülstruktur von MMIm[SeSiMe$_3$] (**6**). Protonen wurden der Übersicht halber nicht abgebildet. Ausgewählte Bindungslängen (in Å) und -winkel (in °): N1-C2 1.331(2), C2-N3 1.331(2), N3-C4 1.375(2), C4-C5 1.346(2), C5-N1 1.378(2), N1-C7 1.464(2), N3-C6 1.464(2), Se1-Si1 2.212(1), Si1-C8 1.878(2), Si1-C9 1.880(2), Si1-C10 1.874(2), Se1-Si1-C8 113.49(6), Se1-Si1-C9 111.69(6), Se1-Si1-C10, Se1-Si1-C10 111.55(6), C8-Si1-C9 107.43(7), C9-Si1-C10 107.42(8), C10-Si1-C8 104.83(8). C2-Se1 7.610(2), N1-C2-Se1 101.09(9), C5-N1-C2-Se1 –59.4(1), C2-Se1-Si1 39.60(2), N1-C2-Se1-Si1 2.06(8).

6.2 Homoleptische Gruppe 13 Metallate mit Trimethylsilylchalkogenolat Liganden [M(ESiMe$_3$)$_4$] (M = Ga, In; E = S, Se): Präkursoren für die Synthese chalkogenbasierter Materialien bei niedrigen Temperaturen

6.2.1 Cat[M(ESiMe$_3$)$_4$] (Cat = DMPyr (M = Ga, E = Se); Cat = Ph$_4$P (M = In, E = S, Se))

DMPyr[Ga(SeSiMe$_3$)$_4$]
CCDC: 1939702

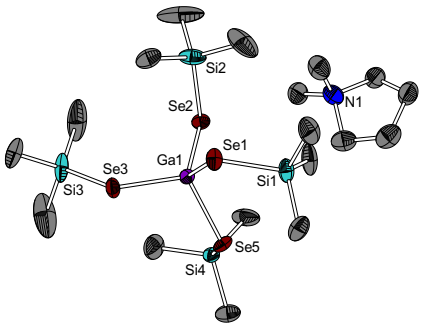

Kristallographisch bestimmte Molekülstruktur von DMPyr[Ga(SeSiMe$_3$)$_4$] (**2**). Protonen wurden der Übersicht halber nicht abgebildet. Ausgewählte Bindungslängen (in Å) und -winkel (in °) für ein repräsentatives Anion **2**: Ga1-Se1 2.3997(8); Ga1-Se2 2.3883(9); Ga1-Se3 2.4158(8); Ga-Se4 2.399(3); Se1-Si1 2.268(2); Se2-Si2 2.274(2); Se3-Si3 2.259(2); Se4-Si4 2.261(2); Se1-Ga1-Se2 115.02(3); Se2-Ga1-Se3 117.29(3); Se3-Ga1-Se4 112.77(6); Se4-Ga1-Se1 104.34(5).

Ph$_4$P[In(SSiMe$_3$)$_4$]
CCDC: 1939703

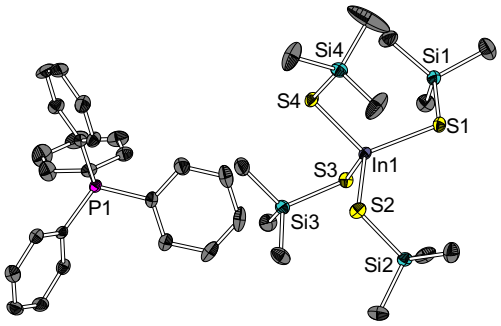

Kristallographisch bestimmte Molekülstruktur von Ph$_4$P In(SSiMe$_3$)$_4$ (**3**) Protonen wurden der Übersicht halber nicht abgebildet. Ausgewählte Bindungslängen (in Å) und -winkel (in °) für ein repräsentatives Anion: In1-S1 2.452(1); In1-S2 2.447(1); In1-S3 2.453(8); In1-S4 2.4577(9); S1-Si1 2.146(1); S2-Si2 2.124(1); S3-Si3 2.121 (1); S4-Si4 2.131(1); S1-In1-S2 113.64(4); S2-In1-S3 111.47(3); S3-In1-S4 111.31(3); S4-In1-S1 113.73(3); In1-S1-Si1 103.39(4); In1-S2-Si2 108.10(4); In1-S3-Si3 106.29(4); In1-S4-Si4 106.57(4).

Ph$_4$P[In(SeSiMe$_3$)$_4$]
CCDC: 1939704

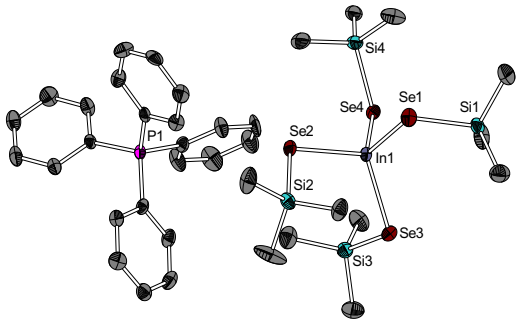

Kristallographisch bestimmte Molekülstruktur von Ph$_4$P[In(SeSiMe$_3$)$_4$] (**4**). Protonen wurden der Übersicht halber nicht abgebildet. Ausgewählte Bindungslängen (in Å) und -winkel (in °) für ein repräsentatives Anion: In1-Se1 2.562(1); In1-Se2 2.5674(9); In1-Se3 2.5632(9); In1-Se4 2.5694(8); Se1-Si1 2.255(2); Se2-Si2 2.268(2); Se3-Si3 2.289(2); Se4-Si4 2.263(2); Se1-In1-Se2 100.86(3); Se2-In1-Se3 113.56(3); Se3-In1-Se4 106.63(3); Se4-In1-Se1 111.30(3); In1-Se1-Si1 104.37(6); In1-Se2-Si2 103.23(6); In1-Se3-Si3 100.20(6); In1-Se4-Si4 102.91(6).

6.2.2 *[Cu(dppe)$_2$] [M(ESiMe$_3$)$_4$] (M = Ga, In; E = S, Se)*

[Cu(dppe)$_2$] [Ga(SSiMe$_3$)$_4$] CCDC: 1939710

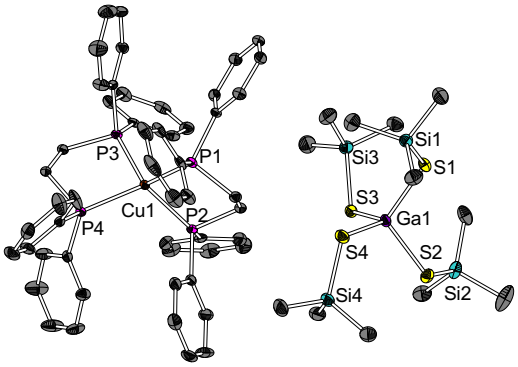

Kristallographisch bestimmte Molekülstruktur von [Cu(dppe)$_2$][Ga(SSiMe$_3$)$_4$]. Protonen wurden der Übersicht halber nicht abgebildet. Ausgewählte Bindungslängen (in Å) und -winkel (in °) für ein repräsentatives Ionenpaar: Ga1-S1 2.280(1); Ga1-S2 2.2598(9); Ga1-S3 2.2791(9); Ga1-S4 2.265(1); S1-Si1 2.122(1); S2-Si2 2.114(1); S3-Si3 2.121(1); S4-Si4 2.124(1); S1-Ga1-S2 108.82(3); S2-Ga1-S3 108.25(3); S3-Ga1-S4 111.53(3); S4-Ga1-S1 110.58(3); Ga1-S1-Si1 110.25(4); Ga1-S2-Si2 106.39(4); Ga1-S3-Si3 110.67(4); Ga1-S4-Si4 105.96(4); Cu1-P1 2.2845(9); Cu1-P2 2.2601(9); Cu1-P3 2.2577(9); Cu1-P4 2.2786(9); P1-Cu1-P2- 89.00(3); P2-Cu1-P3 122.85(3); P3-Cu1-P4 89.93(3); P4-Cu1-P1 128.63(3).

[Cu(dppe)$_2$] [Ga(SeSiMe$_3$)$_4$] CCDC: 1939711

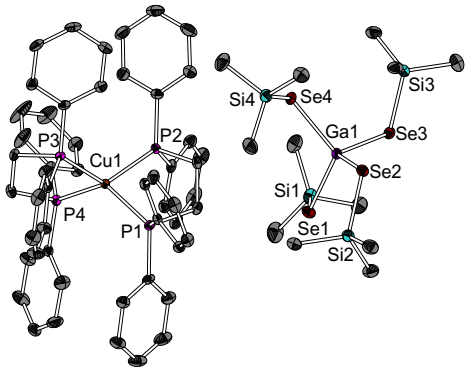

Kristallographisch bestimmte Molekülstruktur von [Cu(dppe)$_2$][Ga(SeSiMe$_3$)$_4$]. Protonen wurden der Übersicht halber nicht abgebildet. Ausgewählte Bindungslängen (in Å) und -winkel (in °) für ein repräsentatives Ionenpaar: Ga1-Se1 2.410(1); Ga1-Se2 2.4249(9); Ga1-Se3 2.4001(9); Ga1-Se4 2.4239(9); Se1-Si1 2.282(1); Se2-Si2 2.2776(9); Se3-Si3 2.272(1); Se4-Si4 2.273(1); Se1-Ga1-Se2 110.25(3); Se2-Ga1-Se3 108.98(3); Se3-Ga1-Se4 106.73(3); Se4-Ga1-Se1 112.18(3); Ga1-Se1-Si1 103.17(3); Ga1-Se2-Si2 108.23(3); Ga1-Se3-Si3 103.01(3); Ga1-Se4-Si4 107.57(3); Cu1-P1 2.3049(9); Cu1-P2 2.274(1); Cu1-P3 2.2698(9); Cu1-P4 2.2991(9); P1-Cu1-P2 89.01(3); P2-Cu1-P3 122.92(3); P3-Cu1-P4 89.94(3); P4-Cu1-P1 128.71(3).

[Cu(dppe)$_2$] [In(SSiMe$_3$)$_4$] CCDC: 1939704

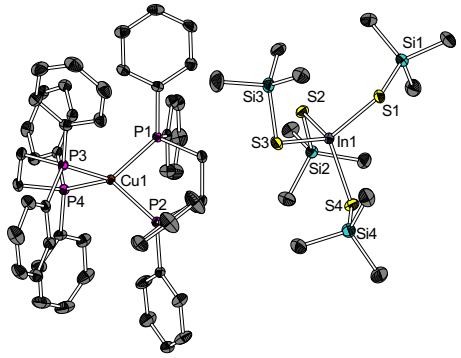

Kristallographisch bestimmte Molekülstruktur von [Cu(dppe)$_2$][In(SSiMe$_3$)$_4$] (**5**) Protonen wurden der Übersicht halber nicht abgebildet. Ausgewählte Bindungslängen (in Å) und -winkel (in °) für ein repräsentatives Ionenpaar: In1-S1 2.4683(6); In1-S2 2.4682(6); In1-S3 2.4510(6); In1-S4 2.4564(7); S1-Si1 2.1356(7); S2-Si2 2.1320(7); S3-Si3 2.1283(7); S4-Si4 2.1397(7); S1-In1-S2 112.53(2); S2-In1-S3 108.38(2); S3-In1-S4 105.53(2); S4-In1-S1 112.06(2); In1-S1-Si1 108.58(3); In1-S2-Si2 108.84(2); In1-S3-Si3 104.42(3); In1-S4-Si4 104.25(3); Cu1-P1 2.2687(6); Cu1-P2 2.2950(6); Cu1-P3 2.2726(6); Cu1-P4 2.3001(6); P1-Cu1-P2 2.2687(6); P2-Cu1-P3 115.19(2); P3-Cu1-P4 88.99(2); P4-Cu1-P1 114.695(2).

[Cu(dppe)$_2$] [In(SeSiMe$_3$)$_4$] CCDC: 1939712

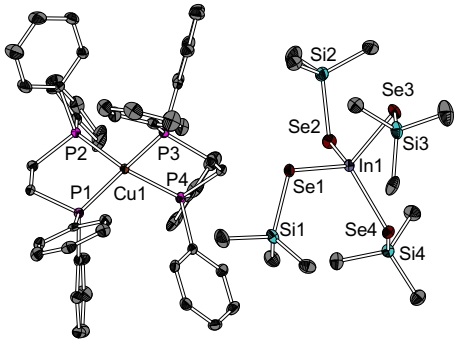

Kristallographisch bestimmte Molekülstruktur von [Cu(dppe)$_2$][In(SeSiMe$_3$)$_4$]. Protonen wurden der Übersicht halber nicht abgebildet. Ausgewählte Bindungslängen (in Å) und -winkel (in °) für ein repräsentatives Ionenpaar: In1-Se1 2.5903(9); In1-Se2 2.578(1); In1-Se3 2.570(1); In1-Se4 2.591(1); Se1-Si1 2.272(1); Se2-Si2 2.282(1); Se3-Si3 2.271(1); Se4-Si4 2.2742(9); Se1-In1-Se2 112.53(3); Se2-In1-Se3 106.46(3); Se3-In1-Se4 108.46(3); Se4-In1-Se1 112.49(3); In1-Se1-Si1 105.51(3); In1-Se2-Si2 101.46(3(); In1-Se3-Si3 101.01(3); In1-Se4-Si4 106.76(3); Cu1-P1 2.268(1); Cu1-P2 2.299(1); Cu1-P3 2.271(1); Cu1-P4 2.305(1); P1-Cu1-P2 90.02(3); P2-Cu1-P3 114.69(4); P3-Cu1-P4 88.89(4); P4-Cu1-P1 114.97(4).

6.2.3 [Cu(dmpe)$_2$] [M(ESiMe$_3$)$_4$] (M = Ga, In; E = S, Se)

[(η-dmpe)Cu(μ-dmpe)$_2$]$_2$[Ga(SSiMe$_3$)$_4$]$_2$
CCDC: 1939706

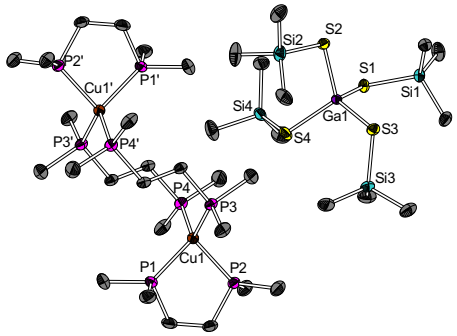

Kristallographisch bestimmte Molekülstruktur von [(η^2-dmpe)Cu(μ^2-dmpe)]$_2$[Ga(SSiMe$_3$)$_4$]$_2$ (**6**). Ein Anion und Protonen wurden der Übersicht halber nicht abgebildet. Ausgewählte Bindungslängen (in Å) und -winkel (in °) für ein repräsentatives Anion und ein Kupferzentrum: Ga1-S1 2.2748(9); Ga1-S2 2.286(1); Ga1-S3 2.281(1); Ga1-S4 2.272(1); S1-Si1 2.124(1); S2-Si2 2.126(1); S3-Si3 2.137(1); S4-Si4 2.128(1); S1-Ga1-S2 105.77(3); S2-Ga1-S3 105.64(3); S3-Ga1-S4 109.38(4); S4-Ga1-S1 110.04(4); Ga1-S1-Si1; 106.90(5); Ga1-S2-Si2 106.20(5); Ga1-S3-Si3 105.90(5); Ga1-S4-Si4 108.82(5); Cu1-P1 2.258(1); Cu1-P2 2.277(1); Cu1-P3 2.239(1); Cu1-P4 2.251(7); P1-Cu1-P2 89.90(4); P2-Cu1-P3 112.09(4); P3-Cu1-P4 112.14(4); P4-Cu1-P1 115.20(4).

[Cu(dmpe)$_2$] [Ga(SeSiMe$_3$)$_4$]
CCDC: 1939707

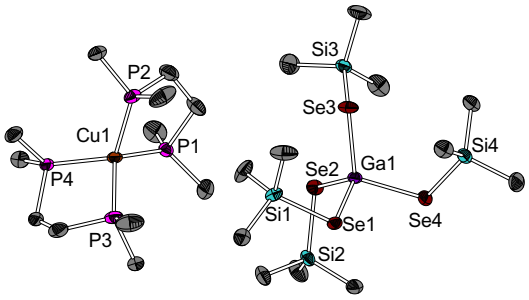

Kristallographisch bestimmte Molekülstruktur von [(dmpe)$_2$Cu][Ga(SeSiMe$_3$)$_4$]$_2$. Protonen wurden der Übersicht halber nicht abgebildet. Ausgewählte Bindungslängen (in Å) und -winkel (in °) für ein repräsentatives Ionenpaar: Ga1-Se1 2.4099(7); Ga1-Se2 2.395(1); Ga1-Se3 2.3939(8); Ga1-Se4 2.4188(9); Se1-Si1 2.268(1); Se2-Si2 2.268(1); Se3-Si3 2.260(1); Se4-Si4 2.261(1); Se1-Ga1-Se2 113.54(3); Se2-Ga1-Se3 110.89(2); Se3-Ga1-Se4 114.24(3); Se4-Ga1-Se1 104.81(3); Ga1-Se1-Si1 102.87(4); Ga1-Se2-Si2 102.25(3); Ga1-Se3-Si3 105.57(4); Ga1-Se4-Si4 104.54(4); Cu1-P1 2.252(1); Cu1-P2 2.261(1); Cu1-P3 2.257(1); Cu1-P4 2.254(1); P1-Cu1-P2 90.67(4); P2-Cu1-P3 119.93(4); P3-Cu1-P4 90.59(4); P4-Cu1-P1 126.08(5).

[(η-dmpe)Cu(μ-dmpe)$_2$]$_2$[In(SSiMe$_3$)$_4$]$_2$
CCDC: 1939708

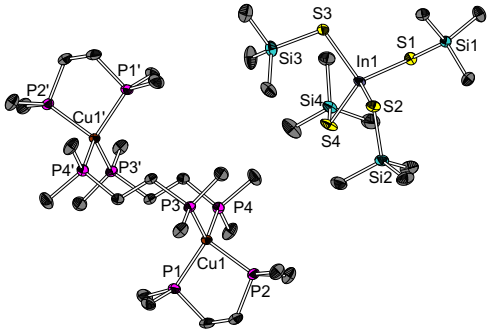

Kristallographisch bestimmte Molekülstruktur von [(η^2-dmpe)Cu(μ^2-dmpe)]$_2$[In(SSiMe$_3$)$_4$]$_2$. Ein Anion und Protonen wurden der Übersicht halber nicht abgebildet. Ausgewählte Bindungslängen (in Å) und -winkel (in °) für ein repräsentatives Anion und ein Kupferzentrum: In1-S1 2.452(2); In1-S2 2.467(2); In1-S3 2.468(2); In1-S4 2.454(2); S1-Si1 2.127(2); S2-Si2 2.139(2); S3-Si3 2.123(2); S4-Si4 2.129(2); S1-In1-S2 113.86(4); S2-In1-S3 105.69(4); S3-In1-S4 111.74(5); S4-In1-S1 110.54(6); In1-S1-Si1 105.45(6); In1-S2-Si2 104.26(5); In1-S3-Si3 105.71(6); In1-S4-Si4 107.73(6); Cu1-P1 2.266(2); Cu1-P2 2.283(2); Cu1-P3 2.243(2); Cu1-P4 2.249(2); P1-Cu1-P2 89.76(5); P2-Cu1-P3 111.52(5); P3-Cu1-P4 112.43(5); P4-Cu1-P1 110.23(5).

[Cu(dmpe)$_2$] [In(SeSiMe$_3$)$_4$]
CCDC: 1939709

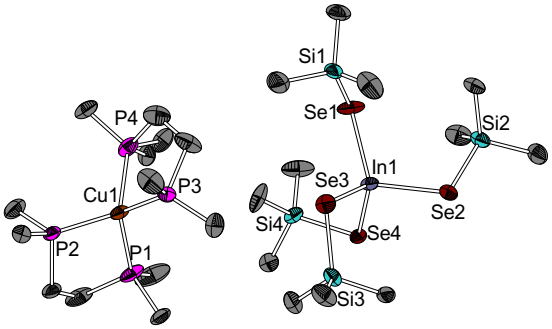

Kristallographisch bestimmte Molekülstruktur von [(dmpe)$_2$Cu][In(SeSiMe$_3$)$_4$]$_2$. Protonen wurden der Übersicht halber nicht abgebildet. Ausgewählte Bindungslängen (in Å) und -winkel (in °) für ein repräsentatives Ionenpaar: In1-Se1 2.5687(9); In1-Se2 2.593(1); In1-Se3 2.5696(8); In1-Se4 2.5840(9); Se1-Si1 2.258(2); Se2-Si2 2.268(2); Se3-Si3 2.275(2); Se4-Si4 2.269(2); Se1-In1-Se2 113.63(3); Se2-In1-Se3 107.62(3); Se3-In1-Se4 112.68(2); Se4-In1-Se1 106.74(2); In1-Se1-Si1 103.71(6); In1-Se2-Si2 103.07(5); In1-Se3-Si3 100.34(5); In1-Se4-Si4 101.62(5); Cu1-P1 2.262(2); Cu1-P2 2.263(2); Cu1-P3 2.257(2); Cu1-P4 2.274(2); P1-Cu1-P2 90.64(7); P2-Cu1-P3 126.14(6); P3-Cu1-P4 90.45(6); P4-Cu1-P1 119.15(7).

6.3 Homoleptische Trimethylsilylchalkogenolatometallate $[Zn(ESiMe_3)_3]^-$ und $[Sn(ESiMe_3)_3]^-$ (E = S, Se) als mögliche molekulare Vorstufen für die Niedrigtemperatursynthese von Cu_2ZnSnS_4 (CZTS)

6.3.1 $Ph_4P[M(ESiMe_3)_3]$ (M = Zn, Sn; E = S, Se)

$Ph_4P[Zn(SSiMe_3)_3]$
CCDC: 1940534

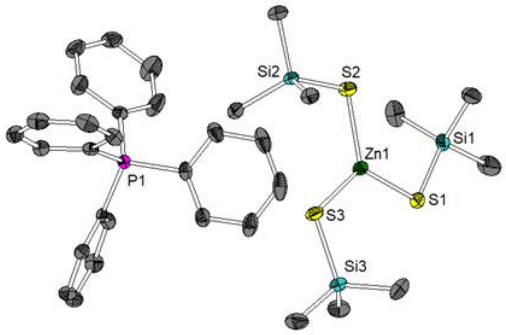

Kristallographisch bestimmte Molekülstruktur von $Ph_4P[Zn(SSiMe_3)_3]$ (**1a**). Protonen wurden der Übersicht halber nicht abgebildet. Ausgewählte Bindungslängen (in Å) und -winkel (in °) für ein repräsentatives Anion: Zn1-S1 2.2543(7); Zn1-S2 2.2536(8); Zn1-S3 2.2534(7); S1-Si1 2.1240(8); S2-Si2 2.1176(7); S3-Si3 2.1055(9); S1-Zn1-S2 120.64(2); S2-Zn1-S3 117.65(2); S3-Zn1-S1 121.72(2); Zn1-S1-Si1 104.42(3); Zn1-S2-Si2 105.12(2); Zn1-S3-Si3 108.95(2).

$(Ph_4P)_2[Zn(SeSiMe_3)_2(\mu_2\text{-}SeSiMe_3)]_2$
CCDC: 1940535

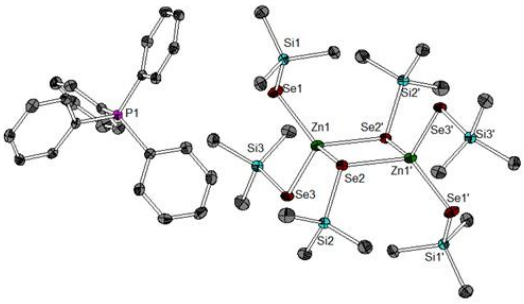

Kristallographisch bestimmte Molekülstruktur von $Ph_4P[Zn(SeSiMe_3)_3]$ (**1b**). Gezeigt ist das Dianion $[(Me_3SiSe)_2Zn(\mu\text{-}SeSiMe_3)]_2^{2-}$ mt einem Kation. Protonen wurden der Übersicht halber nicht abgebildet. Ausgewählte Bindungslängen (in Å) und -winkel (in °) für ein repräsentatives Anion: Zn1-Se1 2.414(1); Zn1-Se2 2.528(1); Zn1-Se3 2.447(1); Zn1-Se2' 2.571(1); Se1-Si1 2.243(2); Se2-Si2 2.273(1); Se3-Si3 2.243(1); Se1-Zn1-Se2 115.68(3); Se2-Zn1-Se3 114.42(3); Se3-Zn1-Se1 108.72(3): Se1-Zn1-Se2' 119.28(3); Zn1-Se1-Si1 109.14(3); Zn1-Se2-Si2 117.03(4); Zn1-Se3-Si3 103.96(4); Se2-Zn1-Se2' 89.66(3); Zn1-Se2-Zn1' 90.34(3).

$Ph_4P[Sn(SSiMe_3)_3]$
CCDC: 1940536

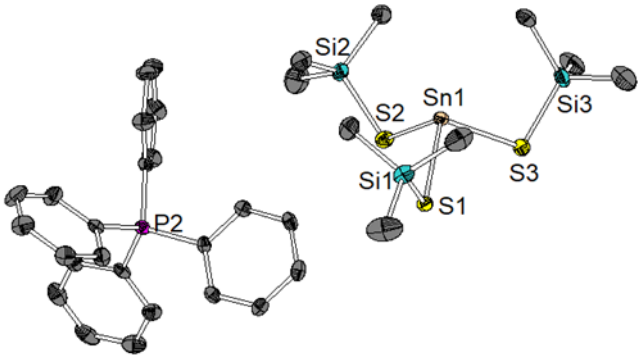

Kristallographisch bestimmte Molekülstruktur von $Ph_4P[Sn(SSiMe_3)_3]$ (**2a**). Protonen wurden der Übersicht halber nicht abgebildet. Ausgewählte Bindungslängen (in Å) und -winkel (in °) für ein repräsentatives Anion: Sn1-S1 2.5521(9); Sn1-S2 2.5372(1); Sn1-S3 2.5366(6); S1-Si1 2.116(1); S2-Si2 2.113(1); S3-Si3 2.114(2); S1-Sn1-S2 94.24(3); S2-Sn1-S3 93.01(3); S1-Sn1-S3 95.38(3); Sn1-S1-Si1 97.55(4); Sn1-S2-Si2 100.69(5); Sn1-S3-Si3 100.32(5).

6.4 Eine Serie Linear koordinierter homoleptischer Münzmetallatkomplexe Cat[M(ESiMe$_3$)$_2$] (M = Cu, Ag, Au; E = S, Se)

6.4.1 Cat[M(ESiMe$_3$)$_2$] (Cat = Ph$_4$P, PPN; M = Cu, Ag, Au; E = S, Se)

Ph$_4$P[Cu(SSiMe$_3$)$_2$]
CCDC: 1940498

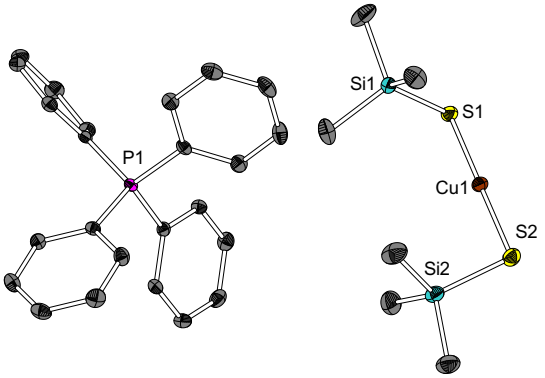

Kristallographisch bestimmte Molekülstruktur von Ph$_4$P[Cu(SSiMe$_3$)$_2$] (1). Protonen wurden der Übersicht halber nicht abgebildet. Ausgewählte Bindungslängen (in Å) und -winkel (in °) für ein repräsentatives Anion: Cu1-S1 2.1412(6), Cu1-S2 2.1475(6), S1-Si1 2.1081(8), S2-Si2 2.1129(7), S1-Cu1-S2 176.63(2), Cu1-S1-Si1 100.34(2), Cu1-S2-Si2 97.14(2), Si1-S1-S2-Si2 48.86(3).

Ph$_4$P[Ag(SSiMe$_3$)$_2$]
CCDC: 1940499

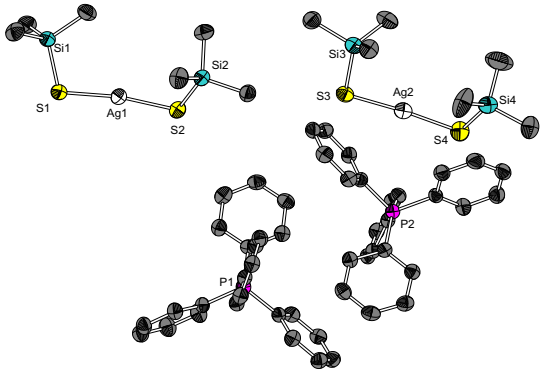

Kristallographisch bestimmte Molekülstruktur von Ph$_4$P[Ag(SSiMe$_3$)$_2$] (2). Protonen wurden der Übersicht halber nicht abgebildet. Ausgewählte Bindungslängen (in Å) und -winkel (in °) für zwei repräsentative Anionen: Ag1-S1 2.341(1), Ag1-S2 2.356(1), S1-Si1 2.111(1), S2-Si2 2.108(2), S1-Ag1-S2 171.70(4), Ag1-S1-Si1 106.28(5), Ag1-S2-Si2 98.59(5), Si1-S1-S2-Si2 51.27(7), Ag2-S3 2.357(1), Ag2-S4 2.368(1), S3-Si3 2.118(2), S4-Si4 2.099(2), S3-Ag2-S4 175.56(4), Ag2-S3-Si3 100.07(5), Ag2-S4-Si4 98.19(6), Si3-S3-S4-Si4 27.82(7).

PPN[Au(SSiMe$_3$)$_2$]
CCDC: 1940500

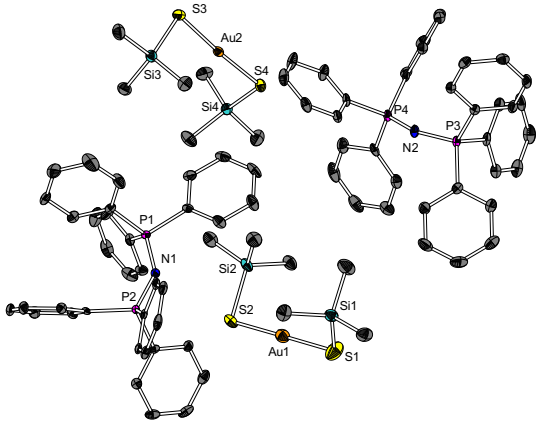

Kristallographisch bestimmte Molekülstruktur von PPN[Au(SSiMe$_3$)$_2$] (3-PPN). Protonen wurden der Übersicht halber nicht abgebildet. Ausgewählte Bindungslängen (in Å) und -winkel (in °) für zwei repräsentative Anionen: Au1-S1 2.289(1), Au1-S2 2.308(1), S1-Si1 2.107(2), S2-Si2 2.112(2), S1-Au1-S2 178.79(4), Au1-S1-Si1 103.80(5), Au1-S2-Si2 94.71(5), Si1-S1-S2-Si2 62.15(6), Au2-S3 2.299(1), Au2-S4 2.2985(9), S3-Si3 2.119(1), S4-Si4 2.119(1), S3-Au2-S4 176.52(3), Au2-S3-Si3 100.38(5), Au2-S4-Si4 102.44(4), Si3-S3-S4-Si4 77.21(5).

PPN[Cu(SeSiMe$_3$)$_2$]
CCDC: 1940501

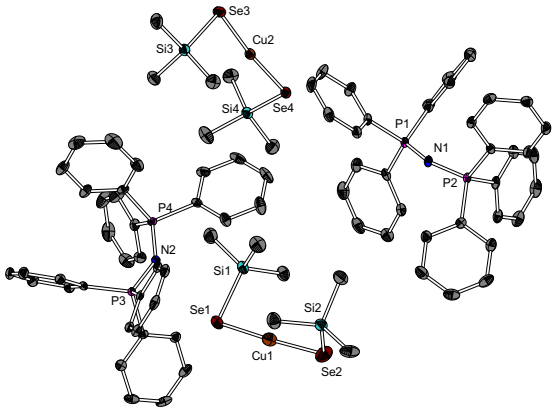

Kristallographisch bestimmte Molekülstruktur von PPN[Cu(SeSiMe$_3$)$_2$] (4-PPN). Protonen wurden der Übersicht halber nicht abgebildet. Ausgewählte Bindungslängen (in Å) und -winkel (in °) für zwei repräsentative Anionen: Cu1-Se1 2.2836(6), Cu1-Se2 2.2613(7), Se1-Si1 2.247(1), Se2-Si2 2.2540(9), Se1-Cu1-Se2 174.98(3), Cu1-Se1-Si1 88.30(3), Cu1-Se2-Si2 101.24(3), Si1-Se1-Se2-Si2 77.45(3), Cu2-Se3 2.2653(6), Cu2-Se4 2.2634(6), Se3-Si3 2.253(1), Se4-Si4 2.2561(8), Se3-Cu2-Se4 174.16(2), Cu2-Se3-Si3 99.20(3), Cu2-Se4-Si4 101.97(3), Si3-Se3-Se4-Si4 75.97(3).

PPN[Ag(SeSiMe$_3$)$_2$]
CCDC: 1940502

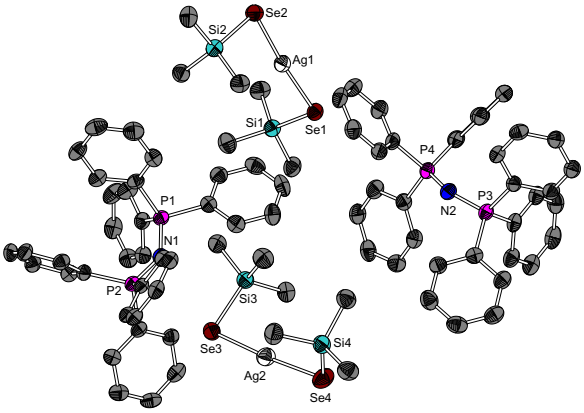

Kristallographisch bestimmte Molekülstruktur von PPN[Ag(SeSiMe$_3$)$_2$] (5-PPN). Protonen wurden der Übersicht halber nicht abgebildet. Ausgewählte Bindungslängen (in Å) und -winkel (in °) für zwei repräsentative Anionen: Ag1-Se1 2.4487(6), Ag1-Se2 2.4498(7), Se1-Si1 2.254(1), Se2-Si2 2.253(2), Se1-Ag1-Se2 175.29(2), Ag1-Se1-Si1 101.79(4), Ag1-Se2-Si2 96.68(4), Si1-Se1-Se2-Si2 73.82(5), Ag2-Se3 2.4745(6), Ag2-Se4 2.4521(8), Se3-Si3 2.247(2), Se4-Si4 2.256(2), Se3-Ag2-Se4 174.66(3), Ag2-Se3-Si3 87.93(4), Ag2-Se4-Si4 100.25(5), Si3-Se3-Se4-Si4 74.75(6).

PPN[Au(SeSiMe$_3$)$_2$]$_2$
CCDC: 1940503

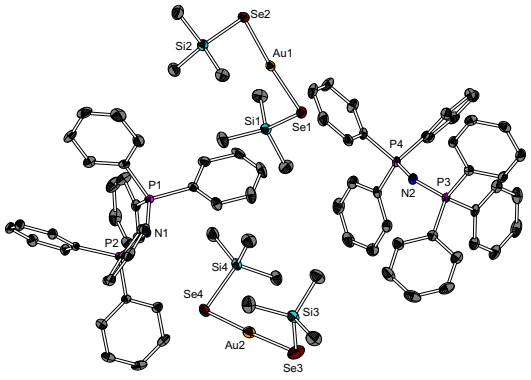

Kristallographisch bestimmte Molekülstruktur von PPN[Au(SeSiMe$_3$)$_2$] (6-PPN). Protonen wurden der Übersicht halber nicht abgebildet. Ausgewählte Bindungslängen (in Å) und -winkel (in °) für zwei repräsentative Anionen: Au1-Se1 2.3980(6), Au1-Se2 2.4015(6), Se1-Si1 2.255(1), Se2-Si2 2.256(1), Se1-Au1-Se2 175.46(2), Au1-Se1-Si1 101.36(3), Au1-Se2-Si2 97.68(3), Si1-Se1-Se2-Si2 75.21(4), Au2-Se3 2.3956(7), Au2-Se4 2.4139(6), Se3-Si3 2.258(1), Se4-Si4 2.255(1), Se3-Au2-Se4 176.14(3), Au2-Se3-Si3 100.79(3), Au2-Se4-Si4 90.29(3), Si3-Se3-Se4-Si4 72.49(4).

6.5 Dinukleare Chalkogenidoorganotrielate DMPyr$_2$[Me$_2$M(μ$_2$-E)]$_2$ durch Indierung und Gallierung organischer Hydrochalkogenid Salze DMPyr[EH] (E = S, Se) mit Trimethyltrielen Me$_3$M (M = Ga, In)

6.5.1 DMPyr[EH] (E = S, Se)

DMPyr[SH]
CCDC: 1910798
Gelöst von *Dr. Lars H. Finger* im Zuge meiner Masterarbeit

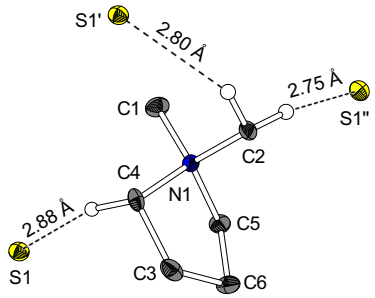

Kristallographisch bestimmte Molekülstruktur von DMPyr[SH] (1). Nur in Wasserstoffbrückenbindungen aktive Protonen wurden abgebildet. Ausgewählte Bindungslängen (in Å) und -winkel (in °): C1-N1 1.493(2), C2-N1 1.503(1), C4-N1 1.511(1), C5-N1 1.511(1), C4-C3 1.527(2), C3-C6 1.550(2), C5-C6 1.526(2), C1-N1-C2 109.95(8), C1-N1-C5 111.67(8), C1-N1-C5-C6 -161.66(9), C5-C6-C3 104.96(9), C5-C6-C3-C4 –2.2(1), C6-C3-C4 105.59(9), C6-C3-C4-N1 –23.7(1), C3-C4-N1-C2 –77.3(1), S1-C4 3.776(1), S1-C4-N1 94.00(6), S1-C4-N1-C5 –64.6(7). Symmetrieoperationen I: -1+x, y, z; II: -1/2+x, 1/2-y, 1/2+z.

DMPyr[SeH]
CCDC: 1910797

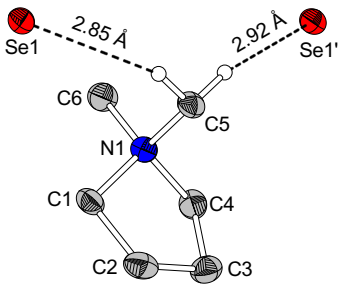

Kristallographisch bestimmte Molekülstruktur von DMPyr[SeH] (2). Nur in Wasserstoffbrückenbindungen aktive Protonen wurden abgebildet. Ausgewählte Bindungslängen (in Å) und -winkel (in °): C6-N1 1.495(4), C5-N1 1.497(4), C1-N1 1.511(4), C4-N1 1.513(4), C1-C2 1.529(5), C2-C3 1.546(5), C4-C3 1.528(5), C6-N1-C5 109.9(2), C6-N1-C4 111.3(2), C6-N1-C4-C3 –159.4(3), C4-C3-C2 105.8(2), C4-C3-C2-C1 3.9(3), C3-C2-C1 104.9(3), C3-C2-C1-N1 –28.7(3), C2-C1-N1-C5 –75.0(3), Se1-C5 3.758(3), Se1-C5-N1 92.8(2), Se1-C5-N1-C4 –170.6(2). Symmetrieoperationen I: 1/2+x, 1/2-y, 1/2+z.

6.5.2 DMPyr$_2$[Me$_2$M(μ_2-E)]$_2$ (M = Ga, In; E = S, Se)

DMPyr$_2$[Me$_2$Ga(μ_2-S)]$_2$
CCDC: 1910795
Gelöst von *Dr. Lars H. Finger* im Zuge meiner Masterarbeit

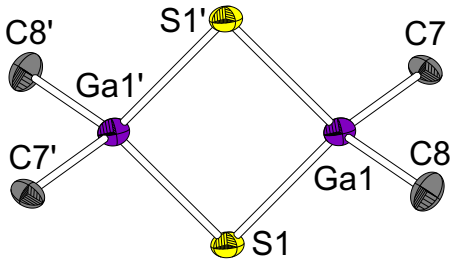

Kristallographisch bestimmte Molekülstruktur des Dianions in DMPyr$_2$[Me$_2$Ga(μ_2-S)]$_2$ (3). Kationen und Protonen wurden der aufgrund unübersichtlicher Fehlordnung nicht abgebildet. Ausgewählte Bindungslängen (in Å) und -winkel (in °): Ga1-S1 2.3225(5), Ga1-S1' 2.3293(4), S1-Ga1-S1' 97.27(1), Ga1-S1'-Ga1' 82.73(1), Ga1-C7 2.032(2), Ga1-C8 2.012(2), C7-Ga1-C8 108.62(7), Ga1'-S1'-Ga1-C7 117.38(5), Ga1'-S1-Ga1-C8 119.00(5). Symmetrieoperationen I: 1-x, -y, 1-z.

DMPyr$_2$[Me$_2$Ga(μ_2-Se)]$_2$
CCDC: 1910796

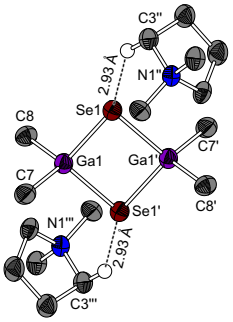

Kristallographisch bestimmte Molekülstruktur von DMPyr$_2$[Me$_2$Ga(μ_2-Se)]$_2$ (4). Nur in Wasserstoffbrückenbindungen aktive Protonen wurden abgebildet. Ausgewählte Bindungslängen (in Å) und -winkel (in °): Ga1-Se1 2.453(1), Ga1-Se1' 2.461(1), Se1-Ga1-Se1' 82.41(4), Ga1-Se1-Ga1' 82.59(4), Ga1-C7 2.017(9), Ga1-C8 2.014(9), C7-Ga1-C8 109.0(4), Ga1'-Se1'-Ga1-C7 –118.4(3), Ga1'-Se1-Ga1-C8 –117.6(3). Symmetrieoperationen I: 1-x, 1-y, 1-z; II: -1/2+x, 1/2-y, ½+z; III: 3/2-x, 1/2+y, 1/2-z.

DMPyr$_2$[Me$_2$In(μ_2-S)]$_2$
CCDC: 1910796
Gelöst von *Dr. Lars H. Finger* im Zuge meiner Masterarbeit

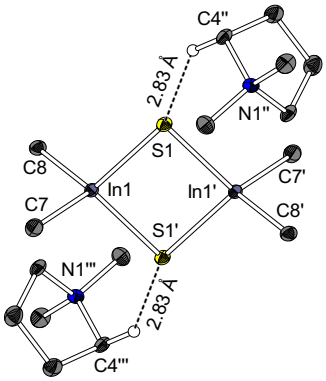

Kristallographisch bestimmte Molekülstruktur von DMPyr$_2$[Me$_2$In(μ_2-S)]$_2$ (5). Nur in Wasserstoffbrückenbindungen aktive Protonen wurden abgebildet. Ausgewählte Bindungslängen (in Å) und -winkel (in °): In1-S1 2.5040(5), In1-S1' 2.5067(4), S1-In1-S1' 96.15(1), In1-S1-In1' 83.85(1), In1-C7 2.206(2), In1-C8 2.205(2), C7-In1-C8 108.45(6), In1'-S1'-In1-C7 –118.81(5), In1'-S1-In1-C8 116.64(4). Symmetrieoperationen I: -x, -y, -z; II: 1-x, -y, -z; III: -1+x, y, z.

DMPyr$_2$[Me$_2$In(μ_2-Se)]$_2$
CCDC: 1910794
Gelöst von *Dr. Lars H. Finger* und Bestandteil seiner Dissertation.

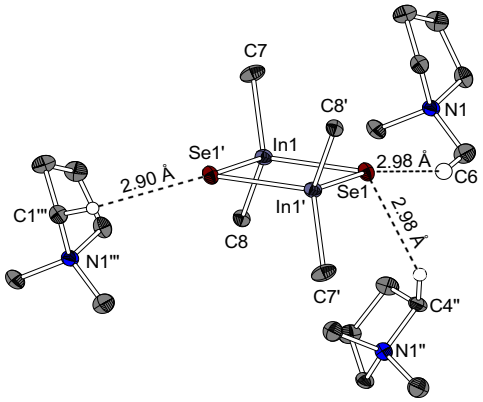

Kristallographisch bestimmte Molekülstruktur von DMPyr$_2$[Me$_2$In(μ_2-Se)]$_2$ (6). Nur in Wasserstoffbrückenbindungen aktive Protonen wurden abgebildet. Ausgewählte Bindungslängen (in Å) und -winkel (in °): In1-Se1 2.6208(4), In1-Se1' 2.6177(4), Se1-In1-Se1' 96.72(1), In1-Se1-In1' 83.28(1), In1-C7 2.209(3), In1-C8 2.212(3), C7-In1-C8 110.2(1), In1'-Se1'-In1-C7 –117.35(9), In1'-Se1-In1-C8 –116.58(8). Symmetrieoperationen I: 2-x, -y, 2-z; II: 1/2+x, ½-y, 1/2+z; III: 1+x, y, z.

6.5.3 *DMPyr$_2$[(Me$_2$In)$_6$(μ$_3$-S)$_4$]*

DMPyr$_2$[(Me$_2$In)$_6$(μ$_3$-S)$_4$]
CCDC: 1910799
Gelöst von *Dr. Lars H. Finger* im Zuge meiner Masterarbeit

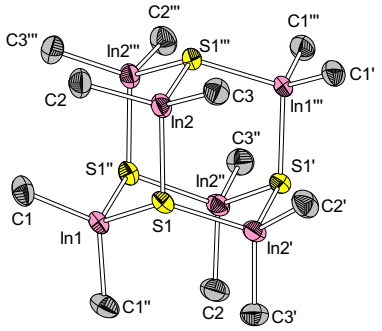

Kristallographisch bestimmte Molekülstruktur von DMPyr$_2$[(Me$_2$In)$_6$(μ^3-S)$_4$] (11). Kationen und Protonen wurden der aufgrund unüberlichtlicher Fehlordnung nicht abgebildet. Ausgewählte Bindungslängen (in Å) und -winkel (in °): S1-In1 2.522(1), S1-In2 2.522(1), S1-In2' 2.522(1), S1''-In1-S1 106.96(4), S1-In2-S1''' 107.15(4), In1-S1-In2' 111.80(5), In1-S1-In2 109.60(5), In1-C1 2.174(5), In2-C2 2.177(6), In2-C3 2.181(5), C1-In1-C1'' 118.5(2), C2-In2-C3 118.0(2), S1-In1-C1 108.2(1), S1-In1-C1'' 107.3(1), In2-S1-In1-C1'' 177.9(2), C1-In1-S1-In2' –176.0(2), C2-In2-S1-In2' 174.4(2), C2-In2-S1-In1 178.8(2), In1-S1-In2'-S1' 59.65(6), In1-S1-In2-S1'''-63.5(6). Symmetrieoperationen I: 3/4–y, –1/4+x, 1/4–z; II: 1–x, 1/2–y, z; III: 1/4+y, 3/4–x, 1/4–z.

6.5.4 *DMPyr$_3$[(Me$_2$In)(μ$_3$-SInMe$_3$)]$_3$*

DMPyr$_3$[(Me$_2$In)(μ$_3$-SInMe$_3$)$_4$]$_3$
Unvollst. gelöst von *Dr. Klaus Harms*.
Kristallqualität erlaubt nur qualitative Strukturdiskussion

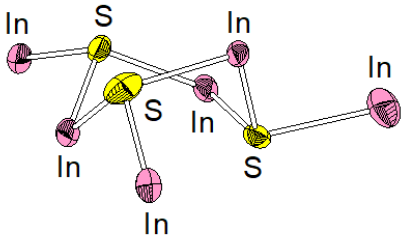

Kristallographisch bestimmte Molekülstruktur des Anionengrundgerüts von DMPyr$_3$[(Me$_2$In)(μ^3-SInMe$_3$)]$_3$. Die Qulität der Kristalldaten erlaubt nur eine qualitative Diskussion der Schweratomlagen. Verzwillingung und Fehlordnungen unterbinden eine verbindliche Analyse der Bindungslängen und -Winkel.

6.6 Organische Methylcarbonat-Salze mit nicht-methylierten Kationen Cat[OCO_2Me] (Cat = Ph_4P^+, PPN^+, TBA^+) über Fluorid-induzierte Demethylierung von Dimethylcarbonat

6.6.1 Cat[OCO_2Me]

PPN[OCO_2Me] · 0.5 MeCN

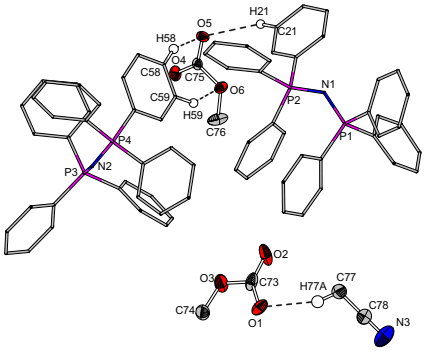

Kristallographisch bestimmte Molekülstruktur von PPN[OCO2Me] · 0.5 MeCN. Der Übersicht halber halber sind nur H-Atome in Wasserstoffbrückenbindungen gezeigt und nur ausgewählte Atome als 50%-Ellipsoid dargestellt. Ausgewählte Bindungslängen (in Å) und -winkel (in °): O1-C73 1.244(3), O2-C73 1.238(3), O3-C73 1.415(3), O3-C74 1.410(3), O1-C73-O2 130.8(2), O1-C73-O3 115.4(2), O2-C73-O3 113.8(2), C73-O3-C74 117.0(2), C74-O3-C73-O1 4.0(3), C74-O3-C73-O2 -175.4(2), N3-C78 1.132(3), C78-C77 1.441(4), N3-C78-C77 179.1(3), C77-H77A 0.98, C78-C77-H77A 160.9(2), H77A-O1 2.406(2), C77-H77A-O1 160.9(2), C73-O1-H77A 94.6(2), C73-O1-H77A-C77 32.2(6), O4-C75 1.231(3), O5-C75 1.231(3), O6-C75 1.406(3), O6-C76 1.421(3), O4-C75-O5 130.6(2), O4-C75-O6 116.9(2), O5-C75-O6 112.5(2), C75-O6-C76 116.1(2), C21-H21 0.95, O5-H21 2.50, O5-H21-C21 143.9(1), C75-O5-H21-C21 -81.1(3), C58-H58 0.95, O5-H58 2.34, O5-H58-C58 150.7(1), C75-O5-H58-C58 16.2(3), C59-H59 0.95, O6-H59 2.499(2), C59-H59-O6 140.7(1), C59-H59-O6-C75 -6.6(3).

TBA[OCO_2Me]

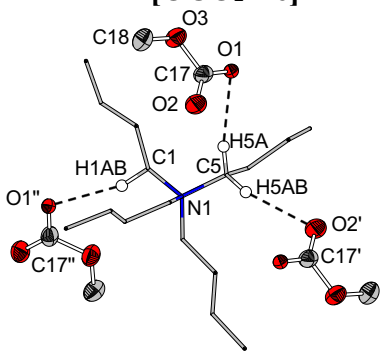

Kristallographisch bestimmte Molekülstruktur von TBA[OCO_2Me]. Der Übersicht halber sind nur H-Atome in Wasserstoffbrückenbindungen gezeigt und nur ausgewählte Atome als 50%-Ellipsoid dargestellt. Ausgewählte Bindungslängen (in Å) und -winkel (in °): O1-C17 1.247(2), O2-C17 1.240(2), O3-C17 1.404(2), O1-C17-O2 130.4(2), O2-C17-O3 116.8(2), O1-C17-O3 112.8(2), O3-C18 1.424(3), C18-O3-C17 115.5(2), C5-H5A 0.97, O1-H5A 2.44, O1-H5A-C5 166.1(1), C17-O1-H5A-C5 -173.3(4), C5-H5AB 0.97, H5A-C5-H5AB 107.4, H5AB-O2' 2.439(1), C5-H5AB-O2' 149.3(1), C5-H5AB-O2'-C17' -153.4(2), C1-H1AB 0.97, O1''-H1AB 2.40, O1''-H1AB-C1 161.6(1), C17''-O1''-H1AB-C1 118.5(3). Symmetrieoperationen: I: 1-x, 1-y, 1-z; II: 1/2-x, 1/2+y, 1/2-z.

6.6.2 $Ph_4P[ESiMe_3]$ (E = S, Se, Te)

$Ph_4P[SSiMe_3]$

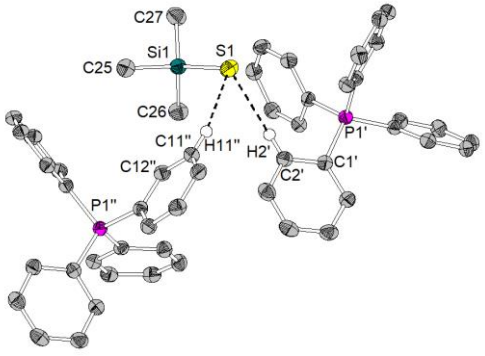

Kristallographisch bestimmte Molekülstruktur von $Ph_4P[SSiMe_3]$. Der Übersicht halber halber sind nur H-Atome in Wasserstoffbrückenbindungen gezeigt. Ausgewählte Bindungslängen (in Å) und -winkel (in °): S1-Si1 2.0647(8), Si1-C25 1.885(2), Si1-C26 1.885(2), Si1-C27 1.884(2), S1-Si1-C25 115.37(7), S1-Si1-C26 111.30(7), S1-Si1-C27 111.43(7), C25-Si1-C26 106.14(9), C26-Si1-C27 108.7(1), C27-Si1-C25 103.4(1), S1-H2' 2.82, C2'-H2' 0.93, S1-H2'-C2' 143(1), Si1-S1-H2'-C2' -138.9(2), C1'-C2' 1.393(3), C1'-C2'-H2' 120.3(2), C1'-C2'-H2'-S1' -120.2(2), S1-H11'' 2.85, C11''-H11'' 0.93, Si1-S1-H11''-C11'' 22.8(3), C12''-C11'' 1.385(3), C12''-C11''-H11'' 120.2(2), C12''-C11''-H11''-S1 -1.7(4). Symmetrieoperationen: I: 1/2+x, y, 1/2-z; II: 1-x, -1/2+y, 1/2-z.

$Ph_4P[SeSiMe_3]$

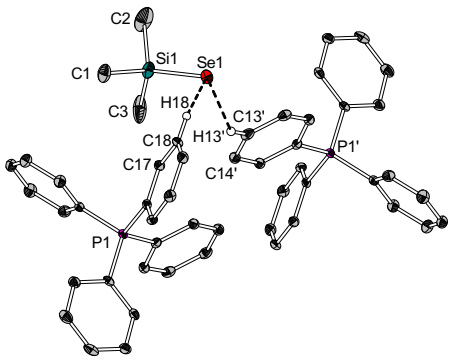

Kristallographisch bestimmte Molekülstruktur von $Ph_4P[SeSiMe_3]$. Der Übersicht halber halber sind nur H-Atome in Wasserstoffbrückenbindungen gezeigt. Ausgewählte Bindungslängen (in Å) und -winkel (in °): Se1-Si1 2.2102(9), Si1-C1 1.882(2), Si1-C2 1.880(3), Si1-C3 1.880(3), Se1-Si1-C1 113.75(7), Se1-Si1-C2 111.0(1), Se1-Si1-C3 112.9(8), C1-Si1-C2 111.01(1), C2-Si1-C3 108.0(2), C3-Si1-C1 106.0(1), Se1-H13' 2.93, C13'-H13' 0.95, Se1-H13'-C13', 144.9(1), Si1-Se1-H13'-C13' 108.6(2), C14'-C13' 1.389(3), C14'-C13'-H13' 119.9, C14'-C13'-H13'-Se1 -147,5(1), Se1-H18 2.92, Se1-H18-C18 132,4(1), Si1-Se1-H18-C18 70.1(1), C17-C18 1.385(2), C17-C18-H18 120.0, C17-C18-H18-Se1 -21.6(2). Symmetrieoperationen: I: 2-x, 1-y, 1-z.

$Ph_4P[TeSiMe_3]$

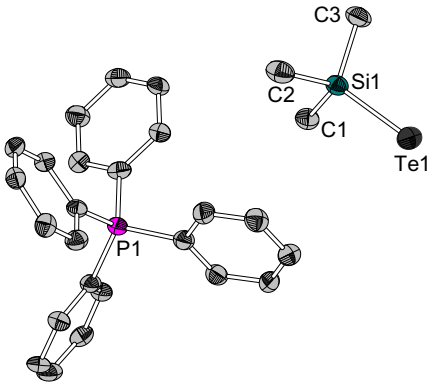

Kristallographisch bestimmte Molekülstruktur von $Ph_4P[SSiMe_3]$. Der Übersicht halber halber sind H-Atome nicht gezeigt. Ausgewählte Bindungslängen (in Å) und -winkel (in °): Te1-Si1 2.447(2), Si1-C1 1.884(9), Si1-C2 1.89(1), Si1-C3 1.89(1), Te1-Si1-C1 111.7(3), Te1-Si1-C2 113.8(3), Te1-Si1-C3 113.8(3), C1-Si1-C2 106.9(4), C2-Si1-C3 104.5(4), C3-Si1-C1 105.5(4).

6.7 Weitere Strukturen

6.7.1 $Ph_4P[Cp_3LaSSiMe_3]$ (E = S, Se, Te)

	$Ph_4P[Cp_3LaSSiMe_3]$	**$Ph_4P[Cp_3LaSeSiMe_3]$**	**$Ph_4P[Cp_3LaTeSiMe_3]$**
Identification code	jghw14_0m_a_Ph4PCp3LaSSiMe3	jg360loesen_Ph4PCp3LaSeSiMe3	jg359la_0m_a_Ph4PCp3LaTeSiMe3
Empirical formula	$C_{42}H_{44}LaPSSi$	$C_{42}H_{44}LaPSeSi$	$C_{84}H_{88}La_2P_2Si_2Te_2$
Formula weight	778.80	825.70	1748.68
Temperature/K	100(2)	100(2)	100(2)
Crystal system	monoclinic	monoclinic	monoclinic
Space group	$P2_1/c$	$P2_1/n$	$P2_1$
a/Å	14.343(3)	14.1259(9)	9.803(2)
b/Å	15.449(3)	17.0307(9)	14.101(3)
c/Å	16.998(3)	17.0151(11)	13.880(3)
α/°	90.00(3)	90	90
β/°	100.44(3)	111.185(5)	102.94(3)
γ/°	90.00(3)	90	90
Volume/Å^3	3704.3(13)	3816.8(4)	1869.8(7)
Z	4	4	1
ρ_{calc}g/cm^3	1.396	1.437	1.553
μ/mm^{-1}	1.313	10.633	2.010
F(000)	1592.0	1664.0	868.0
Crystal size/mm^3	0.323 × 0.211 × 0.154	0.192 × 0.146 × 0.078	0.396 × 0.166 × 0.128
Radiation	MoKα (λ = 0.71073)	CuKα (λ = 1.54178)	MoKα (λ = 0.71073)
2Θ range for data collection/°	4.322 to 51.506	7.004 to 133.186	4.172 to 51.518
Index ranges	$-17 \le h \le 17$, $-18 \le k \le 18$, $-20 \le l \le 20$	$-16 \le h \le 16$, $-18 \le k \le 20$, $-20 \le l \le 16$	$-11 \le h \le 11$, $-17 \le k \le 17$, $-16 \le l \le 16$
Reflections collected	98887	35700	54772
Independent reflections	7056 [R_{int} = 0.0503, R_{sigma} = 0.0191]	6749 [R_{int} = 0.0480, R_{sigma} = 0.0356]	7109 [R_{int} = 0.0320, R_{sigma} = 0.0211]
Data/restraints/parameters	7056/0/418	6749/0/418	7109/1/418
Goodness-of-fit on F^2	1.064	0.958	1.070
Final R indexes [I>=2σ (I)]	R_1 = 0.0208, wR_2 = 0.0449	R_1 = 0.0328, wR_2 = 0.0807	R_1 = 0.0150, wR_2 = 0.0352
Final R indexes [all data]	R_1 = 0.0273, wR_2 = 0.0466	R_1 = 0.0382, wR_2 = 0.0821	R_1 = 0.0158, wR_2 = 0.0355
Largest diff. peak/hole / e Å^{-3}	0.37/-0.43	0.98/-0.56	0.56/-0.53

6.7.2 DMPyr$_2$[S(CuPh)$_2$]

	DMPyr$_2$[(PhCu)$_2$S]
Identification code	jg389loesen_DMPyr2Ph2Cu2S
Empirical formula	$C_{24}H_{38}Cu_2N_2S$
Formula weight	513.70
Temperature/K	293(2)
Crystal system	orthorhombic
Space group	$P2_12_12_1$
a/Å	10.6864(2)
b/Å	11.8364(2)
c/Å	19.5298(5)
α/°	90
β/°	90
γ/°	90
Volume/Å^3	2470.29(9)
Z	4
ρ_{calc}g/cm^3	1.381
μ/mm^{-1}	2.986
F(000)	1080.0
Crystal size/mm^3	0.138 × 0.190 × 0.192
Radiation	CuKα (λ = 1.54178)
2Θ range for data collection/°	9.056 to 151.886
Index ranges	$-8 \leq h \leq 13$, $-14 \leq k \leq 14$, $-24 \leq l \leq 22$
Reflections collected	23703
Independent reflections	5066 [R_{int} = 0.0358, R_{sigma} = 0.0303]
Data/restraints/parameters	5066/0/266
Goodness-of-fit on F^2	1.068
Final R indexes [I>=2σ (I)]	R_1 = 0.0390, wR_2 = 0.1008
Final R indexes [all data]	R_1 = 0.0434, wR_2 = 0.1025
Largest diff. peak/hole / e Å^{-3}	0.34/-0.43
Flack parameter	-0.017(15)

6.7.3 [IMes-Sn(SSiMe$_3$)$_2$]

	[IMes-Sn(SSiMe$_3$)$_2$]
Identification code	jg325_0m_a_NHCSnSSiMe3_2
Empirical formula	$C_{27}H_{42}N_2S_2Si_2Sn$
Formula weight	633.61
Temperature/K	100(2)
Crystal system	monoclinic
Space group	$P2_1/n$
a/Å	10.0486(13)
b/Å	14.3467(14)
c/Å	23.364(3)
α/°	90
β/°	95.863(4)
γ/°	90
Volume/Å^3	3350.6(7)
Z	4
ρ_{calc}g/cm^3	1.256
μ/mm^{-1}	0.975
F(000)	1312.0
Crystal size/mm^3	1.393 × 0.201 × 0.199
Radiation	MoKα (λ = 0.71073)
2Θ range for data collection/°	4.51 to 50.048
Index ranges	$-11 \le h \le 11$, $-17 \le k \le 17$, $-27 \le l \le 27$
Reflections collected	72237
Independent reflections	5907 [R_{int} = 0.0356, R_{sigma} = 0.0138]
Data/restraints/parameters	5907/0/319
Goodness-of-fit on F^2	1.057
Final R indexes [I>=2σ (I)]	R_1 = 0.0196, wR_2 = 0.0441
Final R indexes [all data]	R_1 = 0.0235, wR_2 = 0.0457
Largest diff. peak/hole / e Å^{-3}	0.56/-0.34

6.7.4 Cat[SCS$_2$tBu] (Cat = MMIm, Ph$_3$PMe, Ph$_4$P)

	MMIm[SCS$_2$*t*Bu]	**Ph$_3$PMe [SCS$_2$*t*Bu]**	**Ph$_4$P[SCS$_2$*t*Bu]**
Identification code	jghw17loesen	jgvtnh09loesen	jgvtnh11loesen
Empirical formula	$C_{10}H_{18}N_2S_3$	$C_{23}H_{27}PS_3$	$C_{29}H_{29}PS_3$
Formula weight	262.44	442.60	504.67
Temperature/K	100(2)	100(2)	100(2)
Crystal system	triclinic	monoclinic	monoclinic
Space group	P-1	$P2_1$	$P2_1/c$
a/Å	8.4971(4)	9.2099(4)	9.8409(2)
b/Å	8.6437(4)	14.1370(5)	9.30580(10)
c/Å	10.6184(5)	9.5524(4)	28.8281(5)
α/°	74.738(4)	90	90
β/°	89.219(4)	113.948(3)	95.646(2)
γ/°	63.013(4)	90	90
Volume/Å^3	665.35(6)	1136.66(8)	2627.20(8)
Z	2	2	4
ρ_{calc}g/cm^3	1.310	1.293	1.276
μ/mm^{-1}	4.860	3.689	3.261
F(000)	280.0	468.0	1064.0
Crystal size/mm^3	0.207 × 0.154 × 0.104	0.309 × 0.252 × 0.220	0.301 × 0.234 × 0.187
Radiation	CuKα (λ = 1.54178)	CuKα (λ = 1.54178)	CuKα (λ = 1.54178)
2Θ range for data collection/°	8.698 to 132.97	10.132 to 151.876	9.03 to 127.372
Index ranges	$-10 \le h \le 9$, $-10 \le k \le 4$, $-12 \le l \le 12$	$-11 \le h \le 11$, $-17 \le k \le 8$, $-11 \le l \le 12$	$-7 \le h \le 11$, $-10 \le k \le 10$, $-33 \le l \le 33$
Reflections collected	10914	10792	21331
Independent reflections	2325 [R_{int} = 0.0395, R_{sigma} = 0.0238]	3197 [R_{int} = 0.0238, R_{sigma} = 0.0172]	4324 [R_{int} = 0.0341, R_{sigma} = 0.0188]
Data/restraints/parameters	2325/0/141	3197/1/258	4324/0/302
Goodness-of-fit on F^2	1.087	1.068	1.100
Final R indexes [I>=2σ (I)]	R_1 = 0.0515, wR_2 = 0.1469	R_1 = 0.0266, wR_2 = 0.0722	R_1 = 0.0377, wR_2 = 0.1067
Final R indexes [all data]	R_1 = 0.0546, wR_2 = 0.1492	R_1 = 0.0270, wR_2 = 0.0724	R_1 = 0.0394, wR_2 = 0.1080
Largest diff. peak/hole / e Å^{-3}	0.70/-0.61	0.23/-0.32	0.21/-0.31
Flack parameter	x	0.09(2)	x

6.7.5 [IMes$_2$CuS(H)]

	[(IMes)$_2$CuSH]
Identification code	jg320a_0m_a
Empirical formula	$C_{46}H_{59}CuN_4OS$
Formula weight	779.57
Temperature/K	100(2)
Crystal system	orthorhombic
Space group	Pccn
a/Å	18.010(5)
b/Å	32.999(9)
c/Å	14.570(5)
α/°	90
β/°	90
γ/°	90
Volume/Å^3	8659(4)
Z	8
ρ_{calc}g/cm^3	1.196
μ/mm^{-1}	0.590
F(000)	3328.0
Crystal size/mm^3	0.456 × 0.240 × 0.166
Radiation	MoKα (λ = 0.71073)
2Θ range for data collection/°	4.34 to 50.052
Index ranges	-21 ≤ h ≤ 18, -39 ≤ k ≤ 35, -17 ≤ l ≤ 17
Reflections collected	110324
Independent reflections	7657 [R_{int} = 0.0592, R_{sigma} = 0.0257]
Data/restraints/parameters	7657/82/545
Goodness-of-fit on F^2	1.085
Final R indexes [I>=2σ (I)]	R_1 = 0.0433, wR_2 = 0.1010
Final R indexes [all data]	R_1 = 0.0561, wR_2 = 0.1069
Largest diff. peak/hole / e Å^{-3}	0.43/-0.34

7 Anhang: Volltexte der diskutierten Manuskripte

Im Folgenden befinden sich die sechs im Zuge dieser Arbeit besprochenen Manuskripte in Originalform und die entsprechenden Supporting Information in Graustufen. Die Erlaubnis zur gedruckten und elektronischen Veröffentlichung der bereits veröffentlichten Arbeiten 1 und 2 wurde eingeholt. Die Arbeiten 3 und 4 wurden kürzlich eingereicht und sind im Templat der jeweiligen Zeitschrift wiedergegeben. Die Erlaubnis zur Reproduktion dieses Entwurfes wurde eingeholt. Die übrigen Manuskripte 5 und 6 wurden noch nicht eingereicht und sind in den Templaten geeigneter Zeitschriften eingebunden.

1.) „Systematic study on anion–cation interactions via doubly ionic H-bonds in 1,3-dimethylimidazolium salts comprising chalcogenolate anions MMIm[ER] (E = S, Se; R = H, *t*Bu, $SiMe_3$)“ reproduced from „J. Guschlbauer, T. Vollgraff, J. Sundermeyer**;** *Dalton Trans.*, **2019**, 48, 10971-10978“ with permission from the Royal Society of Chemistry.

2.) „Homoleptic Group 13 Metalates $[M(ESiMe_3)_4]^-$ (M = Ga, In; E = S, Se): Metastable Precursors for Low Temperature Syntheses of Chalcogenide Based Materials“ reprinted with permission from „J. Guschlbauer, T. Vollgraff, J. Sundermeyer; *Inorg. Chem.,* **2019**, DOI: 10.1021/acs.inorgchem.9b02453.“ Copyright 2019 American Chemical Society.

3.) J. Guschlbauer, T. Vollgraff, J. Sundermeyer; „Homoleptic Trimethylsilylchalcogenolato Zinkates $[Zn(ESiMe_3)_3]^-$ and Stannanides $[Sn(ESiMe_3)_3]^-$ (E = S, Se): Precursors in Solution Based Low-Temperature Cu_2ZnSnS_4 (CZTS) Synthesis“, *Submitted (24th October 2019).*

4.) J. Guschlbauer, T. Vollgraff, X. Xie, F. Weigend, J. Sundermeyer; „A Series of Homoleptic Linear Coinage Metal Trimethylsilylchalcogenolate Complexes $Cat[Me_3E\text{-}M\text{-}ESiMe_3]$ (M = Cu, Ag, Au; E = S, Se), *Submitted (14th November 2019).*

5.) J. Guschlbauer, L. H. Finger, T. Vollgraff, K. Harms, J. Sundermeyer; „Dimethylpyrrolidinium Chalcogenido-Dimethylgallates and -indates $DMPyr_2[Me_2M(\mu_2\text{-}E)]_2$ (M = Ga, In; E = S, Se): Their use in the Synthesis of Higher or Lower Order Chalcogenidoindates“*, in preparation.*

6.) J. Guschlbauer, T. Vollgraff, A. Fetoh, J. Sundermeyer; „Organic Methylcarbonate Salts Comprising Non-methylated Onium Cations $Cat[OCO_2Me]$ (Cat = Ph_4P^+, PPN^+, TBA^+) via Fluoride-Induced Demethylation of Dimethylcarbonate”, *in preparation.*

Dalton Trans., **2019**, 48, 10971-10978.

Systematic study on anion–cation interactions *via* doubly ionic H-bonds in 1,3-dimethylimidazolium salts comprising chalcogenolate anions MMIm[ER] (E = S, Se; R = H, *t*Bu, $SiMe_3$)

Jannick Guschlbauer, Tobias Vollgraff, Jörg Sundermeyer

Dalton Transactions

PAPER

View Article Online
View Journal

Cite this: DOI: 10.1039/c9dt01586h

Systematic study on anion–cation interactions *via* doubly ionic H-bonds in 1,3-dimethylimidazolium salts comprising chalcogenolate anions MMIm [ER] (E = S, Se; R = H, *t*Bu, $SiMe_3$)†‡

Jannick Guschlbauer, Tobias Vollgraff and Jörg Sundermeyer *

Received 15th April 2019,
Accepted 7th June 2019

DOI: 10.1039/c9dt01586h

rsc.li/dalton

We present convenient syntheses of so far inaccessible, crystalline and highly pure 1,3-dialkylimidazolium salts with extremely nucleophilic thiolate and selenolate anions $[ER]^-$ (R = H, *t*Bu, $SiMe_3$). While non existent for E = O, the title compounds exist as slightly less basic E = S and Se homologues. The anion cation H-bond interactions in the crystalline state have been studied systematically in six related ionic compounds of varying anion basicity and steric bulk, namely MMIm [SH] (**1**), MMIm [S*t*Bu] (**2**), and MMIm [$SSiMe_3$] (**3**), as well as MMIm [SeH] (**4**), MMIm [Se*t*Bu] (**5**) and MMIm [$SeSiMe_3$] (**6**). The chalcogenolate title compounds **3**, **5**, and **6** are prepared by the newly introduced method of desilylation of Me_3Si-ER (E = S, Se) by the super-nucleophile MMIm [S*t*Bu] (**2**), which is easily accessible *via* deprotonation of HS*t*Bu with *in situ* generated NHC 1,3-dimethylimidazolidin-2-ylidene. Focus is put on the role of the most acidic imidazolium proton C2–H as structural director and as ^{1}H NMR shift indicator. These salts show an unusually high volatility and tendency to sublime under vacuum without irreversible decay.

Introduction

Organic salts containing an easily modifiable cation and a highly nucleophilic unsolvated chalcogenolate anion, such as [EH], [$ESiMe_3$] or [E*t*Bu] (E = S, Se, Te), constitute a growing class of compounds with no existing oxygen homologues (E = O).[1–4] The applicability of organic hydrosulfide based ionic liquids (ILs) as fluxes could be established in metal mixed chalcogenide cluster synthesis,[5] and in the formation of polychalcogenide redox materials.[2] The synthetic access to these chalcogenide based organic salts and ionic liquids (ILs) *via* methylcabonates avoids their contamination with halide, metal ions and water.[1,2] Typically, the methylcarbonate anion serves as deprotonation[2] or desilylation[1] agent towards H_2E or $E(SiMe_3)_2$ (E = S, Se, Te) respectively (Scheme 1, top). While many methylcarbonate salts are simply synthesized *via* solvothermal methylation of amines, phosphines or guanidines with dimethylcarbonate,[1,2,6,7] restrictions arise when highly CH acidic protons are present in the organic cation, a common problem in 1,3-dialkylimidazolium cations (Scheme 1, bottom).[8]

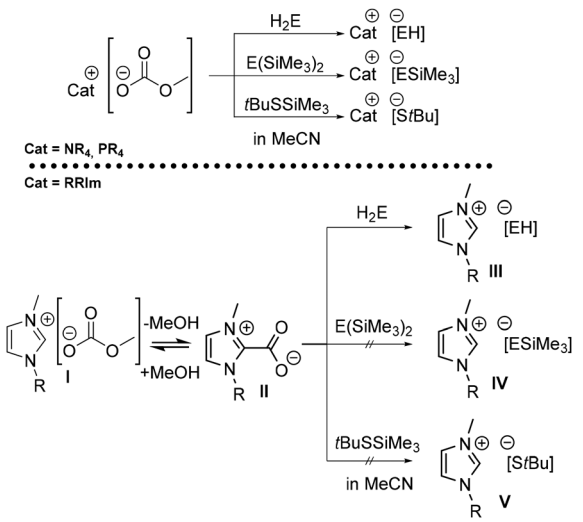

Scheme 1 Top: Synthesis of chalcogenide based organic salts with Cat = $MeNR_3$ or $MePR_3$ (R = alkyl; E = S, Se, Te).[1,2,9] Bottom: In sharp contrast, 1,3-dialkylimidazolium methylcarbonate **I** is converted to rather stable adduct NHC-CO_2 **II** by removal of anion stabilising methanol.[2,8,9] This prevents subsequent reactions with silylated chalcogen precursors.

Fachbereich Chemie and Materials Science Center, Philipps-Universität Marburg, Hans-Meerwein-Straße 4, 35043 Marburg, Germany.
E-mail: JSU@staff.uni-marburg.de

†Dedicated to Professor Hansjörg Grützmacher on the occasion of his 60th birthday.

‡Electronic supplementary information (ESI) available: NMR-spectra, DSC-TGA measurements, single-crystal X-Ray structures, supporting experimental word, illustrative representations of ion pair structures, discussion on literature known structures of similar compounds. CCDC 1908993–1908998. For ESI and crystallographic data in CIF or other electronic format see DOI: 10.1039/c9dt01586h

The methylcarbonate anion present in such highly concentrated methanolic solution of 1,3-dialkylimidazolium methylcarbonates **I** is sufficiently basic to preferably deprotonate the C2-attached proton, in particular when the anion stabilizing solvent methanol is removed.[8] *In situ* formed NHC is then trapped by CO_2 and the adduct NHC-CO_2 **II** is formed (Scheme 1, bottom).[8]

The rather stable adduct NHC-CO_2 **II** is basic enough to react with H_2E in methanol under decarboxylation,[2] it is however not nucleophilic or basic enough to form the chalcogenolates **IV** or **V** *via* desilylation or deprotonation in the presence or absence of methanol.[9] As a consequence, the key intermediate of this paper, MMIm [S*t*Bu] (**2**) and related 1,3-RR′Im [S*t*Bu] salts remained inaccessible up to date. Competing imidazole ring carboxylation by methylcarbonate made it impossible, to generate 1,3-imidazolium salt EMIm [$SSiMe_3$][10] as a pure compound so far. However, when imidazole C2-position was protected by a methyl group, fairly pure acetonitrile soluble 1-ethyl-2,3-dimethylimidazolium (EMMIm) methylcarbonate EMMIm [OCO_2Me] could be isolated in the absence of solvating MeOH and used for the syntheses of fairly pure EMMIm [$SSiMe_3$].[9] In order to avoid cation carboxylation side reactions *in situ* generation of very basic N-heterocyclic olefins (NHO) from 1,3-dialkyl-2-methylimidazolium salts or of N-heterocyclic carbenes (NHC) from 1,3-dialkylimidazolium salts offers an alternative strategy to form highly pure organic salts *via* deprotonation of even weak acids.[9,11,12]

The physical properties of imidazolium salts and ionic liquids are mainly determined by their anion cation interactions and lattice energy. Main influencers are anion cation coulombic and dipole interactions, π interactions[13] or dispersion interactions[14] and the sum and strength of H-bonds[13,15–17] between the H-bond donor, the CH-acidic imidazolium cation, and the H-bond acceptor, the anion. Doubly ionic H-bonds ($[Y–H]^+\cdots[X]^-$) arise between interacting H-bond acceptors ($[X]^-$) and H-bond donors ($[Y–H]^+$) located at complementarily charged ions.[15,17] Thereby the electrostatic interactions support the noncovalent bonding contributions affecting the physical properties of the ionic compounds.[13,15,17,18] A detailed discussion on noncovalent interactions within ionic systems can be found elsewhere.[4,13,15,17–19]

We applied three complementary techniques, XRD analyses, NMR spectroscopy and thermal analyses, in order to study the effects of sterics, basicity and H-bond strengths between imidazolium cations and anions on the properties of these salts. A very suitable approach is to study their solid-state lattice structures in a systematic manner. The crystalline lattice resembles a state close to the energetic minimum. 1,3-Dialkylimidazolium salts with $[OH]^-$, [*O*-alkyl]$^-$, and $[OSiMe_3]^-$ anions have never been characterized for a simple reason: their most acidic C2–H bond gets fully deprotonated by these very basic unsolvated anions.[20] In this study, we therefore choose the slightly less basic anions $[SH]^-$, [S-CMe_3]$^-$, [S-$SiMe_3$]$^-$, and their selenium homologues to systematically investigate their anion cation interactions to 1,3-dimethylimidazolium cations. Another point of interest is the surprising volatility of certain chalcogenide based imidazolium salts, like EMIm [SH], that could be traced back on the formation of a gas phase ion pair, a charge transfer π complex arising from interaction of the HOMO located at the sulfur atom and the LUMO at the aromatic imidazolium core.[4]

Results and discussion

Syntheses of the title compounds

The key compound MMIm [S*t*Bu] (**2**) of this report is quantitatively precipitating by deprotonation of HS*t*Bu with freshly prepared 1,3-dimethylimidazolidin-2-ylidene (MMIm-NHC) (Scheme 2). After filtration MMIm [S*t*Bu] (**2**) is obtained as colourless powder, washed with diethyl ether and then dried *in vacuo*.

This highly nucleophilic reagent MMIm [S*t*Bu] (**2**) can be used to prepare MMIm [Se*t*Bu] (**5**) by performing a quantitative desilylation of Me_3Si-Se*t*Bu in acetonitrile (Scheme 2, top). This strategy uses differences in the hardness and basicity of the negatively charged electron donors [S*t*Bu]$^-$ *versus* [Se*t*Bu]$^-$ towards the trimethylsilyl group, hard in its Lewis acidic character. The obtained colourless solid MMIm [Se*t*Bu] (**5**) was sublimed at 100 °C and 1×10^{-3} mbar for purification.

The same strategy is successful in the synthesis of MMIm [$SSiMe_3$] (**3**) and MMIm [$SeSiMe_3$] (**6**). The higher nucleophilicity, higher basicity and harder character of the anion [S*t*Bu]$^-$ *versus* [$SSiMe_3$]$^-$ or [$SeSiMe_3$]$^-$ leads to selective desilylation of $S(SiMe_3)_2$ and $Se(SiMe_3)_2$ (Scheme 2). This reaction can be performed simply by adding $E(SiMe_3)_2$ to a cooled suspension of MMIm [S*t*Bu] (**2**) in tetrahydrofuran. The suspension rapidly leads to a clear solution after a few minutes of stirring at room temperature. After removing all volatiles *in vacuo*, the target compounds MMIm [$SSiMe_3$] (**3**) and MMIm [$SeSiMe_3$] (**6**) are obtained as colourless powders. This synthesis strategy can

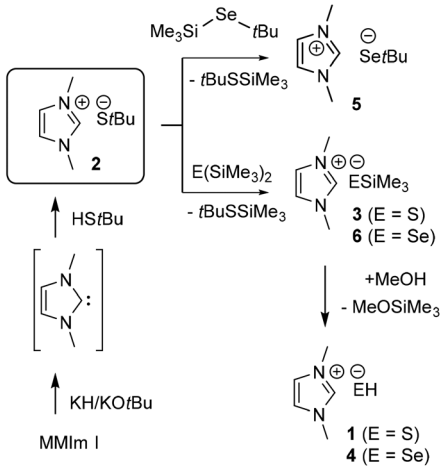

Scheme 2 Preparation of MMIm [S*t*Bu] (**2**) by deprotonation of HS*t*Bu with freshly prepared MMIm-NHC and its use in the preparation of MMIm [Se*t*Bu] (**2**), MMIm [$SSiMe_3$] (**3**) and MMIm [$SeSiMe_3$] (**6**) by desilylation of $Me_3SiSetBu$ and $E(SiMe_3)_2$ (E = S, Se).

also be transferred to prepare the tellurium homologue MMIm [TeSiMe$_3$] (**7**), as described in the ESI.‡ The conversion of trimethylsilylchalcogenolates MMIm [SSiMe$_3$] (**3**) and MMIm [SeSiMe$_3$] (**6**) into the hydrochalcogenides MMIm [SH] (**1**) and MMIm [SeH] (**4**) is simply managed by methanolysis.[1,2]

The target compounds are obtained when all volatiles are removed *in vacuo*. 1,3-Imidazolium hydrochalcogenides are also accessible by metathetic sodium chloride elimination in acetonitrile,[3] or deprotonation of H_2E (E = S, Se) with dialkylimidazolium methylcarbonates in MeOH.[2,4,9]

Crystallographically determined structures of the title compounds

Symmetric 1,3-dimethylimidazolium cations were chosen in order to provide a good chance for crystalline products throughout this series of compounds. Single crystals suitable for XRD analysis for the *tert*-butylchalcogenolates MMIm [E*t*Bu] **2** (E = S, Fig. 1) and **5** (E = Se, Fig. 2) were obtained by diffusion of pentane *via* the gas phase into a saturated solution of the target compound in a mixture of MeCN/THF. Single crystals suitable for X-ray diffraction of trimethylsilylchalcogenolates MMIm [ESiMe$_3$] **3** (E = S, Fig. 3) and **6** (E = Se, Fig. 4) were grown by slow gas phase diffusion of pentane into a diluted solution of the target compound in THF. Finally, single crystals of hydrochalcogenides MMIm [EH] **1** (E = S, Fig. 5) and **4** (E = Se, Fig. 6) developed by carefully layering diethyl ether over the same volume of a saturated solution of the target compound in a 1 : 1 MeCN/THF solution at 4 °C. While **5** crystallizes in the triclinic space group $P\bar{1}$ with $Z = 2$, the other five compounds crystallize in the monoclinic space group $P2_1/n$ with $Z = 4$ (MMIm [Se*t*Bu] (**5**) was solved as non-merohedral twin). Table 1 lists observed C–H···E bonds of the

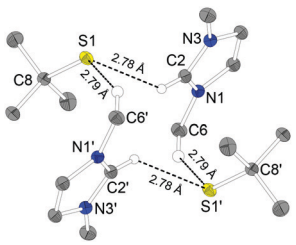

Fig. 1 Molecular structure of the hydrogen bond dimer of MMIm [S*t*Bu] (**2**). Each [S*t*Bu]$^-$ anion is noncovalently bonded to two cations by two H-bonds. Ellipsoids are shown at the 50% probability level. Only protons active in H-bonds are shown (S1–C8 1.845(1) Å). Symmetry operation: I: 1 – *x*, 1 – *y*, 1 – *z*.

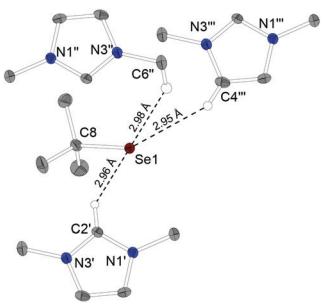

Fig. 2 Molecular structure of MMIm [Se*t*Bu] (**5**). Each [Se*t*Bu]$^-$ anion is bonded to three cations; three H-bond modes are observed. Ellipsoids are shown at the 50% level. Only protons active in H-bonds are shown (Se1–C8 1.994(4) Å). Symmetry operations: I: 1 – *x*, 1 – *y*, 1 – *z*; II: 1 + *x*, 1 + *y*, *z*; III: 1 – *x*, 1 + *y*, –*z*.

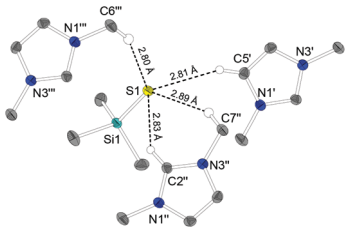

Fig. 3 Molecular structure of MMIm [SSiMe$_3$] (**3**). One [SSiMe$_3$]$^-$ anion is bonded to three cations by four H-bonds. Ellipsoids are shown at the 50% level. Only protons active in H-bonds are shown (S1–Si1 2.0747(8) Å). Symmetry operations: I: –*x*, 1 – *y*, 1 – *z*; II: 1/2 – *x*, 1/2 + *y*, 3/2 – *z*; III: –1/2 + *x*, 1/2 – *y*, 1/2 + *z*.

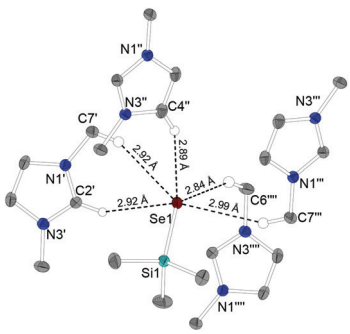

Fig. 4 Molecular structure of MMIm [SeSiMe$_3$] (**6**). One [SeSiMe$_3$]$^-$ anion is bonded to four cations by three H-bonds. Ellipsoids are shown at the 50% level. Only protons active in H-bonds are shown (Se1–Si1 2.2117(8) Å). Symmetry operations: I: 3/2 – *x*, 1/2 + *y*, 1/2 – *z*; II: 2 – *x*, 1 – *y*, 1 – *z*; III: 1 + *x*, *y*, *z*; IIII: 1/2 + *x*, 1/2 – *y*, –1/2 + *z*.

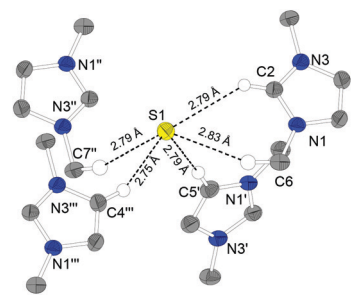

Fig. 5 Molecular structure of MMIm [SH] (**1**). One [SH]$^-$ anion is bonded to four cations by five H-bonds. Ellipsoids are shown at the 50% level (only protons active in H-bonds are depicted, note that the sulfur attached proton is not located *via* Fourier analysis and not shown. Symmetry operations: I: 1/2 – *x*, –1/2 + *y*, 1/2 – *z*; II: 1 – *x*, –*y*, 1 – *z*; III: –1 + *x*, *y*, *z*.

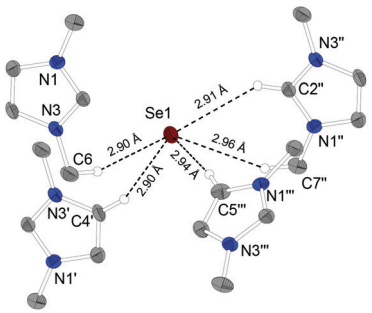

Fig. 6 Molecular structure of MMIm [SeH] (**4**). One $[SeH]^-$ anion is bonded to four cations by five H-bonds. Ellipsoids are shown in 50% level (only protons active in H-bonds are depicted, note that the selenium attached proton is not located *via* Fourier analysis and not shown). Symmetry operations: I: $-x, -y, 1-z$, II: $1-x, -y, 1-z$; III: $1/2+x, 1/2-y, 1/2+z$.

Table 1 H-Bonds of the title compounds **1–6**. Bonding and dihedral angles regarding the H-bond are shown (distances in Å, angles in °). Chelate-like bonding modes are marked with asterisk (*). Refer to the corresponding figures for symmetry operations

Compound/H-bond (···)	*d*(H/C···E) [Å]	C–H···E/N–C–H···E [°]
MMIm [SH] (1)		
*(N1)–C2–H2···S1	2.79/3.572(4)	139.9(2)/39.4(5)
(N3‴)–C4‴–H4‴···S1	2.75/3.626(4)	153.5(2)/16.4(7)
(N3″)–C7″–H7″···S1	2.79/3.733(4)	160.5(2)/−11.5(8)
(N1′)–C5′–H5′···S1	2.79/3.735(3)	173.8(2)/116(2)
*(N1)–C6–H6···S1	2.83/3.745(3)	155.3(2)/−0.2(6)
MMIm [SeH] (4)		
*(N1″)–C2″–H2″···Se1	2.91/3.690(5)	142.2(3)/−38.2(7)
(N3′)–C4′–H4′···Se1	2.90/3.766(5)	155.2(3)/−20(1)
(N3)–C6–H6···Se1	2.90/3.826(4)	161.5(2)/−25(1)
(N1‴)–C5‴–H5‴···Se1	2.94/3.855(4)	170.0(3)/−130(1)
*(N1″)–C7″–H7″···Se1	2.96/3.856(4)	155.6(3)/−23.3(8)
MMIm [S*t*Bu] (2)		
(N1)–C2–H2···S1	2.78/3.541(1)	137.3(7)/132.0(1)
(N1′)–C6′–H6′···S1	2.79/3.633(2)	144.29(7)/−13.2(2)
MMIm [Se*t*Bu] (5)		
(N3′)–C2′–H2′···Se1	2.96/3.692(4)	137(2)/−132(3)
(N3″)–C6″–H6″···Se1	2.98/3.790(4)	143(2)/16(5)
(N3‴)–C4‴–H4‴···Se1	2.95/3.795(4)	151(2)/−9(7)
MMIm [$SSiMe_3$] (3)		
*(N1″)–C2″–H2″···S1	2.83/3.569(2)	137.36(9)/−135.1(1)
(N1′)–C5′–H5′···S1	2.81/3.678(2)	136.8(9)/−15.1(3)
(N1‴)–C6‴–H6‴···S1	2.80/3.682(2)	152.82(9)/−9.3(3)
*(N3″)–C7″–H7″···S1	2.79/3.770(2)	153.74(9)/−4.5(3)
MMIm [$SeSiMe_3$] (6)		
*(N3′)–C2′–H2′···Se1	2.92/3.684(2)	138.25(9)/−137.5(1)
(N3⁗)–C6⁗–H6⁗···Se1	2.84/3.734(2)	152.3(1)/7.1(3)
(N3″)–C4″–H4″···Se1	2.89/3.771(2)	154.10(9)/19.6(3)
*(N1′)–C7′–H7′···Se1	2.92/3.839(2)	155.79(9)/0.6(3)
(N1‴)–C7‴–H7‴···Se1	2.99/3.874(2)	151.23(9)/−14.7(3)

title compounds in the order of increasing C2–E distances in each compound. As the C–H protons' positions are not obtained by explicit refinement of the crystallographic data, the calculated positions are used for the following discussion. H-Bonds were identified by S···H–C or Se···H–C bond lengths that fall below 2.9 Å or 3.0 Å respectively, the sum of these atoms' van der Waal radii.[21] In the ESI‡ crystallographic details and further bond distances and angles are provided.

All title compounds show H-bonding modes that form up a three-dimensional H-bond grid throughout the crystal lattice, except MMIm [S*t*Bu] (**2**) which arranges as a zero-dimensional H-bond dimer. A comparative analysis of bond distances and angles listed in Table 1 reveals that the shortest crystallographically determined distance between the chalcogen atom E and a carbon atom of the imidazolium cation is without any exception the C2–E distance. Interestingly, the distance between the corresponding calculated ideal C2 proton position and the chalcogen atom E does not follow this trend, because the protons are located out of this C2–E axis. The ideal C2 proton positions of the cations are calculated in the aromatic imidazolium plane. Therefore, a non-linear arrangement of C, H, and E with smallest C–H–E angles correlate with long H–E distances (Fig. 7). For all title compounds except for MMIm [$SSiMe_3$] (**3**) the C2–H–E angle is the smallest of all identified C–H–E angles connected to all the identified H-bonds. This explains the surprising trends observed for the C–E and connected H–E distances. In **3** as exception the smallest C–H–E angle 136.8° is observed between the anion $[SSiMe_3]^-$ and the C5-attached proton. These C2–H–E angles range from 137° for **2**, **3**, and **5** to 142° for **4**. The largest C–H–E angle is 173.8° is found for the interaction between the $[SH]^-$ anion and the C5-attached proton in **1**. The comparable interaction for the selenium homologue **2** between $[SeH]^-$ and H5 also shows the largest angle connected to this ion pair. For the $[ESiMe_3]^-$ anions **3** and **6** the largest C–H–E angles 153.7° and 155.8° belong to interactions with an aliphatic C7-attached proton of an N–Me group engaged in a C2–H/C7–H chelate ring towards the chalcogen atom. Interestingly this kind of chelating bonding mode can be observed for all title compounds except for the sterically most demanding anions $[EtBu]^-$ in **2** and **5**. The C2–S distance in **2** (3.541 Å) represents the shortest doubly ionic H-bond of all six title compounds. As expected corresponding C2–Se in **5** (3.692 Å) is larger. The sterically less hindered anions in MMIm [SeH] (**4**) (3.690 Å) and MMIm [$SeSiMe_3$] (**6**) (3.684 Å) display shorter Se–C2 contacts. These trends in the deviation of aromatic C2–H, C4–H and C5–H bond vectors from C2–E, C4–E and C5–E vectors (Fig. 7) might be explained by a charge transfer contribution of the chalcogenide HOMO into the imidazolium π* LUMO[4] as add-on to the doubly ionic H-bond pattern of non-covalent interactions:

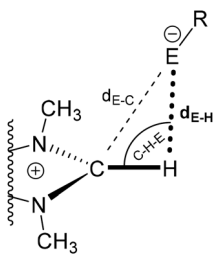

Fig. 7 Correlation of crystallographically determined distances d_{E-C} and d_{H-E} based on calculated C–H positions and C–H–E angles of the C2–H–E interaction: small d_{E-C} and small angles C–H–E correlate with longer distances d_{H-E}.

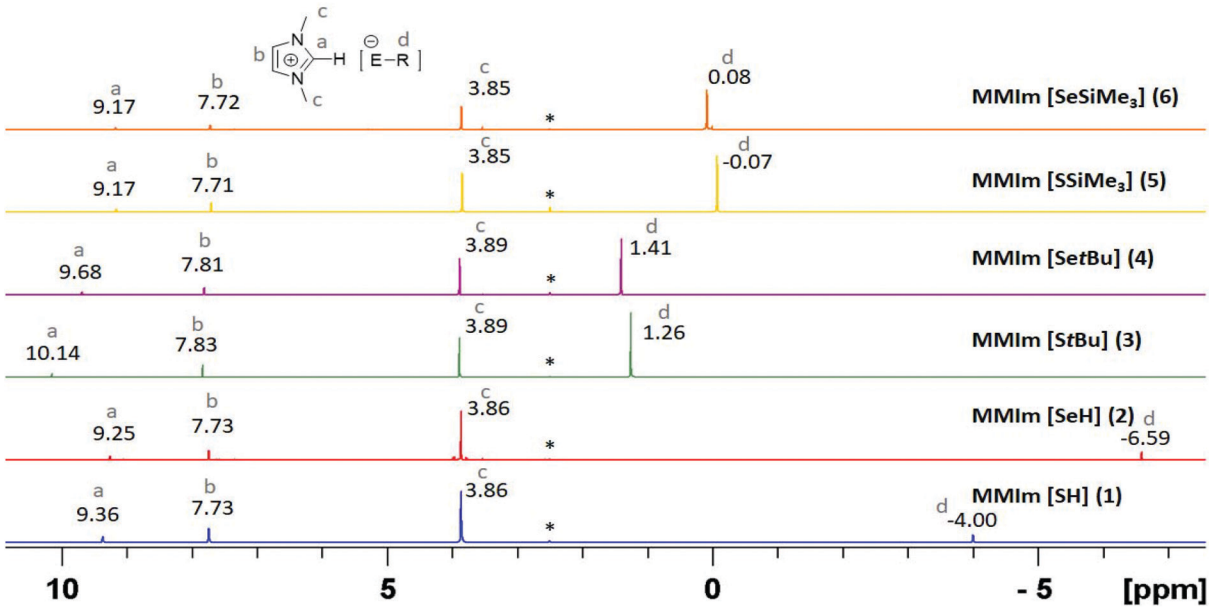

Fig. 8 ^{1}H NMR (300.1 MHz for **1–3**, 300.3 for **4–6**, *[d_6]DMSO) spectra for The title compounds **1–6**. The H2-shifts (a) depend on the anions' basicities, implying a pronounced interaction between anion and cation in solution (concentration: 30 mg probe in 0.6 mL [d_6]DMSO).

with a more pronounced π contribution the C_{ar}–H–E angles get smaller.

Here the term coordination number of H-bond donors towards an electron donor E is used in an inverse manner than in its classical meaning in coordination chemistry, namely the number of dative bonds of an electron pair donor towards a Lewis acid. Similar to coordination chemistry, we observe a correlation between the number of bonding interactions or coordination numbers (cn) and the strength of a particular interaction (bond length): the shortest crystallographically observed CH···E distances are found in the *tert*-butylchalcogenolates **2** and **3** with the smallest cn, but at the same time these are the most basic anions. Typically the solid-state structures of the title compounds show a characteristic dependence of the number of H-bonds of the chalcogenolate anions and their steric bulk: the smallest anions $[EH]^-$ reveal E-cn of **6** (Fig. 5 and 6), the more bulky anions the $[ESiMe_3]^-$ reveal S-cn of **4** and Se-cn of **5** (Fig. 3 and 4), while the sterically most congested, at the same time most basic anions $[EtBu]^-$ display S-cn of **3** and Se-cn of **4** (Fig. 1 and 2), as expected, higher Se homologues show longer H-bonds than S analogues.

A dependence of the E-cn on both, E atomic radius and steric demand, finally on the electron withdrawing group (H^+, CMe_3^+, $SiMe_3^+$) attached to E^{2-}, results in similar H-bond patterns of MMIm [Se*t*Bu] (**5**) and MMIm [$SSiMe_3$] (**3**). The $SiMe_3$ group is sterically less demanding than *t*Bu at the same time more electron withdrawing. Consequently, combinations $[Se\text{-}CMe_3]^-$ and $[S\text{-}SiMe_3]^-$ give rise to similar donor character and similar steric demand, both ion pairs show the same E-cn of **4**. In accord with these arguments the sterically most demanding and electron releasing *tert*-butyl group attached to the smaller and stronger donor S (compared to Se) is leading to the lowest cn **2** at S and the shortest C2–H–S distance 3.541(1), consequently a molecular H-bond dimer instead of a 3D H-bond pattern characteristic for all other ionic title compounds.

A more detailed discussion of these XRD lattice structures is presented in the electronic supplement. A reinvestigation of already published XRD lattice structures of imidazolium hydrochalcogenides[2] reveals the same trends as discussed here (see ESI‡).

^{1}H-NMR shift of the C2-attached proton

The crystallographically determined H-bonding interactions in the title compounds only refer to the solid state. However, even in strongly solvating solvents such as DMSO, ion pair interactions can be observed in solution as well: the ^{1}H NMR shifts of the C2-attached proton depend on the nature of the anion (Fig. 8): the more basic the interacting anion, the larger the low-field shift of the C2–H resonance, while the C4/5–H and C6/7–H shifts are only slightly affected. The anion $[StBu]^-$ affects the C2–H proton shift more than less basic $[SetBu]^-$ and more than less basic $[SH]^-$ and least basic $[SSiMe_3]^-$. The same trend is seen in shifts $[SetBu]^- > [SeH]^- > [SeSiMe_3]^-$. Are the most weakly basic anions $[SSiMe_3]^-$ and $[SeSiMe_3]^-$ solvated in DMSO into completely solvent separated ion pairs as they show the same C2–H resonance? Probably not, but the sulfur atom is better stabilized by the negative hyperconjugative α-silicon effect than the larger Se atom. The salt MMIm $[PF_6]$ with weakly or non-coordinating anion in DMSO may be taken as a reference for completely dissociated anions and cations. It shows a C2–H resonance at 9.01 ppm in DMSO under same conditions. All these observations are in accord with NMR spectra of the homologues EMIm [EH]

(E = S, Se, Te) showing a decreasing C2–H low field shift following the trend $[SH]^-$ > $[SeH]^-$ > $[TeH]^-$ (ref. 2) and with other reports for imidazolium based salts.[16,22]

The low field shifts of the C2–H proton are dependend on the concentration, in particular for the most basic anions $[StBu]^-$ (**2**) and $[SetBu]^-$ (**5**). Higher concentrations lead to larger low field shifts due to stronger anion cation interactions (see ESI‡). In contrast to Cremer *et al.*[22b] no such trends can be observed for the associated ^{13}C NMR shifts of the corresponding C2 nuclei. The ^{77}Se NMR spectra of the selenolates show a distinct trend in ^{77}Se nuclei chemical shift. With increasing basicity of the anion, the signals get more and more shielded reaching an extreme shift for the solvated extremely electron-rich anion $[SetBu]^-$: δ = −414.0 ppm for MMIm $[SeSiMe_3]$ (**6**), −310.2 ppm for MMIm [SeH] (**4**) and +322.1 ppm for MMIm [Se*t*Bu] (**5**) *versus* Me_2Se standard.

Thermal stability and volatility

The DSC and TGA diagrams of all ionic title compounds are presented in the electronic supplement. Fig. 9 summarises the onset temperatures of thermal decay and the melting process. While there is no trend for the melting temperature, the thermal decay temperatures follow the same trend discussed in the C2–H proton shifts: salts with the least basic anions $[ESiMe_3]^-$ (**3** + **6**) are thermally the most stable ones, followed by $[EH]^-$ (**1** + **4**). The most basic anions $[ECMe_3]^-$ (**2** + **5**) lead to thermally most unstable salts. The latter show no physical melting point below their beginning decomposition, the other four salts reveal melting points below 100 °C and well below their decomposition temperatures. Therefore **1**, **3**, **4** and **6** can be considered as highly reactive ionic liquids. All salts **1–6** can be purified by sublimation at 1×10^{-3} mbar at 50–100 °C. As no loss of yield under dynamic vacuum is observed, we assume, that the volatile species are not uncharged decomposition products MMIm-NHC and RSH but the discussed π complex ion pairs already half the way preformed in the solid state lattice structures of these salts. Corresponding quaternary ammonium and phosphonium salts do not show this volatility but decompose *via* cation dealkylation by nucleophilic attack of $[ER]^-$.

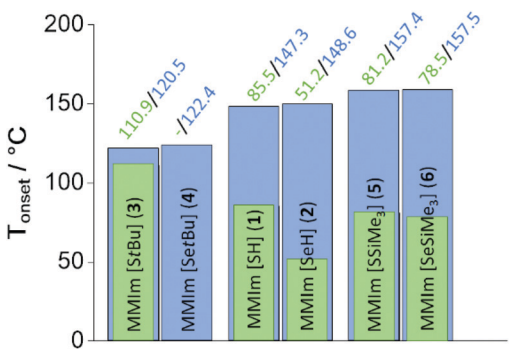

Fig. 9 Onset temperatures (TGA, °C) of the thermal decay (blue) and melting processes (green) of the title compounds **1–6** at 10 °C min^{-1}.

Conclusions

Convenient syntheses of so far inaccessible, crystalline and highly pure 1,3-dialkylimidazolium salts with extremely nucleophilic anions $[ER]^-$ (E = S, Se; R = H, *t*Bu, $SiMe_3$) have been introduced. The title compounds **3**, **5**, and **6** are prepared *via* desilylation of Me_3Si-ER (E = S, Se) by the super-nucleophile MMIm[S*t*Bu] (**2**), which is easily accessible *via* deprotonation of HS*t*Bu with *in situ* generated NHC 1,3-dimethylimidazolidin-2-ylidene. The complete series of ionic compounds has been systematically studied with respect to their anion cation interaction in the crystalline state (XRD) and in solution (NMR). The shortest anion cation contact is always defined by C2H···E. The number of doubly ionic H-bonds in the lattice is determined more by steric than by electronic properties such as anion basicity. Contrastingly, interactions of DMSO solvated anions and cations are determined by the anion basicity. The most basic anions, namely in salts MMIm [S*t*Bu] (**2**), and MMIm [Se*t*Bu] (**5**), lead to the strongest low field shifts in C2–H resonances and to the lowest onset temperatures with respect to the thermal stability of these salts. The four salts with weaker basic anions $[ESiMe_3]^-$ and $[EH]^-$ are reactive ionic liquids with melting points well below their decomposition points. However, all six salts can be sublimed in vacuum, a fact believed to refer to the formation of π complex ion pairs in the gas phase.

Experimental section

X-ray analysis

The data collection for the single-crystal structure determination was performed on a Stoe Stadivari diffractometer or a Bruker D8 Quest diffractometer by the X-ray service of Fachbereich Chemie, Universität Marburg. Information concerning the used hardware, and software used for data collection, cell refinement and data reduction as well as structure refinement can be reviewed in the electronic supplement Tables S1 and S2 and CCDC 1908993–1908998.‡ After solution (SHELXT[23]) and refinement process (SHELXL 2017/1)[24] the data was validated by using Platon.[25] All graphic representations were created with Diamond 4.[26]

Methods and devices

All preparative operations were conducted by using standard Schlenk techniques and freshly dried solvents. All solvents were dried according to common procedures[27] and passed through columns of aluminium oxide, 3 Å molecular sieves and R3-11G-catalyst (BASF) or stored over molecular sieves (3 Å or 4 Å). *tert*-Butylthiol was distilled and stored over 3 Å molecular sieve. Other reagents were used as received unless stated otherwise. Literature known procedures were used as reported or slightly modified to synthesize MMIm [I][28] and $E(SiMe_3)_2$ (E = S, Se).[29]

Elemental analyses (C, H, N, S) were carried out by the service department for routine analysis with a vario MICRO

cube (Elementar). Samples for the elemental analysis were weighted into tin capsules inside a nitrogen filled glovebox (slightly higher N values). ^{1}H and proton decoupled ^{13}C-NMR spectra were recorded in automation with a Bruker Avance II 300 spectrometer, ^{29}Si and ^{77}Se NMR spectra were recorded by the service department for NMR analyses with a Bruker Avance II HD 300, DRX 400 or Avance III 500 spectrometer. All spectra were recorded at ambient temperature. ^{1}H and ^{13}C NMR spectra were calibrated using residual proton signals of the solvent (DMSO[d_6]: δ_H 2.50 ppm, δ_C 39.52 ppm). ^{29}Si NMR spectra were referenced externally ($SiMe_4$: δ_{Si} 0.00 ppm) just as ^{77}Se NMR spectra (Me_2Se δ_{Se} 0.00 ppm). TGA measurements were conducted with a DSC-TGA 3 (Mettler Toledo) in a glovebox with a heating rate of 10 K min^{-1}. Melting points and decomposition temperatures, both at ambient pressure, were determined using data of the DSC-TGA. Refer to the ESI‡ for a more detailed discussion of the DSC-TGA measurements.

Synthesis of 1,3-dimethylimidazolium *tert*-butylthiolate MMIm [S*t*Bu] (2). A mixture of 1,3-dimethylimiadzolium iodide (1.20 g, 5.37 mmol, 1.0 equiv.), potassium hydride (0.27 g, 6.73 mmol, 1.3 equiv.), and potassium *tert*-butanolate (0.04 g, 0.35 mmol, 0.1 equiv.) was suspended in thf (15 mL) and stirred for 66 h under exclusion of light and air. The reaction mixture was filtered. *tert*-Butylthiol (0.58 g, 6.4 mmol, 1.2 equiv.) was slowly added to the filtrate at 0 °C. The reaction mixture was stirred for 30 min at 0 °C and a further 30 min at ambient temperature. The reaction mixture was filtered, and the residue was washed two times with diethyl ether (5 mL) and dried under fine vacuum. MMIm [S*t*Bu] (**1**) was obtained as a light-yellow powder in a yield of 0.89 g (4.78 mmol, 89%). M.p. (T_{onset}): 110.9 °C (10 K min^{-1}, decomp. T_{onset} 120.5 °C), ^{1}H NMR (300.1 MHz, [D_6]DMSO): δ = 9.67 (s, 1H, C2–*H*), 7.75 (s, 2H, C4/5–H), 3.87 (s, 6H, 2 × NCH_3), 1.25 (s, 9H, SC(CH_3)$_3$) ppm; ^{13}C NMR (75.5 MHz, [D_6]DMSO): δ = 137.9 (s, C2–*H*), 123.2 (s, C4/5–H), 40.5 (s, SC(*C*H_3)$_3$), 38.2 (s, S*C*(CH$_3$)$_3$), 35.5 (s, 2 × N*C*H$_3$) ppm; elemental analysis calcd (%) for $C_9H_{18}N_2S$ (186.32 g mol^{-1}): C 58.0, H 9.7, N 15.0, S 17.2; found: C 57.2, H 9.5, N 15.4, S 16.5 (note that the crude product was used).

Synthesis of 1,3-dimethylimidazolium trimethylsilylthiolate MMIm [SSiMe$_3$] (3). MMIm [S*t*Bu] (**2**) (200 mg, 1.07 mmol, 1.0 equiv.) was suspended in thf (5 mL). $S(SiMe_3)_2$ (211 mg, 1.18 mmol, 1.1 equiv.) was added to the suspension at 0 °C. The mixture was stirred for 30 min at 0 °C and a further 30 min at ambient temperature until a clear solution is obtained. All volatiles were removed *in vacuo* and the residue was dried under fine vacuum. MMIm [SSiMe$_3$] (**2**) was obtained as colourless powder in a yield of 203 mg (1.00 mmol, 93%). M.p. (T_{onset}): 81.2 °C (10 K min^{-1}, decomp. T_{onset} 157.4 °C), ^{1}H NMR (300.1 MHz, [D_6]DMSO): δ = 9.17 (s, 1H, C2–*H*), 7.71 (s, 2H, C4/5–H), 3.85 (s, 6H, 2 × NCH_3), −0.07 (s, 9H, SSi(CH_3)$_3$) ppm; ^{13}C NMR (125.8 MHz, [D_6]DMSO): δ = 137.1 (s, C2–*H*), 123.4 (s, C4/5–H), 35.7 (s, 2 × N*C*H$_3$), 8.9 (s, SSi(*C*H$_3$)$_3$) ppm; ^{29}Si NMR (99.4 MHz, [D_6]DMSO): δ = −0.9 (s, S*Si*(CH$_3$)$_3$) ppm; elemental analysis calcd (%) for $C_8H_{18}N_2SSi$ (202.39 g mol^{-1}): C 47.5, H 9.0, N 13.8, S 15.8; found: C 47.0, H 8.6, N 14.4, S 15.7 (note that the crude product was used).

Synthesis of 1,3-dimethylimidazolium hydrosulfide MMIm [SH] (1). MMIm [SSiMe$_3$] (**3**) (200 mg, 1.00 mmol, 1.0 equiv.) was solved in MeOH (3 mL) and the solution was stirred for 1 h at ambient temperature. All volatiles were removed *in vacuo* and the colourless residue was dried under fine vacuum. MMIm [SH] (**3**) was obtained as a colourless solid in a yield of 125 mg (0.96 mmol, 97%). M.p. (T_{onset}): 85.5 °C (10 K min^{-1}, decomp. T_{onset} 147.3 °C), ^{1}H NMR (300.1 MHz, [D_6]DMSO): δ = 9.36 (s, 1H, C2–*H*), 7.73 (s, 2H, C4/5–H), 3.86 (s, 6H, 2 × NCH_3), −4.00 (s, 1H, S*H* ppm; ^{13}C NMR (75.5 MHz, [D_6]DMSO): δ = 137.1 (s, C2–*H*), 123.3 (s, C4/5–H), 35.6 (s, 2 × N*C*H$_3$) ppm; elemental analysis calcd (%) for $C_5H_{10}N_2S$ (130.21 g mol^{-1}): C 46.1, H 7.7, N 21.5, S 24.6; found: C 45.9, H 7.5, N 21.8, S 24.3.

Synthesis of 1,3-dimethylimidazolium *tert*-butylselenolate MMIm [Se*t*Bu] (5). At 0 °C a 1.88 M solution of *t*BuLi in pentane (0.50 mL, 0.94 mmol, 1.1 equiv.) was added to a suspension of grey elemental selenium (74 mg, 0.90 mmol, 1.1 equiv.) in diethyl ether (20 mL). The reaction mixture is slowly warmed to room temperature and stirred at room temperature for 18 h to obtain a solution of LiSe*t*Bu. To this solution $ClSiMe_3$ (102 mg, 0.4 mmol, 1.1 equiv.) is added at 0 °C. The mixture is slowly warmed to room temperature and stirred at room temperature for 18 h to get a solution of *t*BuSeSiMe$_3$ by elimination of LiCl. To remove the LiCl all volatiles of the obtained colourless suspension were collected by condensation. The diethyl ether of the obtained clear solution was removed by careful distillation and the residual *t*BuSeSiMe$_3$ was diluted in MeCN (10 mL). This solution was added to a solution of MMIm [S*t*Bu] (**2**) in MeCN (10 mL) under continuous stirring at −20 °C. The mixture was kept at −20 °C for 2 h and then for a further 30 min warmed at room temperature. All volatiles were removed in fine vacuum until a colourless residue is obtained that was sublimated at 100 °C under a pressure of 10^{-3} mbar. The sublimated target compound MMIm [Se*t*Bu] (**5**) was obtained in a yield of 118 mg (0.50 mmol, 59%). Decomposition before melting (T_{onset} decomposition 122.4 °C, 10 K min^{-1}), ^{1}H NMR (300.3 MHz, [D_6]DMSO): δ = 9.68 (s, 1H, C2–*H*), 7.81 (d, $^{3}J_{HH}$ = 1.6 Hz, 2H, C4/5–H), 3.89 (s, 6H, 2 × NCH_3), 1.41 (s, 9H, SeC(CH_3)$_3$) ppm; ^{13}C NMR (75.5 MHz, [D_6]DMSO): δ = 137.1 (s, C2–*H*), 123.3 (s, C4/5–H), 41.6 (s, SeC(*C*H$_3$)$_3$), 35.5 (s, 2 × N*C*H$_3$), 26.1 (s, Se*C*(CH$_3$)$_3$) ppm; ^{77}Se NMR (57.3 MHz, [D_6]DMSO): δ = 322.1 (s, *Se*C(CH$_3$)$_3$); elemental analysis calcd (%) for $C_9H_{18}N_2Se$ (233.22 g mol^{-1}): C 46.4, H 7.8, N 12.0; found: C 46.2, H 7.6, N 12.8.

Synthesis of 1,3-dimethylimidazolium trimethylsilylselenolate MMIm [SeSiMe$_3$] (6). MMIm [S*t*Bu] (**2**) (150 mg, 0.80 mmol, 1.0 equiv.) was suspended in thf (5 mL). $Se(SiMe_3)_2$ (199 mg, 0.88 mmol, 1.1 equiv.) was added to the suspension at 0 °C. The mixture was stirred for 30 min at 0 °C and a further 30 min at ambient temperature until a clear solution is obtained. All volatiles were removed *in vacuo* and the residue was dried under fine vacuum. MMIm [SeSiMe$_3$] (**6**) was obtained as colourless powder in a yield of 192 mg (0.77 mmol, 96%). M.p. (T_{onset}): 78.5 °C (10 K min^{-1}, decomp. T_{onset} 157.5 °C), ^{1}H NMR (300.3 MHz, [D_6]DMSO): δ = 9.17 (s,

1H, C2–*H*), 7.72 (d, $^{3}J_{HH}$ = 1.6 Hz, 2H, C4/5–H), 3.85 (s, 6H, 2 × NCH_3), −0.08 (s, 9H, SeSi(CH_3)$_3$) ppm; ^{13}C NMR (75.5 MHz, [D$_6$]DMSO): δ = 137.0 (s, C2–*H*), 123.4 (s, C4/5–H), 35.7 (s, 2 × NCH_3), 9.2 (s, SeSi(CH_3)$_3$) ppm; ^{29}Si NMR (59.7 MHz, [D$_6$]DMSO): δ = −5.2 (s, S*Si*(CH$_3$)$_3$) ppm; ^{77}Se NMR (57.3 MHz, [D$_6$]DMSO): δ = −414.0 (s, *Se*Si(CH$_3$)$_3$) ppm; elemental analysis calcd (%) for $C_8H_{18}N_2SeSi$ (249.29 g mol^{-1}): C 38.5, H 7.3, N 11.2; found: C 36.4, H 6.9, N 11.0 (note that the crude product was used for elemental analyses).

Synthesis of 1,3-dimethylimidazolium hydroselenide MMIm [SeH] (4). MMIm [SeSiMe$_3$] (**6**) (100 mg, 0.40 mmol, 1.0 equiv.) was solved in MeOH (3 mL) and the solution was stirred for 18 h at ambient temperature. All volatiles were removed *in vacuo* and the colourless residue was dried under fine vacuum. MMIm [SeH] (**6**) was obtained as a pale greenish solid in a yield of 59 mg (0.33 mmol, 83%). M.p. (T_{onset}): 51.2 °C (10 K min^{-1}, decomp. T_{onset} 148.6 °C), ^{1}H NMR (300.3 MHz, [D$_6$]DMSO): δ = 9.25 (s, 1H, C2–*H*), 7.73 (d, $^{3}J_{HH}$ = 1.6 Hz, 2H, C4/5–H), 3.86 (s, 6H, 2 × NCH_3), −6.59 (s, 1H, Se*H*) ppm; ^{13}C NMR (75.5 MHz, [D$_6$]DMSO): δ = 137.0 (s, C2–*H*), 123.4 (s, C4/5–H), 35.7 (s, 2 × NCH_3) ppm; ^{77}Se NMR (57.3 MHz, [D$_6$]DMSO): δ = −310.2 (s, *Se*H); elemental analysis calcd (%) for $C_5H_{10}N_2Se$ (177.11 g mol^{-1}): C 33.9, H 5.7, N 15.8; found: C 34.1, H 5.6, N 16.2.

Conflicts of interest

There are no conflicts to declare.

Acknowledgements

We thank Deutsche Forschungsgemeinschaft, priority program SPP 1708: 'Material Synthesis near Room Temperature' for financial support. We thank Maria Gutschke and Haowen Wang for performing students research practical work. Dr Klaus Harms is acknowledged for support in questions of XRD refinement.

References

1 L. H. Finger, B. Scheibe and J. Sundermeyer, *Inorg. Chem.*, 2015, **54**, 9568–9575.
2 L. H. Finger and J. Sundermeyer, *Chem. – Eur. J.*, 2016, **22**, 4218–4230.
3 M. D. Hartle, D. J. Meininger, L. N. Zakharov, Z. J. Tonzetich and M. D. Pluth, *Dalton Trans.*, 2015, **44**, 19782–19785.
4 L. H. Finger, F. Wohde, E. I. Grigoryev, A.-K. Hansmann, R. Berger, B. Roling and J. Sundermeyer, *Chem. Commun.*, 2015, **51**, 16169–16172.
5 C. Donsbach, G. Thiele, L. H. Finger, J. Sundermeyer and S. Dehnen, *Inorg. Chem.*, 2016, **55**, 6725–6730.
6 B. Oelkers and J. Sundermeyer, *Green Chem.*, 2011, **13**, 608.
7 R. Kalb, US8075803B2, 2004.
8 J. D. Holbrey, W. M. Reichert, I. Tkatchenko, E. Bouajila, O. Walter, I. Tommasi and R. D. Rogers, *Chem. Commun.*, 2003, 28–29.
9 L. H. Finger, J. Guschlbauer, K. Harms and J. Sundermeyer, *Chem. – Eur. J.*, 2016, **22**, 16292–16303.
10 J. Sundermeyer and L. H. Finger, EP2876081A1, 2013.
11 (*a*) T. Linder and J. Sundermeyer, *Chem. Commun.*, 2009, 2914–2916; (*b*) T. Linder and J. Sundermeyer, DE102006023649A1, 2006.
12 J. M. Earle and R. K. Seddon, WO2001077081A1, 2000.
13 R. P. Matthews, T. Welton and P. A. Hunt, *Phys. Chem. Chem. Phys.*, 2014, **16**, 3238–3253.
14 J. Kohanoff, C. Pinilla, T. G. A. Youngs, E. Artacho and J. M. Soler, *J. Chem. Phys.*, 2011, **135**, 154505.
15 P. A. Hunt, C. R. Ashworth and R. P. Matthews, *Chem. Soc. Rev.*, 2015, **44**, 1257–1288.
16 A. Wulf, K. Fumino and R. Ludwig, *Angew. Chem., Int. Ed.*, 2010, **49**, 449–453.
17 R. P. Matthews, T. Welton and P. A. Hunt, *Phys. Chem. Chem. Phys.*, 2015, **17**, 14437–14453.
18 N. J. Singh, S. K. Min, D. Y. Kim and K. S. Kim, *J. Chem. Theory Comput.*, 2009, **5**, 515–529.
19 M. Deetlefs, C. Hardacre, M. Nieuwenhuyzen, A. A. H. Padua, O. Sheppard and A. K. Soper, *J. Phys. Chem. B*, 2006, **110**, 12055–12061.
20 K. M. Hugar, H. A. Kostalik and G. W. Coates, *J. Am. Chem. Soc.*, 2015, **137**, 8730–8737.
21 M. Mantina, A. C. Chamberlin, R. Valero, C. J. Cramer and D. G. Truhlar, *J. Phys. Chem. A*, 2009, **113**, 5806–5812.
22 (*a*) J. Wang, Y. Liu, W. Li and G. Gao, *RSC Adv.*, 2018, **8**, 28604–28612; (*b*) T. Cremer, C. Kolbeck, K. R. J. Lovelock, N. Paape, R. Wölfel, P. S. Schulz, P. Wasserscheid, H. Weber, J. Thar, B. Kirchner, F. Maier and H.-P. Steinrück, *Chem. – Eur. J.*, 2010, **16**, 9018–9033.
23 G. M. Sheldrick, *Acta Crystallogr., Sect. C: Struct. Chem.*, 2015, **71**, 3–8.
24 C. B. Hübschle, G. M. Sheldrick and B. Dittrich, *J. Appl. Crystallogr.*, 2011, **44**, 1281–1284.
25 A. L. Spek, *Acta Crystallogr., Sect. D: Biol. Crystallogr.*, 2009, **65**, 148–155.
26 H. P. K. Brandenburg, *Diamond*, Crystal Impact GbR, Bonn, 2012.
27 W. L. F. Armarego and D. D. Perrin, *Purification of Laboratory Chemicals*, Butterworth-Heinemann, Oxford, 4th edn, 1997.
28 S. Gardner, T. Kawamoto and D. P. Curran, *J. Org. Chem.*, 2015, **80**, 9794–9797.
29 J.-H. So and P. Boudjouk, *Synthesis*, 1989, 306–307.

Electronic Supplementary Material (ESI) for Dalton Transactions.

Supporting Information

Systematic Study on Anion-Cation Interactions via Doubly Ionic H-Bonds in 1,3-Dimethylimidazolium Salts Comprising Chalcogenolate Anions MMIm [ER] (E = S, Se; R = H, *t*Bu, $SiMe_3$)

Jannick Guschlbauer,[a] Tobias Vollgraff,[a] and Jörg Sundermeyer*[a]

[a] J. Guschlbauer, T. Vollgraff, Prof. Dr. J. Sundermeyer
Fachbereich Chemie and Materials Science Center
Philipps-Universität Marburg, Hans-Meerwein-Straße 4
35043 Marburg (Germany)
E-Mail: JSU@staff.uni-marburg.de

Inhalt

1. NMR Spectra

*a. MMIm [SH] (**1**)*

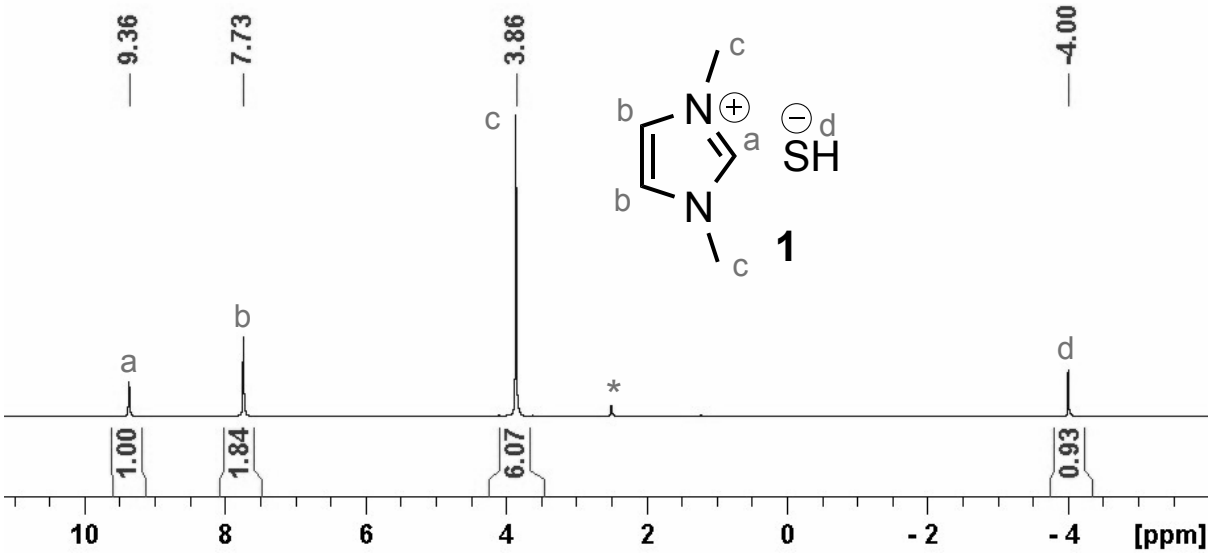

Figure S1. ^{1}H-NMR (300.1 MHz, [D_6]DMSO*) of MMIm [SH] (**1**).

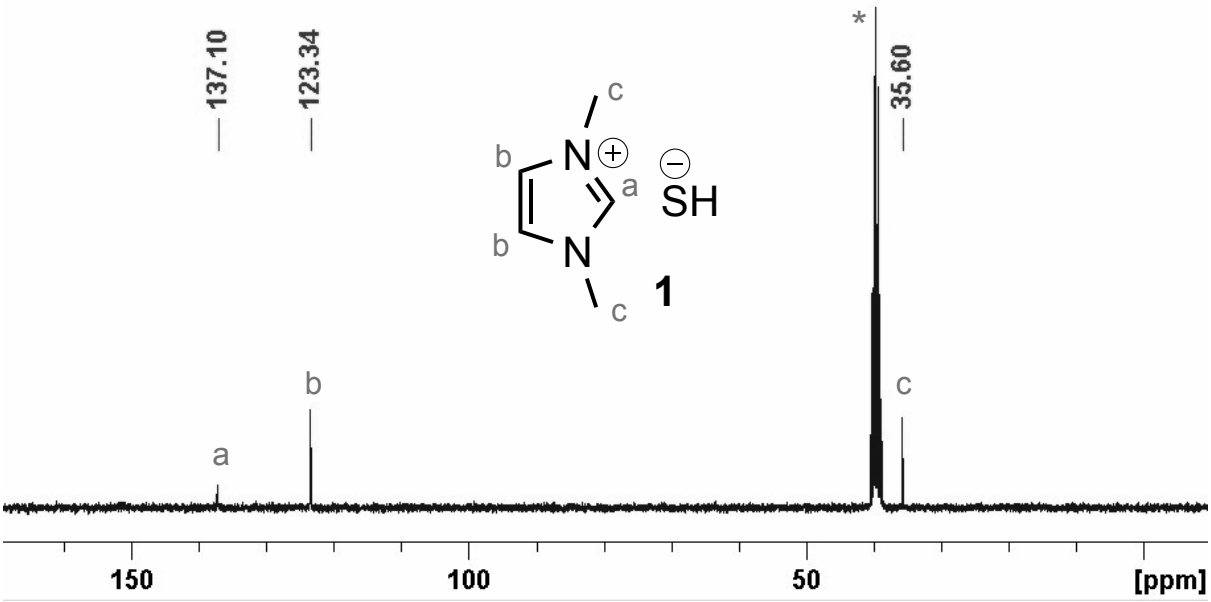

Figure S2. ^{13}C-NMR (75.5 MHz, [D_6]DMSO*) of MMIm [SH] (**1**).

*b. MMIm [StBu] (**2**)*

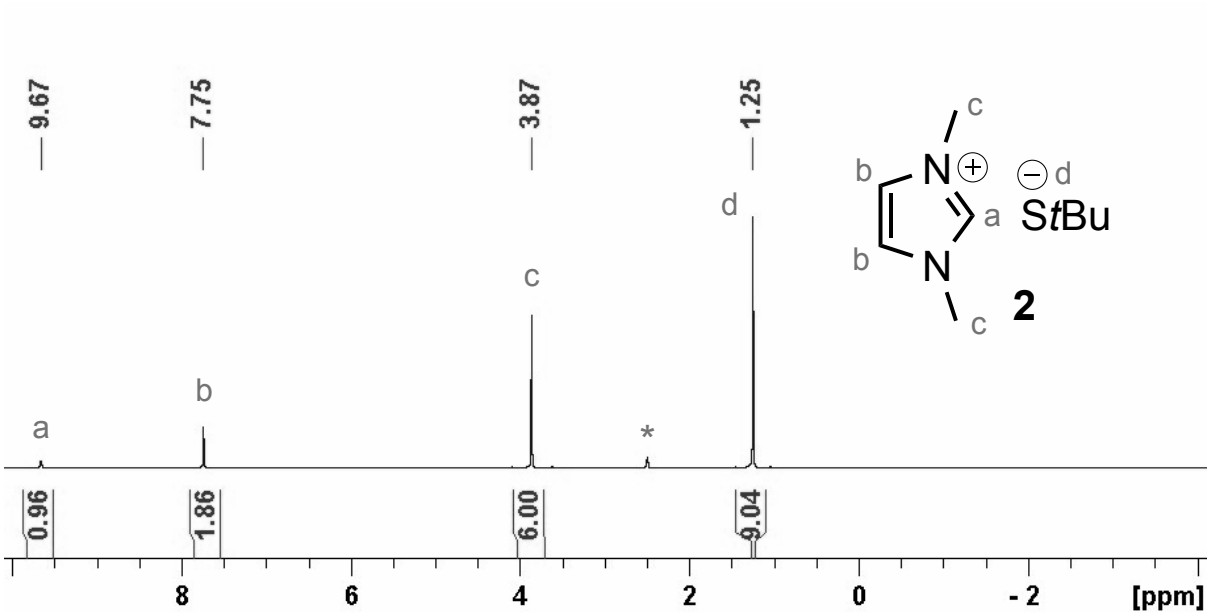

Figure S3. ^{1}H-NMR (300.1 MHz, [D_6]DMSO*) of MMIm [S*t*Bu] (**2**).

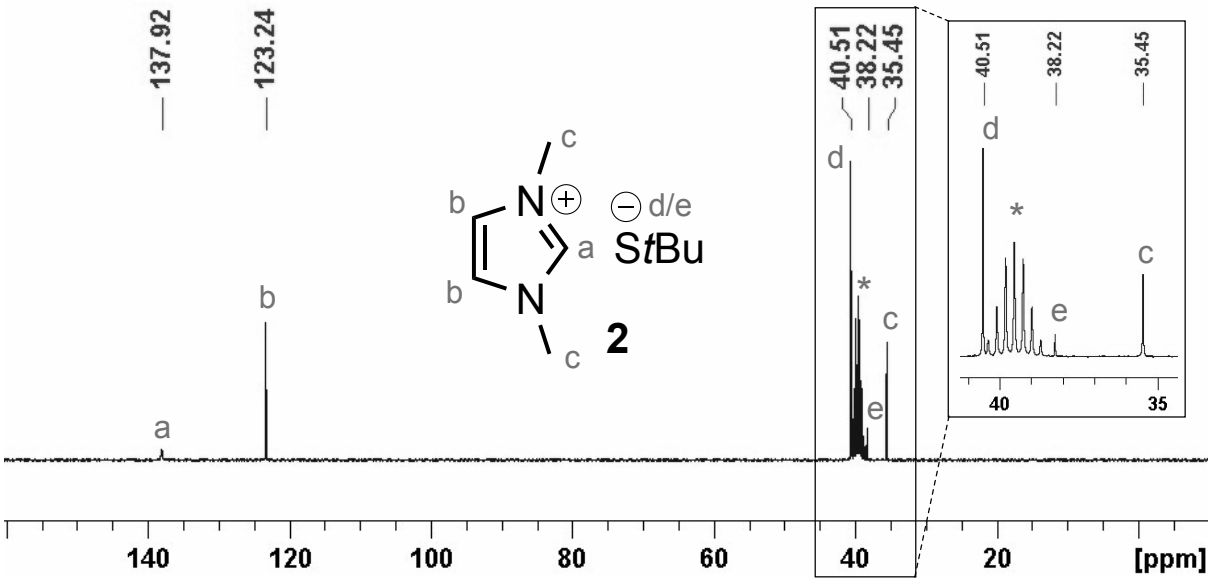

Figure S4. ^{13}C-NMR (75.5 MHz, [D_6]DMSO*) of MMIm [S*t*Bu] (**2**).

*c. MMIm [SSiMe$_3$] (**3**)*

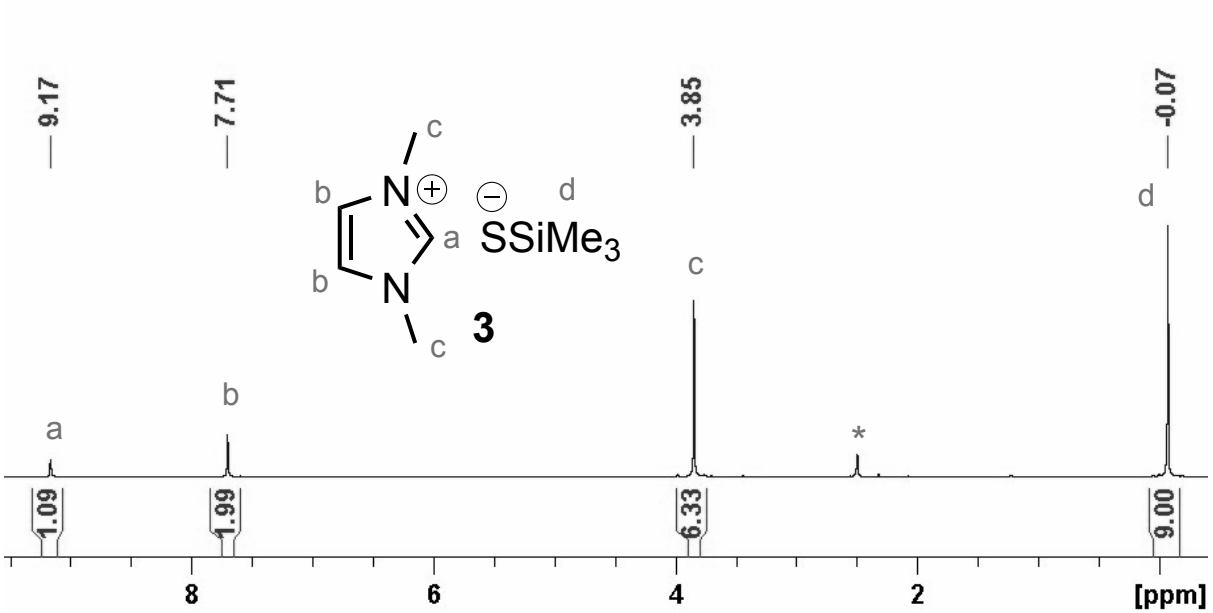

Figure S5. ^{1}H-NMR (300.1 MHz, [D$_6$]DMSO*) of MMIm [SSiMe$_3$] (**3**).

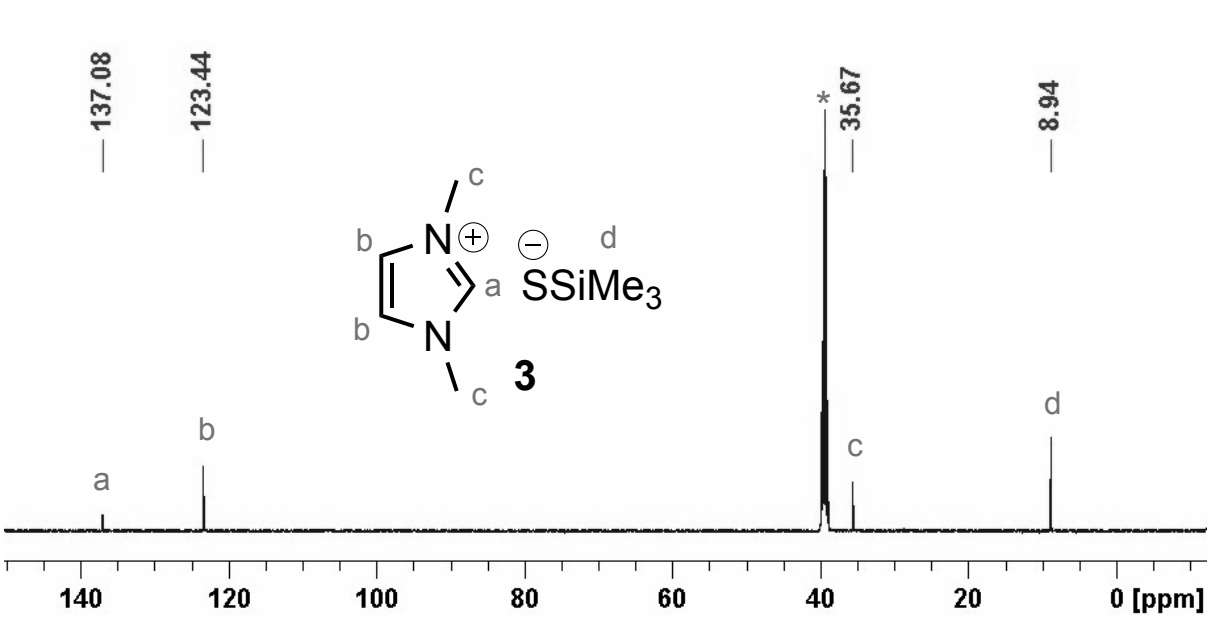

Figure S6. ^{13}C-NMR (125.8 MHz, [D$_6$]DMSO*) of MMIm [SSiMe$_3$] (**3**).

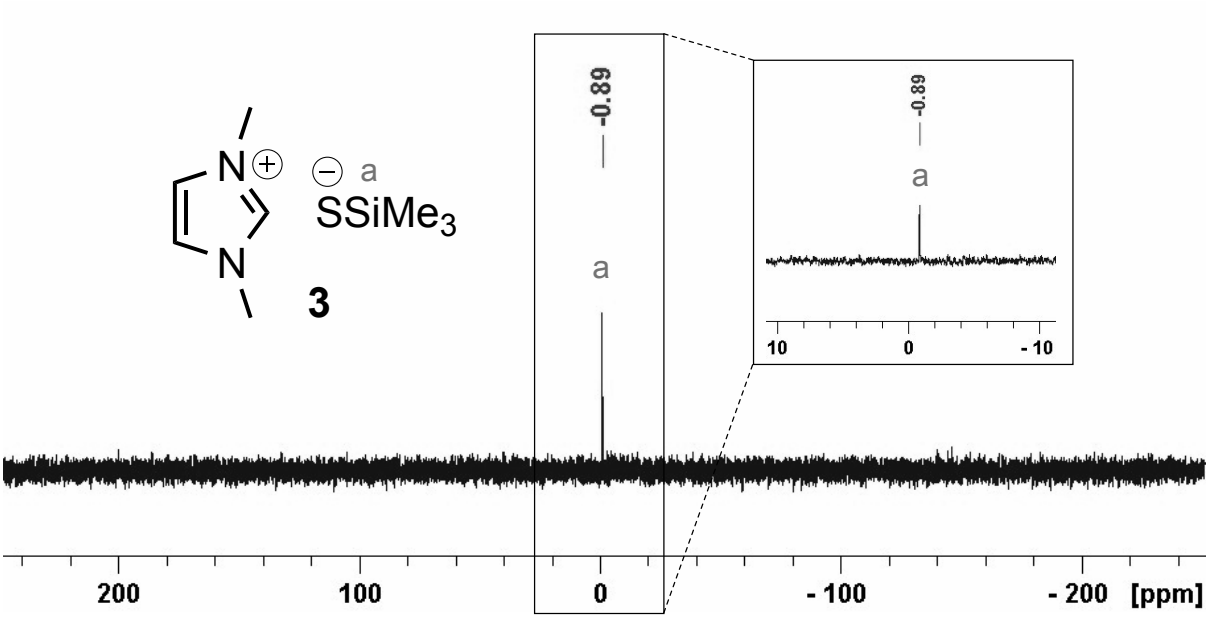

Figure S7. ^{29}Si-NMR (99.4 MHz, [D_6]DMSO) of MMIm [$SSiMe_3$] (**3**).

*d. MMIm [SeH] (**4**)*

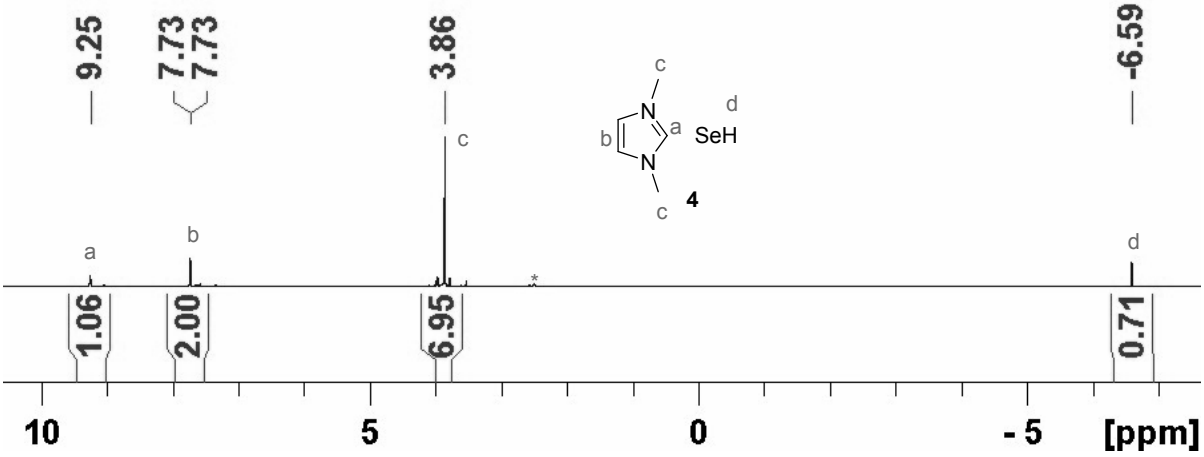

Figure S8. ^{1}H-NMR (300.3 MHz, [D_6]DMSO) of MMIm [SeH] (**4**).

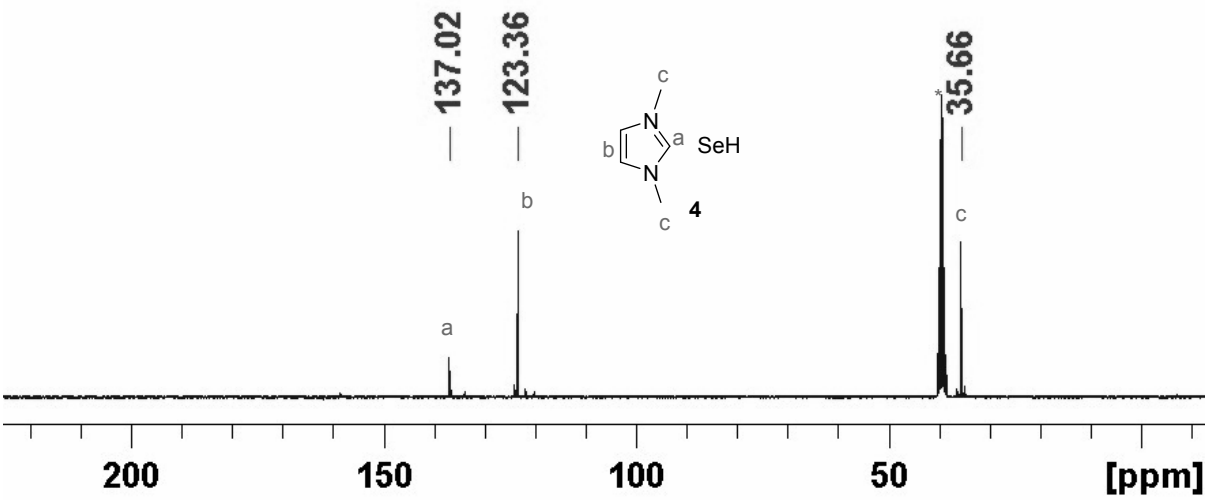

Figure S9. ^{13}C-NMR (75.5 MHz, [D_6]DMSO*) of MMIm [SeH] (**4**).

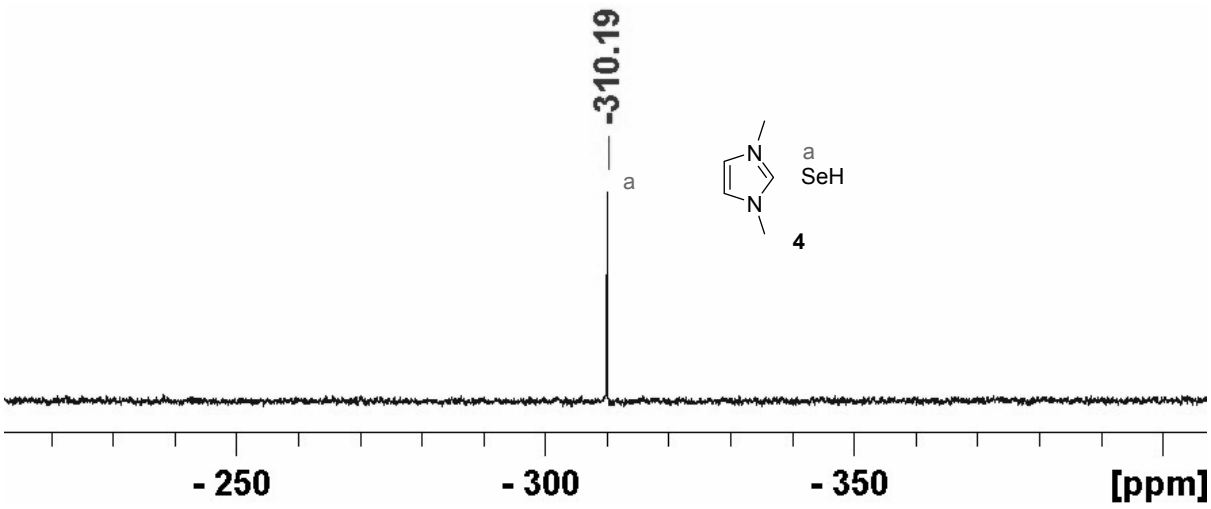

Figure S10. ^{77}Se-NMR (57.3 MHz, [D_6]DMSO) of MMIm [SeH] (**4**).

*e. MMIm [SetBu] (**5**)*

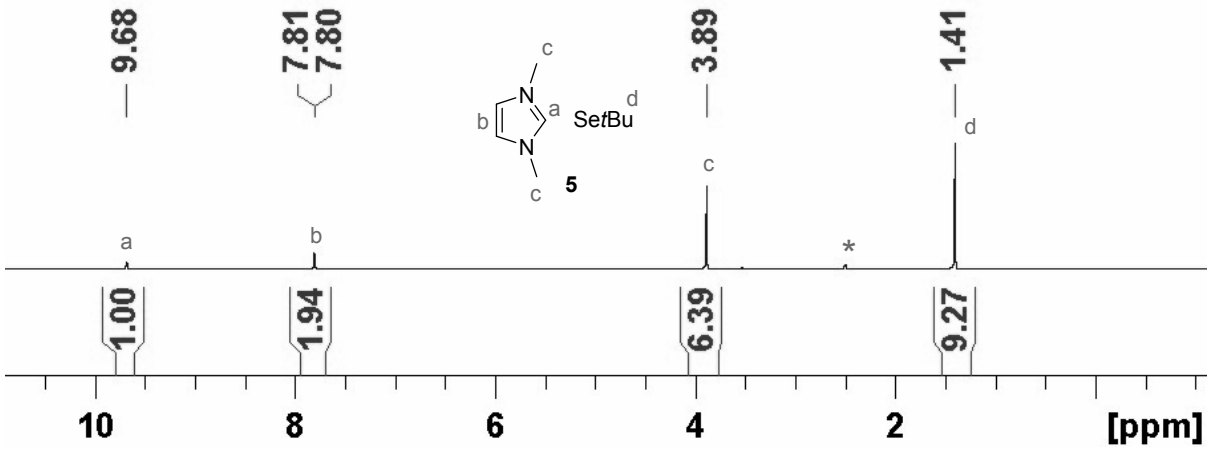

Figure S11. ^{1}H-NMR (300.3 MHz, [D_6]DMSO*) of MMIm [Se*t*Bu] (**5**).

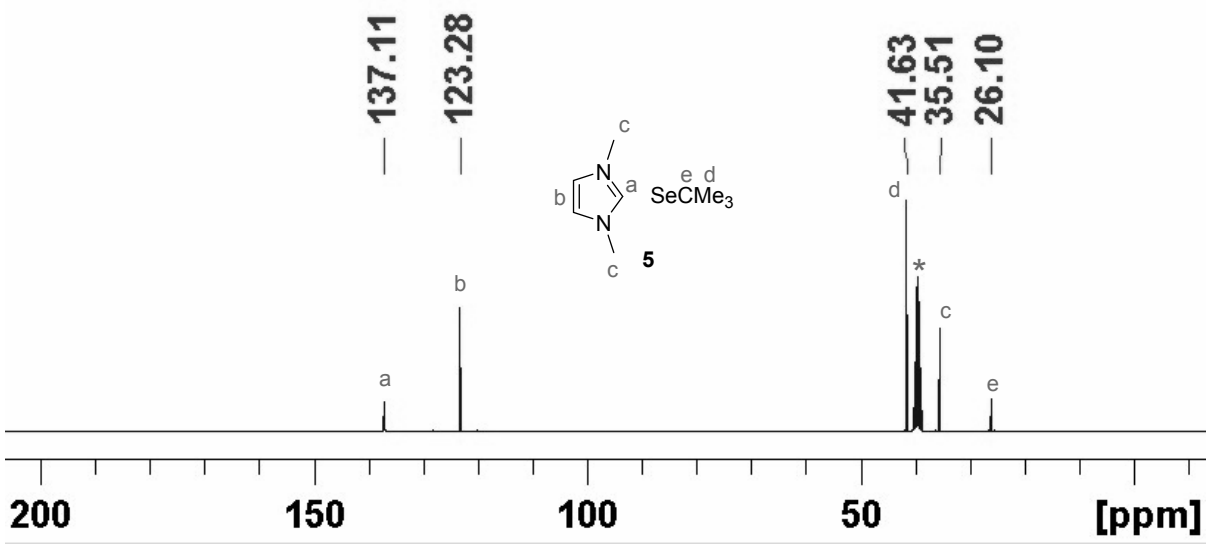

Figure S12. ^{13}C-NMR (75.5 MHz, [D_6]DMSO) of MMIm [Se*t*Bu] (**5**).

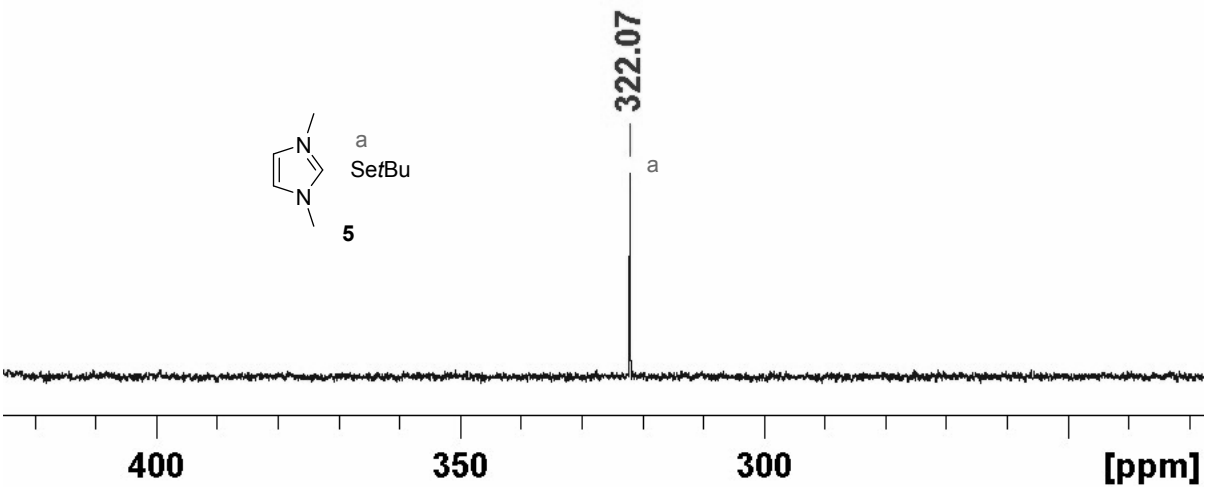

Figure S13. ^{77}Se-NMR (57.3 MHz, [D_6]DMSO) of MMIm [Se*t*Bu] (**5**).

*f. MMIm [SeSiMe$_3$] (**6**)*

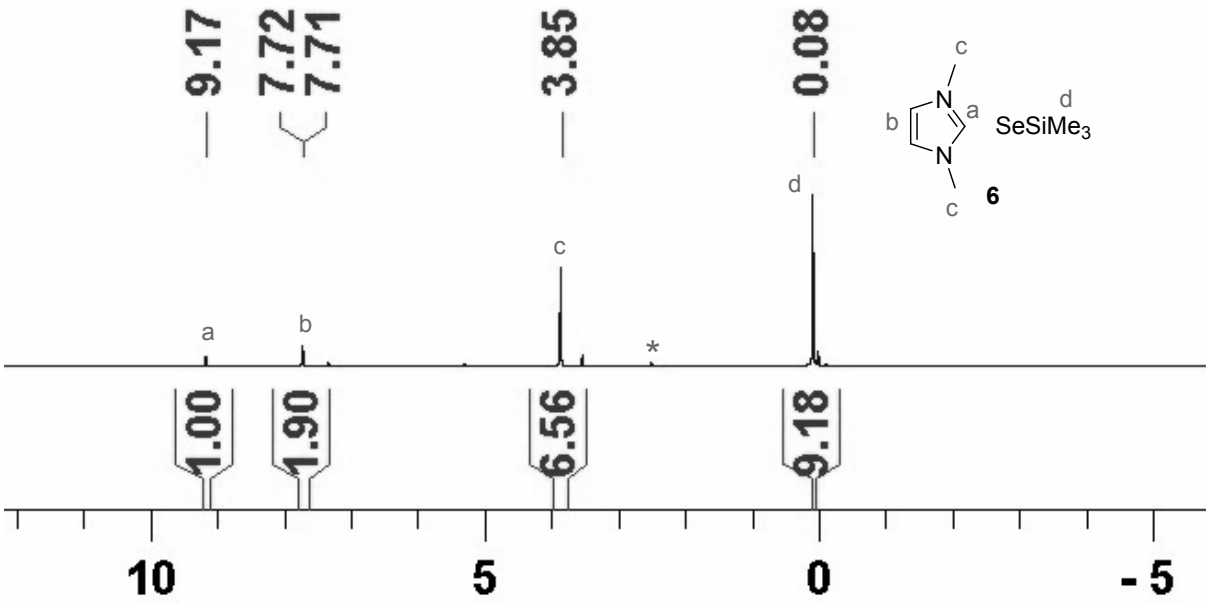

Figure S14. ^{1}H-NMR (300.3 MHz, [D_6]DMSO*) of MMIm [SeSiMe$_3$] (**6**).

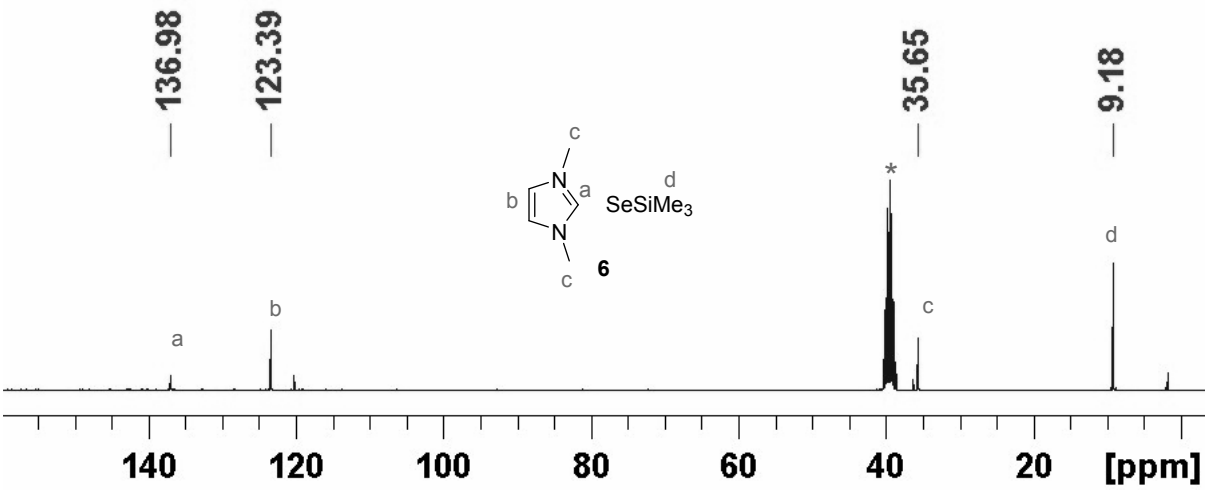

Figure S15. ^{13}C-NMR (75.5 MHz, [D_6]DMSO*) of MMIm [SeSiMe$_3$] (**6**).

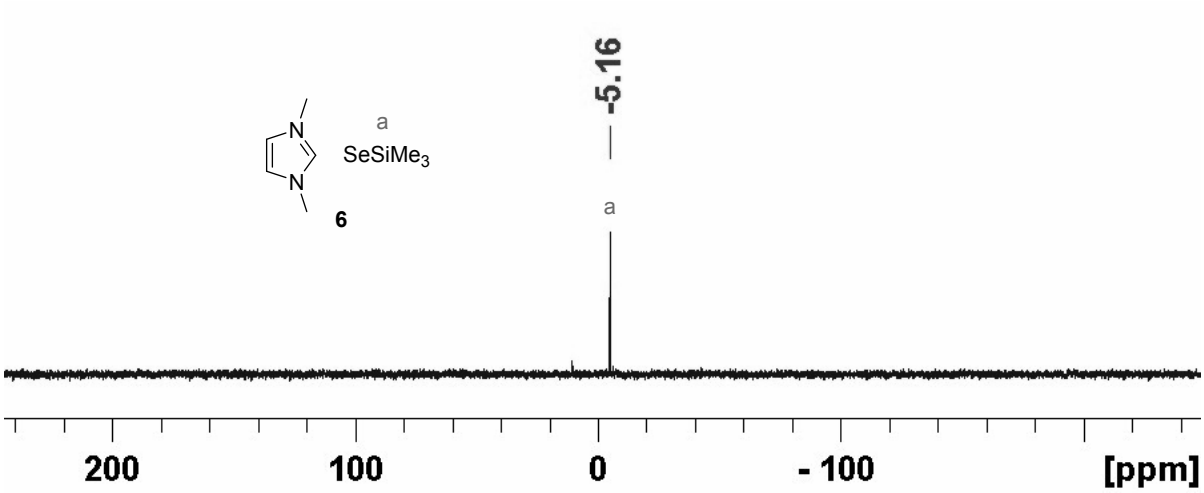

Figure S16. ^{29}Si-NMR (59.7 MHz, [D_6]DMSO) of MMIm [$SeSiMe_3$] (**6**).

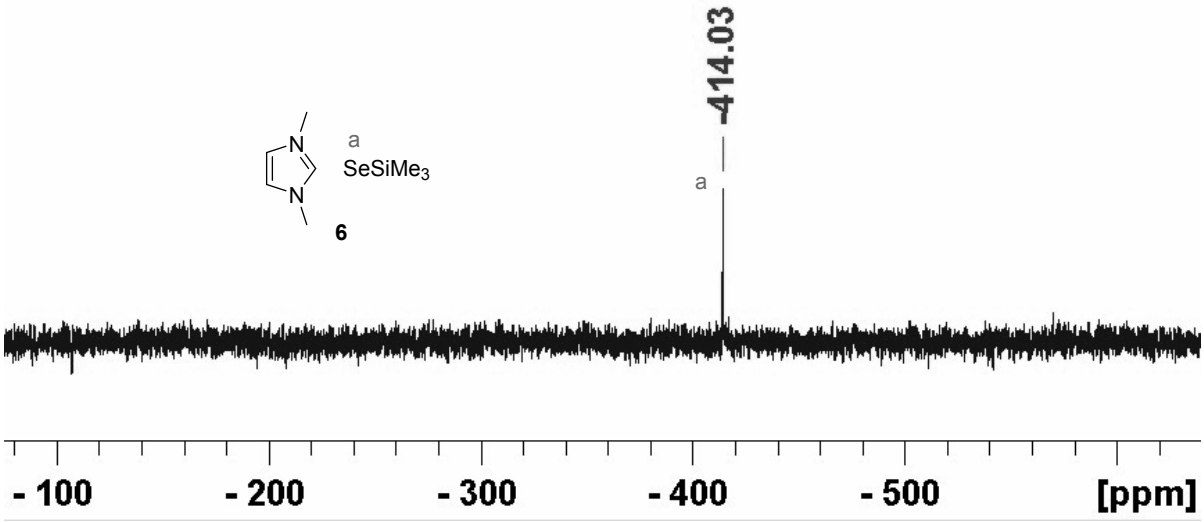

Figure S17. ^{77}Se-NMR (57.3 MHz, [D_6]DMSO) of MMIm [$SeSiMe_3$] (**6**).

g. Discussion of the concentration dependence of the ^{1}H-NMR-shift of the C2-attached proton

To support the assumed dependence of the shift of the C2-attached proton at MMIm [S*t*Bu] (**2**) two ^{1}H-NMR samples of varying concentration were measured: 10 mg **2** in 0.6 mL [D6]DMSO and 30 mg **2** in 0.6 mL [D6]DMSO (figure S7). The signal for the C2-attached proton appears at different shifts (9.67 ppm and 10.14 ppm respectively). A more and more pronounced low filed shift can be observed with increasing concentration. It is plausible to assume that the connection can be traced back on interactions between the differently charged ions. It must be mentioned, that the remaining title compounds **1** and **3** do not show this kind of correlation, due to less pronounced interactions.

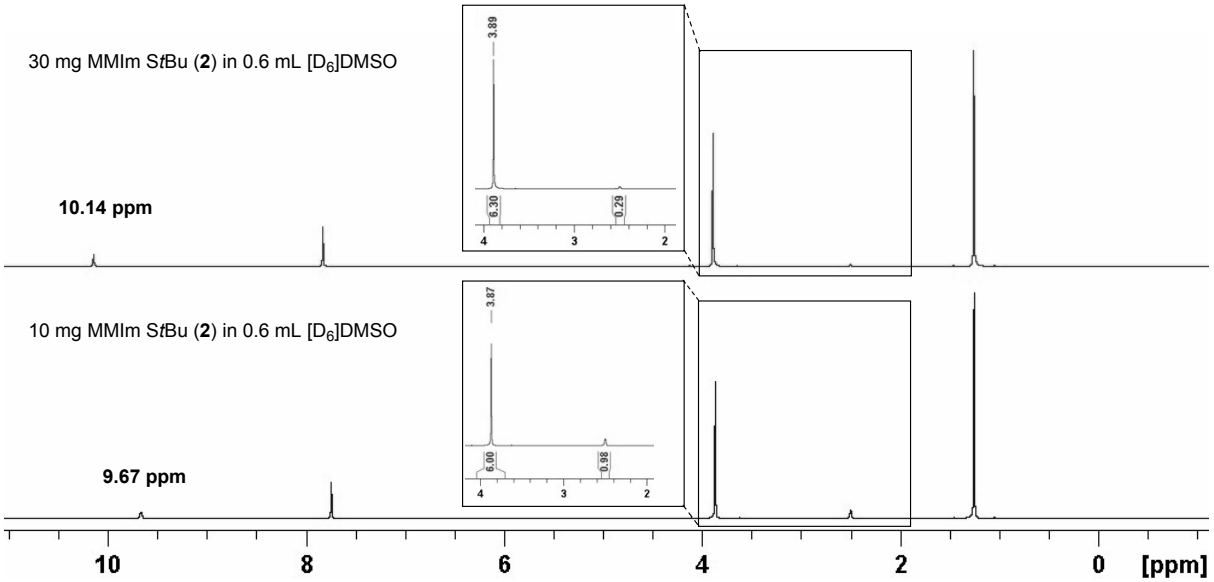

Figure S18. ^{1}H-NMR (300.1 MHz, [D$_6$]DMSO) of two different concentrated samples of MMIm [S*t*Bu] (**2**). A higher concentration leads to a low field shift. Bottom: low concentration sample (10 mg **2** in 0.6 mL [D$_6$]DMSO), top: high concentration sample (30 mg **2** in 0.6 mL [D$_6$]DMSO). The residual proton peak of [D$_6$]DMSO was integrated next to the signal of the nitrogen attached methyl groups to give an coarse measure for the concentration.

2. DSC-TGA measurements

All DSC-TGA measurements were performed on a with a DSC-TGA 3 (Mettler Toledo) in a glovebox with a heating rate of 10K / min.

*a. DSC-TGA of MMIm [SH] (**1**)*

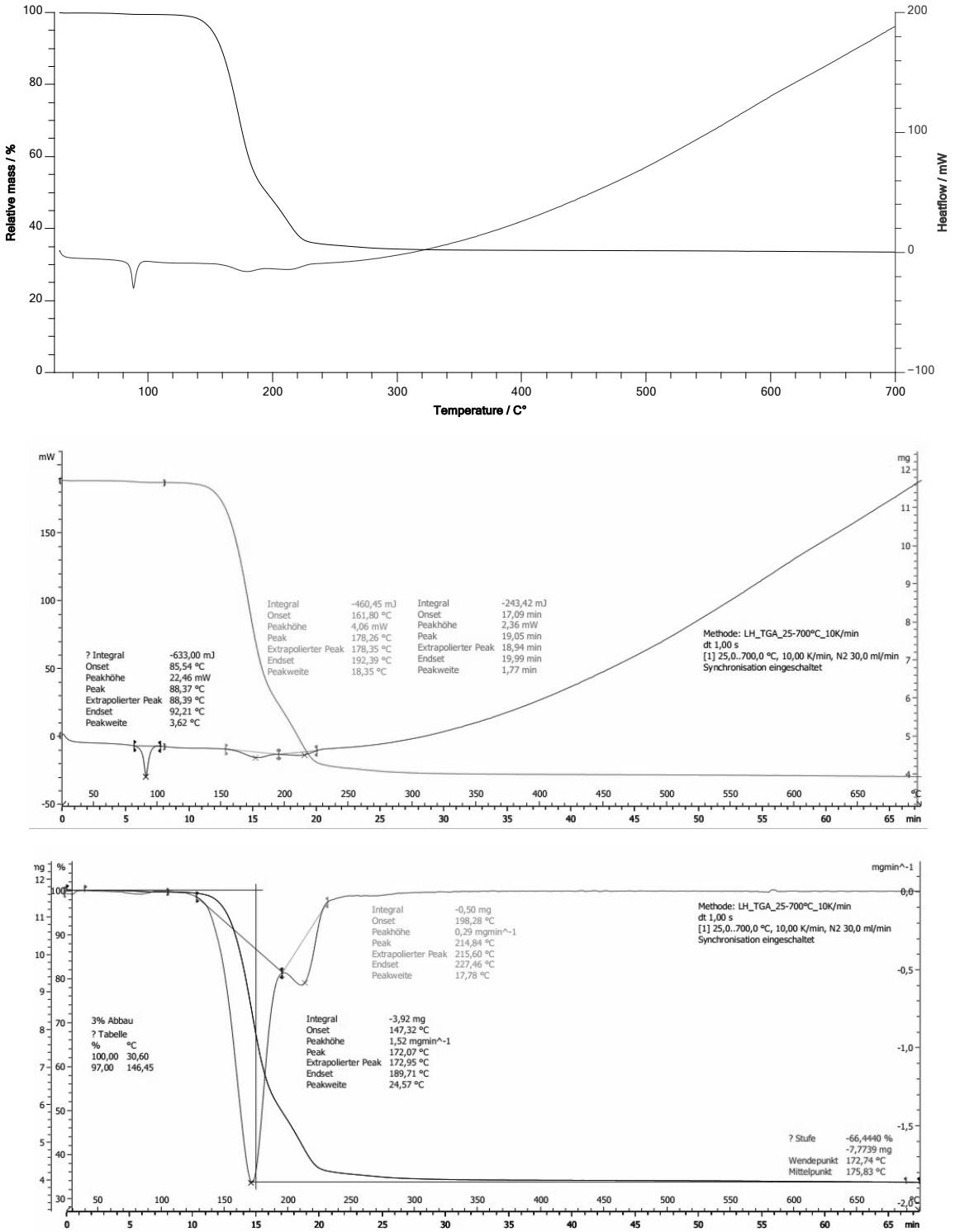

Figure S19. DSC-TGA of MMIm [SH] (**1**) with a heating rate of 10 K/min (top row), evaluation of the DSC-curve (middle row), and evaluation of the DTG-curve (bottom row). The sample melts (T_{onset} 85.5 °C) before decomposition (T_{onset} 147.3 °C).

*b. DSC-TGA of MMIm [StBu] (**2**)*

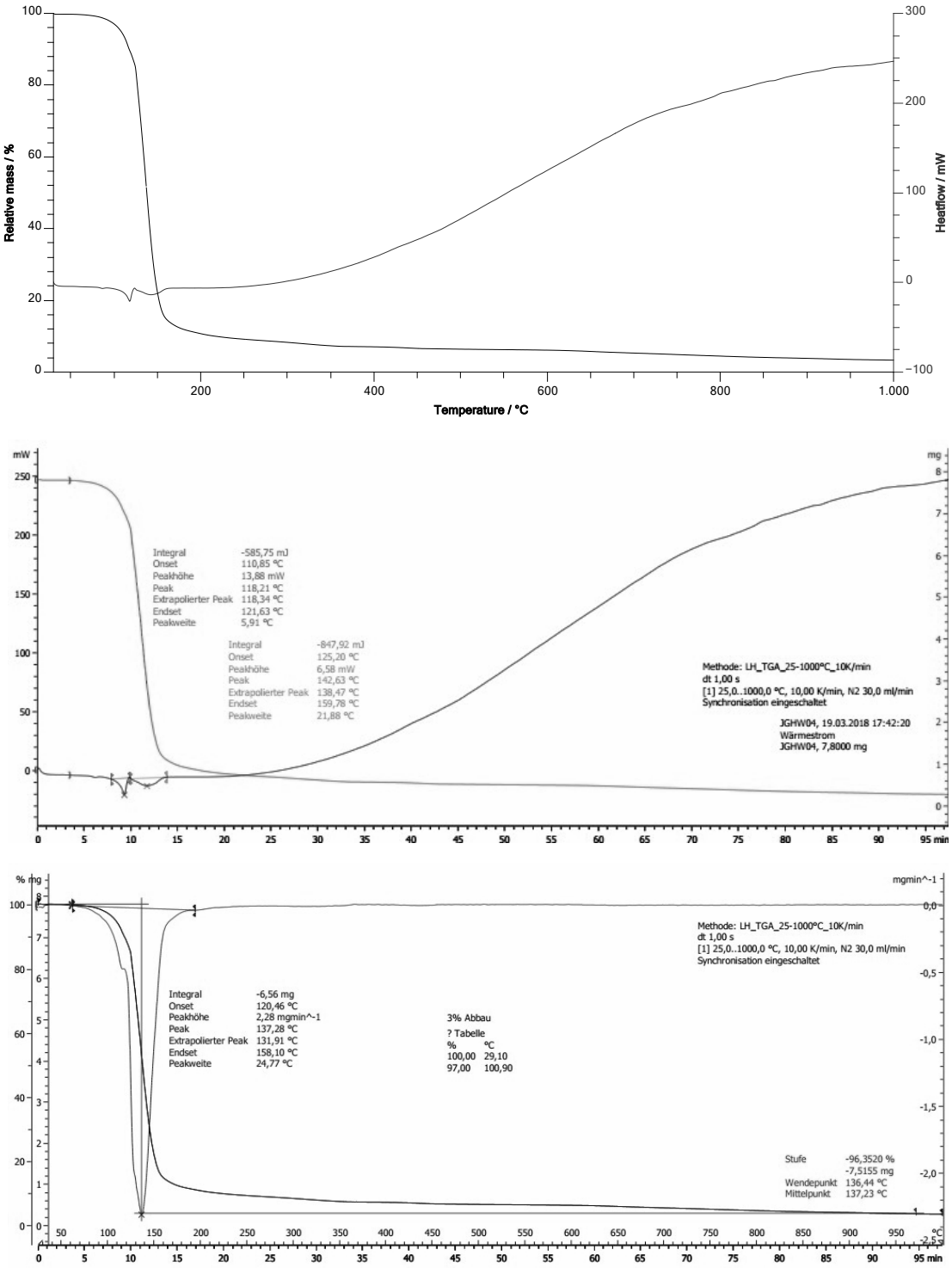

Figure S20. DSC-TGA of MMIm [S*t*Bu] (**2**) with a heating rate of 10 K/min (top row), evaluation of the DSC-curve (middle row), and evaluation of the DTG-curve (bottom row). The melting temperature (T_{onset} 110.9 °C) and and the decomposition temperature (T_{onset} 120.5 °C) are not uniquely distinguishable as they both fall beyond the temperature upon which 3% of mass loss is detectd.

*c. DSC-TGA of MMIm [SSiMe$_3$] (**3**)*

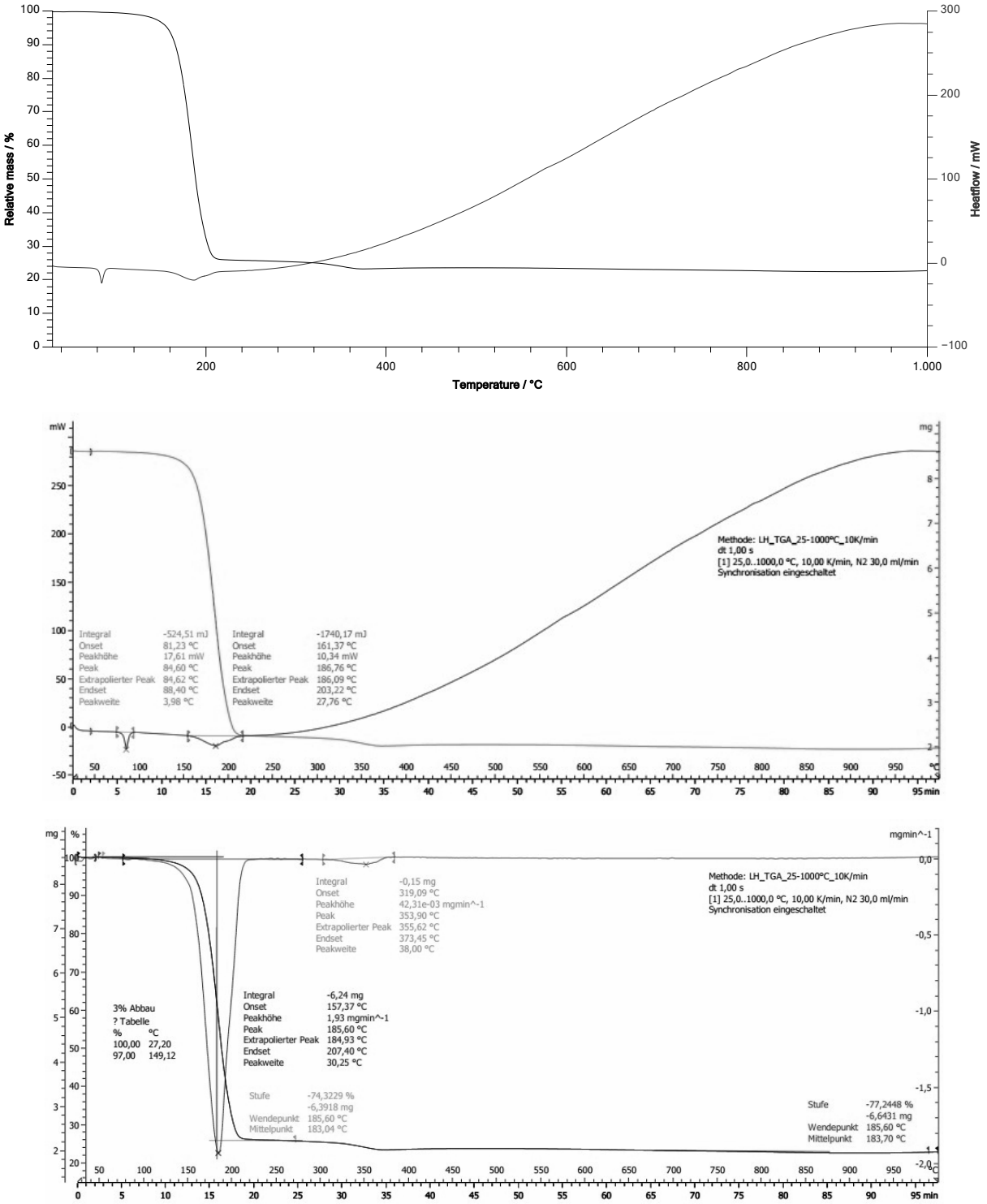

Figure S21. DSC-TGA of MMIm [SSiMe$_3$] (**3**) with a heating rate of 10 K/min (top row), evaluation of the DSC-curve (middle row), and evaluation of the DTG-curve (bottom row). The sample melts (T_{onset} 81.2 °C) before decomposition (T_{onset} 157.4 °C).

*d. DSC-TGA of MMIm [SeH] (**4**)*

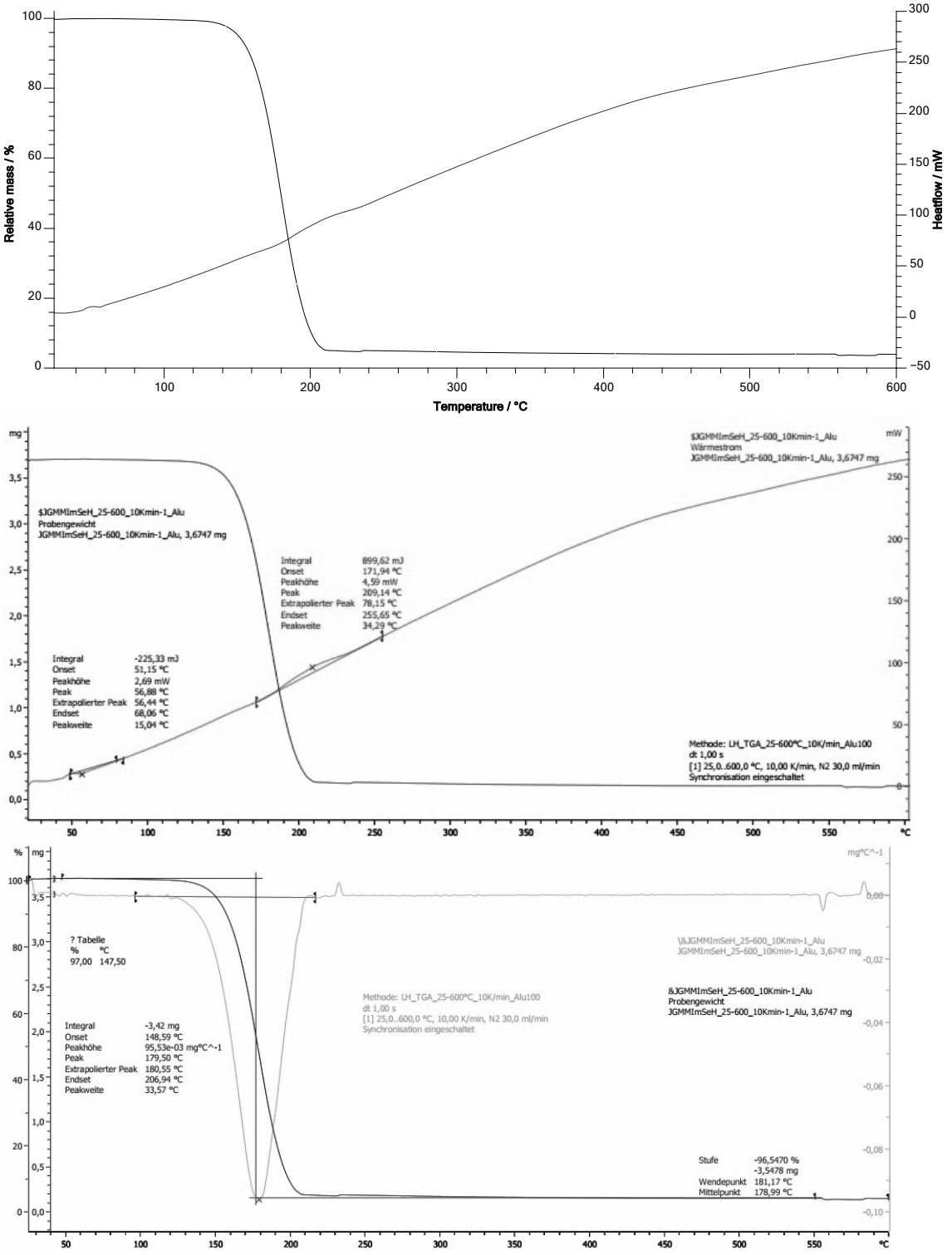

Figure S22. DSC-TGA of MMIm [SeH] (**4**) with a heating rate of 10 K/min (top row), evaluation of the DSC-curve (middle row), and evaluation of the DTG-curve (bottom row). The sample melts (T_{onset} 51.2 °C). The melting point could be experimentally confirmed, as it is not clearly visible in the DSC-curve. Decomposition (T_{onset} 148.6 °C).

*e. DSC-TGA of MMIm [SetBu] (**5**)*

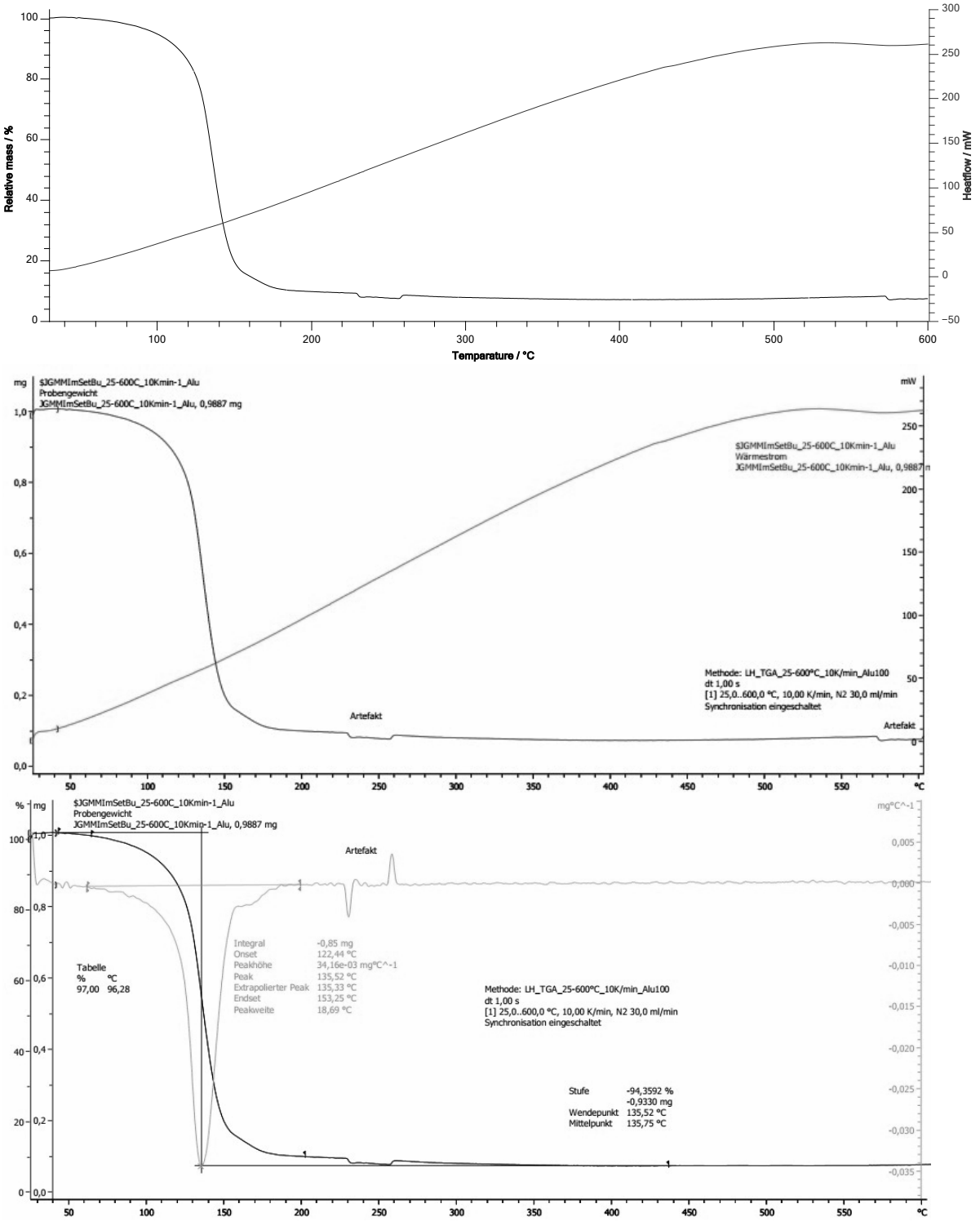

Figure S23. DSC-TGA of MMIm [S*t*Bu] (**5**) with a heating rate of 10 K/min (top row), evaluation of the DSC-curve (middle row), and evaluation of the DTG-curve (bottom row). The sample does not melt before decomposition occurs (T_{onset} 122.4°C).

*f. DSC-TGA of MMIm [SeSiMe$_3$] (**6**)*

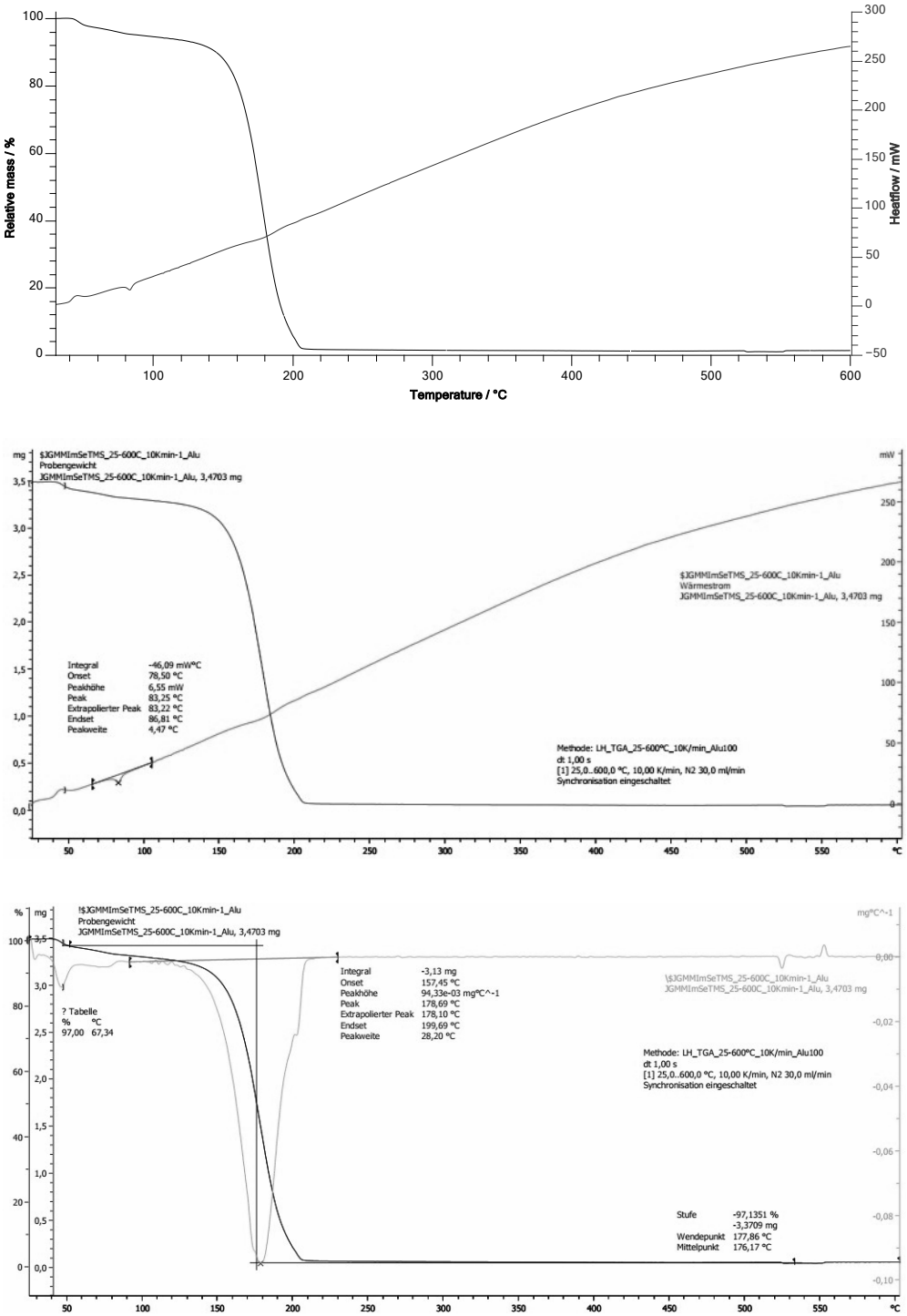

Figure S24. DSC-TGA of MMIm [SeSiMe$_3$] (**6**) with a heating rate of 10 K/min (top row), evaluation of the DSC-curve (middle row), and evaluation of the DTG-curve (bottom row). The sample melts (T_{onset} 78.50 °C) before decomposition occurs (T_{onset} 157.5°C).

Note that we did not determine the decomposition products and therefore cannot claim a sophisticated decomposition mechanism. Refer to previous work dealing with hydrosulfide ILs for information to get information about possible decomposition mechanisms. [1,2]

3. Single crystal x-ray structures

a. Crystal Data

Table S1. XRD-Data of the sulfur-based title compounds **1-3**.

	MMIm [SH] (**1**)	MMIm [S*t*Bu] (**2**)	MMIm [$SSiMe_3$] (**3**)
CCDC code	1908996	1908997	1908998
Identification code	1	2	3
Empirical formula	C5 H10 N2 S	C9 H18 N2 S	C8 H18 N2 S Si
Formula weight	130.21	186.31	202.39
Temperature	100(2) K	100(2) K	100(2) K
Wavelength	1.54186 Å	0.71073 Å	1.54186 Å
Crystal system	Monoclinic	Monoclinic	Monoclinic
Space group	P 21/n	P 21/n	P 21/n
Unit cell dimensions	a = 8.8528(18) Å	a = 8.475(2) Å	a = 8.1442(16) Å
	b = 7.7659(16) Å	b = 8.816(2) Å	b = 12.800(3) Å
	c = 10.851(2) Å	c = 15.127(3) Å	c = 11.871(2) Å
	α = 90°.	α = 90°.	α = 90°.
	β = 103.30(3)°.	β = 104.40(3)°.	β = 106.35(3)°.
	γ = 90°.	γ = 90°.	γ = 90°.
Volume	726.0(3) Å3	1094.7(4) $Å^3$	1187.4(4) $Å^3$
Z	4	4	4
Density (calculated)	1.191 Mg/m^3	1.130 Mg/m^3	1.132 Mg/m^3
Absorption coefficient	3.180 mm^{-1}	0.251 mm^{-1}	3.037 mm^{-1}
F(000)	280	408	440
Crystal size	0.101 x 0.089 x 0.067 mm^3	0.558 x 0.329 x 0.144 mm^3	0.430 x 0.278 x 0.157 mm^3
Theta range for data collection	5.834 to 66.464°.	2.525 to 26.043°.	5.198 to 66.492°.
Index ranges	-10<=h<=8, -9<=k<=8, -10<=l<=12	-10<=h<=10, -10<=k<=10, -18<=l<=18	-9<=h<=9, -15<=k<=15, -10<=l<=14
Reflections collected	6362	27138	5903
Independent reflections	1282 [R(int) = 0.0388]	2162 [R(int) = 0.0304]	2078 [R(int) = 0.0268]
Completeness to theta = x	100.0 % (x = 66.464°)	99.9 % (x = 26.043°)	99.3 % (x = 66.492°)
Absorption correction	Semi-empirical from equivalents	Semi-empirical from equivalents	Semi-empirical from equivalents
Max. and min. transmission	1.0000 and 0.2148	0.7453 and 0.6800	1.0000 and 0.4641
Refinement method	Full-matrix least-squares on F2	Full-matrix least-squares on F2	Full-matrix least-squares on F2
Data / restraints / parameters	1282 / 0 / 79	2162 / 0 / 114	2078 / 0 / 114
Goodness-of-fit on F2	1.100	1.117	1.046
Final R indices [I>2sigma(I)]	R1 = 0.0448, wR2 = 0.1172	R1 = 0.0258, wR2 = 0.0685	R1 = 0.0382, wR2 = 0.1091
R indices (all data)	R1 = 0.0564, wR2 = 0.1219	R1 = 0.0282, wR2 = 0.0699	R1 = 0.0409, wR2 = 0.1124
Extinction coefficient	n/a	n/a	n/a
Largest diff. peak and hole	0.366 and -0.373 $e.Å^{-3}$	0.239 and -0.227 $e.Å^{-3}$	0.629 and -0.443 $e.Å^{-3}$

Table S2. XRD-Data of the selenium-based title compounds **4-6**.

	MMIm [SeH] (**4**)	MMIm [Se*t*Bu] (**5**)	MMIm [$SeSiMe_3$] (**6**)
CCDC code	1908993	1908994	1908995
Identification code	4	5	6
Empirical formula	C5 H10 N2 Se	C9 H18 N2 Se	C8 H18 N2 Se Si
Formula weight	177.11	233.21	249.29
Temperature	100(2) K	100(2) K	100(2) K
Wavelength	0.71073 Å	0.71073 Å	0.71073 Å
Crystal system	Monoclinic	Triclinic	Monoclinic
Space group	P 21/n	P -1	P 21/n
Unit cell dimensions	a = 9.1327(10) Å	a = 7.9370(16) Å	a = 8.125(2) Å
	b = 7.8090(5) Å	b = 8.6020(17) Å	b = 13.039(3) Å
	c = 10.9949(12) Å	c = 9.0870(18) Å	c = 12.038(2) Å
	α = 90°.	a= 92.68(3)°.	α= 90°.
	β = 101.428(9)°.	b= 102.93(3)°.	β= 105.72(3)°.
	γ = 90°.	g = 108.73(3)°.	γ = 90°.
Volume	768.58(13) $Å^3$	567.9(2) $Å^3$	1227.6(5) $Å^3$
Z	4	2	4
Density (calculated)	1.531 Mg/m^3	1.364 Mg/m^3	1.349 Mg/m^3
Absorption coefficient	4.795 mm^{-1}	3.262 mm^{-1}	3.116 mm^{-1}
F(000)	352	240	512
Crystal size	0.316 x 0.237 x 0.077 mm^3	0.375 x 0.225 x 0.218 mm^3	0.341 x 0.336 x 0.189 mm^3
Theta range for data collection	3.222 to 24.999°.	2.319 to 25.778°.	2.351 to 25.740°.
Index ranges	-10<=h<=10, -8<=k<=9, -13<=l<=13	-9<=h<=9, -10<=k<=10, 0<=l<=11	-9<=h<=9, -15<=k<=15, -14<=l<=14
Reflections collected	6171	2170	31330
Independent reflections	1345 [R(int) = 0.0595]	2170 [R(int) = ?]	2344 [R(int) = 0.0370]
Completeness to theta = x	99.3 % (x = 24.999°)	100.0 % (x = 25.778°)	100.0 % (x = 25.740°)
Absorption correction	Semi-empirical from equivalents	Semi-empirical from equivalents	Semi-empirical from equivalents
Max. and min. transmission	1.0000 and 0.1296	0.7453 and 0.5678	0.59 and 0.46
Refinement method	Full-matrix least-squares on F2	Full-matrix least-squares on F2	Full-matrix least-squares on F2
Data / restraints / parameters	1345 / 0 / 79	2170 / 0 / 115	2344 / 0 / 114
Goodness-of-fit on F2	1.092	1.199	1.056
Final R indices [I>2sigma(I)]	R1 = 0.0412, wR2 = 0.1067	R1 = 0.0277, wR2 = 0.0636	R1 = 0.0178, wR2 = 0.0448
R indices (all data)	R1 = 0.0563, wR2 = 0.1151	R1 = 0.0342, wR2 = 0.0675	R1 = 0.0215, wR2 = 0.0464
Extinction coefficient	n/a	n/a	n/a
Largest diff. peak and hole	1.222 and -0.545 $e.Å^{-3}$	0.394 and -0.340 $e.Å^{-3}$	0.253 and -0.295 $e.Å^{-3}$

b. *Molecular structures of the title compounds*

MMIm [SH] (1)

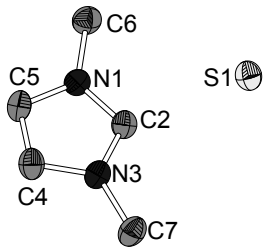

Figure S25. Reduced cell of the crystallographically determined molecular structure of MMIm [SH] (**1**). Protons are not shown. Selected bond lengths (in Å) and bond angles (in °): N1-C2 1.332(4), C2-N3 1.333(4), N3-C4 1.377(4), C4-C5 1.354(4), C5-N1 1.368(4), N1-C6 1.459(4), N3-C7 1.474(4), C2-S1 3.572(4), N1-C2-S1 101.0(2), C5-N1-C2-S1 161.4(2).

MMIm [StBu] (2)

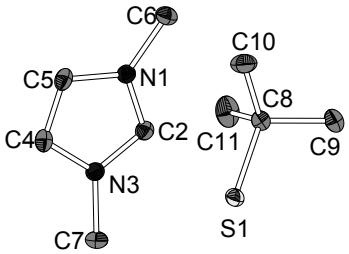

Figure S26. Reduced cell of the crystallographically determined molecular structure of MMIm [StBu] (**2**). Protons are not shown. Selected bond lengths (in Å) and bond angles (in °): N1-C2 1.329(2), C2-N3 1.3301(1), N3-C4 1.378(2), C4-C5 1.352(2), C5-N1 1.376(2), N1-C6 1.463(1), N3-C7 1.465(2), S1-C8 1.845(1), C8-C9 1.527(2), C8-C10 1.526(2), C8-C11 1.531(2), S1-C8-C9 110.38(8), S1-C8-C10 109.78(8), S1-C8-C11 110.17(8), C9-C8-C10 108.4(1), C10-C8-C11 109.3(1), C9-S1-C11 108.7(1), N1-C2-S1 141.76(8), C2-S1 3.541(1), C5-N1-C2-S1 141.1(1), C2-S1-C8 98.10(4), N1-C2-S1-C8 0.9(1).

MMIm [$SSiMe_3$] (3)

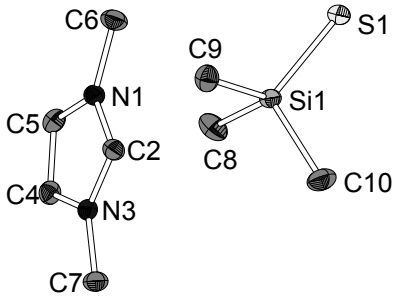

Figure S27. Reduced cell of the crystallographically determined molecular structure of MMIm [$SSiMe_3$] (**3**). Protons are not shown. Selected bond lengths (in Å) and bond angles (in °): N1-C2: 1.330(2), C2-N3 1.334(2), N3-C4 1.389(2), C4-C5 1.352(2), C5-N1 1.377(2), N1-C6 1.466(2), 1.462(2), S1-Si1 2.075(8), Si1-C8 1.882(2), Si1-C9 1.884(2), Si1-C10 1.879(2), S1-Si1-C8 112.07(6), S1-Si1-C9 114.28(6), S1-Si1-C10 111.79(6), C8-Si1-C9 106.78(7), C9-Si1-C10 104.40(7), C10-Si1-C8 106.96(8), C2-S1 7.544(2), N1-C2-S1 56.58(8), C5-N1-C2-S1 90.9(1). C2-S1-Si1 39.45(2), N1-C2-S1-Si1 –103.5(1).

MMIm [SeH] (4)

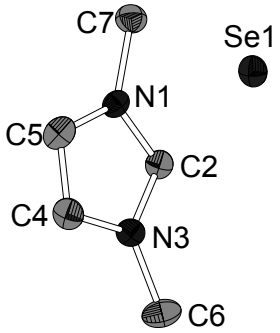

Figure S28. Reduced cell of the crystallographically determined molecular structure of MMIm [SeH] (**4**). Protons are not shown. Selected bond lengths (in Å) and bond angles (in °): N1-C2 1.335(5), C2-N3 1.339(6), N3-C4 1.381(5), C4-C5 1.351(7), C5-N1- 1.369(6), N1-C7 1.468(6), N3-C6 1.458(6), C2-Se1 3.690(5), N1-C2-Se1 102.3(3), C5-N1-C2-Se1 162.7(3).

MMIm [Se*t*Bu] (5)

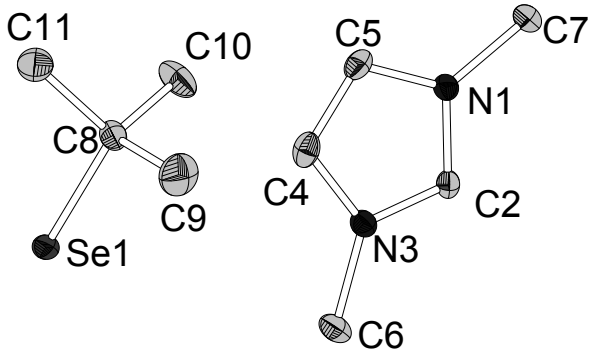

Figure S29. Reduced cell of the crystallographically determined molecular structure of MMIm [SetBu] (**5**). Protons are not shown. Selected bond lengths (in Å) and bond angles (in °): N1-C2 1.333(5), C2-N3 1.331(5), N3-C4 1.383(5), C4-C5 1.349(6), C5-N1 1.380(5), N1-C7 1.464(5), N3-C6 1.467(6), Se1-C8 1.994(4), C8-C9 1.525(4), C8-C10 1.529(5), C8-C11 1.530(6), Se1-C8-C9 110.4(3), Se1-C8-C10 109.1(3), 109.5(3), C2-Se1 6.889(4), N1-C2-Se1 102.7(2), C5-N1-C2-Se1 61.6(2), N1-C2-Se1-C8 1.5(2).

MMIm [SeSiMe$_3$] (6)

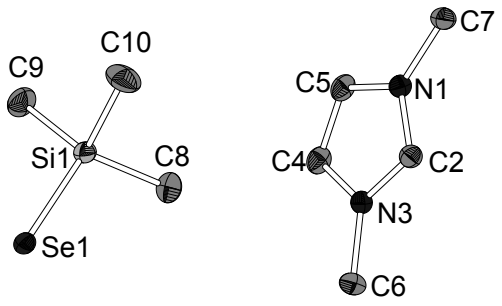

Figure S30. Reduced cell of the crystallographically determined molecular structure of MMIm [SeSiMe$_3$] (**6**). Protons are not shown. Selected bond lengths (in Å) and bond angles (in °): N1-C2 1.331(2), C2-N3 1.331(2), N3-C4 1.375(2), C4-C5 1.346(2), C5-N1 1.378(2), N1-C7 1.464(2), N3-C6 1.464(2), Se1-Si1 2.212(1), Si1-C8 1.878(2), Si1-C9 1.880(2), Si1-C10 1.874(2), Se1-Si1-C8 113.49(6), Se1-Si1-C9 111.69(6), Se1-Si1-C10, Se1-Si1-C10 111.55(6), C8-Si1-C9 107.43(7), C9-Si1-C10 107.42(8), C10-Si1-C8 104.83(8). C2-Se1 7.610(2), N1-C2-Se1 101.09(9), C5-N1-C2-Se1 –59.4(1), C2-Se1-Si1 39.60(2), N1-C2-Se1-Si1 2.06(8).

4. Supporting experimental work

The observation of hydrochalcogenide anions being more basic than the corresponding trimethylsilylchalcogenolate anions can be used in synthesis. In a short experiment we could prove this by desilylating $S(SiMe_3)_2$ with MMIm [SH] (**1**) to get MMIm [$SSiMe_3$] (**3**) in acetonitrile (scheme 1). The formal byproduct $HSSiMe_3$ could not be identified, instead $S(SiMe_3)_2$ could be detected via NMR. Obviously $HSSiMe_3$ decomposes in ambient conditions to hydrogen sulfide and $S(SiMe_3)_2$.

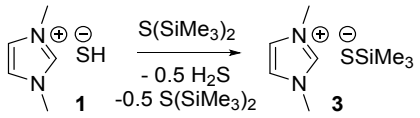

Scheme 1. Desilylation of $S(SiMe_3)_2$ with the hydrosulfide anion in **1** to get the trimethylsilylthiolate anion in **2**.

*a. Preparation of MMIm [$SSiMe_3$] (**3**) via desilylation of $S(SiMe_3)_2$ with MMIm [SH] (**1**)*

MMIm [SH] (**1**) (100 mg, 0.77 mmol, 1.0 equiv) was suspended in thf (5 mL). $S(SiMe_3)_2$ (206 mg, 1.15 mmol, 1.5 equiv) was added to the suspension at 0 °C. The mixture was stirred for 30 min at 0 °C and a further 30 min at ambient temperature until a clear solution is obtained. All volatiles were removed in vacuo and the residue was dried under fine vacuum. MMIm [$SSiMe_3$] (**3**) was obtained as a colourless powder in a yield of 139 mg (0.69 mmol, 90%). ^{1}H NMR (300.1 MHz, [D_6]DMSO): δ = 9.17 (s, 1H, C2-*H*), 7.71 (s, 2H, C4/5-H), 3.85 (s, 6H, 2x NCH_3), –0.07 (s, 9H, SSi(CH_3)$_3$) ppm; ^{13}C NMR (125.8 MHz, [D_6]DMSO): δ = 137.1 (s, C2), 123.4 (s, C4/5-H), 35.7 (s, 2x NCH_3), 8.9 (s, SSi(*C*H_3)$_3$) ppm.

*b. Desilylation of $S(SiMe_3)_2$ with MMIm [SH] (**1**) and MMIm [StBu] (**2**)*

To get information about the sideproducts that arise during the desilylation reactions the corresponding reactions were performed in small scale within [D_3]MeCN with exact amounts of the educts according to stochiometry:

Desilylation of $S(SiMe_3)_2$ with MMIm [S*t*Bu] (2): To a solution of MMIm [S*t*Bu] (**2**) (53 mg, 0.3 mmol, 1 equiv) in [D_3]MeCN (2 mL) $S(SiMe_3)_2$ (50 mg, 0.3 mmol, 1 equiv) was slowly added at 0 °C. The reaction mixture was stirred for 30 min at 0 °C and a further 30 min at ambient temperature. All volatiles were condensed into a liquid nitrogen cooled flask. After recovering ambient temperature, a ^{1}H NMR and a ^{13}C NMR spectra were recorded that confirmed the presence of *t*BuSSiMe$_3$ (Figure S31). ^{1}H NMR (300.1 MHz, [D_3]MeCN): δ = 1.42 (s, 9H,SC(CH_3)$_3$), 0.32 (s, 9H, SSi(CH_3)$_3$) ppm. ^{13}C NMR (75.5 MHz, [D_3]MeCN): δ = 45.2 (s, S*C*(CH$_3$)$_3$), 35.7 (s, SC(*C*H$_3$)$_3$) 3.0 (s, SSi(*C*H$_3$)$_3$) ppm.

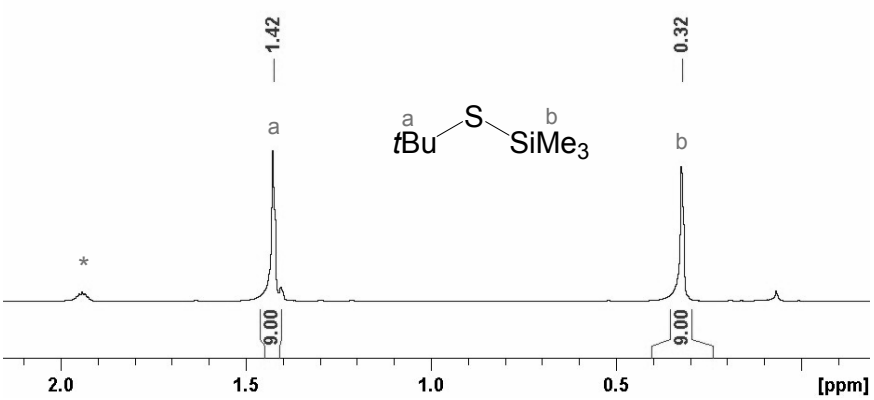

Figure S31. ^{1}H NMR (300.1 MHz, [D_3]MeCN*) of the volatiles after the desilylation of $S(SiMe_3)_2$ with MMIm [StBu] (**2**) to yield MMIm [$SSiMe_3$] (**3**).

Desilylation of $S(SiMe_3)_2$ with MMIm [SH] (1): To a solution of MMIm [SH] (**1**) (37 mg, 0.3 mmol, 1 equiv) in [D_3]MeCN (2 mL) $S(SiMe_3)_2$ (50 mg, 0.3 mmol, 1 equiv) was slowly added at 0 °C. The reaction mixture was stirred for 30 min at 0 °C and a further 30 min at ambient temperature. All volatiles were condensed into a liquid nitrogen cooled flask. After recovering ambient temperature, a ^{1}H NMR and a ^{13}C NMR spectra were recorded that confirmed the presence of $S(SiMe_3)_2$ as the same signals could be observer for an authentic sample of $S(SiMe_3)_2$. A ^{1}H NMR measurement could identify the remaining solid as MMIm [$SSiMe_3$] (**3**). Condensed sample: ^{1}H NMR (300.1 MHz, [D_3]MeCN): δ = 0.34 (s, 18H, $S(Si(CH_3)_3)_2$) ppm. ^{13}C NMR (75.5 MHz, [D_3]MeCN): δ = 4.3 (s, $SSi(CH_3)_3)_2$) ppm. Remaining solid: ^{1}H NMR (300.1 MHz, [D_6]DMSO): δ = 9.17 (s, 1H, C2-*H*), 7.71 (s, 2H, C4/5-H), 3.85 (s, 6H, 2x NCH_3), –0.07 (s, 9H, $SSi(CH_3)_3$) ppm.

c. Sublimation procedure for the title compounds

To sublime the title compounds ca. 30 mg of the crude product were weighted into a Schlenk flask which was modified with a cooling finger. Under fine vacuum the flask was evacuated until a constant pressure of 10^{-3} mbar is obtained. While maintaining the pressure using dynamic vacuum the sample was annealed at 50 °C (for **1**-**3** and **6**), 60 °C (for **4**) and 100 °C (for **5**). After two hours a reasonable amount of sublimate can be observed to be present on the cooling finger. As an example, figure S32 shows the sublimed MMIm [$SSiMe_3$] (**2**). The sublimate is scratched off the surface of the cooling finger and identified via NMR spectroscopy.

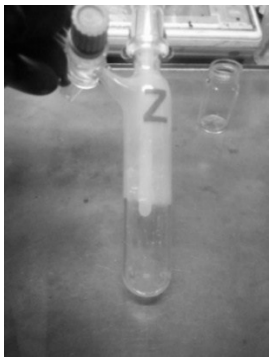

Figure S32. MMIm $SSiMe_3$ (**3**) after two hours of sublimation at 50 °C /10^{-3} mbar.

For additional information about the sublimation procedure refer to the references.[1] We want to point out, that the sublimation of the selenolates is only for MMIm [SetBu] (**5**) at 100°C at a pressure of 10^{-3} mbar possible without problems. The crude products of MMIm [SeH] and MMIm [$SSiMe_3$] turn quite dark after a few minutes at 60 °C, though the sublimate is the intended product.

*d. Synthesis of MMIm [$TeSiMe_3$] (**7**)*

In analogy to the synthesis of MMIm [$SeSiMe_3$] (**6**) the tellurium homologue was prepared by desilylation of $Te(SiMe_3)_2$ with MMIm [S*t*Bu] (**2**).

To a suspension of MMIm [S*t*Bu] (**2**) (125 mg, 0.7 mmol, 1.00 euqiv.) in thf (10mL) $Te(SiMe_3)_2$ (193 mg, 0.7 mmol, 1.05 equi.) is added dropwise at 0°C under exclusion of light. After 30 min. a clear solution is obtained that is stirred at room temperature for a further 30 min. All volatiles were removed in fine vacuum until a slightly grey powder is obtained with a yield of 194 mg (0.7 mmol, 97%). ^{1}H-NMR (250.1 MHz, [D_6]DMSO, figure S33): δ = 9.07 (s, 1H, C2-*H*), 7.69 (s, 2H, C4/5-*H*), 3.85 (s, 6H, 2x NCH_3), 0.32 (s, 9H, $TeSi(CH_3)_3$) ppm. ^{13}C-NMR (62.9 MHz, [D_6]DMSO, figure S34): δ = 137.0 (s, C2), 123.4 (s, C4/5), 35.7 (s, 2x NCH_3), 10.2 (s, $TeSiMe_3$) ppm. ^{29}Si-NMR (56.7 MHz, [D_6]DMSO, figure S35): δ = –27.9 (s, *Te*$Si(CH_3)_3$) ppm. ^{125}Te-NMR (94.7 MHz, [D_6]DMSO, figure S36): δ = –1137.6 (s, *Te*$Si(CH_3)_3$) ppm. elemental

analysis calcd (%) for $C_8H_{18}N_2TeSi$ (297.93 g mol^{-1}): C 32.3, H 6.1, N 9.4; found: C 31.3, H 5.7, N 9.7 (note that the crude product was used).

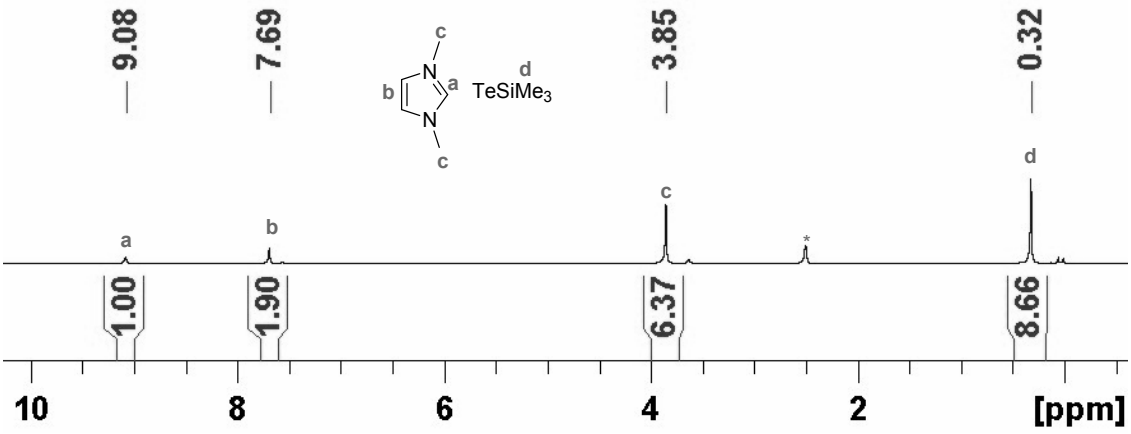

Figure S33. ^{1}H-NMR (250.1 MHz, [D_6]DMSO*) of MMIm [$TeSiMe_3$].

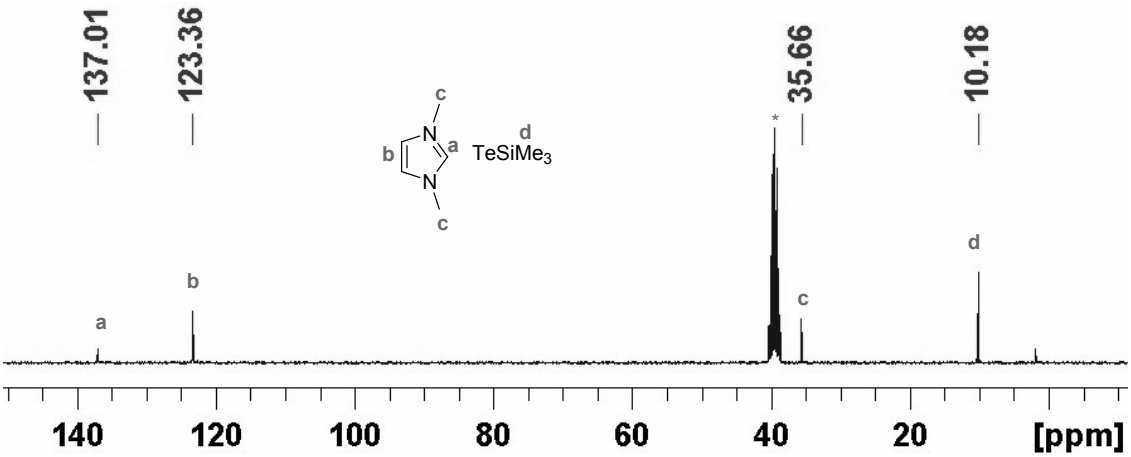

Figure S34. ^{13}C-NMR (62.9 MHz, [D_6]DMSO*) of MMIm [$TeSiMe_3$].

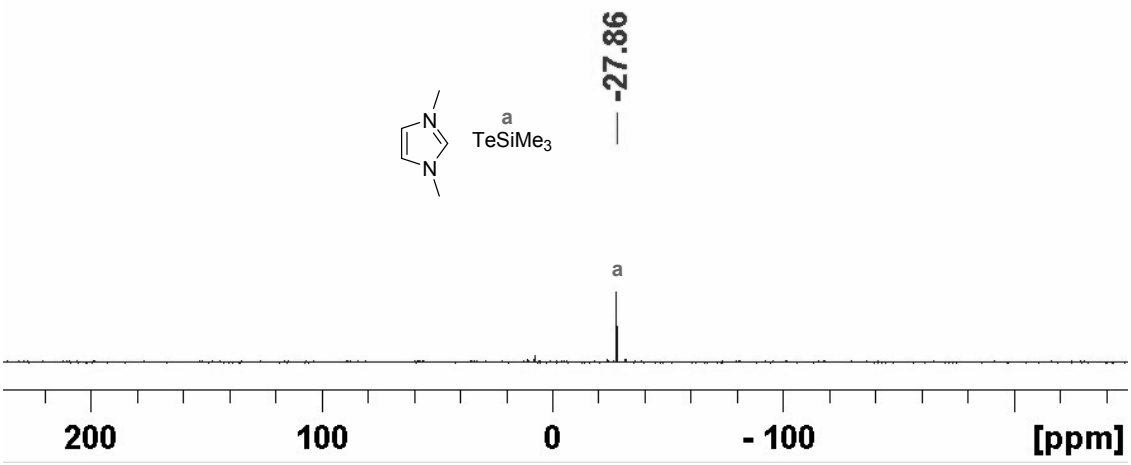

Figure S35. ^{29}Si-NMR (94.7 MHz, [D_6]DMSO*) of MMIm [$TeSiMe_3$].

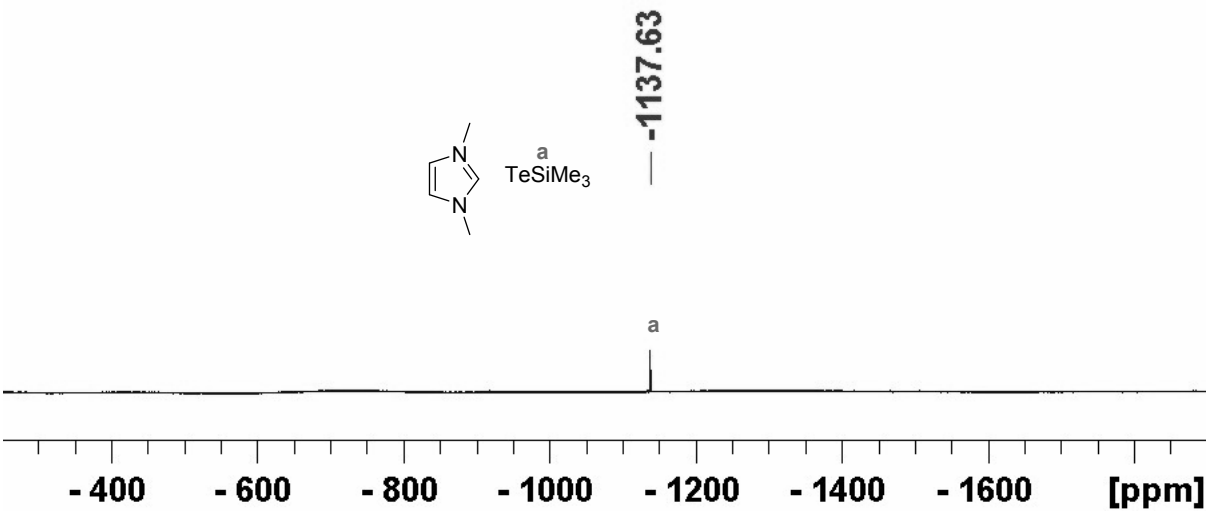

Figure S36. ^{125}Te-NMR (250.1 MHz, [D$_6$]DMSO*) of MMIm [TeSiMe$_3$].

5. Discussion on the literature known representatives of some similar compounds

*a. Comparison of H-bonding in MMIm [StBu] (**2**) and EMMIm [StBu][3]*

In figure S33 the crystallographically determined molecular structures of the title compounds MMIm [S*t*Bu] (**2**) and the literature known C2-methylated homologue EMMIm [S*t*Bu] are shown together with H-bonds. In EMIm [SH] the [SH]$^-$ anion acts as a H-bond acceptor for three protons of three cations. Qualitatively, these H-bonding modes can be observed comparably for the selenium homologue EMIm [SeH] (shown in the supporting information).[1,2] By considering steric effects, it also can be explained, that the amount of H-bonds decreases with increasing steric demand of the N-substituents, going from MMIm [SH] (S cn of 5 to 4 cations) via EMIm [SH] (S cn of 3 to 3 cations per anion)[2] to BMIm [SH] (S cn of 2 to 2 cations per anion).[2] In the only comparable literature known representative of a alkylchalcogenolate salt with imidazolium cation, EMMIm S*t*Bu, the H-bonding modes are strongly determined by the aliphatic methylene unit and interactions with solvent molecules.[3] As MMIm Se*t*Bu (**5**) is the first crystallographically identified example of a free [Se*t*Bu]$^-$ anion, no structures are available for comparison.

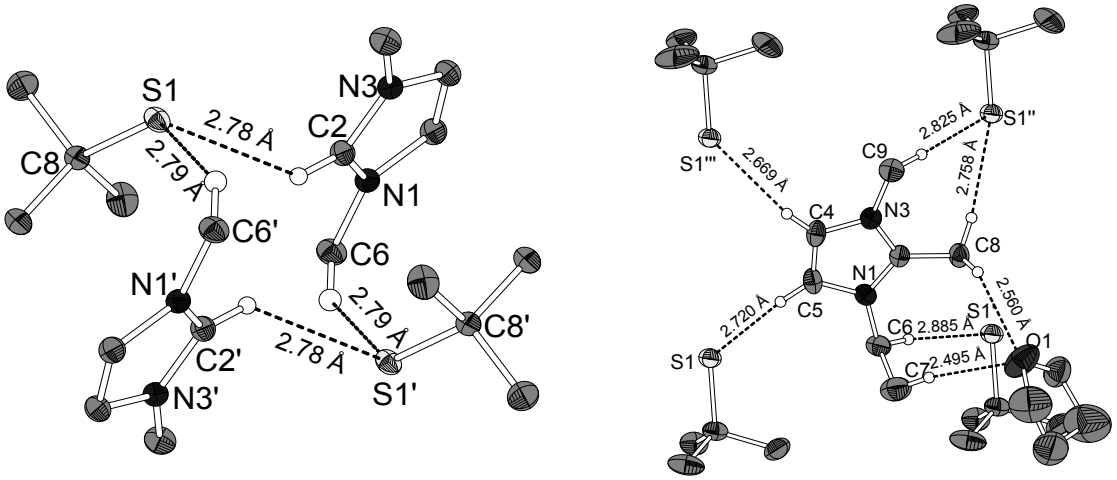

Figure S33. Left: Molecular structure of the hydrogen bond dimer of MMIm [S*t*Bu] (**2**). There are two kinds of hydrogen bonds. Ellipsoids are shown at 50% level. Only protons active in hydrogen bonds are shown (S1-C8 1.845(1) Å). Symmetry operation: I: 1-x, 1-y, 1-z.
Right: Molecular structure of EMMIm [StBu].[3] One S*t*Bu anion is bond to four EMMIm cations with different kinds of hydrogen bonds. Furthermore one thf-molecule acts a H-bond acceptor towards the EMMIm cation. Ellipsoids are shown in 50% level (only protons active in hydrogen bonds are depicted, disordered atoms are neglected). For clarity the H-bonding modes are illustrated from a cation's perspective. Symmetry operations: I: x, -1+y, z; II: 1-x, 1-y, 2-z; III: 1-x, 2-y, 2-z.

While the dimer reported for EMMIm [S*t*Bu][3] (not shown here) only arises when the shortest hydrogen-bonds are considered, the dimer of **2** includes every identified hydrogen bond. It must be mentioned, that a tetrahydrofuran molecule cocrystallized with EMMIm [S*t*Bu] which has an impact on the noncovalent interactions. In table S3 the bond lengths and angles of the identified hydrogen bonds of **2** and EMMIm [S*t*Bu][3] are listed.

Table S3. Hydrogen bond lengths and the corresponding distances between the crystallographically identified positions of the sulfur atom and the carbon atoms of MMIm [StBu] (**2**) and EMMIm [S*t*Bu].[3]Angles at the hydrogen atom and the hydrogen carbon bond are shown (distances in Å, angles in °).Chelate-like bonding modes are marked with asterisk (*). Refer to the corresponding figures for symmetry operations.

Compound / H-bond (•••)	**d(H/C•••E) [Å]**	**C-H•••E/N-C-H•••E [°]**
MMIm [S*t*Bu] (2)		
(N1)-C2-H2•••S1	2.78 / 3.541(1)	137.3(7) / 132.0(1)
(N1')-C6'-H6'•••S1	2.79 / 3.633(2)	144.29(7) / –13.2(2)
EMMIm [S*t*Bu] [3]		
(N3)-C4-H4•••S1‴	2.67 / 3.525(2)	150.1(1) / –87.1(3)
(N1)-C5-H5•••S1	2.72 / 3.592(2)	152.9(1) / 50.5(4)
(N1)-C6-H6•••S1‘	2.89 / 3.869(2)	172.8(1) / –166.5(8)
*(C1)-C8-H8•••S1“	2.76 / 3.715(2)	165.6(1) / –68.2(6)
*(N3)-C9-H9•••S1“	2.83 / 3.785(2)	166.7(1) / 43-8(6)

*b. Comparison of H-bonding in MMIm [SSiMe$_3$] (**3**) and EMMIm [SSiMe$_3$][3]*

In figure S34 the crystallographically determined molecular structures of the title compounds MMIm [SSiMe$_3$] (**3**) and the literature known C2-methylated homologue EMMIm [SSiMe$_3$] are shown together with H-bonds.

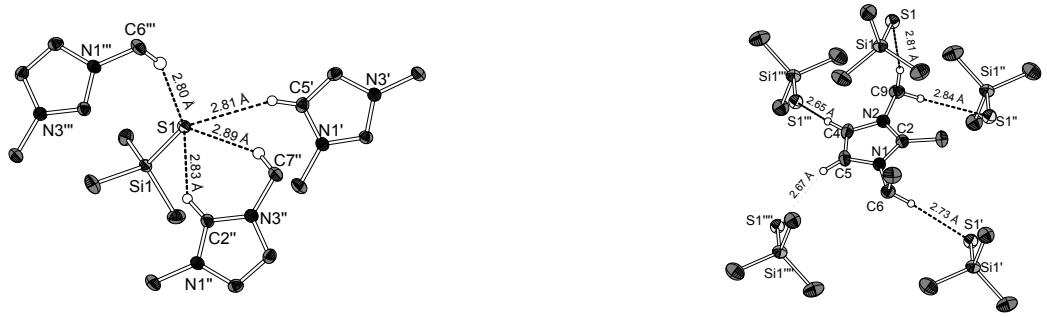

Figure S34. Left: Molecular structure of MMIm [SSiMe$_3$] (**3**). One SSiMe$_3$ anion is bond to three MMIm cations with different kinds of hydrogen bonds. Ellipsoids are shown in 50% level. Only protons active in hydrogen bonds are shown. Symmetry operations: I: -x, 1-y, 1-z; II: 1/2-x, 1/2+y, 3/2-z; III: -1/2+x, 1/2-y, 1/2+z. Right: Molecular structure of EMMIm [SSiMe$_3$]. One SSiMe$_3$ anion is bond to four EMIm cations with different kinds of hydrogen bonds. Ellipsoids are shown in 50% level (only protons active in hydrogen bonds are depicted). For clarity the H-bonding modes are illustrated from a cation's perspective. Symmetry operations: I: x, -1/2-y, 1/2+z; II: 1-x, -1/2+y, 1/2-z; III: 1-x, 1/2-x, 1/2+y, ½-z; IIII: x, 1/2-y, 1/2+z.

MMIm [SSiMe$_3$] (**3**) shows a more focused H-bonding behavior compared to the EMMIm [SSiMe$_3$] analogon. It is surprising that the hydrogen bond lengths involving the aromatic protons are throughout shorter for the EMMIm [SSiMe$_3$] than for **3**. In table S4 the lengths and angles of the identified hydrogen bonds of **3** and EMMIm [SSiMe$_3$][3] are listed.

Table S4. H-bond lengths and the corresponding distances between the crystallographically identified positions of the sulphur atom and the carbon atoms of MMIm [SSiMe$_3$] (**3**) and EMMIm [SeSiMe$_3$] (**6**).[3] Angles at the hydrogen atom and the hydrogen carbon bond are shown (distances in Å, angles in °).Chelate-like bonding modes are marked with asterisk (*). Refer to the corresponding figures for symmetry operations.

Compound / H-bond (•••)	**d(H/C•••E) [Å]**	**C-H•••E/N-C-H•••E [°]**
MMIm [SSiMe$_3$] (3)		
(N1')-C5'-H5'•••S1	2.81 / 3.678(2)	136.8(9) / –15.1(3)
*(N1'')-C2''-H2''•••S1	2.83 / 3.569(2)	137.36(9) / –135.1(1)
*(N3'')-C7''-H7''•••S1	2.79 / 3.770(2)	153.74(9) / –4.5(3)
(N1''')-C6'''-H6'''•••S1	2.80 / 3.682(2)	152.82(9) / –9.3(3)
EMMIm [SSiMe$_3$] [3]		

(N2)-C4-H4•••S1‘‘‘	2.65 / 3.524(3)	153.6(1) / –54.3(5)
(N1)-C5-H5•••S1‘‘‘‘	2.67 / 3.544(3)	152.6(1) / –84.1(4)
(N2)-C9-H9•••S1	2.81 / 3.748(3)	160.6(1) / 19.3(6)
(N2)-C9-H9•••S1‘‘	2.84 / 3.818(3)	178(2) / 115(5)
N1-C6-H6•••S1‘	2.73 / 3.713(3)	175.5(2) / –99(2)

*c. Comparison of H-bonding in MMIm [SH] (**1**) and EMIm [SH] [3]*

In figure S35 the crystallographically determined molecular structures of the title compounds MMIm [SH] (**1**) and the literature known homologue EMIm [$SSiMe_3$] are shown together with H-bonds.

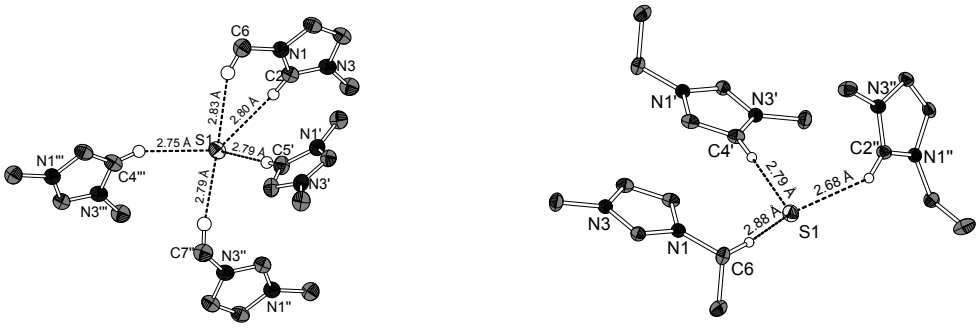

Figure S35: Left: Molecular structure of MMIm [SH] (**1**). One SH anion is bond to four MMIm cations with different kinds of hydrogen bonds. Ellipsoids are shown in 50% level (only protons active in hydrogen bonds are depicted, note that the sulfur attached proton is also not shown). Symmetry operations: I: 1/2-x, -1/2+y, 1/2-z; II: 1-x, -y, 1-z; III: -1+x, y, z. Right: Molecular structure of EMIm [SH].[2] One SH anion is bond to three EMIm cations with different kinds of hydrogen bonds. Ellipsoids are shown in 50% level (only protons active in hydrogen bonds are depicted, note that the sulfur attached proton is also not shown). Symmetry operations: I: 1-x, 1-y, 1-z; II: -1/2+x, 3/2-y, 1/2+z.

Surprisingly the H-bonding modes observed for EMIm [SH] are more focused compared to MMIm [SH] (**1**). It is unexpected that in EMIm [SH] the C5-attached proton remains completely uncoordinated, while in **1** all available chemically equivalent protons are noncovalently connected to hydrosulfide anions. Further it is interesting, that in EMIm [SH] the anion does not act as bridging hydrogen bond acceptor for the protons attached to C2 and C8 while this bonding mode is observed for **1**. In table S5 the bond lengths and angles of the identified hydrogen bonds of MMIm [SH] **1** and EMIm [SH] are listed.

Table S5. Hydrogen bond lengths and the corresponding distances between the crystallographically identified positions of the sulfur atom and the carbon atoms of MMIm [SH] (**1**) and EMIm [SH].[2] Bonding and dihedral angles regarding the H-bond are shown (distances in Å, angles in °). Chelate-like bonding modes are marked with asterisk (*). Refer to the corresponding figures for symmetry operations.

Compound / H-bond (•••)	**d(H/C•••E) [Å]**	**C-H•••E/N-C-H•••E [°]**
MMIm [SH] (1)		
(N3’’’)-C4’’’-H4’’’•••S1	2.75 / 3.625(4)	153.4(2) / 16.4(7)
(N1’)-C5’-H5’•••S1	2.79 / 3.736(3)	173.8(2) / 116(2)
*(N1)-C2-H2•••S1	2.80 / 3.573(4)	139.8(2) / 39.4(5)
*(N1)-C6-H6•••S1	2.83 / 3.744(3)	155.3(2) / –0.2(6)
(N3’’)-C7’’-H7’’•••S1	2.79 / 3.732(4)	160.7(2) / –11.5(8)
EMIm [SH][2]		
(N1’’)-C2’’-H2’’•••S1	2.68 / 3.520(1)	148.23(7) / 37.3(2)
(N3’)-C4’-H4’•••S1	2.79 / 3.731(1)	172.7(7) / 145.4(5)
(N1’’)-C6’’-H6’’•••S1	2.88 / 3.786(1)	152.63(7) / 52.8(2)

The H-bonding modes for the Se-homologue EMIm [SeH] are very similar to those observed in EMIm [SH] (refere to supporting information of the corresponding literature), supporting the assumption that steric aspects play a crucial role for the detectable H-bonding modes (figure S36). [2]

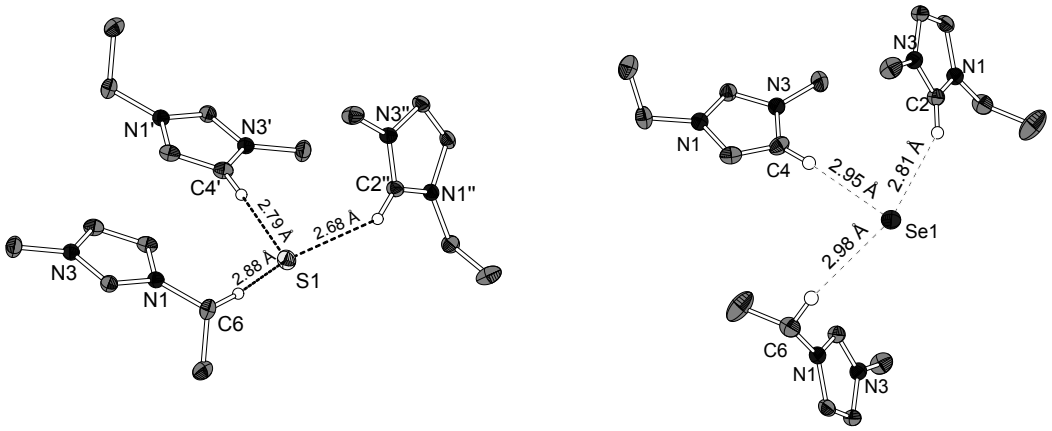

Figure S36: Left: H-bonding modes for EMIm [SH], [2] right: H-bonding modes for EMIm [SeH].[2] The pronounced similarity supports the assumption that steric aspects determine the H-bonding.

d. H-bond aggregates of the title compounds from the perspective of the basic dimeric framework

MMIm [SH] (**1**)

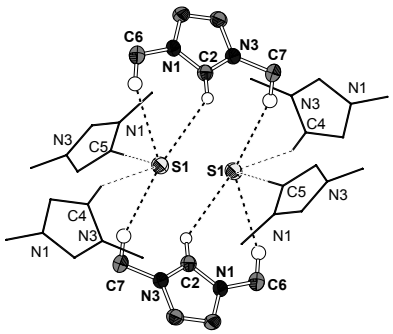

MMIm [SeH] (**4**)

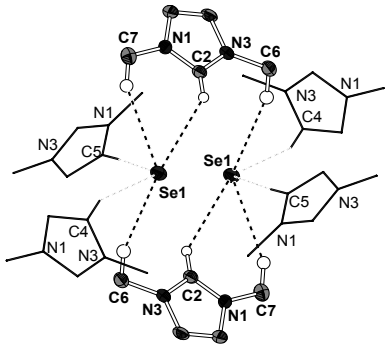

MMIm [S*t*Bu] (**2**)

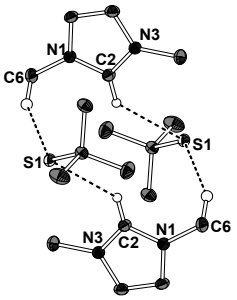

MMIm [Se*t*Bu] (**5**)

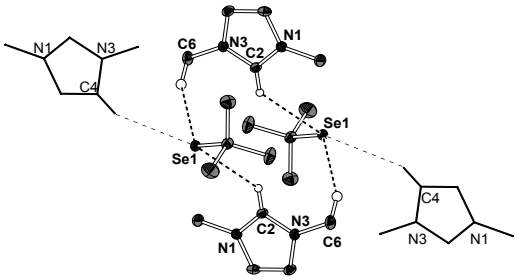

MMIm [SSiMe$_3$] (**3**)

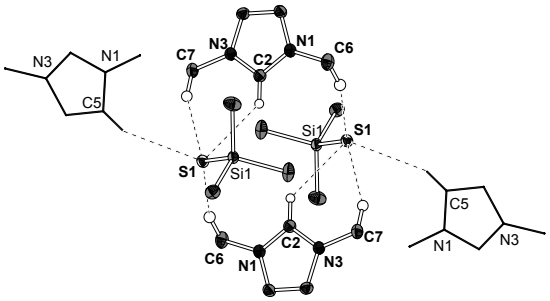

MMIm [SeSiMe$_3$] (**6**)

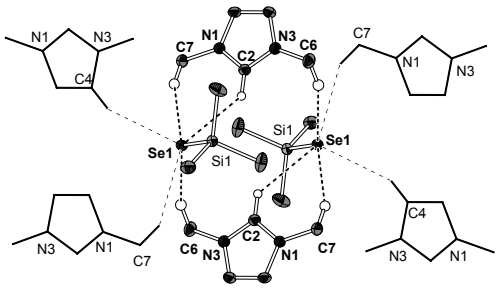

Figure S36: H-bond aggregates of the title compounds illustrated with the basic dimeric arrangement observed for MMIm [StBu] (**2**). The ion pairs of the basic dimer are represented with elliposids shown in 50% level. The symmetrically developed cations are represented as wire and sticks model for clarity. Only protons attached to the anions of the dimer are shown. These representations illustrate the pronounced steric influence of the chalcogen atoms' substituents on the H-bonding modes.

6. References

1 L. H. Finger, F. Wohde, E. I. Grigoryev, A.-K. Hansmann, R. Berger, B. Roling and J. Sundermeyer, *Chem. Commun.*, 2015, **51**, 16169–16172.
2 L. H. Finger and J. Sundermeyer, *Chem. - Eur. J.*, 2016, **22**, 4218–4230.
3 L. H. Finger, J. Guschlbauer, K. Harms and J. Sundermeyer, *Chem. - Eur. J.*, 2016, **22**, 16292–16303.

Inorg. Chem., accepted 22.10.2019, DOI: 10.1021/acs.inorgchem.9b02453.

Homoleptic Group 13 Metalates $[M(ESiMe_3)_4]^-$ (M = Ga, In; E = S, Se): Metastable Precursors for Low Temperature Syntheses of Chalcogenide Based Materials

Jannick Guschlbauer, Tobis Vollgraff, Jörg Sundermeyer

Inorganic Chemistry
Article
Cite This: Inorg. Chem. XXXX, XXX, XXX−XXX
pubs.acs.org/IC

Homoleptic Group 13 Trimethylsilylchalcogenolato Metalates $[M(ESiMe_3)_4]^-$ (M = Ga, In; E = S, Se): Metastable Precursors for Low-Temperature Syntheses of Chalcogenide-Based Materials

Jannick Guschlbauer, Tobias Vollgraff, and Jörg Sundermeyer*

Department of Chemistry and Material Science Center, Philipps-Universität Marburg, Hans-Meerwein-Straße 4, 35032 Marburg, Germany

Supporting Information

ABSTRACT: We communicate the synthesis and full characterization of so far unknown tetrakis-(trimethylsilylsulfido) and -(trimethylsilylselenido) gallates and indates in form of their organic salts $Cat^+[M(ESiMe_3)_4]^-$ (M = Ga, In; E = S, Se; Cat = dimethylpyrrolidinium ($DMPyr^+$), Ph_4P^+, $(dppe)_2Cu^+$, $(dmpe)_2Cu^+$). These thermally metastable silylchalcogenolatometalates can act as modular precursors for an ionic-liquid- or organic-solution-based low-temperature synthesis of multinary metal chalcogenide materials such as the CIGS species $Cu(In_xGa_{1-x})(S_ySe_{1-y})_2$.

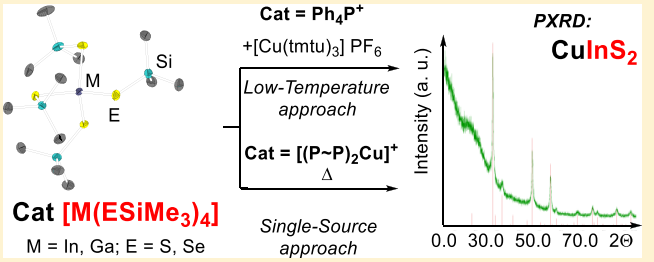

INTRODUCTION

Main-group and transition-metal compounds containing two geminal hydrosulfide and hydroselenide groups, $[M(EH)_2]$ (E = S, Se), are typically too labile with respect to elimination of H_2E and precipitation of binary metal chalcogenides $[M_xE_y]$, in particular if clusters or metal chalcogenides of high lattice energy can be formed.[1] Organochalcogenolato complexes, on the other hand, are thermally rather stable in their M−E−C ligand backbone, so that higher temperatures are needed for a more or less selective E−C bond cleavage needed in the formation of bi- or multinary metal chalcogenide materials.[2−10] It is a challenge to synthesize compounds of an intermediate thermal stability, well balanced between these extremes, to act as precursors for the synthesis of metal chalcogenide materials. We have identified so far unknown homoleptic gallium and indium complexes containing simple trimethylsilylchalcogenido ligands as targets, anticipating that condensation of $[M(ESiMe_3)_2]$ building blocks to [M(E)] units and $(Me_3Si)_2E$ would allow a low-temperature solution-based chalcogenide material synthesis.[11,12] Such an optimized approach could provide organic solutions (or inks) for the elements E = S, Se, Te in the form of their soluble salts $Cat[ESiMe_3]$.[13] Furthermore, binary metastable precursors for element combinations such as GaS, GaSe, InS, and InSe would be desirable for the synthesis of films of the binary chalcogenide M_xE_y; finally solutions of other metal ions M′ are needed to synthesize ternary or even multinary chalcogenide materials in a solution (e.g., inkjet or slot print)-based printed electronics technology.

A few heteroleptic neutral complexes containing the reactive trimethylsilylchalcogenolate moiety $L_xM(ESiMe_3)_y$ (L = auxiliary ligand; E = S, Se, Te; M = Zn,[14−16] Cd,[17] Cu,[18,19] Ag,[19] Au,[20] Mn,[21] Co)[21] are known as versatile precursors for binary materials $ME_{0.5y}$ and as starting materials for chalcogenide metal cluster synthesis.[11,14,18,20,22] This is attributed to the driving force behind the thermally inducible intra- or intermolecular elimination of volatile $E(SiMe_3)_2$ and the formation of the corresponding metal chalcogenides (Scheme 1, eq 1)[16,17] and the facile removability of the $SiMe_3$ moiety by compounds containing silicon affine nucleophiles X in the compound M′X (X = e. g. OAc) (Scheme 1, eq 2).[15,16,21−28] Among the known examples for $ESiMe_3$-containing complexes,[11,12,15,19,21,29,30] only heteroleptic trimethylsilylchalcogenolate (E) complexes containing high-priced organogallium and organoindium units (R_nM) have been described, namely four-membered rings such as $[tBu_2M(\mu_2\text{-}SeSiMe_3)]_2$,[29a] the spirocyclic M/E-heterocyclic compounds $[(Me_2M)_6E(ESiMe_3)_4]$,[29b] and the polynuclear compound $[R_3PCu(\mu_2\text{-}ESiMe_3)MMe_3]$; the last compound decomposes at room temperature.[31] Furthermore, only one example of a homoleptic trimethylsilylchalcogenidometalate anion, namely $[(tmeda)Li]_2[Mn(SSiMe_3)_4]$, has been reported.[21] Herein we report three strategies to synthesize and structurally characterize previously unknown simple gallates and indates of the type $[M(ESiMe_3)_4]^-$ (E = S, Se). The corresponding cation is either a quaternary ammonium or phosphonium (Scheme 1, eq 3a) or the copper(I) phosphine cation $[CuL_4]^+$ (Scheme 1, eq 3b). It will be demonstrated that these metastable soluble sources of the elements Ga, In, S, and Se can be combined with suitable semistabilized sources of

Received: August 13, 2019

DOI: 10.1021/acs.inorgchem.9b02453
Inorg. Chem. XXXX, XXX, XXX−XXX

Scheme 1. Neutral $ESiMe_3$ Complexes with Auxiliary Ligands and Novel Homoleptic Metalates as Precursors for Binary Materials (Eq 1),[16,17] Clusters (Eq 2),[11,19,20] and Ternary CIGS Materials (Eq 3, This Work)

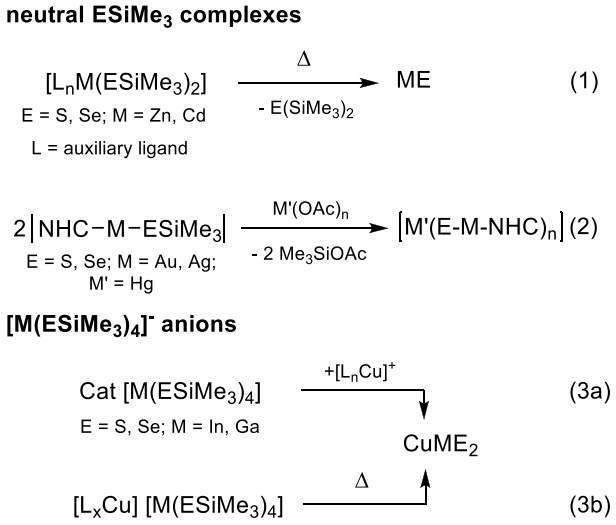

copper, $[L_nCu]^+$, in a low-temperature synthesis of CIGS particles.

This approach is of fundamental interest, as group 13 chalcogenide materials are important semiconductors for optosensoric[32] and photovoltaic applications.[33] Among the most prominent representatives are the CIGS materials $Cu(In_xGa_{1-x})(S_ySe_{1-y})_2$, which are commercially established solar absorbers in thin-film photovoltaic devices.[33] The preparation of CIGS materials is connected with some difficulties, such as the difference in chalcogenophilicity between Cu and In/Ga that can lead to phase impurities by e.g. Cu_2E.[34,35] One convenient way to prepare CIGS materials avoiding high-temperature gas-phase reactions with a large excess of sulfur and selenium sources is the thermal decomposition of single-source precursors, which are mainly based on phosphine-stabilized copper(I) cations and group 13 alkanethiolate anions $L_nCuM(ER)_m$ (M = Ga, In; R = alkyl; L = auxiliary ligand).[36−40] In the following, we communicate that any combination of the elements Ga/In and S/Se in the form of their metalates can be used as modular building blocks for selective material coprecipitation approaches toward CIGS materials (Scheme 1, eq 3a) at low temperature. Furthermore, we present single-source precursors to prepare $CuME_2$ (Scheme 1, eq 3b).

RESULTS AND DISCUSSION

$Li[In(SSiMe_3)_4]$ is prepared by reacting $InCl_3$ with 4 equiv of $LiSSiMe_3$ in diethyl ether (Supporting Information). The intended subsequent cation exchange with $Ph_4P[Cl]$ to get the uncoordinated $[In(SSiMe_3)_4]^-$ anion turned out to be problematic, as uncoordinated chloride anions tend to induce a desilylation and precipitation of indium sulfide rather than form lithium chloride. To overcome this restriction, the title compounds were synthesized by introducing the cation while—or before—metalate anion formation. By treatment of 1 equiv of $GaCl_3$ with 1 equiv of the ionic liqud $DMPyr[ESiMe_3]$ and 3 equiv of $LiESiMe_3$ at −78 °C for 18 h in tetrahydrofuran, the gallates $DMPyr[Ga(SSiMe_3)_4]$ (**1**) and $DMPyr[Ga(SeSiMe_3)_4]$ (**2**) are obtained after extraction with diethyl ether (Scheme 2). It is assumed that at low temperature the first reaction step is the formation of the

Scheme 2. Preparation of $DMPyr[Ga(SSiMe_3)_4]$ (1) and $DMPyr[Ga(SeSiMe_3)_4]$ (2)

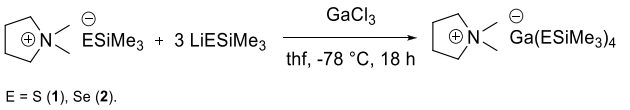

gallate $DMPyr[Cl_3Ga(ESiMe_3)]$. While the system is still cooled at −78 °C, the chlorido ligands become consecutively substituted by $LiESiMe_3$. Thereby intermolecular desilylation and precipitation of Ga_2S_3 is inhibited, as is observed for the equimolar conversion of $DMPyr[SeSiMe_3]$ and $InCl_3$ at room temperature (Supporting Information). Though the eliminated lithium chloride is soluble in tetrahydrofuran, it does not react with the target compound that is precipitating.

$DMPyr[Ga(SeSiMe_3)_4]$ (**2**) crystallizes in the monoclinic space group $P2_1/c$ with eight ion pairs per unit cell (Figure 1). The inner core of such an anion has only been observed once in $Li[Ga(SSiR_3)_4]$ (R = O*t*Bu), but its properties are not at all comparable to those of **1**.[41]

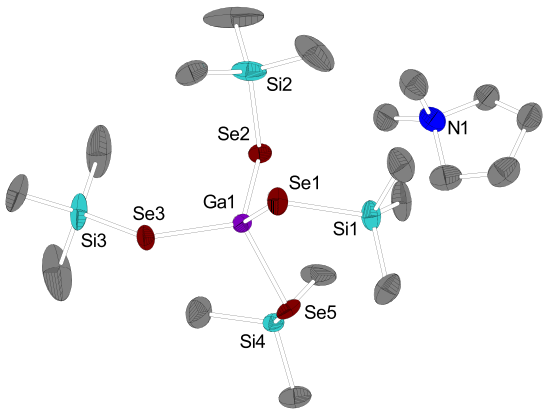

Figure 1. Molecular structure of $DMPyr[Ga(SeSiMe_3)_4]$ (**2**). Protons and disordered atoms are neglected for clarity. Ellipsoids are shown at the 50% probability level. Selected bond lengths (Å) and angles (deg) for a representative anion of **2**: Ga1−Se1 2.3997(8); Ga1−Se2 2.3883(9); Ga1−Se3 2.4158(8); Ga−Se4 2.399(3); Se1−Si1 2.268(2); Se2−Si2 2.274(2); Se3−Si3 2.259(2); Se4−Si4 2.261(2); Se1−Ga1−Se2 115.02(3); Se2−Ga1−Se3 117.29(3); Se3−Ga1−Se4 112.77(6); Se4−Ga1−Se1 104.34(5).

So far, organic salts of the type $Cat[ESiMe_3]$ have been restricted to quaternary monomethylammonium or -phosphonium cations.[13] Cations such as Ph_4P^+ and $N(PPh_3)_2^+$ that combine aspects of crystallizing tendency and lipophilicity were not accessible. Since the indate compounds do not crystallize well with $DMPyr^+$ cations, we introduced the Ph_4P^+ cation by addition of $Ph_4P[Cl]$ and $InCl_3$ to form the tetrachloroindate $Ph_4P[InCl_4]$.

The target compounds $Ph_4P[In(SSiMe_3)_4]$ (**3**) and $Ph_4P[In(SeSiMe_3)_4]$ (**4**) are obtained by substitution of the chloride atoms in tetrahydrofuran with 4 equiv of $LiESiMe_3$ and subsequent extraction into diethyl ether (Scheme 3).

$Ph_4P[In(SeSiMe_3)_4]$ (**4**) crystallizes in the orthorhombic space group $Pna2_1$ with eight ion pairs per unit cell (Figure 2).

DOI: 10.1021/acs.inorgchem.9b02453
Inorg. Chem. XXXX, XXX, XXX−XXX

Scheme 3. Preparation of $Ph_4P[In(SSiMe_3)_4]$ (3) and $Ph_4P[In(SeSiMe_3)_4]$ (4)

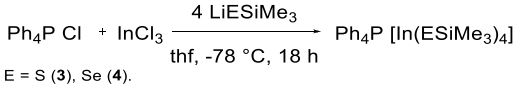

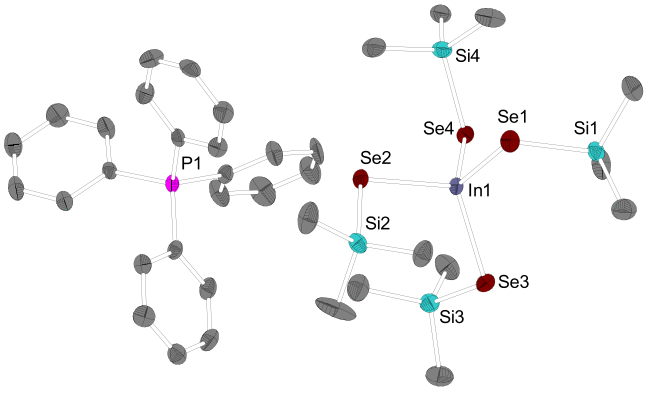

Figure 2. Molecular structure of $Ph_4P[In(SeSiMe_3)_4]$ (**4**). Protons and disordered atoms are neglected for clarity. Ellipsoids are shown at the 50% probability level. Selected bond lengths (Å) and angles (deg) for a representative anion of **4**: In1−Se1 2.562(1); In1−Se2 2.5674(9); In1−Se3 2.5632(9); In1−Se4 2.5694(8); Se1−Si1 2.255(2); Se2−Si2 2.268(2); Se3−Si3 2.289(2); Se4−Si4 2.263(2); Se1−In1−Se2 100.86(3); Se2−In1−Se3 113.56(3); Se3−In1−Se4 106.63(3); Se4−In1−Se1 111.30(3); In1−Se1−Si1 104.37(6); In1−Se2−Si2 103.23(6); In1−Se3−Si3 100.20(6); In1−Se4−Si4 102.91(6).

With **1**−**4** we have all Ga/In/S/Se combinations as binary metastable building blocks in hand. With the exception of **1** they could also be structurally characterized (Supporting Information). For the preparation of CIGS materials via the strategy in Scheme 1 eq 3a, a copper(I) source has to be provided externally. To achieve a selective formation of the desired material, a source of sufficiently masked copper(I) ions is necessary to prevent premature precipitation of Cu_2E.[19,24,31,42] $[Cu(tmtu)_3][PF_6]$ (tmtu = *N,N,N′,N′*-tetramethylthiourea) was found to be suitable in terms of both lipophilicity and stability. By adding an equimolar amount of $[Cu(tmtu)_3][PF_6]$[43] to a solution of $Ph_4P[In(SSiMe_3)_4]$ (**3**) in tetrahydrofuran at −78 °C, a clear solution is obtained that rapidly turns into a red suspension. After the red solid was annealed at 80 °C for 11 days, the isolated black powder was identified as $CuInS_2$ via PXRD with only a small amount of unassignable impurities (Supporting Information). Assuming that the reactive trimethylsilylthiolate ligands are responsible for the deficient selectivity during the precipitation of $CuInS_2$, we chose to thermolyze the anion $[In(SSiMe_3)_4]^-$ into a partially desilylated intermediate, which was obtained by harshly heating $Ph_4P[In(SSiMe_3)_4]$ (**3**) without solvent at 200 °C for 1 min prior to coprecipitation. In contrast to **3**, this residue is soluble in acetonitrile. This solution led to a more selective coprecipitation, when a solution of $[Cu(tmtu)_3][PF_6]$ in acetonitrile was added at −20 °C. Directly after the addition a slightly yellowish solution was obtained that rapidly turned into a reddish suspension (Supporting Information). After the residue was annealed at 110 °C for 3 days, $CuInS_2$ could be identified via PXRD (Scheme 4). Refer to the Supporting Information for a detailed description of this procedure.

Scheme 4. Low-Temperature Synthesis of $CuInS_2$ by Coprecipitation of Prethermolyzed $Ph_4P[In(SSiMe_3)_4]$ (3) with $[Cu(tmtu)_3][PF_6]$

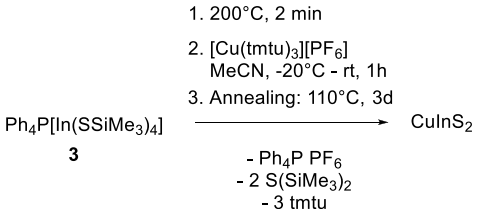

This new strategy could turn out to be of general interest for solution-based or ionic-liquid-based CIGS material syntheses. As the organic cations are variable and all Ga/In/S/Se combinations are accessible as binary precursors, a process where the ionic liquid $Cat[PF_6]$ is formed as a byproduct and flux can be envisaged. The auxiliary ligand tmtu can simply be recovered by sublimation under reduced pressure (Scheme 5).

Scheme 5. General Strategy for the Preparation of CIGS Materials in ILs Using the Title Anions

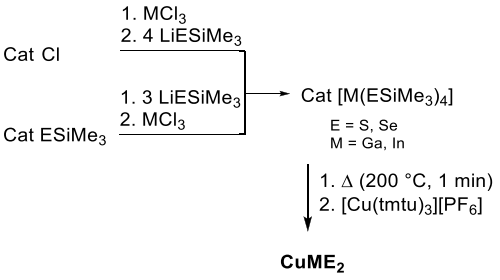

The residue obtained by thermolysis of $Ph_4P[In(SSiMe_3)_4]$ (**3**) has not yet been fully characterized. We do not have any evidence that after desilylation a coordination polymer with edge-bridged tetrahedral $[InS_2]^-$ anions in a SiS_2-like polymeric strand, as observed for $Cs[GaSe_2]$,[44] or a 2D arrangement of corner-connected heteroadamantane subunits with bridging chalcogen atoms, as observed for $Tl[MSe_2]$ (M = Ga, In),[45] is formed. Instead, NMR spectra suggest a thermal dissociation of $Ph_4P[In(SSiMe_3)_4]$ into $Ph_4P[SSiMe_3]$ and $[In(SSiMe_3)_3]$, which spontaneously eliminates $S(SiMe_3)_2$ to form the oligomer $[In(S)(SSiMe_3)]_n$ (see the Supporting Information). This is in accord with a TGA study, the results of an elemental analysis, and the fact that crystals of the flux $Cat[SSiMe_3]$ are often observed via XRD as a byproduct of this decay.

One aspect that positively affects the selectivity of low-temperature ternary chalcogenide material precipitation is a homogeneous solution of an equimolar amount of the anions in **1**−**4** and the copper source before precipitation occurs. In principle this can also be achieved on a molecular level by designing ionic single-source precursors for $CuMS_2$ materials displaying copper(I)-based cations and one of the title complexes as an anion. In order to stabilize these compounds from rapid decomposition, strongly binding auxiliary ligands are needed to protect the copper(I) complex cations from instant precipitation as Cu_2S. The sterically demanding phosphine chelate ligands dppe (bis(diphenylphosphino)-ethylene) and dmpe (bis(dimethylphosphino)ethylene) were found to match this purpose, as they stabilize the metastable ion pairs at ambient and slightly elevated temperatures.

DOI: 10.1021/acs.inorgchem.9b02453
Inorg. Chem. XXXX, XXX, XXX−XXX

We synthesized the $CuInS_2$ single-source precursor $[Cu(dppe)_2][In(SSiMe_3)_4]$ (**5**) by stirring a mixture of CuCl and 2 equiv of dppe in tetrahydrofuran. The colorless suspension that formed immediately dissolved after addition of 1 equiv of $InCl_3$. This can probably be attributed to the formation of the soluble $[Cu(dppe)_2][InCl_4]$. Without isolation this intermediate was treated with 4 equiv of $LiSSiMe_3$ in order to obtain the target compound $[Cu(dppe)_2][In(SSiMe_3)_4]$ (**5**) after extraction into diethyl ether (Scheme 6).

Scheme 6. Preparation of the $CuInS_2$ Single-Source Precursor $[Cu(dppe)_2][In(SSiMe_3)_4]$ (5)

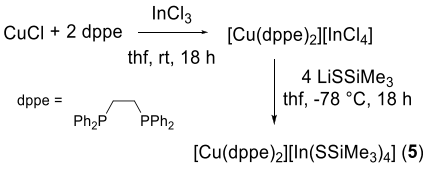

The crystallographically determined molecular structure confirms the assumptions concerning the configuration (Figure 3). $[Cu(dppe)_2][In(SSiMe_3)_4]$ (**5**) crystallizes in the monoclinic space group $P2_1/c$ with four ion pairs per unit cell.

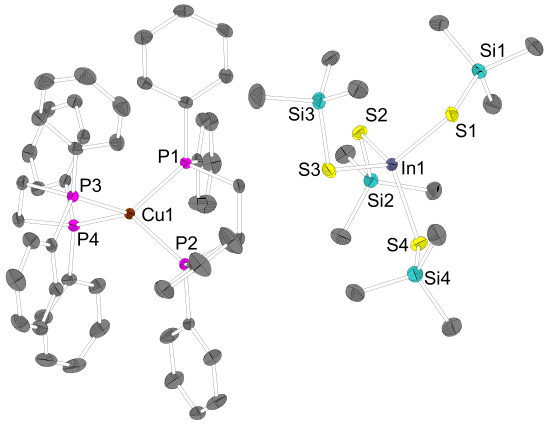

Figure 3. Molecular structure of $[Cu(dppe)_2][In(SSiMe_3)_4]$ (**5**) (In–S, 2.4510(6)–2.4683(6) Å; S–In–S, 105.53(2)–112.53(2)°). Protons are neglected for clarity. Ellipsoids are shown at the 50% probability level. Selected bond lengths (Å) and angles (deg) for a representative ion pair of **5**: In1–S1 2.4683(6); In1–S2 2.4682(6); In1–S3 2.4510(6); In1–S4 2.4564(7); S1–Si1 2.1356(7); S2–Si2 2.1320(7); S3–Si3 2.1283(7); S4–Si4 2.1397(7); S1–In1–S2 112.53(2); S2–In1–S3 108.38(2); S3–In1–S4 105.53(2); S4–In1–S1 112.06(2); In1–S1–Si1 108.58(3); In1–S2–Si2 108.84(2); In1–S3–Si3 104.42(3); In1–S4–Si4 104.25(3); Cu1–P1 2.2687(6); Cu1–P2 2.2950(6); Cu1–P3 2.2726(6); Cu1–P4 2.3001(6); P1–Cu1–P2 2.2687(6); P2–Cu1–P3 115.19(2); P3–Cu1–P4 88.99(2); P4–Cu1–P1 114.695(2).

The TGA measurement of $[Cu(dppe)_2][In(SSiMe_3)_4]$ (**5**) shows that the thermal decomposition takes place in two steps: (1) decomposition of the $[In(SSiMe_3)_4]^-$ anion and (2) thermolysis (complete desilylation, cleavage of the dppe ligands, evaporation of emerging volatiles, and incorporation of Cu(I) into the binary In/S matrix to yield $CuInS_2$). After annealing at 550 °C for 30 min $CuInS_2$ could be identified by PXRD (Figure 4) after comparison with the known reference pattern.[47]

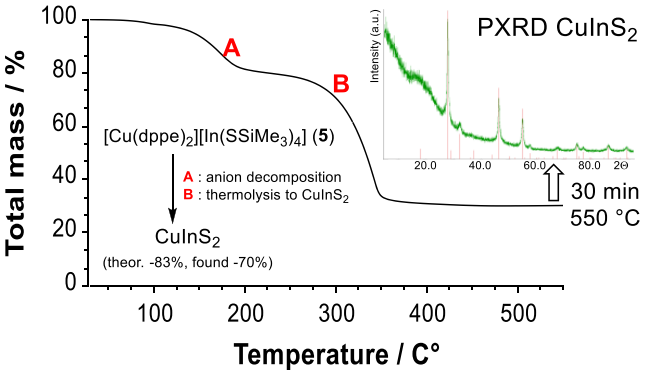

Figure 4. TGA measurement of $[Cu(dppe)_2][In(SSiMe_3)_4]$ (**5**) and PXRD of the residue that could be identified as $CuInS_2$.[46]

As dppe decomposes prior to evaporation, we assume that the observed excess mass might arise due to nonvolatile impurities that emerge during this decay. This was indirectly confirmed by the clean decomposition that was observed for the related $CuGaS_2$ single-source precursor $[(\eta^2\text{-dmpe})Cu(\mu_2\text{-dmpe})]_2[Ga(SSiMe_3)_4]_2$ (**6**), which was prepared analogously to the synthesis of **5**, but with $GaCl_3$ and dmpe ligands instead of dppe (Scheme 7).

Scheme 7. Preparation of the $CuGaS_2$ Single-Source Precursor $[(\eta^2\text{-dmpe})Cu(\mu_2\text{-dmpe})]_2[Ga(SSiMe_3)_4]_2$ (6)

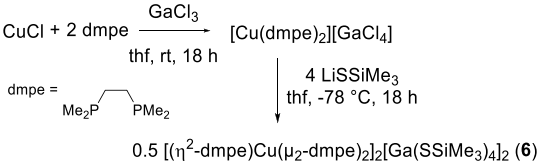

Though the electron donor ability of dmpe leads to stronger P–Cu bonds, its higher volatility (bp 180 °C) allowed their full removal during thermolysis. The TGA measurement of **6** shows a two-step decomposition similar to that for **5**. After the TGA residue was annealed at 600 °C for 30 min, $CuGaS_2$ was identified (Supporting Information).

6 crystallizes in the triclinic space group $P\bar{1}$ with one ion pair per unit cell (Figure 5). A centrosymetric dication with bridging and chelating dmpe ligands is observed.

Following the same strategy, all representatives of single-source precursors with dmpe- and dppe-containing Cu^+, with gallium and indium as the central atoms and sulfur and selenium in the silylated ligands, could be prepared by simple one-pot syntheses; all of them were structurally characterized via XRD (Supporting Information). This is a favorable aspect, when a solution-based synthesis of CIGS materials $Cu(In_xGa_{1-x})(S_ySe_{1-y})_2$ with varying Ga/In and S/Se ratios is considered.

CONCLUSION

In summary, we have prepared and structurally characterized the novel set of homoleptic metalate anions $[M(ESiMe_3)_4]^-$ comprising triel atoms Ga or In and simple, cheap, and reactive trimethylsilylchalcogenolate ligands. These can be considered as metastable binary Ga–S, Ga–Se, In–S, and In–Se building blocks in solution-based low-temperature chalcogenide material syntheses. We have shown that the title compound $Ph_4P[In(SSiMe_3)_4]$ (**3**) can be used as a precursor for the

DOI: 10.1021/acs.inorgchem.9b02453
Inorg. Chem. XXXX, XXX, XXX–XXX

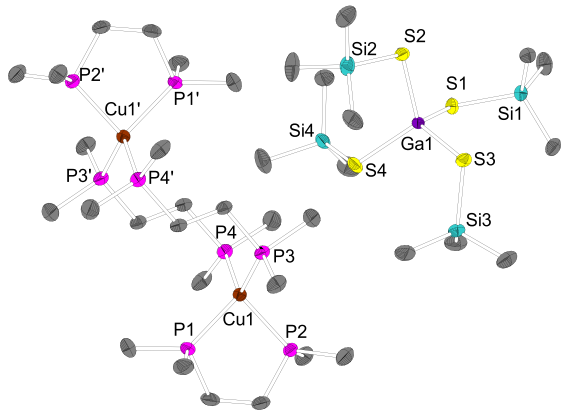

Figure 5. Molecular structure of $[(\eta^2\text{-dmpe})Cu(\mu_2\text{-dmpe})]_2[Ga(SSiMe_3)_4]_2$ (**6**) (Ga−S, 2.272(1)−2.286(1) Å; S−Ga−S, 105.65(3)−114.00(4)°). One anion and the protons are not displayed for clarity. Ellipsoids are shown at the 50% probability level. Selected bond lengths (Å) and angles (deg) for a representative anion and copper center of **6**: Ga1−S1 2.2748(9); Ga1−S2 2.286(1); Ga1−S3 2.281(1); Ga1−S4 2.272(1); S1−Si1 2.124(1); S2−Si2 2.126(1); S3−Si3 2.137(1); S4−Si4 2.128(1); S1−Ga1−S2 105.77(3); S2−Ga1−S3 105.64(3); S3−Ga1−S4 109.38(4); S4−Ga1−S1 110.04(4); Ga1−S1−Si1; 106.90(5); Ga1−S2−Si2 106.20(5); Ga1−S3−Si3 105.90(5); Ga1−S4−Si4 108.82(5); Cu1−P1 2.258(1); Cu1−P2 2.277(1); Cu1−P3 2.239(1); Cu1−P4 2.251(7); P1−Cu1−P2 89.90(4); P2−Cu1−P3 112.09(4); P3−Cu1−P4 112.14(4); P4−Cu1−P1 115.20(4).

coprecipitation of $CuInS_2$ by treatment with $[Cu(tmtu)_3][PF_6]$ in acetonitrile at low temperature. By a combination of the title anions with copper(I)-based cations that are protected with more strongly binding auxiliary ligands (L = dppe, dmpe), single-source precursors of the type $[CuL_2][M(ESiMe_3)_4]$ are obtained. Thermal decompositions of $[Cu(dppe)_2][In(SSiMe_3)_4]$ (**5**) and $[(\eta^2\text{-dmpe})Cu(\mu_2\text{-dmpe})]_2[Ga(SSiMe_3)_4]_2$ (**6**) yield $CuInS_2$ and $CuGaS_2$, respectively. This new strategy of designing homoleptic metastable silylchalcogenolato metalates as molecular precursors for solution-based material synthesis is of general interest, as it can be further developed into a spray-coating or inkjet printing technology. It will be demonstrated soon that this strategy can be extended to other metal chalcogenide semiconductor materials that also form sulfides and selenides of high lattice energy.

EXPERIMENTAL SECTION

General considerations regarding starting materials, solvents, analytical devices, and the preparation of the homologues are provided as Supporting Information. Here the syntheses of the title compounds are presented.

Synthesis of DMPyr[Ga(SSiMe$_3$)$_4$] (1). With continuous stirring at 0 °C *n*-BuLi (2.9 M, 0.35 mL, 1.02 mmol, 3.0 equiv) was added dropwise to a solution of $S(SiMe_3)_2$ (187 mg, 1.05 mmol, 3.1 equiv) in thf (10 mL). After the mixture was stirred for 30 min at 0 °C and another 30 min at ambient temperature, all volatiles were removed under fine vacuum with the help of diethyl ether and pentane until a colorless powder was obtained. DMPyr[$SSiMe_3$] (70 mg, 0.34 mmol, 1.0 equiv) was added to the residue, and the mixture was suspended in thf (10 mL). With continuous stirring at −78 °C a solution of $GaCl_3$ (60 mg, 0.34 mmol, 1.0 equiv) in thf (10 mL) was added dropwise to the suspension. The reaction mixture was stirred within the −78 °C cooling bath (dry ice/acetone) and thereby allowed to obtain ambient temperature very slowly within 18 h. All volatiles were removed under fine vacuum, and the colorless residue was suspended in diethyl ether (60 mL). The mixture was filtered off from the crude product and the filtrate was stored at −30 °C for 24 h to obtain colorless crystals. The mother liquor was filtered off from the product and reused for further extraction cycles of the crude product. Four to five repetitions yielded colorless crystals of DMPyr[Ga(SSiMe$_3$)$_4$] (**1**) with a yield of 156 mg (0.26 mmol, 78%) after drying under fine vacuum.

^{1}H NMR (300.3 MHz, THF[d_8]): δ 3.73 (m, 4H, $[(CH_2CH_2)_2N(CH_3)_2]^+$), 3.32 (s, 6H, $[(CH_2CH_2)_2N(CH_3)_2]^+$), 2.31 (m, 4H, $[(CH_2CH_2)_2N(CH_3)_2)]^+$), 0.32 (s, 36H, $[Ga(SSi(CH_3)_3)_4]^-$) ppm. ^{13}C NMR (75.5 MHz, THF[d_8]): δ 66.4 (s, $[(CH_2CH_2)_2N(CH_3)_2)]^+$), 52.6 (s, $[(CH_2CH_2)_2N(CH_3)_2)]^+$), 22.6 (s, $[(CH_2CH_2)_2N(CH_3)_2)]^+$), 5.7 (s, $[Ga(SSi(CH_3)_3)_4]^-$) ppm. ^{29}Si NMR (59.7 MHz, THF[d_8]): δ 10.2 (s, $[Ga(SSi(CH_3)_3)_4]^-$) ppm. Note that the low solubility of **1** in THF led to very weak signals in the ^{13}C NMR spectra, preventing the observation of coupling of ^{13}C with ^{15}N, and a vanishingly low visibility of the signal at 66.4 ppm. Anal. Calcd for $C_{18}H_{50}GaNS_4Si_4$: C, 36.59; H, 8.53; N, 2.37; S, 21.70. Found: C, 36.54; H, 8.28; N, 2.68; S, 22.14.

Synthesis of DMPyr[Ga(SeSiMe$_3$)$_4$] (2). With continuous stirring at 0 °C *n*-BuLi (2.9 M, 0.27 mL, 0.77 mmol, 3.0 equiv) was added dropwise to a solution of $Se(SiMe_3)_2$ (180 mg, 0.80 mmol, 3.1 equiv) in thf (10 mL). After the mixture was stirred for 30 min at 0 °C and another 30 min at ambient temperature, all volatiles were removed under fine vacuum with the help of diethyl ether and pentane until a colorless powder was obtained. DMPyr[$SeSiMe_3$] (65 mg, 0.26 mmol, 1.0 equiv) was added to the residue, and the mixture was suspended in thf (10 mL). With continuous stirring at −78 °C a solution of $GaCl_3$ (45 mg, 0.26 mmol, 1.0 equiv) in thf (10 mL) was added dropwise to the suspension. The reaction mixture was stirred within the −78 °C cooling bath (dry ice/acetone) and thereby allowed to obtain ambient temperature very slowly within 18 h. All volatiles were removed under fine vacuum, and the colorless residue was suspended in diethyl ether (60 mL). The mixture was filtered off from the crude product, and the filtrate was stored at −30 °C for 24 h to obtain colorless crystals. The mother liquor is filtered off from the product and reused for further extraction cycles of the crude product. Four to five repetitions yielded colorless crystals of DMPyr[Ga(SeSiMe$_3$)$_4$] (**2**) with a yield of 136 mg (0.17 mmol, 68%) after drying under fine vacuum. Single crystals suitable for X-ray diffraction of **2** were grown from a saturated solution in diethyl ether after storing the mixture at room temperature for 2 days.

^{1}H NMR (300.3 MHz, THF[d_8]): δ 3.70 (m, 4H, $[(CH_2CH_2)_2N(CH_3)_2]^+$), 3.30 (s, 6H, $[(CH_2CH_2)_2N(CH_3)_2]^+$), 2.31 (m, 4H, $[(CH_2CH_2)_2N(CH_3)_2)]^+$), 0.44 (s, 36H, $[Ga(SeSi(CH_3)_3)_4]^-$) ppm. ^{13}C NMR (75.5 MHz, THF[d_8]): δ 66.4 (s, $[(CH_2CH_2)_2N(CH_3)_2)]^+$), 52.62 (t, $^1J_{CN}$ = 3.9 Hz, $[(CH_2CH_2)_2N(CH_3)_2)]^+$), 22.6 (s, $[(CH_2CH_2)_2N(CH_3)_2)]^+$), 5.8 (s, $[Ga(SeSi(CH_3)_3)_4]^-$)ppm. ^{29}Si NMR (59.7 MHz, THF[d_8]): δ 7.4 (s, $[Ga(SeSi(CH_3)_3)_4]^-$) ppm. Note that we could not observe any signals in the ^{77}Se NMR spectra, as mentioned in the general considerations, and that the low solubility of **2** in THF led to a vanishingly low visibility of the signal at 66.4 ppm. Anal. Calcd for $C_{18}H_{50}GaNSe_4Si_4$: C, 27.77; H, 6.47; N, 1.80. Found: C, 28.22; H, 6.36; N, 1.85.

Synthesis of Ph$_4$P[In(SSiMe$_3$)$_4$] (3). A mixture of $Ph_4P[Cl]$ (86 mg, 0.23 mmol, 1.0 equiv) and $InCl_3$ (51 mg, 0.23 mmol, 1.0 equiv) in thf (10 mL) was stirred for 18 h at ambient temperature to yield a clear solution of $Ph_4P[InCl_4]$. To a solution of $S(SiMe_3)_2$ (167 mg, 0.94 mmol, 4.1 equiv) in thf (10 mL) was added *n*-BuLi (2.9 M, 0.32 mL, 0.91 mmol, 4.0 equiv) dropwise with continuous stirring at 0 °C. After the mixture was stirred for 30 min at 0 °C and another 30 min at ambient temperature, all volatiles were removed under fine vacuum with the help of diethyl ether and pentane until a colorless powder was obtained. This powder was diluted in thf (10 mL) and the solution added dropwise to the $Ph_4P[InCl_4]$ solution at −78 °C. The reaction mixture was stirred within the −78 °C cooling bath (dry ice/acetone) and thereby allowed to obtain ambient temperature very slowly within 18 h. All volatiles were removed under fine vacuum, and the colorless residue was suspended in diethyl ether (60 mL). The mixture was filtered off from the crude product, and the filtrate was stored at −30 °C for 24 h to obtain colorless crystals. The mother

DOI: 10.1021/acs.inorgchem.9b02453
Inorg. Chem. XXXX, XXX, XXX−XXX

liquor was filtered off from the product and reused for further extraction cycles of the crude product. Four to five repetitions yielded colorless crystals of $Ph_4P[In(SSiMe_3)_4]$ (**3**) with a yield of 178 mg (0.20 mmol, 89%) after drying under fine vacuum. Single crystals of $Ph_4P[In(SSiMe_3)_4]$ (**3**) suitable for X-ray analyses could be obtained by layering pentane over a saturated solution of **3** in diethyl ether at −30 °C for some days.

^{1}H NMR (300.3 MHz, THF[d_8]): δ 7.96−7.81 (m, 20H, Ph_4P^+), 0.28 (s, 36H, $[In(SSi(CH_3)_3)_4]^-$) ppm. ^{13}C NMR (75.5 MHz, THF[d_8]): δ 136.2 (d, $^4J_{CP}$ = 3.0 Hz, $P(C(CHCH)_2(CH))_4$), 135.5 (d, $^3J_{CP}$ = 10.7 Hz, $P(C(CHCH)_2(CH))_4$), 131.3 (d, $^2J_{CP}$ = 13.0 Hz, $P(C(CHCH)_2(CH))_4$), 118.9 (d, $^1J_{CP}$ = 89.2 Hz, $P(C(CHCH)_2(CH))_4$), 6.0 (s, $[In(SSi(CH_3)_3)_4]^-$) ppm. ^{29}Si NMR (59.7 MHz, THF[d_8]): δ 13.7 (s, $[In(SSi(CH_3)_3)_4]^-$) ppm. Anal. Calcd for $C_{36}H_{56}InPS_4Si_4$: C, 49.40; H, 6.45; S, 14.65. Found: C, 49.34; H, 6.02; S, 14.48.

Synthesis of $Ph_4P[In(SeSiMe_3)_4]$ (4). A mixture of $Ph_4P[Cl]$ (71 mg, 0.19 mmol, 1.0 equiv) and $InCl_3$ (42 mg, 0.18 mmol, 1.0 equiv) in thf (10 mL) was stirred for 18 h at ambient temperature to yield a clear solution of $Ph_4P[InCl_4]$. To a solution of $Se(SiMe_3)_2$ (174 mg, 0.77 mmol, 4.1 equiv) in thf (10 mL) was added dropwise *n*-BuLi (2.9 M, 0.26 mL, 0.75 mmol, 4.0 equiv) with continuous stirring at 0 °C. After the mixture was stirred for 30 min at 0 °C and another 30 min at ambient temperature, all volatiles were removed under fine vacuum with the help of diethyl ether and pentane until a colorless powder was obtained. This powder was diluted in thf (10 mL) and added dropwise to the $Ph_4P[InCl_4]$ solution at −78 °C. The reaction mixture was stirred within the −78 °C cooling bath (dry ice/acetone) and thereby allowed to obtain ambient temperature very slowly within 18 h. All volatiles were removed under fine vacuum, and the colorless residue was suspended in diethyl ether (60 mL). The mixture was filtered off from the crude product, and the filtrate was stored at −30 °C for 24 h to obtain colorless crystals. The mother liquor was filtered off from the product and reused for further extraction cycles of the crude product. Four to five repetitions yielded colorless crystals of $Ph_4P[In(SeSiMe_3)_4]$ (**4**) with a yield of 147 mg (0.14 mmol, 74%) after drying under fine vacuum. Single crystals of $Ph_4P[In(SeSiMe_3)_4]$ (**4**) suitable for X-ray analyses could be obtained by layering pentane over a saturated solution of **4** in diethyl ether and storing the mixture at 0 °C for some days.

^{1}H NMR (300.3 MHz, THF[d_8]): δ 7.96−7.81 (m, 20H, Ph_4P^+), 0.40 (s, 36H, $[In(SeSi(CH_3)_3)_4]^-$) ppm. ^{13}C NMR (75.5 MHz, THF[d_8]): δ 136.3 (d, $^4J_{CP}$ = 3.0 Hz, $P(C(CHCH)_2(CH))_4$), 135.5 (d, $^3J_{CP}$ = 10.6 Hz, $P(C(CHCH)_2(CH))_4$), 131.3 (d, $^2J_{CP}$ = 12.9 Hz, $P(C(CHCH)_2(CH))_4$), 118.9 (d, $^1J_{CP}$ = 89.2 Hz, $P(C(CHCH)_2(CH))_4$), 6.5 (s, $[In(SeSi(CH_3)_3)_4]^-$) ppm. ^{29}Si NMR (59.7 MHz, THF[d_8]): δ 6.9 (s, $[In(SeSi(CH_3)_3)_4]^-$) ppm. Note that we could not observe any signals in the ^{77}Se NMR spectra, as mentioned in the general considerations. Anal. Calcd for $C_{36}H_{56}InPSe_4Si_4$: C, 40.64; H, 5.31. Found: C, 40.41; H, 5.12.

Synthesis of $[Cu(dppe)_2][In(SSiMe_3)_4]$ (5). A mixture of CuCl (14 mg, 0.14 mmol, 1.00 equiv) and dppe (114 mg, 0.29 mmol, 2.00 equiv) in thf (5 mL) was stirred at ambient temperature for 18 h to yield a colorless suspension. To this suspension was added a solution of $InCl_3$ (32 mg, 0.14 mmol, 1.00 equiv) in thf (5 mL). The reaction mixture was stirred for 24 h at room temperature to yield a colorless solution of $[Cu(dppe)_2][InCl_4]$. To a solution of $S(SiMe_3)_2$ (105 mg, 0.59 mmol, 4.1 equiv) in thf (5 mL) was added dropwise *n*-BuLi (2.9M, 0.20 mL, 0.57 mmol, 4.0 equiv) with continuous stirring at 0 °C . After the mixture was stirred for 30 min at 0 °C and another 30 min at ambient temperature, all volatiles were removed under fine vacuum with the help of diethyl ether and pentane until a colorless powder was obtained. This powder was diluted in thf (10 mL), and the solution was added dropwise to the $[Cu(dppe)_2][InCl_4]$ solution at −78 °C. The reaction mixture was stirred within the −78 °C cooling bath (dry ice/acetone) and thereby allowed to obtain ambient temperature very slowly within 18 h. All volatiles were removed under fine vacuum, and the colorless residue was suspended in diethyl ether (60 mL). The mixture was filtered off from the crude product, and the filtrate was stored at −30 °C for 24 h to obtain colorless crystals. The mother liquor was filtered off the product and reused for further extraction cycles of the crude product. Two repetitions yieldeds colorless crystals of $[Cu(dppe)_2][In(SSiMe_3)_4]$ (**5**) with a yield of 162 mg (0.12 mmol, 81%) after drying under fine vacuum. Single crystals suitable for X-ray analysis were grown by layering pentane over a saturated solution of **5** in diethyl ether and storing this mixture at 0 °C for several days.

^{1}H NMR (300.2 MHz, THF[d_8]): δ 7.32−7.20 (m, 40H, $2(C_6H_5)_2PCH_2CH_2P(C_6H_5)_2$), 2.56 (m, 8H, $2(C_6H_5)_2PCH_2CH_2P(C_6H_5)_2$), 0.30 (s, 36H, $[In(SSi(CH_3)_3)_4]^-$) ppm. ^{13}C NMR (75.5 MHz, THF[d_8]): δ 133.4 (m) and 133.1 (m) and 131.0 (s) and 129.7 (m) and 129.0 (m) ($(C_6H_5)_2PCH_2CH_2P(C_6H_5)_2$), 27.3 (s, $(C_6H_5)_2PCH_2CH_2P(C_6H_5)_2$), 6.3 (s, $[In(SSi(CH_3)_3)_4]^-$) ppm. ^{29}Si NMR (59.7 MHz, THF[d_8]): δ 10.8 (s, $[In(SSi(CH_3)_3)_4]^-$) ppm. Anal. Calcd for $C_{64}H_{84}CuInP_4S_4Si_4$: C, 55.06; H, 6.06; S, 9.81. Found: C, 55.32; H, 5.72; S, 7.52. Note that the deviation in the sulfur value might be traced back to stable sulfide-containing materials that form during combustion.

Synthesis of $[(\eta^2\text{-dmpe})Cu(\mu_2\text{-dmpe})_2]_2[Ga(SSiMe_3)_4]_2$ (6). To a suspension of CuCl (35 mg, 0.35 mmol, 1.00 equiv) in thf (3 mL) was added a solution of dmpe (105 mg, 0.70 mmol, 2.00 equiv) in thf (2 mL), and the mixture was stirred at ambient temperature for 18 h to yield a colorless suspension. To this suspension was added a solution of $GaCl_3$ (62 mg, 0.35 mmol, 1.00 equiv) in thf (5 mL). The reaction mixture was stirred for 24 h at room temperature to yield a colorless solution of $[Cu(dmpe)_2][GaCl_4]$. To a solution of $S(SiMe_3)_2$ (257 mg, 1.44 mmol, 4.1 equiv) in thf (10 mL) was added dropwise *n*-BuLi (2.9 M, 0.48 mL, 1.40 mmol, 4.0 equiv) with continuous stirring at 0 °C. After the mixture was stirred for 30 min at 0 °C and another 30 min at ambient temperature, all volatiles were removed under fine vacuum with the help of diethyl ether and pentane until a colorless powder was obtained. This powder was diluted in thf (10 mL) and added dropwise to the $[Cu(dmpe)_2][GaCl_4]$ solution at −78 °C. The reaction mixture was stirred within the −78 °C cooling bath (dry ice/acetone) and thereby allowed to obtain ambient temperature very slowly within 18 h. All volatiles were removed under fine vacuum, and the colorless residue was suspended in diethyl ether (60 mL). The mixture was filtered off from the crude product and the filtrate was stored at −30 °C for 24 h to obtain colorless crystals. The mother liquor is filtered off from the product and reused for further extraction cycles of the crude product. Three repetitions yielded colorless crystals of $[(\eta^2\text{-dmpe})Cu(\mu_2\text{-dmpe})_2]_2[Ga(SSiMe_3)_4]_2$ (**6**) with a yield of 138 mg (0.08 mmol, 69%) after drying under fine vacuum. Single crystals suitable for X-ray diffraction were grown from diethyl ether after a few days at ambient temperature.

^{1}H NMR (300.3 MHz, THF[d_8]): δ 1.83 (m, 8H, $2(CH_3)_2PCH_2CH_2P(CH_3)_2$), 1.38 (s, 24H, $2(CH_3)_2PCH_2CH_2P(CH_3)_2$), 0.31 (2*s**, 36H, $[Ga(SSi(CH_3)_3)_4]^-$) ppm. ^{13}C NMR (75.5 MHz, THF[d_8]): δ 29.0 (m, $(CH_3)_2PCH_2CH_2P(CH_3)_2$)), 14.4 (m, $(CH_3)_2PCH_2CH_2P(CH_3)_2$), 5.8 and 5.5 (2*s**, $[Ga(SSi(CH_3)_3)_4]^-$) ppm. ^{29}Si NMR (59.7 MHz, THF[d_8]): δ 10.6 and 9.7 (2*s**, $[Ga(SSi(CH_3)_3)_4]^-$) ppm. *Note that the two singlet signals could be attributed to equilibria caused by exchange with the dmpe ligands in solution. Anal. Calcd for $C_{48}H_{136}Cu_2Ga_2P_8S_8Si_8$: C, 33.73; H, 8.02, S, 15.01. Found: C, 33.15; H, 7.89; S, 13.45. Note that the deviation in the carbon content might be caused by the high phosphorus content, which is a known disruptive factor in combustion elemental analysis. Further, the deviation in the sulfur value might be traced back on stable sulfide-containing materials that form during combustion.

■ ASSOCIATED CONTENT

Supporting Information

The Supporting Information is available free of charge on the ACS Publications website at DOI: 10.1021/acs.inorgchem.9b02453.

X-ray crystallographic data of the presented compounds and homologues (CCDC 1939702−1939712), details

DOI: 10.1021/acs.inorgchem.9b02453
Inorg. Chem. XXXX, XXX, XXX−XXX

on devices, methods, starting materials, synthetic procedures, and analytical data for the introduced compounds, representation of NMR spectra and TGA-DSC curves, XRD details, and the preparation of materials and their characterization via PXRD (PDF)

Accession Codes

CCDC 1939702−1939712 contain the supplementary crystallographic data for this paper. These data can be obtained free of charge via www.ccdc.cam.ac.uk/data_request/cif, or by emailing data_request@ccdc.cam.ac.uk, or by contacting The Cambridge Crystallographic Data Centre, 12 Union Road, Cambridge CB2 1EZ, UK; fax: +44 1223 336033.

AUTHOR INFORMATION

Corresponding Author

*E-mail for J.S.: jsu@staff.uni-marburg.de.

ORCID

Jörg Sundermeyer: 0000-0001-8244-8201

Notes

The authors declare no competing financial interest.

ACKNOWLEDGMENTS

We thank the Deutsche Forschungsgemeinschaft DFG and its priority program SPP 1708 "Material Synthesis Near Room Temperature" for financial support. We thank K. Harms for his advice in the refinement of nontrivial XRD data. We wish to dedicate this paper to Professor Stefanie Dehnen on the occasion of her 50th birthday.

REFERENCES

(1) Peruzzini, M.; Rios, I. D. L.; Romerosa, A.; Karlin, K. D. Coordination Chemistry of Transition Metals with Hydrogen Chalcogenide and Hydrochalcogenido Ligands. *Prog. Inorg. Chem.* **2007**, 169−453.

(2) Fuhr, O.; Dehnen, S.; Fenske, D. Chalcogenide clusters of copper and silver from silylated chalcogenide sources. *Chem. Soc. Rev.* **2013**, *42*, 1871−1906.

(3) Dehnen, S.; Eichhöfer, A.; Fenske, D. Chalcogen-Bridged Copper Clusters. *Eur. J. Inorg. Chem.* **2002**, *2002*, 279−317.

(4) Fuhrmann, D.; Dietrich, S.; Krautscheid, H. Copper Zinc Thiolate Complexes as Potential Molecular Precursors for Copper Zinc Tin Sulfide (CZTS). *Chem. - Eur. J.* **2017**, *23*, 3338−3346.

(5) Fuhrmann, D.; Dietrich, S.; Krautscheid, H. Zinc Tin Chalcogenide Complexes and Their Evaluation as Molecular Precursors for Cu_2ZnSnS_4 (CZTS) and $Cu_2ZnSnSe_4$ (CZTSe). *Inorg. Chem.* **2017**, *56*, 13123−13131.

(6) Kischel, M.; Dornberg, G.; Krautscheid, H. Trialkylphosphine-stabilized copper(I) dialkylaluminum(III) ethanedithiolate complexes: single-source precursors and a novel modification of copper aluminum disulfide. *Inorg. Chem.* **2014**, *53*, 1614−1623.

(7) Kluge, O.; Grummt, K.; Biedermann, R.; Krautscheid, H. Trialkylphosphine-stabilized copper(I) phenylchalcogenolate complexes–crystal structures and copper-chalcogenolate bonding. *Inorg. Chem.* **2011**, *50*, 4742−4752.

(8) Kluge, O.; Krautscheid, H. Trialkylphosphine-stabilized copper-(I) gallium(III) phenylchalcogenolate complexes: Crystal structures and generation of ternary semiconductors by thermolysis. *Inorg. Chem.* **2012**, *51*, 6655−6666.

(9) Hossain, S.; Niihori, Y.; Nair, L. V.; Kumar, B.; Kurashige, W.; Negishi, Y. Alloy Clusters: Precise Synthesis and Mixing Effects. *Acc. Chem. Res.* **2018**, *51*, 3114−3124.

(10) Veselska, O.; Demessence, A. d^{10} coinage metal organic chalcogenolates: From oligomers to coordination polymers. *Coord. Chem. Rev.* **2018**, *355*, 240−270.

(11) DeGroot, M. W.; Corrigan, J. F. Metal-Chalcogenolate Complexes with Silyl Functionalities: Synthesis and Reaction Chemistry. *Z. Anorg. Allg. Chem.* **2006**, *632*, 19−29.

(12) Babcock, J. R.; Zehner, R. W.; Sita, L. R. A Heterocumulene Metathesis Route to $Cd[ESiMe_3]_2$ and Passivated CdE (E = S and Se) Nanocrystals. *Chem. Mater.* **1998**, *10*, 2027−2029.

(13) Finger, L. H.; Scheibe, B.; Sundermeyer, J. Synthesis of organic (trimethylsilyl)chalcogenolate salts CatTMS-E (E = S, Se, Te): The methylcarbonate anion as a desilylating agent. *Inorg. Chem.* **2015**, *54*, 9568−9575.

(14) DeGroot, M. W.; Taylor, N. J.; Corrigan, J. F. Zinc chalcogenolate complexes as capping agents in the synthesis of ternary II-II'-VI nanoclusters: structure and photophysical properties of $(N,N'\text{-tmeda})_5Zn_5Cd_{11}Se_{13}(SePh)_6(thf)_2$. *J. Am. Chem. Soc.* **2003**, *125*, 864−865.

(15) DeGroot, M. W.; Corrigan, J. F. Coordination Complexes of Zinc with Reactive $ESiMe_3$ (E = S, Se, Te) Ligands. *Organometallics* **2005**, *24*, 3378−3385.

(16) DeGroot, M. W.; Khadka, C.; Rösner, H.; Corrigan, J. F. ZnS and ZnSe Nanoparticles via Solid-State and Solution Thermolysis of Zinc Silylchalcogenolate Complexes. *J. Cluster Sci.* **2006**, *17*, 97−110.

(17) Turner, E. A.; Rösner, H.; Huang, Y.; Corrigan, J. F. Accessing Binary CdE [E = S, Se, Te] and Ternary $Cd_xZn_{1-x}E$ [E = S, Se] Materials in Mesoporous Architectures Using Silylated-Chalcogen Reagents. *J. Phys. Chem. C* **2007**, *111*, 7319−7329.

(18) Fard, M. A.; Weigend, F.; Corrigan, J. F. Simple but effective: thermally stable Cu-$ESiMe_3$ via NHC ligation. *Chem. Commun.* **2015**, *51*, 8361−8364.

(19) AzizpoorFard, M.; Levchenko, T. I.; Cadogan, C.; Humenny, W. J.; Corrigan, J. F. Stable -$ESiMe_3$ Complexes of Cu(I) and Ag(I) (E = S, Se) with NHCs: Synthons in Ternary Nanocluster Assembly. *Chem. - Eur. J.* **2016**, *22*, 4543−4550.

(20) Polgar, A. M.; Weigend, F.; Zhang, A.; Stillman, M. J.; Corrigan, J. F. A N-Heterocyclic Carbene-Stabilized Coinage Metal-Chalcogenide Framework with Tunable Optical Properties. *J. Am. Chem. Soc.* **2017**, *139*, 14045−14048.

(21) Khadka, C. B.; Macdonald, D. G.; Lan, Y.; Powell, A. K.; Fenske, D.; Corrigan, J. F. Trimethylsilylchalcogenolates of Co(II) and Mn(II): From mononuclear coordination complexes to clusters containing -ESiMe3 moieties (E = S, Se). *Inorg. Chem.* **2010**, *49*, 7289−7297.

(22) Polgar, A. M.; Khadka, C. B.; AzizpoorFard, M.; Nikkel, B.; O'Donnell, T.; Neumann, T.; Lahring, K.; Thompson, K.; Cadogan, C.; Weigend, F.; et al. A Controlled Route to a Luminescent 3 d10−5 d10Sulfido Cluster Containing Unique $AuCu_2(\mu_3\text{-}S)$ Motifs. *Chem. - Eur. J.* **2016**, *22*, 18378−18382.

(23) Khadka, C. B.; Eichhöfer, A.; Weigend, F.; Corrigan, J. F. Zinc chalcogenolate complexes as precursors to ZnE and Mn/ZnE (E = S, Se) clusters. *Inorg. Chem.* **2012**, *51*, 2747−2756.

(24) Tran, D. T. T.; Beltran, L. M. C.; Kowalchuk, C. M.; Trefiak, N. R.; Taylor, N. J.; Corrigan, J. F. Ternary Nanoclusters of CuHgS, CuHgSe, and CuInS. *Inorg. Chem.* **2002**, *41*, 5693−5698.

(25) Zhai, J.; Filatov, A. S.; Hillhouse, G. L.; Hopkins, M. D. Synthesis, structure, and reactions of a copper-sulfido cluster comprised of the parent Cu_2S unit: $\{(NHC)Cu\}_2(\mu\text{-}S)$. *Chem. Sci.* **2016**, *7*, 589−595.

(26) Kuiper, J. L.; Shapley, P. A.; Rayner, C. M. Synthesis, Structure, and Reactivity of the Ruthenium(VI)-Nickel(II) Complex $(dppe)Ni(\mu_3\text{-}S)_2\{Ru(N)Me_2\}_2$. *Organometallics* **2004**, *23*, 3814−3818.

(27) Jacobsen, H.; Fink, M. J. Decomposition Cascades of Dicoordinate Copper(I) Chalcogenides. *Eur. J. Inorg. Chem.* **2007**, *2007*, 5294−5299.

(28) DeGroot, M. W.; Taylor, N. J.; Corrigan, J. F. Controlled synthesis of ternary II-II'-VI nanoclusters and the effects of metal ion distribution on their spectral properties. *Inorg. Chem.* **2005**, *44*, 5447−5458.

(29) (a) Stoll, S.; Bott, S. G.; Barron, A. R. Selenide and selenolate compounds of indium: a comparative study of In-Se bond-forming reactions. *J. Chem. Soc., Dalton Trans.* **1997**, *8*, 1315−1321. (b) Kluge,

DOI: 10.1021/acs.inorgchem.9b02453
Inorg. Chem. XXXX, XXX, XXX−XXX

O.; Puidokait, M.; Biedermann, R.; Krautscheid, H. Synthese und Kristallstruktur der spirocyclischen Gallium- und Indium-Chalkogen-Heterocyclen $[(Me_2Ga)_6S(SSiMe_3)_4]$, $[(Me_2Ga)_6Se(SeSiMe_3)_4]$ und $[(Me_2In)_6S(SSiMe_3)_4]$. *Z. Anorg. Allg. Chem.* **2007**, *633*, 2138−2140.
(30) Niebel, T.; Macdonald, D. G.; Khadka, C. B.; Corrigan, J. F. Synthesis and Characterization of trans-PdIITrimethylsilylchalcogenolates. *Z. Anorg. Allg. Chem.* **2010**, *636*, 1095−1099.
(31) Biedermann, R.; Kluge, O.; Fuhrmann, D.; Krautscheid, H. Synthesis and Crystal Structures of $[(iPr_3P)_2Cu(\mu\text{-}ESiMe_3)(InMe_3)]$ (E = S, Se): Lewis Acid-Base Adducts with Chalcogen Atoms in Planar Coordination. *Eur. J. Inorg. Chem.* **2013**, *2013*, 4727−4731.
(32) Jacobs-Gedrim, R. B.; Shanmugam, M.; Jain, N.; Durcan, C. A.; Murphy, M. T.; Murray, T. M.; Matyi, R. J.; Moore, R. L.; Yu, B. Extraordinary photoresponse in two-dimensional $In_{(2)}Se_{(3)}$ nanosheets. *ACS Nano* **2014**, *8*, 514−521.
(33) Ramanujam, J.; Singh, U. P. Copper indium gallium selenide based solar cells - a review. *Energy Environ. Sci.* **2017**, *10*, 1306−1319.
(34) Al-Shakban, M.; Matthews, P. D.; Zhong, X. L.; Vitorica-Yrezabal, I.; Raftery, J.; Lewis, D. J.; O'Brien, P. On the phase control of $CuInS_2$ nanoparticles from Cu-/In-xanthates. *Dalton Trans.* **2018**, *47*, 5304−5309.
(35) Binsma, J. J. M.; Giling, L. J.; Bloem, J. Phase relations in the system Cu_2S-In_2S_3. *J. Cryst. Growth* **1980**, *50*, 429−436.
(36) Banger, K. K.; Jin, M. H.-C.; Harris, J. D.; Fanwick, P. E.; Hepp, A. F. A new facile route for the preparation of single-source precursors for bulk, thin-film, and nanocrystallite I-III-VI semiconductors. *Inorg. Chem.* **2003**, *42*, 7713−7715.
(37) Sun, C.; Cevher, Z.; Zhang, J.; Gao, B.; Shum, K.; Ren, Y. One-pot synthesis and characterization of chalcopyrite $CuInS_2$ nanoparticles. *J. Mater. Chem. A* **2014**, *2*, 10629−10633.
(38) Zhao, X.; Huang, Y.; Corrigan, J. F. Facile Preparation of Wurtzite $CuInE_2$(E = S, Se) Nanoparticles Under Solvothermal Conditions. *Inorg. Chem.* **2016**, *55*, 10810−10817.
(39) Fujdala, K. L.; Chomitz, W. A.; Zhu, Z.; Kuchta, M. C. *Polymeric precursors for CIS and CIGS photovoltaics*. EP 2462149A2, 2010.
(40) Hirpo, W.; Dhingra, S.; Sutorik, A. C.; Kanatzidis, M. G. Synthesis of mixed copper-indium chalcogenolates. Single-source precursors for the photovoltaic materials $CuInQ_2$ (Q = S, Se). *J. Am. Chem. Soc.* **1993**, *115*, 1597−1599.
(41) Baranowska, K.; Chojnacki, J.; Wojnowski, W.; Wurster, E. Lithium tetrakis(tri-tert-butoxysilanethiolato)gallate(III). *Acta Crystallogr., Sect. E: Struct. Rep. Online* **2002**, *58*, m728−m729.
(42) Kluge, O.; Biedermann, R.; Holldorf, J.; Krautscheid, H. Organo-gallium/indium chalcogenide complexes of copper(I): Molecular structures and thermal decomposition to ternary semiconductors. *Chem. - Eur. J.* **2014**, *20*, 1318−1331.
(43) JCPDS File No. 65-2732.
(44) JCPDS File No. 27-0159.
(45) Friedrich, D.; Schlosser, M.; Näther, C.; Pfitzner, A. In Situ X-ray Diffraction Study of the Thermal Decomposition of Selenogallates $Cs_2[Ga_2(Se_2)_{2-x}Se_{2+x}]$ (x = 0, 1, 2). *Inorg. Chem.* **2018**, *57*, 5292−5298.
(46) Krebs, B. Thio- and Seleno-Compounds of Main Group Elements - Novel Inorganic Oligomers and Polymers. *Angew. Chem., Int. Ed. Engl.* **1983**, *22*, 113−134.
(47) JCPDS File No. 25-0279.

DOI: 10.1021/acs.inorgchem.9b02453
Inorg. Chem. XXXX, XXX, XXX−XXX

Supporting Information:

Homoleptic Group 13 Trimethylsilylchalcogenolato Metalates $[M(ESiMe_3)_4]^-$ (M = Ga, In; E = S, Se): Metastable Precursors for Low Temperature Syntheses of Chalcogenide Based Materials

Jannick Guschlbauer, Tobias Vollgraff, Jörg Sundermeyer*

Fachbereich Chemie and Material Science Center, Philipps-Universität Marburg, Hans-Meerwein-Straße 4, 35032 Marburg (Germany). Email: JSU@staff.uni-marburg.de

Content

General Considerations

All preparative operations were conducted by using standard Schlenk techniques and freshly dried solvents. Solvents were dried according to common procedures[1] and passed through columns of aluminium oxide, R3-11G-catalyst (BASF) or molecular sieves (3 Å or 4 Å). Elemental analyses (C, H, N, S) were carried out by the service department for routine analysis from the department of chemistry at the university of Marburg with a vario MICRO cube (Elementar). Samples for elemental analysis were weighted into tin capsules inside a nitrogen filled glovebox. ^{1}H and proton decoupled ^{13}C NMR spectra were recorded in automation with a Bruker Avance II 300 spectrometer, ^{29}Si NMR spectra were recorded by the service department for NMR analyses with a Bruker Avance II HD 300, DRX 400 or Avance III 500 spectrometer. All spectra were recorded at ambient temperature. ^{1}H and ^{13}C NMR spectra were calibrated using residual proton signals of the solvent (THF[d_8]: δ_H 3.58 & 1.72 ppm, δ_C 67.21 & 25.31 ppm). ^{29}Si NMR spectra were referenced externally ($SiMe_4$: δ_{Si} 0.00 ppm). For NMR-Solvents other than THF[d_8], like DMSO[d_6], MeCN[d_3], $CDCl_3$, and CD_2Cl_2, decomposition of the title anions was observed. Other inert solvents like C_6D_6 are not polar enough to dissolve the compounds. THF[d_8] does only slightly dissolve the target compounds. Silicon grease impurities that are indicated in the NMR spectra are not attributed to impure substances, as proven by elemental analysis, but rather to the low solubility of the compounds in THF[d_8]. For the selenium containing complexes we tried to get ^{77}Se NMR-spectra but could never observe a signal. We assume that this is an effect of the quadrupole momentum of the gallium and indium nuclei when symmetrically coordinated by trimethylsilylselenolate ligands. We could always prove the presence of selenium within the presented selenolates by the precipitation of red elemental selenium when treating the probe with a solution of bromine in methanol.

TGA measurements were conducted with a DSC-TGA 3 (Mettler Toledo) in a glovebox. Decomposition temperatures were determined using data of the DSC-TGA.

All solvents were dried according to common procedures and passed through columns of aluminium oxide, 3 Å molecular sieves and R3-11G catalyst (BASF) or stored over molecular sieves (3 Å or 4 Å). The reagents were used as received unless stated otherwise. $[Cu(tmtu)_3][PF_6]$,[2] dppe,[3] DMPyr[$ESiMe_3$],[4] $E(SiMe_3)_2$,[5] $LiESiMe_3$[6] (E = S, Se; tmtu = *N,N,N',N'*-dimethylthiourea, DMPyr = dimethylpyrrolidinium) were prepared according to literature known procedures or slightly modified.

The data collection for the single-crystal structure determination was performed on a Stoe Stadivari diffractometer or a Bruker D8 Quest diffractometer by the X-ray service department

of the department of chemistry at the university of Marburg. Information concerning the used hardware, and software used for data collection, cell refinement and data reduction as well as structure solution and refinement can be reviewed in the attached CIF-files. After the solution (Shelxt)[7] and refinement process (Shelxl 2017/1)[8] the data was validated by using Platon.[9] All graphic representations were created with Diamond 4.[10]

PXRD measurements were conducted by giving a small amount of the sample between two layers of Scotch tape. The diffractograms were recorded on a Stoe Stadi MP using Cu or Mo-$K_{\alpha 1}$ radiation that passed a bent focusing monochromator and a high sensitivity Mythen-detector. The transmission diffractograms were recorded from 2theta = 5° - 105° (5°min^{-1}).

Experimental Section

The usage of acetonitrile, dimethylsulfoxide, dichlormethane or chloroform resulted in the decomposition of the title anions $[M(ESiMe_3)_4]^-$ (M = Ga, In; E = S, Se) and are avoided throughout the described procedures.

Additional experiments

Our first attempts to synthesize the title anions were inspired by the synthesis of $Li_2Mn(SSiMe_3)_4$.[11] By preparing $Li[In(SSiMe_3)_4]$ from $InCl_3$ and four equivalents of $LiSSiMe_3$ in diethyl ether a white solid could be extracted. The intended subsequent cation exchange with Ph_4P Cl turned out to be a problematic step because uncoordinated chloride anions are more likely to desilylate the target compound than to form lithium chloride.

For the preparation of the gallates DMPyr $[Ga(SSiMe_3)_4]$ (**1**) and DMPyr $[Ga(SeSiMe_3)_4]$ (**2**) we made use of an addition step, in which the chalcogenolate based ionic liquid DMPyr $[ESiMe_3]$ is utilized.[4] We found out, that the equimolar conversion of $GaCl_3$ and DMPyr $[SeSiMe_3]$ at ambient temperature leads to the formation of the reactive intermediate DMPyr $[Cl_3Ga(SeSiMe_3)]$ that suddenly undergoes an intramolecular elimination of $ClSiMe_3$ to form a compound with ternary anion $DMPyr_3[SeGaCl_2]_3$.[12] To prevent this intramolecular elimination, it is necessary to properly cool down the reaction mixture as long as the intermediates of the type Cat $[Cl_{4-x}M(ESiMe_3)_x]$ (x = 1 - 4) are present.

Further we found out, that the conversion of one equivalent $GaCl_3$ and four equivalents of DMPyr $[SSiMe_3]$ does not quantitatively yield the target compound **1**. This might be attributed to the electrostatic repulsion between the $[ESiMe_3]^-$ and the $[Cl_{4-x}M(ESiMe_3)_x]^-$ (x = 1 - 4)

anions. To avoid this repulsion the neutral compound $LiESiMe_3$ was used to substitute the chloratoms of the metal center.[6]

In addition to the compounds presented in the main text, we prepared and characterized further homologues of the single source precursors of the type $[L_2Cu]_n[M(ESiMe_3)_4]$ (L = dppe, dmpe, M = Ga, In; E = S, Se) analogously to the preparation of the presented title compounds **5** and **6**.

Synthesis of Li[In(SeSiMe$_3$)$_4$] • 0.5 thf and Li[In(SSiMe$_3$)$_4$] • 0.25 thf

n-BuLi (2.9M, 0.38 mL, 1.10 mmol, 4.00 equiv.) was dropwise added to a solution of $Se(SiMe_3)_2$ (253 mg, 1.12 mmol, 4.10 equiv.) in thf (10 mL) at 0 °C and stirred for 30 min at 0 °C and further 1 h at ambient temperature. All volatiles were removed under reduced pressure until a colorless powder is obtained. The residue was diluted in diethyl ether (10 mL) and given into a solution of $InCl_3$ (61 mg, 0.27 mmol, 1.00 equiv.) in diethyl ether (10 mL) at –78 °C. The reaction mixture is stirred within the –78 °C cooling bath (dry ice/acetone) and thereby allowed to obtain ambient temperature very slowly within 18 h. Lithium chloride is removed by filtration and all the volatiles of the obtained solution are removed under reduced pressure. After drying in fine vacuum Li $[In(SeSiMe_3)_4]$ • 0.5 thf is obtained as colorless solid with a yield of 184 mg (0.32 mmol, 87%). ^{1}H NMR (500.20 MHz, THF[d_8]): δ = 3.62 (m, 2H. 0.5 x $(CH_2)_2(CH_2)_2O)$), 1.77 (m, 2H. 0.5 x $(CH_2)_2(CH_2)_2O)$), 0.18 (s, 36 H, $[In(SeSiMe_3)_4]^-$)* ppm. ^{13}C NMR (125.78 MHz, THF[d_8]): δ= 68.0 (s, 0.5 x $(CH_2)_2(CH_2)_2O)$), 26.2 (s, 0.5 x $(CH_2)_2(CH_2)_2O)$), 8.6 (s, $[In(SeSiMe_3)_4]^-$)* ppm. ^{29}Si NMR (99.38 MHz, THF[d_8]): δ= –2.3 (s, $[In(SeSiMe_3)_4]^-$)* ppm. *Note that the shift of the $[In(SeSiMe_3)_4]^-$ anion is not the same as for $Ph_4P[In(SeSiMe_3)_4]$ (**4**). The differences are most likely caused by coordination of the anion to the lithium cation, as observed for comparable compounds.[11] Anal. Calcd. for $C_{14}H_{40}InLiO_{0.5}Se_4Si_4$: C, 21.94; H, 5.26. Found: C, 22.46, H, 5.26.

The reaction was transferred to the sulfur homologue by using 81 mg $InCl_3$ (0.37 mmol, 1.00 equiv.), 270 mg $S(SiMe_3)_2$ (1.51 mmol, 4.1 equiv.), and 0.51 mL *n*-BuLi (2.9M, 1.47 mmol, 4.00 equiv.) to obtain 172 mg of $Li[In(SSiMe_3)_4]$ • 0.25 thf (0.31 mmol, 83%). ^{1}H NMR (300.25 MHz, THF[d_8]): δ= 3.62 (m, 1H. 0.25 x $(CH_2)_2(CH_2)_2O)$), 1.78 (m, 1H. 0.25 x $(CH_2)_2(CH_2)_2O)$), 0.31 (s, 36 H, $[In(SSiMe_3)_4]^-$)* ppm. ^{13}C NMR (75.50 MHz, THF[d_8]): δ= 68.0 (s, 0.25 x $(CH_2)_2(CH_2)_2O)$), 26.2 (s, 0.5 x $(CH_2)_2(CH_2)_2O)$), 6.24 (s, $[In(SSiMe_3)_4]^-$)* ppm. ^{29}Si NMR (59.65 MHz, THF[d_8]): δ = –11.0 (s, $[In(SSiMe_3)_4]^-$)* ppm. *Note that the shift of the $[In(SSiMe_3)_4]^-$ anion is not the same as for $Ph_4P[In(SSiMe_3)_4]$ (**3**). The differences might

be caused by coordination of the anion to the lithium cation, as observed for comparable compounds.[11]

No successful exchange of the Li-cation could be realized by using Ph_4PCl in diethyl ether.

Reaction of $InCl_3$ with one equivalent DMPyr [$SeSiMe_3$]

A solution of $GaCl_3$ (55 mg, 0.31 mmol, 1.00 equiv.) in 10 mL thf was given dropwise to DMPyr [$SeSiMe_3$] (78 mg, 0.31 mmol, 1.00 equiv.) at –78 °C and stirred for 10 min. The suspension was warmed to room temperature and stirred for a further 30 min until a yellowish precipitate arises. All volatiles were removed under reduced pressure and the residue was dried in fine vacuum. DMPyr [Cl_2GaSe] was obtained as yellow powder with a yield of 95 mg (0.31 mmol, 95%) that is very low soluble in thf and MeCN. Anal. Calcd. for $C_6H_{14}C_{l2}GaNSe$: C, 22.54; H, 4.41; N, 4.38. Found: C, 21.94; H, 4.18; N, 4.51. Note that the crude product was investigated.

We assume the anion in the product DMPyr [Cl_2GaSe] to be trimeric, as described in literature.[12] The herein presented procedure can be considered an alternative for the established processes.

Reaction of $GaCl_3$ with four equivalents of DMPyr [$SSiMe_3$]

To a suspension of DMPyr [$SSiMe_3$] (70 mg, 0.34 mmol, 4.00 equiv.) in thf (5 mL) a solution of $GaCl_3$ (15 mg, 0.09 mmol, 1.00 equiv.) was added dropwise at –78 °C. The reaction mixture is stirred within the –78 °C cooling bath (dry ice/acetone) and thereby allowed to obtain ambient temperature very slowly within 18 h. The obtained suspension was filtered and all volatiles were removed from the filtrate to obtain a colorless solid with a yield of 30 mg (0.05 mmol, 60%). ^{1}H NMR (300.3 MHz, THF[d_8]): δ = 3.69 (m, 4H, $[(CH_2CH_2)_2N(CH_3)_2]^+$), 3.29 (s, 6H, $[(CH_2CH_2)_2N(CH_3)_2]^+$), 2.30 (m, 4H, $[(CH_2CH_2)_2N(CH_3)_2)]^+$), 0.32 (s, 27H, $[Ga(SSi(CH_3)_3)_4]^-$)* ppm; ^{29}Si NMR(59.7 MHz, THF[d_8]): δ = 11.2 (s, $[Ga(SSi(CH_3)_3)_4]^-$) ppm. Due to the low concentration no ^{13}C NMR could be obtained. *The integral of the anion's signal indicates an incomplete conversion of the educts or unselective processes. We assume the electrostatic repulsion between the assumed $[Cl_{4-x}M(ESiMe_3)_x]^-$ intermediates and the $[ESiMe_3]^-$ anion to be the reason for this incomplete conversion. Other possibilities are nucleophilic desilylation processes or nucleophilic attacks at the metal center by the eliminated, uncoordinated chloride anions. Though we know that DMPyr [Cl] is practically insoluble in thf, these side reactions could be an effect of a very small amount of diluted DMPyr [Cl].

Homologues of the single source precursors

Synthesis of $[Cu(dppe)_2][Ga(SSiMe_3)_4]$

The preparation of $[Cu(dppe)_2][Ga(SSiMe_3)_4]$ was realized analogously to the synthesis of $[Cu(dppe)_2][In(SSiMe_3)_4]$ (**5**) by substitution of the corresponding homologues and the same amount of solvent: 15 mg CuCl (0.15 mmol, 1.0 eq.), 118 mg dppe (0.30 mmol, 2.0 eq.), 26 mg $GaCl_3$ (0.15 mmol, 1.0 eq.), 108 mg $S(SiMe_3)_2$ (0.61 mmol, 4.1 eq.), 0.20 mL of a 2.9M-*n*-BuLi solution (0.59 mmol, 4.0 eq.). 133 mg $[Cu(dppe)_2][Ga(SSiMe_3)_4]$ (0.10 mmol, 67%) were obtained as colorless crystalline blocks. Single crystals suitable for XRD analysis were grown by layering pentane over a saturated solution of the product in diethyl ether and storing the mixture at –30°C for several days.

^{1}H NMR (500.2 MHz, THF[d_8]): δ = 7.36 – 7.19 (m, 40H, 2 x $(C_6H_5)_2PCH_2CH_2P(C_6H_5)_2$), 2.57 (m, 8H, 2 x $(C_6H_5)_2PCH_2CH_2P(C_6H_5)_2$), 0.31 (s, 36H, $[Ga(SSi(CH_3)_3)_4]^-$) ppm. ^{13}C NMR (125.8 MHz, THF[d_8]): δ = 133.2 (m) & 133.1 (m) & 131.0 (s) & 129.7 (m) ($(C_6H_5)_2PCH_2CH_2P(C_6H_5)_2$), 27.3 (s, $(C_6H_5)_2PCH_2CH_2P(C_6H_5)_2$), 5.8 & 5.5 (2 x s, $[Ga(SSi(CH_3)_3)_4]^-$) ppm. ^{29}Si NMR (99.4 MHz, THF[d_8]): δ = 10.6 & 9.72 (s, $[Ga(SSi(CH_3)_3)_4]^-$) ppm. In the NMR-spectra two signals that can be assigned to the anion. We assume either dynamic interactions between the dppe ligands and the metalate center, or a partial rearrangement of chalcogenolate- and phosphine ligand in solution. Anal. calcd. for $C_{64}H_{84}CuGaP_4S_4Si_4$: C, 56.89; H, 6.27; S, 9.49. Found: C, 56.64; H, 6.06; S, 8.24. Note that the deviation in the sulfur value might be traced back on stable sulfide containing materials that form during combustion.

Synthesis of $[Cu(dppe)_2][Ga(SeSiMe_3)_4]$

The preparation of $[Cu(dppe)_2][Ga(SeSiMe_3)_4]$ was realized analogously to the synthesis of $[Cu(dppe)_2][In(SSiMe_3)_4]$ (**5**) by substitution of the corresponding homologues and the same amount of solvent: 13 mg CuCl (0.13 mmol, 1.0 eq.), 104 mg dppe (0.26 mmol, 2.0 eq.), 23 mg $GaCl_3$ (0.13 mmol, 1.0 eq.), 120 mg $Se(SiMe_3)_2$ (0.53 mmol, 4.1 eq.), 0.18 mL of a 2.9M-*n*-BuLi solution (0.52 mmol, 4.0 eq.). 143 mg $[Cu(dppe)_2][Ga(SeSiMe_3)_4]$ (0.09 mmol, 72%) were obtained as colorless crystalline blocks. Single crystals suitable for XRD analysis were grown by layering pentane over a saturated solution of the product in diethyl ether and storing the mixture at –30°C for several days.

^{1}H NMR (300.3 MHz, THF[d_8]): δ = 7.37 – 7.18 (m, 40H, 2 x $(C_6H_5)_2PCH_2CH_2P(C_6H_5)_2$), 2.56 (m, 8H, 2 x $(C_6H_5)_2PCH_2CH_2P(C_6H_5)_2$), 0.42 (s, 36H, $[Ga(SeSi(CH_3)_3)_4]^-$) ppm. ^{13}C NMR (75.5 MHz, THF[d_8]): δ = 133.4 (m) & 133.1 (m) & 131.0 (s) & 129.7 (m) & 129.0

((C_6H_5)$_2$PCH$_2$CH$_2$P(C_6H_5)$_2$), 27.3 (s, (C_6H_5)$_2$P*C*H$_2$*C*H$_2$P(C_6H_5)$_2$), 5.9 (2 x s*, [Ga(SeSi(*C*H$_3$)$_3$)$_4$]$^-$) ppm. ^{29}Si NMR (59.7 MHz, THF[d$_8$]): δ = 6.52 (s, [Ga(Se*Si*(CH$_3$)$_3$)$_4$]$^-$) ppm. *In the NMR-spectra two signals that can be assigned to the anion. We assume either dynamic interactions between the dppe ligands and the metalate center, or a partial rearrangement of chalcogenolate- and phosphine ligand in solution.

Synthesis of [Cu(dppe)$_2$][In(SeSiMe$_3$)$_4$]

The preparation of [Cu(dppe)$_2$][In(SeSiMe$_3$)$_4$] was realized analogously to the synthesis of [Cu(dppe)$_2$][In(SSiMe$_3$)$_4$] (**5**) by substitution of the corresponding homologues and the same amount of solvent: 13 mg CuCl (0.13 mmol, 1.0 eq.), 101 mg dppe (0.25 mmol, 2.0 eq.), 28 mg InCl$_3$ (0.13 mmol, 1.0 eq.), 117 mg Se(SiMe$_3$)$_2$ (0.52 mmol, 4.1 eq.), 0.17 mL of a 2.9M-*n*-BuLi solution (0.51 mmol, 4.0 eq.). 139 mg [Cu(dppe)$_2$][In(SeSiMe$_3$)$_4$] (0.09 mmol, 70%) were obtained as colorless crystalline blocks. Single crystals suitable for XRD analysis were grown by layering pentane over a saturated solution of the product in diethyl ether and storing the mixture at –30°C for several days.

^{1}H NMR (300.3 MHz, THF[d$_8$]): δ = 7.32 – 7.19 (m, 40H, 2 x (C_6H_5)$_2$PCH$_2$CH$_2$P(C_6H_5)$_2$), 2.54 (m, 8H, 2 x (C_6H_5)$_2$PC*H*$_2$C*H*$_2$P(C_6H_5)$_2$), 0.42 (s, 36H, [In(SeSi(C*H*$_3$)$_3$)$_4$]$^-$) ppm. ^{13}C NMR (75.5 MHz, THF[d$_8$]): δ = 133.6 & 133.5 & 133.4 & 133.1 & 131.0 & 129.7 & 129.3 & 128.9 (m, (*C*$_6$H$_5$)$_2$PCH$_2$CH$_2$P(*C*$_6$H$_5$)$_2$), 27.3 (s, (C_6H_5)$_2$P*C*H$_2$*C*H$_2$P(C_6H_5)$_2$), 6.6 & 4.5 (2 x s*, [In(SeSi(*C*H$_3$)$_3$)$_4$]$^-$) ppm. ^{29}Si NMR (59.7 MHz, THF[d$_8$]): δ = 11.0 & 6.9 (2 x s*, [In(Se*Si*(CH$_3$)$_3$)$_4$]$^-$) ppm. *In the NMR-spectra two signals that can be assigned to the anion. We assume either dynamic interactions between the dppe ligands and the metalate center, or a partial rearrangement of chalcogenolate- and phosphine ligand in solution.

Synthesis of [(dmpe)$_2$Cu][Ga(SeSiMe$_3$)$_4$]

The preparation of [(dmpe)$_2$Cu][Ga(SeSiMe$_3$)$_4$] was realized analogously to the synthesis of [(η^2-dmpe)Cu(μ_2-dmpe)$_2$]$_2$[Ga(SSiMe$_3$)$_4$]$_2$ (**6**) by substitution of the corresponding homologues and the same amount of solvent: 19 mg CuCl (0.19 mmol, 1.0 eq.), 58 mg dmpe (0.38 mmol, 2.0 eq.), 34 mg GaCl$_3$ (0.19 mmol, 1.0 eq.), 177 mg Se(SiMe$_3$)$_2$ (0.79 mmol, 4.1 eq.), 0.26 mL of a 2.9M-*n*-BuLi solution (0.77 mmol, 4.0 eq.). 156 mg [Cu(dmpe)$_2$][Ga(SeSiMe$_3$)$_4$] (0.14 mmol, 78%) were obtained as colorless crystalline blocks. Single crystals suitable for XRD analysis were grown by layering pentane over a saturated solution of the product in diethyl ether and storing the mixture at –30°C for several days.

^{1}H NMR (300.3 MHz, THF[d_8]): δ = 1.83 (m, 8H, 2 x $(H_3C)_2PCH_2CH_2P(CH_3)_2$), 1.39 (s, 24H, 2 x $(H_3C)_2PCH_2CH_2P(CH_3)_2$), 0.43 & 42 (2 x s*, 36H, $[Ga(SeSi(CH_3)_3)_4]^-$) ppm. ^{13}C NMR (75.5 MHz, THF[d_8]): δ = 29.0 (m, $(H_3C)_2PCH_2CH_2P(CH_3)_2$), 14.5 (m, $(H_3C)_2PCH_2CH_2P(CH_3)_2$), 5.9 & 5.7 (2 x s*, $[Ga(SeSi(CH_3)_3)_4]^-$) ppm. ^{29}Si NMR (59.7 MHz, THF[d_8]): δ = 7.5 & 6.8 (2 x s*, $[Ga(SeSi(CH_3)_3)_4]^-$) ppm. *In the NMR-spectra two signals that can be assigned to the anion. We assume either dynamic interactions between the dmpe ligands and the metalate center, or a partial rearrangement of chalcogenolate- and phosphine ligand in solution. Anal. calcd. for $C_{24}H_{68}CuGaP_4Se_4Si_4$: C, 27.7; H, 6.6 Found: C, 27.7; H, 6.4.

Synthesis of $[(\eta^2\text{-dmpe})Cu(\mu_2\text{-dmpe})_2]_2[In(SSiMe_3)_4]_2$

The preparation of $[(\eta^2\text{-dmpe})Cu(\mu_2\text{-dmpe})_2]_2[In(SSiMe_3)_4]_2$ was realized analogously to the synthesis of $[(\eta^2\text{-dmpe})Cu(\mu_2\text{-dmpe})_2]_2[Ga(SSiMe_3)_4]_2$ (**6**) by substitution of the corresponding homologues and the same amount of solvent: 22 mg CuCl (0.22 mmol, 1.0 eq.), 67 mg dmpe (0.44 mmol, 2.0 eq.), 49 mg $InCl_3$ (0.22 mmol, 1.0 eq.), 162 mg $S(SiMe_3)_2$ (0.91 mmol, 4.1 eq.), 0.31 mL of a 2.9M-*n*-BuLi solution (0.89 mmol, 4.0 eq.). 112 mg $[(\eta^2\text{-dmpe})Cu(\mu_2\text{-dmpe})_2]_2[In(SSiMe_3)_4]_2$ (0.06 mmol, 56%) were obtained as colorless crystalline blocks. Single crystals suitable for XRD analysis were grown by layering pentane over a saturated solution of the product in diethyl ether and storing the mixture at –30°C for several days.

^{1}H NMR (300.3 MHz, THF[d_8]): δ = 1.82 (m, 8H, 2 x $(H_3C)_2PCH_2CH_2P(CH_3)_2$), 1.38 (s, 24H, 2 x $(H_3C)_2PCH_2CH_2P(CH_3)_2$), 0.31 (s, 36H, $[In(SSi(CH_3)_3)_4]^-$) ppm. ^{13}C NMR (75.5 MHz, THF[d_8]): δ = 29.0 (m, $(H_3C)_2PCH_2CH_2P(CH_3)_2$), 14.4 (m, $(H_3C)_2PCH_2CH_2P(CH_3)_2$), 6.4 & 6.1 (2 x s*, $[In(SSi(CH_3)_3)_4]^-$) ppm. ^{29}Si NMR (59.7 MHz, THF[d_8]): δ = 12.0 & 11.0 (2 x s*, $[In(SSi(CH_3)_3)_4]^-$) ppm. *In the NMR-spectra two signals that can be assigned to the anion. We assume either dynamic interactions between the dmpe ligands and the metalate center, or a partial rearrangement of chalcogenolate- and phosphine ligand in solution. Anal. calcd. for $C_{24}H_{68}CuInP_4S_4Si_4$: C, 32.0; H, 7.6; S, 14.3 Found: C, 31.6; H, 7.1; S, 12.9. Note that the deviation in the sulfur value might be traced back on stable sulfide containing materials that form during combustion.

Synthesis of $[(dmpe)_2Cu][In(SeSiMe_3)_4]$

The preparation of $[(dmpe)_2Cu][In(SeSiMe_3)_4]$ was realized analogously to the synthesis of $[(\eta^2\text{-dmpe})Cu(\mu_2\text{-dmpe})_2]_2[Ga(SSiMe_3)_4]_2$ (**6**) by substitution of the corresponding homologues and the same amount of solvent: 18 mg CuCl (0.18 mmol, 1.0 eq.), 55 mg dmpe

(0.37 mmol, 2.0 eq.), 41 mg $InCl_3$ (0.18 mmol, 1.0 eq.), 170 mg $Se(SiMe_3)_2$ (0.75 mmol, 4.1 eq.), 0.25 mL of a 2.9M-*n*-BuLi solution (0.74 mmol, 4.0 eq.). 117 mg $[Cu(dmpe)_2][In(SeSiMe_3)_4]$ (0.10 mmol, 59%) were obtained as colorless crystalline blocks. Single crystals suitable for XRD analysis were grown by layering pentane over a saturated solution of the product in diethyl ether and storing the mixture at –30°C for several days.

^{1}H NMR (300.3 MHz, THF[d_8]): δ = 1.83 (m, 8H, 2 x $(H_3C)_2PCH_2CH_2P(CH_3)_2$), 1.38 (s, 24H, 2 x $(H_3C)_2PCH_2CH_2P(CH_3)_2$), 0.44 (s, 36H, $[In(SeSi(CH_3)_3)_4]^-$) ppm. ^{13}C NMR (75.5 MHz, THF[d_8]): δ = 29.0 (m, $(H_3C)_2PCH_2CH_2P(CH_3)_2$), 14.5 (m, $(H_3C)_2PCH_2CH_2P(CH_3)_2$), 6.6 (s, $[In(SeSi(CH_3)_3)_4]^-$) ppm. ^{29}Si NMR (59.7 MHz, THF[d_8]): δ = 7.3 (s, $[In(SeSi(CH_3)_3)_4]^-$) ppm. Anal. calcd. for $C_{24}H_{68}CuInP_4Se_4Si_4$: C, 26.5; H, 6.3 Found: C, 26.5; H, 5.9.

NMR Spectra

*DMPyr [Ga(SSiMe$_3$)$_4$] (**1**)*

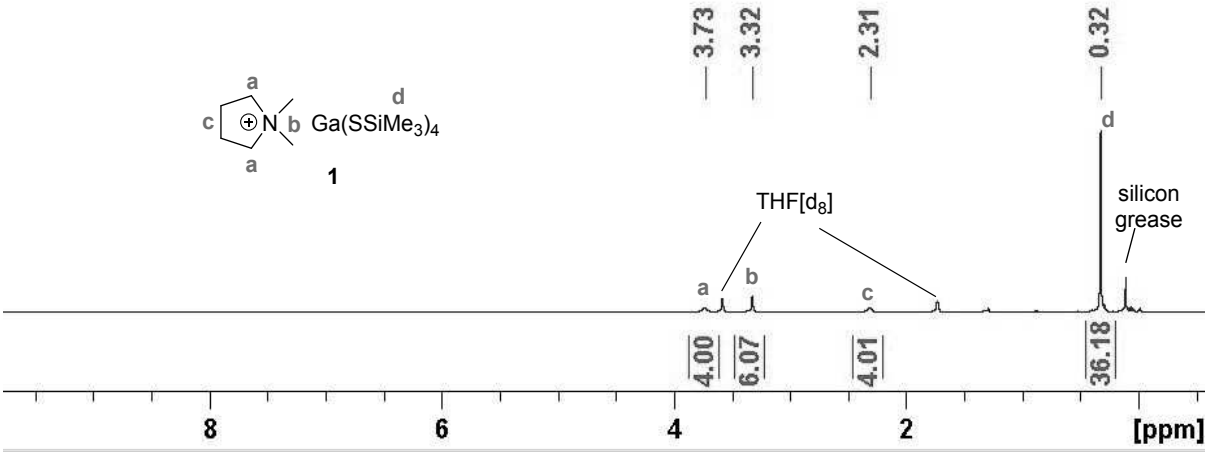

Figure S1. ^{1}H NMR (300.3 MHz, THF[d$_8$]) of **1**.

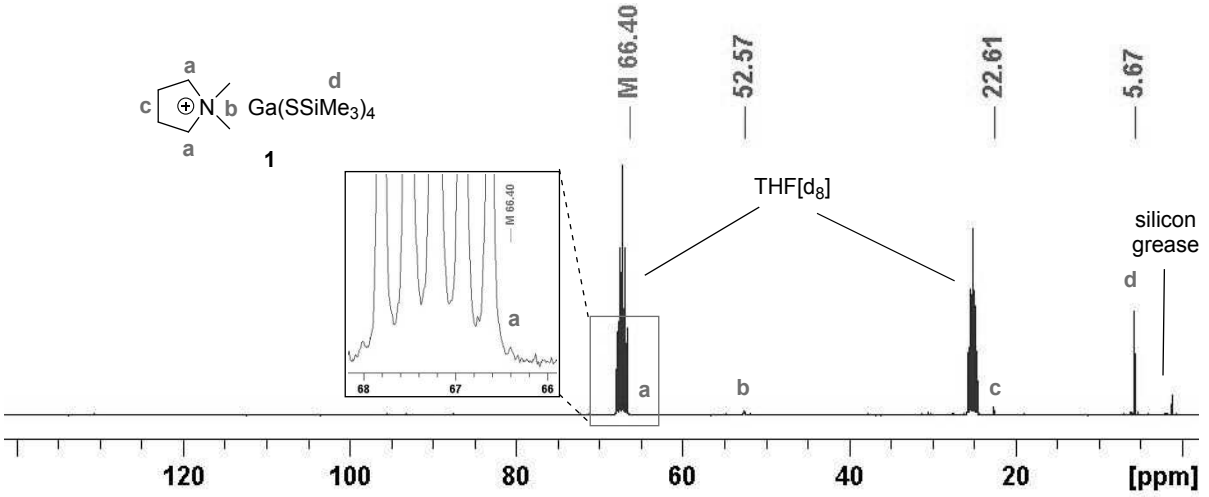

Figure S2. ^{13}C NMR (75.5 MHz, THF[d$_8$]) of **1**.

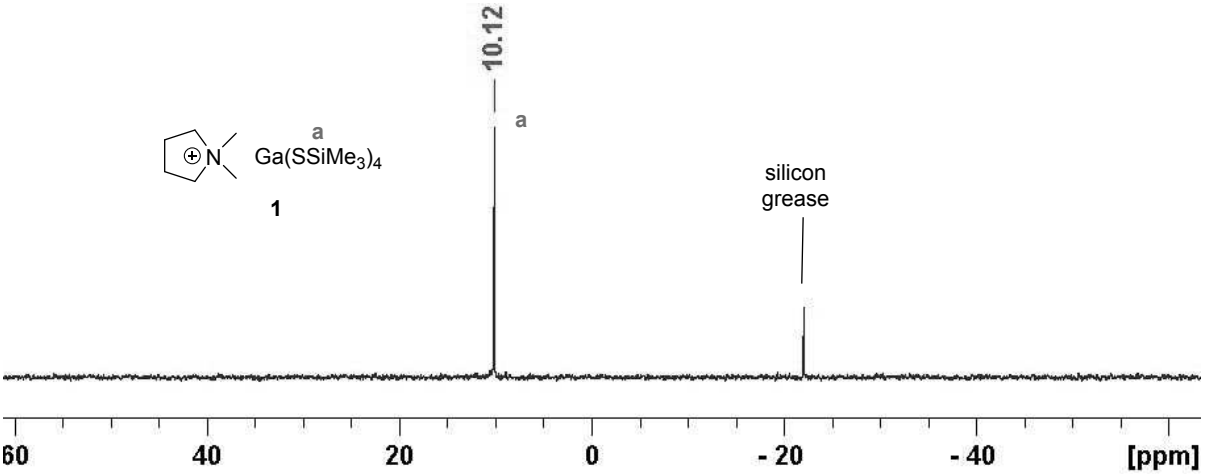

Figure S3. ^{29}Si NMR (59.7 MHz, THF[d$_8$]) of **1**.

*DMPyr [Ga(SeSiMe$_3$)$_4$] (**2**)*

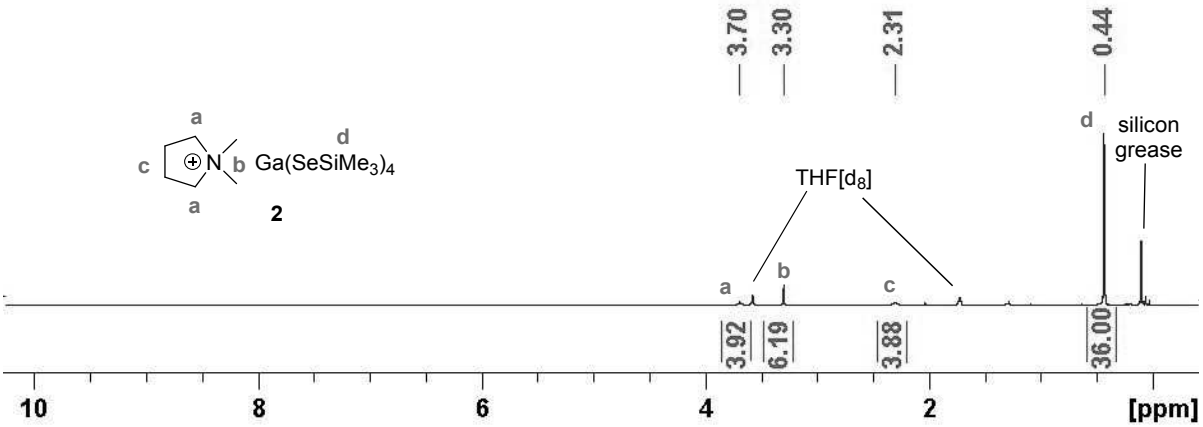

Figure S4. ^{1}H NMR (300.3 MHz, THF[d_8]) of **2**.

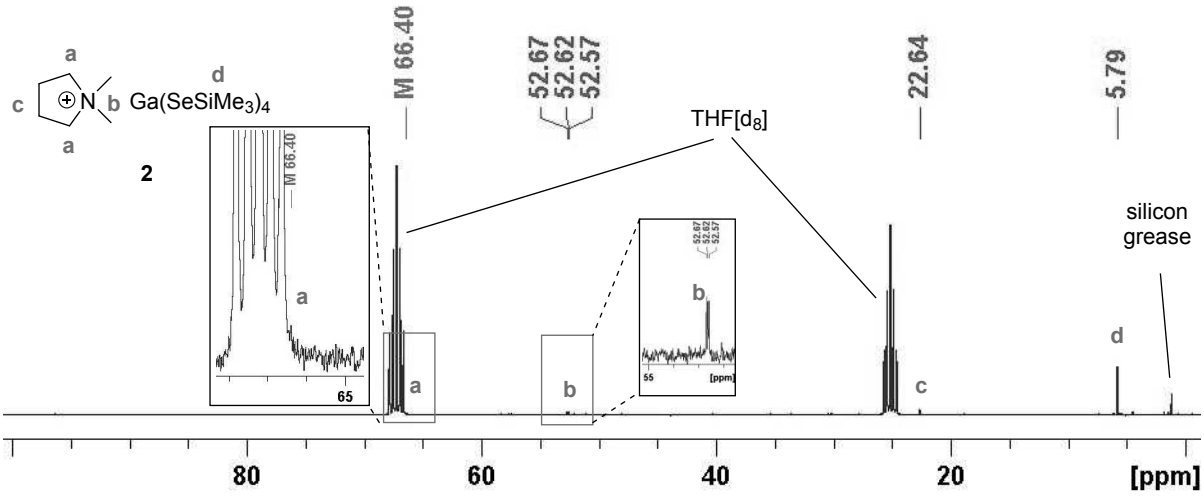

Figure S5. ^{13}C NMR (75.5 MHz, THF[d_8]) of **2**.

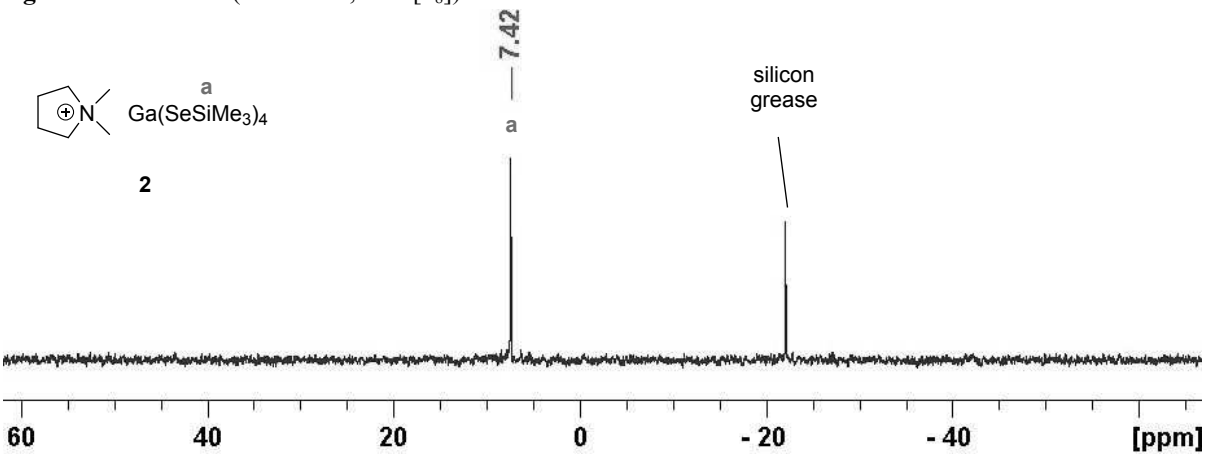

Figure S6. ^{29}Si NMR (59.7 MHz, THF[d_8]) of **2**.

*Ph_4P [$In(SSiMe_3)_4$] (**3**)*

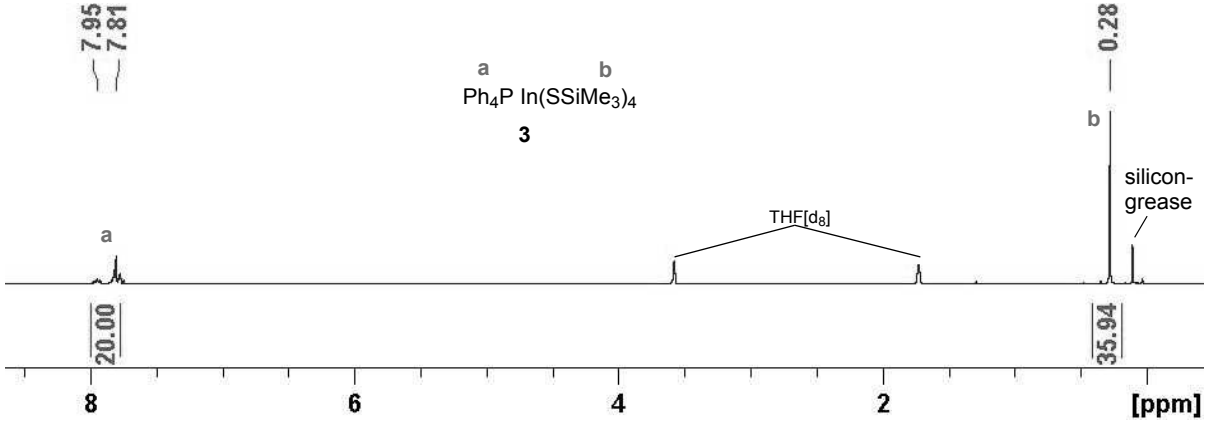

Figure S7. ^{1}H NMR (300.3 MHz, THF[d_8]) of **3**.

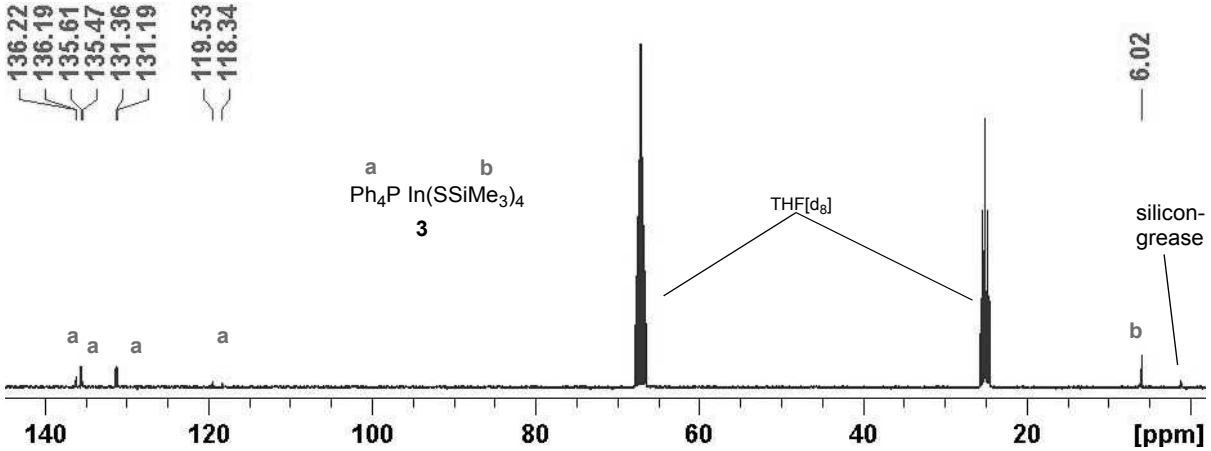

Figure S8. ^{13}C NMR (75.5 MHz, THF[d_8]) of **3**.

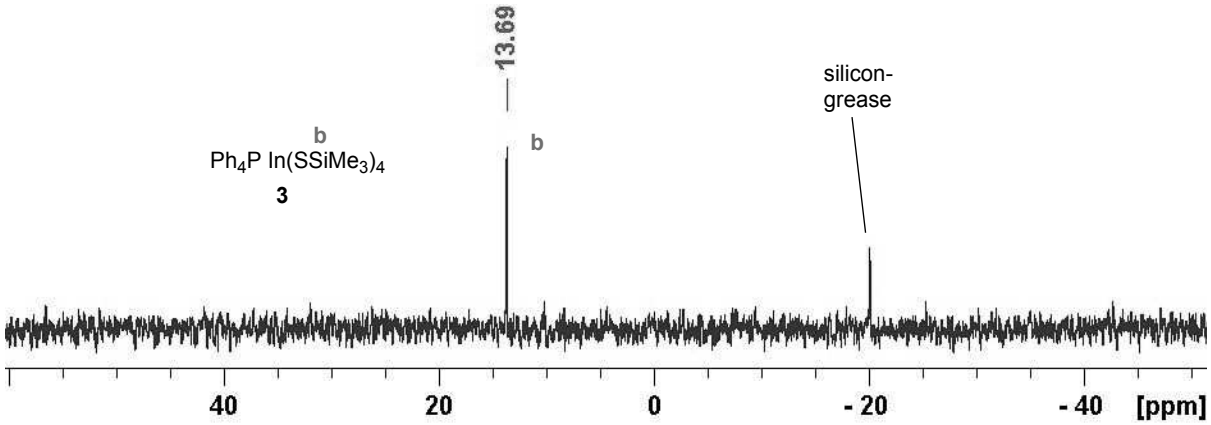

Figure S9. ^{29}Si NMR (59.7 MHz, THF[d_8]) of **3**.

*Ph_4P [$In(SeSiMe_3)_4$] (**4**)*

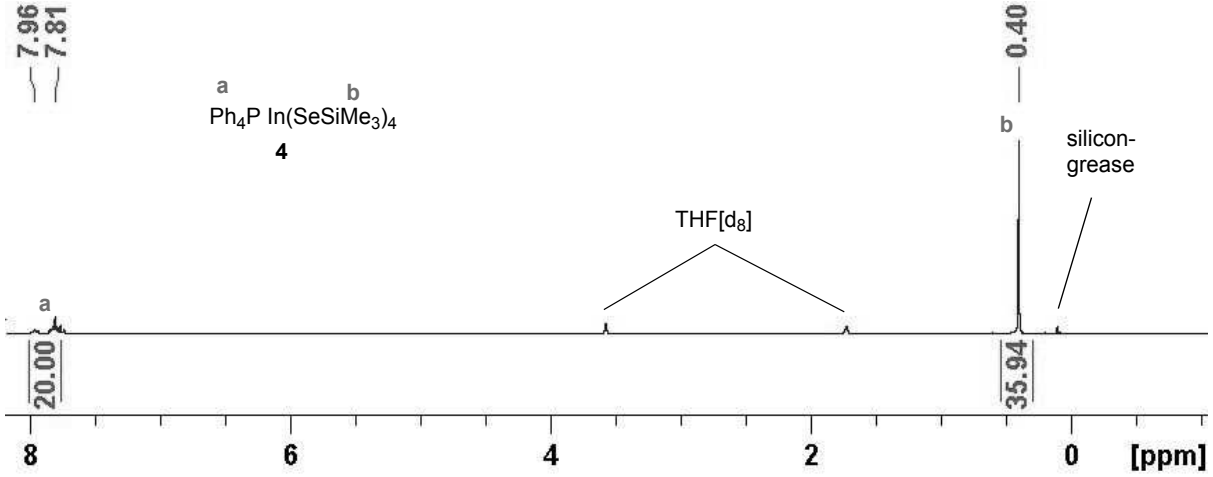

Figure S10. ^{1}H NMR (300.3 MHz, THF[d_8]) of **4**.

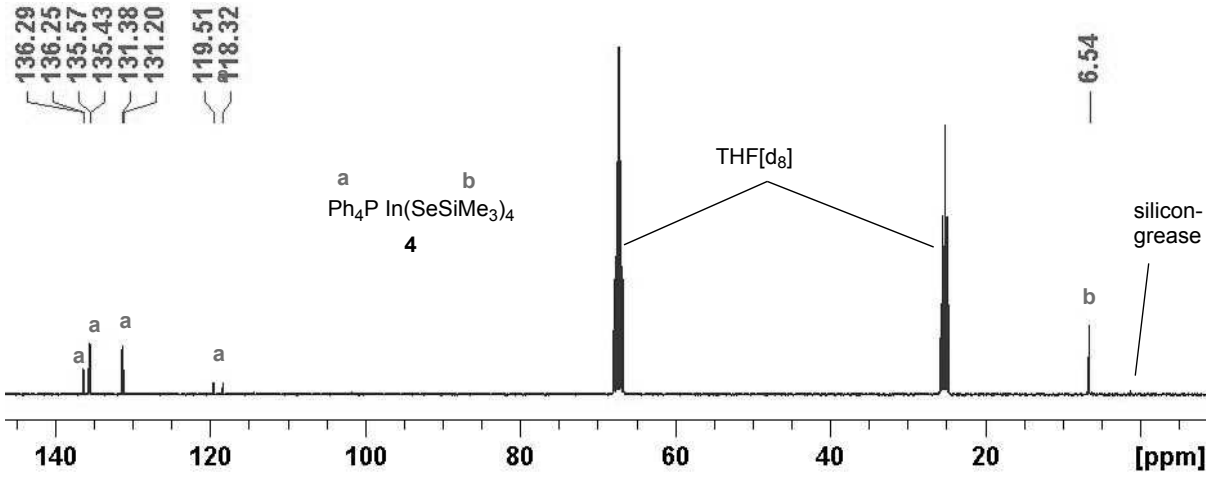

Figure S11. ^{13}C NMR (75.5 MHz, THF[d_8]) of **4**.

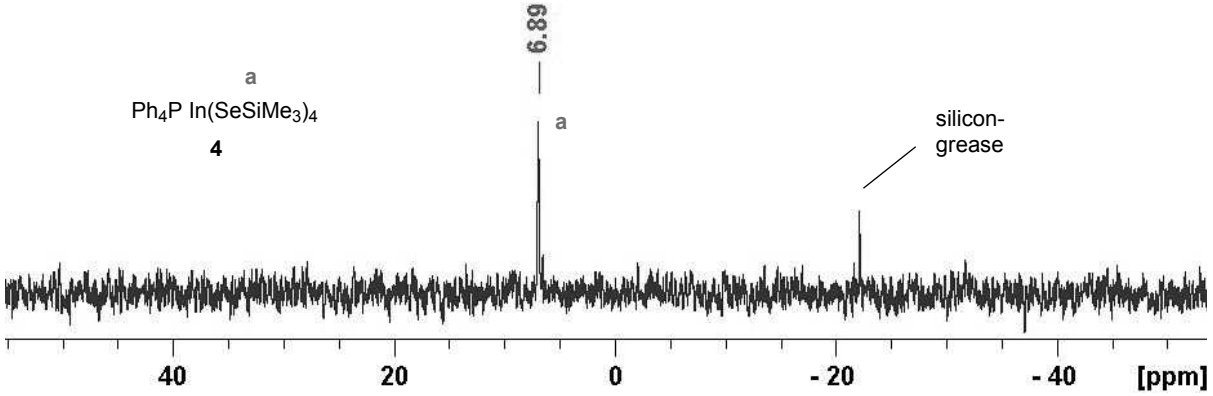

Figure S12. ^{29}Si NMR (59.7 MHz, THF[d_8]) of **4**.

*[Cu(dppe)$_2$][In(SSiMe$_3$)$_4$] (**5**)*

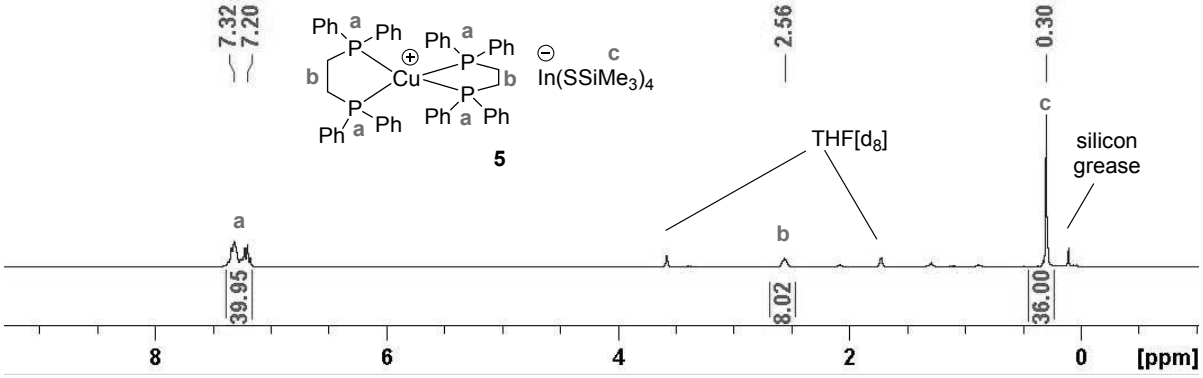

Figure S13. ^{1}H NMR (300.2 MHz, THF[d$_8$]) of **5**.

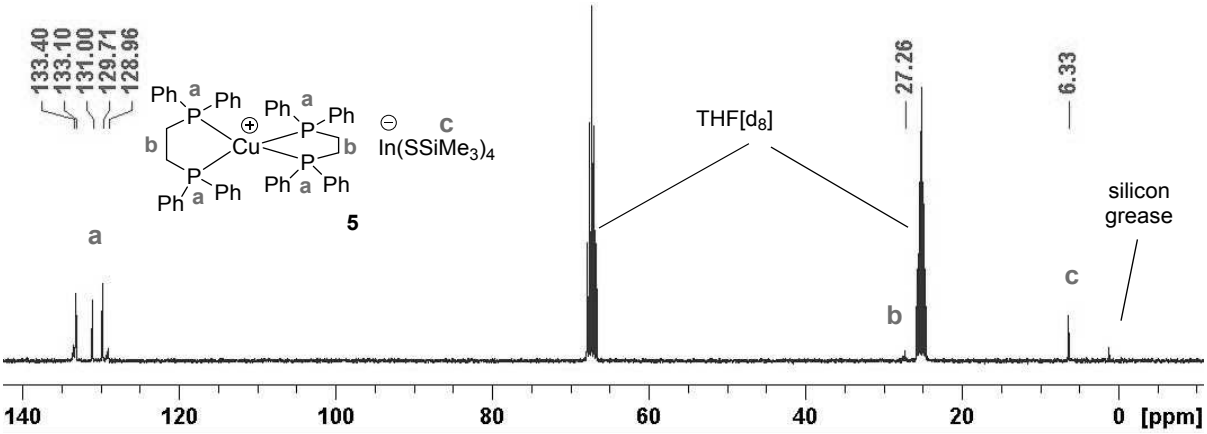

Figure S14. ^{13}C NMR (75.5 MHz, THF[d$_8$]) of **5**.

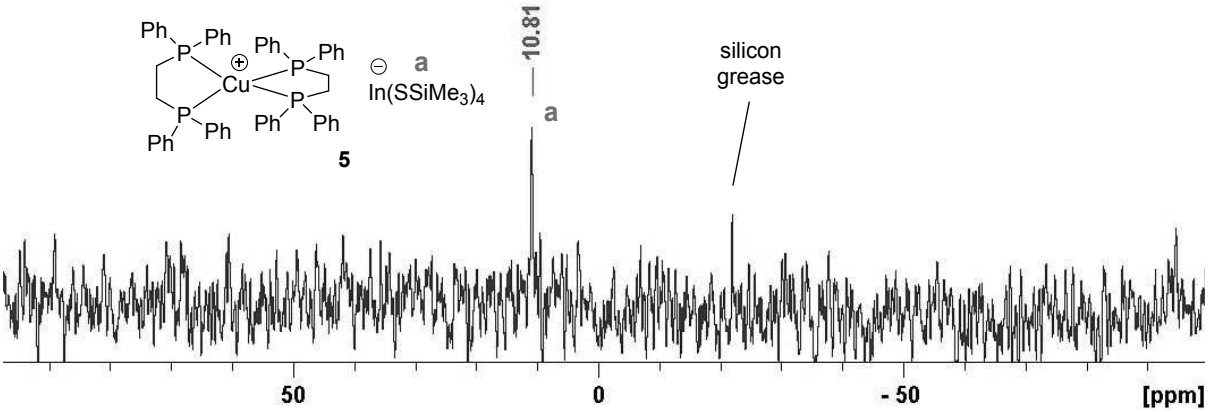

Figure S15. ^{29}Si NMR (99.7 MHz, THF[d$_8$]) of **5**.

[(η²-dmpe)Cu(μ₂-dmpe)₂]₂[Ga(SSiMe₃)₄]₂ ***(6)***

For clarity we assume the $[Cu(dmpe)_2]^+$ cation to be the present species in solution, not the dimer.

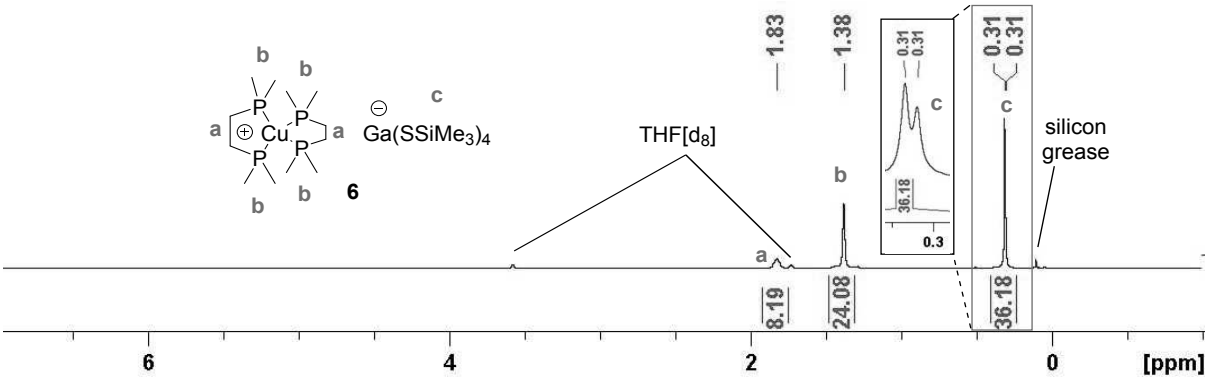

Figure S16. ^{1}H NMR (300.3 MHz, $THF[d_8]$) of **6**.

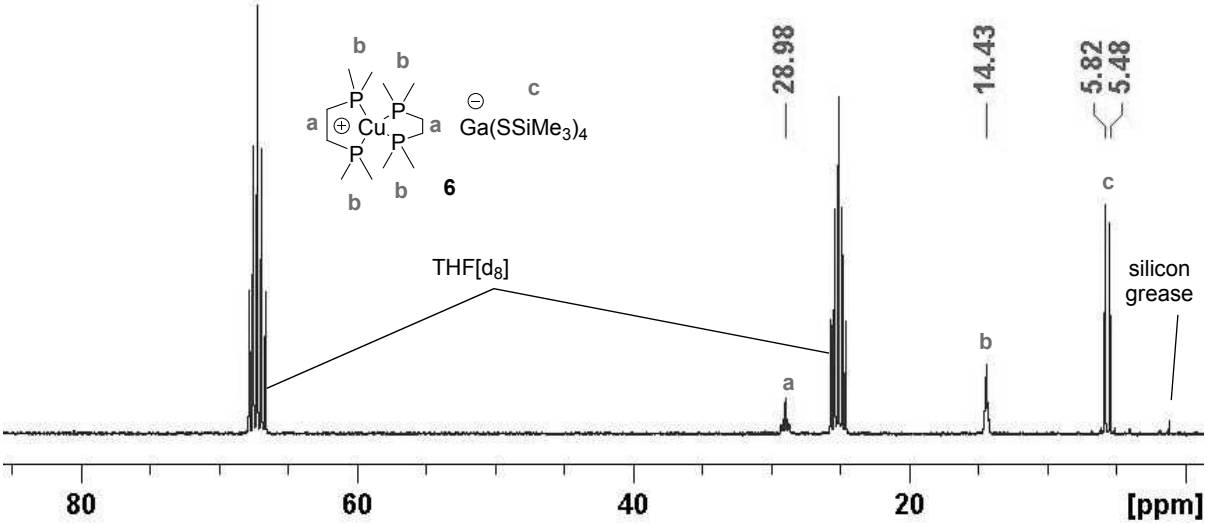

Figure S17. ^{13}C NMR (75.5 MHz, $THF[d_8]$) of **6**.

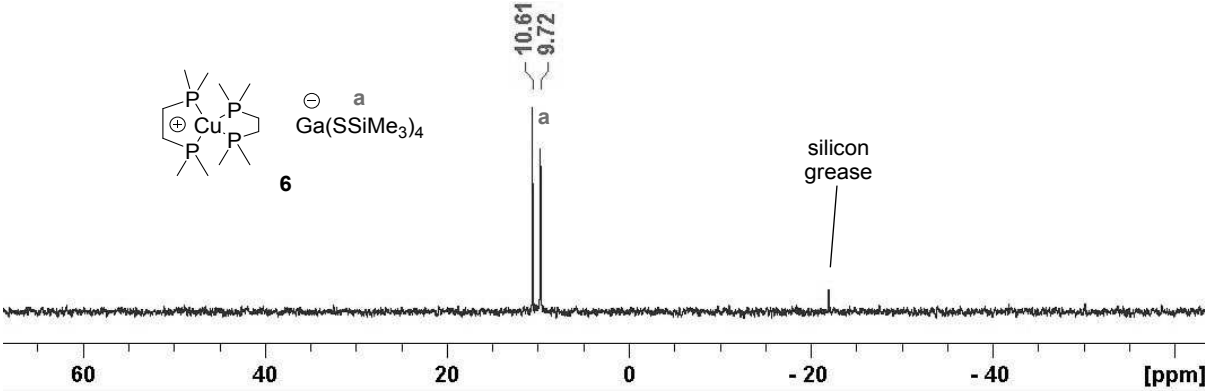

Figure S18. ^{29}Si NMR (59.7 MHz, $THF[d_8]$) of **6**.

^{1}H NMR spectra of the homologue [(dppe)$_2$Cu][M(ESiMe$_3$)$_4$] (M = Ga, In; E = S, Se) SSPs

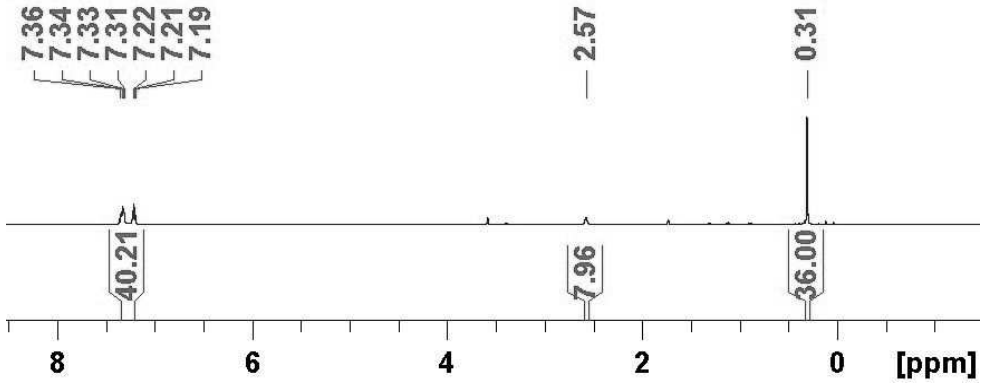

^{1}H NMR (500.2 MHz, THF[d_8]) of [dppe$_2$Cu][Ga(SSiMe$_3$)$_4$].

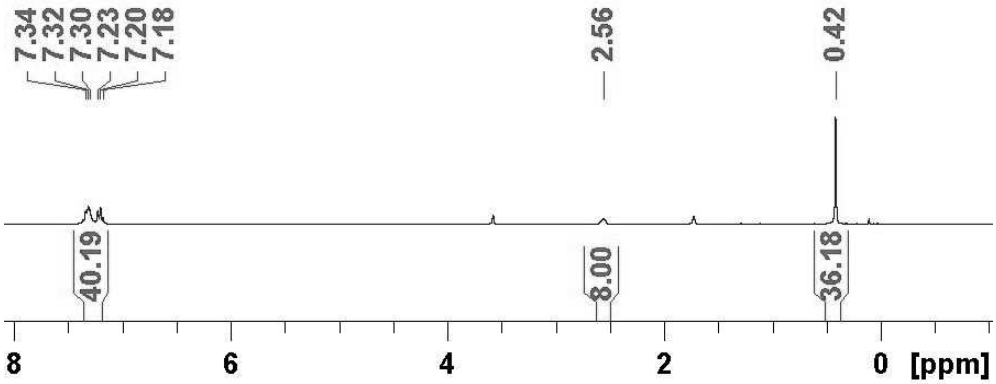

^{1}H NMR (300.3 MHz, THF[d_8]) of [dppe$_2$Cu][Ga(SeSiMe$_3$)$_4$].

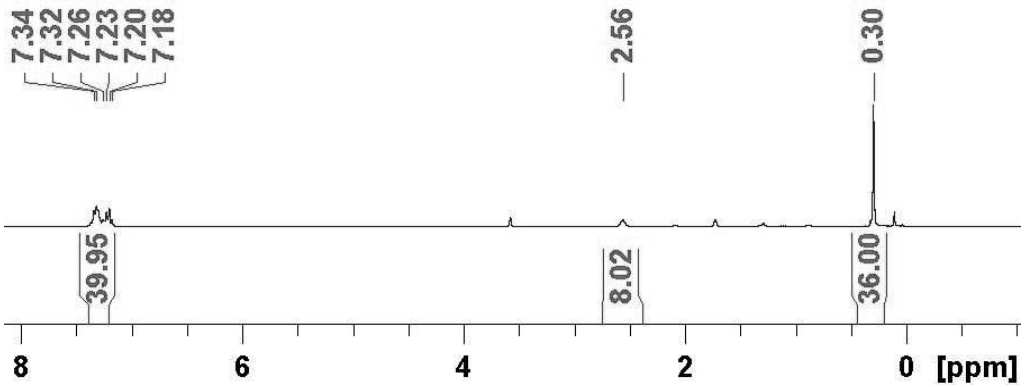

^{1}H NMR (300.3 MHz, THF[d_8]) of [dppe$_2$Cu][In(SSiMe$_3$)$_4$] (**5**).

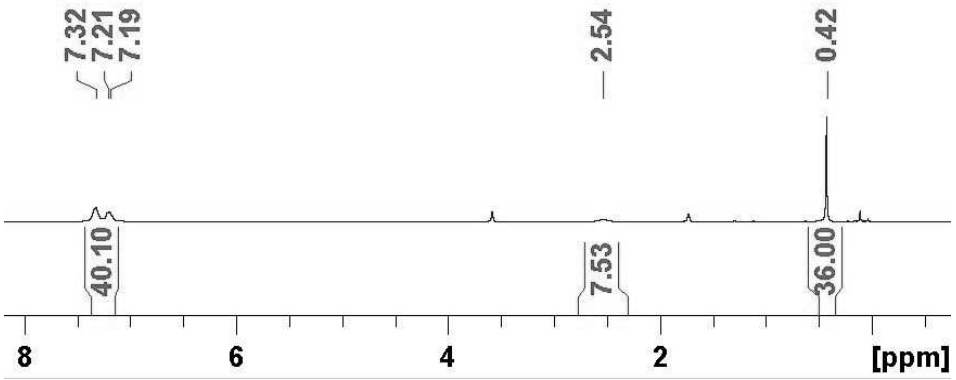

^{1}H NMR (300.3 MHz, THF[d_8]) of [dppe$_2$Cu][In(SeSiMe$_3$)$_4$].

^{13}C NMR spectra of the homologue $[(dppe)_2Cu][M(ESiMe_3)_4]$ (M = Ga, In; E = S, Se) SSPs

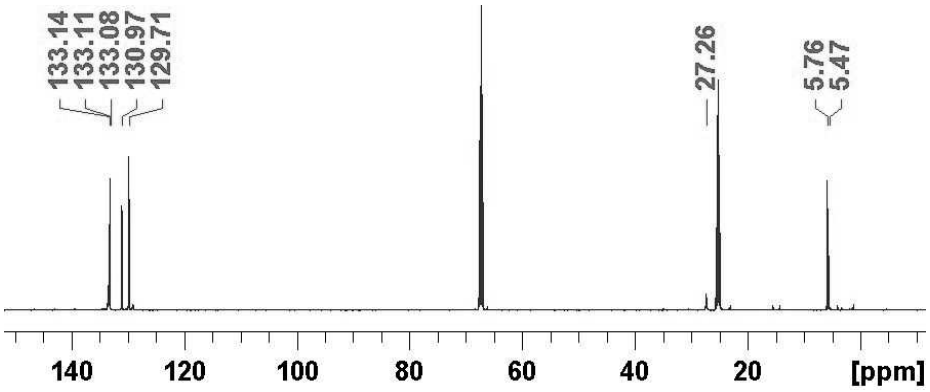

^{13}C NMR (125.8 MHz, $THF[d_8]$) of $[dppe_2Cu][Ga(SSiMe_3)_4]$.

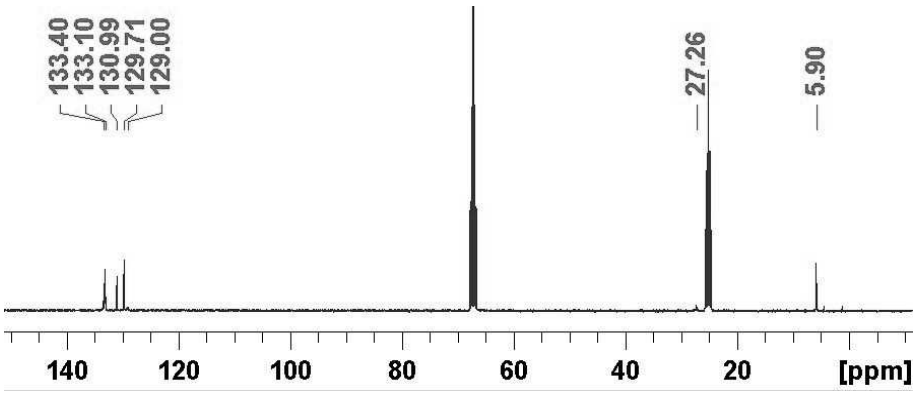

^{13}C NMR (75.5 MHz, $THF[d_8]$) of $[dppe_2Cu][Ga(SeSiMe_3)_4]$.

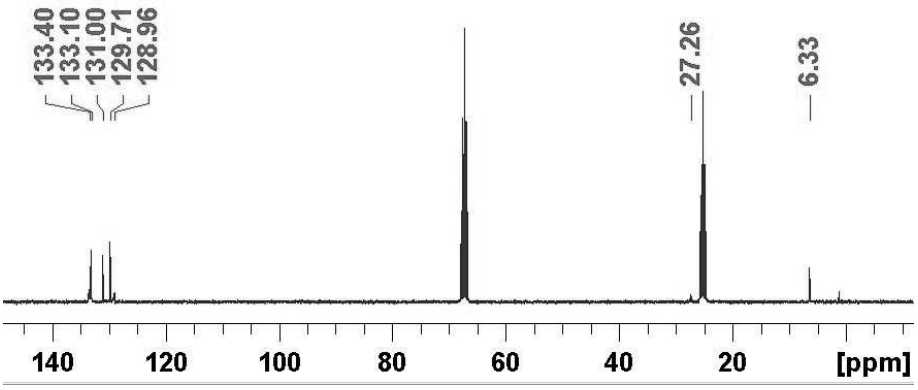

^{13}C NMR (75.5 MHz, $THF[d_8]$) of $[dppe_2Cu][In(SSiMe_3)_4]$ (**5**).

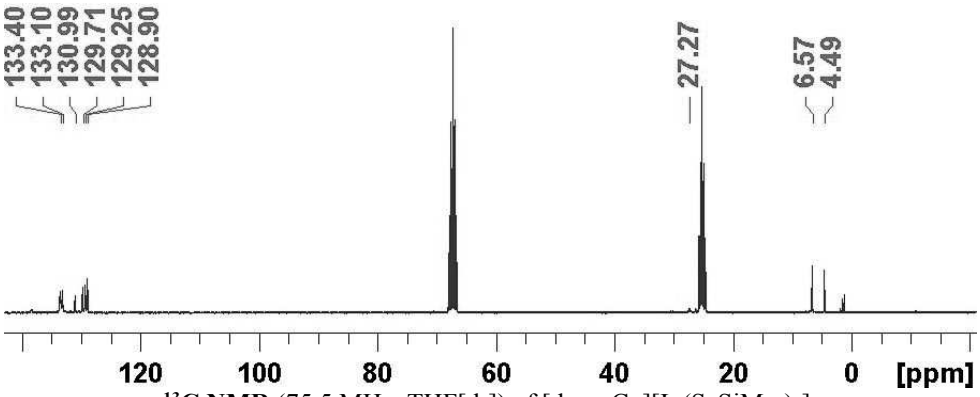

^{13}C NMR (75.5 MHz, $THF[d_8]$) of $[dppe_2Cu][In(SeSiMe_3)_4]$.

^{29}Si NMR spectra of the homologue [(dppe)$_2$Cu][M(ESiMe$_3$)$_4$] (M = Ga, In; E = S, Se) SSPs

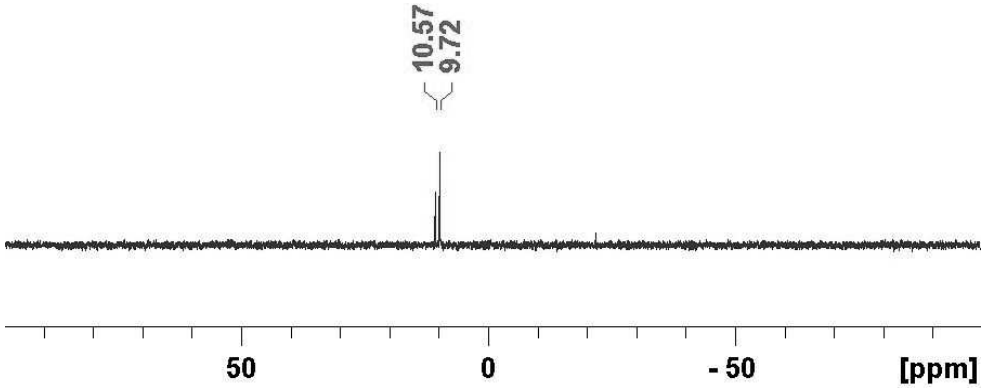

^{29}Si NMR (99.4 MHz, THF[d$_8$]) of [dppe$_2$Cu][Ga(SSiMe$_3$)$_4$].

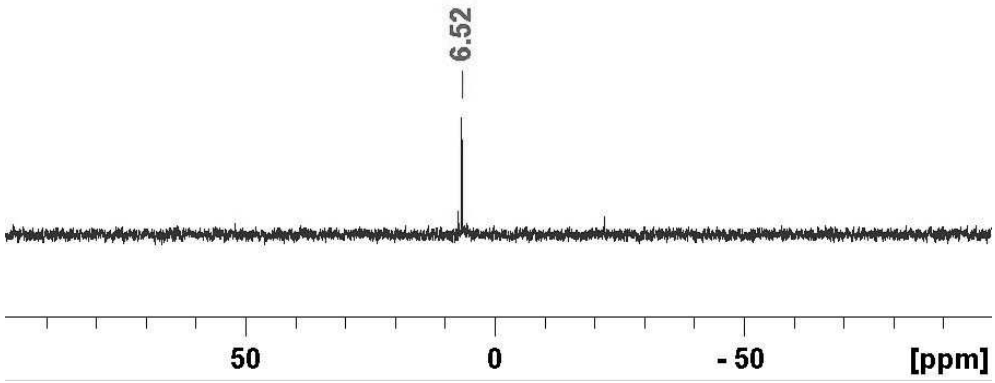

^{29}Si NMR (59.7 MHz, THF[d$_8$]) of [dppe$_2$Cu][Ga(SeSiMe$_3$)$_4$].

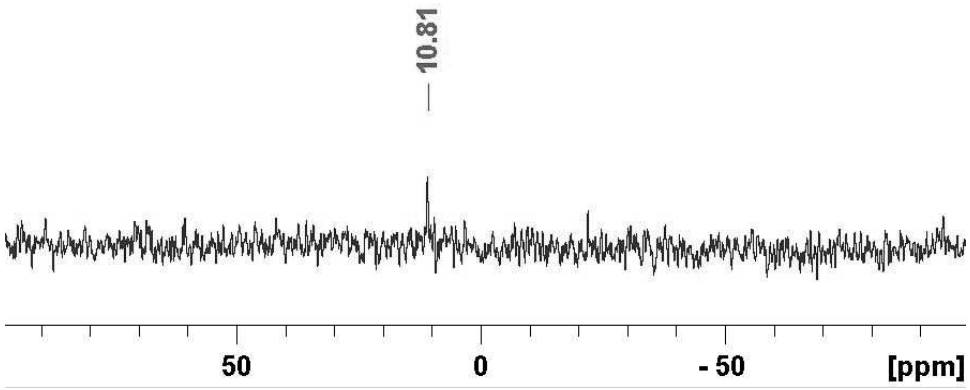

^{29}Si NMR (59.7 MHz, THF[d$_8$]) of [dppe$_2$Cu][In(SSiMe$_3$)$_4$] (**5**).

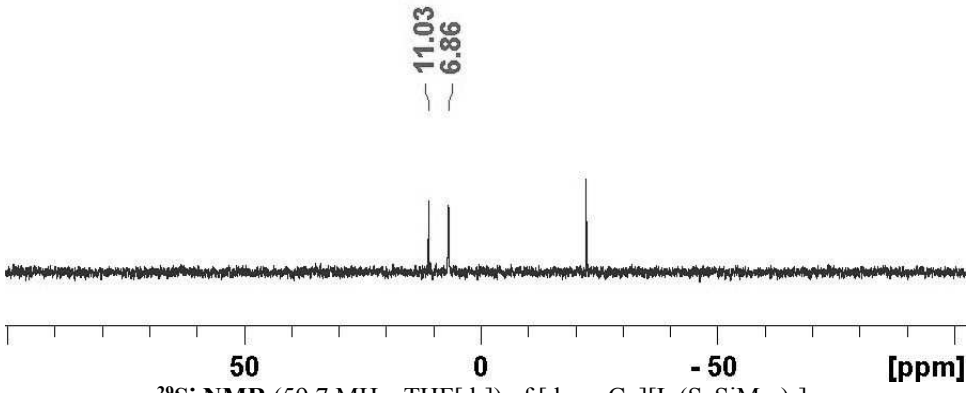

^{29}Si NMR (59.7 MHz, THF[d$_8$]) of [dppe$_2$Cu][In(SeSiMe$_3$)$_4$].

^{1}H NMR spectra of the homologue [(dmpe)$_2$Cu][M(ESiMe$_3$)$_4$] (M = Ga, In; E = S, Se) SSPs

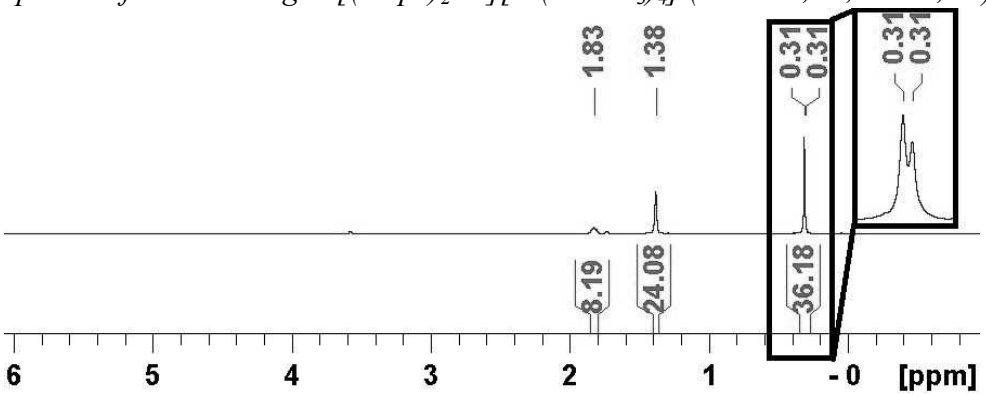

^{1}H NMR (300.3 MHz, THF[d_8]) of [(η^2-dmpe)Cu(μ_2-dmpe)$_2$]$_2$[Ga(SSiMe$_3$)$_4$]$_2$.

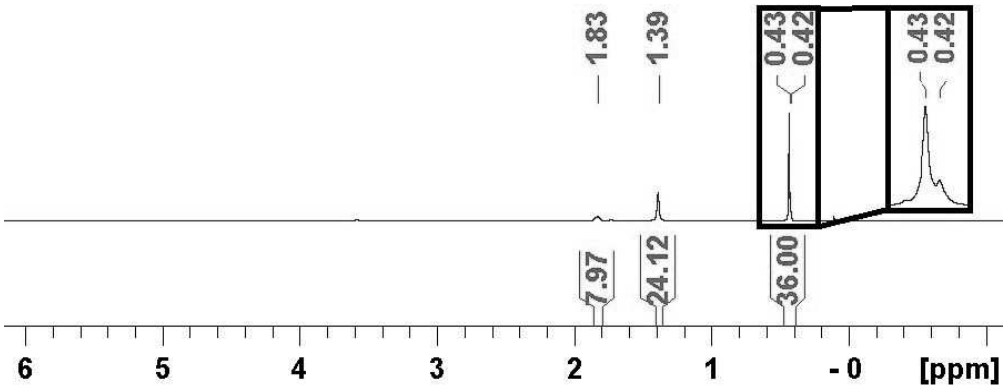

^{1}H NMR (300.3 MHz, THF[d_8]) of [(dmpe)$_2$Cu][Ga(SeSiMe$_3$)$_4$].

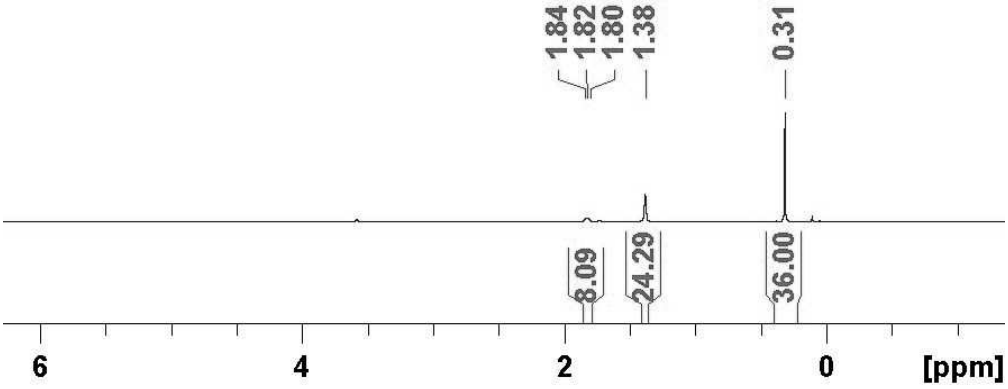

^{1}H NMR (300.3 MHz, THF[d_8]) of [(η^2-dmpe)Cu(μ_2-dmpe)$_2$]$_2$[In(SSiMe$_3$)$_4$]$_2$.

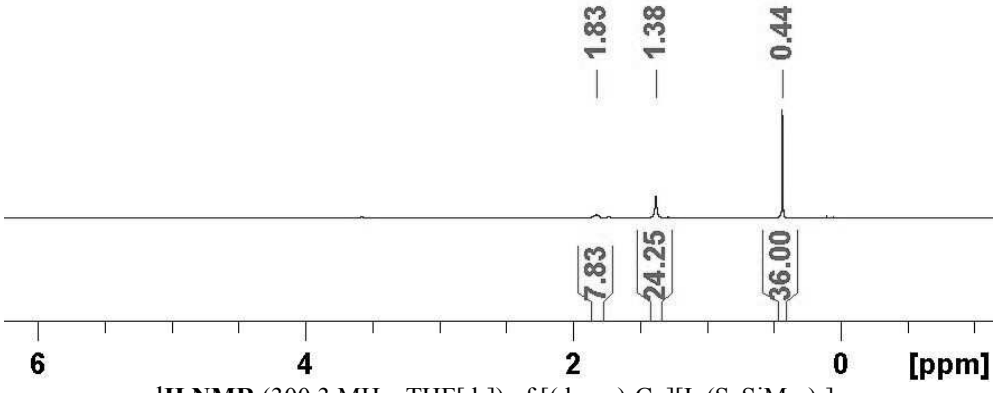

^{1}H NMR (300.3 MHz, THF[d_8]) of [(dmpe)$_2$Cu][In(SeSiMe$_3$)$_4$].

^{13}C NMR spectra of the homologue $[(dmpe)_2Cu][M(ESiMe_3)_4]$ (M = Ga, In; E = S, Se) SSPs

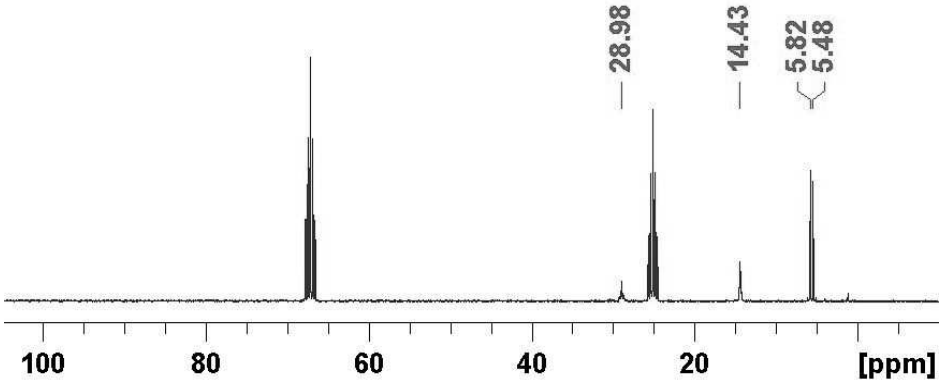

^{13}C NMR (75.5 MHz, THF[d_8]) of $[(\eta^2\text{-dmpe})Cu(\mu_2\text{-dmpe})_2]_2[Ga(SSiMe_3)_4]_2$.

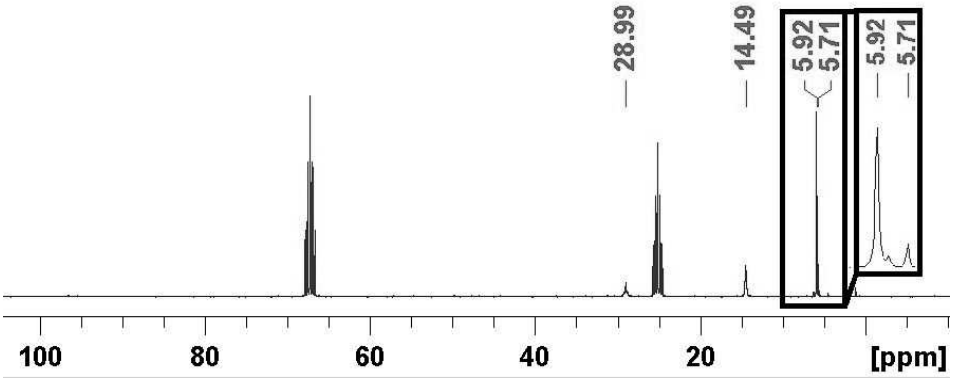

^{13}C NMR (75.5 MHz, THF[d_8]) of $[(dmpe)_2Cu][Ga(SeSiMe_3)_4]$.

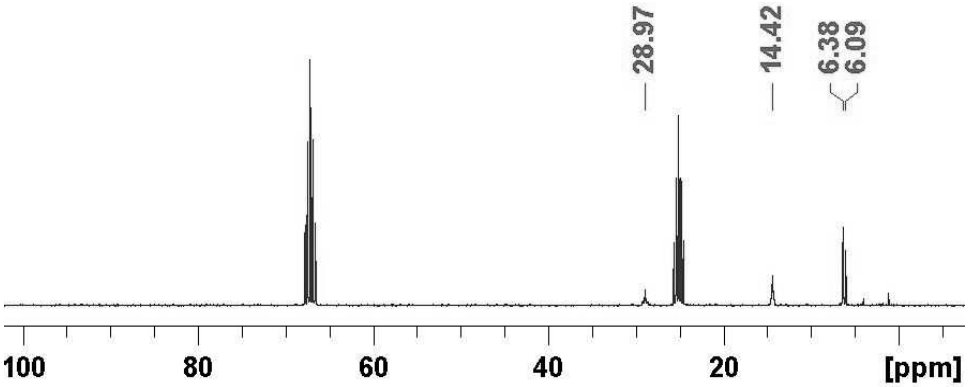

^{13}C NMR (75.5 MHz, THF[d_8]) of $[(\eta^2\text{-dmpe})Cu(\mu_2\text{-dmpe})_2]_2[In(SSiMe_3)_4]_2$.

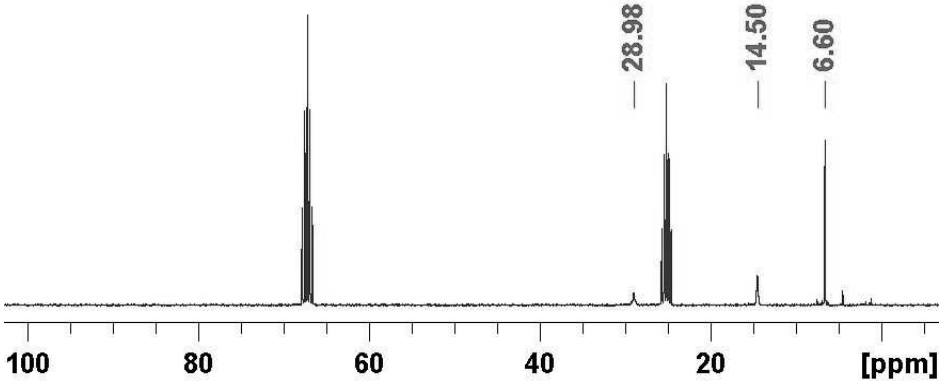

^{13}C NMR (75.5 MHz, THF[d_8]) of $[(dmpe)_2Cu][In(SeSiMe_3)_4]$.

^{29}Si NMR spectra of the homologue [(dmpe)$_2$Cu][M(ESiMe$_3$)$_4$] (M = Ga, In; E = S, Se) SSPs

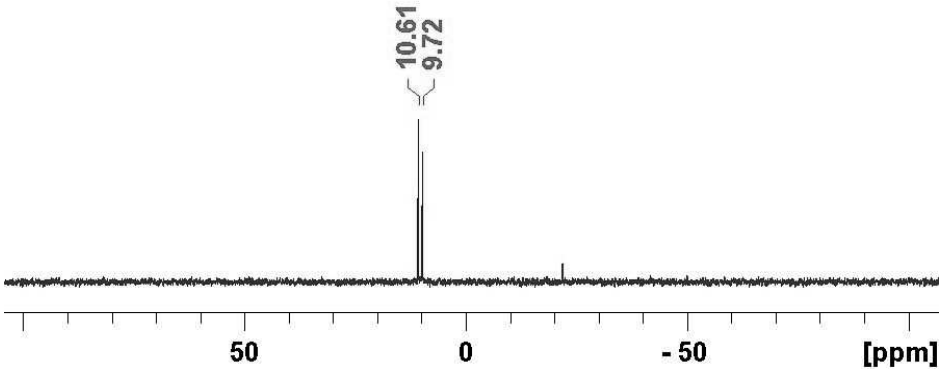

^{29}Si NMR (59.7 MHz, THF[d_8]) of [(η^2-dmpe)Cu(μ_2-dmpe)$_2$]$_2$[Ga(SSiMe$_3$)$_4$]$_2$.

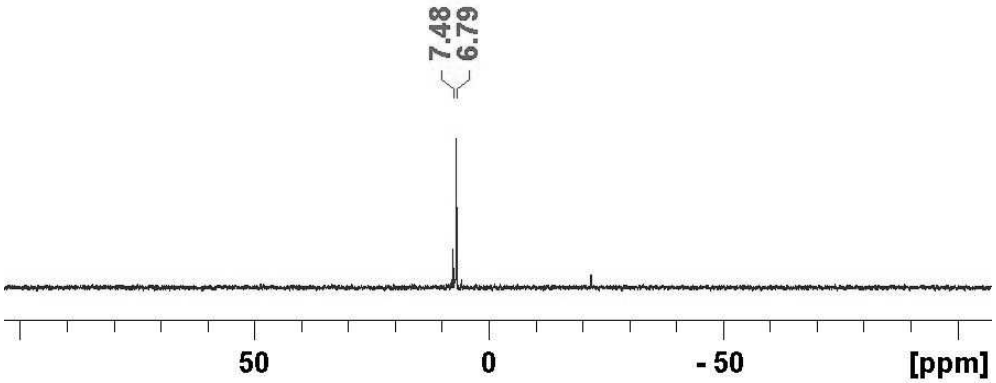

^{29}Si NMR (59.7 MHz, THF[d_8]) of [(dmpe)$_2$Cu][Ga(SeSiMe$_3$)$_4$].

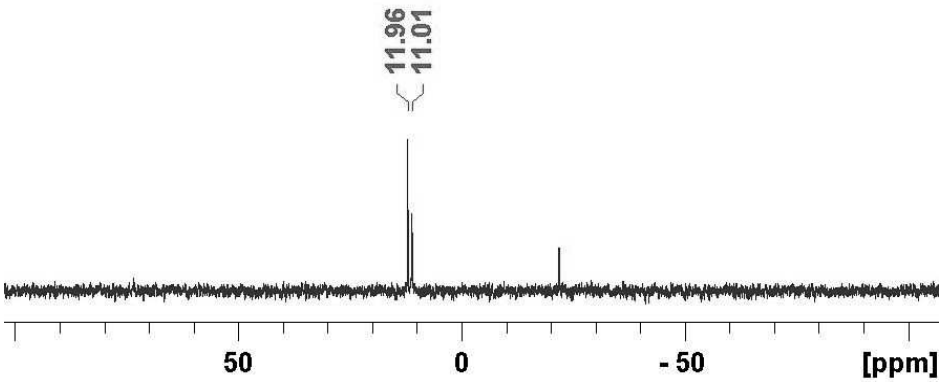

^{29}Si NMR (59.7 MHz, THF[d_8]) of [(η^2-dmpe)Cu(μ_2-dmpe)$_2$]$_2$[In(SSiMe$_3$)$_4$]$_2$.

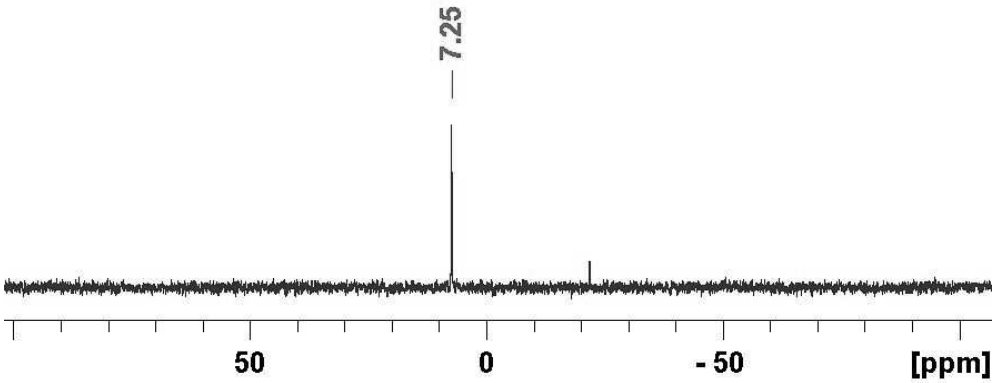

^{29}Si NMR (59.7 MHz, THF[d_8]) of [(dmpe)$_2$Cu][In(SeSiMe$_3$)$_4$].

Thermogravimetric measurements

*DMPyr [Ga(SSiMe$_3$)$_4$] (**1**)*

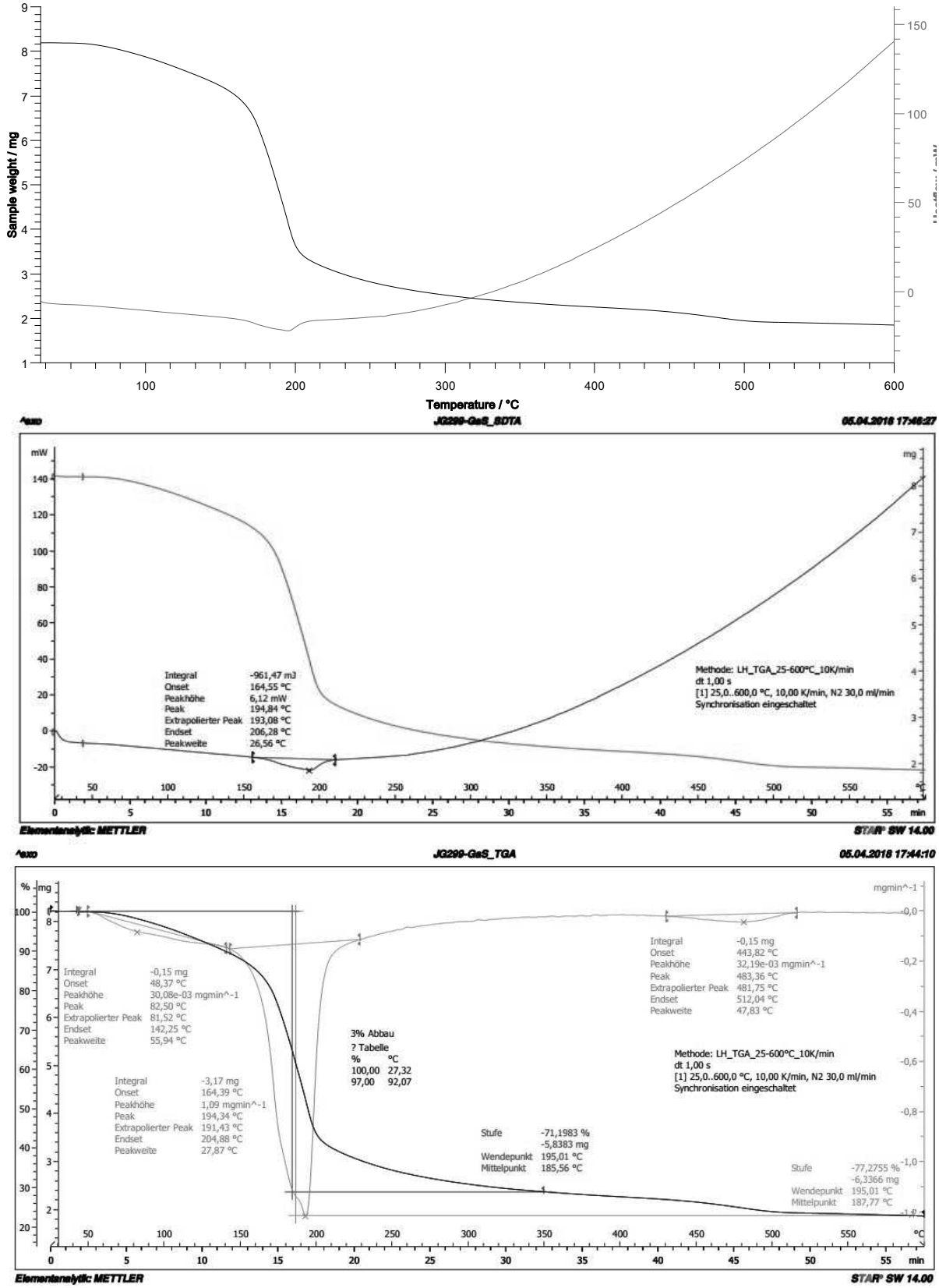

Figure S19. TGA-DSC of **1** (heating rate 10 K min^{-1}; 30 °C - 600 °C).

*DMPyr [Ga(SeSiMe$_3$)$_4$] (**2**)*

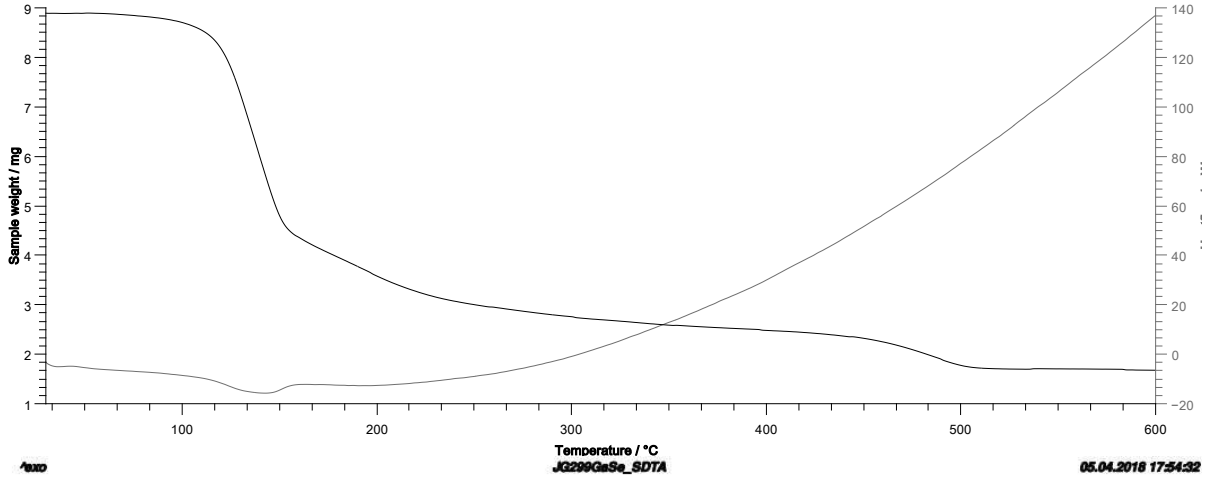

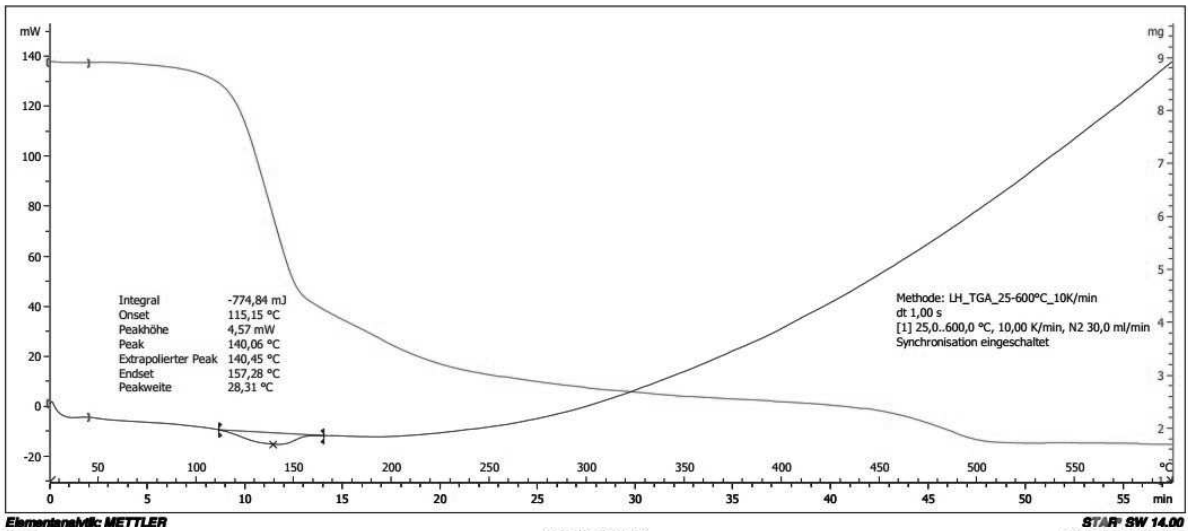

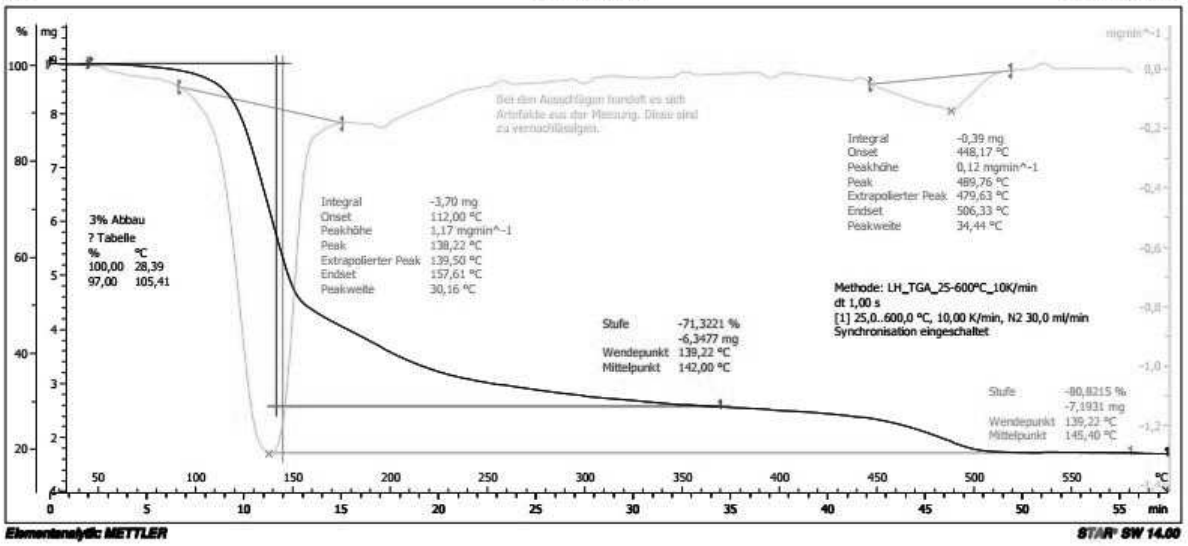

Figure S20. TGA-DSC of **2** (heating rate 10 K min^{-1}; 30 °C - 600 °C).

*Ph_4P [$In(SSiMe_3)_4$] (**3**)*

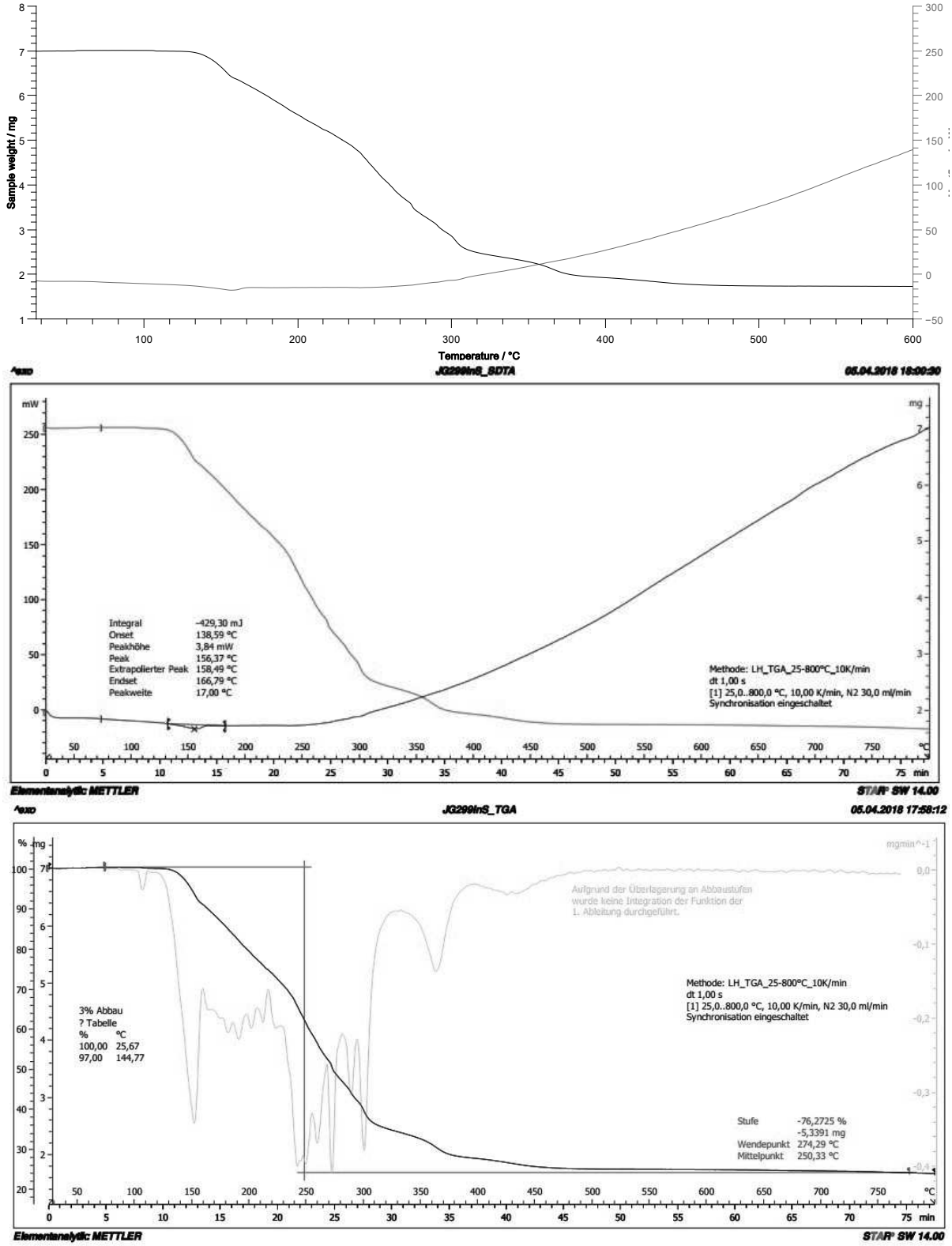

Figure S21. TGA-DSC of **3** (heating rate 10 K min^{-1}; 30 °C - 600 °C).

*Ph_4P [$In(SeSiMe_3)_4$] (**4**)*

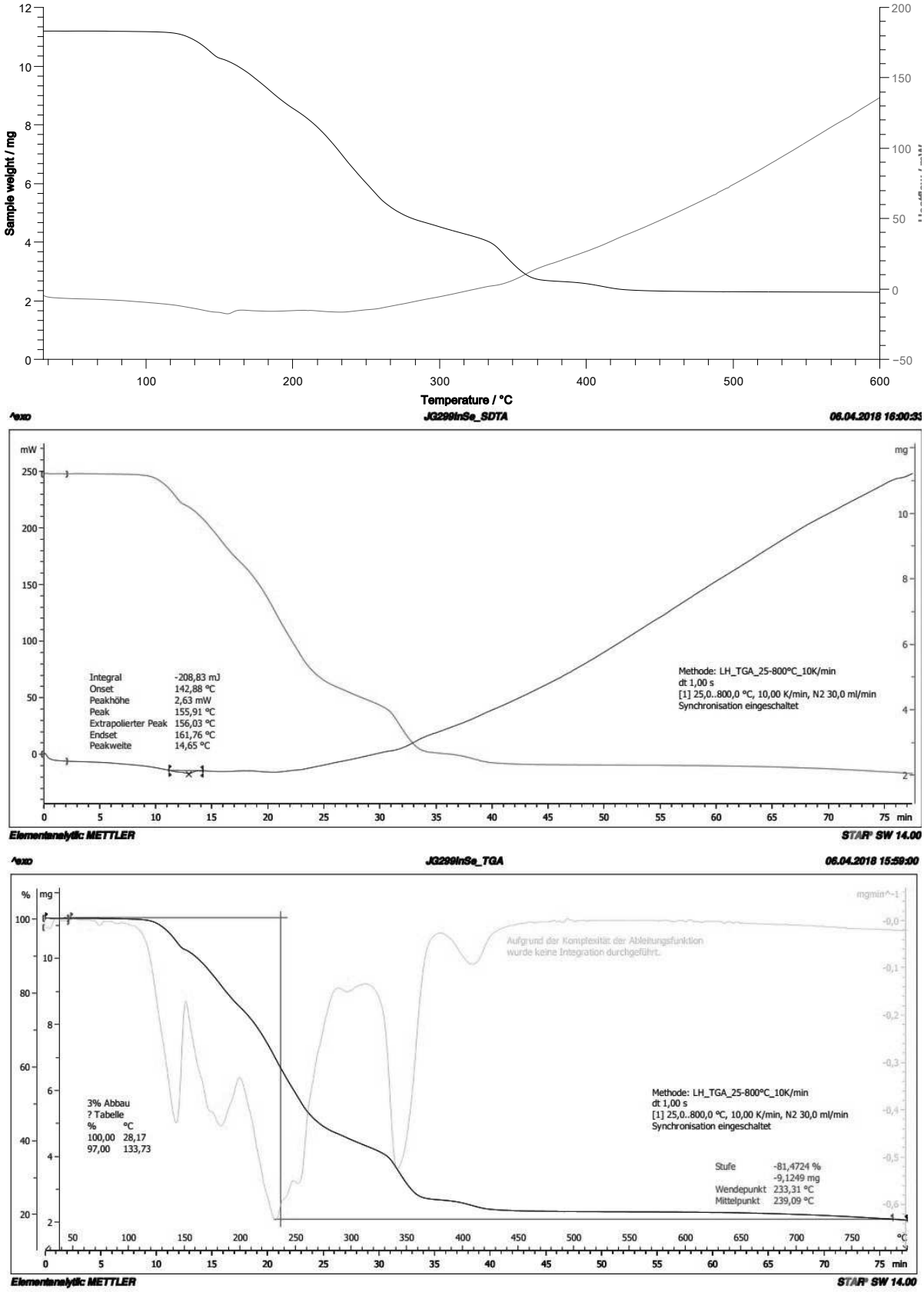

Figure S22. TGA-DSC of **4** (heating rate 10 K min^{-1}; 30 °C - 600 °C).

*[Cu(dppe)$_2$][In(SSiMe$_3$)$_4$] (**5**)*

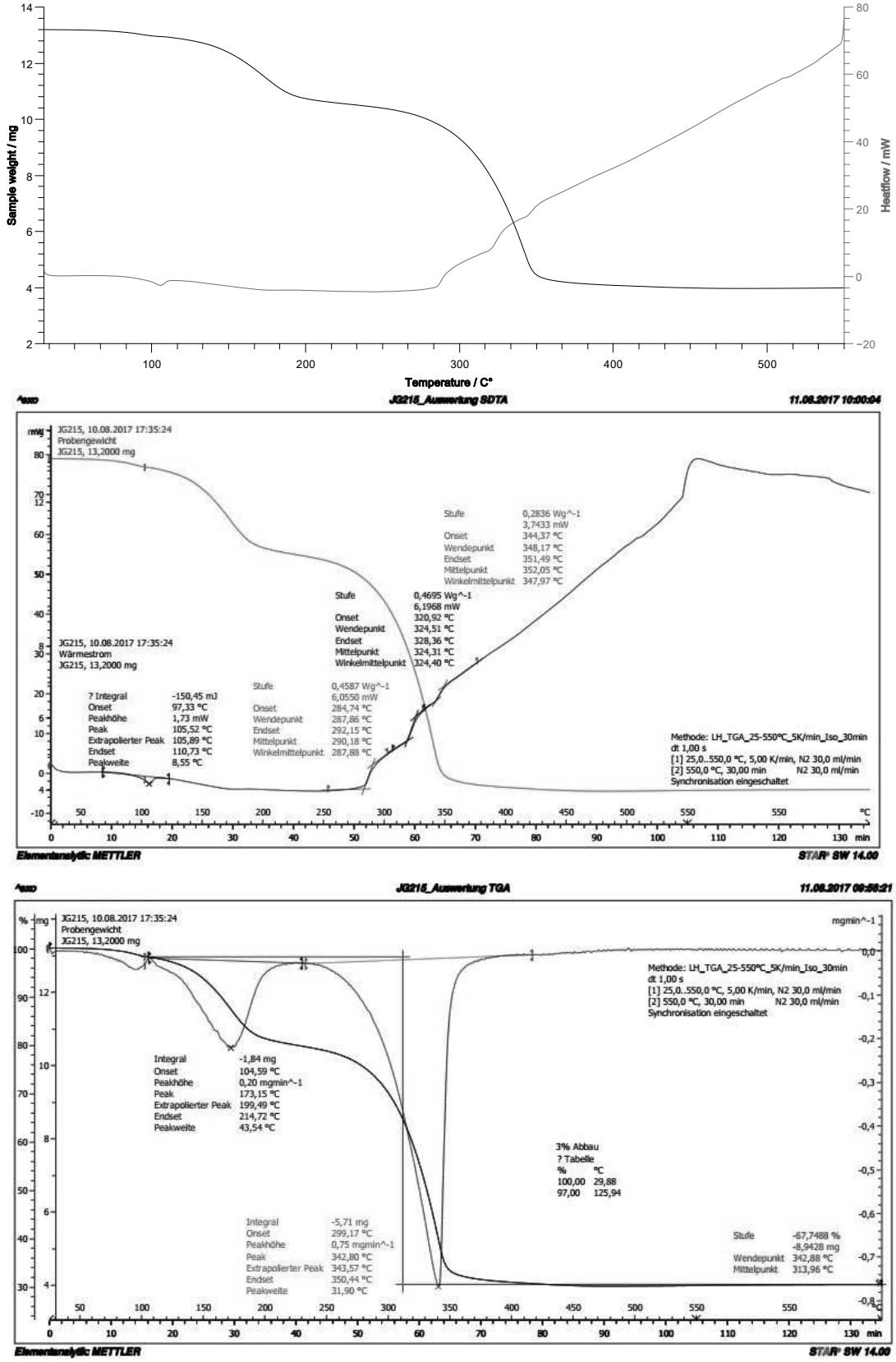

Figure S23. TGA-DSC of **5** (heating rate 5 K min^{-1}; 30 °C - 550 °C, then 30 min at 550 °C).

[(η²-dmpe)Cu(μ₂-dmpe)₂]₂[Ga(SSiMe₃)₄]₂ (**6**)

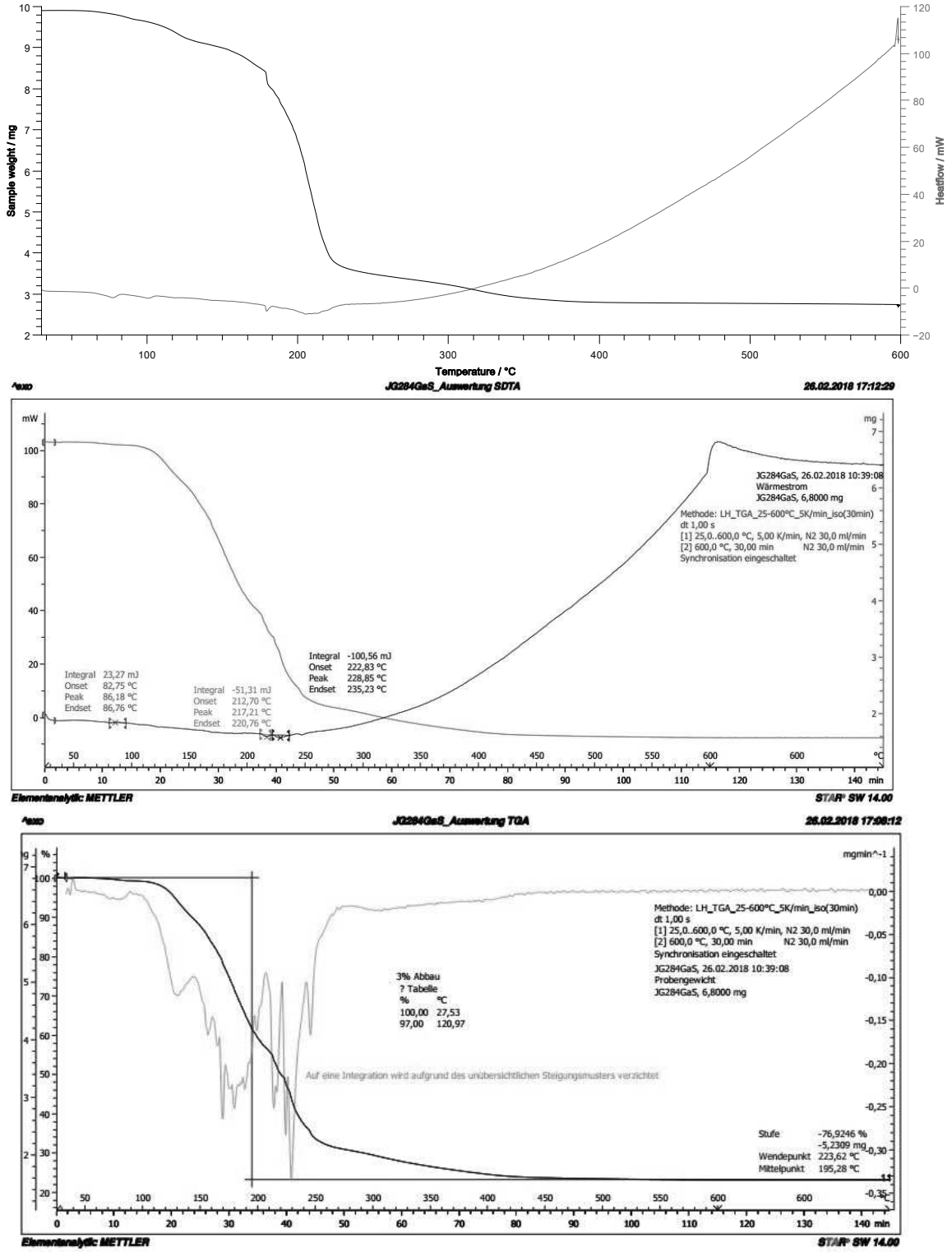

Figure S24. TGA-DSC of **6** (heating rate 5 K min^{-1}; 30 °C - 600 °C, then 30 min at 600 °C).

Material preparations

*Coprecipitation of $CuInS_2$ from **3** and $[Cu(tmtu)_3]PF_6$*

To a solution of Ph_4P $[In(SSiMe_3)_4]$ (**3**) (50 mg, 0.06 mmol, 1.00 equiv.) in thf (5 mL) a suspension of $[Cu(tmtu)_3][PF_6]$ (35 mg, 0.06 mmol, 1.00 equiv.) in thf (5 mL) is slowly added at –78 °C. The solution is stirred for 18 h and allowed to slowly obtain ambient temperature within this time. A reddish suspension is obtained. This suspension is annealed at 80 °C for eleven days and turns to black (note that the boiling point of thf is about 66 °C. Usage of an autoclave should be considered). The solution was removed via canula and the residue was washed with acetonitrile (5 mL) PXRD of the black powder confirms the presence of $CuInS_2$ (Figure S25).

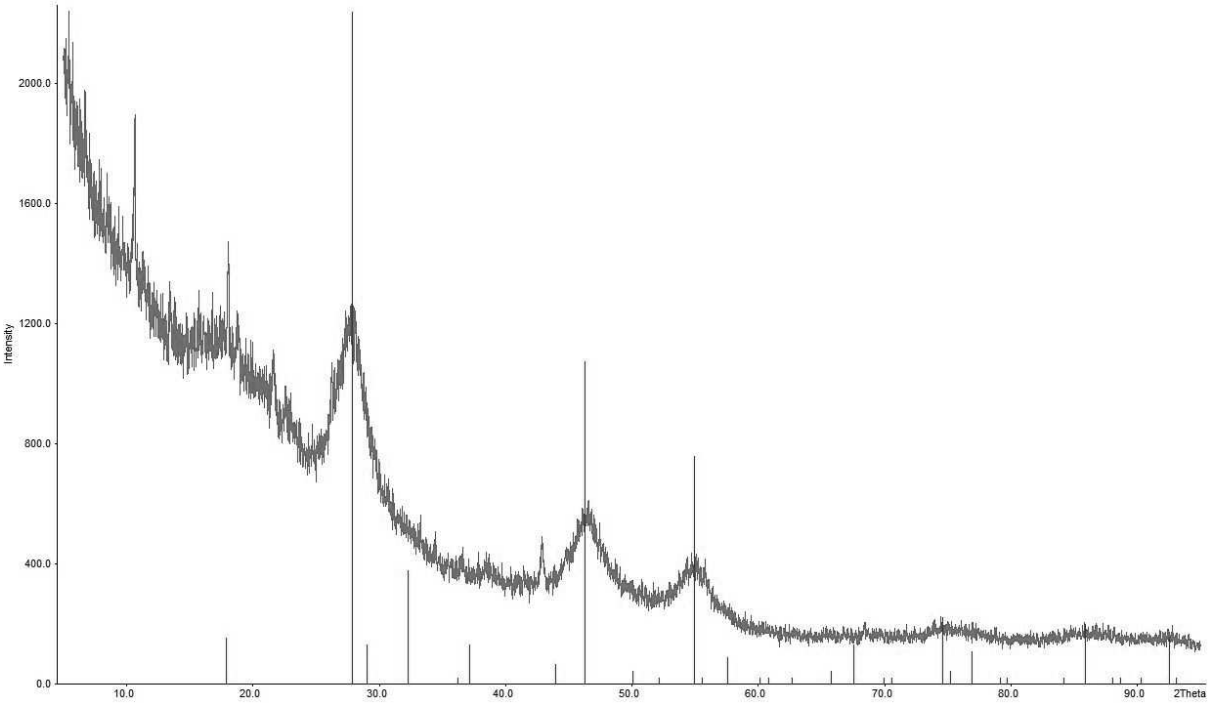

Figure S25. PXRD of the precipitate obtained by coprecipitation of **3** with $[Cu(tmtu)_3][PF_6]$ and annealing for eleven days at 80 °C. The presence of $CuInS_2$ is indicated.[13]

*Coprecipitation of $CuInS_2$ from partially thermolyzed **3** and $[Cu(tmtu)_3][PF_6]$*

Ph_4P $[In(SSiMe_3)_4]$ (**3**) (50 mg, 0.06 mmol, 1.00 equiv.) was heated at 200 °C for 1 minute under reduced pressure, until a pale-yellow liquid emerges, which solidifies when cooled down to ambient temperature. This solid was unsuccessfully tried to dilute in thf (5 mL), but successfully diluted by adding the same amount of acetonitrile, indicating the conversion of the educt compound (Figure S26). As discussed later, the nature of the thermolyzed 3 is a stoichiometrical equivalent for a "Ph_4P $[InS_2]$"-compound. For simplification of the we use this inadequate abbreviation in the following. See the following section for a discussion on the thermolysis product of the title anions.

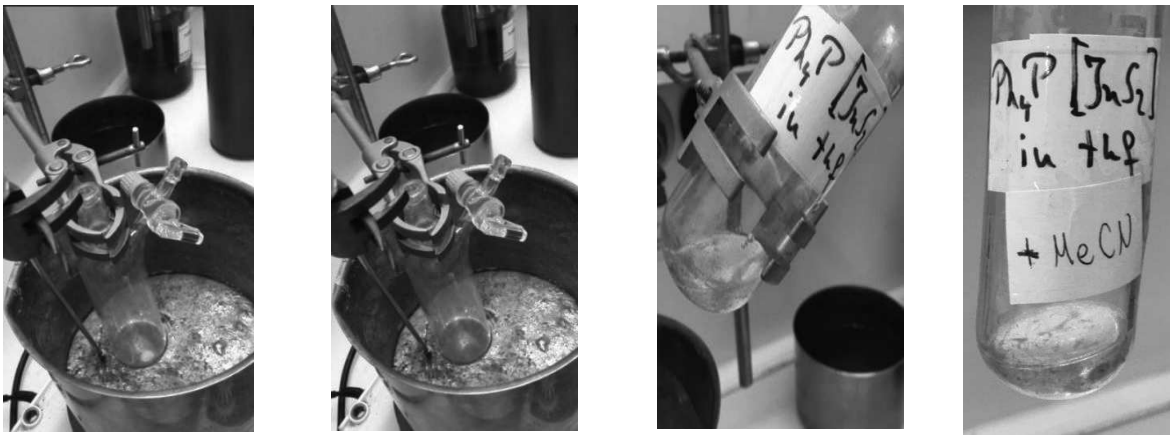

Figure S26. Ph_4P [$In(SSiMe_3)_4$] (**3**) (**A**) is warmed to 200 °C for one minute until a pale-yellow liquid emerges (**B**). After cooling down to ambient temperature a thf-insoluble solid is obtained (**C**), that forms a colorless solution by the same volume of adding acetonitrile (**D**).

To this clear solution of Ph_4P [InS_2] a solution of [$Cu(tmtu)_3$][PF_6] (35 mg, 0.06 mmol, 1.00 equiv.) in 5 mL acetonitrile was added at –20 °C. The solution rapidly obtained a yellow color and within one minute the precipitation of a reddish solid is observed (Figure S27).

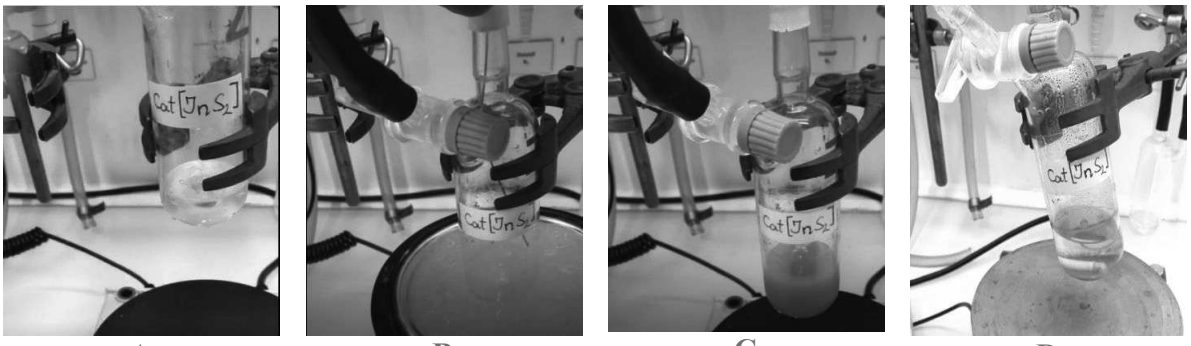

Figure S27. To a clear solution of Ph_4P[InS_2] in acetonitrile (**A**) a solution of [$Cu(tmtu)_3$][PF_6] is added. The solution gets pale-yellow (**B**) and rapidly turns into a reddish suspension when heated up to ambient temperature (**C**). After sedimentation a clear, colorless solution and a red solid are obtained (**D**).

The mixture is filtered, and the residue is suspended in diglyme (10 mL) for better heat transfer. The suspension is heated at 110 °C for 72 h. The supernatant solution is removed, and the black residue is investigated by PXRD. The presence of phase pure $CuInS_2$ is confirmed (Figure S28).

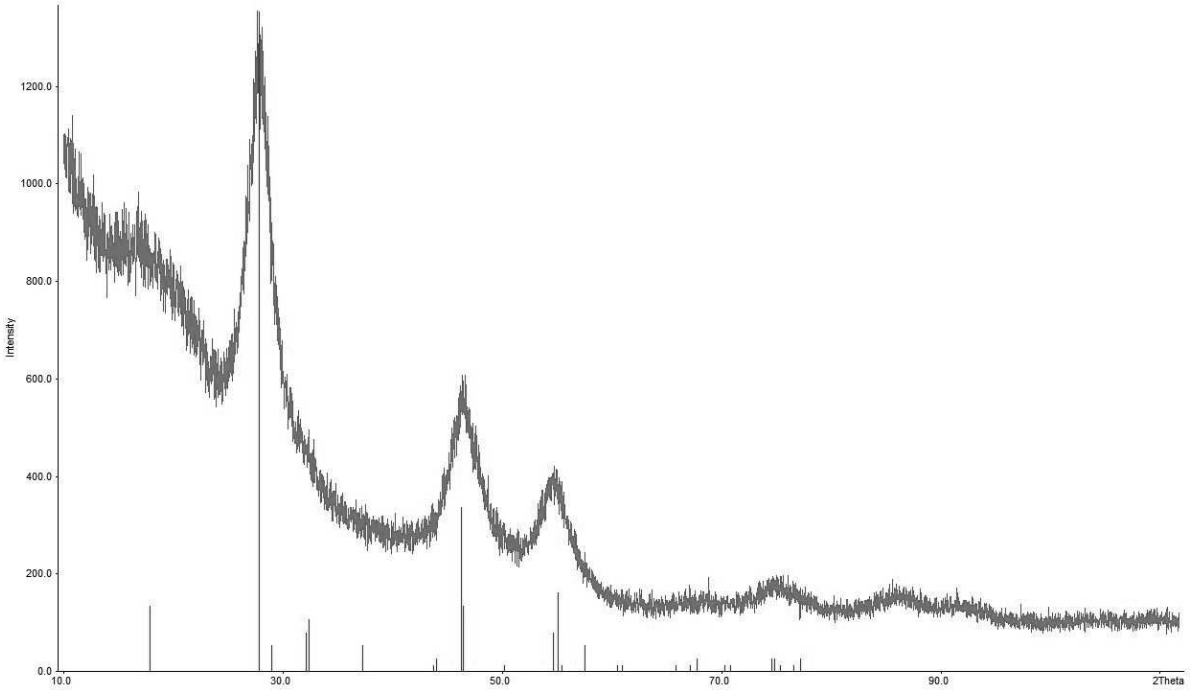

Figure S28. PXRD of the precipitate obtained by coprecipitation of freshly prepared $Ph_4P[InS_2]$ (by thermolysis of **3**) with $[Cu(tmtu)_3][PF_6]$ in acetonitrile and annealing for 72 h at 110 °C that confirms the presence of $CuInS_2$.[14]

*$CuInS_2$ from **5***

The residue of the DSC-TGA measurement of $[Cu(dppe)_2][In(SSiMe_3)_4]$ (**5**) (30 °C – 600 °C with a heating rate of 5 K min^{-1} and subsequent annealing at 600 °C for 30 min) was investigated by PXRD. Phase pure $CuInS_2$ was detected (Figure S29).

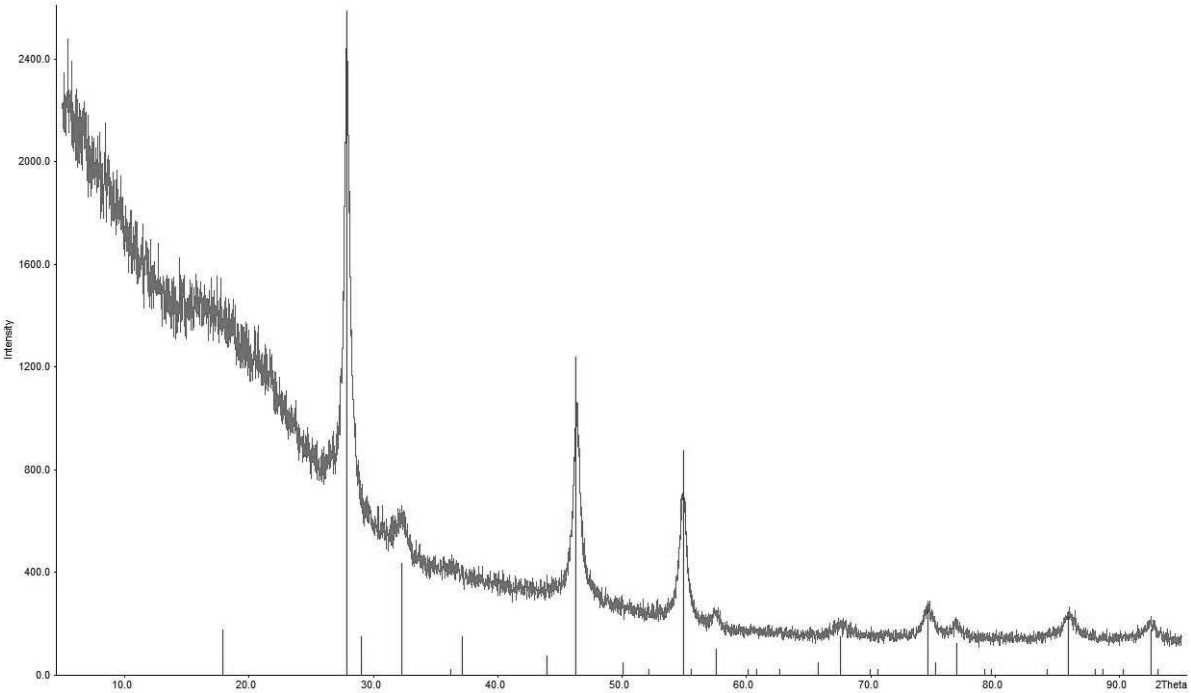

Figure S29. PXRD of the residue obtained from the DSC-TGA measurement of $[Cu(dppe)_2][In(SSiMe_3)_4]$ (**5**) that confirms the presence of $CuInS_2$.[13]

*$CuGaS_2$ from **6***

The residue of the DSC-TGA measurement of $[(\eta^2\text{-dmpe})Cu(\mu_2\text{-dmpe})_2]_2[Ga(SSiMe_3)_4]_2$ (**6**) (30 °C - 550 °C with a heating rate of 5 K min^{-1} and subsequent annealing at 550 °C for 30 min) was investigated by PXRD. Phase pure $CuGaS_2$ was detected (Figure S30).

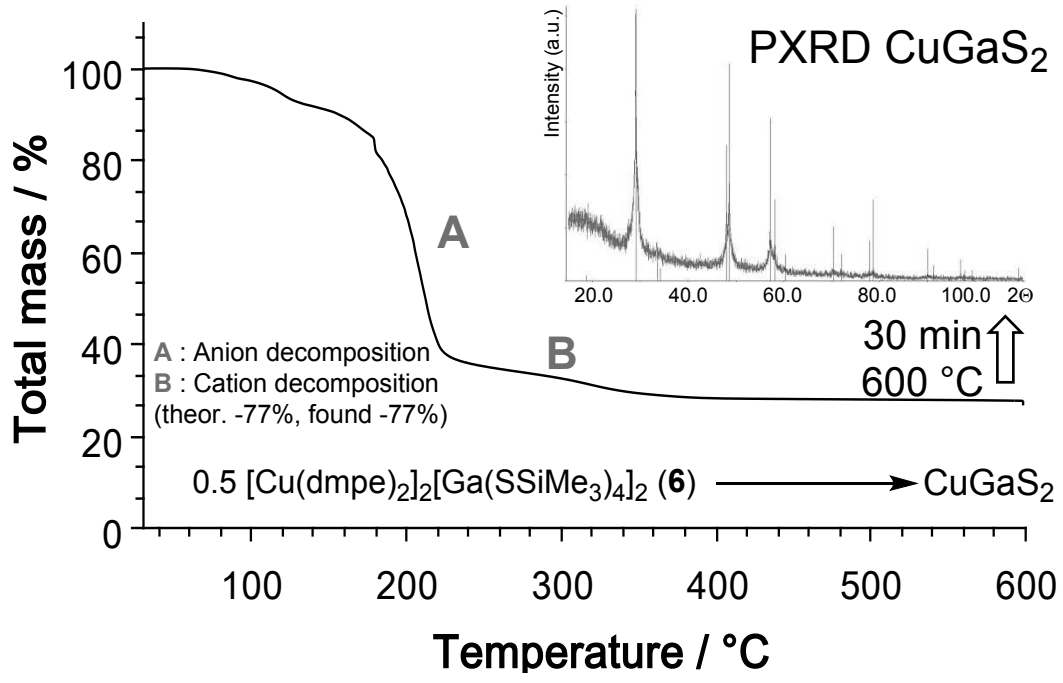

Figure S30. PXRD of the residue obtained from the DSC-TGA measurement of $[(\eta^2\text{-dmpe})Cu(\mu_2\text{-dmpe})_2]_2[Ga(SSiMe_3)_4]_2$ (**6**) that confirms the presence of $CuGaS_2$.[15]

Comment on the decomposition mechanism of the title anions

In our effort to get crystallographic data of the partially desilylated thermolysis products of the $[M(ESiMe_3)_4]^-$ anions we could not get any suitable crystals. However, it was possible to grow crystals that could be identified as ionic liquid like compounds like Ph_4P $[SSiMe_3]$ or DMPyr $[SeSiMe_3]$ of very poor quality. Further an elemental analysis of the residue obtained by treating $(Ph_3P)_2N$ $In(SSiMe_3)_4$ (obtained by the same route as for the synthesis of **3** with $(Ph_3P)_2N$ Cl instead of Ph_4P Cl) for 2 min. at 200 °C gave rise to the idea, that no quantitative intramolecular desilylation takes place, as the elemental analysis fits to a mixture of the partial desilylation product $SIn(SSiMe_3)_2$ and $(Ph_3P)_2N$ $[SSiMe_3]$

Anal. calcd. For $C_{42}H_{48}In_1N_1P_2S_3Si_2$: C, 56.3; H, 5.4; N, 1.6; S, 10.7. Found: C, 56.5; H, 5.1; N, 1.9; S, 10.7.

To investigate the presence of remaining trimethylsilyl groups and the elemental composition of the title compound's defined thermal decomposition residues we investigated the residues obtained by treating 50 mg of Ph_4P $In(SSiMe_3)_4$ (**3**) and 50 mg of Ph_4P $In(SeSiMe_3)_4$ (**4**) at 200 °C for 2 min. The obtained residues were dried in fine vacuum and subsequently investigated via ^1H NMR. For both residues a plausible decomposition mechanism can be formulated by assuming a decomposition of the Ph_4P $[M(ESiMe_3)_4]$ into Ph_4P $ESiMe_3$ and the neutral compound $In(ESiMe_3)_3$, and the corresponding condensation products of the latter, assuming the intermolecular elimination of $E(SiMe_3)_2$. The degree of condensation differs, depending on the decomposed anion when having the same decomposition conditions.

The ^1H NMR spectra (figure S31) of the defined residue of Ph_4P $[In(SSiMe_3)_4]$ (**3**) shows signals that can be assigned to a mixture of one equivalent of Ph_4P $[SSiMe_3]$ (literature known anion) [4] and one equivalent of $[SInSiMe_3]$, before and after extraction with toluene. This proves the fact, that two independent species are present that are – in principle – separable by extraction. However, as Ph_4P $[SSiMe_3]$ is slightly soluble in toluene, another cation should be used, when an isolation of the neutral compound is intended.

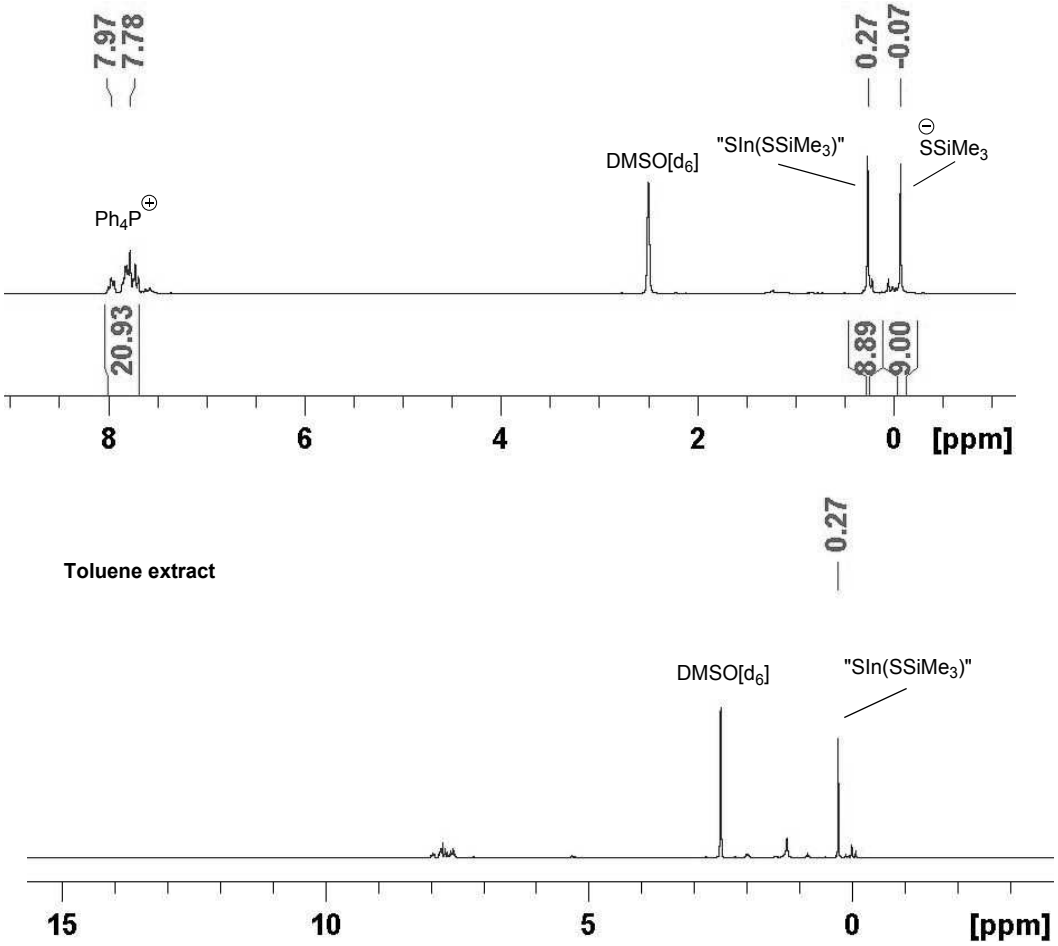

Figure S31. ^1H NMR (250.1 MHz, DMSO[d_6]) spectra of the residue of the defined thermal decomposition of Ph_4P $In(SSiMe_3)_4$ (**3**) at 200 °C for two minutes (top), and of the product obtained after extraction of the residue with toluene (down). A significant enrichment of the signal assigned to the neutral compound can be observed.

These observations can be rationalized by an onefold elimination of $S(SiMe_3)_2$ from each equivalent of $[In(SSiMe_3)_3]$ after decomposition of Ph_4P $[In(SSiMe_3)_4]$ into Ph_4P $[SSiMe_3]$ and $In(SSiMe_3)_3$ (**scheme S1**).

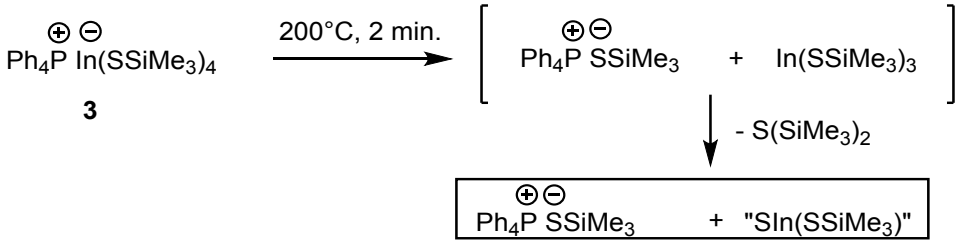

Scheme S1: Assumed mechanism of the defined thermal decomposition of the $[In(SSiMe_3)_4]^-$ anion.

For the decomposed residue of Ph_4P $[In(SeSiMe_3)_4]$ the degree of condensation is further evolved, as the elemental analysis can be explained by the presence of a mixture of four equivalents of Ph_4P $[SeSiMe_3]$ and one equivalent of $Se_5In_4(SeSiMe_3)_2$ (**scheme S2**).

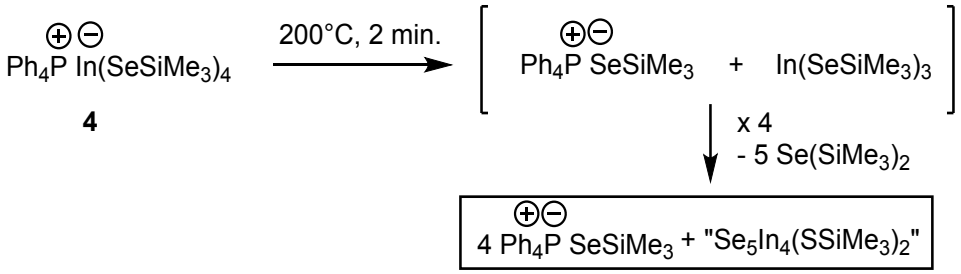

Scheme S2: Assumed mechanism of the thermal decomposition of the $[In(SeSiMe_3)_4]^-$ anion.

Elemental analysis of thermolysis residue of Ph_4P $[In(SeSiMe_3)_4]$ to a assumed mixture of four equivalents Ph_4P $[SeSiMe_3]$ and one equivalent of $Se_5In_4(SeSiMe_3)_2$:

Anal. calcd. For $C_{114}H_{134}In_4P_4Se_{11}Si_6$: C, 43.8; H, 4.3. Found: C, 42.5; H, 4.3.

This is supported by the NMR spectra that shows two signals at 0.06 ppm and 0.01 ppm with an intensity of 9H:4.5H (with the signal for the Ph_4P^+ cation calibrated to 20H) (figure S32). The signal with the higher intensity can be assigned to the free $[SeSiMe_3]^-$ anion though we want to point out that the shift is not exactly as reported (observed: 0.06 ppm, reported 0.09 ppm).[4]

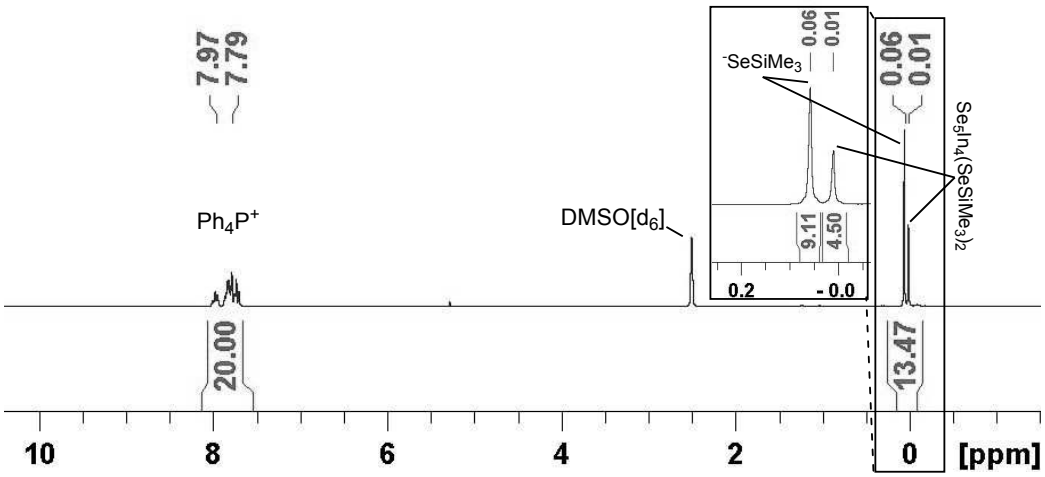

Figure S32. ^{1}H NMR (250.1 MHz, DMSO[d_6]) spectra of the residue of the thermal decomposition of Ph_4P $In(SeSiMe_3)_4$ (**4**).

Our assumptions are supported by the fact that a complete thermal treatment, as achieved in the TGA measurement of Ph_4P [$In(SSiMe_3)_4$] (**3**), every silylated moiety is cleaved under the formation of the binary metalchalcogenide (In_2S_3). The residue of the TGA measurement was investigated via PXRD and In_2S_3 was identified, with minor PXRD-active impurities (figure S33). This proves that in principle the title compounds **1**-**4** can be used as precursors for M_2E_3 material. The arising byproduct Cat $ESiMe_3$ decomposes at temperatures below 300°C, as reported.[4]

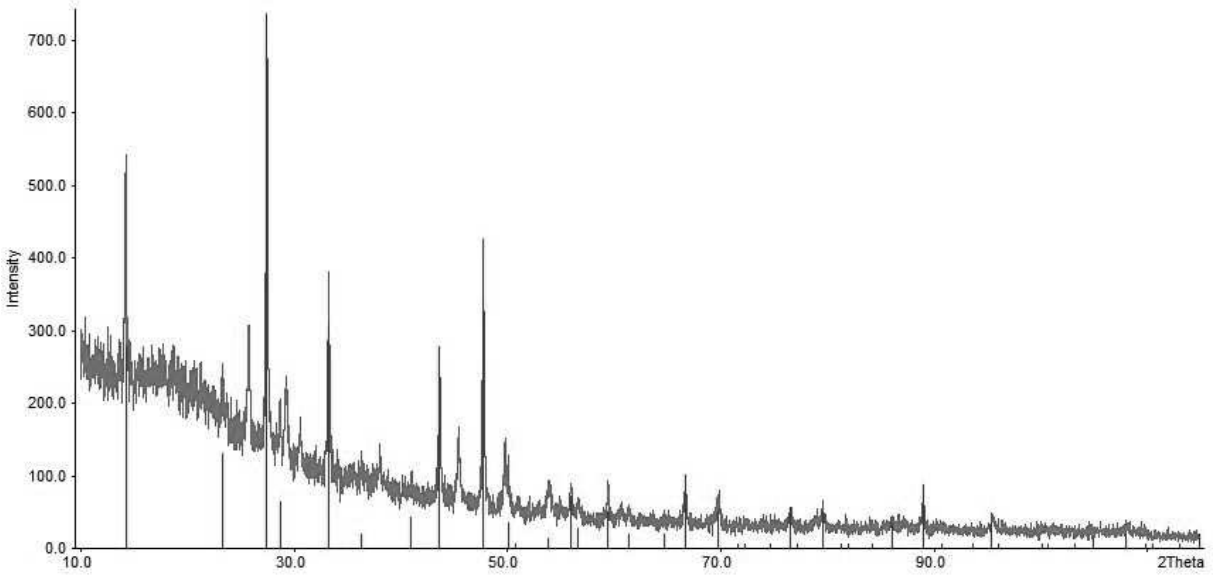

Figure S33. PXRD of the residue obtained from the DSC-TGA measurement of Ph_4P [$In(SSiMe_3)_4$] (**3**) that confirms the presence of In_2S_3.[16]

For the described coprecipitation procedure we assume a mixture of Ph_4P [$SSiMe_3$] and [$SIn(SSiMe_3)$] to be present and homogeniously diluted in acetonitrile. When adding [$Cu(tmtu)_3$][PF_6] the highly nucleophile [$SSiMe$]$^-$ anion attacks the copper atom under

formation of a $[(tmtu)_xCuSSiMe_3]$ compound and the formation of $Ph_4P\,[PF_6]$ as shown in **scheme S3**.

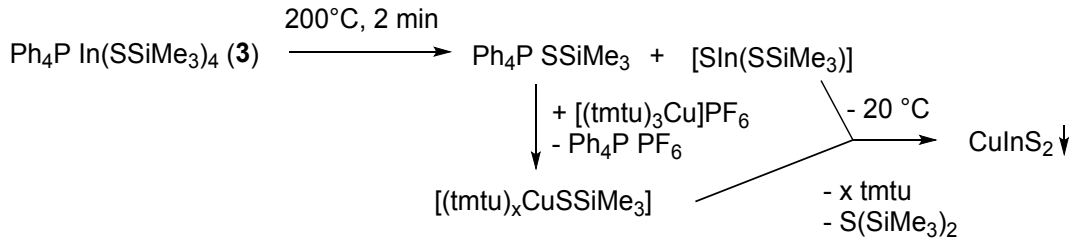

Scheme S3: Assumed mechanism of the coprecipitation procedure to get $CuInS_2$.

These assumptions can be transferred on the material formation using the presented single source precursors. Though more detailed investigation is currently under process we have reasons to assume a thermal transformation of $[Cu(dppe)_2][In(SSiMe_3)_4]$ (**5**) into partially desilylated representatives of $[S_{0.5x}In(SSiMe_3)_{3-x}]$ and 0.5 $[(\eta^2\text{–dppe})Cu(SSiMe_3)]_2(\mu_2\text{-dppe})$. After further thermal treatment $CuInS_2$ arises and the dppe and $S(SiMe_3)_2$ residues evaporate.

Single crystal XRD data

All combinations of the presented single source precursors with dmpe and dppe auxiliary ligand containing gallium, indium and sulfur, selenium could be structurally identified by single crystal x-ray analysis. All representatives of the dppe single-source-precursors are structurally comparable to the title compound $[Cu(dppe)_2][In(SSiMe_3)_4]$ (**5**) presented in the main text.

Surprisingly, there is a difference for the dmpe single-source-precursors. While the indium-sulfur homologue $[(\eta^2\text{-dmpe})Cu(\mu_2\text{-dmpe})_2]_2[In(SSiMe_3)_4]_2$ shows the same dimeric arrangement of the copper-cation as the title compound $[(\eta^2\text{-dmpe})Cu(\mu_2\text{-dmpe})_2]_2[Ga(SSiMe_3)_4]_2$ (**6**), the selenium homologues for both, gallium and indium, show a monomeric $[Cu(dmpe)_2]^+$ cation, as observed for the dppe analogons. As no interaction between the anion and the cation besides the electrostatic attraction could be detected in the XRD-data, we assume this phenomenon to be caused by packing effects, attributed to the bigger radii that are achieved by the selenium anions.

Further the title compound $Ph_4P\,[In(SSiMe_3)_4]$ (**3**) could be structurally characterized, showing a structure comparable to the selenium homologue $Ph_4P\,[In(SeSiMe_3)_4]$ (**4**).

In the following **Table S1** – **Table S6** the crystal and refinement data are provided, and the subsequent figures **Figure S33** – **Figure S43** show the structures and list the most important bond lengths and anlges of the following compounds:

DMPyr [$Ga(SeSiMe_3)_4$] (**2**, **Table S1**, **Figure S34**)

Ph_4P [$In(SSiMe_3)_4$] (**3**, **Table S3**, **Figure S35**)

Ph4P [$In(SeSiMe_3)_4$] (**4**, **Table S1**, **Figure S36**)

[$Cu(dppe)_2$] [$Ga(SSiMe_3)_4$] (**Table S3**, **Figure S37**)

[$Cu(dppe)_2$] [$Ga(SeSiMe_3)_4$] (**Table S4**, **Figure S38**)

[$Cu(dppe)_2$] [$In(SSiMe_3)_4$] (**5**, **Table S2, Figure S39**)

[$Cu(dppe)_2$] [$In(SeSiMe_3)_4$] (**Table S4**, **Figure S40**)

[(η^2-dmpe)Cu(μ_2-dmpe)$_2$]$_2$ [$Ga(SSiMe_3)_4$]$_2$ (**6**, **Table S2**, **Figure S41**)

[$Cu(dmpe)_2$] [$Ga(SeSiMe_3)_4$] (**Table S5**, **Figure S42**)

[(η^2-dmpe)Cu(μ_2-dmpe)$_2$]$_2$ [$In(SSiMe_3)_4$]$_2$ (**Table S5**, **Figure S43**)

[$Cu(dmpe)_2$] [$In(SeSiMe_3)_4$] (**Table S6**, **Figure S44**)

Table S1. XRD crystal and refinement data of DMPyr [$Ga(SeSiMe_3)_4$] (**2**) and Ph_4P [$In(SeSiMe_3)_4$] (**4**).

	DMPyr [$Ga(SeSiMe_3)_4$] (**2**) (**Figure S34**)		Ph_4P [$In(SeSiMe_3)_4$] (**4**) (**Figure S36**)	
CCDC-code	1939702		1939704	
Identification code	jg122_0m		jg159_0m_a	
Empirical formula	C18 H50 Ga N Se4 Si4		C36 H56 In P Se4 Si4	
Formula weight	778.51		1062.79	
Temperature	100(2) K		110(2) K	
Wavelength	0.71073 Å		0.71073 Å	
Crystal system	Monoclinic		Orthorhombic	
Space group	*P* 21/*c*		P n a 21	
Unit cell dimensions	a = 17.9769(7) Å	α= 90°.	a = 21.8628(10) Å	α= 90°.
	b = 19.0143(7) Å	β= 103.3670(10)°.	b = 11.9715(6) Å	β= 90°.
	c = 20.4031(8) Å	γ = 90°.	c = 35.2914(17) Å	γ = 90°.
Volume	6785.2(5) $Å^3$		9236.8(8) $Å^3$	
Z	8		8	
Density (calculated)	1.524 Mg/m^3		1.529 Mg/m^3	
Absorption coefficient	5.251 mm^{-1}		3.825 mm^{-1}	
F(000)	3104		4224	
Crystal size	0.401 x 0.259 x 0.206 mm^3		0.371 x 0.250 x 0.208 mm^3	
Theta range for data collection	2.315 to 25.769°.		2.192 to 25.027°.	
Index ranges	-21<=h<=21, -23<=k<=23, -24<=l<=24		-24<=h<=26, -14<=k<=13, -38<=l<=42	
Reflections collected	114138		66330	
Independent reflections	12969 [R(int) = 0.0529]		14564 [R(int) = 0.0390]	
Completeness to theta = 25.000°	99.9 %		99.9 %	
Absorption correction	Semi-empirical from equivalents		Semi-empirical from equivalents	
Max. and min. transmission	0.7453 and 0.5040		0.7453 and 0.6857	
Refinement method	Full-matrix least-squares on F2		Full-matrix least-squares on F2	
Data / restraints / parameters	12969 / 549 / 628		14564 / 160 / 893	
Goodness-of-fit on F2	1.046		1.110	
Final R indices [I>2sigma(I)]	R1 = 0.0440, wR2 = 0.1063		R1 = 0.0283, wR2 = 0.0621	
R indices (all data)	R1 = 0.0641, wR2 = 0.1169		R1 = 0.0346, wR2 = 0.0680	
Largest diff. peak and hole	2.139 and -1.173 $e.Å^{-3}$		0.909 and -0.848 $e.Å^{-3}$	

Table S2. XRD crystal and refinement data of $Cu(dppe)_2][In(SSiMe_3)_4]$ (**5**) and $[(\eta^2\text{-dmpe})Cu(\mu_2\text{-dmpe})_2]_2[Ga(SSiMe_3)_4]_2$ (**6**).

	$[Cu(dppe)_2][In(SSiMe_3)_4]$ (**5**) (**Figure S39**)	$[(\eta_2\text{-dmpe})Cu(\mu^2\text{-dmpe})_2]_2[Ga(SSiMe_3)_4]_2$ (**6**) (**Figure S41**)
CCDC-code	1939704	1939706
Identification code	jg215loesen	JG284GaS_0m_a
Empirical formula	C64 H84 Cu In P4 S4 Si4	C48 H136 Cu2 Ga2 P8 S8 Si8
Formula weight	1396.15	1709.04
Temperature	100(2) K	100(2) K
Wavelength	0.71073 Å	0.71073 Å
Crystal system	Monoclinic	Triclinic
Space group	*P* 21/*c*	*P* -1
Unit cell dimensions	a = 20.1339(10) Å α= 90°. b = 15.3675(7) Å β= 91.886(2)°. c = 22.9005(10) Å γ = 90°.	a = 12.589(4) Å α= 77.883(12)°. b = 12.686(5) Å β= 84.024(10)°. c = 15.475(6) Å γ = 72.599(9)°.
Volume	7081.8(6) $Å^3$	2303.5(14) $Å^3$
Z	4	1
Density (calculated)	1.309 Mg/m^3	1.232 Mg/m^3
Absorption coefficient	0.938 mm^{-1}	1.485 mm^{-1}
F(000)	2904	904
Crystal size	0.468 x 0.372 x 0.174 mm^3	0.429 x 0.205 x 0.116 mm^3
Theta range for data collection	2.219 to 25.758°.	2.120 to 25.767°.
Index ranges	-24<=h<=24, -18<=k<=18, -27<=l<=27	-15<=h<=14, -15<=k<=15, -18<=l<=18
Reflections collected	249732	62992
Independent reflections	13525 [R(int) = 0.0450]	8805 [R(int) = 0.0508]
Completeness to theta = 25.000°	99.9 %	99.9 %
Absorption correction	Semi-empirical from equivalents	Semi-empirical from equivalents
Max. and min. transmission	0.7453 and 0.6767	0.7453 and 0.6857
Refinement method	Full-matrix least-squares on F2	Full-matrix least-squares on F2
Data / restraints / parameters	13525 / 0 / 715	8805 / 0 / 363
Goodness-of-fit on F2	1.043	1.013
Final R indices [I>2sigma(I)]	R1 = 0.0246, wR2 = 0.0561	R1 = 0.0345, wR2 = 0.0777
R indices (all data)	R1 = 0.0310, wR2 = 0.0589	R1 = 0.0487, wR2 = 0.0832
Largest diff. peak and hole	0.771 and -0.585 $e.Å^{-3}$	1.929 and -0.938 $e.Å^{-3}$

Table S3. XRD crystal and refinement data of Ph_4P $[In(SSiMe_3)_4]$ (**3**) and $[Cu(dppe)_2][Ga(SSiMe_3)_4]$.

.

	Ph_4P $[In(SSiMe_3)_4]$ (**3**) (**Figure S35**)		$[Cu(dppe)_2][Ga(SSiMe_3)_4]$ (**Figure S37**)	
CCDC-code	1939703		1939710	
Identification code	jg138in		JG245S_0m_a	
Empirical formula	C36 H56 In P S4 Si4		C64 H84 Cu Ga P4 S4 Si4	
Formula weight	875.19		1351.05	
Temperature	100(2) K		100(2) K	
Wavelength	0.71073 Å		0.71073 Å	
Crystal system	Orthorhombic		Monoclinic	
Space group	P n a 21		P 21/c	
Unit cell dimensions	a = 21.588(4) Å	α= 90°.	a = 19.973(4) Å	α= 90°.
	b = 11.767(2) Å	β= 90°.	b = 15.216(3) Å	β= 91.66(3)°.
	c = 35.199(7) Å	γ = 90°.	c = 22.687(5) Å	γ = 90°.
Volume	8941(3) $Å^3$		6892(2) $Å^3$	
Z	8		4	
Density (calculated)	1.300 Mg/m^3		1.302 Mg/m^3	
Absorption coefficient	0.882 mm^{-1}		1.020 mm^{-1}	
F(000)	3648		2832	
Crystal size	0.456 x 0.437 x 0.300 mm^3		0.500 x 0.171 x 0.092 mm^3	
Theta range for data collection	2.213 to 25.796°.		2.240 to 25.931°.	
Index ranges	-26<=h<=26, -14<=k<=14, -42<=l<=42		-24<=h<=24, -18<=k<=18, -27<=l<=27	
Reflections collected	109938		171575	
Independent reflections	17102 [R(int) = 0.0271]		13395 [R(int) = 0.1239]	
Completeness to theta = 25.000°	99.9 %		99.9 %	
Absorption correction	Semi-empirical from equivalents		Semi-empirical from equivalents	
Max. and min. transmission	0.7453 and 0.6534		0.7453 and 0.6501	
Refinement method	Full-matrix least-squares on F2		Full-matrix least-squares on F2	
Data / restraints / parameters	17102 / 7 / 854		13395 / 0 / 715	
Goodness-of-fit on F2	1.058		1.011	
Final R indices [I>2sigma(I)]	R1 = 0.0193, wR2 = 0.0442		R1 = 0.0400, wR2 = 0.0710	
R indices (all data)	R1 = 0.0203, wR2 = 0.0445		R1 = 0.0708, wR2 = 0.0797	
Largest diff. peak and hole	0.574 and -0.608 $e.Å^{-3}$		0.575 and -0.478 $e.Å^{-3}$	

Table S4. XRD crystal and refinement data of $[Cu(dppe)_2][Ga(SeSiMe_3)_4]$ and $[Cu(dppe)_2][In(SeSiMe_3)_4]$.

	$[Cu(dppe)_2][Ga(SeSiMe_3)_4]$ (**Figure S38**)		$[Cu(dppe)_2][In(SeSiMe_3)_4]$ (**Figure S40**)	
CCDC-code	1939711		1939712	
Identification code	jg245se_0m_a		jg244_0m_a	
Empirical formula	C64 H84 Cu Ga P4 Se4 Si4		C64 H84 Cu In P4 Se4 Si4	
Formula weight	1538.65		1583.75	
Temperature	100(2) K		100(2) K	
Wavelength	0.71073 Å		0.71073 Å	
Crystal system	Monoclinic		Monoclinic	
Space group	P 21/c		P 21/c	
Unit cell dimensions	a = 20.156(4) Å	α= 90°.	a = 20.180(4) Å	α= 90°.
	b = 15.502(3) Å	β= 91.56(3)°.	b = 15.544(3) Å	β= 91.70(3)°.
	c = 22.937(5) Å	γ = 90°..	c = 22.973(5) Å	γ = 90°.
Volume	7164(3) $Å^3$		7203(3) $Å^3$	
Z	4		4	
Density (calculated)	1.427 Mg/m^3		1.460 Mg/m^3	
Absorption coefficient	2.897 mm^{-1}		2.827 mm^{-1}	
F(000)	3120		3192	
Crystal size	0.660 x 0.181 x 0.133 mm^3		0.632 x 0.127 x 0.116 mm^3	
Theta range for data collection	2.209 to 25.712°.		2.205 to 25.724°.	
Index ranges	-24<=h<=24, -18<=k<=18, -27<=l<=27		-24<=h<=24, -18<=k<=18, -26<=l<=28	
Reflections collected	198940		231576	
Independent reflections	13621 [R(int) = 0.0677]		13689 [R(int) = 0.0715]	
Completeness to theta = 25.000°	99.9 %		99.9 %	
Absorption correction	Semi-empirical from equivalents		Semi-empirical from equivalents	
Max. and min. transmission	0.7453 and 0.5551		0.7453 and 0.6134	
Refinement method	Full-matrix least-squares on F2		Full-matrix least-squares on F2	
Data / restraints / parameters	13621 / 0 / 715		13689 / 0 / 715	
Goodness-of-fit on F2	1.015		1.016	
Final R indices [I>2sigma(I)]	R1 = 0.0239, wR2 = 0.0472		R1 = 0.0245, wR2 = 0.0480	
R indices (all data)	R1 = 0.0354, wR2 = 0.0504		R1 = 0.0367, wR2 = 0.0515	
Largest diff. peak and hole	0.395 and -0.337 $e.Å^{-3}$		0.744 and -0.390 $e.Å^{-3}$	

Table S5. XRD crystal and refinement data of $[Cu(dmpe)_2][Ga(SeSiMe_3)_4]$ and $[(\eta^2\text{-dmpe})Cu(\mu_2\text{-dmpe})_2]_2[In(SSiMe_3)_4]_2$.

	$[Cu(dmpe)_2][Ga(SeSiMe_3)_4]$ (**Figure S42**)		$[(\eta^2\text{-dmpe})Cu(\mu_2\text{-dmpe})_2]_2[In(SSiMe_3)_4]_2$ (**Figure S43**)	
CCDC-code	1939707		1939708	
Identification code	JG284GaSe_0m_a		JG284InS_0m_a	
Empirical formula	C24 H68 Cu Ga P4 Se4 Si4		C24 H68 Cu In P4 S4 Si4	
Formula weight	1042.12		899.62	
Temperature	100(2) K		100(2) K	
Wavelength	0.71073 Å		0.71073 Å	
Crystal system	Monoclinic		Triclinic	
Space group	C c		P -1	
Unit cell dimensions	a = 10.663(2) Å	α= 90°.	a = 12.713(10) Å	α= 76.77(2)°.
	b = 23.494(5) Å	β= 103.34(3)°.	b = 12.953(11) Å	β= 83.62(2)°.
	c = 19.045(4) Å	γ = 90°.	c = 15.413(13) Å	γ = 71.868(18)°.
Volume	4642.4(17) $Å^3$		2346(3) $Å^3$	
Z	4		2	
Density (calculated)	1.491 Mg/m^3		1.274 Mg/m^3	
Absorption coefficient	4.430 mm^{-1}		1.376 mm^{-1}	
F(000)	2096		940	
Crystal size	0.390 x 0.279 x 0.166 mm^3		0.458 x 0.294 x 0.124 mm^3	
Theta range for data collection	2.146 to 25.795°.		2.173 to 25.746°.	
Index ranges	-13<=h<=13, -28<=k<=28, -23<=l<=23		-15<=h<=15, -15<=k<=15, -18<=l<=18	
Reflections collected	56952		51867	
Independent reflections	8860 [R(int) = 0.0345]		8925 [R(int) = 0.0474]	
Completeness to theta = 25.000°	100.0 %		99.9 %	
Absorption correction	Semi-empirical from equivalents		Semi-empirical from equivalents	
Max. and min. transmission	0.7453 and 0.5150		0.7453 and 0.6232	
Refinement method	Full-matrix least-squares on F2		Full-matrix least-squares on F2	
Data / restraints / parameters	8860 / 2 / 364		8925 / 0 / 363	
Goodness-of-fit on F2	1.008		1.005	
Final R indices [I>2sigma(I)]	R1 = 0.0167, wR2 = 0.0369		R1 = 0.0262, wR2 = 0.0554	
R indices (all data)	R1 = 0.0188, wR2 = 0.0375		R1 = 0.0413, wR2 = 0.0611	
Largest diff. peak and hole	0.407 and -0.310 $e.Å^{-3}$		0.426 and -0.476 $e.Å^{-3}$	

Table S6. XRD crystal and refinement data of $[Cu(dmpe)_2][In(SeSiMe_3)_4]$.

	$[Cu(dmpe)_2][In(SeSiMe_3)_4]$ (**Figure S39**)	
CCDC-code	1939709	
Identification code	JG284InSe_0m_a	
Empirical formula	C24 H68 Cu In P4 Se4 Si4	
Formula weight	1087.22	
Temperature	100(2) K	
Wavelength	0.71073 Å	
Crystal system	Monoclinic	
Space group	C c	
Unit cell dimensions	a = 10.725(3) Å	α= 90°.
	b = 23.524(6) Å	β= 102.828(7)°.
	c = 19.271(4) Å	γ = 90°.
Volume	4740(2) $Å^3$	
Z	4	
Density (calculated)	1.523 Mg/m^3	
Absorption coefficient	4.257 mm^{-1}	
F(000)	2168	
Crystal size	0.878 x 0.425 x 0.305 mm^3	
Theta range for data collection	2.131 to 25.698°.	
Index ranges	-13<=h<=13, -28<=k<=28, -23<=l<=22	
Reflections collected	79208	
Independent reflections	8502 [R(int) = 0.0529]	
Completeness to theta = 25.000°	99.9 %	
Absorption correction	Semi-empirical from equivalents	
Max. and min. transmission	0.75 and 0.61	
Refinement method	Full-matrix least-squares on F2	
Data / restraints / parameters	8502 / 8 / 374	
Goodness-of-fit on F2	1.027	
Final R indices [I>2sigma(I)]	R1 = 0.0237, wR2 = 0.0528	
R indices (all data)	R1 = 0.0281, wR2 = 0.0547	
Largest diff. peak and hole	0.668 and -0.557 $e.Å^{-3}$	

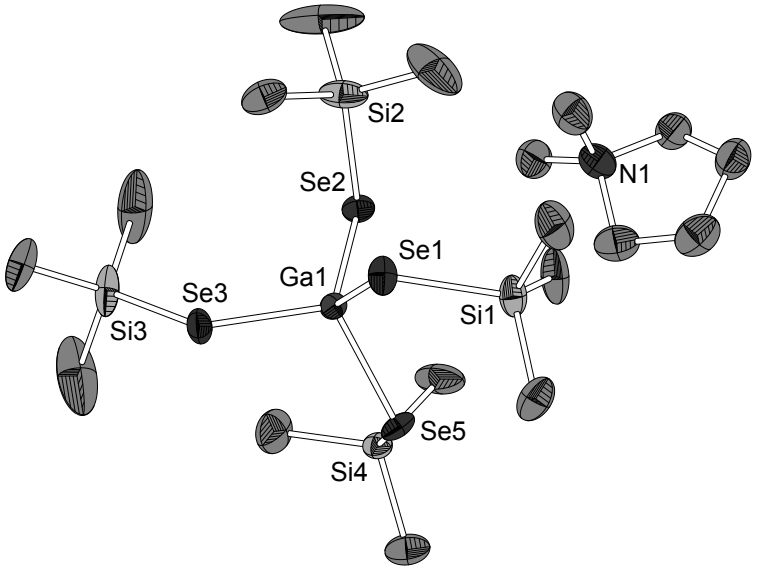

Figure S34: Molecular structure of DMPyr [$Ga(SeSiMe_3)_4$] (**2**). Protons and disordered atoms are neglected for clarity. Monoclinic space group $P2_1/c$ with eight ion pairs per unit cell. Ellipsoids are shown in 50% level. Selected bond lengths (Å) and angles (°) for a representative anion of **2**: Ga1-Se1 2.3997(8); Ga1-Se2 2.3883(9); Ga1-Se3 2.4158(8); Ga-Se4 2.399(3); Se1-Si1 2.268(2); Se2-Si2 2.274(2); Se3-Si3 2.259(2); Se4-Si4 2.261(2); Se1-Ga1-Se2 115.02(3); Se2-Ga1-Se3 117.29(3); Se3-Ga1-Se4 112.77(6); Se4-Ga1-Se1 104.34(5).

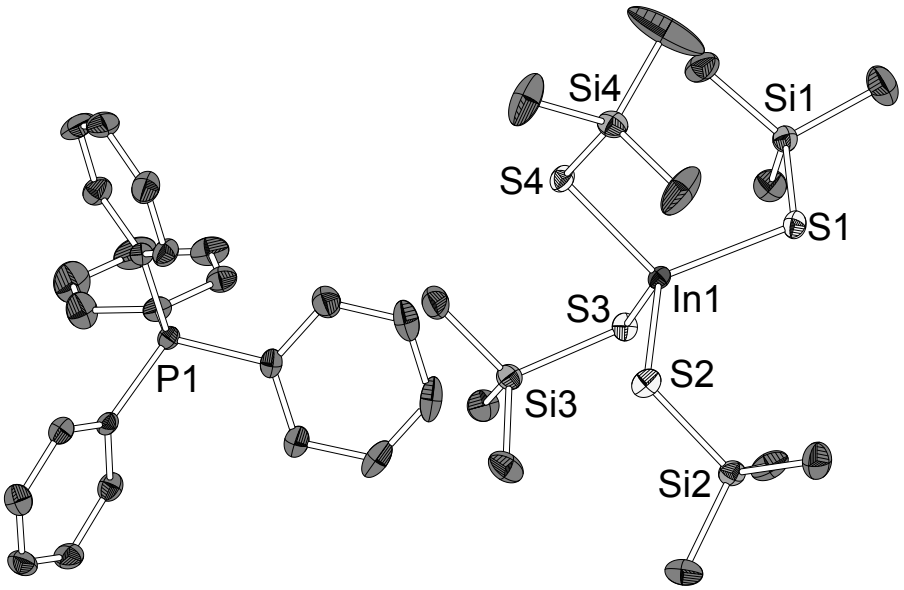

Figure S35: Molecular structure of Ph_4P [$In(SSiMe_3)_4$] (**3**) (In-S: 2.447(1) Å to 2.4577(9) Å, S-In-S: 111.31(3)° to 113.73(3)°). Protons are neglected for clarity. Ellipsoids are shown in 50% level. Orthorhombic space-group $Pna2_1$, eight formula units per unit cell. Selected bond lengths (Å) and angles (°) for a representative ion pair: In1-S1 2.452(1); In1-S2 2.447(1); In1-S3 2.453(8); In1-S4 2.4577(9); S1-Si1 2.146(1); S2-Si2 2.124(1); S3-Si3 2.121 (1); S4-Si4 2.131(1); S1-In1-S2 113.64(4); S2-In1-S3 111.47(3); S3-In1-S4 111.31(3); S4-In1-S1 113.73(3); In1-S1-Si1 103.39(4); In1-S2-Si2 108.10(4); In1-S3-Si3 106.29(4); In1-S4-Si4 106.57(4).

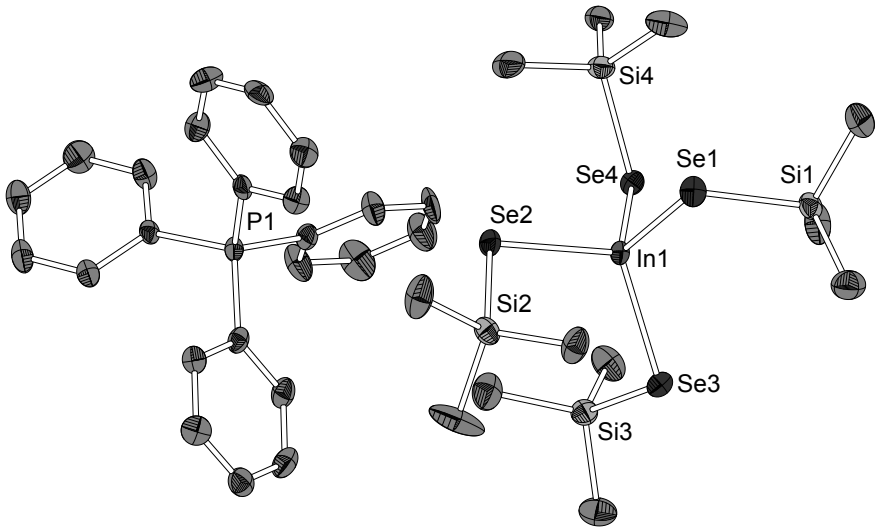

Figure S36: Molecular structure of Ph_4P $[In(SeSiMe_3)_4]$ (**4**) (In-Se: 2.562(1) Å to 2.5694(8) Å, Se-In-Se: 100.86(3)° to 113.56(3)°). Protons and disordered atoms are neglected for clarity. Ellipsoids are shown in 50% level. Orthorhombic space group *Pna*2 with eight ion pairs per unit cell. Selected bond lengths (Å) and angles (°) for a representative anion of **4**: In1-Se1 2.562(1); In1-Se2 2.5674(9); In1-Se3 2.5632(9); In1-Se4 2.5694(8); Se1-Si1 2.255(2); Se2-Si2 2.268(2); Se3-Si3 2.289(2); Se4-Si4 2.263(2); Se1-In1-Se2 100.86(3); Se2-In1-Se3 113.56(3); Se3-In1-Se4 106.63(3); Se4-In1-Se1 111.30(3); In1-Se1-Si1 104.37(6); In1-Se2-Si2 103.23(6); In1-Se3-Si3 100.20(6); In1-Se4-Si4 102.91(6).

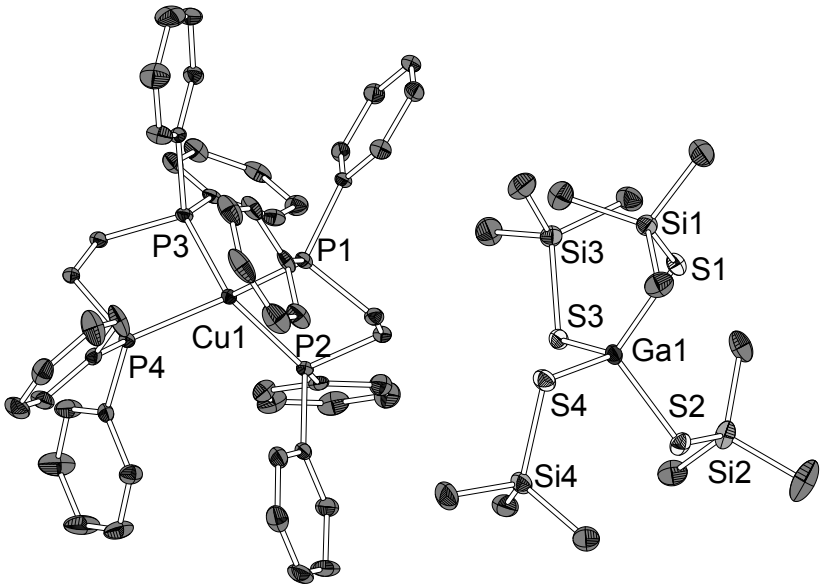

Figure S37: Molecular structure of $[Cu(dppe)_2][Ga(SSiMe_3)_4]$ (Ga-S: 2.2598(9) Å to 2.280(1) Å, S-Ga-S: 108.82(3)° to 111.53(3)°). Protons are neglected for clarity. Ellipsoids are shown in 50% level. Monoclinic space-group *P*21/*c*, four formula units per unit cell. Selected bond lengths (Å) and angles (°) for a representative ion pair: Ga1-S1 2.280(1); Ga1-S2 2.2598(9); Ga1-S3 2.2791(9); Ga1-S4 2.265(1); S1-Si1 2.122(1); S2-Si2 2.114(1); S3-Si3 2.121(1); S4-Si4 2.124(1); S1-Ga1-S2 108.82(3); S2-Ga1-S3 108.25(3); S3-Ga1-S4 111.53(3); S4-Ga1-S1 110.58(3); Ga1-S1-Si1 110.25(4); Ga1-S2-Si2 106.39(4); Ga1-S3-Si3 110.67(4); Ga1-S4-Si4 105.96(4); Cu1-P1 2.2845(9); Cu1-P2 2.2601(9); Cu1-P3 2.2577(9); Cu1-P4 2.2786(9); P1-Cu1-P2- 89.00(3); P2-Cu1-P3 122.85(3); P3-Cu1-P4 89.93(3); P4-Cu1-P1 128.63(3).

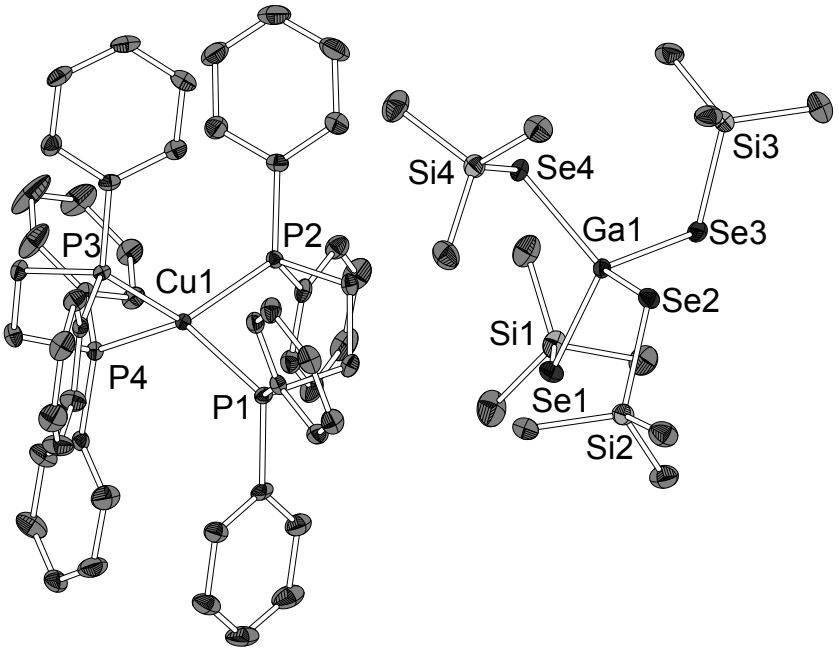

Figure S38: Molecular structure of $[Cu(dppe)_2][Ga(SeSiMe_3)_4]$ (Ga-Se: 2.4001(9) Å to 2.4249(9) Å, Se-Ga-Se: 106.73(3)° to 112.18(3)°). Protons are neglected for clarity. Ellipsoids are shown in 50% level. Monoclinic space-group *P*21/*c*, four formula units per unit cell. Selected bond lengths (Å) and angles (°) for a representative ion pair: Ga1-Se1 2.410(1); Ga1-Se2 2.4249(9); Ga1-Se3 2.4001(9); Ga1-Se4 2.4239(9); Se1-Si1 2.282(1); Se2-Si2 2.2776(9); Se3-Si3 2.272(1); Se4-Si4 2.273(1); Se1-Ga1-Se2 110.25(3); Se2-Ga1-Se3 108.98(3); Se3-Ga1-Se4 106.73(3); Se4-Ga1-Se1 112.18(3); Ga1-Se1-Si1 103.17(3); Ga1-Se2-Si2 108.23(3); Ga1-Se3-Si3 103.01(3); Ga1-Se4-Si4 107.57(3); Cu1-P1 2.3049(9); Cu1-P2 2.274(1); Cu1-P3 2.2698(9); Cu1-P4 2.2991(9); P1-Cu1-P2 89.01(3); P2-Cu1-P3 122.92(3); P3-Cu1-P4 89.94(3); P4-Cu1-P1 128.71(3).

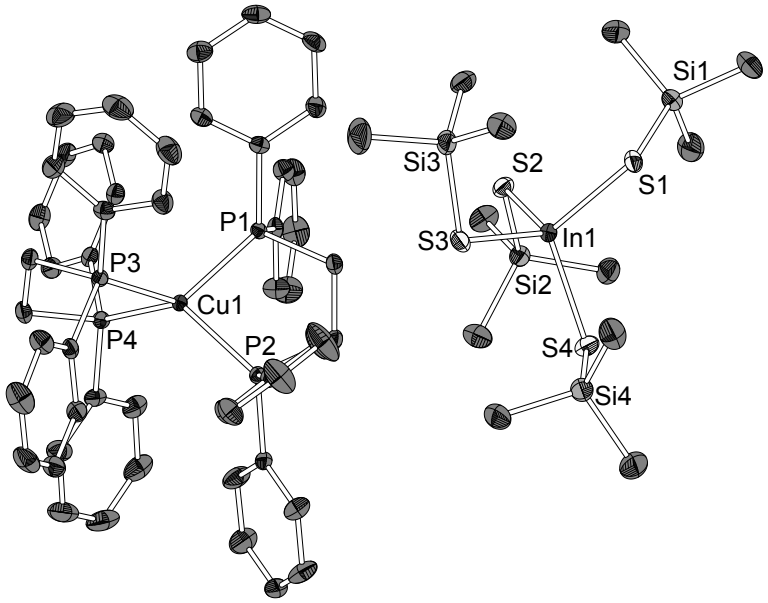

Figure S39: Molecular structure of $[Cu(dppe)_2][In(SSiMe_3)_4]$ (**5**) (In-S: 2.4510(6) Å to 2.4683(6) Å, S-In-S: 105.53(2)° to 112.53(2)°). Protons are neglected for clarity. Ellipsoids are shown in 50% level. Monoclinic space group $P2_1/c$ with four ion pairs per unit cell. Selected bond lengths (Å) and angles (°) for a representative ion pair of **5**: In1-S1 2.4683(6); In1-S2 2.4682(6); In1-S3 2.4510(6); In1-S4 2.4564(7); S1-Si1 2.1356(7); S2-Si2 2.1320(7); S3-Si3 2.1283(7); S4-Si4 2.1397(7); S1-In1-S2 112.53(2); S2-In1-S3 108.38(2); S3-In1-S4 105.53(2); S4-In1-S1 112.06(2); In1-S1-Si1 108.58(3); In1-S2-Si2 108.84(2); In1-S3-Si3 104.42(3); In1-S4-Si4 104.25(3); Cu1-P1 2.2687(6); Cu1-P2 2.2950(6); Cu1-P3 2.2726(6); Cu1-P4 2.3001(6); P1-Cu1-P2 2.2687(6); P2-Cu1-P3 115.19(2); P3-Cu1-P4 88.99(2); P4-Cu1-P1 114.695(2).

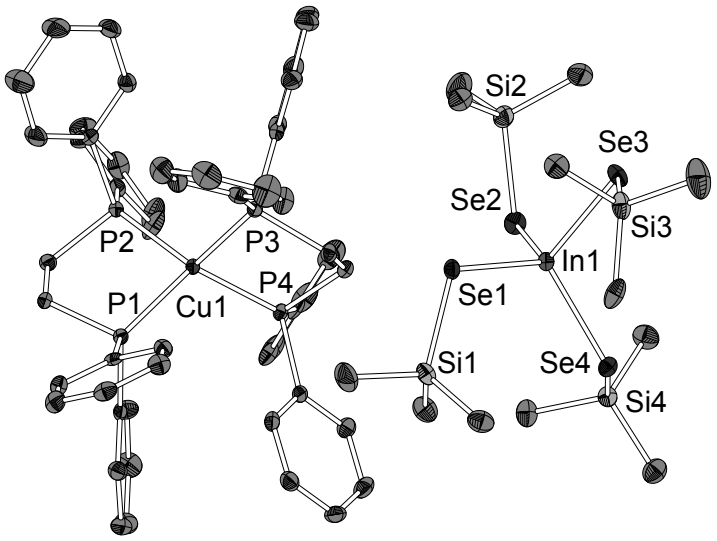

Figure S40: Molecular structure of $[Cu(dppe)_2][In(SeSiMe_3)_4]$ (In-Se: 2.570(1) Å to 2.591(1) Å, Se-In-Se: 106.46(3)° to 112.53(3)°). Protons are neglected for clarity. Ellipsoids are shown in 50% level. Monoclinic space-group *P*21/*c*, four formula units per unit cell. Selected bond lengths (Å) and angles (°) for a representative ion pair: In1-Se1 2.5903(9); In1-Se2 2.578(1); In1-Se3 2.570(1); In1-Se4 2.591(1); Se1-Si1 2.272(1); Se2-Si2 2.282(1); Se3-Si3 2.271(1); Se4-Si4 2.2742(9); Se1-In1-Se2 112.53(3); Se2-In1-Se3 106.46(3); Se3-In1-Se4 108.46(3); Se4-In1-Se1 112.49(3); In1-Se1-Si1 105.51(3); In1-Se2-Si2 101.46(3(); In1-Se3-Si3 101.01(3); In1-Se4-Si4 106.76(3); Cu1-P1 2.268(1); Cu1-P2 2.299(1); Cu1-P3 2.271(1); Cu1-P4 2.305(1); P1-Cu1-P2 90.02(3); P2-Cu1-P3 114.69(4); P3-Cu1-P4 88.89(4); P4-Cu1-P1 114.97(4).

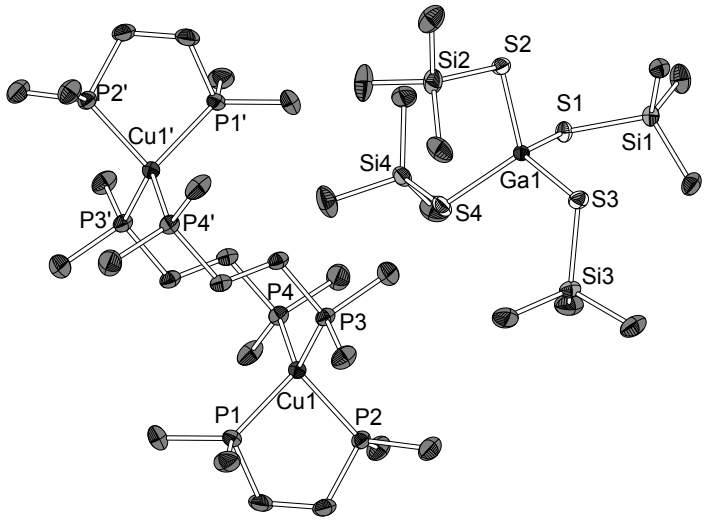

Figure S41: Molecular structure of $[(\eta^2\text{-dmpe})Cu(\mu_2\text{-dmpe})]_2[Ga(SSiMe_3)_4]_2$ (**6**) (Ga-S: 2.272(1) Å – 2.286(1) Å, S-Ga-S: 105.65(3)° - 114.00(4)°). One anion and protons are neglected for clarity. Ellipsoids are shown in 50% level. Triclinic space group *P*-1 with one ion pair per unit cell. Selected bond lengths (Å) and angles (°) for a representative anion and copper centre of **6**: Ga1-S1 2.2748(9); Ga1-S2 2.286(1); Ga1-S3 2.281(1); Ga1-S4 2.272(1); S1-Si1 2.124(1); S2-Si2 2.126(1); S3-Si3 2.137(1); S4-Si4 2.128(1); S1-Ga1-S2 105.77(3); S2-Ga1-S3 105.64(3); S3-Ga1-S4 109.38(4); S4-Ga1-S1 110.04(4); Ga1-S1-Si1; 106.90(5); Ga1-S2-Si2 106.20(5); Ga1-S3-Si3 105.90(5); Ga1-S4-Si4 108.82(5); Cu1-P1 2.258(1); Cu1-P2 2.277(1); Cu1-P3 2.239(1); Cu1-P4 2.251(7); P1-Cu1-P2 89.90(4); P2-Cu1-P3 112.09(4); P3-Cu1-P4 112.14(4); P4-Cu1-P1 115.20(4).

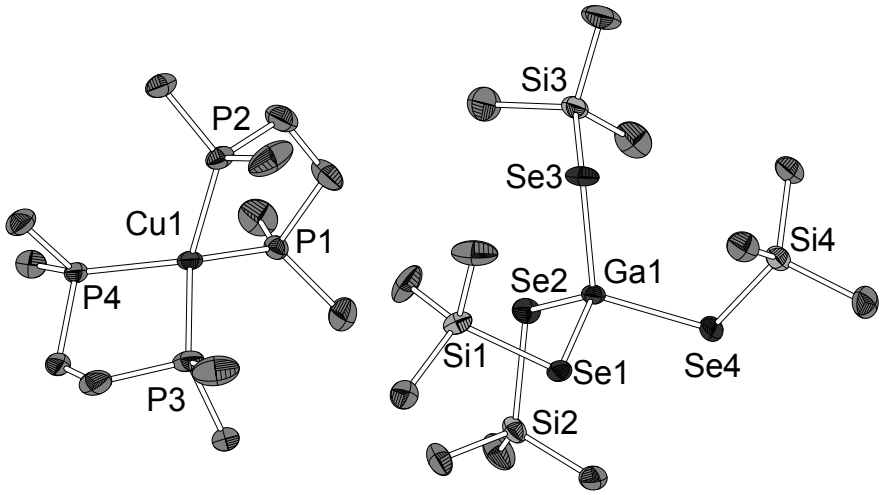

Figure S42: Molecular structure of $[(dmpe)_2Cu][Ga(SeSiMe_3)_4]_2$ (Ga-Se: 2.3939(8) Å – 2.4188(9) Å, Se-Ga-Se: 104.81(3)° - 114.24(3)°). Protons are neglected for clarity. Ellipsoids are shown in 50% level. Monoclinic space group *Cc* with four ion pairs per unit cell. Selected bond lengths (Å) and angles (°) for a representative anion and anion: Ga1-Se1 2.4099(7); Ga1-Se2 2.395(1); Ga1-Se3 2.3939(8); Ga1-Se4 2.4188(9); Se1-Si1 2.268(1); Se2-Si2 2.268(1); Se3-Si3 2.260(1); Se4-Si4 2.261(1); Se1-Ga1-Se2 113.54(3); Se2-Ga1-Se3 110.89(2); Se3-Ga1-Se4 114.24(3); Se4-Ga1-Se1 104.81(3); Ga1-Se1-Si1 102.87(4); Ga1-Se2-Si2 102.25(3); Ga1-Se3-Si3 105.57(4); Ga1-Se4-Si4 104.54(4); Cu1-P1 2.252(1); Cu1-P2 2.261(1); Cu1-P3 2.257(1); Cu1-P4 2.254(1); P1-Cu1-P2 90.67(4); P2-Cu1-P3 119.93(4); P3-Cu1-P4 90.59(4); P4-Cu1-P1 126.08(5).

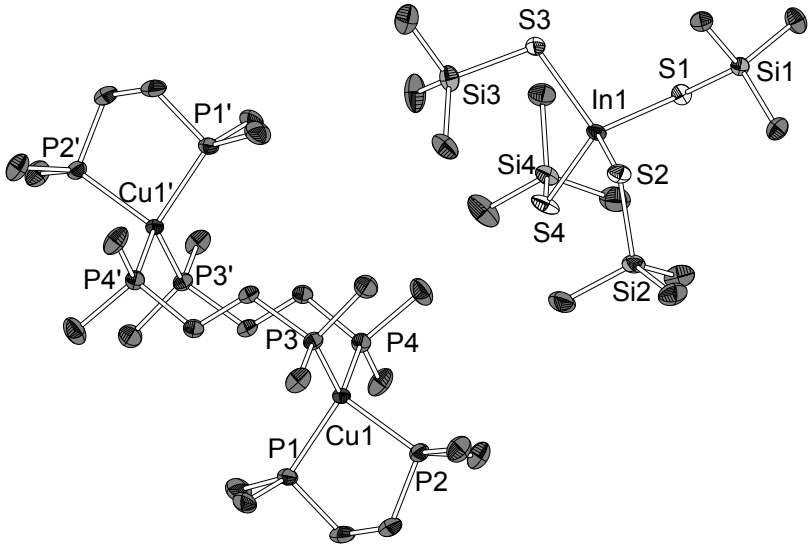

Figure S43: Molecular structure of $[(\eta^2\text{-dmpe})Cu(\mu_2\text{-dmpe})]_2[In(SSiMe_3)_4]_2$ (In-S: 2.452(2) Å – 2.468(2) Å, S-In-S: 105.69(4)° - 113.86(4)°). One anion and protons are neglected for clarity. Ellipsoids are shown in 50% level. Triclinic space-group *P*-1, two formula units per unit cell. Selected bond lengths (Å) and angles (°) for a representative anion and copper center: In1-S1 2.452(2); In1-S2 2.467(2); In1-S3 2.468(2); In1-S4 2.454(2); S1-Si1 2.127(2); S2-Si2 2.139(2); S3-Si3 2.123(2); S4-Si4 2.129(2); S1-In1-S2 113.86(4); S2-In1-S3 105.69(4); S3-In1-S4 111.74(5); S4-In1-S1 110.54(6); In1-S1-Si1 105.45(6); In1-S2-Si2 104.26(5); In1-S3-Si3 105.71(6); In1-S4-Si4 107.73(6); Cu1-P1 2.266(2); Cu1-P2 2.283(2); Cu1-P3 2.243(2); Cu1-P4 2.249(2); P1-Cu1-P2 89.76(5); P2-Cu1-P3 111.52(5); P3-Cu1-P4 112.43(5); P4-Cu1-P1 110.23(5).

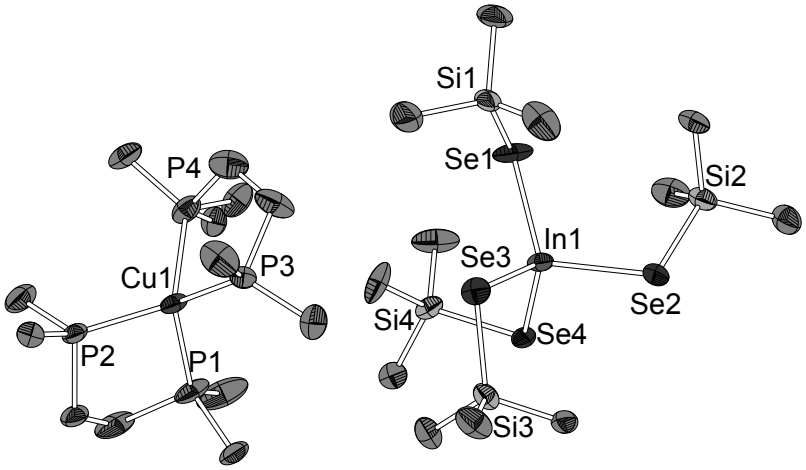

Figure S44: Molecular structure of $[(dmpe)_2Cu][In(SeSiMe_3)_4]_2$ (In-Se: 2.5687(9) Å – 2.593(1) Å, Se-In-Se: 106.74(2)° - 113.63(3)°). Protons are neglected for clarity. Ellipsoids are shown in 50% level. Monoclinic space group *Cc* with four ion pairs per unit cell. Selected bond lengths (Å) and angles (°) for a representative anion and anion: In1-Se1 2.5687(9); In1-Se2 2.593(1); In1-Se3 2.5696(8); In1-Se4 2.5840(9); Se1-Si1 2.258(2); Se2-Si2 2.268(2); Se3-Si3 2.275(2); Se4-Si4 2.269(2); Se1-In1-Se2 113.63(3); Se2-In1-Se3 107.62(3); Se3-In1-Se4 112.68(2); Se4-In1-Se1 106.74(2); In1-Se1-Si1 103.71(6); In1-Se2-Si2 103.07(5); In1-Se3-Si3 100.34(5); In1-Se4-Si4 101.62(5); Cu1-P1 2.262(2); Cu1-P2 2.263(2); Cu1-P3 2.257(2); Cu1-P4 2.274(2); P1-Cu1-P2 90.64(7); P2-Cu1-P3 126.14(6); P3-Cu1-P4 90.45(6); P4-Cu1-P1 119.15(7).

References

(1) Armarego, W. L. F.; Perrin, D. D. *Purification of laboratory chemicals*, 4th ed., paperback ed.; Butterworth-Heinemann: Oxford, 1997.

(2) Weininger, M. S.; Hunt, G. W.; Amma, E. L. Crystal and molecular structure of tris(ethylenethiourea)copper(I) sulphate and tris(tetramethylthiourea)copper(I) tetrafluoroborate [examples of trigonal planar copper(I) stereochemistry. *J. Chem. Soc., Chem. Commun.* **1972**, 1140.

(3) Huang, S.-H.; Keith, J. M.; Hall, M. B.; Richmond, M. G. Ortho-Metalation Dynamics and Ligand Fluxionality in the Conversion of $Os_3(CO)_{10}$(dppm) to $HOs_3(CO)_8[\mu\text{-}PhP(C_6H_4\text{-}\mu_2,\eta^1)CH_2PPh_2]$: Experimental and DFT Evidence for the Participation of Agostic C−H and π-Aryl Intermediates at an Intact Triosmium Cluster. *Organometallics* **2010**, *29*, 4041–4057.

(4) Finger, L. H.; Scheibe, B.; Sundermeyer, J. Synthesis of Organic (Trimethylsilyl)chalcogenolate Salts Cat[TMS-E] (E = S, Se, Te): the Methylcarbonate Anion as a Desilylating Agent. *Inorg. Chem.* **2015**, *54*, 9568–9575.

(5) So, J.-H.; Boudjouk, P. Convenient Syntheses of Hexamethyldisilathiane and Tetramethyldisilathiane. *Synthesis* **1989**, *1989*, 306–307.

(6) Taher, D.; Wallbank, A. I.; Turner, E. A.; Cuthbert, H. L.; Corrigan, J. F. Alk-2-ynyl Trimethylsilyl Chalcogenoethers by Nucleophilic Substitution of Propargyl Bromides. *Eur. J. Inorg. Chem.* **2006**, *2006*, 4616–4620.

(7) Sheldrick, G. M. Crystal structure refinement with SHELXL. *Acta Cryst. Sect. C* **2015**, *71*, 3–8.

(8) Hübschle, C. B.; Sheldrick, G. M.; Dittrich, B. S. ShelXle: a Qt graphical user interface for SHELXL. *J. Appl. Cryst.* **2011**, *44*, 1281–1284.

(9) Spek, A. L. Structure validation in chemical crystallography. *Acta Cryst. Sect. D* **2009**, *65*, 148–155.

(10) K. Brandenburg, H. P. *Diamond*; Crystal Impact GbR: Bonn, **2012**.

(11) Khadka, C. B.; Macdonald, D. G.; Lan, Y.; Powell, A. K.; Fenske, D.; Corrigan, J. F. Trimethylsilylchalcogenolates of Co(II) and Mn(II): From Mononuclear Coordination Complexes to Clusters Containing $-ESiMe_3$ Moieties (E = S, Se). *Inorganic chemistry* **2010**, *49*, 7289–7297.

(12) Krebs, B.; Bobb, W.; Wellmer, H.-J.; Wiesmann, K. Chalkogenohalogenogallate(III) und -indate(III): Eine neue Verbindungsklasse in der dritten Hauptgruppe. Synthese und Struktur von $[Ph_4P]_2[In_2SX_6]$, $[Et_4N]_3[In_3E_3C_{l6}] \cdot MeCN$ und $[Et_4N]_3[Ga_3S_3Cl_6] \cdot THF$ (X = Cl, Br; E = S, Se). *Z. anorg. allg. Chem.* **1994**, *620*, 1234–1246.

(13) JCPDS File No. 65-2732.

(14) JCPDS File No. 27-0159.

(15) JCPDS File No. 25-0279.

(16) JCPDS File No. 65-0459.

Manuscript submitted (24.10.2019)

Homoleptic Trimethylsilylchalcogenolato Zinkates $[Zn(ESiMe_3)_3]^-$ and Stannanides $[Sn(ESiMe_3)_3]^-$ (E = S, Se): Precursors in Solution Based Low-Temperature Cu_2ZnSnS_4 (CZTS) Synthesis

Jannick Guschlbauer, Tobias Vollgraff, Jörg Sundermeyer

ARTICLE

Homoleptic Trimethylsilylchalcogenolato Zincates $[Zn(ESiMe_3)_3]^-$ and Stannanides $[Sn(ESiMe_3)_3]^-$ (E = S, Se): Precursors for Chalcogenide Based Materials Containing Sn and Zn

Received 00th January 20xx,
Accepted 00th January 20xx

DOI: 10.1039/x0xx00000x

Jannick Guschlbauer,[a] Tobias Vollgraff [a] and Jörg Sundermeyer [a] *

Organic cation salts with homoleptic zincate and stannanide anions, Ph_4P $[Zn(ESiMe_3)_3]$ (E = S (**1a**), Se (**1b**)) and Cat $[Sn(ESiMe_3)_3]$ (Cat = Ph_4P^+ (E = S (**2a-Ph₄P**); Cat = PPN^+ (E = S **2a-Ph₄P**, Se (**2a**)) are presented and structurally characterized. Efforts to isolate neutral thermally metastable stannane precursors $[Sn(ESiMe_3)_4]$ (E = S (**3**), Se(**4**)) are reported as well. The thermal decomposition of the presented compounds to yield different binary sulfides and selenides of zinc and tin are described. The potential ability of the title anions to act as precursors in solution-based low-temperature synthesis of Cu_2ZnSnS_4 (CZTS) by coprecipitation with $[Cu(tmtu)_3]PF_6$ and subsequent annealing is shortly discussed. The presented compounds might be of interest as binary M / E building block precursors for chalcogenide based materials.

Introduction

Metal complexes containing trimethylsilyl chalcogenolato ligands $ESiMe_3$ (E = S, Se) are an emerging class of metastable molecular compounds. V*ia* low-temperature desilylation and condensation steps these may serve as precursors for molecular clusters or metal chalcogenide materials.[1,2,3] So far, focus was put on uncharged heteroleptic complexes with strongly binding coligands such as $[(tmeda)Zn(SSiMe_3)_2]$, which decomposes thermally to ZnS nanoparticles,[4] or $[(Mes_2NHC)AuS\text{-}SiMe_3]$, which serves as starting material for the synthesis of multinary chalcogenide metal clusters with variable optical properties.[5] Despite these perspectives there is only one report on a charged coordination compounds with cheap and easily accessible trimethylsilylchalcogenolate ligands $ESiMe_3$ (E = S, Se) – namely $Li_2[Mn(SSiMe_3)_4$.[6a] We are interested to develop a new class of simple homoleptic metalate complexes with metals typically used in metal chalcogenide semiconductor and solar absorber materials. As new examples, we introduced organic cation gallates and indates $[M(E\text{-}SiMe_3)_4]^-$ (M = Ga, In; E = S, Se) and successfully used them to prepare materials of the CIGS family.[6b] Herein we present the corresponding zincates $[Zn(E\text{-}SiMe_3)_3]^-$ and stannanides $[Sn(E\text{-}SiMe_3)_3]^-$ (E = S, Se) as organic cation salts. We also present an approach to uncharged thermally metastable tin(IV) derivatives $[Sn(E\text{-}SiMe_3)_4]$. We demonstrate, that the presented compounds can be thermally decomposed to the corresponding binary sulfides ZnS and SnS and selenides ZnSe, SnSe, and $SnSe_2$. By having precursors for the aforementioned binary semiconductors at hand, a novel approach to prepare Cu_2ZnSnS_4 (CZTS) is in principle accessible. CZTS is a photovoltaic absorber material with kesterite structure made up by earth abundant and nontoxic elements only.[7] CZTS has gained recent interest in cadmium-free thin film solar cells with efficiencies more than 10%.[8] The performance can be enhanced by partial replacement of sulphur by selenium to form CZTSSe materials with an efficiency of up to 12.6%.[9] The direct band gap can be tuned from 1.04 eV to 1.48 eV by varying the chalcogen ratio of the solid solution system $Cu_2ZnSnS_xSe_{4-x}$.[10,11] Only few molecules containing at least two of the elements present in CZTS are known to be suitable for this purpose.[12,13] The herein presented compounds can be seen as an extension of the previously reported $[M(ESiMe_3)_{n+1}]^-$ complexes for M = Ga, In[6b] that provide further binary M / E building blocks for the preparation of multinary chalcogenide-based materials.

Results and Discussion

Syntheses and Structures of Cat $[M(E\text{-}SiMe_3)_3]$ (M = Zn, Sn; E = S, Se)

The zincates $Ph_4P[Zn(SSiMe_3)_3]$ (**1a**) and $Ph_4P[Zn(SeSiMe_3)_3]$ (**1b**), and the stannanides $Cat[Sn(SSiMe_3)_3]$ (**2a-Cat**), and $PPN[Sn(SeSiMe_3)_3]$ (**2b**) (Cat = PPN^+ = $[Ph_3PNPPh_3]^+$) were prepared by treating *in situ* prepared chlorometalates $Cat[MCl_3]$ (M = Zn, Sn(II)) with three equivalents of LiE-$SiMe_3$ (E = S, Se) in tetrahydrofuran and allowing the reaction mixture slowly to reach ambient temperature (Scheme 1). Cooling of the reaction mixture and a slow warm up are important, as partly substituted intermediates $[MCl_x(ESiMe_3)_{3-x}]^-$ tend to eliminate trimethylsilylchloride and to condense with precipitation of the

[a] *Fachbereich Chemie and Materials Science Center, Philipps-Universität, Hans-Meerwein-Str. 4, 35032 Marburg, Germany. E-mail:JSU@staff.uni-marburg.de.*

Electronic Supplementary Information (ESI) available: experimental details on the decompositions of $Sn(ESiMe_3)_4$, NMR spectra, XRD data, Thermal decompostition of the title anions, attempt to prepare CZTS and comment on the mechanism of condensation of the binary anions The CIF files of the presented structures are provided. See DOI: 10.1039/x0xx00000x

corresponding metal chalcogenides at ambient or slightly higher temperatures.

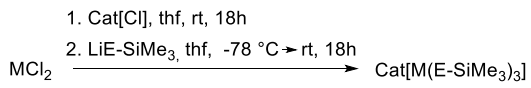

1a: M = Zn, Cat = Ph_4P^+, E = S.
1b: M = Zn, Cat = Ph_4P^+, E = Se.
2a-cat: M = Sn, E = S, Cat = Ph_4P^+/PPN^+
2b: M = Sn, E = Se, Cat = PPN^+.

Scheme 1. General procedure for the preparation of the title compounds $Cat[M(ESiMe_3)_3]^-$ (M = Zn, Sn; E = S, Se).

In order to separate the desired product from lithium chloride, thf is removed from the reaction mixture and the lipophilic title compounds are extracted into diethyl ether. The highly reactive anions are stable towards hydrocarbons or ethers but they decompose in chlorinated or protic solvents, even in dipolar aprotic MeCN and DMSO. Therefore, the yield in the extraction and separation process can be optimized using lipophilic cations typically applied in ionic liquid technology. In this fundamental study however, we intended to use higher symmetry organic cations Ph_4P^+ and PPN^+ in order to induce higher melting points and crystallinity for XRD analytical reasons. On the other hand, the cation has an influence on the stability of theses salts: Stannanides **2a, b** are prepared in much better yields and can be stored at ambient temperature for long periods of time if the PPN^+ cation instead of Ph_4P^+ is used. Ph_4P^+ representatives are only accessible in minor yields. They decompose slowly under inert gas at ambient temperature which is indicated by a pronounced darkening of the colourless powders after a few days (inert gas, 25°C).

$Ph_4P[Zn(SSiMe_3)_3]$ (**1a**) crystallizes in the monoclinic space group $P2_1/n$ with four formula units and two equivalents of diethyl ether per unit cell (Figure 1). No intermolecular bonding interactions could be detected. The zinc atom is trigonal planar coordinated by three -$SSiMe_3$ ligands. The Zn-S bond lengths range from 2.2534(8) Å to 2.2543(7) Å and the S-Zn-S angles from 117.65(2)° to 121.72(2)°. The sum of all three S-Zn-S angles is 360°, indicating the planarity of the anion. Though trigonal planar coordinated neutral zinc complexes[14,15] and supersilyl stabilised zincates like $[L_xLi]\{Zn[SSi(SiMe_3)_3]_3\}$[16] are known, **1a** is the first metastable zincate with organic cation and technologically available, cheap and reactive $SSiMe_3$ ligands – an important aspect, if applications in sustainable materials synthesis are envisaged. It is a commonly observed fact, that compounds with -$ESiR_3$ (E = S, Se) substituents of decreasing steric demand of R display an increasing lability and decreasing thermostability.[1] This makes the lightest representatives based on -$ESiMe_3$ exceptionally attractive for thermally metastable precursors in low temperature solvothermal synthesis of chalcogenide materials.

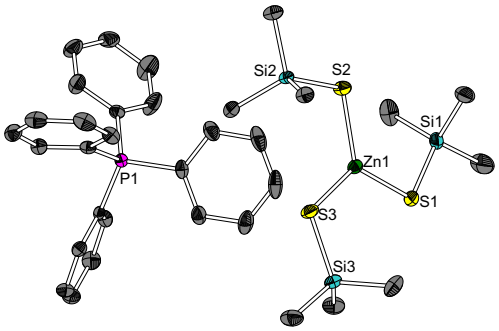

Figure 1. Molecular structure of $Ph_4P[Zn(SSiMe_3)_3]$ (**1a**). Atoms are shown as ellipsoids with 50% probability. Hydrogen atoms and half a molecule of diethyl ether are omitted for clarity. Selected bond lengths (Å) and angles (°) for **1a**: Zn1-S1 2.2543(7); Zn1-S2 2.2536(8); Zn1-S3 2.2534(7); S1-Si1 2.1240(8); S2-Si2 2.1176(7); S3-Si3 2.1055(9); S1-Zn1-S2 120.64(2); S2-Zn1-S3 117.65(2); S3-Zn1-S1 121.72(2); Zn1-S1-Si1 104.42(3); Zn1-S2-Si2 105.12(2); Zn1-S3-Si3 108.95(2).

The charged nature of the $[Zn(SSiMe_3)_3]^-$ anion prevents fast condensation at ambient temperature. In contrast to the corresponding neutral zinc complexes $[L_xZn(SSiMe_3)_2]$,[3,17] **1a** can be stored without cooling for some days.

The selenium homologue $Ph_4P[Zn(SeSiMe_3)_3]$ (**1b**) crystallizes as crystallographically imposed centrosymmetric dianionic dimer $[(Me_3SiSe)_2Zn(\mu\text{-}SeSiMe_3)]_2^{2-}$ in the triclinic space group *P*-1 with two formula units per unit cell. Surprisingly, selenium with its larger atomic radius and higher polarisability compared to sulfur leads to tetracoordinate zinc atoms and the formation of a four membered ring structure with bridging μ-$SeSiMe_3$ ligands. Both zincate centres display a distorted tetrahedral configuration. As expected, the two terminal -$SeSiMe_3$ substituents reveal shorter Zn-Se bond distances of 2.414(1) Å to 2.447(1) Å and an Se-Zn-Se angle of 108.72(3)°), while the two bridging μ-$SeSiMe_3$ ligands show Zn-Se bond distances of 2.528(1) Å, and 2.571(1) Å, and an Se-Zn-Se' angle of 89.66(3)°, while the Zn-Se-Zn' angle is 90.34(3)° (Figure 2). The -$SiMe_3$ moieties of the bridging ligands are oriented in a *anti* fashion with an angle of 49.50(4)° towards the Zn_2Se_2-ring plane. No non-ionic bonding interaction between cation and anion can be observed (shortest C-C distance between anion cation is 3.984(6) Å). The dinuclear nature of the dianion $[(Me_3SiSe)_2Zn(\mu\text{-}SeSiMe_3)]_2^{2-}$ is most likely not preserved in thf solution, as the $^1H/^{13}C/^{29}Si$ NMR spectra show just one sharp signal for the $SeSiMe_3$ groups. This might be explained by dynamic ligand exchange or dimer dissociation/association in thf solution. Another obvious explanation is, that the affinity of Zn^{2+} towards thf as donor ligand is high enough to prevent dimer formation in thf solutions. The $[Zn(ESiMe_3)_3]^-$ (E = S, Se) anion is one of the very few systems in which the selenium homologue shows a different structural motif as the corresponding sulfur representative. The presented compounds are closing the gap of knowledge between polynuclear silylchalcogenolato complexes of zinc[14,15] and structurally comparable alkylthiolatozincates.[18,19] To the best of our knowledge, dianionic dinuclear compounds with the central $[(RSe)_2Zn(\mu\text{-}SeR)_2Zn(SeR)_2]^{2-}$ core have not yet been observed: The coulomb repulsion of two approaching monoanions is probably higher for more electron rich R = alkyl derivatives than

for R = trimethylsilyl derivatives. In nearly all of such structurally characterised four-membered ring compounds, the substituents at the bridging chalcogen atoms show *anti* configuration. There is one example for *syn* configuration.[19]

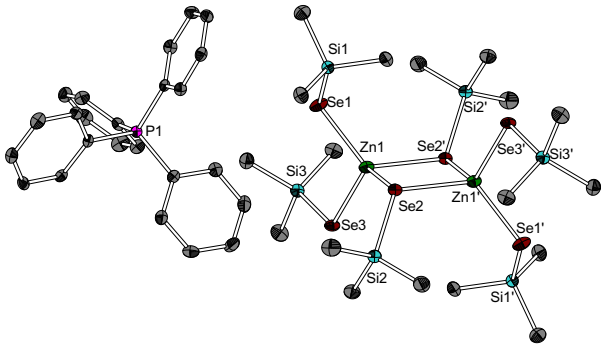

Figure 2. Molecular structure of $Ph_4P[Zn(SeSiMe_3)_3]$ (**1b**). Shown is the dianion $[(Me_3SiSe)_2Zn(\mu\text{-}SeSiMe_3)]_2^{2-}$ with one cation. Atoms are shown as ellipsoids with 50% probability. Hydrogen atoms, disordered atoms and one cation are omitted for clarity. Selected bond lengths (Å) and angles (°) for **1b**: Zn1-Se1 2.414(1); Zn1-Se2 2.528(1); Zn1-Se3 2.447(1); Zn1-Se2' 2.571(1); Se1-Si1 2.243(2); Se2-Si2 2.273(1); Se3-Si3 2.243(1); Se1-Zn1-Se2 115.68(3); Se2-Zn1-Se3 114.42(3); Se3-Zn1-Se1 108.72(3): Se1-Zn1-Se2' 119.28(3); Zn1-Se1-Si1 109.14(3); Zn1-Se2-Si2 117.03(4); Zn1-Se3-Si3 103.96(4); Se2-Zn1-Se2' 89.66(3); Zn1-Se2-Zn1' 90.34(3). Symmetry operation: I: 2-x, 1-y, 2-z.

$Ph_4P[Sn(SSiMe_3)_3]$ (**2a-Ph₄P**) crystallizes in the triclinic space group $P_{\bar{1}}$ with four formula units per unit cell (Figure 3). In accord with VSEPR model the tin(II) centre is trigonal pyramidally (or pseudo tetrahedrally) coordinated by three $SSiMe_3$ moieties with Sn-S bond lengths ranging from 2.543(1) Å to 2.554(9) Å and S-Sn-S angles ranging from 90.34(3)° to 96.57(3)°.

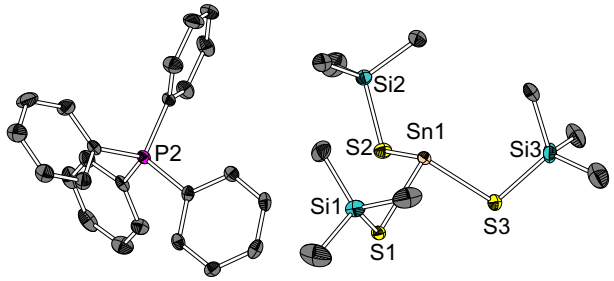

Figure 3. Molecular structure of $Ph_4P[Sn(SSiMe_3)_3]$ (**2a**). Atoms are shown as ellipsoids with 50% probability. Hydrogen atoms and disordered atoms are omitted for clarity. Selected bond lengths (Å) and angles (°) for **2a**: Sn1-S1 2.5521(9); Sn1-S2 2.5372(1); Sn1-S3 2.5366(6); S1-Si1 2.116(1); S2-Si2 2.113(1); S3-Si3 2.114(2); S1-Sn1-S2 94.24(3); S2-Sn1-S3 93.01(3); S1-Sn1-S3 95.38(3); Sn1-S1-Si1 97.55(4); Sn1-S2-Si2 100.69(5); Sn1-S3-Si3 100.32(5).

This is the first structurally characterised example of a $ESiMe_3$ (E = S, Se) moiety attached to tin. Sn-S-E linkages were however isolated in sterically highly congested $[Sn(\mu_2\text{-}S)(SSi(OtBu)_3)_2]_2$[20a] and supersilyl derivatives $\{Sn[ESi(SiMe_3)_3]_2\}_2$ and $\{Me_3P\text{-}Sn[ESi(SiMe_3)_3]_2\}$.[20b] As **2a-Ph₄P** reveals a rather low solubility even in thf and at the same time low thermal stability, we neither could get acceptable NMR spectra nor an acceptable elemental analysis of this particular compound. Therefore we synthesised better soluble $PPN[Sn(SSiMe_3)_3]$ (**2a-PPN**) in order to provide the non-structural analytical and spectroscopic data.

The ^{29}Si NMR spectra in d_8-thf show a singlet at 8.3 ppm which is superimposed by a doublet with a coupling constant of $^2J_{SiSn}$ = 41.8 Hz that arises due to coupling of the I = +1/2 spin isotope ^{29}Si with the I = +1/2 spin nuclei ^{119}Sn and ^{117}Sn. In the ^{119}Sn NMR spectra a singlet at 228.5 ppm is superimposed by a doublet with the corresponding coupling constant $^2J_{SnSi}$ = 41.4 Hz.

Despite tremendous effort we were not able to grow XRD diffractive crystals of the selenium homologue $PPN[Sn(SeSiMe_3)_3]$ (**2b**). In d_8-thf only one signal was detected in multinuclear NMR spectra: ^{119}Sn NMR (297.4 ppm, superimposed singlet and doublet, $^1J_{SeSn}$ = 808.6 Hz), ^{77}Se NMR (–263.0 ppm, singlet) and ^{29}Si NMR (4.3 ppm, superimposed singlet and doublet, $^2J_{SiSn}$ = 44.2 Hz). Therefore, we assume a monomeric form of **2b** to be present in tetrahydrofuran solution.

Thermal decomposition of Cat[M(E-SiMe₃)₃] (M = Zn, Sn; E = S, Se)

To investigate the thermal decomposition behavior of the metallates **1a** – **2b**, TGA measurements of the title compounds were conducted. The residues obtained by these measurements were investigated via PXRD. The TGA measurements of the zincates **1a** and **1b** are shown in Figure 4. For both compounds, decomposition starts below 160 °C. At 500 °C no more mass loss can be detected. We trace back the rather broad temperature range on the decomposition of the title compound into a neutral compound $M(ESiMe_3)_2$ and an ionic compound $Ph_4P[ESiMe_3]$, as shown in Scheme S2 in analogy to the decomposition of the comparable trielate compound $Ph_4P[In(SSiMe_3)_4]$ in a previous study.[6b] The thermal decomposition behaviour of $Ph_4P[ESiMe_3]$ is substance of current investigations within our working group and first results have shown a thermal decomposition with a similar large temperature range in the TGA with a negliable residual mass of approximately 5% for both, E = S and Se as discussed in the supporting information (Figure S9). Comparable organic salts with chalcogenolate based anions and e. g. imidazolium cations are known to also decompose with only minor residues as indicate and discussed in several reports.[34]

The total mass losses were found to be 77% for $Ph_4P[Zn(SSiMe_3)_3]$ (**1a**) and 83% for $Ph_4P[Zn(SeSiMe_3)_3]$ (**1b**), which is comparable to the theoretical mass losses connected to the complete thermolyses of 86% (**1a** to ZnS) and 83% (**1b** to ZnSe), considering the coarse accuracy of the measurement process and the residual mass of the $Ph_4P[ESiMe_3]$ compounds. The residues of the TGA measurements of **1a** and **1b** were identified as ZnS and ZnSe respectively by PXRD (supporting information Figure S7).

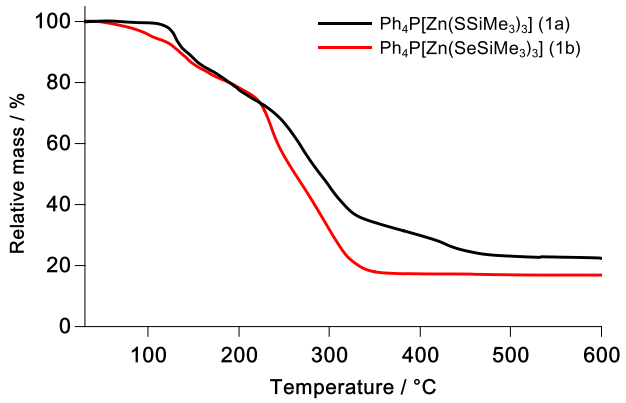

Figure 4. TGA measurements (25°C-600°C, 10 K min^{-1}) of $Ph_4P[Zn(SSiMe_3)_3]$ (**1a**, black) and $Ph_4P[Zn(SeSiMe_3)_3]$ (**1b**, red).

The TGA measurements of the stannanides **2a-PPN** and **2b** are shown in Figure 5. For both compounds the decomposition process starts below 160 °C. At 500 °C no more mass loss can be detected. The mass loss is less rapid compared to the zincates **1a** and **1b** which might be an effect of the PPN^+ cations that are usually found to be of higher thermal stability than corresponding representatives with Ph_4P^+ cations. The total mass losses were found to be 83% for $PPN[Sn(SSiMe_3)_3]$ (**2a-PPN**) and 77% for $PPN[Sn(SeSiMe_3)_3]$ (**1b**), which is close to the theoretical mass losses connected to quantitative thermolyses that are 85% (**2a-PPN** to SnS) and 83% (**2b** to SnSe), considering some minor contamination with residual mass by thermolysis of the cation. Both residues could be identified as SnS and SnSe respectively by PXRD (supporting information Figure S8).

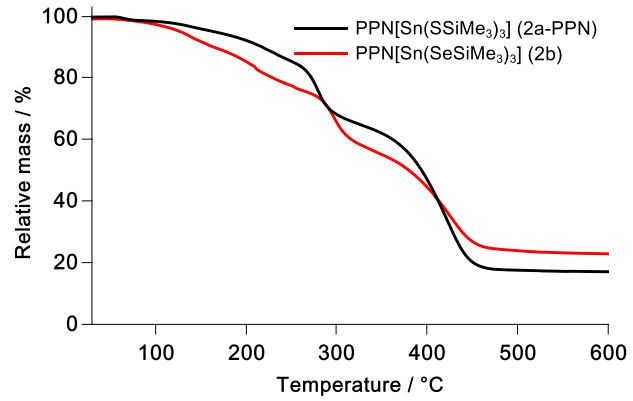

Figure 5. TGA measurements (25°C-600°C, 10 K min^{-1}) of $PPN[Sn(SSiMe_3)_3]$ (**2a-PPN**, black) and $PPN[Sn(SeSiMe_3)_3]$ (**2b**, red).

Theses binary building block precursors were evaluated in the synthesis of photovoltaic quaternary material CZTS in a solution-based low-temperature coprecipitation pathway according to a previously published method, in which the ternary species $CuInS_2$ could be synthesised.[6b] A mixture was prepared using **2a-PPN** priorly treated with one atom equivalent of elemental sulfur to turn Sn(II) into Sn(IV) and **1a-PPN** in acetonitrile. To this mixture two equivalents of $[Cu(tmtu)_3][PF_6]$ dissolved in acetonitrile were added at –20°C. After thermal annealing and washing the emerged black precipitate, the prepared sample was investigated by PXRD and Raman spectroscopy and compared to reported data,[21,22] giving some hints that CZTS syntheses might be possible by this method. Further optimization is necessary to gain well defined phase pure particles (Scheme S1). This experiment is described in the supporting information in the chapter *Attempts to prepare CZTS with the title compounds*.

Syntheses of $[Sn(ESiMe_3)_4]$ (E = S, Se)

As tin in several interesting materials like SnS_2 or Cu_2ZnSnS_4 (CZTS) occurs in oxidation state four, we were interested to develop trimethylsilylchalcogenide precursors containing Sn(IV), ideally the unknown neutral homoleptic stannanes $[Sn(ESiMe_3)_4]$ with E = S (**3**) and Se(**4**). Two examples of homoleptic supersilylchalcogenolates $Sn\{ESi(SiMe_3)_3\}_4$ (E = S, Se) were mentioned in a monograph.[23] However they were not fully characterized by elemental analyses and MS or XRD methods. We reacted $SnCl_4$ in toluene with 4 eq. of $LiSSiMe_3$ and $LiSeSiMe_3$ applying a 18 h temperature gradient starting at -80°C towards +20°C. After filtration at 0°C and evaporation of toluene at room temperature or below, we obtained pentane soluble waxy solids in about 89% and 83% yield assumed to be spectroscopically pure and analytically nearly pure $[Sn(SSiMe_3)_4]$ (**3**) (colourless) and $[Sn(SeSiMe_3)_4]$ (**4**) (pale yellow).

In ^{29}Si NMR spectra of $[Sn(ESiMe_3)_4]$ in C_6D_6 singlets with superimposed doublets at 21.6 ppm with $^2J_{SiSn}$ = 32.8 Hz (E = S, **3**) and at 17.7 ppm with $^2J_{SiSn}$ = 33.8 Hz (E = Se, **4**) are observed. The ^{119}Sn NMR spectrum of $[Sn(SSiMe_3)_4]$ (**3**) shows a singlet with the corresponding superimposed doublet at 50.5 ppm with $^2J_{SnSi}$ = 33.6 Hz. Under standard conditions, this coupling cannot be observed in the ^{119}Sn NMR spectrum of $[Sn(SeSiMe_3)_4]$ (**4**). Instead a singlet at -307.5 ppm with a superimposed doublet ($^1J_{SnSe}$ = 1570.3 Hz) is observed, which is caused by the coupling of the I = +1/2 spin isotope ^{119}Sn with the I = +1/2 spin nucleus ^{77}Se. This assignment is confirmed by a corresponding signal in the ^{77}Se NMR spectrum. Besides the singlet at -114.6 ppm, two superimposing doublets are observed with $^1J_{SeSn}$ coupling constants of 1565.1 Hz and 1496.9 Hz to both abundant ^{119}Sn and ^{117}Sn nuclei. Due to quite low natural abundance of these NMR active heteronuclei, the spin statistically expected quintets are not resolved.

Under inert conditions, compounds **3** and **4** are metastable at temperatures higher than 0°C and start to lose $(Me_3Si)_2E$. This is confirmed by TGA and elemental analysis of $[Sn(SSiMe_3)_4]$ (**3**) showing a slightly too low mass content for S, C and H. Deviations from calculated mass contents of **3** are about one percent. In order to prove that, even on their transport to the CHN analyser combustion chamber, there is a certain loss of $(Me_3Si)_2S$ at ambient temperature we followed that loss of mass by TGA at 25°C in a glovebox. It starts without heating. With a heating rate of 10 K min^{-1} we observe an accelerated decay and two-step process. This behaviour makes it impossible to get a reliable offset temperature without active cooling. At 121 °C a plateau is reached, roughly referring to the formation of SnS_2 (calc. -66%/ obs. -41%). Further heating leads to a second thermal decay step referring to loss of S and formation of SnS

(calc. -6% relative to starting point of measurement, figure 6). This thermal conversion of SnS_2 to SnS, is well documented in literature.[24] We explain the mismatch between calc. and lower observed mass loss in step 1 by the fact, that the measurement was started at room temperature, when already part of **3** had lost $(Me_3Si)_2S$. Furthermore, we believe, that step 2 having only a share of 6% referring to the starting point of measurement (not of pure **3**) is too small because thermal decay of **3** does not follow a purely redox neutral elimination of $(Me_3Si)_2S$ but parallel a reductive elimination of disulfide $(Me_3Si)_2S_2$. In fact, PXRD of the substance recovered from the first plateau is revealing a mix of SnS_2 and SnS. For this reason, the mass loss is not matching with theory, starting from pure SnS_2 (14%, Scheme 2), but is lower (only 10% relative to the plateau).

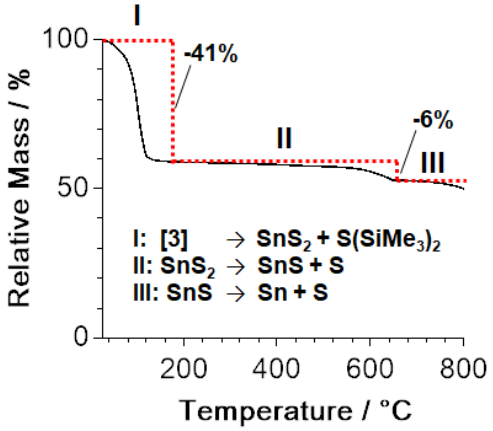

Figure 6. TGA of [Sn(SSiMe3)4] (3) (heating rate 10 K min-1.

Another indication for a parallel occurring reductive elimination mechanism is gained, when $[Sn(SSiMe_3)_4]$ (**3**) is thermally decomposed not at 1 bar with slow heating rate (TGA) but under reduced pressure (0.01 mbar) and a very fast heating to 180°C (dumping a flask in a preheated oil bath). Such annealing of the obtained residue under inert gas at 180°C for three days leads to a black powder identified via PXRD as SnS with only traces of SnS_2 as contamination (supporting information Figure S2). This can be explained by reductive elimination of $(Me_3Si)_2S_2$ from molecular Sn(IV)→Sn(II) intermediates as suggested in Scheme 2.

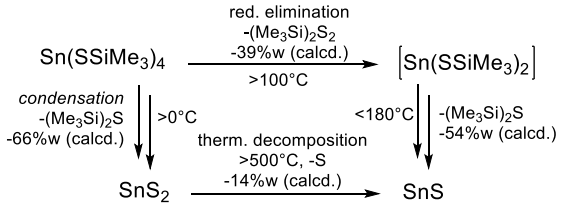

Scheme 2. Parallel thermal decomposition paths discussed: 1. elimination of $(Me_3Si)_2S$ and 2. reductive elimination of $(Me_3Si)_2S_2$ towards Sn(II) species (PXRD in the SI).

Certainly, a more elaborate study with focus on DFT calculations analysing barriers of different decay mechanisms and on TGA-MS experiments under inert gas coupled with extensive PXRD studies will have to follow to fully understand these preliminary experimental results.

$[Sn(SeSiMe_3)_4]$ (**4**) has an even higher thermal, moisture and oxygen sensitivity than sulfur analogue **3**. Therefore, this species was only characterized by elemental analysis and multinuclear NMR so far. Contrastingly, when decomposing $[Sn(SeSiMe_3)_4]$ (**4**) at 200 °C for two days under reduced pressure, only the expected solid $SnSe_2$ could be identified by PXRD (refer to SI for details). Unfortunately, even very soft MS ionisation techniques such as liquid injection field desorption (LIFDI) did not allow to observe the molecular ions of both precursor molecules **3** and **4** or of defined higher molecular tin chalcogenide clusters as intermediates of the condensation process, so far: It is characteristic, that silyl groups are too labile upon ionisation. As a matter of fact, such neutral pentane soluble compounds $[Sn(ESiMe_3)_4]$ are difficult to crystallize even at -80°C. They show a much higher tendency to condense to higher nuclear clusters and, driven by the high lattice energy, finally to SnE_2 than the four isoelectronic anions in salts $Cat[M(ESiMe_3)_4]$ (M = Ga, In).[6b] The thermal decay of **3** and **4** in pentane is observable, as clear colourless solutions become cloudy and ochre coloured with time at ambient temperature under inert gas. Addition of non-dried aprotic or protic solvents such as MeOH leads to quantitative desilylation, formation of Me_3SiOMe, H_2E and rapid precipitation of canary yellow SnS_2 or brownish-black $SnSe_2$ particles from purely organic solvents. This is another perspective of using these highly reactive, highly lipophilic and thermally metastable Sn/S/Se precursors in coating techniques.

Conclusions

Novel trimethylsilylthio- and seleno zincates $[Zn(ESiMe_3)_3]^-$ (E = S, Se) and corresponding stannanides $[Sn(ESiMe_3)_3]^-$ (E = S, S), were isolated and fully characterized as their organic cation salts. Interestingly, thiolato zincate $Ph_4P[Zn(SSiMe_3)_3]$ (**1a**) reveals a trigonal planar configuration in the XRD analysis, selenolato zincate (**1b**) reveals a tetrahedral configuration at zinc forming the dianionic dinuclear complex $[(Me_3SiSe)_2Zn(\mu\text{-}SeSiMe_3)]_2^{2-}$. As expected for a main group element, trimethylsilylthiolato stannanide $Ph_4P[Sn(SSiMe_3)_3]$ (**2a**) is coordinated in a trigonal pyramidal (pseudotetrahedral) fashion. The thermal decomposition of title salts **1a**, **1b** and **2a-PPN** and **2b** has been investigated by TGA measurements. The residues have been identified as corresponding binary chalcogenides ZnS, ZnSe, SnS and SnSe by PXRD. While these metalates are thermally rather stable, neutral tin(IV) derivatives $[Sn(ESiMe_3)_4]$ (E = S (**3**), Se (**4**)) are metastable at room temperature. Nevertheless, they can be synthesised, NMR spectroscopically fully characterised and used as sources to precipitate SnS_2 and $SnSe_2$ from organic solution containing water or MeOH. Thermal decay of **3** and **4** does not allow storing them for extended periods of time as inks at room temperature. Therefore a different solution based approach towards CZTS particles starting from tin(II) derivative $PPN[Sn(SSiMe_3)_3]$ **2a-PPN**, its oxidation by elemental sulfur, subsequent additions of 1 eq. zincate $PPN[Zn(SSiMe_3)_3]$ and 2 eq. of copper source

$[Cu(tmtu)_3][PF_6]$ in MeCN was performed. Though further optimization is needed to get phase pure microcrystalline quaternary chalcogenide material CZTS, this work is a very basic study on an optional sol-gel-type condensation approach towards such multinary materials. There are plenty of options by modifying the organic cations and used solvents without changing the novel anionic Zn / Sn / S / Se sources described here.

Experimental section

Materials and methods

All preparative operations were conducted by using standard Schlenk techniques and freshly dried solvents. Solvents were dried according to common procedures[26] and passed through columns of aluminium oxide, R3-11G-catalyst (BASF) or molecular sieves (3 Å or 4 Å). Elemental analyses (C, H, N, S) were carried out by the service department for routine analysis from the department of chemistry at the university of Marburg with a vario MICRO cube (Elementar). Samples for elemental analysis were weighted into tin capsules inside a nitrogen filled glovebox. ^{1}H and proton decoupled ^{13}C NMR spectra were recorded in automation with a Bruker Avance II 300 spectrometer, ^{29}Si NMR spectra were recorded by the service department for NMR analyses with a Bruker Avance II HD 300, DRX 400 or Avance III 500 spectrometer. All spectra were recorded at ambient temperature. ^{1}H and ^{13}C NMR spectra were calibrated using residual proton signals of the solvent (thf[d_8]: δ_H 3.58 & 1.72 ppm, δ_C 67.21 & 25.31 ppm, C_6D_6: δ_H 7.16 ppm, δ_C 128.06 ppm). ^{29}Si NMR spectra were referenced externally ($SiMe_4$: δSi 0.00 ppm). For NMR solvents other than thf[d_8], such as DMSO[d_6], MeCN[d_3], $CDCl_3$, and CD_2Cl_2, decomposition of the title anions was observed. C_6D_6 is not polar enough to dissolve the ionic compounds, while thf[d_8] only slightly dissolves the ionic target compounds. Silicon grease impurities that in some samples are indicated in the NMR spectra are not attributed to impure substances, as proven by elemental analysis, but rather to the low solubility of the compounds in thf[d_8].

TGA measurements starting at 25°C were conducted with a DSC-TGA 3 (Mettler Toledo) in a glovebox. Decomposition temperatures were determined using data of the DSC-TGA.

All solvents were dried according to common procedures and passed through columns of aluminium oxide, 3 Å molecular sieves and R3-11G catalyst (BASF) or stored over molecular sieves (3 Å or 4 Å). The reagents were used as received unless stated otherwise. $[Cu(tmtu)_3][PF_6]$,[27] $E(SiMe_3)_2$,[28] $LiESiMe_3$[29](E = S, Se; tmtu = *N,N,N′,N′*-tetramethylthiourea) were prepared according to literature known procedures or slightly modified.

The data collection for the single-crystal structure determination was performed on a Stoe Stadivari diffractometer or a Bruker D8 Quest diffractometer by the X-ray service department of the department of chemistry at the university of Marburg. Information concerning the used hardware, and software used for data collection, cell refinement and data reduction as well as structure solution and refinement can be reviewed in the attached CIF. After the solution (Shelxt)[30] and refinement process (Shelxl 2017/1)[31] the data was validated by using Platon.[32] All graphic representations were created with Diamond 4.[33]

PXRD measurements were conducted by giving a small amount of the sample between two layers of Scotch tape. The diffractograms were recorded on a Stoe Stadi MP using Cu or Mo-$K_{\alpha1}$ radiation that passed a bent focusing monochromator and a high sensitivity Mythen-detector. The transmission diffractograms were recorded from 2theta = 5° - 105° (5° min^{-1}). Raman Spectra were recorded using an InVia Raman microscope from Renishaw utilized with a frequency doubled Nd-YAG laser with a wavelength of 532 nm.

Preparation of $Ph_4P[Zn(SSiMe_3)_3]$ (1a). A mixture of $ZnCl_2$ (38 mg, 0.28 mmol, 1.0 equiv.) and $Ph_4P[Cl]$ (104 mg, 0.28 mmol, 1.0 equiv.) in thf (10 mL) is stirred for 18 h at room temperature. To a solution of $S(SiMe_3)_2$ (153 mg, 0.86 mmol, 3.1 equiv.) in thf (5 mL) a 2.9M solution of *n*-BuLi in hexane (0.29 mL, 0.83 mmol, 3.0 equiv.) is added dropwise at 0 °C in a separate reactor. After 30 min at 0 °C and further 30 min at ambient temperature, all volatiles were removed under fine vacuum with the help of diethyl ether (2 mL) and pentane (2 mL). The obtained colourless powder is dissolved in thf (10 mL) and added dropwise to the suspension of $Ph_4P[ZnCl_3]$ in thf (10 mL) at –78 °C. The reaction mixture is stirred for 18 h within the cooling bath and allowed to slowly warm up to ambient temperature at the end of this period. All volatiles are removed in fine vacuum and the residue is extracted with Et_2O (60 mL). After filtration all volatiles were removed from the obtained filtrate in fine vacuum. The residue was washed with pentane and dried in fine vacuum. **1a** is obtained as a colourless solid (119 mg, 0.17 mmol, 60%). X-ray suitable single crystals were grown by layering a saturated solution of **1a** in Et_2O under the same volume of pentane at 0 °C. ^{1}H NMR (300.3 MHz, thf[d_8]): δ = 7.95-7.81 (m, 20 H, *Ph*$_4$P$^+$), 0.19 (s, 27 H, [Zn(SSi*Me*$_3$)$_3$]$^-$) ppm. ^{13}C{^{1}H} NMR (75.5 MHz, thf[d_8]): δ = 136.2 (d, $^4J_{CP}$ = 3.0 Hz, (HC(CH)$_2$(CH)$_2$*C*)$_4$P$^+$), 135.6 (d, $^3J_{CP}$ = 10.4 Hz, (HC(*C*H)$_2$(CH)$_2$C)$_4$P$^+$), 131.3 (d, $^2J_{CP}$ = 13.0 Hz, (HC(CH)$_2$(*C*H)$_2$C)$_4$P$^+$), 118.9 (d, $^1J_{CP}$ = 89.5 Hz, (HC(CH)$_2$(CH)$_2$*C*)$_4$P$^+$), 6.5 (s, [Zn(SSi*Me*$_3$)$_3$]$^-$) ppm. ^{29}Si NMR (59.7 MHz, thf[d_8]): δ = 8.3 (s, [Zn(S*Si*Me$_3$)$_3$]$^-$) ppm. Elemental analysis exp. (calc.): C 55.1 (55.0), H 6.9 (6.6).

Preparation of $Ph_4P[Zn(SeSiMe_3)_3]$ (1b). A mixture of $ZnCl_2$ (32 mg, 0.23 mmol, 1.0 equiv.) and $Ph_4P[Cl]$ (87 mg, 0.23 mmol, 1.0 equiv.) in thf (10 mL) is stirred for 18 h at room temperature. To a solution of $Se(SiMe_3)_2$ (162 mg, 0.72 mmol, 3.1 equiv.) in thf (5 mL) a 2.9M solution of *n*-BuLi in hexane (0.24 mL, 0.70 mmol, 3.0 equiv.) is added dropwise at 0 °C in a separate reactor. The reaction mixture is stirred for 30 min at 0 °C and further 30 min at ambient temperature. All volatiles were removed under fine vacuum. The residue was washed with pentane and dried in fine vacuum. The obtained colourless

powder is dissolved in thf (10 mL) and added dropwise to the suspension of $Ph_4P[ZnCl_3]$ in thf (10 mL) at –78 °C. The reaction mixture is stirred for 18 h and allowed to slowly warm up to ambient temperature at the end of this period. All volatiles are removed in fine vacuum and the residue is extracted with Et_2O (60 mL). After filtration all volatiles were removed from the obtained filtrate in fine vacuum. The residue was washed with pentane and dried in fine vacuum. **1b · 0.5 Et₂O** is obtained as a colourless solid (118 mg, 0.13 mmol, 52%). X-ray suitable single crystals were grown by layering a saturated solution of **1b · 0.5 Et₂O** in Et_2O under the same volume of pentane and storing the mixture at 0 °C for a few days. ^{1}H NMR (300.3 MHz, thf[d_8]): δ = 7.95-7.82 (m, 20 H, *Ph*$_4$P$^+$), 3.39 (q, $^3J_{HH}$ = 7.0 Hz, 1H, 0.5 O(C*H*$_2$CH$_3$)$_2$), 1.12 (t, $^3J_{HH}$ = 7.0 Hz, 1.5 H, 0.5 O(CH$_2$C*H*$_3$)$_2$), 0.33 (s, 27 H, [Zn(SSi*Me*$_3$)$_3$]$^-$) ppm. ^{13}C{^{1}H} NMR (75.5 MHz, thf[d_8]): δ = 136.2 (d, $^4J_{CP}$ = 3.1 Hz, (H*C*(CH)$_2$(CH)$_2$C)$_4$P$^+$), 135.6 (d, $^3J_{CP}$ = 10.4 Hz, (HC(*C*H)$_2$(CH)$_2$C)$_4$P$^+$), 131.3 (d, $^2J_{CP}$ = 12.9 Hz, (HC(CH)$_2$(*C*H)$_2$C)$_4$P$^+$), 118.9 (d, $^1J_{CP}$ = 89.5 Hz, (HC(CH)$_2$(CH)$_2$*C*)$_4$P$^+$), 7.0 (s, [Zn(SeSi*Me*$_3$)$_3$]$^-$) ppm. ^{29}Si-NMR (59.7 MHz, thf[d_8]): δ = 4.3 (s, [Zn(Se*Si*Me$_3$)$_3$]$^-$) ppm. Elemental analysis exp. (calc. $C_{35}H_{52}O_{0.5}PSe_3Si_3Zn$): C 46.9 (46.8), H 5.9 (5.8).

Preparation of Ph₄P [Sn(SSiMe₃)₃] (2a-Ph₄P). A mixture of $SnCl_2$ (49 mg, 0.26 mmol, 1.0 equiv.) and $Ph_4P[Cl]$ (97 mg, 0.26 mmol, 1.0 equiv.) in thf (10 mL) is stirred for 18 h at room temperature. To a solution of S(SiMe$_3$)$_2$ (141 mg, 0.79 mmol, 3.1 equiv.) in thf (5 mL) a 2.9M solution of *n*-BuLi in hexane (0.28 mL, 0.78 mmol, 3.0 equiv.) is added dropwise at 0 °C in a separate reactor. The reaction mixture is stirred for 30 min at 0 °C and further 30 min at ambient temperature. All volatiles were removed under fine vacuum. The residue was washed with pentane and dried in fine vacuum. The obtained colourless powder is directly dissolved in thf (10 mL) and slowly added to the solution of $Ph_4P[SnCl_3]$ in thf (10 mL) at –78 °C. The reaction mixture is stirred for 18 h within the cooling bath and allowed to slowly warm up to ambient temperature at the end of this period. All volatiles are removed in fine vacuum and the residue is extracted with Et_2O (60 mL). Half of the filtrate was kept at 0 °C, layered with the same volume of pentane and this mixture was stored at –30 °C for several days to yield X-ray diffractive single crystals of **2a-Ph₄P** (ca. 30 mg). The crystalline product is too insoluble for multinuclar NMR measurements and thermally too unstable at elevated temperature in solvents, that do not decompose it. In some attempts to force it into solution, spontaneous precipitation of yellow material was observed. Therefore, no satisfying elemental analyses could be obtained.

Preparation of PPN[Sn(SSiMe₃)₃] (2a-PPN). A mixture of $SnCl_2$ (97 mg, 0.51 mmol, 1.0 equiv.) and PPN[Cl] (295 mg, 0.51 mmol, 1.0 equiv.) in thf (10 mL) is stirred for 18 h at room temperature. To a solution of S(SiMe$_3$)$_2$ (284 mg, 1.59 mmol, 3.1 equiv.) in thf (5 mL) a 2.9M solution of *n*-BuLi in hexane (0.53 mL, 1.54 mmol, 3.0 equiv.) is added dropwise at 0 °C in a separate reactor. The reaction mixture is stirred for 30 min at 0 °C and further 30 min at ambient temperature. All volatiles were removed under fine vacuum with the help of diethyl ether and pentane. The obtained colourless powder is directly dissolved in thf (10 mL) and slowly added to the solution of PPN $[SnCl_3]$ in thf (10 mL) at –78 °C. The reaction mixture is stirred for 18 h within the cooling bath and allowed to slowly warm up to ambient temperature at the end of this period. All volatiles are removed in fine vacuum and the residue is extracted with Et_2O (60 mL). After filtration all volatiles were removed from the obtained filtrate in fine vacuum. The residue was washed with pentane and dried in fine vacuum. **2a-PPN** is obtained as a colourless solid (320 mg, 0.32 mmol, 64%). ^{1}H-NMR (300.3 MHz, thf[d_8]): δ = 7.73-7.60 (m, 30 H, PPN$^+$), 0.24 (s, 27 H, [Sn(SSi*Me*$_3$)$_3$]$^-$) ppm. ^{13}C{^{1}H} NMR (75.5 MHz, thf[d_8]): δ = 134.5 (s, ((H*C*(CH)$_2$(CH)$_2$C)$_3$P)$_2$N$^+$), 133.1 (m, ((HC(*C*H)$_2$(CH)$_2$C)$_3$P)$_2$N$^+$), 130.1 (m, ((HC(CH)$_2$(*C*H)$_2$C)$_3$P)$_2$N$^+$), 128.0 (dd, $^1J_{CP}$ = 107.2 Hz, $^2J_{CN}$ = 1.9 Hz, ((HC(CH)$_2$(CH)$_2$*C*)$_3$P)$_2$N$^+$), 6.1 (s, [Sn(SSi*Me*$_3$)$_3$]$^-$) ppm. ^{29}Si NMR (59.7 MHz, thf[d_8]): δ = 8.3 (s with superimposed d, $^2J_{SiSn}$ = 41.8 Hz, [Sn(S*Si*Me$_3$)$_3$]$^-$) ppm. ^{119}Sn NMR (112.0 MHz, thf[d_8]): δ = 228.5 (s with superimposed d, $^2J_{SnSi}$ = 41.4 Hz, [*Sn*(SSiMe$_3$)$_3$]$^-$) ppm. Elemental analysis exp. (calc. $C_{45}H_{57}NP_2S_3Si_3Sn$): C 55.1 (55.6), H 5.6 (5.9), N 1.5 (1.4).

Preparation of PPN [Sn(SeSiMe₃)₃] (2b). A mixture of $SnCl_2$ (85 mg, 0.45 mmol, 1.0 equiv.) and PPN[Cl] (258 mg, 0.45 mmol, 1.0 equiv.) in thf (10 mL) is stirred for 18 h at room temperature. To a solution of Se(SiMe$_3$)$_2$ (314 mg, 1.39 mmol, 3.1 equiv.) in thf (5 mL) a 2.9M solution of *n*-BuLi in hexane (0.46 mL, 1.35 mmol, 3.0 equiv.) is added dropwise at 0 °C in a separate reactor. The reaction mixture is stirred for 30 min at 0 °C and further 30 min at ambient temperature. All volatiles were removed under fine. The obtained colourless powder is directly dissolved in thf (10 mL) and added slowly to the solution of PPN$[SnCl_3]$ in thf (10 mL) at –78 °C. The reaction mixture is stirred for 18 h within the cooling bath and allowed to slowly warm up to ambient temperature at the end of this period. All volatiles are removed in fine vacuum and the residue is extracted with Et_2O (60 mL). After filtration all volatiles were removed from the obtained filtrate in fine vacuum. The residue was washed with pentane and dried in fine vacuum. **2b-PPN** is obtained as a yellow-reddish oil (406 mg, 0.36 mmol, 81%). ^{1}H-NMR (300.3 MHz, thf[d_8]): δ = 7.72-7.55 (m, 30 H, PPN$^+$), 0.34 (s, 27 H, [Sn(SSi*Me*$_3$)$_3$]$^-$) ppm. ^{13}C{^{1}H} NMR (75.5 MHz, thf[d_8]): δ = 134.5 (s, ((H*C*(CH)$_2$(CH)$_2$C)$_3$P)$_2$N$^+$), 133.1 (m, ((HC(*C*H)$_2$(CH)$_2$C)$_3$P)$_2$N$^+$), 130.1 (m, ((HC(CH)$_2$(*C*H)$_2$C)$_3$P)$_2$N$^+$), 128.0 (dd, $^1J_{CP}$ = 108.6 Hz, $^2J_{CN}$ = 2.0 Hz, ((HC(CH)$_2$(CH)$_2$*C*)$_3$P)$_2$N$^+$), 6.0 (s, [Sn(SeSi*Me*$_3$)$_3$]$^-$) ppm. ^{29}Si-NMR (59.7 MHz, thf[d_8]): δ = 4.3 (s with superimposed d, $^2J_{SiSn}$ = 44.2 Hz, [Sn(Se*Si*Me$_3$)$_3$]$^-$) ppm. ^{77}Se-NMR (57.3 MHz, thf[d_8]): δ = –263.0 (s, [Sn(*Se*SiMe$_3$)$_3$]$^-$) ppm. ^{119}Sn-NMR (112.0 MHz, thf[d_8]): δ = 297.4 (s with superimposed d, $^1J_{SnSe}$ = 808.6 Hz, [*Sn*(SeSiMe$_3$)$_3$]$^-$) ppm. Elemental analysis exp. (calc. $C_{45}H_{57}NP_2Se_3Si_3Sn$): C 49.2 (48.5), H 5.5 (5.2), N 1.9 (1.3). According to proton NMR results, the slightly too high C and H content arises from the presence of silicon grease traces, which could not be fully extracted, as **2b-PPN** is an oil.

Preparation of [Sn(SSiMe₃)₄] (3). A 2.43M solution of *n*-BuLi in hexane (0.61mL, 1.48 mmol, 4.0 equiv.) is given dropwise into a

solution of $S(SiMe_3)_2$ (271 mg, 1.52 mmol, 4.1 equiv.) in thf (5 mL) at 0°C. The solution is stirred for 30 min at 0°C and another 30 min at ambient temperature. All volatiles were removed at 40°C / 10^{-3}mbar. After digesting the residue in diethyl ether / pentane and removing all volatiles, the obtained colourless powder is directly dissolved in toluene (10 mL) and added dropwise to a solution of $SnCl_4$ (97 mg, 0.37 mmol, 1.0 equiv.) in toluene (10 mL) at -78 °C. The reaction mixture is stirred within the cooling bath for 18 h, thereby allowed to slowly reach ambient temperature. The suspension is filtered and all volatiles are removed from the filtrate at 15°C / 10^{-4} mbar. **3** is obtained as colourless waxy solid (178 mg, 0.33 mmol, 89%) of remarkable sensitivity towards oxygen, moisture and slightly elevated temperatures. ^{1}H-NMR (300.3 MHz, C_6D_6): δ = 0.55 (s, 36 H, Sn(SSi*Me*$_3$)$_4$) ppm. ^{13}C{^{1}H} NMR (75.5 MHz, C_6D_6): δ = 4.8 (t, $^1J_{CSi}$ = 8.3 Hz, Sn(SSi*Me*$_3$)$_4$) ppm. ^{29}Si-NMR (59.7 MHz, C_6D_6): δ = 21.6 (s with superimposed d, $^2J_{SiSn}$ = 32.8 Hz, Sn(S*Si*Me$_3$)$_4$) ppm. ^{119}Sn-NMR (112.0 MHz, C_6D_6): δ = 50.5 (s with superimposed d, $^2J_{SnSi}$ = 33.6 Hz, *Sn*(SSiMe$_3$)$_4$) ppm. Elemental analysis exp. (calc. $C_{12}H_{36}S_4Si_4Sn$): C 25.7 (26.7), H 6.2 (6.7), S 21.4 (23.8). Low values of C, H and S are due to beginning partial loss of $(Me_3Si)_2S$ even at room temperature.

Preparation of [Sn(SeSiMe$_3$)$_4$] (4). A 2.43M solution of *n*-BuLi in hexane (0.45mL, 1.10 mmol, 4.0 equiv.) is given dropwise into a solution of $Se(SiMe_3)_2$ (254 mg, 1.12 mmol, 4.1 equiv.) in thf (5 mL) at 0°C. The solution is stirred for 30 min at 0°C and another 30 min at ambient temperature. All volatiles were removed at 40°C / 10^{-3}mbar. After digesting the residue in diethyl ether / pentane and removing all volatiles, the obtained colourless powder is directly dissolved in toluene (10 mL) and added dropwise to a solution of $SnCl_4$ (72 mg, 0.27 mmol, 1.0 equiv.) in toluene (10 mL) at –78 °C. The reaction mixture is stirred within the cooling bath for 18 h, thereby allowed to slowly reach ambient temperature. The suspension is filtered and all volatiles were removed from the filtrate at 15°C / 10^{-4} mbar. **4** is obtained as pale yellowish waxy solid (166mg, 0.23 mmol, 83%) of remarkable sensitivity towards oxygen, moisture and slightly elevated temperatures. ^{1}H-NMR (500.2 MHz, C_6D_6): δ = 0.63 (s, 36 H, Sn(SeSi*Me*$_3$)$_4$) ppm. ^{13}C{^{1}H} NMR (125.8 MHz, C_6D_6): δ = 5.0 (s with superimposed d, $^1J_{CSi}$ = 14.0 Hz, Sn(SeSi*Me*$_3$)$_4$) ppm. ^{29}Si-NMR (99.3 MHz, C_6D_6): δ = 17.7 (s with superimposed d, $^2J_{SiSn}$ = 33.8 Hz, Sn(Se*Si*Me$_3$)$_4$) ppm. ^{77}Se-NMR (95.4 MHz, C_6D_6): δ = –114.6 (s with two superimposed d, $^1J_{SeSn}$ = 1496.9 Hz & 1565.1 Hz, Sn(*Se*SiMe$_3$)$_4$) ppm. ^{119}Sn-NMR (186.5 MHz, C_6D_6): δ = 50.5 (s with superimposed d, $^1J_{SnSi}$ = 1570.3 Hz, *Sn*(SeSiMe$_3$)$_4$) ppm. Due to its even more metastable and waxy nature compared to **3**, no satisfying elemental analysis could be obtained.

Conflicts of interest

There are no conflicts to declare.

Acknowledgements

Financial support of the German Research Foundation DFG and its priority program SPP 1708: “Material Synthesis near Room Temperature” is gratefully acknowledged. We thank Melanie Förster for recording the Raman spectra and the service facilities of the chemistry department of the Philipps Universität Marburg for NMR spectroscopy, elemental analysis and XRD for measurements and fruitful discussion.

Notes and references

1 M. W. DeGroot and J. F. Corrigan, *Z. anorg. allg. Chem.*, 2006, **632**, 19–29.
2 a) M. W. DeGroot and J. F. Corrigan, *Angew. Chem. Int. Ed.*, 2004, **43**, 5355–5357; b) M. W. DeGroot, N. J. Taylor and J. F. Corrigan, *J. Am. Chem. Soc.*, 2003, **125**, 864–865.
3 C. B. Khadka, A. Eichhöfer, F. Weigend and J. F. Corrigan, *Inorg. Chem.*, 2012, **51**, 2747–2756.
4 M. W. DeGroot, C. Khadka, H. Rösner and J. F. Corrigan, *J. Clust. Sci.*, 2006, **17**, 97–110.
5 A. M. Polgar, F. Weigend, A. Zhang, M. J. Stillman and J. F. Corrigan, *J. Am. Chem. Soc.*, 2017, **139**, 14045–14048.
6 a) C. B. Khadka, D. G. Macdonald, Y. Lan, A. K. Powell, D. Fenske and J. F. Corrigan, *Inorg. Chem.*, 2010, **49**, 7289–7297. b) J. Guschlbauer, T. Vollgraff and J. Sundermeyer, *Inorg. Chem.*, 2019, **58**, 15385-15392.
7 X. Liu, Y. Feng, H. Cui, F. Liu, X. Hao, G. Conibeer, D. B. Mitzi and M. Green, *Prog. Photovolt.: Res. Appl.*, 2016, **24**, 879–898.
8 X. Cui, K. Sun, J. Huang, J. S. Yun, C.-Y. Lee, C. Yan, H. Sun, Y. Zhang, C. Xue, K. Eder, L. Yang, J. M. Cairney, J. Seidel, N. J. Ekins-Daukes, M. Green, B. Hoex and X. Hao, *Energy Environ. Sci.,* 2019, DOI: 0.1039/c9ee01726g.
9 W. Wang, M. T. Winkler, O. Gunawan, T. Gokmen, T. K. Todorov, Y. Zhu and D. B. Mitzi, *Adv. Energy Mater.*, 2014, **4**, 1301465.
10 W. Sun, X. Geng, J. C. Armstrong, J. Cui and T.-p. Chen, in *2014 IEEE 40th Photovoltaic Specialist Conference (PVSC)*, IEEE, 2014, 421–424.
11 M. Kumar, A. Dubey, N. Adhikari, S. Venkatesan and Q. Qiao, *Energy Environ. Sci.*, 2015, **8**, 3134–3159.
12 D. Fuhrmann, S. Dietrich and H. Krautscheid, *Chem. Eur. J.*, 2017, **23**, 3338–3346.
13 D. Fuhrmann, S. Dietrich and H. Krautscheid, *Inorg. Chem.*, 2017, **56**, 13123–13131.
14 I. E. Medina-Ramírez, M. J. Fink and J. P. Donahue, *Acta Cryst. C*, 2009, **65**, m475-m477.
15 F. Meyer-Wegner, M. Bolte and H.-W. Lerner, *Inorg. Chem. Commun.*, 2013, **29**, 134–137.
16 M. Kotsch, C. Gienger, C. Schrenk and A. Schnepf, *Z. anorg. allg. Chem.*, 2016, **642**, 670–675.
17 M. W. DeGroot and J. F. Corrigan, *Organometallics*, 2005, **24**, 3378–3385.
18 a) I. L. Abrahams, C. D. Garner and W. Clegg, *J. Chem. Soc., Dalton Trans.*, 1987, **6**, 1577-1579; b) W. P. Chung, J. C. Dewan and M. A. Walters, *Inorg. Chem.*, 1991, **30**, 4280–4282; c) M. Gelinsky and H. Vahrenkamp, *Z. anorg. allg. Chem.*, 2002, **628**, 1017-1021; d) Y. Matsunaga, K. Fujisawa, N. Ibi, N. Amir, Y. Miyashita and K.-I. Okamoto, *BCSJ*, 2005, **78**, 1285–1287; e) A. D. Watson, C. P. Rao, J. R. Dorfman and R. H. Holm, *Inorg. Chem.*, 1985, **24**, 2820–2826.
19 X.-Y. Tang, R.-X. Yuan, J.-X. Chen, W. Zhao, A.-X. Zheng, M. Yu, H.-X. Li, Z.-G. Ren and J.-P. Lang, *Dalton Trans.*, 2012, **41**, 6162–6172.

20 a) M. Kloskowska, A. Konitz, W. Wojnowski and B. Becker, *Z. anorg. allg. Chem.*, 2006, **632**, 2424–2428. b) A. L. Seligson and J. Arnold, *J. Am. Chem. Soc.*, 1993, **115**, 8214-8220.
21 X. Yu, A. Ren, F. Wang, C. Wang, J. Zhang, W. Wang, L. Wu, W. Li, G. Zeng and L. Feng, *Int. J. Photoenergy*, 2014, Article ID 861249, 1–6.
22 S. Kumar, V. Kumar, V. Mikli, T. Varema, M. Altosaar and M. Grossberg, *Energy Procedia*, 2016, **102**, 136–143.
23 H. Lange, U. Herzog and G. Roewer, *Organosilicon Chemistry V*, 2003, Wiley-VCH GmbH & Co. KGaA, Weinheim, 288-293.
24 T. Shimada, F. S. Ohuchi, B. A. Parkinson, *J. Vac. Sci. Technol. A*, 1992, ***10***, 539–542.
25 M. Himmrich, H. Haeuseler, *Spectrochim. Act*., 1991, **47A**, 933-942.
26 W. L. F. Armarego and D. D. Perrin, *Purification of laboratory chemicals*, 4th ed., paperback ed.; Butterworth-Heinemann: Oxford, 1997.
27 Weininger, M. S.; Hunt, G. W. and Amma, E. L. *J. Chem. Soc., Chem. Commun.* 1972, **20**, 1140-1141.
28 T. J. Curphey, *Phosphorus Sulfur* 2001, ***173***, 123–142.
29 D. Taher, A. I. Wallbank, E. A. Turner, H. L. Cuthbert and J. F. Corrigan, *Eur. J. Inorg. Chem.* 2006, **22**, 4616–4620.
30 G. M. Sheldrick, *Acta Cryst. A* 2015, **71**, 3–8.
31 G. M. Sheldrick, *Acta Cryst. C,* 2015, ***71***, 3–8.
32 A. L. Spek, *Acta Cryst. D,* 2009, **65**, 148–155.
33 K. Brandenburg, H. P. *Diamond*; Crystal Impact GbR: Bonn, 2012.
34 a) L. H. Finger, F. Wohde, E. I. Grigoryev, A.-K. Hansmann, R. Berger, B. Roling and J. Sundermeyer, *Chem. Commun.*, 2015, **51**, 16169-16172. b) L. H. Finger and J. Sundermeyer, Chem. Eur. J., 2016, **22**, 4218-4230. c) J. Guschlbauer, T. Vollgraff and J. Sundermeyer, *Dalton Trans.*, 2019, **48**, 10971-10978.

Supporting Information

Homoleptic Trimethylsilylchalcogenolato Zincates $[Zn(ESiMe_3)_3]^-$ and Stannanides $[Sn(ESiMe_3)_3]^-$ (E = S, Se): Precursors for Chalcogenide Based Materials Containing Sn and Zn

Jannick Guschlbauer, Tobias Vollgraff, Jörg Sundermeyer*

Fachbereich Chemie and Materials Science Center, Philipps-Universität, Hans-Meerwein-Str. 4, 35032 Marburg, Germany. *E-mail:JSU@staff.uni-marburg.de.

Content

1 Experimental Section

1.1 Experiments with Sn(IV)

In our initial effort to prepare precursors for tin dichalcogenide semiconductors SnS_2 and $SnSe_2$ we prepared tetravalent $Sn(ESiMe_3)_4$ (E = S (**3**), Se(**4**)) by reacting $SnCl_4$ with four equivalents of $LiESiMe_3$. Though we could record NMR spectra that fit the assumed monomeric structures we were not able to get satisfying information the structure of the molecules mass spectrometry or XRD. Despite this circumstance we investigated the thermal decomposition of $Sn(SSiMe_3)_4$ by decomposing the compound at 180°C and annealing the beige solid for 3 days at this temperature. The black residue was identified as SnS in the Herzenbergite structure with minor impurities of SnS_2 in the berndtite structure via PXRD. The detailed experimental procedures are described in the following.

One possible explaination is the oxidation of two -$SSiMe_3$ ligands by the Sn(IV) atom to form Me_3SiS-$SSiMe_3$ and $Sn(SSiMe_3)_2$, and a subsequent elimination of $S(SiMe_3)_2$ to yield SnS. However, the TGA measurement of the assumed $Sn(SSiMe_3)_4$ does not indicate a direct transformation to SnS but rather SnS_2.

1.1.1 Decomposition and material preparation with $[Sn(ESiMe_3)_4]$ (E = S (**3**), Se (**4**))

The TGA of $[Sn(SSiMe_3)_4]$ (**3**) shows, that the investigated compound is not stable at ambient temperature, as a mass loss can be observed directly at the beginning of the measurement (**Figure S1**). When the first thermal process is finished at ca. 120 °C a plateau indicates a stable decomposition product that decomposes at ca. 550 °C, and a further decomposition at ca. 740 °C. As the Assumed that the first step is the intramolecular desilylation that yields SnS_2 (eq. S**1**). The TGA pattern from the end of the first decomposition step equals the TGA of SnS_2, as reported in the literature.[1] The decomposition at ca. 550 °C is attributed to the transformation from SnS_2 to SnS and elemental sulfur (eq. S**2**), while the decomposition from 740 °C on can be assigned to the thermolysis of SnS to the elements Sn and S (eq. S**3**).

$$Sn(SSiMe_3)_4 \rightarrow SnS_2 + 2\ S(SiMe_3)_2 \qquad (S\mathbf{1})$$

$$SnS_2 \rightarrow SnS + S \qquad (S\mathbf{2})$$

$$SnS \rightarrow Sn + S \qquad (S\mathbf{3})$$

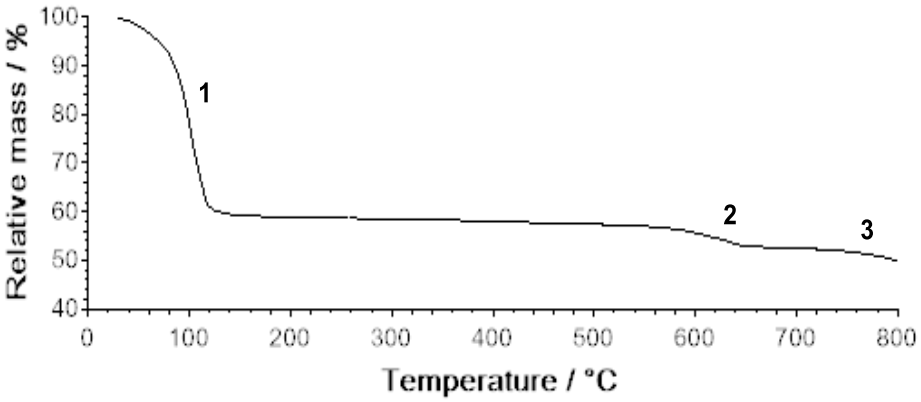

Figure S1: TGA of the assumed $Sn(SSiMe_3)_4$ (**3**) (heating rate of 10 K min^{-1}). The first decomposition (**1**) takes place at ambient temperature before the measurement starts. The second (**2**) and third (**3**) decomposition step is identical with the one, reported for SnS_2.[1]

To investigate the first decomposition product a defined decomposition of the assumed [$Sn(SSiMe_3)_4$] (**3**) was conducted by heating 100 mg of this compound at 180 °C under reduced pressure for approximately five minutes until no more volatiles are produced. The beige residue was annealed at 180 °C for 3 days and subsequently investigated via PXRD (**Figure S2**). The prepared material was identified as SnS in the Herzenbergite structure (JCPDS: 39-0354) with minor impurities of SnS_2 in the Berndtite structure (JCPDS: 21-1231).

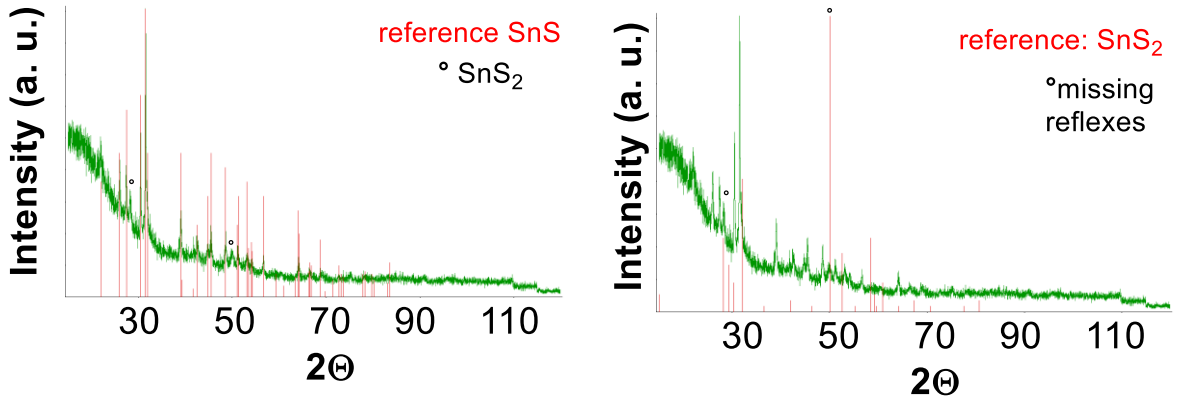

Figure S2: PXRD of the thermolysis product of the assumed $Sn(SSiMe_3)_4$. Top: the most reflexes are attributed to SnS in the herzenbergite structure (JCPDS: 39-0354). Bottom: reflexess that do not fit to the herzenbergite structure can be attributed to minor impurities of SnS_2 in the berndtite structure (JCPDS: 21-1231).

A possible explanation of the reduction of the tin centre is the reductive elimination of the silylated disulfide compound $Me_3SiS\text{-}SSiMe_3$.

To investigate the thermal decomposition product of the assumed selenium homologue [$Sn(SeSiMe_3)_4$] (**4**) a defined thermolysis was conducted by heating a sample of 100 mg at 180 °C under reduced pressure for approximately five minutes until no more volatiles are produced. The black residue was annealed at 200 °C for 2 days and subsequently investigated via PXRD (**Figure S3**). The prepared material was identified as $SnSe_2$ (JCPDS: 89-3197) without any crystallographically active phase impurities. Compared to the decomposition of $Sn(SSiMe_3)_4$, another decomposition mechanism without subsequent reduction has to take place obviously.

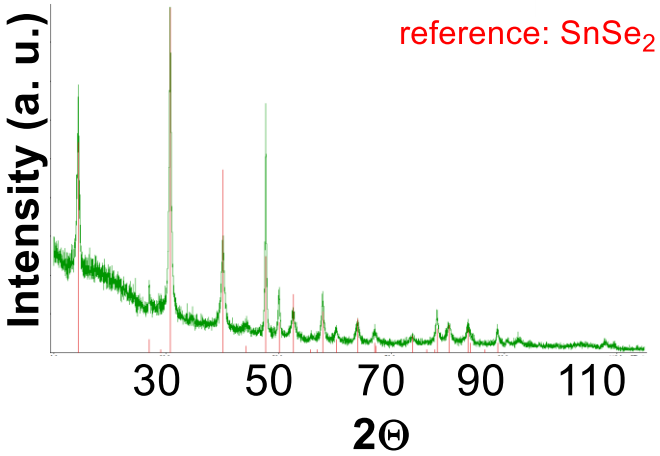

Figure S3: PXRD of the thermolysis product of the assumed $Sn(SeSiMe_3)_4$. After annealing at 200 °C for 2 days. The residue is identified as $SnSe_2$ (JCPDS: 89-3197).

2 NMR Spectra

*2.1 NMR Spectra of $Ph_4P[Zn(SSiMe_3)_3]$ (**1a**)*

Due to the poor solubility of 1a in THF the silicon grease contamination seems to be more severe than it is as proven by elemental analysis (attributed signals: δ_H = 0.11 ppm, δ_C = 1.1 ppm, δ_{Si} = –22 ppm).

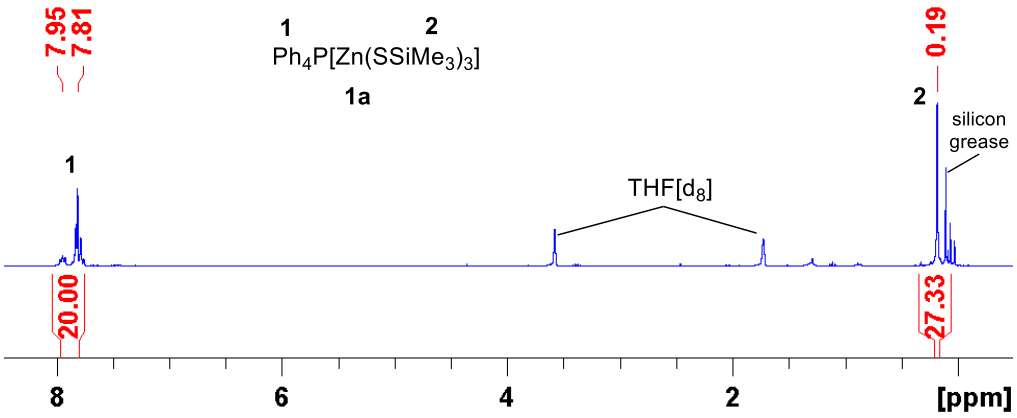

^{1}H-NMR (300.3 MHz, THF[d_8]) of **1a**. Note that the solubility of **1a** is very poor in thf.

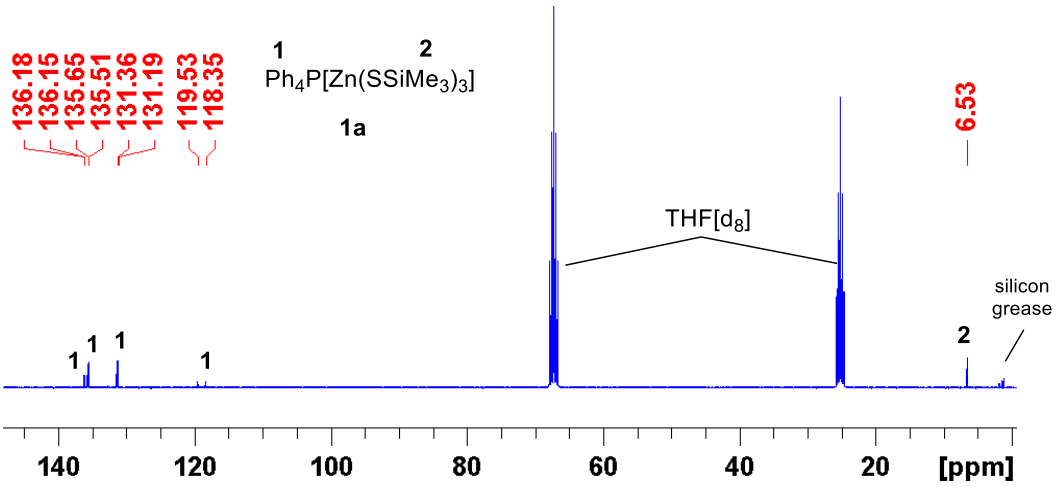

^{13}C{^{1}H}-NMR (75.5 MHz, THF[d_8]) of **1a**. Note that the solubility of **1a** is very poor in thf.

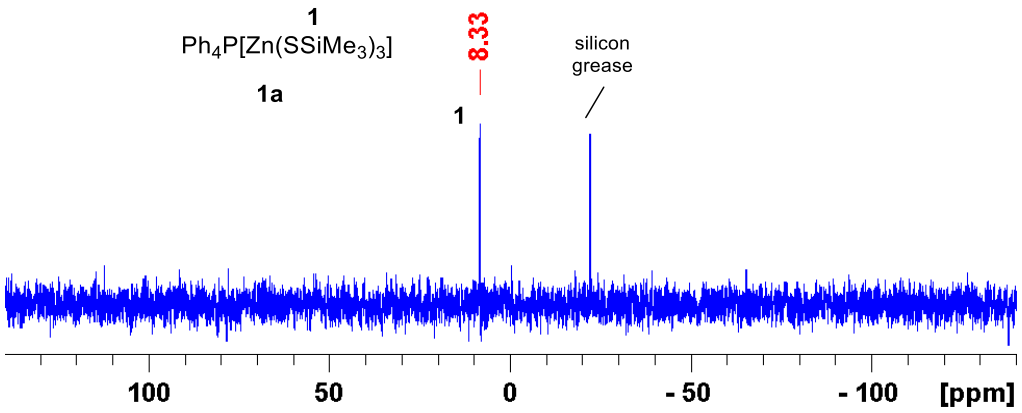

^{29}Si-NMR (59.7 MHz, THF[d_8]) of **1a**. Note that the solubility of **1a** is very poor in thf.

*2.2 NMR Spectra of $Ph_4P[Zn(SeSiMe_3)_3]$ · 0.5 Et_2O (**1b · 0.5 Et_2O**)*

Due to the poor solubility of 1b · 0.5 Et_2O in THF the silicon grease contamination seems to be more severe than it is as proven by elemental analysis (attributed singals: δ_H = 0.11 ppm, δ_C = 1.1 ppm, δ_{Si} = –22 ppm).

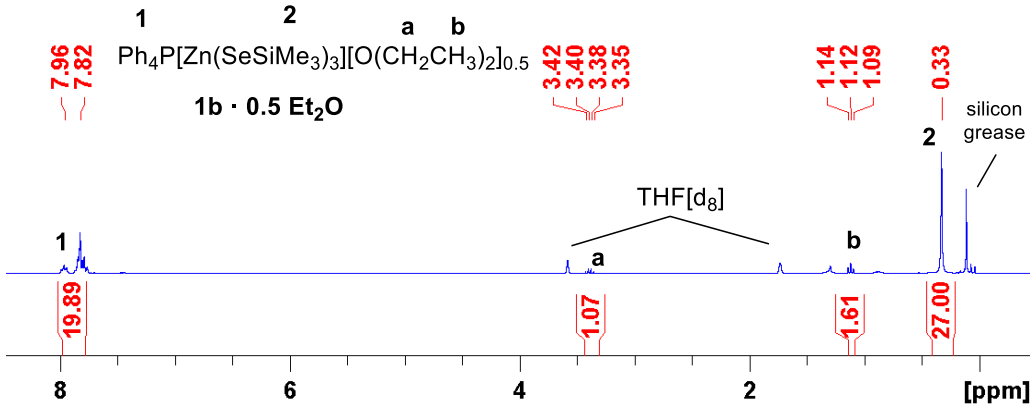

^{1}H-NMR (300.3 MHz, THF[d_8]) of **1b**. The solubility of **1b · 0.5 Et_2O** is very poor in thf.

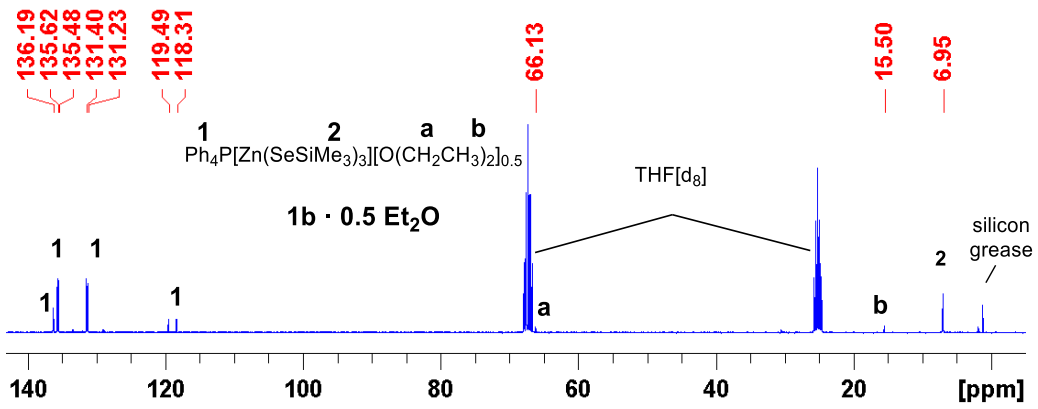

^{13}C{^{1}H}-NMR (75.5 MHz, THF[d_8]) of **1b**. The solubility of **1b · 0.5 Et_2O** is very poor in thf.

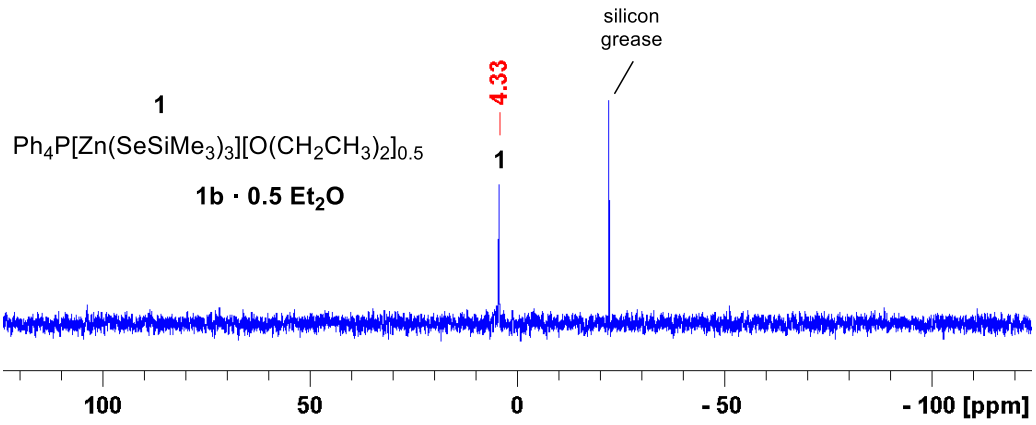

^{29}Si-NMR (59.7 MHz, THF[d_8]) of **1b**. The solubility of **1b · 0.5 Et$_2$O** is very poor in thf.

Several attempts to get a ^{77}Se-NMR spectrum of **1b** failed. We assume that the symmetrically coordinated zinc center causes problems. This is a commonly observed phenomenon for $[M(SeSiMe_3)_x]^-$ metallates that contain a central atom and do not show a dipole momentum.

*2.3 NMR Spectra of PPN[Sn(SSiMe$_3$)$_3$] (**2a-PPN**)*

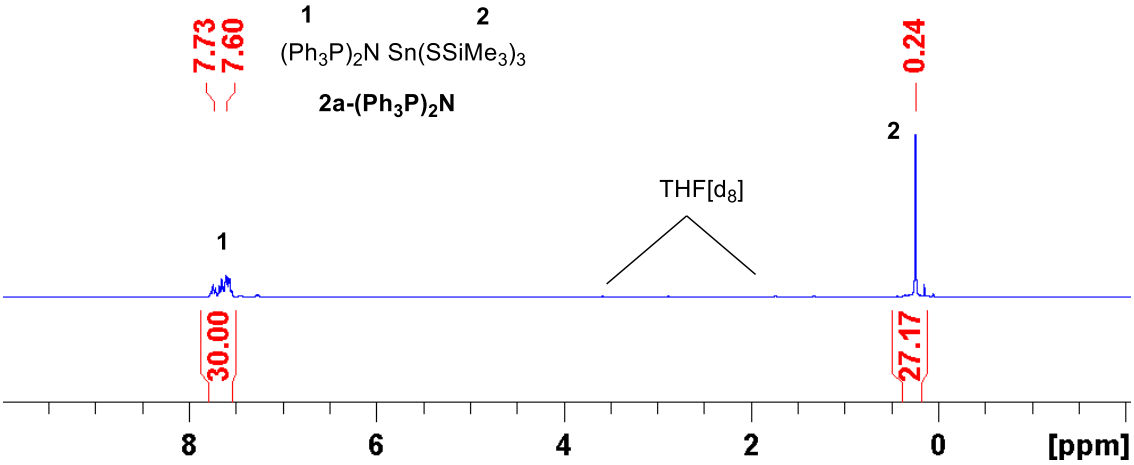

^{1}H-NMR (300.3 MHz, THF[d_8]) of **2a-PPN**.

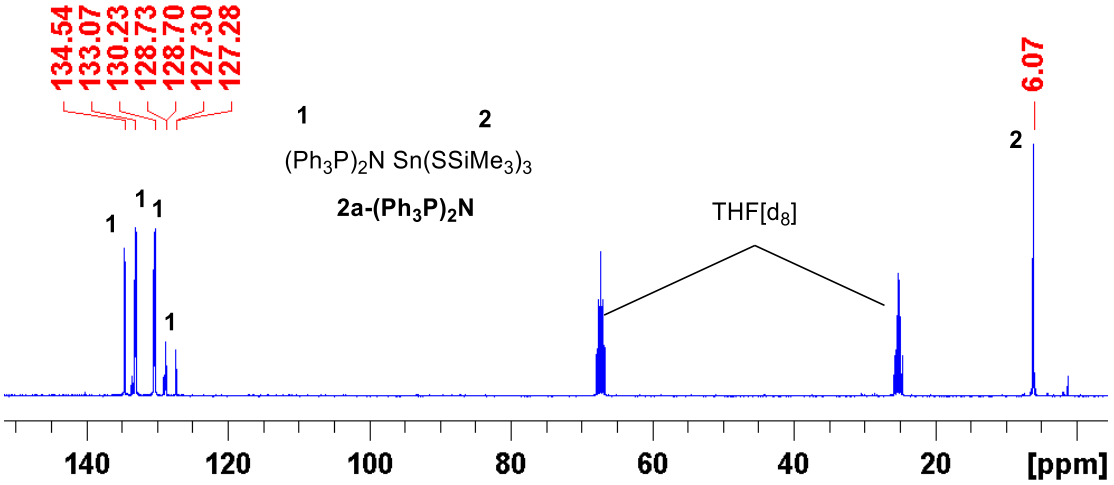

^{13}C{^{1}H}-NMR (75.5 MHz, THF[d_8]) of **2a-PPN**.

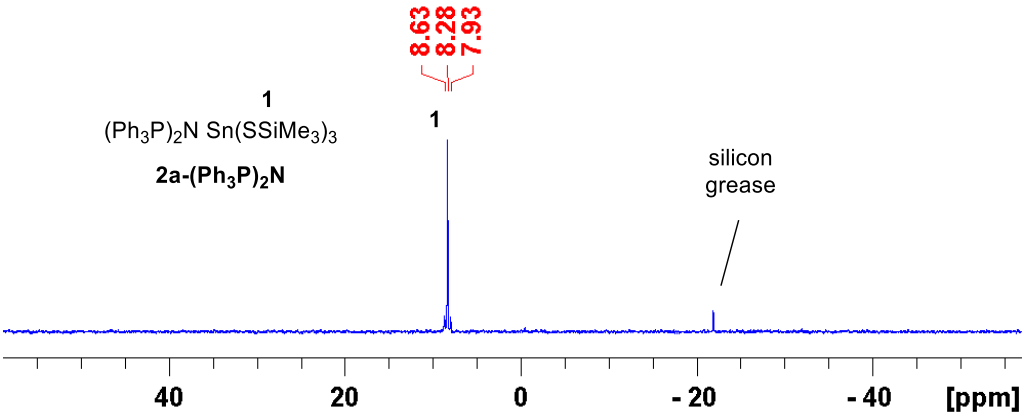

^{29}Si-NMR (59.7 MHz, THF[d_8]) of **2a-PPN**.

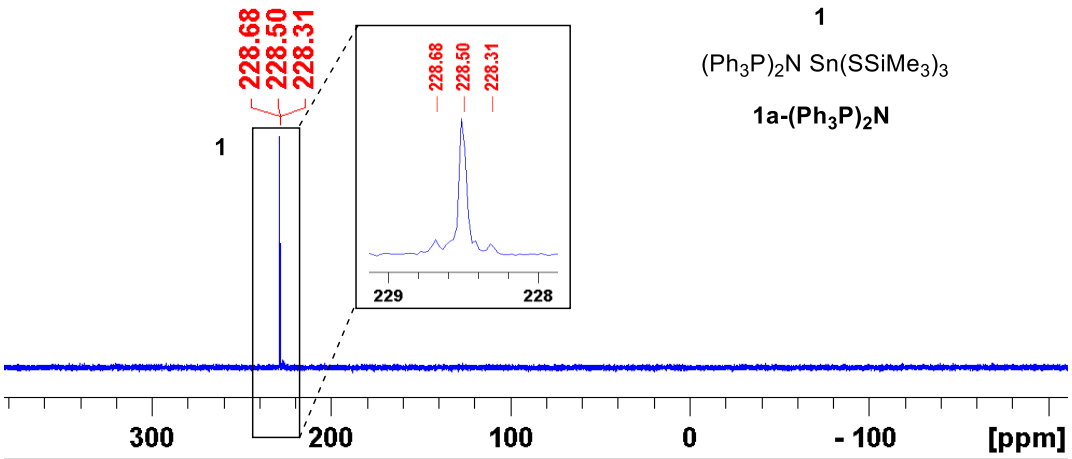

^{119}Sn-NMR (112.0 MHz, THF[d_8]) of **2a-PPN**.

*2.4 NMR Spectra of PPN[Sn(SeSiMe$_3$)$_3$] (**2b**)*

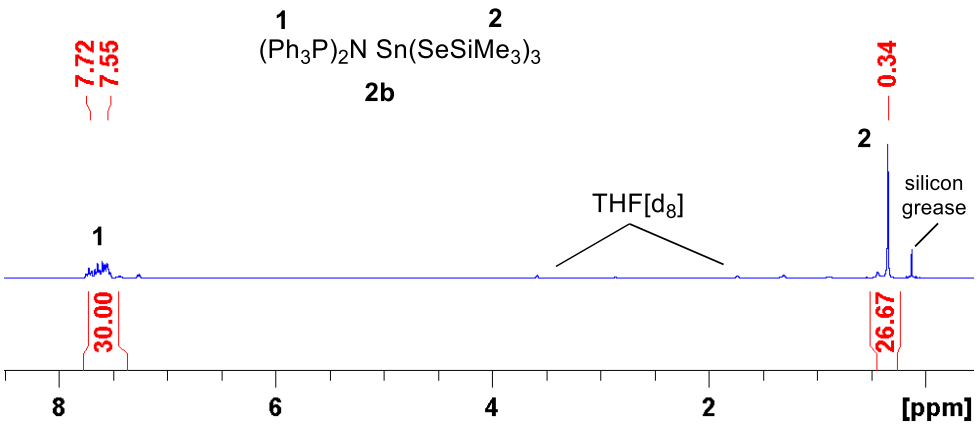

^{1}H-NMR (300.3 MHz, THF[d$_8$]) of **2b**.

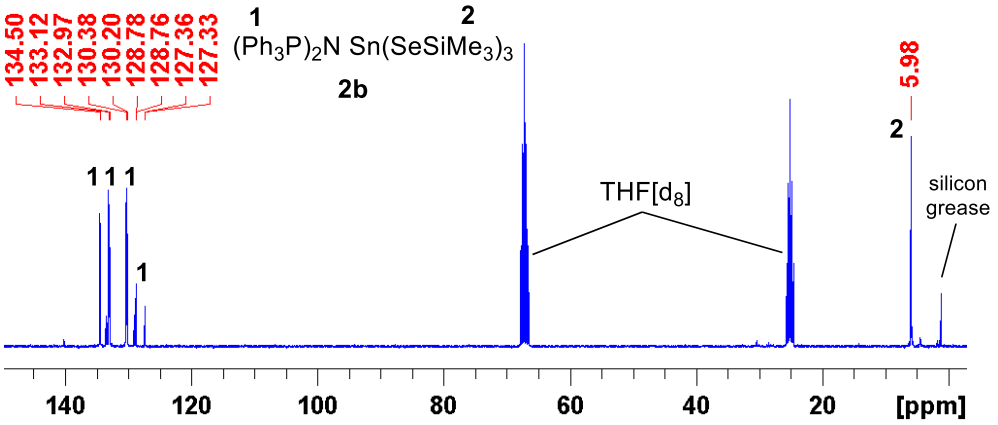

^{13}C{^{1}H}-NMR (75.5 MHz, THF[d$_8$]) of **2b**.

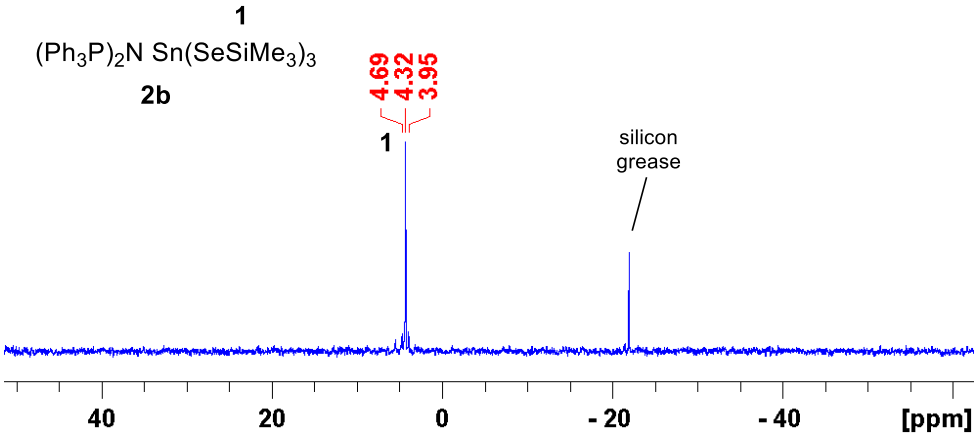

^{29}Si-NMR (59.7 MHz, THF[d$_8$]) of **2b**.

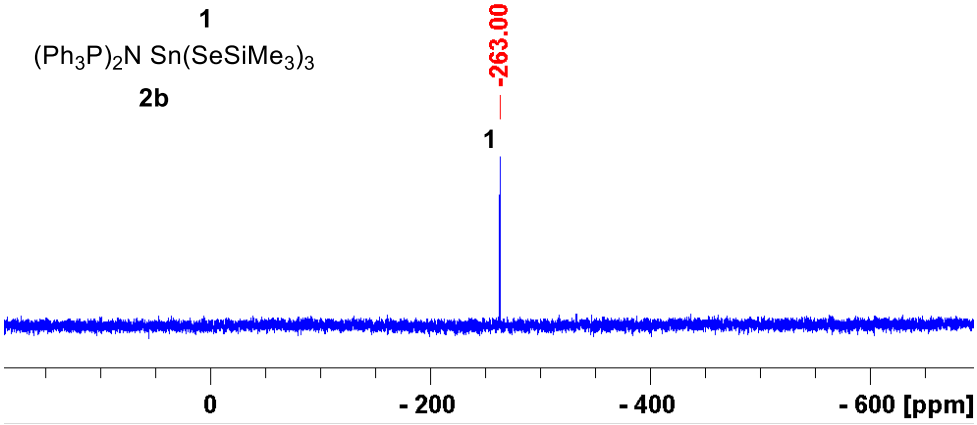

^{77}**Se-NMR** (57.3 MHz, THF[d_8]) of **2b**.

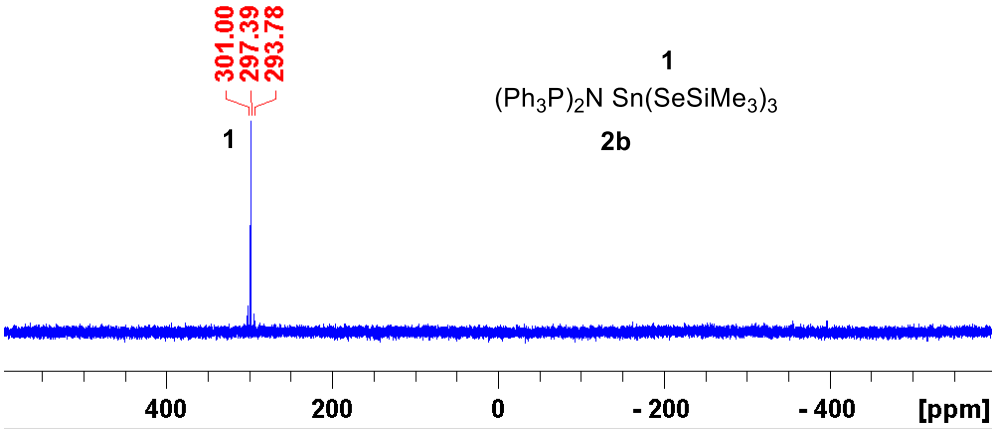

^{119}**Sn-NMR** (112.0 MHz, THF[d_8]) of **2b**.

2.5 NMR for the assumed species $Sn(SSiMe_3)_4$

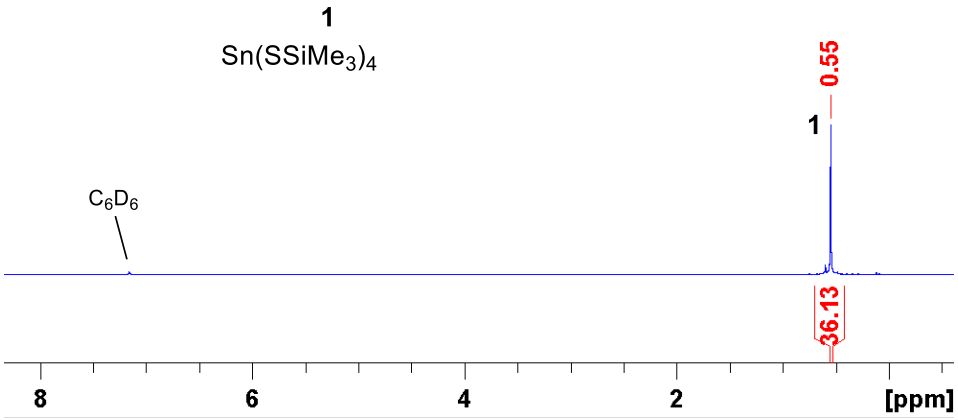

^{1}**H-NMR** (300.3 MHz, C_6D_6) of assumed $Sn(SSiMe_3)_4$.

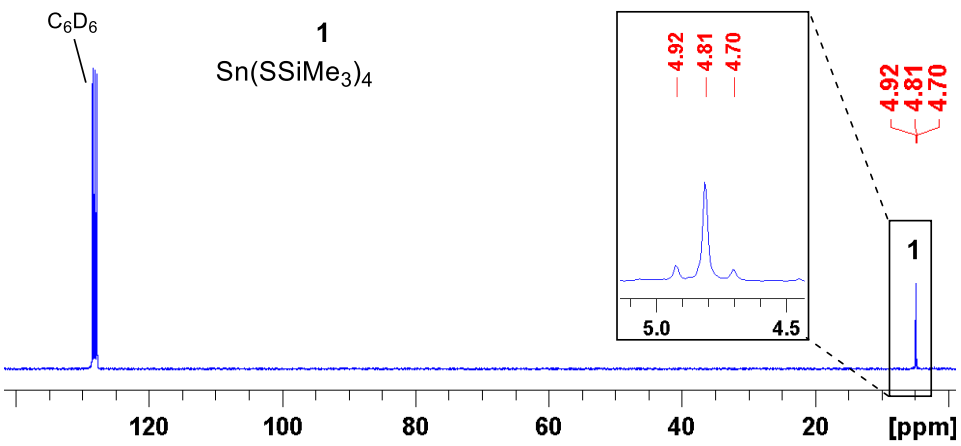

^{13}C{^{1}H}-NMR (75.5 MHz, C_6D_6) of assumed $Sn(SSiMe_3)_4$.

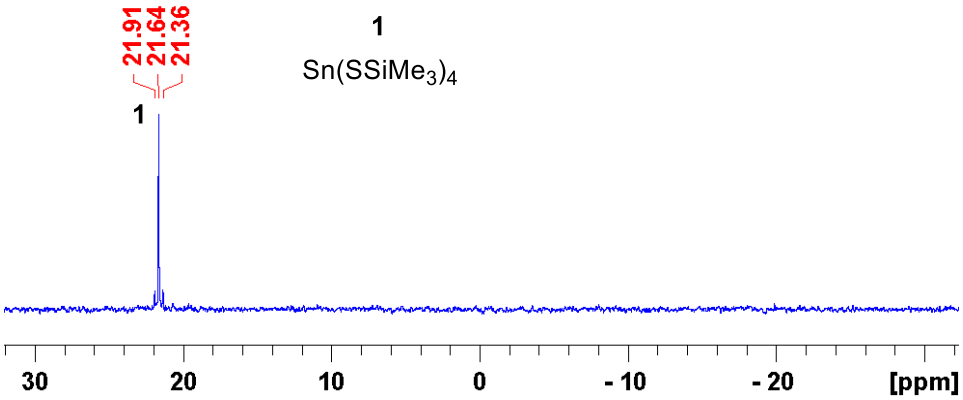

^{29}Si-NMR (59.7 MHz, C_6D_6) of assumed $Sn(SSiMe_3)_4$.

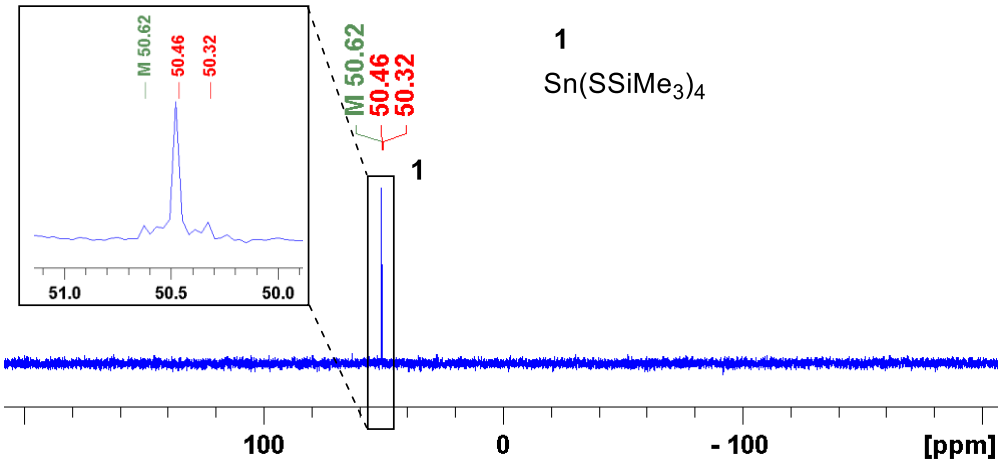

^{119}Sn-NMR (112.0 MHz, C_6D_6) of assumed $Sn(SSiMe_3)_4$.

2.6 NMR for the assumed species $Sn(SeSiMe_3)_4$

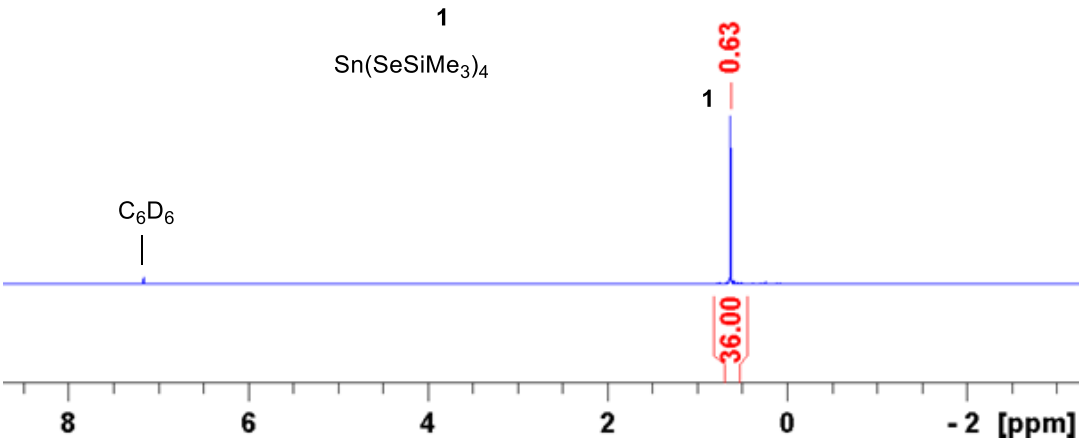

^{1}H-NMR (500.2 MHz, C_6D_6) of assumed $Sn(SeSiMe_3)_4$.

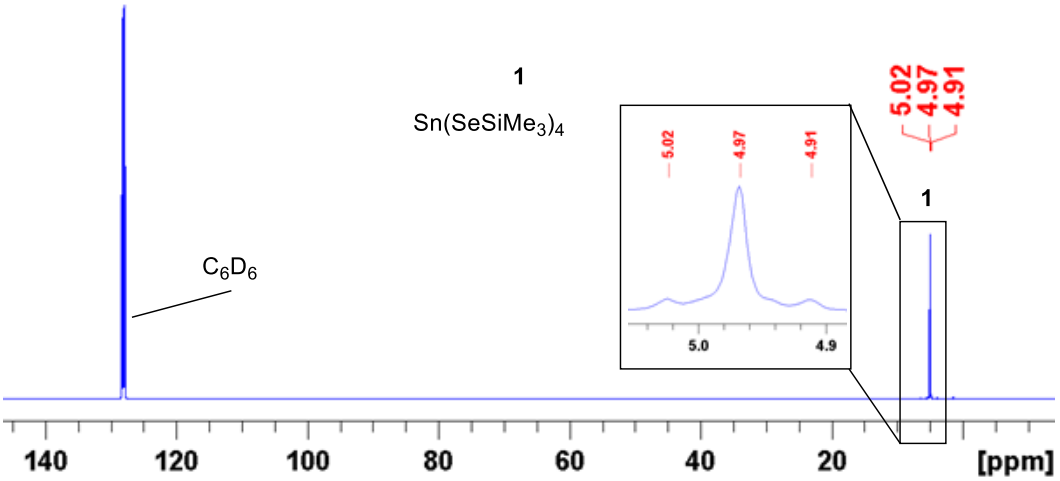

^{13}C{^{1}H}-NMR (125.8 MHz, C_6D_6) of assumed $Sn(SeSiMe_3)_4$.

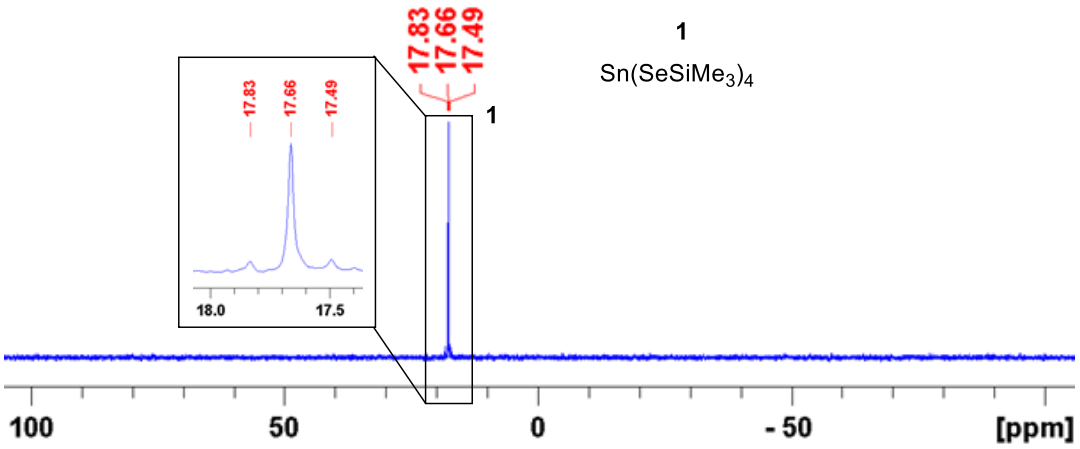

^{29}Si-NMR (99.3 MHz, C_6D_6) of assumed $Sn(SeSiMe_3)_4$.

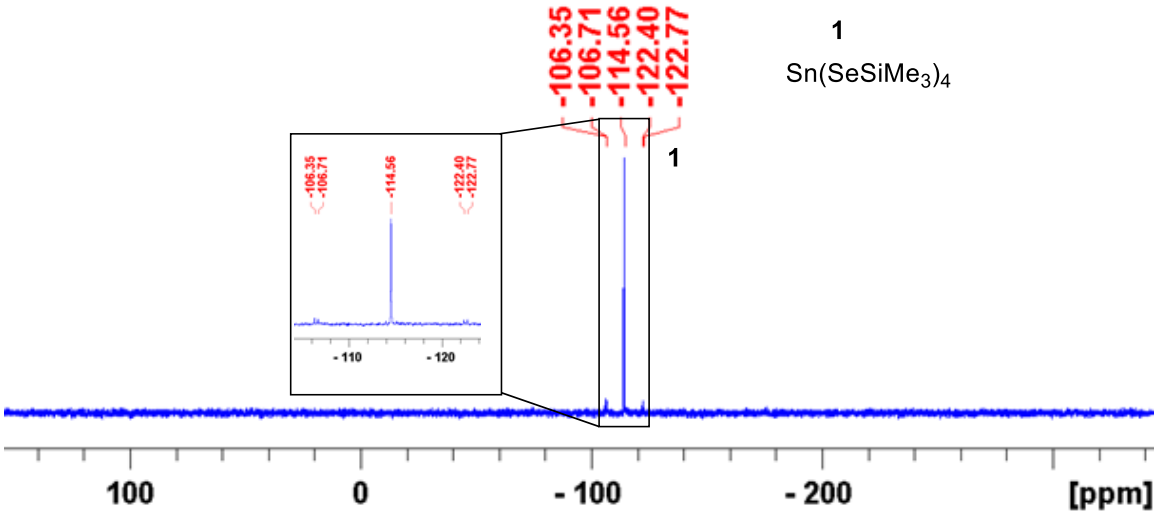

^{77}Se-NMR (95.40 MHz, C_6D_6) of assumed $Sn(SeSiMe_3)_4$.

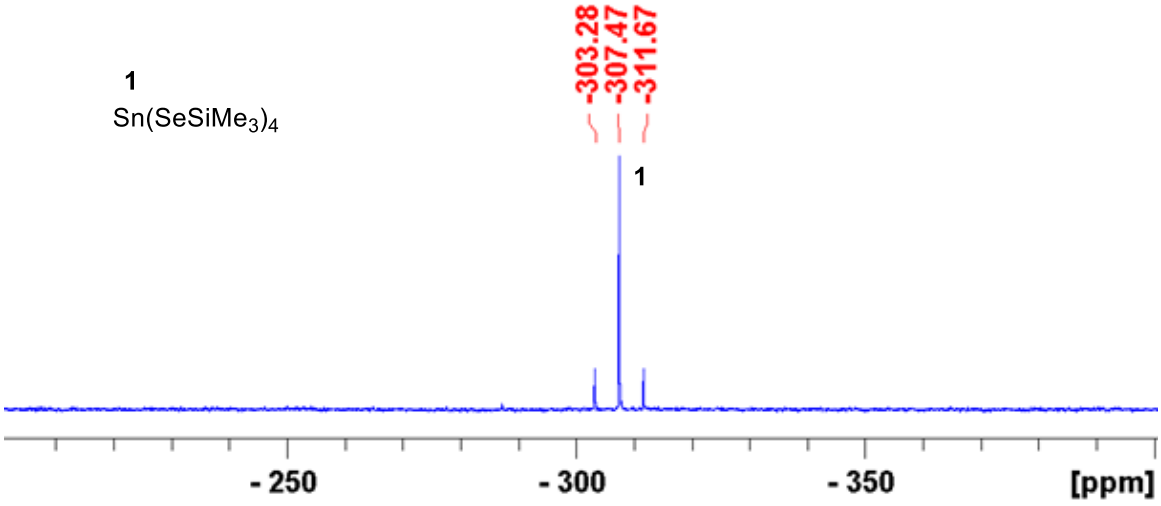

^{119}Sn-NMR (186.5 MHz, C_6D_6) of assumed $Sn(SeSiMe_3)_4$.

3 XRD data

*3.1 XRD of $Ph_4P[Zn(SSiMe_3)_3]$ (**1a**)*

Table S1: Crystallographic data for $Ph_4P[Zn(SSiMe_3)_3]$ (**1a**).

Identification code	**JG176_0m_a**	
CCDC code	**1940534**	
Empirical formula	C70 H104 O P2 S6 Si6 Zn2	
Formula weight	1515.11	
Temperature	100(2) K	
Wavelength	0.71073 Å	
Crystal system	Monoclinic	
Space group	P 21/n	
Unit cell dimensions	a = 11.687(2) Å	α= 90°.
	b = 18.890(4) Å	β= 98.27(3)°.
	c = 18.770(4) Å	γ = 90°.
Volume	4100.7(15) $Å^3$	
Z	2	
Density (calculated)	1.227 Mg/m^3	
Absorption coefficient	0.902 mm-1	
F(000)	1604	
Crystal size	0.403 x 0.212 x 0.150 mm^3	
Theta range for data collection	2.204 to 27.203°.	
Index ranges	-14<=h<=15, -24<=k<=24, -24<=l<=24	
Reflections collected	50367	
Independent reflections	9097 [R(int) = 0.0320]	
Completeness to theta = 25.000°	99.9 %	
Absorption correction	Semi-empirical from equivalents	
Max. and min. transmission	0.7455 and 0.6684	
Refinement method	Full-matrix least-squares on F2	
Data / restraints / parameters	9097 / 75 / 426	
Goodness-of-fit on F2	1.000	
Final R indices [I>2sigma(I)]	R1 = 0.0284, wR2 = 0.0659	
R indices (all data)	R1 = 0.0385, wR2 = 0.0701	
Largest diff. peak and hole	0.517 and -0.321 $e.Å^{-3}$	

*3.2 XRD of $Ph_4P[Zn(SeSiMe_3)_3]$ (**1b**)*

Table S2: Crystallographic data for $Ph_4P[Zn(SeSiMe_3)_3]$ (**1b**).

Identification code	**jg280_0m_a**	
CCDC code	**1940535**	
Empirical formula	C66 H94 P2 Se6 Si6 Zn2	
Formula weight	1722.39	
Temperature	100(2) K	
Wavelength	0.71073 Å	
Crystal system	Triclinic	
Space group	P -1	
Unit cell dimensions	a = 12.360(6) Å	α= 104.645(14)°.
	b = 12.641(6) Å	β= 108.529(13)°.
	c = 14.290(7) Å	γ = 105.841(14)°.
Volume	1890.2(17) $Å^3$	
Z	1	
Density (calculated)	1.513 Mg/m^3	
Absorption coefficient	3.697 mm^{-1}	
F(000)	868	
Crystal size	0.242 x 0.230 x 0.205 mm^3	
Theta range for data collection	2.540 to 25.748°.	
Index ranges	-15<=h<=15, -15<=k<=15, -17<=l<=17	
Reflections collected	53377	
Independent reflections	7214 [R(int) = 0.0633]	
Completeness to theta = 25.000°	99.9 %	
Absorption correction	Semi-empirical from equivalents	
Max. and min. transmission	0.7453 and 0.6145	
Refinement method	Full-matrix least-squares on F2	
Data / restraints / parameters	7214 / 18 / 407	
Goodness-of-fit on F2	1.016	
Final R indices [I>2sigma(I)]	R1 = 0.0285, wR2 = 0.0547	
R indices (all data)	R1 = 0.0426, wR2 = 0.0585	
Largest diff. peak and hole	0.643 and -0.498 $e.Å^{-3}$	

*3.3 XRD of $Ph_4P[Sn(SSiMe_3)_3]$ (**2a-Ph_4P**)*

Table S3: Crystallographic data for $Ph_4P[Sn(SSiMe_3)_3]$ (**2a-Ph_4P**).

Identification code	**JG174**	
CCDC code	**1940536**	
Empirical formula	C33 H47 P S3 Si3 Sn	
Formula weight	773.81	
Temperature	100(2) K	
Wavelength	0.71073 Å	
Crystal system	Triclinic	
Space group	P -1	
Unit cell dimensions	a = 12.1418(7) Å	α= 110.185(2)°.
	b = 16.0663(9) Å	β= 99.200(2)°.
	c = 22.2417(13) Å	γ = 94.620(2)°.
Volume	3976.6(4) $Å^3$	
Z	4	
Density (calculated)	1.293 Mg/m^3	
Absorption coefficient	0.951 mm^{-1}	
F(000)	1600	
Crystal size	0.294 x 0.163 x 0.140 mm^3	
Theta range for data collection	2.195 to 25.027°.	
Index ranges	-14<=h<=14, -19<=k<=17, 0<=l<=26	
Reflections collected	14140	
Independent reflections	14140, the crystal was solved as non-merohedral twin.	
Completeness to theta = 25.000°	99.9 %	
Absorption correction	Semi-empirical from equivalents	
Max. and min. transmission	0.745264 and 0.683693	
Refinement method	Full-matrix least-squares on F2	
Data / restraints / parameters	14140 / 24 / 790	
Goodness-of-fit on F2	1.075	
Final R indices [I>2sigma(I)]	R1 = 0.0304, wR2 = 0.0637	
R indices (all data)	R1 = 0.0386, wR2 = 0.0669	
Largest diff. peak and hole	0.416 and -0.797 $e.Å^{-3}$	

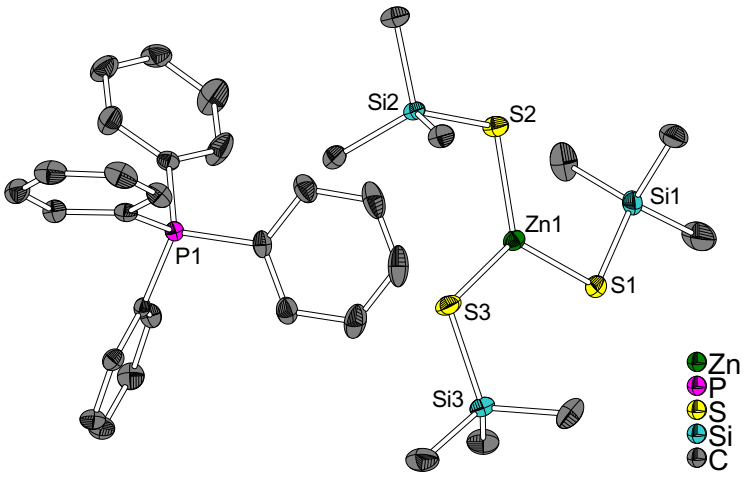

Figure S4: Molecular structure of $Ph_4P[Zn(SSiMe_3)_3]$ (**1a**). Half an equivalent of Et_2O, and hydrogen atoms are omitted for clarity. Relevant bond distances and angles: Zn1-S1: 2.2543(7) Å, Zn1-S2: 2.2536(8) Å, Zn1-S3: 2.2534(7) Å, S1-Si1: 2.1240(8) Å, S2-Si2: 2.1176(7) Å, S3-Si3: 2.1055(9) Å, S1-Zn1-S2: 120.64(2)°, S2-Zn1-S3: 117.65(2)°, S3-Zn1-S1: 121.72(2)°, Zn1-S1-Si1: 104.42(3)°, Zn1-S2-Si2: 105.12(2)°, Zn1-S3-Si3: 108.95(2)°.

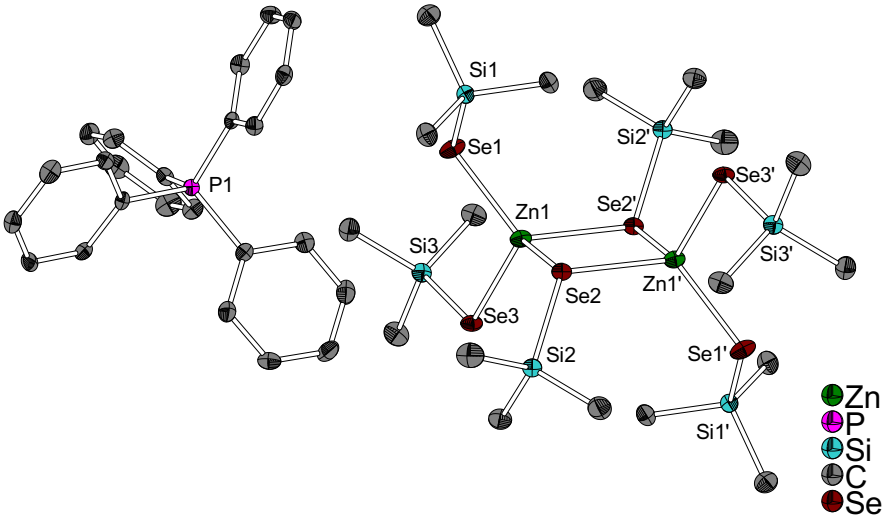

Figure S5: Molecular structure of $Ph_4P[Zn(SeSiMe_3)_3]$ (**1b**). Hydrogen atoms and one Ph_4P-cation are omitted for clarity. Relevant bond distances and angles: Zn1-Se1: 2.414(1) Å, Zn1-Se2: *2.528(1)* Å, Zn1-Se2': 2.571(1) Å, Zn1-Se3: 2.447(1) Å, Se1-Si1: 2.243(2) Å, Se3-Si3: 2.243(1) Å, Se2-Si2: 2.273(1) Å, Se1-Zn1-Se2: 115.68(3)°, Se1-Zn1-Se2': 119.28(3)°, Se1-Zn1-Se3: 108.72(3)°, Se2-Zn1-Se2': 89.66(3)°, Zn1-Se2-Zn1': 90.34(3)°, Zn1-Se1-Si1: 109.14(4)°, Zn1-Se2-Si2: 117.03(4)°, Zn1-Se3-Si3: 103.96(4)°.

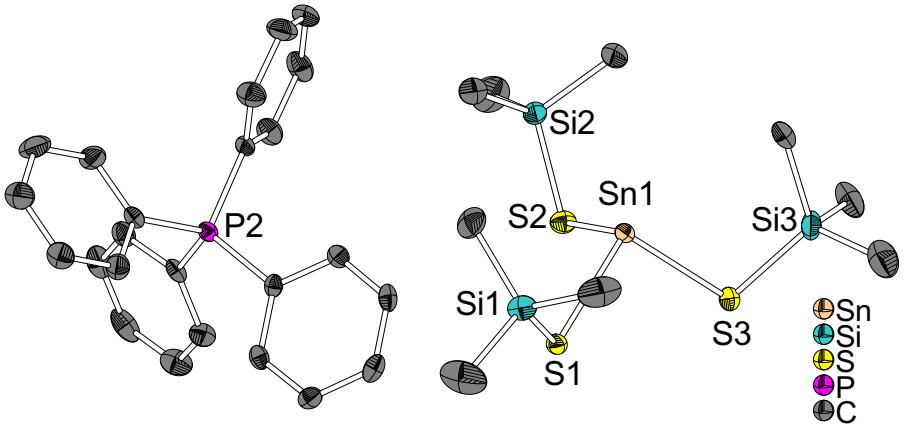

Figure S6: Molecular structure of $Ph_4P[Sn(SSiMe_3)_3]$ (**2a**). Hydrogen atoms and disordered atoms are omitted for clarity. Relevant bond distances and angles: Sn1-S1: 2.5521(9) Å, Sn1-S2: 2.5372(9) Å, Sn1-S3: 2.5366(9) Å, S1-Sn1-S2: 94.24(3)°, S1-Sn1-S3: 94.24(3)°, S2-Sn1-S3: 93.01(3)°, S1-Si1: 2.116(1) Å, S2-Si2: 2.113(1) Å, S3-Si3: 2.114(2) Å, Sn1-S1-Si1: 97.55(4)°, Sn1-S2-Si2: 100.67(5)°, Sn1-S3-Si3: 100.32(5)°.

4 Thermal decomposition of the title anions

To investigate the thermal behavior TGA measurements of the title compounds were conducted. To get further evidence on the mechanism of the title anions' decomposition the residues obtained after the TGA measurement were investigated via PXRD.

The TGA measurements of the zincates $Ph_4P[Zn(SSiMe_3)_3]$ **1a** and $Ph_4P[Zn(SeSiMe_3)_3]$ **1b** are shown in **Figure 4** in the main text. The residues of the TGA measurements could be identified as ZnS (for **1a**) and ZnSe (for **1b**) via PXRD (**Figure S7**).

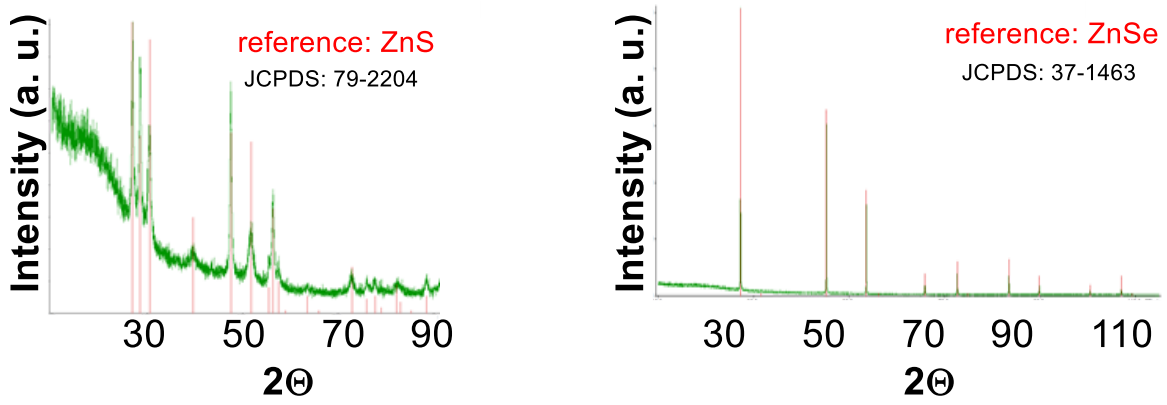

Figure S7: PXRDs of the residues obtained from the TGA measurements of $Ph_4P[Zn(SSiMe_3)_3]$ (**1a**, on the left) and $Ph_4P[Zn(SeSiMe_3)_3]$ (**1b**, on the right). The corresponding binary chalcogenides ZnS (on the left) and ZnSe (on the right) are identified.

The TGA measurements of the stannanides $PPN[Sn(SSiMe_3)_3]$ (**2a-PPN**) and $PPN[Zn(SeSiMe_3)_3]$ (**2b**) are shown in **Figure 5** in the main text. The residues of the TGA measurements could be identified as SnS (for **2a-PPN**) and SnSe (**2b**) via PXRD (**Figure S8**).

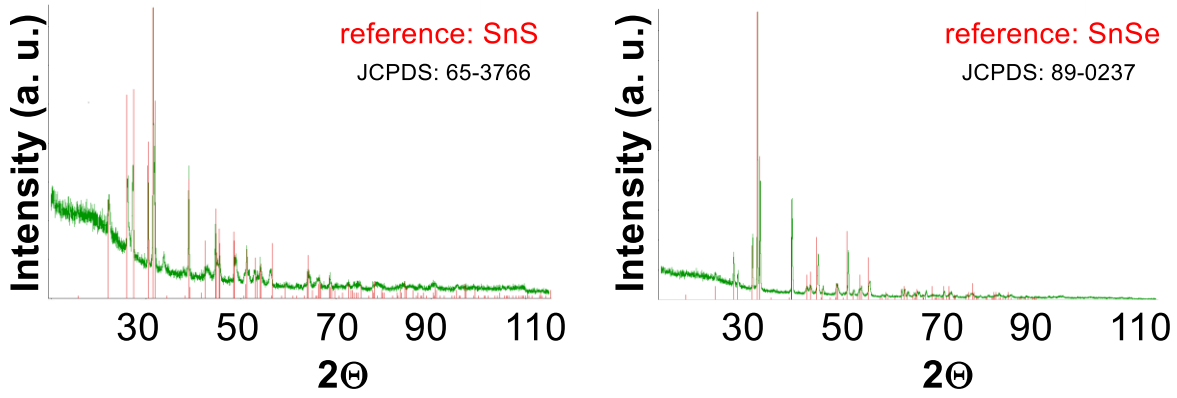

Figure S8: PXRDs of the residues obtained from the TGA measurements of $PPN[Sn(SSiMe_3)_3]$ (**2a-PPN**, on the left) and $PPN[Sn(SeSiMe_3)_3]$ (**2b**, on the right). The corresponding binary chalcogenides SnS (on the left) and SnSe (on the right) are identified.

During ongoing research, the yet unknown compounds $Ph_4P[ESiMe_3]$ were prepared for E = S and Se. We here show the TGA analysis of these compounds to demonstrate that the broadness of the temperature range of the thermal decay of the title anions is mainly caused by the decomposition of $Ph_4P[ESiMe_3]$ (**Figure S9**). As the TGA measurements for the $PPN[ESiMe_3]$ compounds are not available yet a comparison with the PPN^+ salts of the stannanides **2a-PPN** and **2b** is not yet possible.

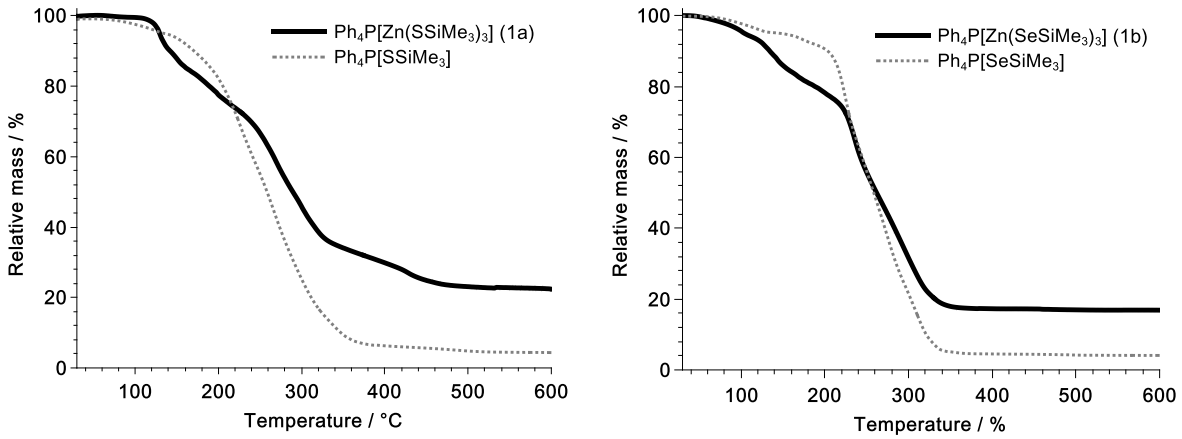

Figure S9: Comparison of the thermal decomposition of the zinkates $Ph_4P[Zn(ESiMe_3)]$ with the corresponding organic salts $Ph_4P[ESiMe_3]$ (E = S, left; Se, right).

The decomposition of $Cat[M(ESiMe_3)_{n+1}]$ compounds into $Cat[ESiMe_3]$ and neutral $M(ESiMe_3)_n$ has been investigated for $Ph_4P[In(ESiMe_3)_4]$ (E = S, Se) by NMR and CHN analysis and is published elsewhere.[2] The $Ph_4P[ESiMe_3]$ compounds decay almost completely into volatiles at 500°C (the Se homologue decomposes slightly faster) with very little residual mass around 5%. The corresponding neutral compounds $M(ESiMe_3)_n$ decompose by condensation induced by elimination of $E(SiMe_3)_2$. While stable intermediates $M(E)_{0.5x}(ESiMe_3)_{n-x}$ might emerge, the complete desilation yield the binary metal chalcogenides $ME_{0.5n}$. This is in accordance with our observations and provides a possible explanation for the outcome of the TGA measurements.

5 Attempts to prepare CZTS with the title compounds

5.1 Attempted preparation of Cu_2ZnSnS_4

An atom efficient and solution based low cost access to CZTS is of interest for the sake of its benefits regarding ecological aspects of sustainability that might be incompatible with expensive vacuum technology and high-temperature gas phase sulfuration or selenation

processes incorporating excess H_2E. Another problem is the challenging preparation of phase pure CZTS, as the presence of binary impurities like Cu_xS, ZnS, or Cu_xSnS_y are common problems,[3] that also arise in molecular precursor decomposition strategies.[4,5] As CZTS is a quaternary compound the preparation is usually performed in a four component system, in which every required element is introduced with a distinct precursor. By using a binary precursor containing the chalcogen atoms in the desired amount, the complexity of the system can be reduced to a three component system.[4] Despite of such interesting application perspectives there are very few metastable precursors known containing two or more of the desired elements in one formula unit.[4,5] Herein we show how the new title compounds act as templates for binary intermediates $[M_xE_y]^-$ (E = S, Se; M = Zn, Sn) that are useful building blocks for solution based preparations of CZTS. This approach avoids vacuum techniques and subsequent treatment with large excess of toxic chalcogen sources such as H_2E at higher temperatures

In the following we describe a short attempt to prepare Cu_2ZnSnS_4 (CZTS) by a coprecipitation strategy comparable to a previously published coprecipitation of $CuInS_2$. Our aim was to use a mixture of the title salts **1a-PPN** and **2a-PPN** in acetonitrile to precipitate the target material by pouring in a solution of $[Cu(tmtu)_3][PF_6]$. Our experiment turned out to be promising, though not satisfyingly good enough to be presented in the main text. We choose to present the obtained results here to provide some valuable information that might be of interest for those who want to prepeare CZTS using the presented precursor strategy.

As the precusors $[Sn(ESiMe_3)_4]$ are too labile for long time storage in a technical printed electronics application, a different protocol was developed involving stannanide anion $[Sn(SSiMe_3)_3]^-$ (**2**) and oxidative addition of one atom equivalent of elemental sulfur. Addition of elemental sulfur leads to a precipitate, not soluble enough to be examined via Si- and Sn-NMR spectroscopy. Based on the faster condensation tendency, we assume, that sulfur is oxidatively added and tin(IV) intermediates are formed. However, it cannot be fully excluded, that sulfur might form so far unknown trimethylsilyldisulfido ligands at tin(II). For simplicity we refer to the *in situ* generated, but not isolated species as "$[Sn(S)(SSiMe_3)_3]^-$" being aware, that such partially silylated thiostannates tend to rapidly condense to more and more insoluble higher nuclear clusters. Planned studies will be revealing, whether a replacement of purely organic cations by alkali cryptand cations will allow to crystallise intermediates of this process. In this study, the focus was put on gaining first proof of concept, that such soluble and metastable sources for the elements Sn / Zn / S / Se can in fact be used in a solution based

approach towards colloids and microcrystalline co-precipitates of CZTS and its building blocks. This would be a precondition for further developing a printed electronics process. In a preliminary experiment, we observed, that thermal pre-treatment of a finely ground 1:1 mixture of "Cat [Sn(S)($SSiMe_3$)$_3$]" and Cat [Zn($SSiMe_3$)$_3$ (160°C, 10 min.) under reduced pressure leads to partial dissociation of the metalates into Cat [$SSiMe_3$] (detected by NMR). The plausible neutral species "[Sn(S)($SSiMe_3$)$_2$]$_n$", and "[Zn($SSiMe_3$)$_2$]$_n$" formally formed are very labile, prone to eliminate (Me_3Si)$_2$E at these conditions and to form metal chalcogenide nano- and microparticles. This characteristic condensation tendency is reduced or even inhibited at room temperature by the presence of Cat[$ESiMe_3$] and formation of more stable metalate complexes. In contrast to the starting materials, the residue of this thermal pre-annealing process can be suspended as thermally stable beige, nearly coloureless dispersion in MeCN. To this dispersion two equivalents of [Cu(tmtu)$_3$]PF_6 (tmtu = *N,N,N',N'*-tetramethylthiourea), dissolved in MeCN, were added dropwise. The suspension immediately turns black. After 18 h at 20°C, the solvent was removed in vacuum, replaced by diglyme and the black dispersion was stirred in diglyme at 160°C/ 5d for equilibrating the nanoparticular phases under a high boiling dispersing agent, that at the same time dissolves LiCl and PPN[PF_6] by-products. Finally, the matured precipitate was centrifuged, washed, dried and annealed at 300 °C for 18 h. The combination of PXRD (**Figure S10**) and Raman spectroscopy (**Figure S11**) gave hints for the presence of microcrystalline, CZTS. As the main signals in the PXRD patterns of orthorhombic CZTS and cubic ZnS are nearly identical,[6] a Raman spectra is useful to check that the sample is not made up of ZnS. The observed signal at 336 cm^{-1} is associated with the totally symmetric M-S vibration in MS_4 tetrahedra in CZTS, and is known to be the by far most dominant peak for CZTS.[7] Both the wavenumber and line half width fit to colloidal nano-powders of CZTS obtained by hot injection methods (**Figure S11**),[8] which is why we claim this result to be promising. Though the absence of a distinct Raman signal at 351 cm^{-1} should indicate that no larger phase impurities of ZnS are present, the large line half width in the PXRD and the Raman spectra indicate small crystalline domains and disorder. However, Raman spectra are not suited to uniquely identify materials. We are therefore not able to make statements concerning the phase purity and the elemental decomposition that also could be impaired by the presence of chloride anions during the precipitation step.

Based on these findings, a co-precipitation process involving no MeCN and no change of the solvent, preferably diglyme, and hot filtration step is suggested for further optimising this synthesis strategy (**Scheme S1**).

Experimental procedure

Preparation of the Zn/S-precursor mix (**Scheme S1**, **A**): A mixture of $ZnCl_2$ (21 mg, 0.15 mmol, 1.0 equiv.) and PPN [Cl] (89 mg, 0.15 mmol, 1.0 equiv.) is stirred in thf (10 mL) for 18 h at ambient temperature. In a separate reaction tube, to a solution of $S(SiMe_3)_2$ (84 mg, 0.47 mmol, 3.1 equiv.) in thf (5 mL) a solution of 2.9M *n*-BuLi in hexane (0.16 mL, 0.46 mmol, 3.0 equiv.) is added dropwise at 0 °C. The reaction mixture is stirred for 30 min at 0 °C and further 30 min at ambient temperature. All volatiles are removed under fine vacuum. The obtained colourless powder is directly dissolved in thf (10 mL) and slowly added to the above solution of PPN [$ZnCl_3$] in thf (10 mL) at –78 °C. The reaction mixture is stirred for 18 h within the cooling bath. During this time the reaction mixture is allowed to slowly reach ambient temperature. A clear, colourless solution of PPN[$Zn(SSiMe_3)_3$] · 3 LiCl in thf (20 mL) is obtained.

Preparation of precursor mix Sn/S (**Scheme S1**, **B**): A mixture of $SnCl_2$ (29 mg, 0.15 mmol, 1.0 equiv.) and PPN[Cl] (89 mg, 0.15 mmol, 1.0 equiv.) is stirred in thf (10 mL) for 18 h at ambient temperature. To a solution of $S(SiMe_3)_2$ (84 mg, 0.47 mmol, 3.1 equiv.) in thf (5 mL) a solution of 2.9M *n*-BuLi in hexane (0.16 mL, 0.46 mmol, 3.0 equiv.) is added dropwise at 0 °C in a separate reactor. The reaction mixture is stirred for 30 min at 0 °C and a further 30 min at ambient temperature. All volatiles were removed under fine vacuum with the help of diethyl ether and pentane. The obtained colourless powder is dissolved in thf (10 mL) and slowly added to the solution of PPN[$SnCl_3$] in thf (10 mL) at –78 °C and the reaction mixture is stirred for 18 h within the cooling bath. During this time the reaction mixture is allowed to slowly reach ambient temperature. A clear, colourless solution of PPN [$Sn(SSiMe_3)_3$] · 3 LiCl in thf (20 mL) is obtained. To this solution a solution of elemental sulfur (5 mg, 0.15 mmol, 1.0 equiv.) in thf (5 mL) is added slowly at –78 °C and stirred for 30 min at this temperature until a green solution is obtained. The mixture is warmed up to ambient temperature and stirred for 1 h. A beige precipitate is obtained. All volatiles were removed in fine vacuum to obtain precursor mix **B**.

Preparation of the multinary sulfidometalate precursor mixture: To the freshly prepared Sn/S precursor mix **B** a solution of Zn/S precursor mix **A** in thf (20 mL) is added and stirred for 10 min at ambient temperature. All volatiles are removed in fine vacuum until a colourless slurry is obtained. This slurry is heated up to 160 °C for 15 min at 10^{-2} mbar

until no more volatiles emerge and a yellow-greenish melt arises. When this mixture is cooled down to ambient temperature a beige varnish-like solid is obtained, which is suspended in MeCN (10 mL). A solution of $[Cu(tmtu)_3]PF_6$ (187 mg, 0.31 mmol, 2.0 equiv.; scheme 2, **C**) in MeCN (10 mL) is added slowly at –20 °C. A spontaneous precipitation of black particles is observed. The mixture is stirred at –20 °C for 1 h, warmed to room temperature and stirred for a further 18 h at ambient temperature, while the precipitation intensifies. All volatiles are removed under reduced pressure and the black residue is suspended with diglyme (10 mL). The suspension is annealed at 160 °C without stirring for 5 d. The suspension is centrifugated and the supernatant is removed via canula. The black residue is washed with MeCN (10 mL), then washed with thf (10 mL) and the black solid is dried in fine vacuum. This residue is annealed at 300 °C under N_2 for a further 18 h and then investigated by PXRD and Raman spectroscopy.

Suggested optimized procedure

It is suggested to use cheaper quaternary ammonium cations "Cat" and not to separate LiCl from *in situ* generated highly reactive species. Sulfur (1/8 S_8 eq.) as oxidant is added to $Cat[Sn(SSiMe_3)_3]\cdot 3LiCl$ *in situ* formed in diglyme to yield a dispersion of Sn(IV) chalcogenide particles. $Cat[Zn(SSiMe_3)_3]\cdot 3LiCl$ is prepared *in situ* in diglyme. Both dispersions are combined on a target and the third solution of $[Cu(tmtu)_3]PF_6$ in diglyme is printed or spray coated on top. The thin film with precipitating nano- and microparticles is thermally annealed at 160°C under the flux of diglyme under inert conditions. Side products such as LiCl and tmu are very soluble in diglyme and are rinsed in washing steps. Annealing of the dried co-precipitate should lead to CZTS. Both, $(Me_3Si)_2E$ and its activated form $Cat[ESiMe_3]$ (E = S, Se) may be added if extra sources of sulfur and selenium are required in such solvent based precipitation and annealing process. According to TGA, excess $Cat[ESiMe_3]$ salts are decomposed with very little residual mass, as discussed above and in the main text. The suggested steps to be further developed into a printed electronics technology are presented in **Scheme S1.**

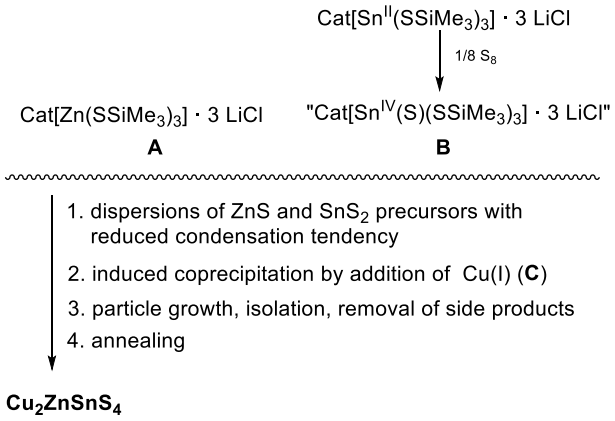

Scheme S1. Procedure to prepare CZTS by using a Cu(I) source **C** and precursor mixtures **A** and **B** prepared from the title anions.

5.1.1 Discussion of the PXRD and Raman spectra

Note that the identity of CZTS cannot be proven by PXRD exclusively as this compound is known to show essentially the same PXRD pattern as ZnS in the Wurtzite modification.[6] By comparing the recorded PXRD pattern with the reference patterns for Kesterite CZTS and Wurtite ZnS all arising reflections can be assigned (**Figure S10**). To prove the identity of CZTS a Raman spectrum needs to be recorded additionally.

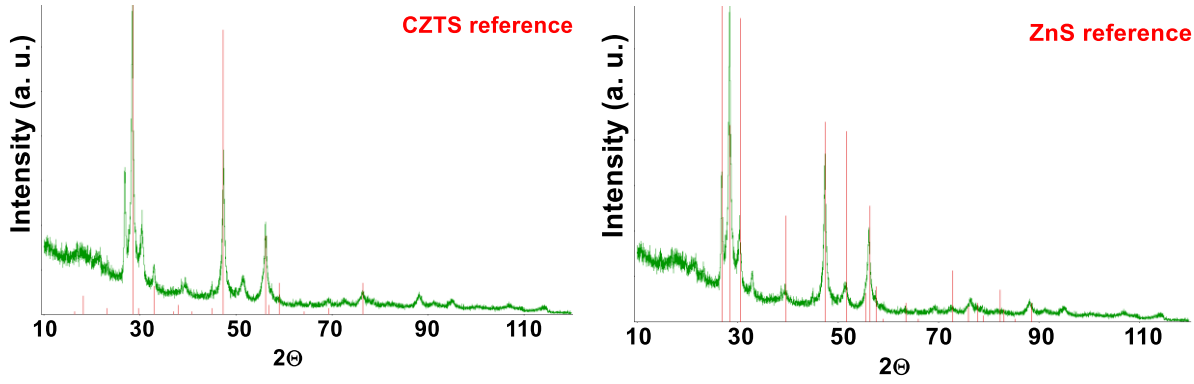

Figure S10: PXRD of the prepared sample, top row: Cu_2ZnSnS_4 reference (JCPDS: 26-0575), bottom row: ZnS reference (JCPDS: 79-2204).

In the Raman spectrum CZTS shows a big signal at 338 cm^{-1}, and a small peak at 287 cm^{-1}, while the absence of a peak at 351 cm^{-1} that is attributed to ZnS, is reported to be an indication for CZTS to be present.[6] In the Raman spectrum of the prepared sample (**Figure S11**) no peak

at 351 cm^{-1} and only one peak at 336 cm^{-1} can be observed. This Raman shift has been reported in literature for samples containing CZTS.[9,10] The small signal at 287 cm^{-1} cannot be detected clearly. Though these results seem to be promising, we need to clarify that these do not provide any information about defects and phase-purity – as mentioned above.

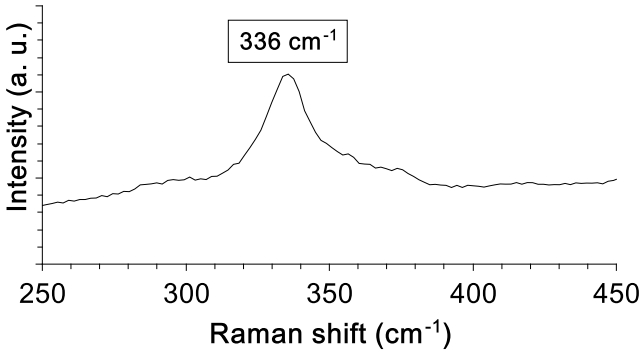

Figure S11: Raman spectrum of the prepared sample.

5.2 Comment on the mechanism of condensation of the binary anions

It is believed, that dissociation of the metalate complexes Cat[$Zn(SSiMe_3)_3$] and Cat[$Sn(SSiMe_3)_3$], after oxidation by S formally Cat[$Sn(S)(SSiMe_3)_3$], into Cat[$SSiMe_3$] and neutral intermediates [$Zn(SSiMe_3)_2$] and "[$Sn(S)(SSiMe_3)_2$]" triggers the rate of condensation, elimination of $S(SiMe_3)_2$ and formation of a matrix of *in statu nascendi* nanocrystalline particles Cu_2S, ZnS and SnS_2. The proposed mechanism is illustrated in **Scheme S2**. The dissociation of $[M(ESiMe_3)_{n+1}]^-$ anions into $M(ESiMe_3)_n$ and $[ESiMe_3]^-$ has been investigated for $Ph_4P[M(ESiMe_3)_4]$ (M = In; E = S) elsewhere.[2]

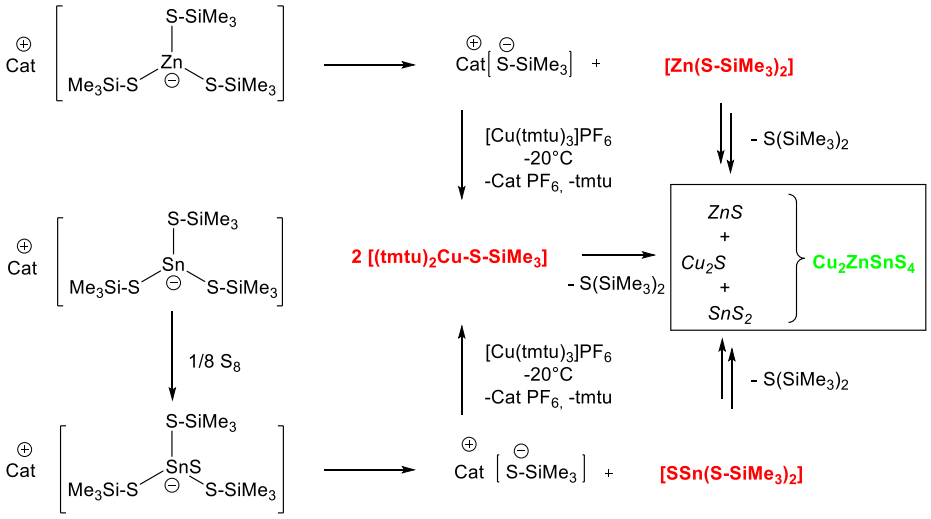

Scheme S2: Proposed mechanism of the coprecipitation of ZnS, Cu_2S and SnS_2 starting from isolated and characterised title metallates.

6 References

(1) T. Shimada, F. S. Ohuchi and B. A. Parkinson, *J. Vac. Sci. Technol. A: Vacuum, Surfaces, and Films*, 1992, **10**, 539–542.

(2) J. Guschlbauer, T. Vollgraff and J. Sundermeyer, *Inorg. Chem.*, 2019, **58**, 15385-15392.

(3) M. Kumar, A. Dubey, N. Adhikari, S. Venkatesan and Q. Qiao, *Energy Environ. Sci.*, 2015, **8**, 3134–3159.

(4) D. Fuhrmann, S. Dietrich and H. Krautscheid, *Chem. Eur. J.*, 2017, **23**, 3338–3346.

(5) D. Fuhrmann, S. Dietrich and H. Krautscheid, *Inorg. Chem.*, 2017, **56**, 13123–13131.

(6) X. Yu, A. Ren, F. Wang, C. Wang, J. Zhang, W. Wang, L. Wu, W. Li, G. Zeng and L. Feng, *Int. J. Photoenergy*, 2014, Article ID 861249, 1–6.

(7) M. Himmrich, H. Haeuseler, *Spectrochim. Act.*, 1991, **47A**, 933-942.

(8) S. Kumar, V. Kumar, V. Mikli, T. Varema, M. Altosaar and M. Grossberg, *Energy Procedia*, 2016, **102**, 136–143.

(9) Y. Wang, Y. Huang, A. Y. S. Lee, C. F. Wang and H. J. Gong, *J. Alloys Compd.* 2012, **539**, 237–241.

(10) Z. Seboui, Y. Cuminal and N. Kamoun-Turki, *J. Renew. Sustain. Energy*, 2013, **5**, 23113.

Manuscript submitted (14.11.2019)

A Series of Homoleptic Linear Coinage Metal Trimethylsilylchalcogenolate Complexes Cat[Me_3E-M-$ESiMe_3$] (M = Cu, Ag, Au; E = S, Se)

Jannick Guschlbauer, Tobias Vollgraff, Xiulan Xie, Florian Weigend, Jörg Sundemeyer

A Novel Series of Homoleptic Linear Coinage Metal Trimethylsilylchalcogenolate Complexes Cat[Me_3SiE-M-$ESiMe_3$] (M = Cu, Ag, Au; E = S, Se)

Jannick Guschlbauer,[a] Tobias Vollgraff,[a] Xiulan Xie,[a] Florian Weigend,[b] Jörg Sundermeyer[a]*

[a] Fachbereich Chemie and Materials Science Center, Philipps-Universität Marburg, Hans-Meerwein-Straße 4, 35043 Marburg.

[b] Karlsruhe Institute of Technology (KIT), Institute of Nanotechnology, Hermann-von-Helmholtz-Platz 1, 76344 Eggenstein-Leopoldshafen, Germany.

ABSTRACT: The syntheses and the crystallographically determined molecular structures of the organic salts Cat[$M(ESiMe_3)_2$] (**1**: M/E = Cu/S, Cat = Ph_4P^+; **2**: M/E = Ag/S, Cat = Ph_4P^+; **3-Cat**: M/E = Au/S; **4-Cat**: M/E = Cu/Se; **5-Cat**: M/E = Ag/Se; **6-Cat**: M/E = Au/Se; Cat = Ph_4P^+ or PPN^+) are presented. Much to our surprise these homoleptic coinage metalate anions are stable enough to be isolated even in the absence of any strongly binding and stabilizing extra ligands. The complete series of metalates has been characterized by XRD analysis. The coinage metal atoms are linearly coordinated by two trimethylsilylchalcogenolate ligands. The silyl moieties of all presented anions show an unexpected *gauche* conformation in the solid state. The energetic preference of the *gauche* conformation is confirmed by quantum chemical calculations. It amounts to about 2-6 kJ/mol (mainly depending on M), which is small. For a model-compound, where $SiMe_3$ is replaced with Cl, this can be rationalized by π-type interactions between the d(M) and the p(E) orbitals, in particular by the reduction of the anti-bonding character of the HOMO for the *gauche* conformation compared to the eclipsed conformation. For the original compound, matters are more complicated, and rather the reduction of the anti-bonding character of neighbor next neighbor Cu-Si interactions as well as effects of electron correlation may serve as rationalization. For the NMR-spectroscopic characterization of the selenium containing anions 2D $^1H/^{77}Se$- and $^1H/^{29}Si$-HMQC methods were used.

INTRODUCTION

Compounds containing thiophilic group 11 metal centers M (M = Cu, Ag, Au) and chalcogenolate based ligands $[ER]^-$ (E = S, Se, Te) constitute a class of compounds mainly dominated by oligomeric and polymeric structural motives.[1,2] Low molecular neutral coinage metal chalcogenolate complexes are rarely observed, and only realizable for bulky and stabilizing substituents attached to the chalcogen atom and strong heteroligands attached to the highly thiophilic coinage metal atom. The formation of higher aggregated oligomers and higher dimensional compounds with increasing steric accessibility of the chalcogen atom can be considered a general trend.[1,3] Though, low-molecular chalcogenide- and chalcogenolate compounds are of great interest: they represent molecular building blocks of solid state materials (as the parental unit for Cu_2S: [(Imes-Cu)$_2$(μ^2S)]),[4] metastable intermediates for the formation of materials (as the ZnS-precursors [(tmeda)Zn($SSiMe_3)_2$]),[5] or representative model systems for metaloproteines (as the tetranuclear "[4Cu:2S]" cluster in the active side of N_2O-reductase).[6] The importance of the understanding of bonding situations in metalloproteins is quite illustrative: while copper is the second most abundant transition metal after iron found in organisms,[7] silver compounds are commonly used as biocides that are not harmful for mammals but toxic for microorganisms,[8] and gold-based low-molecular chalcogenolate compounds are used for pharmaceutical purposes in commercially established drugs, e. g. for the therapy of arthritis.[9]

Complexes containing trimethylsilylchalcogenolate moieties $ESiMe_3$ (E = S, Se, Te) can be used as starting point for the preparation of coinage metal chalcogenide clusters with higher complexity or for nanoparticles,[10] that are of interest due to their photoluminescence behaviour.[11,12] The cleavage of the chalcogen trimethylsilyl linkage can be performed with suitable desilylating agents, like metal acetates, or thermal induced intra- or intermolecular elimination of $E(SiMe_3)_2$.[5,10,11] Up to now, mononuclear neutral compounds containing a coinage-metal attached E-$SiMe_3$ group are made accessible with phosphine or N-heterocyclic carbene (NHC) auxiliary ligands attached to the linearly coordinated metal center. While the phosphine compounds of the type [R_3P-M-$ESiMe_3$] are quite difficult to handle,[13] the NHC analogues [NHC-M-$ESiMe_3$], and the known representatives with cyclic(alkyl)(amino)carbenes (CAAC) [CAAC-M-$ESiMe_3$] are of reasonable stability and allow selective reactions to yield e. g. defined ternary cluster molecules with tunable optical properties.[11,14,15] NHC protected coinage metal halogenido complexes have also been used as precursors for the steady preparation of coinage metal chalcogenide materials M_2E.[16] These materials gain growing interest due to their negligible toxicity and their potential to act as e. g. IR emitters and superionic conductors.[17,18]

Herein we introduce an ionic approach applying low molecular coinage metalate anions that are attached to the functional $ESiMe_3$ moiety. By charge repulsion the necessity of an auxiliary ligand to inhibit condensation and precipitation of high-lattice energy binary metal chalcogenide is by-passed. The synthesis and the crystallographically determined molecular structures of

the first homoleptic coinage metalate complexes in the organic salts Cat $[M(ESiMe_3)_2]$ (**1**: Cat = Ph_4P^+, M = Cu, E = S; **2**: Cat = Ph_4P^+, M = Ag, E = S; **3**: Cat = PPN^+ or Ph_4P^+, M = Ag, E = S; **4**: Cat = PPN^+ or Ph_4P^+, M = Cu, E = Se; **5**: Cat = PPN^+ or Ph_4P^+, M = Ag, E = Se; **6**: Cat = PPN^+ or Ph_4P^+, M = Au, E = Se). The title compounds constitute a complete set of homologue metastable group 11-chalcogenolate compounds with two functional E-$SiMe_3$ moieties, that can be handled at ambient temperature for some time and stored for extended periods of time at –30 °C. Negatively charged homoleptic metalate salts $Cat[M(ESiMe_3)_n]^-$ (M = Ga, In, Zn, Sn(II), E = S, Se) with E-$SiMe_3$ moieties are investigated to act as CIGS- and CZTS-type materials precursors in our working group.

RESULTS AND DISCUSSION

Syntheses, XRD Structures, and DFT Calculations

The structures of a number of linearly coordinated mononuclear anions of the type $[M(ER)_2]^-$ (M = Cu, Ag, Au; E = S, Se, Te; R= bulky organic ligand) are known.[1,19] The intermolecular charge repulsion prevents aggregation, which is observed for corresponding neutral compounds. However, depending on the ligands, the formation of higher charged polynuclear oligomeric anions or higher-coordinated coinage metalate centers can be observed.[19]

For the synthesis of the title compounds a route established within our working group was transferred on the coinage metals (Scheme 1). First, an organic chloride salt Cat Cl is added to the metal chlorides MCl (M = Cu(I), Ag(I), Au(I)) in tetrahydrofuran, yielding the chlorometalates $Cat[MCl_2]$. A twofold elimination of lithium chloride is performed by adding two equivalents of the metalated $ESiMe_3$-precursor $LiESiMe_3$[20] in tetrahydrofuran at –78 °C. After slowly warming the reaction mixture to ambient temperature in an overnight fashion, and removal of all volatiles *in vacuo*, the product can be extracted with diethyl ether. At this point it we want to point out, that the yields obtained by recrystallization are best for all species with Ph_4P^+ cation (supporting information). However, the usage of PPN^+ was indicated to grow suitable single crystals for X-ray analysis.

Scheme 1. General LiCl elimination route to prepare the title compounds $Cat[M(ESiMe_3)_2]$ from the corresponding chlorometalates $Cat[MCl_2]$ and $LiESiMe_3$.

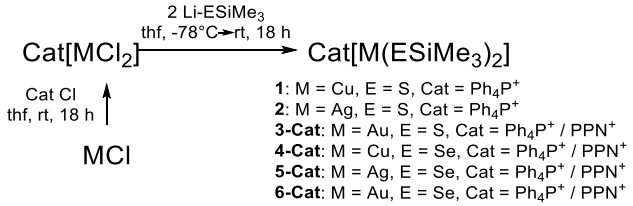

All title compounds crystallize in the triclinic space group P_{-1} with four ion pairs per unit cell (Figure 1 to Figure 6). As an exception, $Ph_4P[Cu(SSiMe_3)_2]$ (**1**) has only two ion pairs per unit cell.

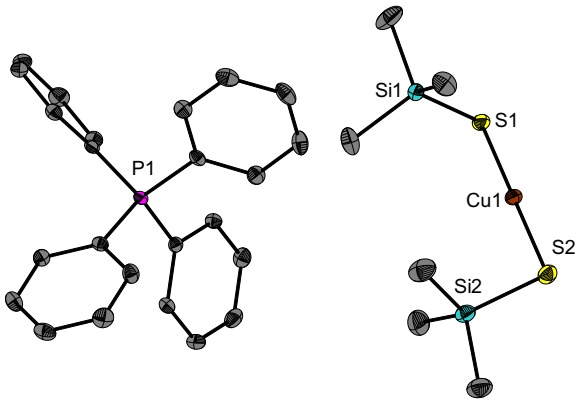

Figure 1. Molecular structure of $Ph_4P[Cu(SSiMe_3)_2]$ (**1**). Protons are neglected for clarity. Ellipsoids are shown at 50% level. Selected bond lengths (Å) and angles (°) of the anion in **1**: Cu1-S1 2.1412(6), Cu1-S2 2.1475(6), S1-Si1 2.1081(8), S2-Si2 2.1129(7), S1-Cu1-S2 176.63(2), Cu1-S1-Si1 100.34(2), Cu1-S2-Si2 97.14(2), Si1-S1-S2-Si2 48.86(3).

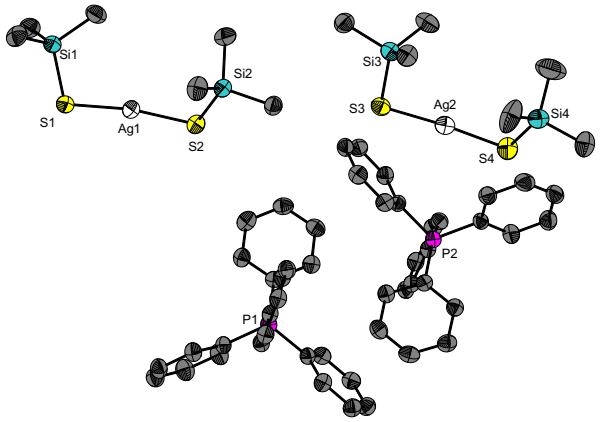

Figure 2. Molecular structure of $Ph_4P[Ag(SSiMe_3)_2]$ (**2**). Protons are neglected for clarity. Ellipsoids are shown at 50% level. Selected bond lengths (Å) and angles (°) of the crystallographically inequivalent anions in the reduced cell in **2**: Ag1-S1 2.341(1), Ag1-S2 2.356(1), S1-Si1 2.111(1), S2-Si2 2.108(2), S1-Ag1-S2 171.70(4), Ag1-S1-Si1 106.28(5), Ag1-S2-Si2 98.59(5), Si1-S1-S2-Si2 51.27(7), Ag2-S3 2.357(1), Ag2-S4 2.368(1), S3-Si3 2.118(2), S4-Si4 2.099(2), S3-Ag2-S4 175.56(4), Ag2-S3-Si3 100.07(5), Ag2-S4-Si4 98.19(6), Si3-S3-S4-Si4 27.82(7).

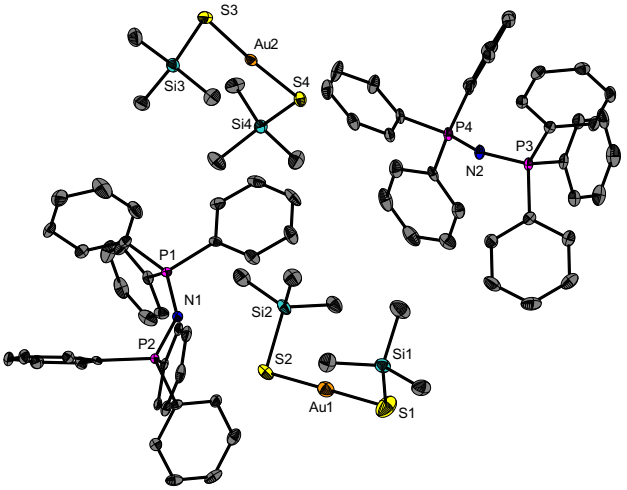

Figure 3. Molecular structure of PPN[Au(SSiMe$_3$)$_2$] (**3-PPN**). Protons are neglected for clarity. Ellipsoids are shown at 50% level. Selected bond lengths (Å) and angles (°) of the two crystallographically inequivalent anions in the reduced cell in **3**: Au1-S1 2.289(1), Au1-S2 2.308(1), S1-Si1 2.107(2), S2-Si2 2.112(2), S1-Au1-S2 178.79(4), Au1-S1-Si1 103.80(5), Au1-S2-Si2 94.71(5), Si1-S1-S2-Si2 62.15(6), Au2-S3 2.299(1), Au2-S4 2.2985(9), S3-Si3 2.119(1), S4-Si4 2.119(1), S3-Au2-S4 176.52(3), Au2-S3-Si3 100.38(5), Au2-S4-Si4 102.44(4), Si3-S3-S4-Si4 77.21(5).

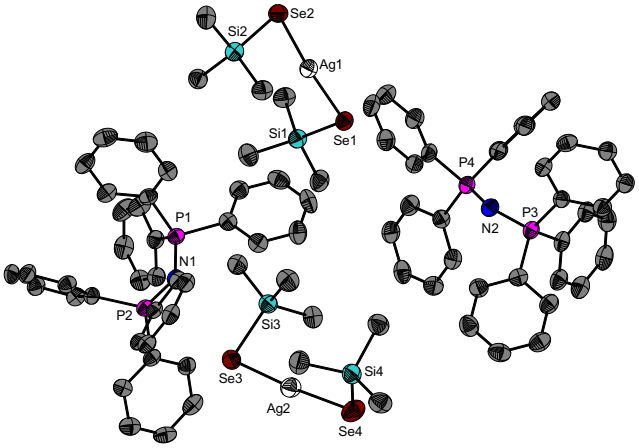

Figure 5. Molecular structure of PPN[Ag(SeSiMe3)2] (**5-PPN**). Protons are neglected for clarity. Ellipsoids are shown at 50% level. Selected bond lengths (Å) and angles (°) of the crystallographically inequivalent anions in the reduced cell in **5**: Ag1-Se1 2.4487(6), Ag1-Se2 2.4498(7), Se1-Si1 2.254(1), Se2-Si2 2.253(2), Se1-Ag1-Se2 175.29(2), Ag1-Se1-Si1 101.79(4), Ag1-Se2-Si2 96.68(4), Si1-Se1-Se2-Si2 73.82(5), Ag2-Se3 2.4745(6), Ag2-Se4 2.4521(8), Se3-Si3 2.247(2), Se4-Si4 2.256(2), Se3-Ag2-Se4 174.66(3), Ag2-Se3-Si3 87.93(4), Ag2-Se4-Si4 100.25(5), Si3-Se3-Se4-Si4 74.75(6).

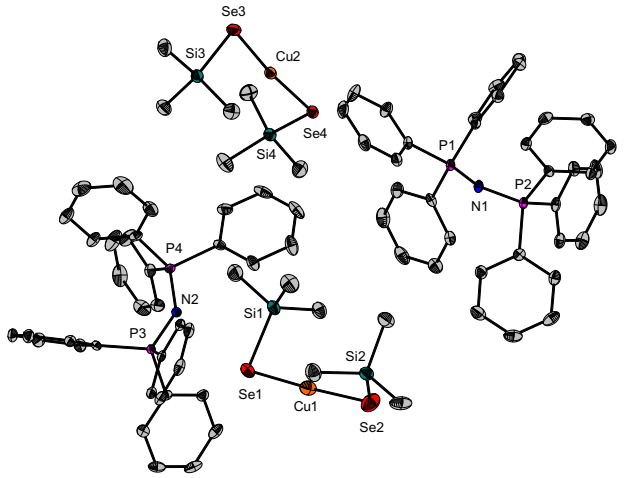

Figure 4. Molecular structure of PPN[Cu(SeSiMe$_3$)$_2$] (**4-PPN**). Protons are neglected for clarity. Ellipsoids are shown at 50% level. Selected bond lengths (Å) and angles (°) of the crystallographically inequivalent anions in the reduced cell in **4**: Cu1-Se1 2.2836(6), Cu1-Se2 2.2613(7), Se1-Si1 2.247(1), Se2-Si2 2.2540(9), Se1-Cu1-Se2 174.98(3), Cu1-Se1-Si1 88.30(3), Cu1-Se2-Si2 101.24(3), Si1-Se1-Se2-Si2 77.45(3), Cu2-Se3 2.2653(6), Cu2-Se4 2.2634(6), Se3-Si3 2.253(1), Se4-Si4 2.2561(8), Se3-Cu2-Se4 174.16(2), Cu2-Se3-Si3 99.20(3), Cu2-Se4-Si4 101.97(3), Si3-Se3-Se4-Si4 75.97(3).

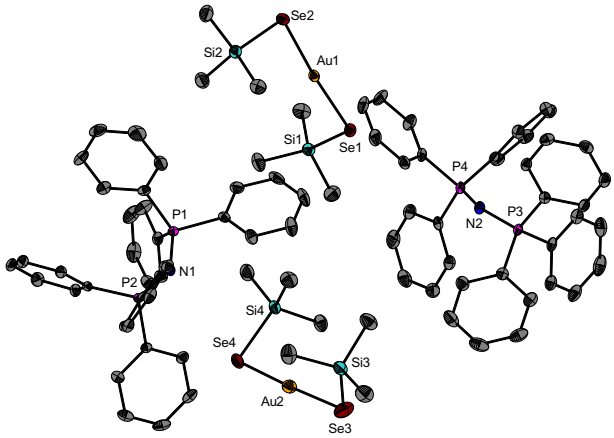

Figure 6. Molecular structure of PPN[Au(SeSiMe$_3$)$_2$] (6-PPN). Protons are neglected for clarity. Ellipsoids are shown at 50% level. Selected bond lengths (Å) and angles (°) of the crystallographically inequivalent anions in the reduced cell in **6**: Au1-Se1 2.3980(6), Au1-Se2 2.4015(6), Se1-Si1 2.255(1), Se2-Si2 2.256(1), Se1-Au1-Se2 175.46(2), Au1-Se1-Si1 101.36(3), Au1-Se2-Si2 97.68(3), Si1-Se1-Se2-Si2 75.21(4), Au2-Se3 2.3956(7), Au2-Se4 2.4139(6), Se3-Si3 2.258(1), Se4-Si4 2.255(1), Se3-Au2-Se4 176.14(3), Au2-Se3-Si3 100.79(3), Au2-Se4-Si4 90.29(3), Si3-Se3-Se4-Si4 72.49(4).

With exception of the x-ray structural data of **1** containing only one ion pair in the reduced cell, all other unit cells reported here contain two crystallographically independent ion pairs. The structural parameters such as the E-M-E angles or the Si-E-E-Si dihedral angles of crystallographically independent anions differ quite noticeably for the thiolatoargentate **2**, as shown in **Table 1**.

Table 1. Comparison of structural parameters of the homologue metalate anions in the title compounds $Ph_4P[Cu(SSiMe_3)_2]$ (**1**), $Ph_4P[Ag(SSiMe_3)_2]$ (**2**), $PPN[Au(SSiMe_3)_2]$ (**3-PPN**), $PPN[Cu(SeSiMe_3)_2]$ (**4-PPN**), $PPN[Ag(SeSiMe_3)_2]$ (**5-PPN**), and $PPN[Au(SeSiMe_3)_2]$ (**6-PPN**).

Anion (M/E)	M-E/Å	E-Si/Å	E-M-E/°	M-E-Si/°	Si-E-E-Si/°
1 (Cu/S)	2.1412(6)-2.1475(6)	2.1081(8)-2.1129(7)	176.63(2)	97.14(2)-100.34(2)	48.86(3)
2 (Ag/S)	2.341(1)-2.368(1)	2.099(2)-2.118(2)	171.70(4)-175.56(4)	98.19(6)-106.28(5)	27.82(7)-51.82(7)
3 (Au/S)	2.289(1)-2.308(1)	2.107(2)-2.119(1)	178.79(4)-176.52(3)	94.71(5)-103.80(5)	62.15(6)-77.21(5)
4 (Cu/Se)	2.2613(7)-2.2836(6)	2.247(1)-2.2561(8)	174.16(2)-174.98(3)	88.30(3)-101.97(3)	75.97(3)-77.45(3)
5 (Ag/Se)	2.4487(6)-2.4745(6)	2.247(2)-2.256(2)	174.66(3)-175.29(2)	87.93(4)-101.79(4)	73.82(5)-74.75(6)
6 (Au/Se)	2.3956(7)-2.4139(6)	2.255(1)-2.258(1)	175.46(2)-176.14(3)	90.29(3)-101.36(3)	72.49(4)-75.21(4)

The experimentally determined torsional angle Si-S-S-Si, α, seemed to be surprising. Though, two known organothiolate coinage metalates $[Cu(StBu)_2]^{-}$[21] and $[Au(SeCF_3)_2]^{-}$[22] also show this *gauche* conformation. Contrastingly, adamantylthiolatocuprate $[Cu(SAd)_2]^{-}$[23] displays an anti-conformation in the solid state. In sharp contrast to these known organothiolates, all of the title compounds of this report spontaneously precipitate monovalent coinage metal chalcogenides from THF or other organic solutions, when methanol or traces of water are added, indicated by the precipitation of dark solids. The formation of Ag_2S by defined methanolysis of **2** is described in the Supporting Information. This opens the perspective for ligand L controlled co-precipitation of $LCu_xAg_yAu_zS_nSe_m$ nanoparticles from homogeneous organic solutions under adjustable protolytic conditions difficult to provide with other precursor molecules.

DFT calculations

For a deeper insight into the phenomenon connected with the gauche-like conformation, the variation of this coordinate was investigated in density functional calculations employing TURBOMOLE.[24] with the TPSS functional[25] and dhf-TZVP basis sets.[26] Structure optimizations were carried out keeping α fixed at -10, 0-,10…270° and optimizing all other coordinates. This was done for M = Cu, Ag, Au and E=S, Se in $[M(ESiMe_3)_2]^{-}$ as well as for the model compound $[Cu(SCl)_2]^{-}$. The resulting energy curves are shown in Figure 7.

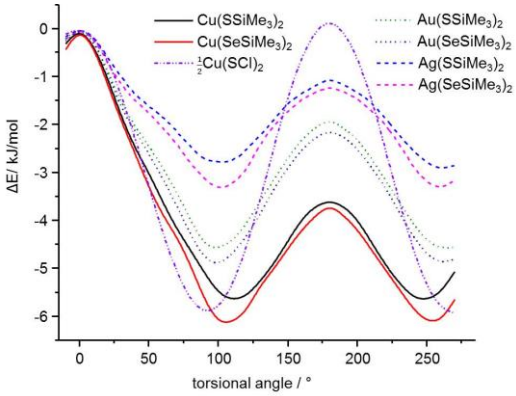

Figure 7. Energy as a function of the torsional angle Si-E-E-Si, *α*, of $[M(ESiMe_3)_2]^{-}$ and Cl-E-E-Cl for $[Cu(SCl)_2]^{-}$, respectively. Energies are given relative to the eclipsed configuration (0°). For $[Cu(SCl)_2]^{-}$, the energies are divided by a factor of two.

The experimentally observed preference of torsional angles in the range of about 100° and 250° is visible also in the calculated energy curves, but it is not very large. The maximum difference amounts to 6 kJ/mol and is found between α=0° and α=100° for $[Cu(SeSiMe_3)_2]^{-}$. For a given M, the results for S and Se are very similar. The impact of the choice of M to the shape of the curves is larger. The energy difference between α=0° and α=100° decreases from Cu via Au to Ag, which is in line with the sequence of the accessibility of the d shell for chemical bonds and thus points to a rationalization involving angle-dependent (π-type) interactions of the d(M) orbitals and the p(E) orbitals. Due to the smallness of the energetic preference of α=100°, the net effect is expected to be small for all compounds. We thus first discuss the electronic structure of the model compound $[Cu(SCl)_2]^{-}$, which shows a similar shape for E(α), but with energy differences between α=0° and α=100° being twice as large as for $[Cu(SeSiMe_3)_2]^{-}$. A Walsh-type diagram for the nine highest occupied MOs and angles between 0° and 90° is shown in Figure 8.

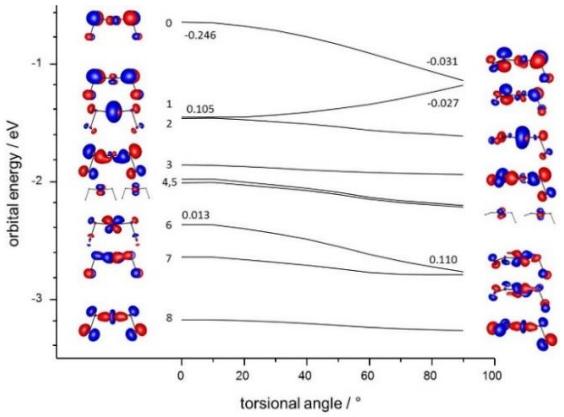

Figure 8. Orbital energies of the highest occupied MOs as a function of the torsional angle Cl-S-S-Cl, α, of $[Cu(SCl)_2]^{-}$. Orbitals are plotted for α=0° (left) and α=90° (right). The numbers in the diagram (-0.246 etc.) denote the sum of the Mulliken overlap population between Cu and the two S atoms (negative numbers indicate antibonding character).

For HOMO, HOMO-1 and HOMO-6 a significant influence of α on the orbital energies is observed. For α=0°, the HOMO is a strongly anti-bonding combination (Mulliken overlap population OP=-0.246 between Cu and S) of d_{zx}(Cu) and p_x(S);

HOMO-1 is a very weakly bonding combination of d_{xy}(Cu) and p_x(S). For α=90°, both orbitals are essentially non-bonding, which in sum increases the overlap and thus the bond strength. This is enhanced by HOMO-6 (d_{yz}(Cu) with p_z(S)), which changes from non-bonding to weakly bonding, accompanied with a lowering of the orbital energy. For this model compound, the preference of α=90° thus is rationalized by the change of the π interactions in these three MOs, in particular by the decrease of the anti-bonding character of the HOMO, and reflected by an increase (α=90° vs. α=0°) of OP by 0.180 for the sum of these MOs. When summing over all MOs, the OP changes by 0.121 (from 1.143 to 1.264), which shows that the dominant changes indeed arise from the three MOs listed above. For completeness we note that the interaction between Cu and the two Cl atoms is weakly antibonding and only slightly dependent from α: OP(0°)=-0.134, OP(90°)=-0.152.

For the original compound $[Cu(SSiMe_3)_2]^-$ matters are by far less obvious (shown in the supporting information, Figure S3). Like for the model compound, the anti-bonding character of the HOMO, which is similar to that of the model compound, is reduced, but this stabilization is compensated by changes in several other MOs. As a consequence, the OPs between Cu and the two S atoms are identical for α=90° and α=0°, 1.195. Here, π interactions between Cu and S alone do not rationalize the (slight) energetic preference for α=90°. An explanation rather may be found in the neighbor next neighbor interactions and further in effects of electron correlation, which are beyond the one-electron picture of orbital considerations. This is supported by the fact that in DFT, where these effects are included, the energy difference between α=0° and α=90° is 5.6 kJ/mol, whereas at Hartree-Fock level, where such effects are neglected, it is only 2.3 kJ/mol.

NMR-spectroscopy

The thiolatometalates **1**-**3** were investigated by ^{1}H-, ^{13}C-, and ^{29}Si-NMR spectroscopy in d^8-THF at ambient temperature. The ^{1}H-NMR signals for the metalate anions range from 0.12 ppm for the argentate **2**, to 0.13 ppm for both, the aurate **3-Ph$_4$P** and the cuprate **1**. The ^{13}C-NMR signals range from 7.4 ppm for the aurate **3-Ph$_4$P** to 8.6 ppm for the argentate **2**, while the chemical shift for the cuprate **1** is at 8.3 ppm. A trend is observed in ^{29}Si-NMR spectra showing an increasingly pronounced low field shift with growing molecular weight. It ranges from 5.2 ppm for the cuprate **1** to 7.7 ppm for the aurate **3-Ph$_4$P** (Figure 9).

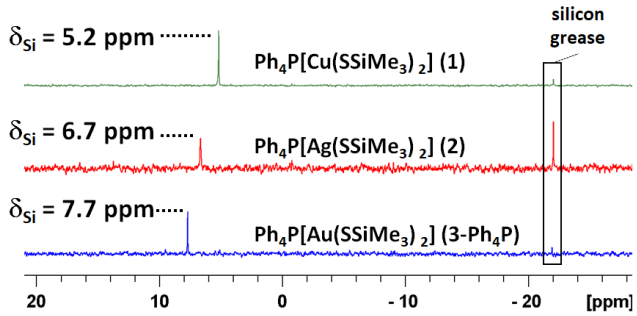

Figure 9. ^{29}Si-NMR (59.7 MHz for **1** and **2**, 99.4 MHz for 3, d^8-THF) spectra of the thiolatometalates $Ph_4P[Cu(SSiMe_3)_2]$ (**1**, top row), $Ph_4P[Ag(SSiMe_3)_2]$ (**2**, middle row), and $Ph_4P[Au(SSiMe_3)_2]$ (**3-Ph$_4$P**, bottom row).

While ^{1}H- and ^{13}C-NMR spectra were routinely recorded for the selenometalates **4**-**6**, detection of ^{29}Si- and the ^{77}Se signals turned out to be very difficult. We therefore applied two-dimensional ^{1}H-^{29}Si-HMQC[27] and ^{1}H-^{77}Se-HMQC methods at 0 °C utilizing the gradient selective coherence transfer from proton to the corresponding heteronuclei. At 0 °C, the ^{1}H-NMR shifts of the selenolatometalate anions are quite similar, ranging from 0.27 ppm for the cuprate **4-Ph$_4$P** as well as 0.31 ppm for the aurate **6-Ph$_4$P**, and 0.30 ppm for the argentate **4-Ph$_4$P**. However, clear identification is possible by the ^{29}Si-NMR shifts that are accessible by the 2D-NMR method quite easily. The ^{29}Si-NMR shifts range from 0.2 ppm for the cuprate **4-Ph$_4$P** to 2.4 ppm for the aurate **6-Ph$_4$P**, while the signal for the argentate **5-Ph$_4$P** is at 1.6 ppm (Figure 10).

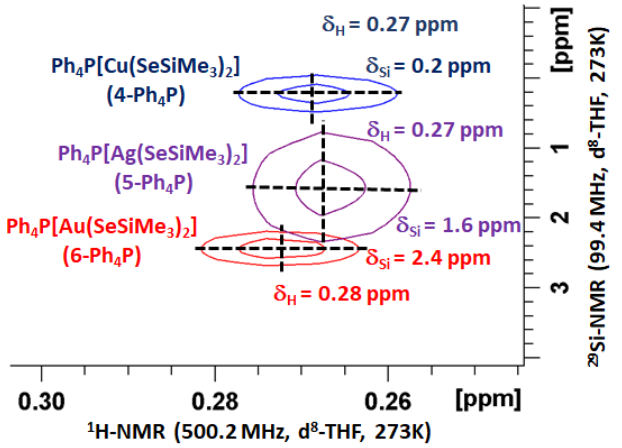

Figure 10. ^{1}H-^{29}Si-HMQC-NMR (99.4 MHz, d^8-THF) spectra of the selenolate compounds **4-Ph$_4$P** - **6-Ph$_4$P** at 273K.

The specific ^{77}Se-NMR signals for the selenolatometalates **4-Ph$_4$P** - **6-Ph$_4$P** in the ^{1}H-^{77}Se-HMQC-NMR spectra also allow an identification, though the does not show a correlation between the molecular weight as for the corresponding ^{29}Si-NMR signals. The most high-field shifted ^{77}Se-NMR signal (–502.2 ppm) is observed for the argentate **5-Ph$_4$P**, while the aurate **6-Ph$_4$P** shows the most low-field shifted signal (–377.9 ppm). The ^{77}Se-NMR signal of the cuprate **4-Ph$_4$P** is at –469.4 ppm (Figure 11).

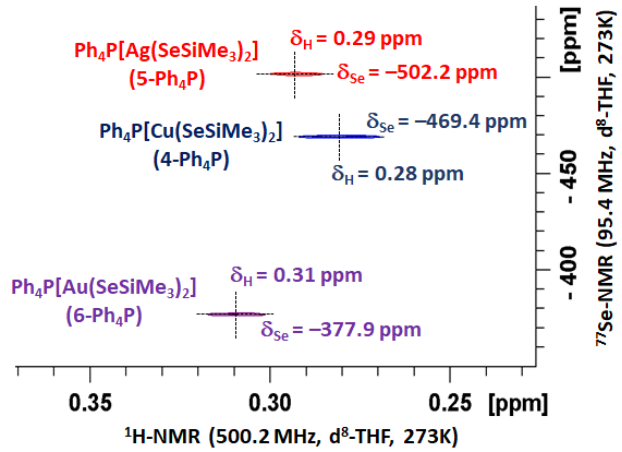

Figure 11. ^{1}H-^{77}Se-HMQC-NMR (500.2 MHz, d^8-THF) spectra of the selenolate compounds **4-Ph$_4$P** - **6-Ph$_4$P** at 273K.

Conclusion

We described the syntheses and crystallographically determined molecular structures of homoleptic trimethylsilylthiolato metalate anions $[M(SSiMe_3)_2]^-$ (M = Cu (**1**), Ag (**2**), Au (**3**)) and corresponding trimethylsilylselenolatometalates $[M(SSiMe_3)_2]^-$ (M = Cu (**4**), Ag (**5**), Au (**6**)) comprising Ph_4P^+ or PPN^+ cations. All metalate anions exhibit a linear coordination with an unexpected *gauche*-like conformation. By DFT calculations the preference of this conformation could be traced back on electronic effects. Furthermore, 2D HMQC methods were applied to detect the otherwise non observable NMR shifts of the ^{29}Si- and ^{77}Se-nuclei of the selenolate compounds **4-Ph$_4$P**, **5-Ph$_4$P**, and **6-Ph$_4$P**. We are convinced, that in future research, the unprecedented metastable chalcogenido metalates disclosed here will qualify as valuable precursors for multinary coinage metal chalcogenide nanoparticle or cluster synthesis from organic solution.

Experimental Section

All preparative operations were conducted by using standard Schlenk techniques and freshly dried solvents. All solvents were dried according to common procedures[28] and passed through columns of aluminium oxide, R3-11G-catalyst (BASF) or stored over molecular sieves (3 Å or 4 Å). Other reagents were used as received unless stated otherwise. $S(SiMe_3)_2$ and $Se(SiMe_3)_2$ were prepared analogously according to the literature known synthesis of $S(SiMe_3)_2$,[29] $LiESiMe_3$ are known precursors for the introduction of E-$SiMe_3$ moieties.[20] We prepared these compounds in a slightly simplified way, as described in the experimental section.

Elemental analyses (C, H, N, S) were carried out by the service department for routine analysis with a vario MICRO cube (Elementar). Samples for the elemental analysis were weighted into tin capsules inside a nitrogen filled glovebox. ^{1}H and proton decoupled ^{13}C-NMR spectra were recorded in automation with a Bruker Avance II 300 spectrometer, ^{29}Si- and ^{77}Se-NMR spectra were recorded by the service department for NMR analyses with a Bruker Avance II HD 300, DRX 400 or Avance III 500 spectrometer. All spectra were recorded at ambient temperature, unless stated otherwise. ^{1}H- and ^{13}C-NMR spectra were calibrated using residual proton signals of the solvent (THF-d^8: δ_H 3.58 & 1.72 ppm, δ_C 67.21 & 25.31 ppm). ^{29}Si-NMR spectra were referenced externally ($SiMe_4$: δ_{Si} 0.00 ppm) just as ^{77}Se-NMR spectra (Me_2Se δ_{Se} 0.00 ppm).

At this point only one representative synthesis of $Ph_4P[Cu(SSiMe_3)_2]$ (**1**) is shown. Please refer to the supporting information for detailed synthetic procedures of all the title compounds.

Ph$_4$P[Cu(SSiMe$_3$)$_2$] (1): A mixture of $Ph_4P[Cl]$ (0.122 g, 0.32 mmol, 1.00 eq.) and CuCl (0.032 g, 0.32 mmol, 1.00 eq.) was suspended in thf (10 mL) and stirred for 18 h at room temperature to obtain a suspension of $Ph_4P[CuCl_2]$. In a separate flask a solution of $S(SiMe_3)_2$ (0.119 g, 0.67 mmol, 2.1 eq.) in thf (5 mL) was stirred at 0 °C and treated with a 2.9M solution of *n*-BuLi in hexane (0.22 mL, 0.64 mmol, 2.0 eq.). The pale-yellow reaction mixture was stirred for 30 min. at 0 °C and for a further 30 min. at room temperatures. All volatiles were removed in fine vacuum until $LiSSiMe_3$ is obtained as a colorless waxy solid and remaining excess of $S(SiMe_3)_2$ is removed quantitatively. The residue is diluted in THF (10 mL) and added dropwise to the previously prepared suspension of $Ph_4P[CuCl_2]$ at –78 °C. The reaction mixture was slowly allowed to obtain room temperature within 18 h. All volatiles were removed in fine vacuum and the residue suspended with diethyl ether (60 mL) and filtrated. The filtrate was stored at –30 °C to obtain the target compound as colorless blocks. The mother liquor can be reused for a further extraction cycle to obtain **1** as colorless crystals with a yield of 0.168 g (0.27 mmol, 84%). **^{1}H-NMR (300.3 MHz, d^8-THF)**: δ = 7.93-7.83 (m, 20 H, $(H_5C_6)_4P^+$), 0.13 (s, 18 H, $[Cu(SSi(CH_3)_3)_2]^-$) ppm. **^{13}C-NMR (75.5 MHz, d^8-THF):** δ = 136.1 (d, $^4J_{PC}$ = 3.2 Hz, $[(HC(CH_2)_2(CH_2)_2C)_4P]^+$)), 135.6 (d, $^3J_{PC}$ = 10.4 Hz, $[(HC(CH_2)_2(CH_2)_2C)_4P]^+$), 131.3 (d, $^2J_{PC}$ = 13.2 Hz, $[(HC(CH_2)_2(CH_2)_2C)_4P]^+$), 118.9 (d, $^1J_{PC}$ = 98.3 Hz, $[(HC(CH_2)_2(CH_2)_2C)_4P]^+$), 8.3 (s, $[Cu(SSi(CH_3)_3)_2]^-$) ppm. **^{29}Si (59.7 MHz, d^8-THF):** δ = 5.2 (s, $[Cu(SSi(CH_3)_3)_2]^-$) ppm. **Elemental analysis:** Calcd. for $C_{30}H_{38}Cu_1P_1S_2Si_2$: C, 58.7; H, 6.2; S, 10.5. Found: C, 58.6; H, 5.8; S, 10.3.

ASSOCIATED CONTENT

Experimental procedures, Crystallographic detail, NMR spectra, the thermal decomposition behavior of **1**, supporting DFT calculation and a detailed description of the Ag_2S precipitation by methanolysis of **2**.

AUTHOR INFORMATION

Corresponding Author

* E-Mail: JSU@staff.uni-marburg.de

Author Contributions

All authors have given approval to the final version of the manuscript.

Funding Sources

DFG (SPP 1708 ‘Material Synthesis near room Temperature’)

ACKNOWLEDGMENT

We thank the German research fund DFG and its priority program SPP 1708 ‘Material Synthesis near room Temperature’ for financial support. Bertram Peters is thanked for his support with PXRD measurements.

REFERENCES

(1) Veselska, O.; Demessence, A. d10 coinage metal organic chalcogenolates: From oligomers to coordination polymers. *Coord. Chem. Rev.* **2018**, *355*, 240–270.

(2) Krebs, B.; Henkel, G. Transition-Metal Thiolates: From Molecular Fragments of Sulfidic Solids to Models for Active Centers in Biomolecules. *Angew. Chem. Int. Ed.* **1991**, 30, 769-788.

(3) Polgar, A. M.; Corrigan, J. F. Recent advances in the self-assembly of polynuclear metal–selenium and –tellurium compounds from 14–16 reagents. *Physical Sciences Reviews*, 4(2), pp. -. Retrieved 13 Aug. 2019, from doi:10.1515/psr-2017-0126.

(4) Zhai, J.; Filatov, A. S.; Hillhouse, G. L.; Hopkins, M. D. Synthesis, structure, and reactions of a copper-sulfido cluster comprised of the parent Cu2S unit: {(NHC)Cu}$_2$(μ-S). *Chem. Sci.* **2016**, *7*, 589–595.

(5) DeGroot, M. W.; Khadka, C.; Rösner, H.; Corrigan, J. F. ZnS and ZnSe Nanoparticles via Solid-State and Solution Thermolysis of Zinc Silylchalcogenolate Complexes. *J. Clust. Sci.* **2006**, *17*, 97–110.

(6) Pomowski, A.; Zumft, W. G.; Kroneck, P. M. H.; Einsle, O. N_2O binding at a 4Cu:2S copper-sulphur cluster in nitrous oxide reductase. *Nature* **2011**, *477*, 234–237.

(7) Festa, R. A.; Thiele, D. J. Copper: An essential metal in biology. *Current biology:CB* **2011**, *21*, R877-83.

(8) Silver, S.; Le Phung, T.; Silver, G. Silver as biocides in burn and wound dressings and bacterial resistance to silver compounds. *J. Ind. Microbiol. Biotechnol.* **2006**, *33*, 627–634.

(9) Shaw, C. F. Gold-Based Therapeutic Agents. *Chem. Rev.* **1999**, *99*, 2589–2600.

(10) DeGroot, M. W.; Corrigan, J. F. Metal-Chalcogenolate Complexes with Silyl Functionalities: Synthesis and Reaction Chemistry. *Z. anorg. allg. Chem.* **2006**, *632*, 19–29.

(11) a) Polgar, A. M.; Weigend, F.; Zhang, A.; Stillman, M. J.; Corrigan, J. F. A N-Heterocyclic Carbene-Stabilized Coinage Metal-Chalcogenide Framework with Tunable Optical Properties. *J. Am. Chem. Soc.* **2017**, *139*, 14045–14048. b) Polgar, A. M.; Zhang, A.; Mack, F.; Weigend, F.; Lebedkin, S.; Stillman, M. J.; Corrigan, J. F. Tuning the Metal/Chalcogen Composition in Copper(I)-Chalcogenide Clusters with Cyclic (Alkyl)(amino)carbene Ligands. *Inorg. Chem.* **2019**, *58*, 3338–3348.

(12) Gimeno, M. C.; Laguna, A. Chalcogenide centred gold complexes. *Chem. Soc. Rev.* **2008**, *37*, 1952–1966.

(13) Borecki, A.; Corrigan, J. F. New copper and silver trimethylsilylchalcogenolates. *Inorg. Chem.* **2007**, *46*, 2478–2484.

(14) Azizpoor Fard, M.; Levchenko, T. I.; Cadogan, C.; Humenny, W. J.; Corrigan, J. F. Stable -ESiMe$_3$ Complexes of Cu(I) and Ag(I) (E=S, Se) with NHCs: Synthons in Ternary Nanocluster Assembly. *Chem. Eur. J.* **2016**, *22*, 4543–4550.

(15) Fard, M. A.; Weigend, F.; Corrigan, J. F. Simple but effective: Thermally stable Cu-ESiMe$_3$ via NHC ligation. *Chem. Commun.* **2015**, *51*, 8361–8364.

(16) Lu, H.; Brutchey, R. L. Tunable Room-Temperature Synthesis of Coinage Metal Chalcogenide Nanocrystals from N-Heterocyclic Carbene Synthons. *Chem. Mater.* **2017**, *29*, 1396–1403.

(17) Gui, R.; Jin, H.; Wang, Z.; Tan, L. Recent advances in synthetic methods and applications of colloidal silver chalcogenide quantum dots. *Coord. Chem. Rev.* **2015**, *296*, 91–124.

(18) Reiss, P.; Carrière, M.; Lincheneau, C.; Vaure, L.; Tamang, S. Synthesis of Semiconductor Nanocrystals, Focusing on Nontoxic and Earth-Abundant Materials. *Chem. Rev.* **2016**, *116*, 10731–10819.

(19) Henkel, G.; Krebs, B. Metallothioneins: Zinc, cadmium, mercury, and copper thiolates and selenolates mimicking protein active site features-structural aspects and biological implications. *Chem. Rev.* **2004**, *104*, 801–824.

(20) Taher, D.; Wallbank, A. I.; Turner, E. A.; Cuthbert, H. L.; Corrigan, J. F. Alk-2-ynyl Trimethylsilyl Chalcogenoethers by Nucleophilic Substitution of Propargyl Bromides. *Eur. J. Inorg. Chem.* **2006**, 22, 4616–4620.

(21) Kohner-Kerten, A.; Tshuva, E. Y. Preparation and X-ray characterization of two-coordinate Cu(I) complex of aliphatic thiolato ligand: Effect of steric bulk on coordination features. *J. Organomet. Chem.* **2008**, *693*, 2065–2068.

(22) Naumann, D.; Tyrra, W.; Quadt, S.; Buslei, S.; Pantenburg, I.; Schäfer, M. Bis(trifluoromethylselenato(0))metallates(I) of Silver and Gold, $[M(SeCF_3)_2]^-$ (M = Ag, Au). *Z. anorg. allg. Chem.* **2005**, *631*, 2733–2737.

(23) Fujisawa, K.; Imai, S.; Kitajima, N.; Moro-oka, Y. Preparation, Spectroscopic Characterization, and Molecular Structure of Copper(I) Aliphatic Thiolate Complexes. *Inorg. Chem.* **1998**, *37*, 168–169.

(24) TURBOMOLE 7.3, TURBOMOLE GmbH **2018**. University of Karlsruhe and Forschungszentrum Karlsruhe, 1989-2007, TURBOMOLE GmbH since 2007.

(25) Tao, J. M.; Perdew, J. P.; Staroverov, V. N.; Scuseria, G. E. Climbing the density functional ladder: Nonempirical meta-generalized gradient approximation designed for molecules and solids. *Phys. Rev. Lett.* **2003**, *91*, 146401.

(26) Weigend, F.; Baldes, A. Segmented contracted basis sets for one- and two-component Dirac-Fock effective core potentials. *J. Chem. Phys.* **2010**, *133*, 174102.

(27) Provera, S.; Davalli, S.; Raza, G. H.; Contini, S.; Marchioro, C. Long-range two-dimensional ^{1}H-^{29}Si heteronuclear shift correlation using gradients. Application to tetra-TMS-α-O-methyl-D-glucopyranose and tetra-TES-α-O-methyl-D-glucopyranose. *Magn. Reson. Chem.* **2001**, *39*, 38–42.

(28) Armarego, W. L. F.; Perrin, D. D. *Purification of laboratory chemicals*, 4th ed., reprint; Butterworth-Heinemann: Oxford, 2002.

(29) So, J.-H.; Boudjouk, P. Convenient Syntheses of Hexamethyldisilathiane and Tetramethyldisilathiane. *Synthesis* **1989**, 4, 306–307.

SYNOPSIS TOC. The syntheses and the crystallographically determined molecular structures of the organic salts Cat[M(ESiMe$_3$)$_2$] (M = Cu, Ag, Au; E = S, Se; Cat = Ph_4P^+ or PPN^+) are presented. The homoleptic coinage metalate anions present in the title compounds are monomeric and the coinage metal atoms are approximately linearly coordinated by two trimethylsilylchalcogenolate ligands. The silyl moieties of all presented anions show an unexpected *gauche*-like conformation in the solid state, which is investigated by DTF calculations. For the facile investigation of ^{77}Se and ^{29}Si nuclei by NMR, ^{1}H/^{77}Se- and ^{1}H/^{29}Si-HMQC NMR methods are used.

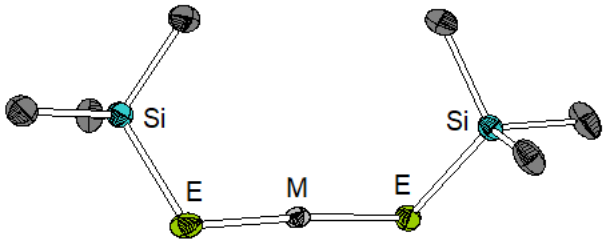

Cat[M(ESiMe$_3$)$_2$]

M = Cu^I, Ag^I, Au^I; E = S, Se

Cat = Ph_4P^+ or PPN^+

Homoleptic linear [ESiMe$_3$]$^-$ coinage metallates

Gauche-like conformation (XRD, DFT)

Selenolates: ^{1}H/^{77}Se HMQC NMR Spectra

A Novel Series of Homoleptic Linear Coinage Metal Trimethylsilylchalcogenolate Complexes Cat[Me_3SiE-M-$ESiMe_3$] (M = Cu, Ag, Au; E = S, Se)

Supporting Information

Jannick Guschlbauer,[a] Tobias Vollgraff,[a] Xiulan Xie, [a] Florian Weigend,[b] Jörg Sundermeyer[a]*

[a] Fachbereich Chemie and Materials Science Center, Philipps-Universität Marburg, Hans-Meerwein-Straße 4, 35043 Marburg.

[b] Karlsruhe Institute of Technology (KIT), Institute of Nanotechnology, Hermann-von-Helmholtz-Platz 1, 76344 Eggenstein-Leopoldshafen, Germany.

Inhalt

1. Experimental Section

Please refer to the main text for the general considerations concerning the methods and devices. All synthetic manipulations must be performed under strict exclusion of moisture and air, as the title compounds decompose quite readily. The title compounds were all prepared analogly. Therefore, a general procedure is described

A mixture of **Cat[Cl]** (**m1**, 1.00 eq.) and **MCl** (**m2**, 1.00 eq.) was suspended in thf (10 mL) and stirred for 18 h at room temperature to obtain a suspension of Cat [MCl_2]. In a separate flask a solution of **E(SiMe$_3$)$_2$** (**m3**, 2.1 eq.) in thf (5 mL) was stirred at 0 °C and treated with a 2.9M solution of *n*-BuLi in hexane (**v1**, 2.0 eq.). The pale-yellow reaction mixture was stirred for 30 min. at 0 °C and for a further 30 min. at room temperatures. All volatiles were removed in fine vacuum until LiESiMe$_3$ is obtained as a colorless (or slightly yellowish for E = Se) waxy solid and remaining excess of E(SiMe$_3$)$_2$ is removed quantitatively. The residue is diluted in thf (10 mL) and added dropwise to the previously prepared suspension of Cat [MCl_2] at –78 °C. The reaction mixture was slowly allowed to obtain room temperature within 18 h. All volatiles were removed in fine vacuum and the residue suspended with diethyl ether (60 mL) and filtrated. The filtrate was stored at –30 °C to obtain the target compound as colourless blocks. The mother liquor can be reused for a further extraction cycle to obtain the target compound as colorless crystals with a yield of **m4**. (For reagents see Table S1, for analytics see **1.1-1.10**).

Table S1: Reagents and yields of the title compounds.

Cat[M(ESiMe$_3$)$_2$]	**Cat[Cl], m1** (m, n)	**MCl, m2** (m, n)	**E(SiMe$_3$)$_2$ m3** (m, n)	**v1** *n*-BuLi [2.9M] (V)	**m4** (m, n, %)
Ph$_4$P[Cu(SSiMe$_3$)$_2$] (**1**)	Ph$_4$P[Cl] 122 mg, 0.32 mmol	CuCl 32 mg, 0.32 mmol	S(SiMe$_3$)$_2$ 119 mg, 0.67 mmol	0.22 mL, 0.64 mmol	168 mg, 0.27 mmol 84%
Ph$_4$P[Ag(SSiMe$_3$)$_2$] (**2**)	Ph$_4$P[Cl] 114 mg, 0.30 mmol	AgCl, 44 mg, 0.30 mmol	S(SiMe$_3$)$_2$ 114 mg, 0.64 mmol	0.21 mL, 0.61 mmol	172 mg, 0.25 mmol, 86%
Ph$_4$P[Au(SSiMe$_3$)$_2$] (**3-Ph$_4$P**)	Ph$_4$P[Cl] 100 mg, 0.27 mmol	AuCl 62 mg, 0.27 mmol	S(SiMe$_3$)$_2$ 100 mg, 0.56 mmol	0.19 mL, 0.54 mmol	168 mg, 0.23 mmol, 84%

continuation **Table S1**

Cat[M(ESiMe$_3$)$_2$]	**Cat[Cl], m1** (m, n)	**MCl, m2** (m, n)	**E(SiMe$_3$)$_2$ m3** (m, n)	**v1** *n*-BuLi [2.9M] (V)	**m4** (m, n, %)
PPN[Au(SSiMe$_3$)$_2$] (**3-PPN**)	Ph$_4$P[Cl] 74 mg, 0.13 mmol	AuCl 30 mg, 0.13 mmol	S(SiMe$_3$)$_2$ 48 mg, 0.27 mmol	0.09 mL, 0.26 mmol	32 mg, 0.03 mmol, 26%
Ph$_4$P[Cu(SeSiMe$_3$)$_2$] (**4-Ph$_4$P**)	Ph$_4$P[Cl] 106 mg, 0.28 mmol	CuCl 28 mg, 0.28 mmol	Se(SiMe$_3$)$_2$ 134 mg, 0.59 mmol	0.20 mL, 0.57 mmol	128 mg, 0.18 mmol 64%
PPN[Cu(SeSiMe$_3$)$_2$] (**4-PPN**)	PPN[Cl] 127 mg, 0.22 mmol	CuCl 22 mg, 0.22 mmol	Se(SiMe$_3$)$_2$ 99 mg, 0.44 mmol	0.15 mL, 0.44 mmol	86 mg, 0.09 mmol 43%
Ph$_4$P[Ag(SeSiMe$_3$)$_2$] (**5-Ph$_4$P**)	Ph$_4$P[Cl] 100 mg, 0.27 mmol	AgCl 38 mg, 0.27 mmol	Se(SiMe$_3$)$_2$ 126 mg, 0.56 mmol	0.18 mL. 0.53 mmol	0.143 mg, 0.19 mmol 72%
PPN[Ag(SeSiMe$_3$)$_2$] (**5-PPN**)	PPN[Cl] 121 mg, 0.21 mmol	AgCl 30 mg, 0.21 mmol	Se(SiMe$_3$)$_2$ 95 mg, 0.42 mmol	0.14 mL, 0.42 mmol	90 mg, 0.09 mmol, 45%
Ph$_4$P[Au(SeSiMe$_3$)$_2$] (**6-Ph$_4$P**)	Ph$_4$P[Cl] 89 mg, 0.24 mmol	AuCl 55 mg, 0.24 mmol	Se(SiMe$_3$)$_2$ 113 mg, 0.50 mmol	0.17 mL, 0.48 mmol	156 mg, 0.19 mmol 78%
PPN[Au(SeSiMe$_3$)$_2$] (**6-PPN**)	PPN[Cl] 83 mg, 0.14 mmol	AuCl 34 mg, 0.14 mmol	Se(SiMe$_3$)$_2$ 67 mg, 0.30 mmol	0.10 mL 0.29 mmol	40 mg. 0.04 mmol 27%

1.1. Ph$_4$P[Cu(SSiMe$_3$)$_2$] (1):

^{1}H-NMR (300.3 MHz, d^8-THF): δ = 7.93-7.83 (m, 20 H, (H_5C$_6$)$_4$P$^+$), 0.13 (s, 18 H, [Cu(SSi(CH_3)$_3$)$_2$]$^-$) ppm. **^{13}C-NMR (75.5 MHz, d^8-THF):** δ = 136.1 (d, $^4J_{PC}$ = 3.2 Hz, [(H*C*(CH$_2$)$_2$(CH$_2$)$_2$C)$_4$P]$^+$)), 135.6 (d, $^3J_{PC}$ = 10.4 Hz, [(HC(*C*H$_2$)$_2$(CH$_2$)$_2$C)$_4$P]$^+$), 131.3 (d, $^2J_{PC}$ = 13.2 Hz, [(HC(CH$_2$)$_2$(*C*H$_2$)$_2$C)$_4$P]$^+$), 118.9 (d, $^1J_{PC}$ = 98.3 Hz, [(HC(CH$_2$)$_2$(CH$_2$)$_2$*C*)$_4$P]$^+$), 8.3 (s, [Cu(SSi(*C*H$_3$)$_3$)$_2$]$^-$) ppm. **^{29}Si (59.7 MHz, d^8-THF):** δ = 5.2 (s, [Cu(S*Si*(CH$_3$)$_3$)$_2$]$^-$) ppm. **Elemental analysis:** Calcd. for C$_{30}$H$_{38}$Cu$_1$P$_1$S$_2$Si$_2$: C, 58.7; H, 6.2; S, 10.5. Found: C, 58.6; H, 5.8; S, 10.3.

1.2. $Ph_4P[Ag(SSiMe_3)_2]$ (2):

^{1}H-NMR (300.3 MHz, d^8-THF): δ = 7.96-7.81 (m, 20 H, $(H_5C_6)_4P^+$), 0.12 (s, 18 H, $[Ag(SSi(CH_3)_3)_2]^-$) ppm. **^{13}C-NMR (75.5 MHz, d^8-THF):** δ = 136.1 (d, $^4J_{PC}$ = 3.2 Hz, $[(HC(CH_2)_2(CH_2)_2C)_4P]^+$)), 135.6 (d, $^3J_{PC}$ = 10.4 Hz, $[(HC(CH_2)_2(CH_2)_2C)_4P]^+$), 131.3 (d, $^2J_{PC}$ = 13.2 Hz, $[(HC(CH_2)_2(CH_2)_2C)_4P]^+$), 118.9 (d, $^1J_{PC}$ = 98.3 Hz, $[(HC(CH_2)_2(CH_2)_2C)_4P]^+$), 8.6 (s, $[Ag(SSi(CH_3)_3)_2]^-$) ppm. **^{29}Si (59.7 MHz, d^8-THF):** δ = 5.2 (s, $[Ag(SSi(CH_3)_3)_2]^-$) ppm. **Anal. calcd.** for $C_{30}H_{38}Ag_1P_1S_2Si_2$: C, 54.8; H, 5.8; S, 9.8. Found: C, 54.7; H, 5.8; S, 10.3.

1.3. $Ph_4P[Au(SSiMe_3)_2]$ (3-Ph_4P):

^{1}H-NMR (300.3 MHz, d^8-THF): δ = 7.92-7.85 (m, 20 H, $(H_5C_6)_4P^+$), 0.13 (s, 18 H, $[Au(SSi(CH_3)_3)_2]^-$) ppm. **^{13}C-NMR (75.5 MHz, d^8-THF):** δ = 136.0 (d, $^4J_{PC}$ = 3.2 Hz, $[(HC(CH_2)_2(CH_2)_2C)_4P]^+$)), 135.4 (d, $^3J_{PC}$ = 10.4 Hz, $[(HC(CH_2)_2(CH_2)_2C)_4P]^+$), 131.3 (d, $^2J_{PC}$ = 13.2 Hz, $[(HC(CH_2)_2(CH_2)_2C)_4P]^+$), 118.9 (d, $^1J_{PC}$ = 98.3 Hz, $[(HC(CH_2)_2(CH_2)_2C)_4P]^+$), 7.4 (s, $[Au(SSi(CH_3)_3)_2]^-$) ppm. **^{29}Si (59.7 MHz, d^8-THF):** δ = 7.7 (s, $[Au(SSi(CH_3)_3)_2]^-$) ppm. **Anal. calcd.** for $C_{30}H_{38}Au_1P_1S_2Si_2$: C, 48.3; H, 5.1; S, 8.6. Found: C, 48.2; H, 5.2; S, 7.9. The deviation in the S-value is most likely an artefact of the measurement.

1.4. $PPN[Au(SSiMe_3)_2]$ (3-PPN):

^{1}H-NMR (500.2 MHz, d^8-THF): δ = 7.71-7.52 (m, 30 H, PPN^+), 0.16 (s, 18 H, $[Au(SSi(CH_3)_3)_2]^-$) ppm. **^{13}C-NMR (125.8 MHz, d^8-THF):** δ = 134.4 (s) & 133.2 (m), 133.1 (m), 128.1 (d, $^1J_{CP}$ = 108.7 Hz) (PPN^+),

7.5 (s, $[Au(SSi(CH_3)_3)_2]^-$) ppm. **^{29}Si (99.4 MHz, d^8-THF):** δ = 7.6 (s, $[Au(SSi(CH_3)_3)_2]^-$) ppm. **Anal. calcd.** for $C_{42}H_{48}Au_1N_1P_2S_2Si_2$: C, 53.3; H, 5.1; N, 1.5; S, 6.8. Found: C, 53.0; H, 5.2; N, 1.7; S, 6.7.

1.5. $Ph_4P[Cu(SeSiMe_3)_2]$ (4-Ph_4P):

^{1}H-NMR (500.2 MHz, d^8-THF, 273K): δ = 7.97-7.84 (m, 20H, $(H_5C_6)_4P^+$), 0.27 (s, 18H, $[Cu(SeSi(CH_3)_3)_2]^-$) ppm. **^{13}C-NMR (125.8 MHz, d^8-THF, 273K):** δ = 136.1 (d, $^4J_{PC}$ = 2.9 Hz, $[(HC(CH_2)_2(CH_2)_2C)_4P]^+$)), 135.6 (d, $^3J_{PC}$ = 10.8 Hz, $[(HC(CH_2)_2(CH_2)_2C)_4P]^+$), 131.3 (d, $^2J_{PC}$ = 13.0 Hz, $[(HC(CH_2)_2(CH_2)_2C)_4P]^+$), 118.8 (d, $^1J_{PC}$ = 89.6 Hz, $[(HC(CH_2)_2(CH_2)_2C)_4P]^+$), 8.8 (s, $[Cu(SeSi(CH_3)_3)_2]^-$) ppm. **^{29}Si (99.4 MHz, d^8-THF, 273K):** δ = 0.23 (s, $[Cu(SeSi(CH_3)_3)_2]^-$) ppm.

Note that extended measurement times were needed to obtain a 1D-^{29}Si-NMR spectrum. However, it was not possible to obtain a ^{77}Se-NMR signal. For the convenient detection of the ^{29}Si- and the ^{77}Se-NMR signal, ^{29}Si/^{1}H- and the ^{77}Se/^{1}H-HMQC measurements were performed:

^{29}Si- / ^{1}H-HMQC-NMR (99.4 MHz / 500.2 MHz, d^8-THF, 273K):

^{1}H 0.27 (s, $[Cu(SeSi(CH_3)_3)_2]^-$) ppm / ^{29}Si 0.2 (s, $[Cu(SeSi(CH_3)_3)_2]^-$) ppm.

^{77}Se- / ^{1}H-HMQC-NMR (95.4 MHz / 500.2 MHz, d^8-THF, 273K):

^{1}H 0.28 (s, $[Cu(SeSi(CH_3)_3)_2]^-$) ppm / ^{77}Se –469.4 (s, $[Cu(SeSi(CH_3)_3)_2]^-$) ppm.

1.6. PPN[Cu(SeSiMe$_3$)$_2$] (4-PPN):

^{1}H-NMR (300.3 MHz, d^8-THF): δ = 7.69-7.53 (m, 30H, PPN^+), 0.29 (s, 18H, $[Cu(SeSi(CH_3)_3)_2]^-$) ppm. **^{13}C-NMR (75.5 MHz, d^8-THF):** δ = 134.4 (s) & 133.1 (m), 130.3 (m), 128.1 (d, $^{1}J_{CP}$ = 107.2 Hz) (PPN^+),

8.9 (s, $[Cu(SeSi(CH_3)_3)_2]^-$) ppm.

No ^{29}Si-NMR and no ^{77}Se-NMR spectra could be obtained.

Anal. calcd. for $C_{42}H_{48}Cu_1N_1P_2Se_2Si_2$: C, 55.7; H, 5.3; N, 1.6. Found: C, 55.3; H, 5.4; N, 2.0.

1.7. Ph$_4$P[Ag(SeSiMe$_3$)$_2$] (5-Ph$_4$P):

^{1}H-NMR (500.2 MHz, d^8-THF, 273K): δ = 7.97-7.83 (m, 20H, $(H_5C_6)_4P^+$), 0.27 (s, 18H, $[Ag(SeSi(CH_3)_3)_2]^-$) ppm. **^{13}C-NMR (75.5 MHz, d^8-THF):** δ = 136.1 (d, $^{4}J_{PC}$ = 3.8 Hz, $[(HC(CH_2)_2(CH_2)_2C)_4P]^+$)), 135.6 (d, $^{3}J_{PC}$ = 10.5 Hz, $[(HC(CH_2)_2(CH_2)_2C)_4P]^+$), 131.3 (d, $^{2}J_{PC}$ = 12.8 Hz, $[(HC(CH_2)_2(CH_2)_2C)_4P]^+$), 118.9 (d, $^{1}J_{PC}$ = 89.1 Hz, $[(HC(CH_2)_2(CH_2)_2C)_4P]^+$), 9.2 (s, $[Ag(SeSi(CH_3)_3)_2]^-$) ppm. **^{29}Si (99.4 MHz, d^8-THF, 273K):** δ = 1.59 (bs, $[Ag(SeSi(CH_3)_3)_2]^-$) ppm. **^{77}Se (95.4 MHz, d^8-THF, 273K)**: δ = –501.5 (bs, $[Ag(SeSi(CH_3)_3)_2]^-$) ppm.

Note that extended measurement times were needed to obtain 1D-^{29}Si-NMR and 1D-^{77}Se-NMR spectra. For the convenient detection of the ^{29}Si- and the ^{77}Se-NMR signal, ^{29}Si/^{1}H- and the ^{77}Se/^{1}H-HMQC measurements were performed:

^{29}Si- / ^{1}H-HMQC-NMR (99.4 MHz / 500.2 MHz, d^8-THF, 273K):

^{1}H 0.27 (s, $[Ag(SeSi(CH_3)_3)_2]^-$) ppm / ^{29}Si 1.6 (s, $[Ag(SeSi(CH_3)_3)_2]^-$) ppm.

^{77}Se- / ^{1}H-HMQC-NMR (95.4 MHz / 500.2 MHz, d^8-THF, 273K):

^{1}H 0.29 (s, $[Ag(SeSi(CH_3)_3)_2]^-$) ppm / ^{77}Se –502.2 (s, $[Ag(SeSi(CH_3)_3)_2]^-$) ppm.

Anal. calcd. for $C_{30}H_{38}Ag_1P_1Se_2Si_2$: C, 47.9; H, 5.1. Found: C, 47.5; H, 4.9.

1.8. PPN[Ag(SeSiMe$_3$)$_2$] (5-PPN):

^{1}H-NMR (300.3 MHz, d^8-THF): δ = 7.67-7.52 (m, 30H, PPN^+), 0.28 (s, 18H, $[Ag(SeSi(CH_3)_3)_2]^-$) ppm. **^{13}C-NMR (75.5 MHz, d^8-THF):** δ = 134.4 (s) & 133.1 (m), 130.2 (m), 128.1 (d, $^{1}J_{CP}$ = 109.5 Hz) (PPN^+),

9.3 (s, $[Ag(SeSi(CH_3)_3)_2]^-$) ppm.

No ^{29}Si-NMR and no ^{77}Se-NMR spectra could be obtained.

Anal. calcd. for $C_{42}H_{48}Ag_1N_1P_2Se_2Si_2$: C, 53.1; H, 5.1; N, 1.5. Found: C, 52.5; H, 5.0; N, 2.8. We think that the deviation in the N-value is an artefact of the measurement process.

1.9. $Ph_4P[Au(SeSiMe_3)_2]$ (6-Ph_4P):

^{1}H-NMR (300.3 MHz, d^8-THF): δ = 7.96-7.78 (m, 20H, $(H_5C_6)_4P^+$), 0.27 (s, 18H, $[Au(SeSi(CH_3)_3)_2]^-$) ppm. **^{13}C-NMR (75.5 MHz, d^8-THF):** δ = 136.1 (d, $^4J_{PC}$ = 3.0 Hz, $[(HC(CH_2)_2(CH_2)_2C)_4P]^+$)), 135.6 (d, $^3J_{PC}$ = 10.2 Hz, $[(HC(CH_2)_2(CH_2)_2C)_4P]^+$), 131.3 (d, $^2J_{PC}$ = 12.9 Hz, $[(HC(CH_2)_2(CH_2)_2C)_4P]^+$), 118.9 (d, $^1J_{PC}$ = 89.5 Hz, $[(HC(CH_2)_2(CH_2)_2C)_4P]^+$), 7.99 (s, $[Au(SeSi(CH_3)_3)_2]^-$) ppm. **^{29}Si (99.4 MHz, d^8-THF, 273K):** δ = 2.4 (bs, $[Au(SeSi(CH_3)_3)_2]^-$) ppm. **^{77}Se (95.4 MHz, d^8-THF, 273K)**: δ = –377.1 (bs, $[Au(SeSi(CH_3)_3)_2]^-$) ppm.

Note that extended measurement times were needed to obtain 1D-^{29}Si-NMR and 1D-^{77}Se-NMR spectra. For the convenient detection of the ^{29}Si- and the ^{77}Se-NMR signal, ^{29}Si/^{1}H- and the ^{77}Se/^{1}H-HMQC measurements were performed:

^{29}Si- / ^{1}H-HMQC-NMR (99.4 MHz / 500.2 MHz, d^8-THF, 273K):

^{1}H 0.27 (s, $[Au(SeSi(CH_3)_3)_2]^-$) ppm / ^{29}Si 2.4 (s, $[Au(SeSi(CH_3)_3)_2]^-$) ppm.

^{77}Se- / ^{1}H-HMQC-NMR (95.4 MHz / 500.2 MHz, d^8-THF, 273K):

^{1}H 0.31 (s, $[Au(SeSi(CH_3)_3)_2]^-$) ppm / ^{77}Se –377.3 (s, $[Au(SeSi(CH_3)_3)_2]^-$) ppm.

Anal. calcd. for $C_{30}H_{38}Au_1P_1Se_2Si_2$: C, 42.9; H, 4.6. Found: C, 42.0; H, 4.5. We think that the minor deviation in the C-value is an artefact of the measurement process.

1.10. PPN[Au(SeSiMe$_3$)$_2$] (6-PPN):

^{1}H-NMR (300.3 MHz, d^8-THF): δ = 7.64-7.53 (m, 30 H, PPN^+), 0.29 (s, 18 H, $[Au(SSi(CH_3)_3)_2]^-$) ppm. **^{13}C-NMR (125.8 MHz, d^8-THF):** δ = 134.4 (s) & 133.2 (m), 130.2 (m), 128.1 (d, $^1J_{CP}$ = 106.3 Hz) (PPN^+), 8.0 (s, $[Au(SeSi(CH_3)_3)_2]^-$) ppm. **^{29}Si (59.7 MHz, d^8-THF):** δ = 2.0 (s, $[Au(SeSi(CH_3)_3)_2]^-$) ppm. **^{29}Si (57.3 MHz, d^8-THF):** δ = –377.1 (s, $[Au(SeSi(CH_3)_3)_2]^-$) ppm.

Anal. calcd. for $C_{42}H_{48}Au_1N_1P_2Se_2Si_2$: C, 48.5; H, 4.8; N, 1.4. Found: C, 48.3; H, 4.8; N, 1.8.

2. Crystallographic Data

	$Ph_4P[Cu(SSiMe_3)_2]$ (1)	$Ph_4P[Ag(SSiMe_3)_2]$ (2)
CCDC code	1940498	1940499
Identification code	JG218_0m_a	jg238a
Empirical formula	C30 H38 Cu P S2 Si2	C30 H38 Ag P S2 Si2
Formula weight	613.41	657.74
Temperature	100(2) K	293(2) K
Wavelength	0.71073 Å	1.54184 Å
Crystal system	Triclinic	Triclinic
Space group	P-1	P-1
Unit cell dimensions	a = 10.5501(19) Å α= 80.854(8)°. b = 12.252(3) Å β= 83.226(7)°. c = 13.035(3) Å γ = 82.567(7)°.	a = 10.4355(6) Å α= 81.408(5)°. b = 15.6356(10) Å β= 88.691(5)°. c = 20.8806(14) Å γ = 73.322(5)°.
Volume	1641.3(6) $Å^3$	3226.3(4) $Å^3$
Z	2	4
Density (calculated)	1.241 Mg/m^3	1.354 Mg/m^3
Absorption coefficient	0.931 mm^{-1}	7.523 mm^{-1}
F(000)	644	1360
Crystal size	0.127 x 0.124 x 0.087 mm^3	0.430 x 0.202 x 0.067 mm^3
Theta range for data collection	2.148 to 27.161°.	4.424 to 75.176°.
Index ranges	-13<=h<=13, -15<=k<=15, -16<=l<=16	-12<=h<=12, -18<=k<=19, -10<=l<=25
Reflections collected	62213	59795
Independent reflections	7278 [R(int) = 0.0446]	12798 [R(int) = 0.0709]
Completeness to theta = 25.000°	99.9 %	98.4 %
Absorption correction	Semi-empirical from equivalents	Semi-empirical from equivalents
Max. and min. transmission	0.7455 and 0.7175	0.0356 and 0.0025
Refinement method	Full-matrix least-squares on F2	Full-matrix least-squares on F2
Data / restraints / parameters	7278 / 0 / 331	12798 / 12 / 661
Goodness-of-fit on F2	1.040	0.925
Final R indices [I>2sigma(I)]	R1 = 0.0278, wR2 = 0.0608	R1 = 0.0423, wR2 = 0.0995
R indices (all data)	R1 = 0.0386, wR2 = 0.0642	R1 = 0.0661, wR2 = 0.1072
Extinction coefficient	n/a	n/a
Largest diff. peak and hole	0.580 and -0.293 $e.Å^{-3}$	0.894 and -0.811 $e.Å^{-3}$

	PPN[Au(SSiMe$_3$)$_2$] (3-PPN)		PPN[Cu(SeSiMe$_3$)$_2$] (4-PPN)	
CCDC code	1940500		1940501	
Identification code	JG241_0m_a		JG292_0m_a	
Empirical formula	C42 H48 Au N P2 S2 Si2		C42 H48 Cu N P2 Se2 Si2	
Formula weight	946.02		906.39	
Temperature	100(2) K		100(2) K	
Wavelength	0.71073 Å		0.71073 Å	
Crystal system	Triclinic		Triclinic	
Space group	P -1		P -1	
Unit cell dimensions	a = 11.3887(19) Å	α= 103.747(5)°.	a = 11.3420(14) Å	α= 104.161(4)°.
	b = 16.358(3) Å	β= 99.464(5)°.	b = 16.426(2) Å	β= 98.596(4)°.
	c = 23.928(4) Å	γ = 98.301(5)°.	c = 24.124(3) Å	γ = 98.710(5)°.
Volume	4192.1(13) Å^3		4225.2(9) Å^3	
Z	4		4	
Density (calculated)	1.499 Mg/m^3		1.425 Mg/m^3	
Absorption coefficient	3.773 mm^{-1}		2.402 mm^{-1}	
F(000)	1904		1848	
Crystal size	0.820 x 0.171 x 0.114 mm^3		0.417 x 0.316 x 0.179 mm^3	
Theta range for data collection	2.213 to 25.781°.		2.204 to 25.751°.	
Index ranges	-13<=h<=13, -20<=k<=20, -29<=l<=29		-13<=h<=13, -20<=k<=20, -29<=l<=29	
Reflections collected	93678		118878	
Independent reflections	16024 [R(int) = 0.0475]		16121 [R(int) = 0.0409]	
Completeness to theta = 25.000°	99.9 %		99.9 %	
Absorption correction	Semi-empirical from equivalents		Semi-empirical from equivalents	
Max. and min. transmission	0.7453 and 0.5588		0.7453 and 0.5774	
Refinement method	Full-matrix least-squares on F2		Full-matrix least-squares on F2	
Data / restraints / parameters	16024 / 0 / 913		16121 / 0 / 913	
Goodness-of-fit on F2	1.025		1.015	
Final R indices [I>2sigma(I)]	R1 = 0.0261, wR2 = 0.0502		R1 = 0.0325, wR2 = 0.0780	
R indices (all data)	R1 = 0.0366, wR2 = 0.0530		R1 = 0.0410, wR2 = 0.0820	
Extinction coefficient	n/a		n/a	
Largest diff. peak and hole	1.221 and -1.484 e.Å^{-3}		1.601 and -1.370 e.Å^{-3}	

	PPN[Ag(SeSiMe$_3$)$_2$] (5-PPN)	PPN[Au(SeSiMe$_3$)$_2$] (6-PPN)
CCDC code	1940502	1940503
Identification code	jg300loesen	JG307_0m_a
Empirical formula	C42 H48 Ag N P2 Se2 Si2	C42 H48 Au N P2 Se2 Si2
Formula weight	950.72	1039.82
Temperature	293(2) K	110(2) K
Wavelength	1.54184 Å	0.71073 Å
Crystal system	Triclinic	Triclinic
Space group	P -1	P -1
Unit cell dimensions	a = 11.3803(3) Å α= 104.225(2)°. b = 16.4691(4) Å β= 98.471(2)°. c = 24.1539(6) Å γ = 98.694(2)°.	a = 11.3626(14) Å α= 104.125(5)°. b = 16.507(2) Å β= 98.810(5)°. c = 24.050(3) Å γ = 98.627(5)°.
Volume	4256.65(19) Å^3	4239.5(9) Å^3
Z	4	4
Density (calculated)	1.484 Mg/m^3	1.629 Mg/m^3
Absorption coefficient	7.224 mm^{-1}	5.349 mm^{-1}
F(000)	1920	2048
Crystal size	0.439 x 0.196 x 0.070 mm^3	0.525 x 0.146 x 0.100 mm^3
Theta range for data collection	2.822 to 71.784°.	2.206 to 25.803°.
Index ranges	-13<=h<=8, -19<=k<=20, -27<=l<=29	-13<=h<=13, -20<=k<=20, -29<=l<=29
Reflections collected	79842	166786
Independent reflections	16310 [R(int) = 0.0792]	16286 [R(int) = 0.0470]
Completeness to theta = 70.000°	98.9 %	99.9 %
Absorption correction	Semi-empirical from equivalents	Semi-empirical from equivalents
Max. and min. transmission	0.0395 and 0.0028	0.7453 and 0.4906
Refinement method	Full-matrix least-squares on F2	Full-matrix least-squares on F2
Data / restraints / parameters	16310 / 0 / 913	16286 / 0 / 913
Goodness-of-fit on F2	1.041	1.023
Final R indices [I>2sigma(I)]	R1 = 0.0505, wR2 = 0.1345	R1 = 0.0235, wR2 = 0.0489
R indices (all data)	R1 = 0.0720, wR2 = 0.1461	R1 = 0.0308, wR2 = 0.0512
Extinction coefficient	n/a	n/a
Largest diff. peak and hole	2.036 and -1.211 e.Å^{-3}	2.300 and -1.413 e.Å^{-3}

3. NMR-Spectra

3.1. $Ph_4P[Cu(SSiMe_3)_2]$ (1)

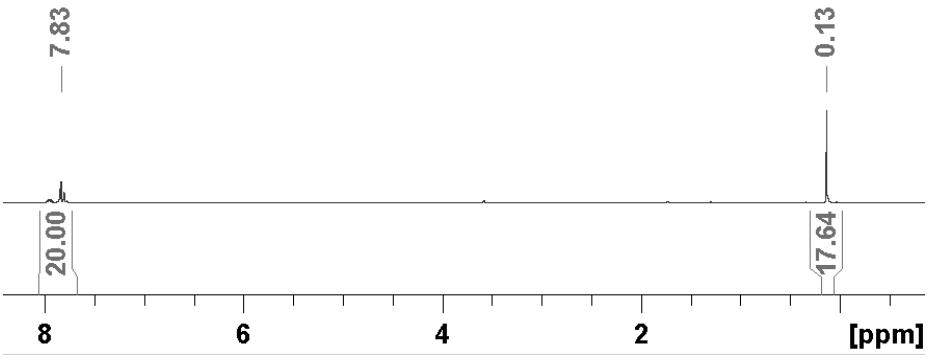

^{1}H-NMR (300.3 MHz, d^8-THF)

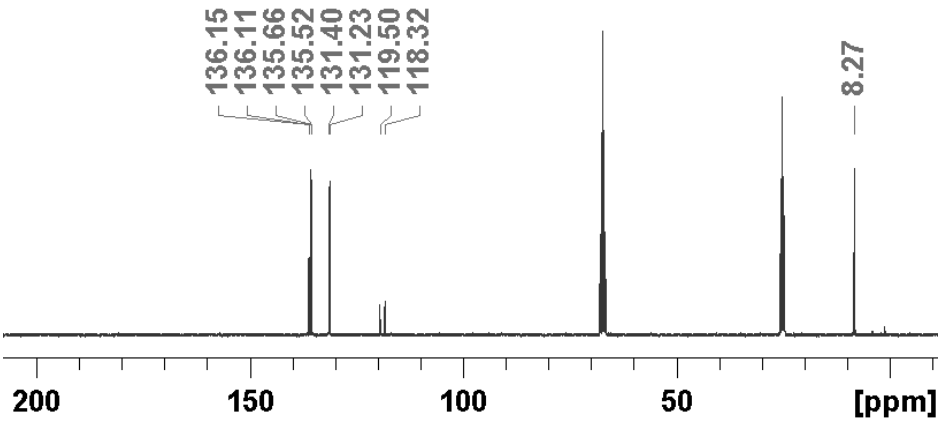

^{13}C-NMR (75.5 MHz, d^8-THF)

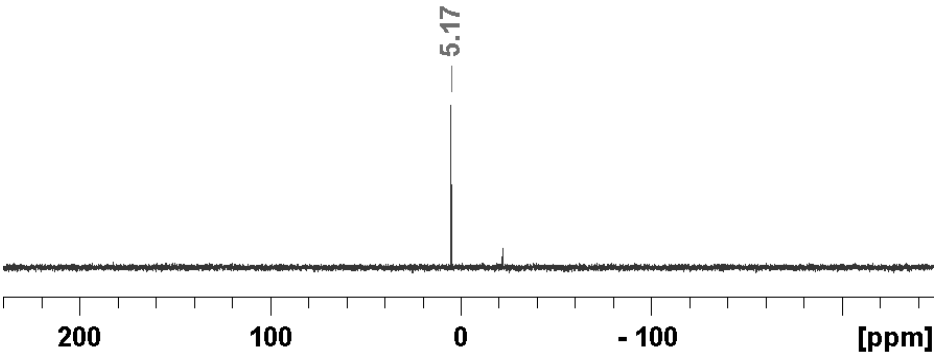

^{29}Si-NMR (59.7 MHz, d^8-THF) (the signal at ca. -22 ppm can be assigned to silicon grease)

3.2. $Ph_4P[Ag(SSiMe_3)_2]$ (2)

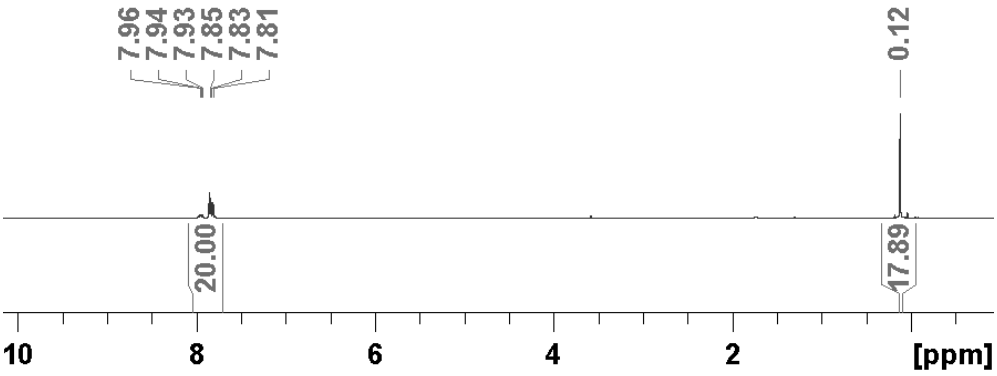

^{1}H-NMR (300.3 MHz, d^{8}-THF)

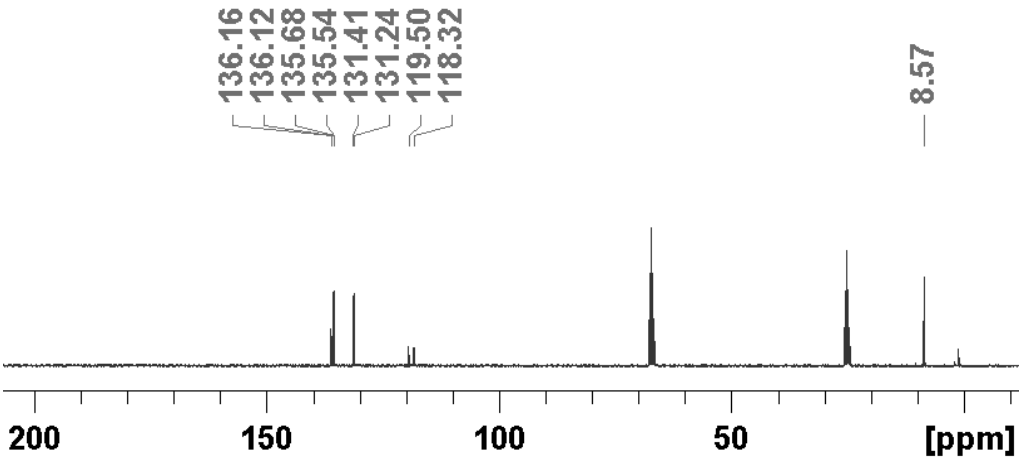

^{13}C-NMR (75.5 MHz, d^{8}-THF)

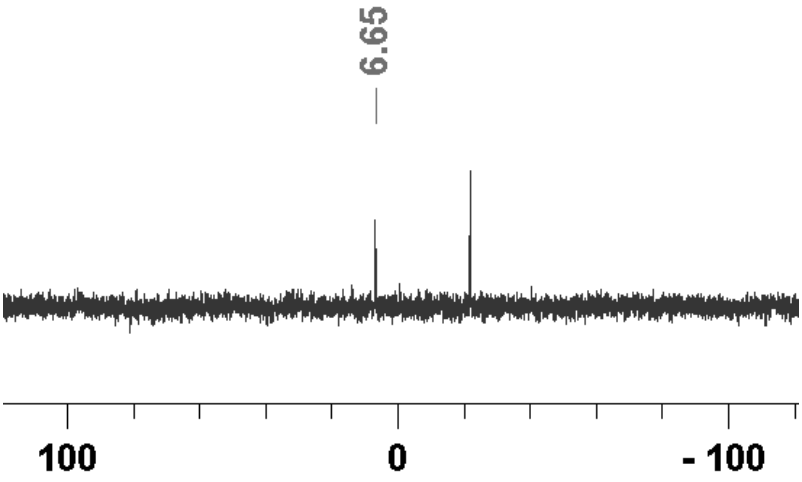

^{29}Si-NMR (59.7 MHz, d^{8}-THF) (the signal at ca. -22 ppm can be assigned to silicon grease)

3.3. PPN[Au(SSiMe$_3$)$_2$] (3-PPN)

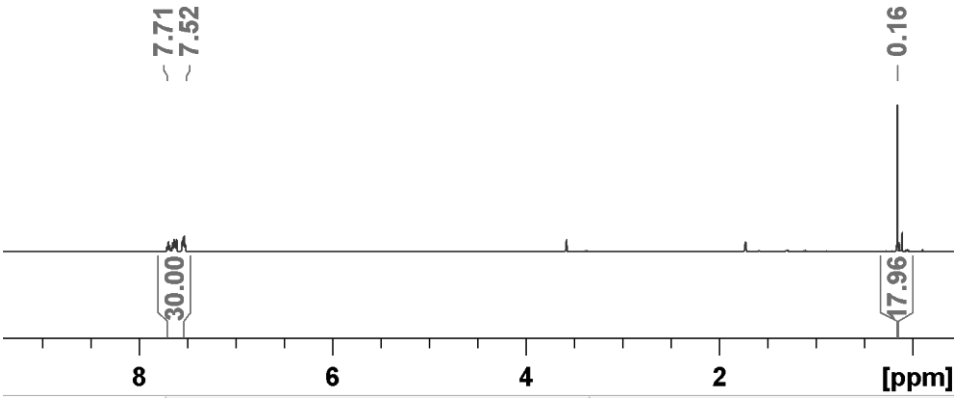

^{1}H-NMR (500.2 MHz, d^{8}-THF)

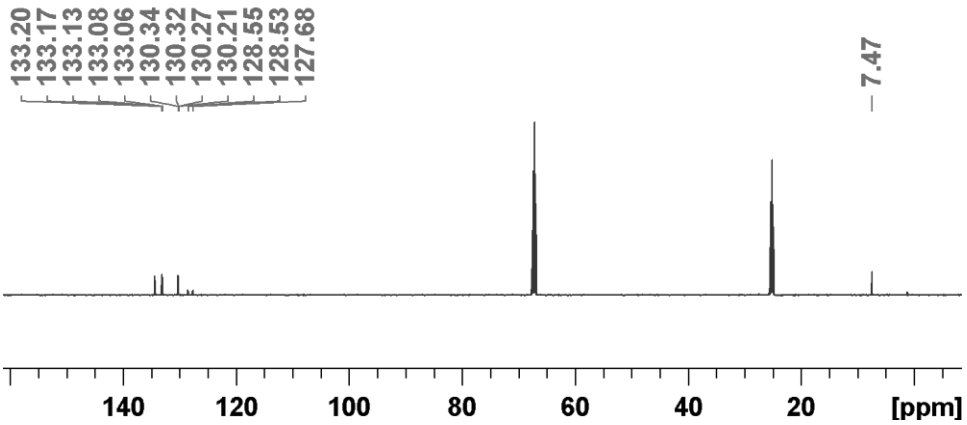

^{13}C-NMR (125.8 MHz, d^{8}-THF)

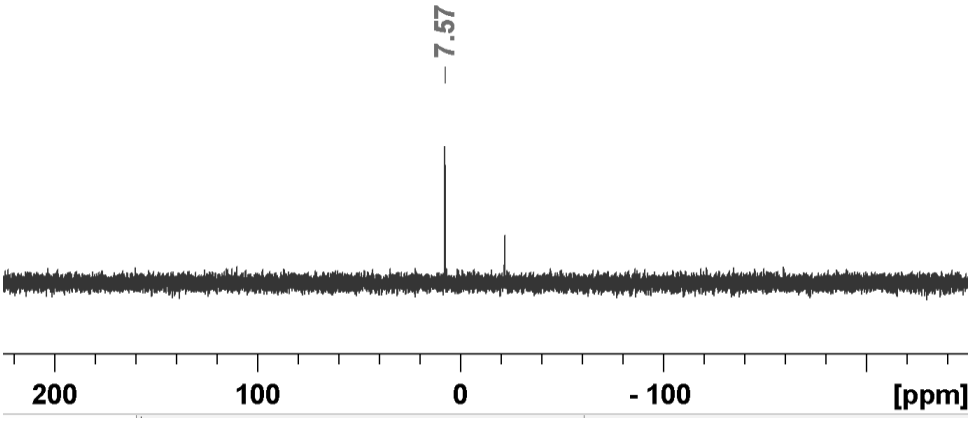

^{29}Si-NMR (99.4 MHz, d^{8}-THF) (the signal at ca. -22 ppm can be assigned to silicon grease)

3.4. $Ph_4P[Au(SSiMe_3)_2]$ (3-Ph_4P)

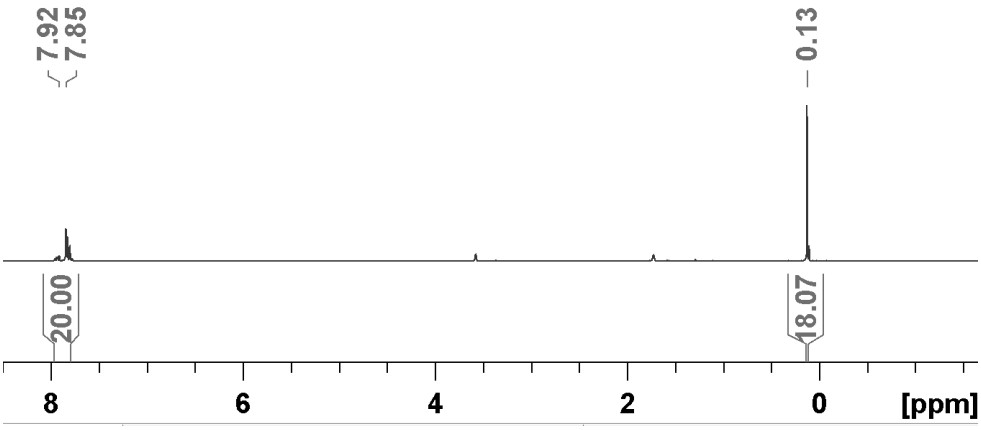

^{1}H-NMR (300.3 MHz, d^{8}-THF)

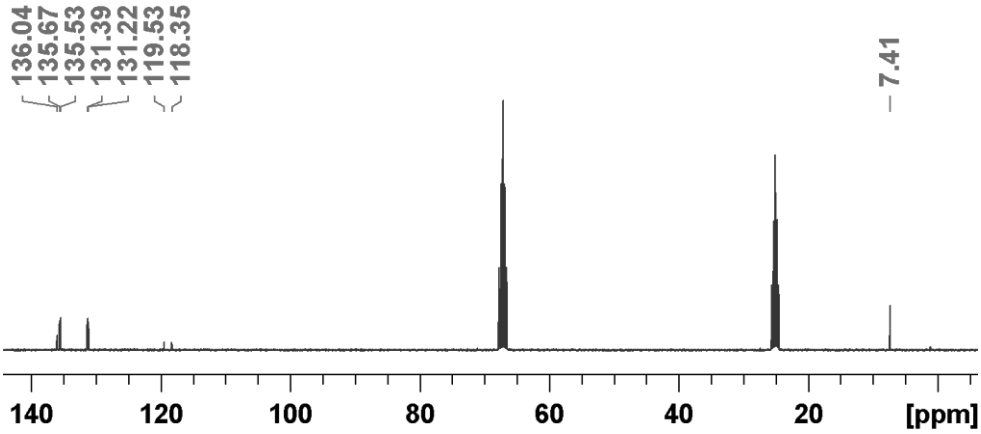

^{13}C-NMR (75.5 MHz, d^{8}-THF)

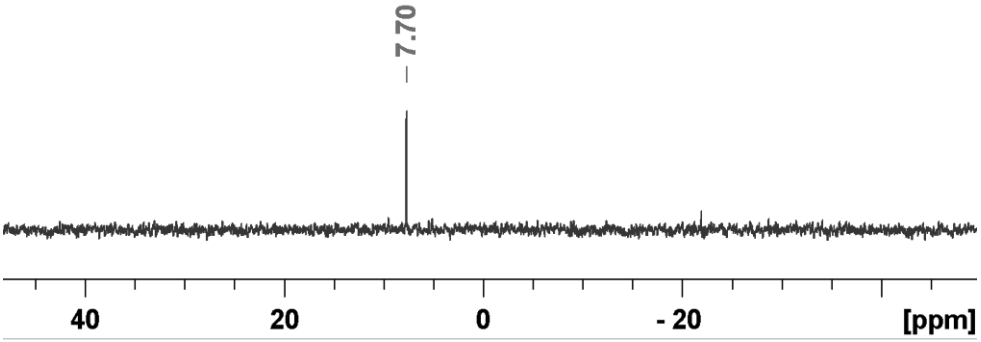

^{29}Si-NMR (59.7 MHz, d^{8}-THF) (the signal at ca. -22 ppm can be assigned to silicon grease)

3.5. PPN[Cu(SeSiMe$_3$)$_2$] (4-PPN)

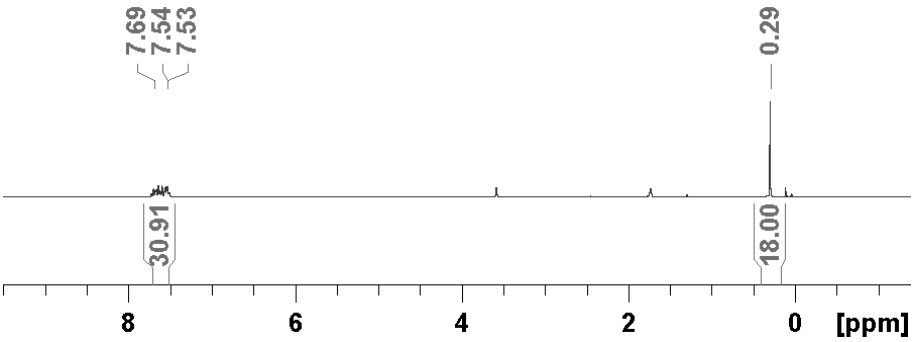

^{1}H-NMR (300.3 MHz, d^{8}-THF)

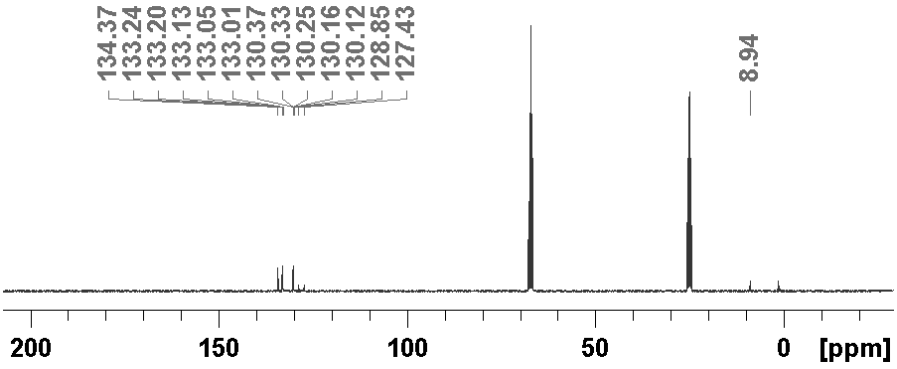

^{13}C-NMR (59.7 MHz, d^{8}-THF)

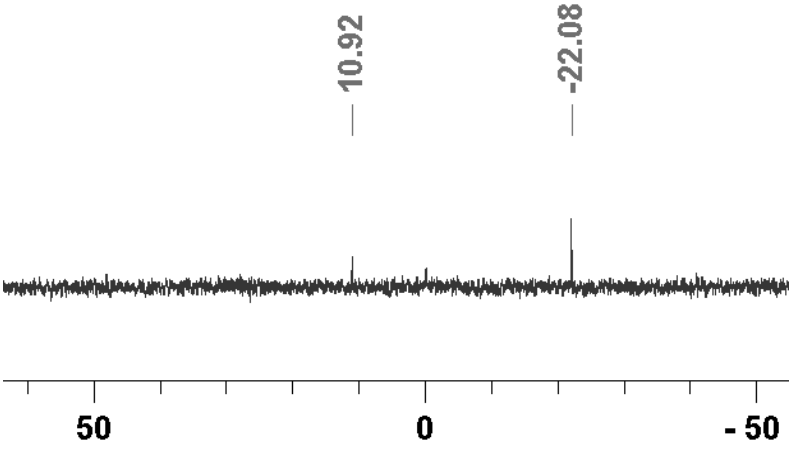

^{29}Si-NMR (59.7 MHz, d^{8}-THF) (the signal at ca. -22 ppm can be assigned to silicon grease)

No Signals could be obtained could be obtained by standard ^{77}Se-NMR-measurements.

3.6. $Ph_4P[Cu(SeSiMe_3)_2]$ (4-Ph_4P)

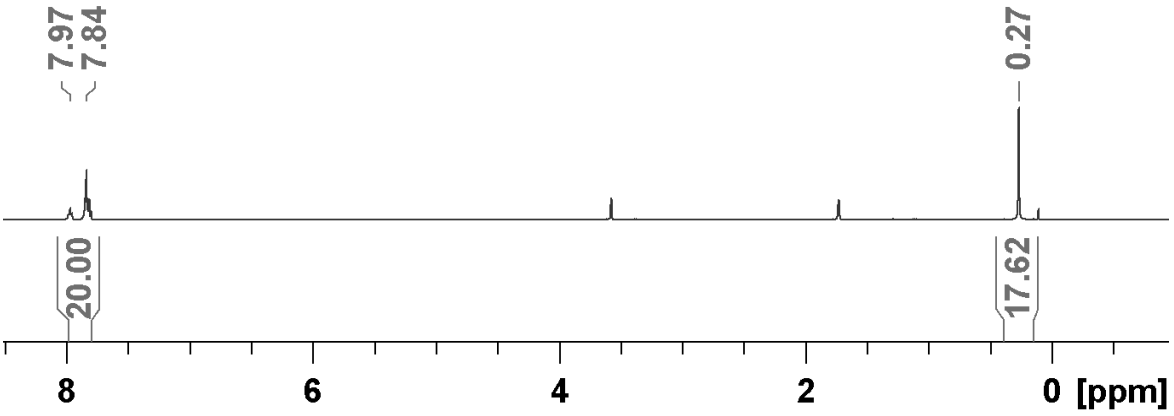

^{1}H-NMR (500.2 MHz, d^8-THF, 273K)

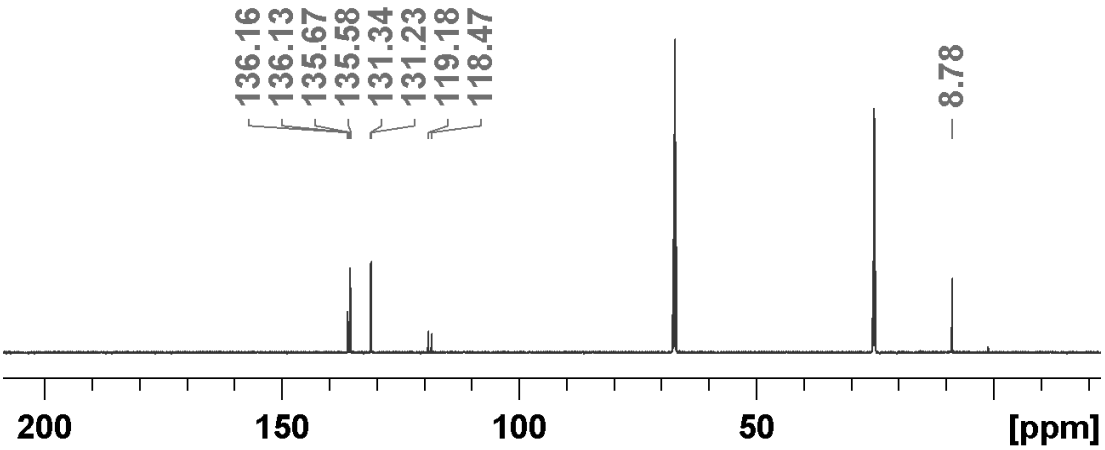

^{13}C-NMR (125.8 MHz, d^8-THF, 273K)

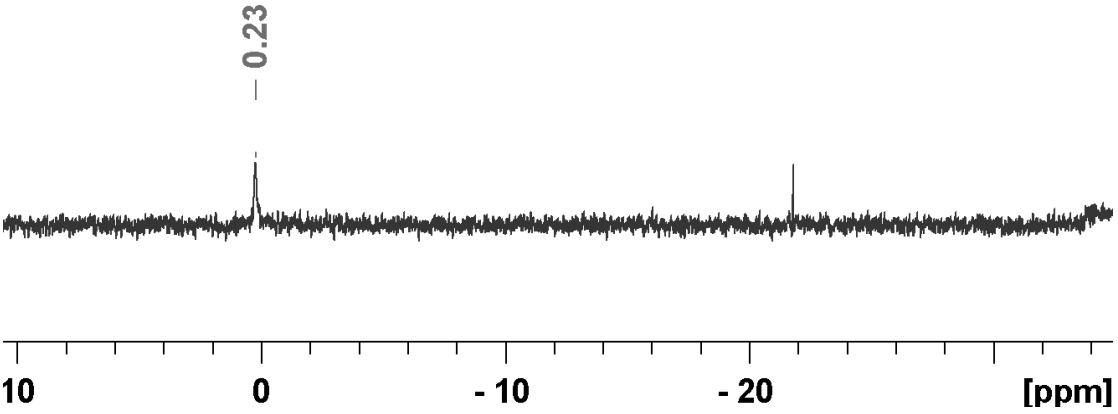

^{29}Si-NMR (99.4 MHz, d^8-THF, 273K) (the signal at ca. -22 ppm can be assigned to silicon grease)

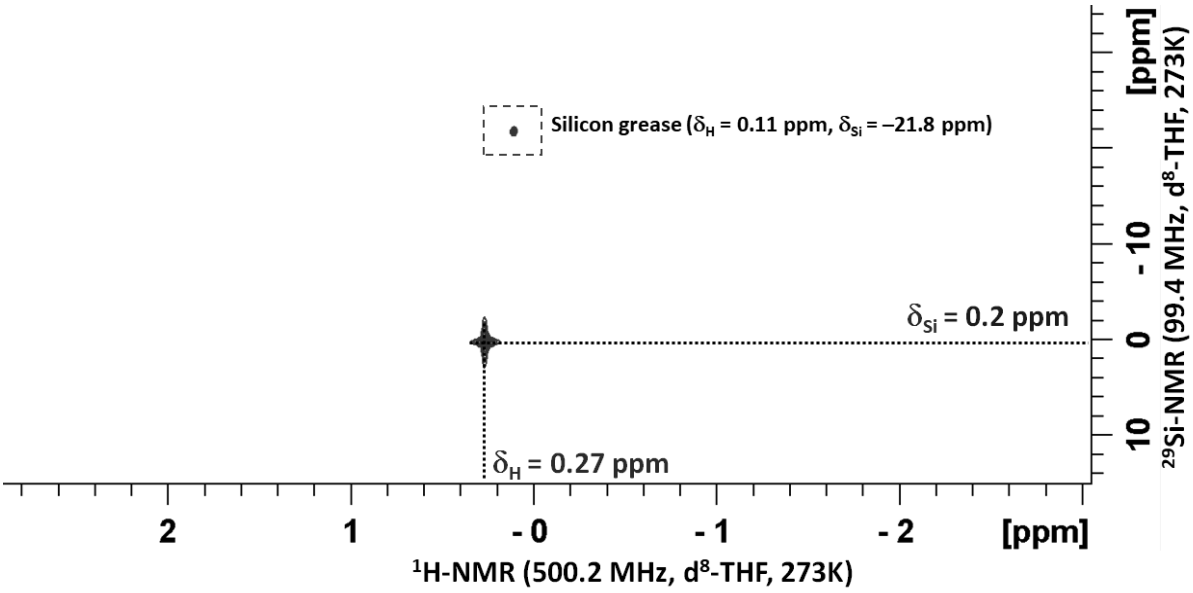

^{29}Si/^{1}H-HMQC-NMR (99.4/500.2 MHz, d^8-THF, 273K)

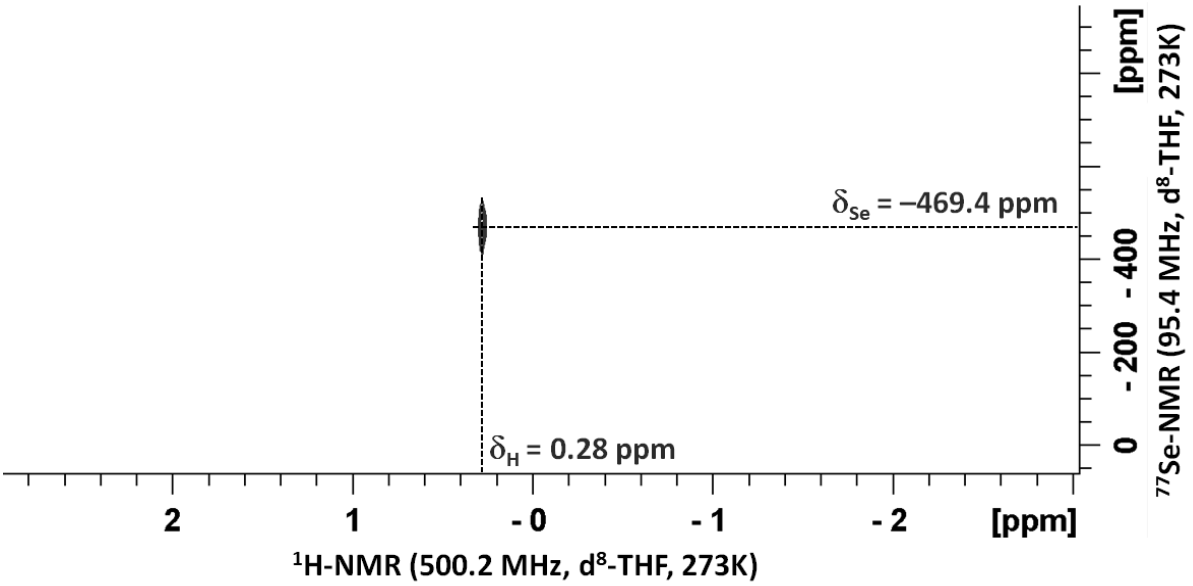

^{77}Se/^{1}H-HMQC-NMR (500.2/95.4 MHz, d^8-THF, 273K)

3.7. PPN[Ag(SeSiMe$_3$)$_2$] (5-PPN)

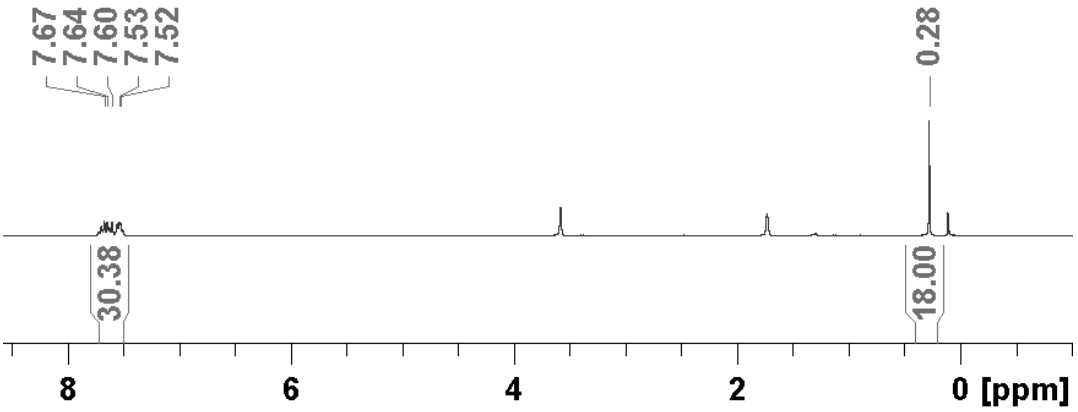

^{1}H-NMR (300.3 MHz, d^{8}-THF)

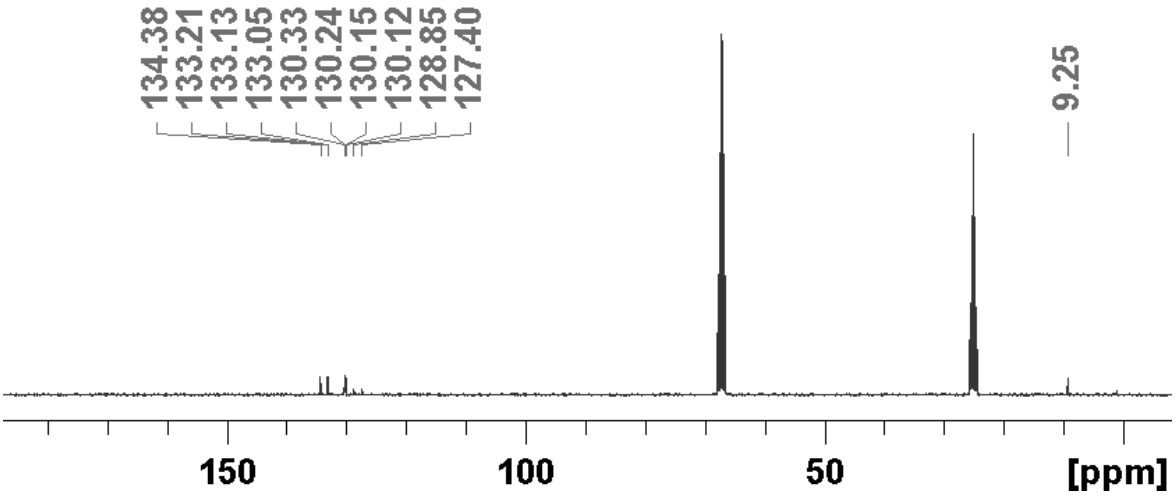

^{13}C-NMR (75.5 MHz, d^{8}-THF)

3.8. $Ph_4P[Ag(SeSiMe_3)_2]$ (5-Ph_4P)

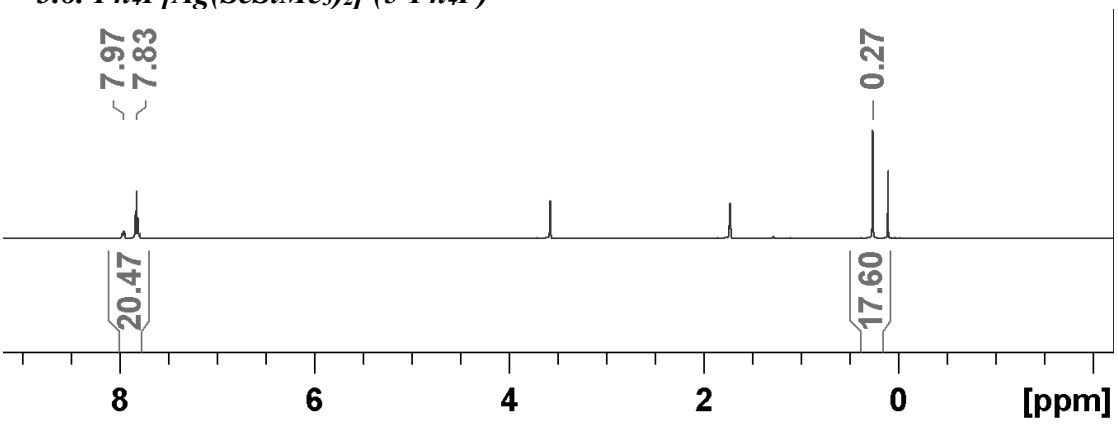

^{1}H-NMR (500.2 MHz, d^{8}-THF, 273K)

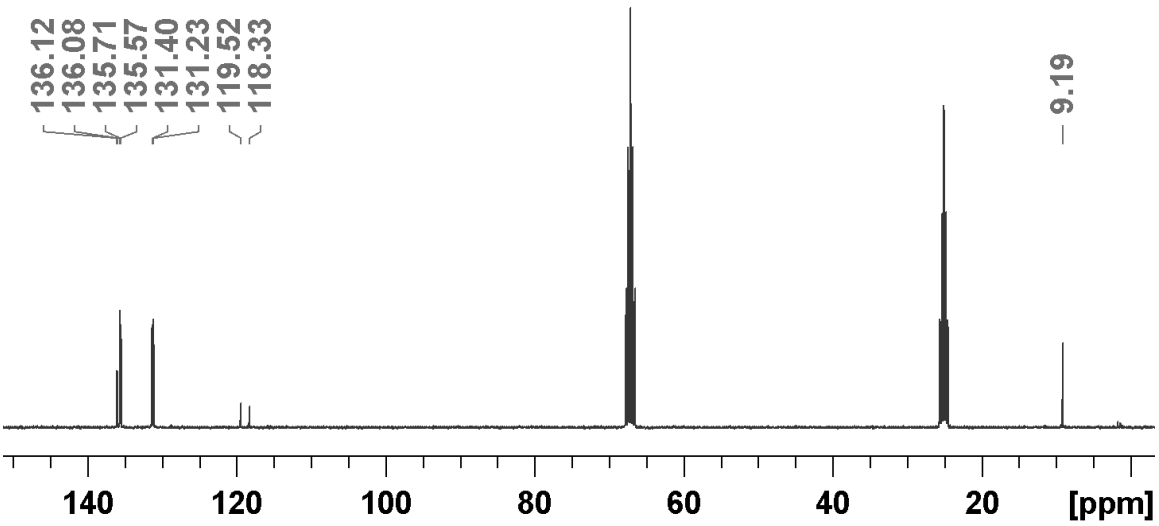

^{13}C-NMR (75.5 MHz, d^{8}-THF)

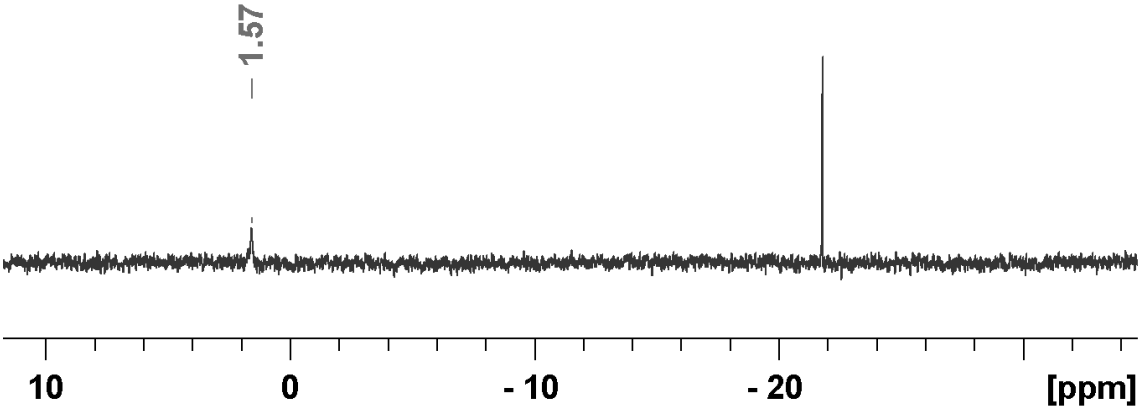

^{29}Si-NMR (99.4 MHz, d^{8}-THF, 273K)

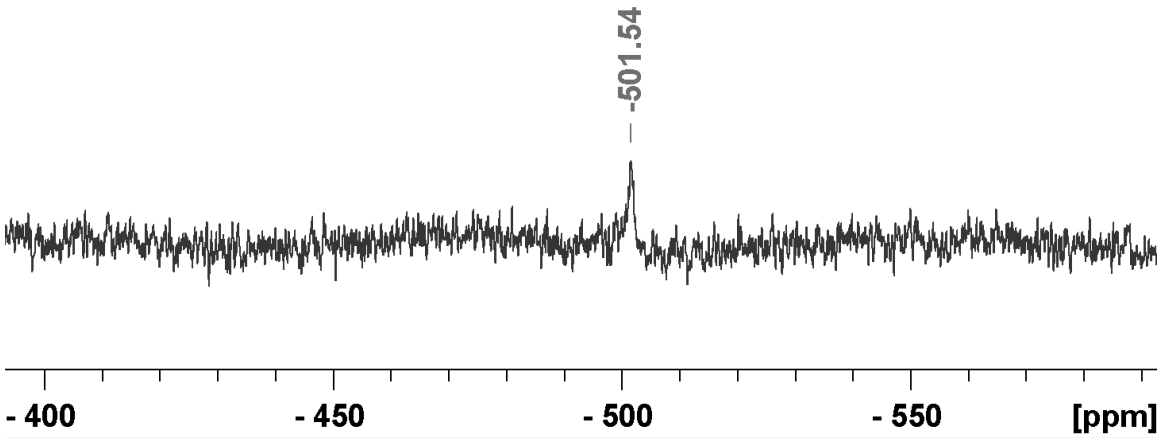

^{77}Se-NMR (95.4 MHz, d^{8}-THF, 273K)

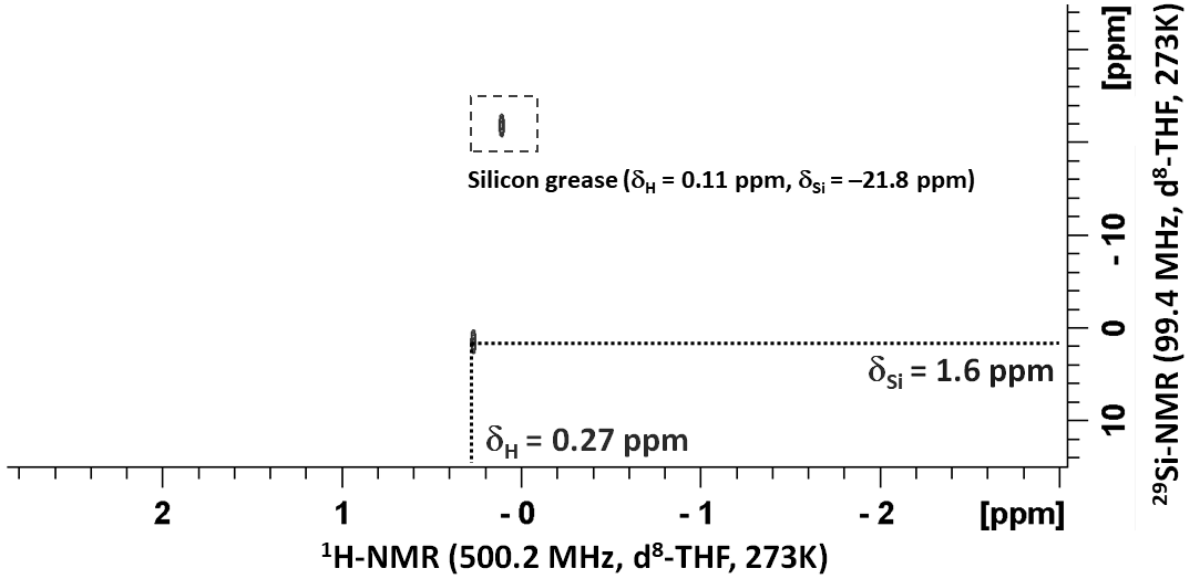

^{29}Si/^{1}H-HMQC-NMR (500.2/99.4 MHz, d^{8}-THF, 273K)

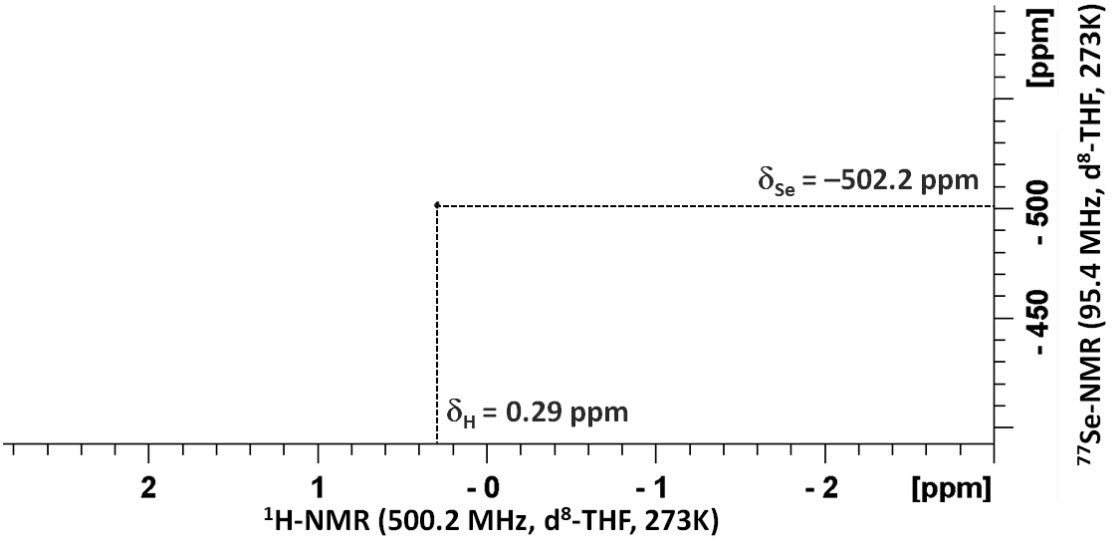

^{77}Se/^{1}H-HMQC-NMR (500.2/95.4 MHz, d^{8}-THF, 273K)

3.9. PPN[Au(SeSiMe$_3$)$_2$] (6-PPN)

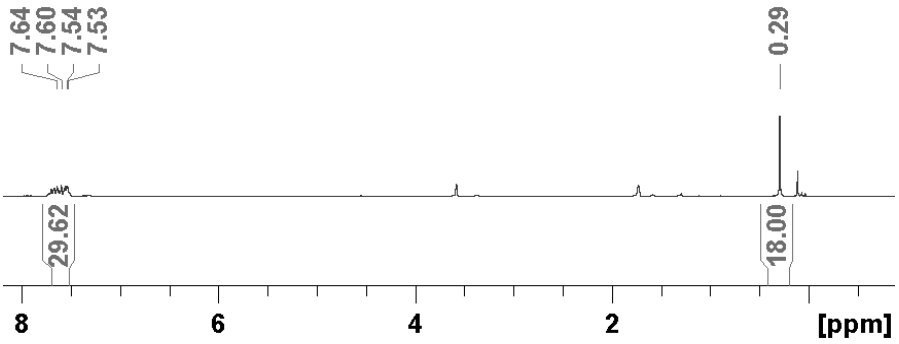

^{1}H-NMR (300.3 MHz, d^{8}-THF)

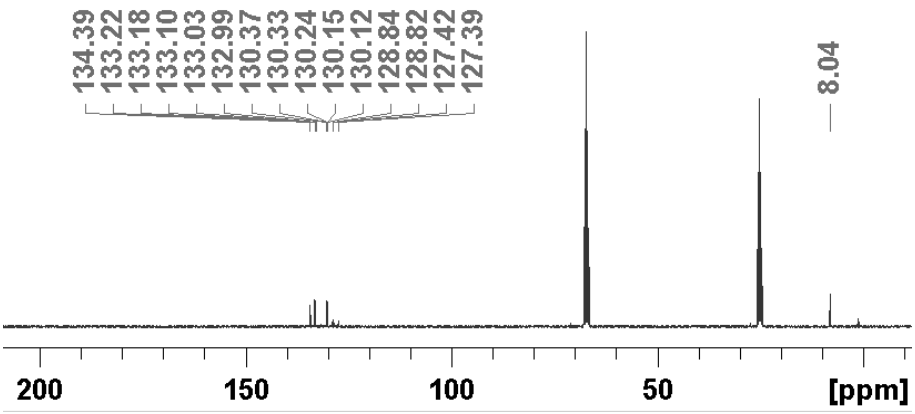

^{13}C-NMR (75.5 MHz, d^{8}-THF)

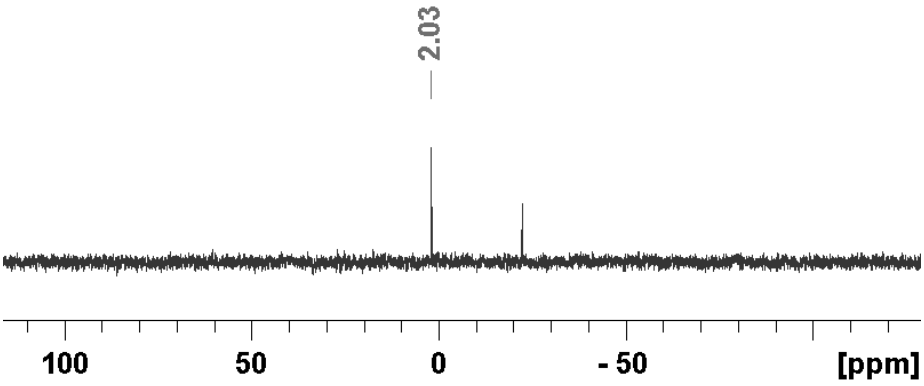

^{29}Si-NMR (59.7 MHz, d^{8}-THF)

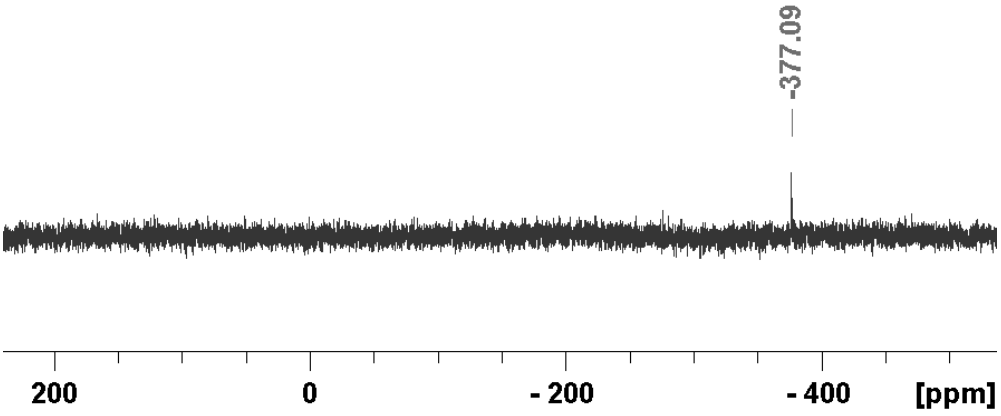

^{77}Se-NMR (57.3 MHz, d^{8}-THF)

3.10. $Ph_4P[Au(SeSiMe_3)_2]$ (6-Ph_4P)

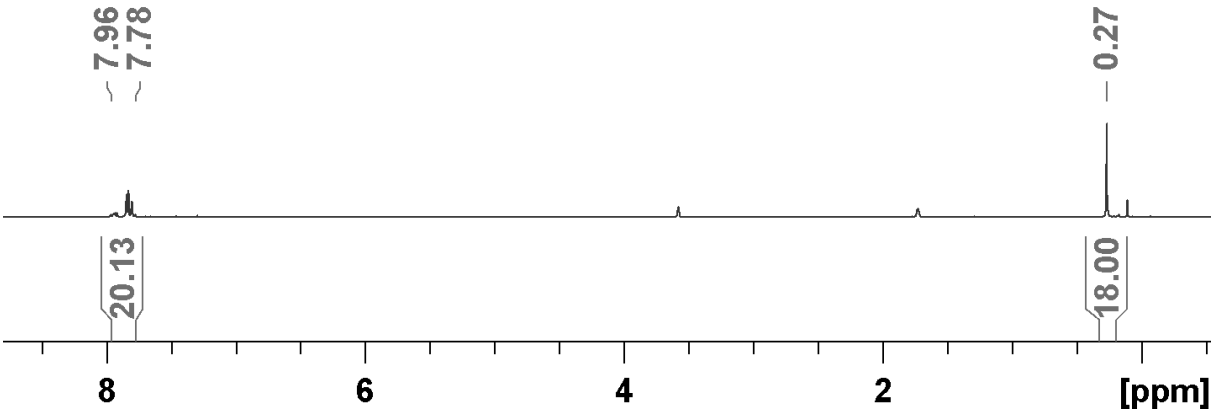

^{1}H-NMR (300.3 MHz, d^{8}-THF)

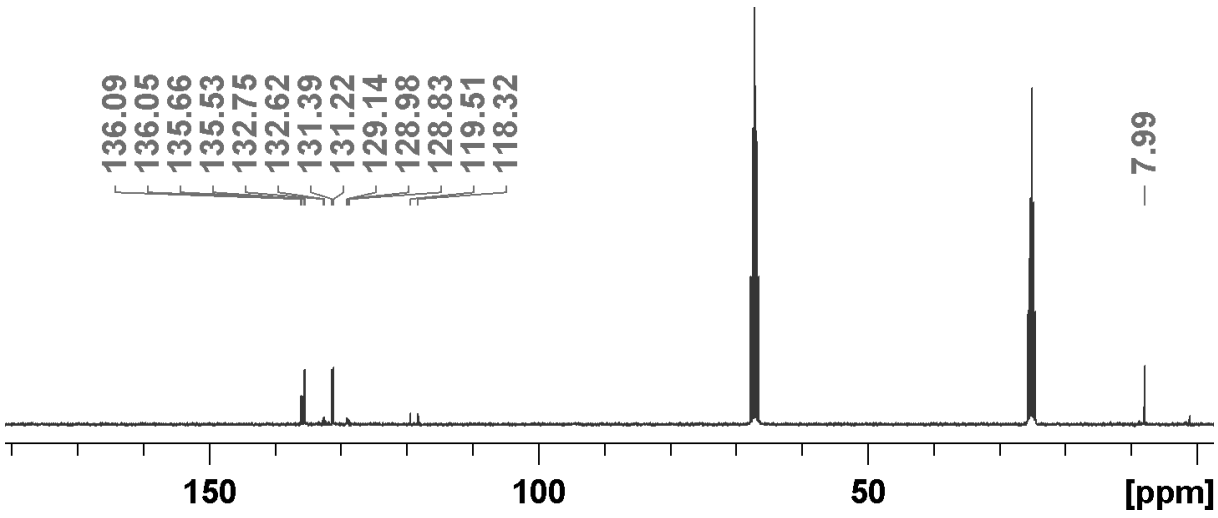

^{13}C-NMR (75.5 MHz, d^8-THF)

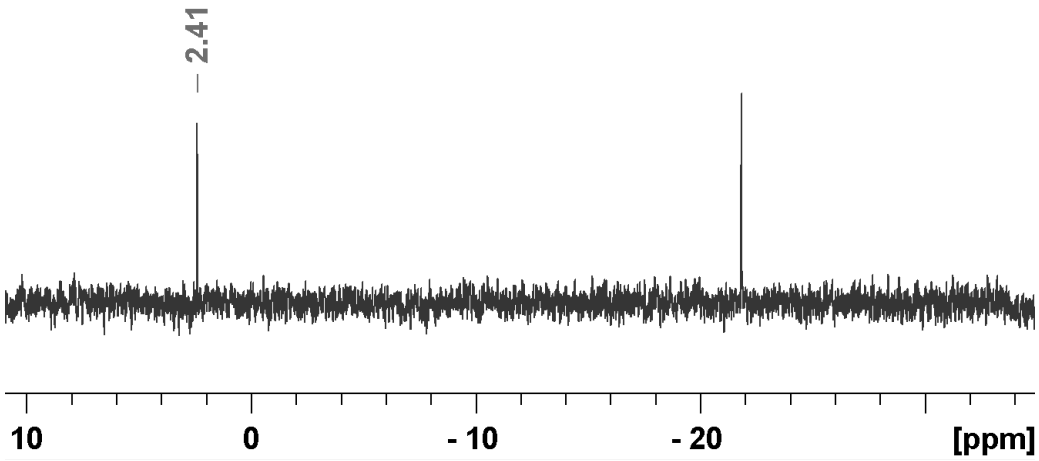

^{29}Si-NMR (99.4 MHz, d^8-THF, 273K)

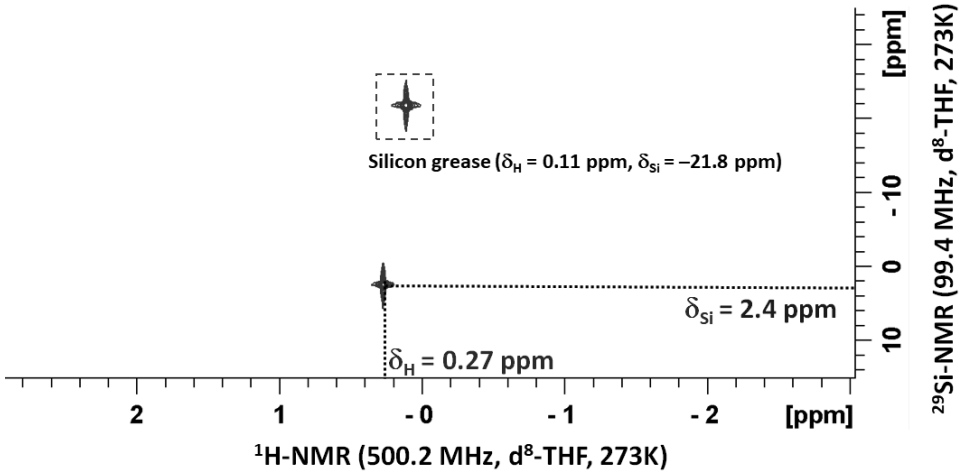

^{29}Si/^{1}H-HMQC-NMR (500.2/99.4 MHz, d^{8}-THF, 273K)

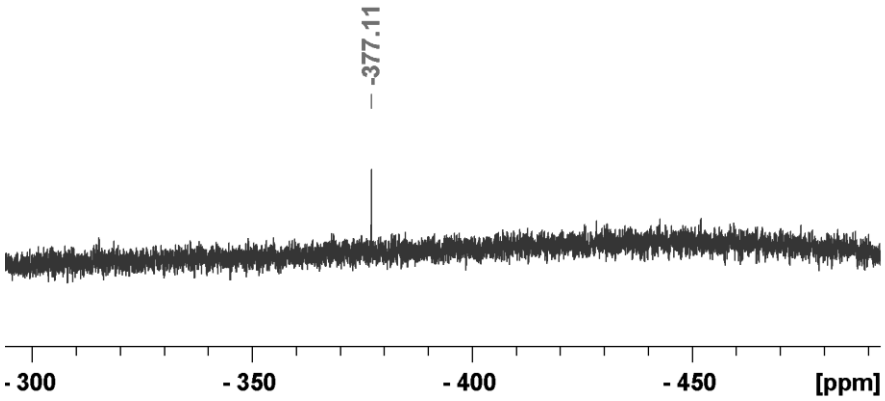

^{77}Se-NMR (95.4 MHz, d^{8}-THF, 273K)

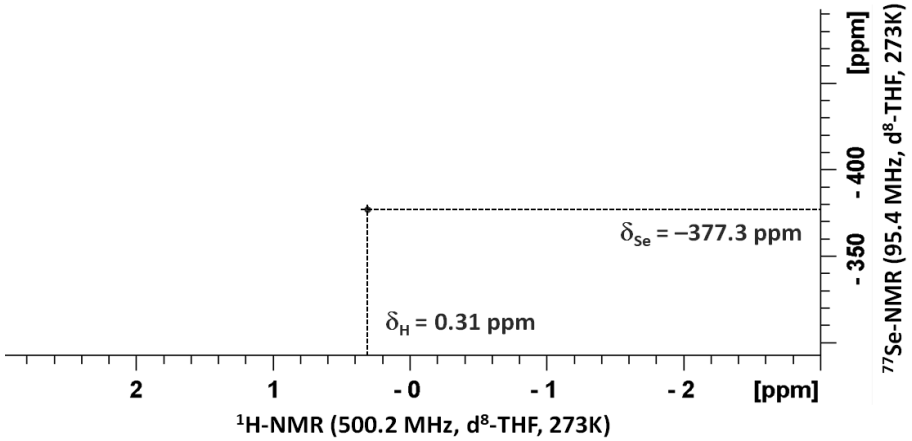

^{77}Se/^{1}H-HMQC-NMR (500.2/95.4 MHz, d^{8}-THF, 273K)

4. Thermal Decomposition of $Ph_4P[Cu(SSiMe_3)_2]$ (1)

In the DSC-TGA curve of $Ph_4P[Cu(SSiMe_3)_2]$ (**1**) shows a defined melting point a 91 °C (T_{onset} = 91.2 °C) and a rapid loss of mass from 179 °C on (T_{onset} = 179.2 °C), indicating the thermal decomposition. From 500 °C on, no further mass loss is detected (Figure S1). The total mass loss is 86%, which coarsely fits to the stoichiometric connected with the formation of Cu_2S (theoretical mass loss: 87%).

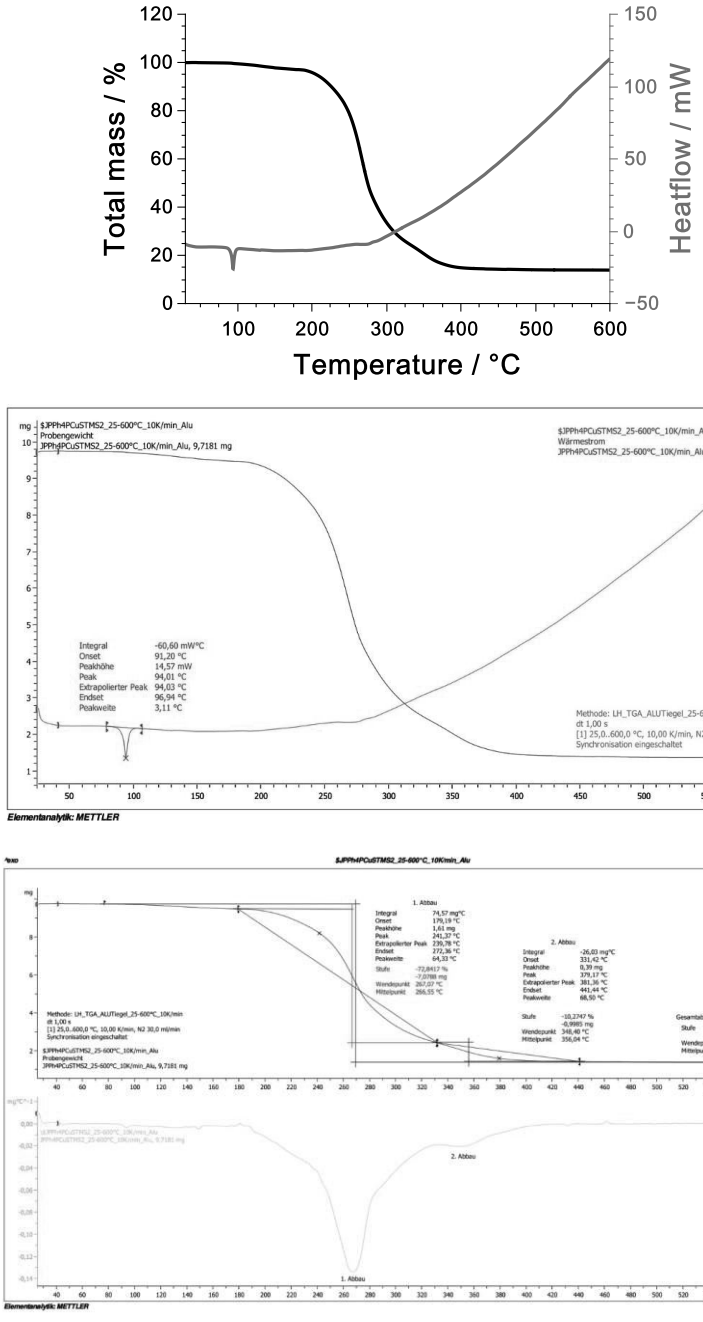

Figure S1. TGA/DSC curve of $Ph_4P[Cu(SSiMe_3)_2]$ (**1**) 25°C to 600 °C with a heating rate of 10 K min^{-1}. **1** melts (T_{onset} = 91.2 °C) before decomposition (T_{onset} = 179.2 °C).

The residue of the TGA-measurement was investigated via powder-XRD and by comparison with reference diffractograms identified as $Cu_{1.81}S$ (JCPDS: 41-0959), a copper-deficient phase of Cu_2S (Figure S2). The theoretical mass loss from $Ph_4P[Cu(SSiMe_3)_2]$ (**1**) to $Cu_{1.81}S$ (88%) is also very close to the observed one. In prior works we investigated the thermal decomposition behavior of monoanionic homoleptic metalates with $ESiMe_3$-moiety $Cat[M(ESiMe_3)_{n+1}]$ (E = S, Se; M = Ga, In, Zn, Sn(II)). Residues were always identified to be the binary metal chalcogenides $ME_{0.5n}$, which was traced back on a formal decomposition of the metalate compounds into the organic salt Cat $ESiMe_3$ and the neutral compound $M(ESiMe_3)_n$. While Cat $ESiMe_3$ decomposes without residue, the neutral $M(ESiMe_3)_n$ intramolecularly decomposes under quantitative desilylation by elimination of $E(SiMe_3)_2$ into the metal chalcogenides $ME_{0.5n}$. This decomposition assumption seems not to apply on $Ph_4P[Cu(SSiMe_3)_2]$ (**1**).

By defined thermolysis of 1 at 180 °C for two minutes at fine vacuum, a yellow waxy solid is obtained. This residue is diluted in DMF and this solution is subsequently layered with approximately twice the volume of diethyl ether. After a few days single crystals could be obtained that were clearly identified crystallographically as the literature-known binary 12:8-copper/sulfur tetraanion containing salt $(Ph_4P)_4[Cu_{12}S_8]$ (P. Betz, B. Krebs, G. Henkel, *Angew. Chem.* **1984**, 96 (4), 293-294). This anion could thermally decompose to four equivalents of Ph_3P and two equivalents of Ph_2S to form one formula unit of Cu_2S. However, in presence of Ph_4P $[SSiMe_3]$ it can be suggested, that $(Ph_4P)_4[Cu_{12}S_8]$ reacts with $Ph_4P[SSiMe_3]$ to form adducts of the kind $(Ph_4P)_{4+n}[Cu_{12}S_8(SSiMe_3)_n]$. At elevated temperatures probably an conversion of two $[SSiMe_3]^-$ ligands to one equivalent of $[S_2]^{2-}$ and $(Me_3Si)_2$ could explain the copper-poor Cu/S phase (Scheme S2): When the $[S_2]^{2-}$ is partially substituting the $[S]^{2-}$ ions in $(Ph_4P)_4[Cu_{12}S_8]$ to yield species of the kind $(Ph_4P)_4[Cu_{12}S_{8-x}(S_2)_x]$, complete thermolysis would yield $Cu_{12}S_{8-x+2x-2}$ (or $Cu_{12}S_{6+x}$). For x = 0.63 the target stoichiometry of $Cu_{1.81}S$ would result.

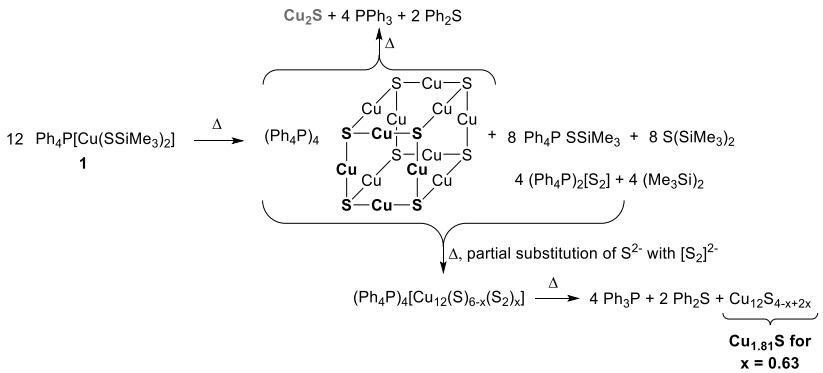

Scheme S2. By thermal treatment of twelve equivalents of $Ph_4P[Cu(SSiMe_3)_2]$ (**1**) one equivalent of the cluster molecule $(Ph_4P)_4[Cu_{12}S_8]$ is obtained by complete desilylation, together with eight equivalents of Ph_4P $SSiMe_3$. We assume that the copper atoms in the cluster molecule are partially attacked by the $SSiMe_3$ anions, thereby increasing the overall sulfur content of the material obtained after complete thermolysis.

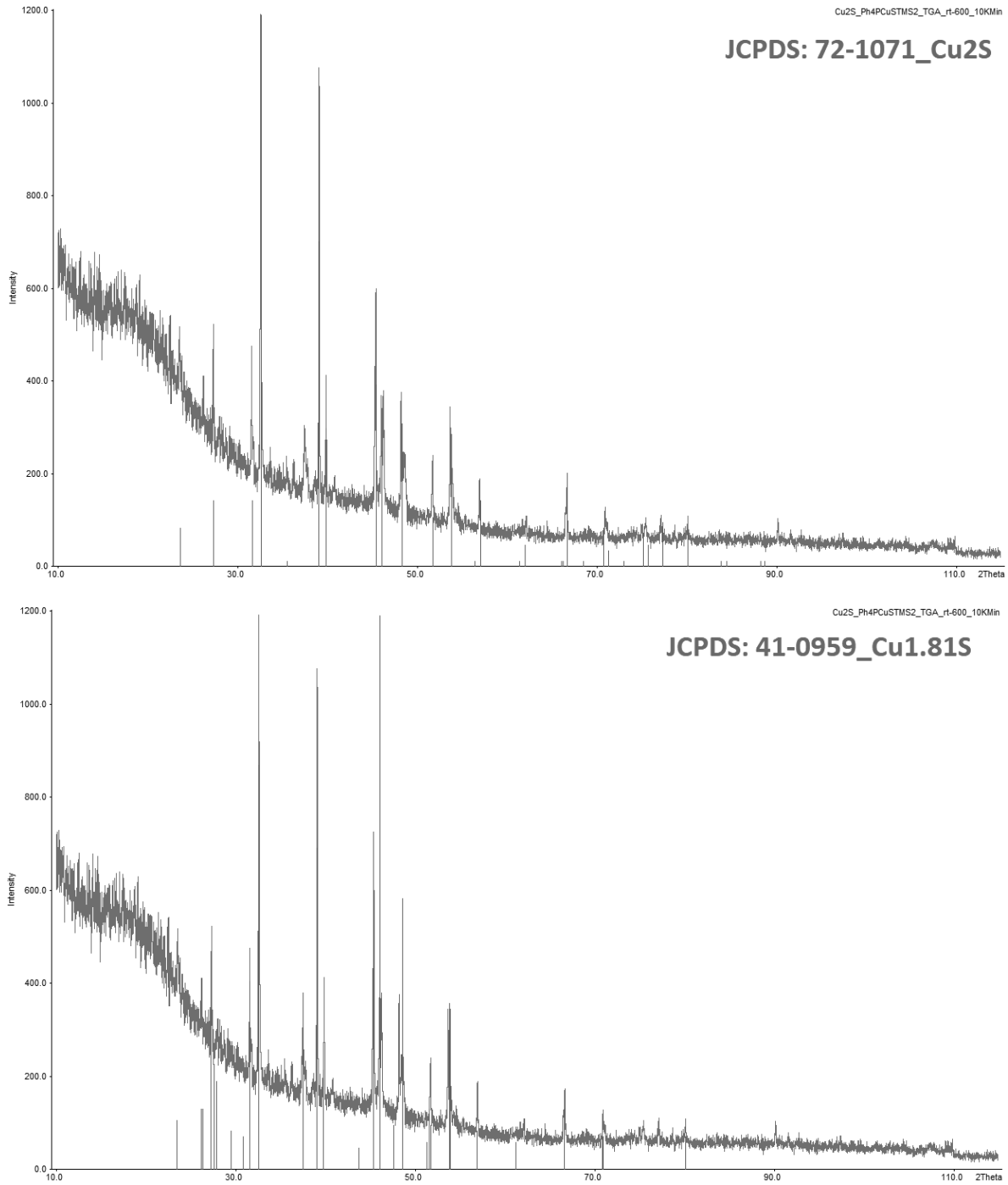

Figure S2. PXRD of the residue obtained by the TGA measurement (25°C to 600 °C with a heating rate of 10 K min^{-1}). The reflexes that can not be assigned to Cu_2S (top, JCPDS: 72-1071) can be assigned to $Cu_{1.81}S$ (bottom, JCPDS: 41-0959).

5. Quantumchemical calculations

Figure S3 shows the orbital energies of the highest occupied MOs of $[Cu(SSiMe_3)_2]^-$ as a function of the torsional angle Si-S-S-Si, α, of $[Cu(SSiMe_3)_2]^-$, in the same way as Figure 8 for the model compound $[Cu(SCl)_2]^-$ in the main paper. The labeling of MOs in Figure S3 is in line with that in Figure 8, as far as possible. The underlying density functional calculations were done with TURBOMOLE employing the TPSS functional and dhf-TZVP basis sets, that is, structure optimizations were carried out keeping α fixed at -10, 0-,10…270° while all other coordinates were optimized.

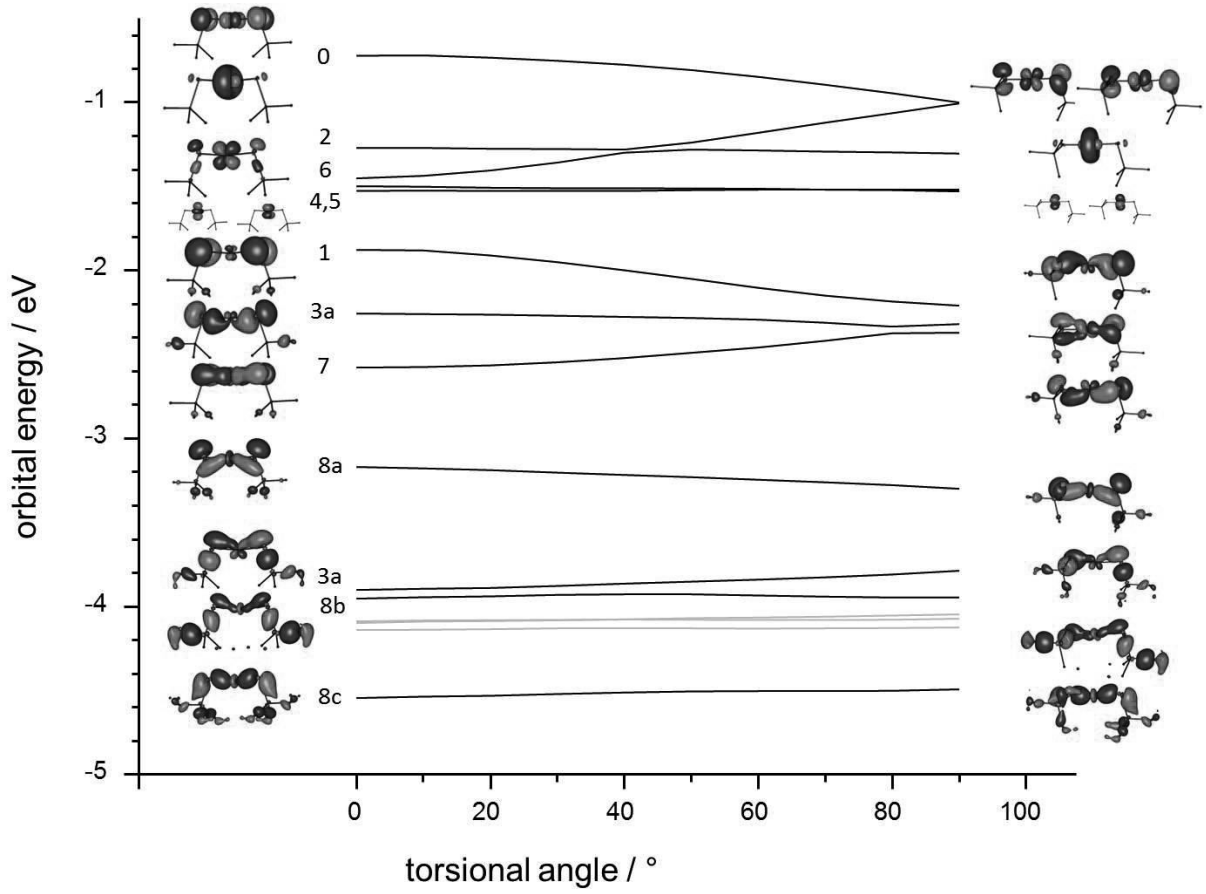

Figure S3. Orbital energies of the highest occupied MOs as a function of the torsional angle Si-S-S-Si, α, of $[Cu(SSiMe_3)_2]^-$. Orbitals are plotted for α=0° (left) and α=90° (right).

6. Methanolysis of $Ph_4P[Ag(SSiMe_3)_2]$ (2) and formation of Ag_2S

When dry methanol (15 mL) is added to the colorless powder $Ph_4P[Ag(SSiMe_3)_2]$ (50 mg, 0.08 mmol) under inert gas conditions at room temperature, a rapid change in color due to the precipitation of black silver sulfide indicates the formation of Ag_2S (Figure S4, top row). After centrifugation of the suspension the supernatant solution is removed. The black residue is washed twice with thf (10 mL) and stored for 3 days as 140°C under vacuum. The identity of Ag_2S is proven by PXRD (Figure S4, bottom row).

Precipitation:

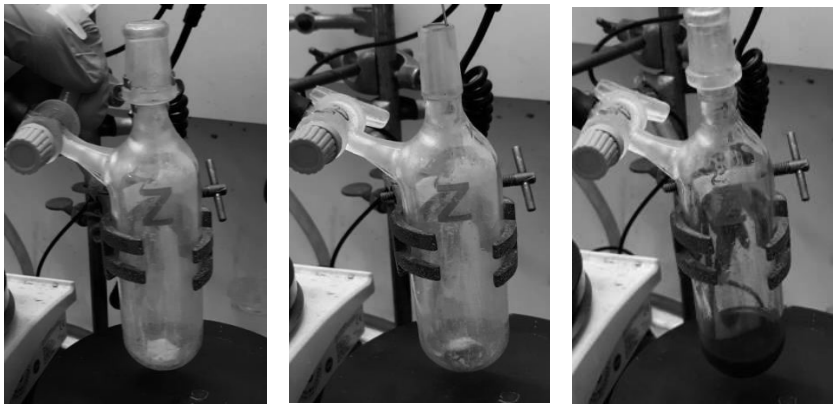

PXRD:

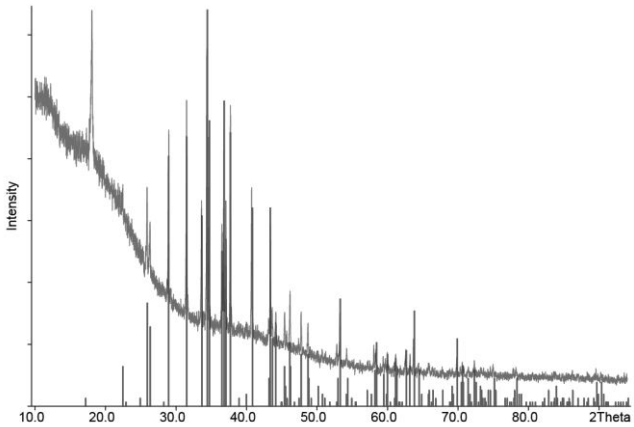

Figure S4. Top row: $Ph_4P[Ag(SSiMe_3)_2]$ (left) is treated with MeOH (middle) to yield a black suspension of Ag_2S (right). Bottom row: The isolated black residue is identified as Ag_2S by PXRD (green: observed, red: reference for Ag_2S) after isolation and annealing (3d, 140°C).

It is a commonly observed phenomenon among the title compounds, that contact with protic solvents or moisture from air induces the precipitation of black solids. This has been observed in all the corresponding NMR-sample tubes after measurement, due to the diffusion of moisture into the tube. We state, that this is a convenient method to prepare coinage metal chalcogenide materials M_2E (M = Cu, Ag, Au; E = S, Se) from lipophilic solvents. A solution of $Cat[M(ESiMe_3)_2]$ in tetrahydrofuran can be used to precipitate the corresponding M_2E material by slowly adding methanol.

In preparation

Dimethylpyrrolidinium Chalcogenido-Dimethylgallates and -indates $DMPyr_2[Me_2M(\mu_2\text{-}E)]_2$ (M = Ga, In; E = S, Se): Their use in the Synthesis of Higher or Lower Order Chalcogenidoindates

Jannick Guschlbauer, Lars H. Finger, Tobias Vollgraff, Klaus Harms, Jörg Sundermeyer

Dimethylpyrrolidinium Chalcogenido-Dimethylgallates and -indates $DMPyr_2[Me_2M(\mu_2\text{-}E)]_2$ (M = Ga, In; E = S, Se): Their use in the Synthesis of Higher or Lower Order Chalcogenidoindates

Jannick Guschlbauer, Lars H. Finger, Tobias Vollgraff, Klaus Harms, Jörg Sundermeyer*

Philipps-Universität Marburg, Hans-Meerwein-Straße 4, 35032 Marburg, Germany

ABSTRACT: Reactions of *N,N*-dimethylpyrrolidinium hydrochalcogenide salts DMPyr [SH] (**1**) and DMPyr [SeH] (**2**) with trimethygallium and trimethylindium lead to metalation of $[EH]^-$, methane elimination and formation of a new series of chalcogenido metalates $DMPyr_2[Me_2Ga(\mu_2\text{-}S)]_2$ (**3**), $DMPyr_2[Me_2Ga(\mu_2\text{-}Se)]_2$ (**4**), $DMPyr_2[Me_2In(\mu_2\text{-}S)]_2$ (**5**), and $DMPyr_2[Me_2In(\mu_2\text{-}Se)]_2$ (**6**). The crystallographically determined molecular structures of **3**, **4**, **5**, and **6** show the presence of dinuclear dianions with four-membered ring structures displaying highly nucleophilic bridging chalcogenide ligands. Some representative reactions of these building blocks with nucleophiles and electrophiles were studied: Addition of two equivalents of $E(SiMe_3)_2$ (E = S, Se) to the indates $DMPyr_2[Me_2In(\mu_2\text{-}S)]_2$ (**5**) and $DMPyr_2[Me_2In(\mu_2\text{-}Se)]_2$ (**6**) leads to a cleavage of the ring, E silylation and formation of mononuclear, monoanionic trimethylsilylchalcogenido dimethylindates $DMPyr[Me_2In(SSiMe_3)_2]$ (**7**), $DMPyr[Me_2In(SeSiMe_3)_2]$ (**8**), and even a mixed thio-selenido dimethylindate $DMPyr[Me_2In(SSiMe_3)(SeSiMe_3)]$ (**9**). Reaction of $DMPyr_2[Me_2In(\mu_2\text{-}S)]_2$ (**5**) with two equivalents Lewis acid Me_3In leads to charge delocalization, ring expansion and formation of six-membered ring $DMPyr_3[Me_2In(\mu_3\text{-}S\text{-}InMe_3)]_3$ (**10**). The latter is a key intermediate in the formation of dianionic sulfidoindate $DMPyr_2[(Me_2In)_6(\mu_3\text{-}S)_4]$ (**11**) displaying an unusual inverse heteroadamantane structure with four capping sulfido ligands.

Introduction

Molecular compounds of group 13 and 16 elements are of interest due to their potential to act as precursors for triel-chalcogenide-based semiconductor materials.[1] The sesquiselenide In_2Se_3, or members of the CIGS-family $Cu(In_xGa_{1-x})(S_y,Se_{1-y})_2$, show remarkable performance in optoelectronic[2] and photovoltaic[3] devices, respectively.

The most common strategies to incorporate purely inorganic chalcogen atoms into molecular compounds or clusters is either the deprotonation of H_2E (E = S, Se) with precursors containing basic leaving groups,[3] or salt eliminations of the corresponding alkali metal chalcogenides M_2E or MEH (M = Li-Cs) or $LiESiMe_3$[4] and $NaESiMe_3$ with group 13 metal halides.[5,6] Furthermore, desilylation of $E(SiMe_3)_2$ with desilylating metal acetates or halides are a common strategy.[7] Trimethylgallium and -indium are widely used group 13 precursors that can be decomposed thermally to yield high purity materials in MOCVD processes.[8] Alkyltrieles are *Lewis*-acidic, but can also act as *Brønsted* bases towards suitable *Brønsted* acids under elimination of the corresponding alkanes.[9,10] Scheme 1 shows representative reaction patterns between selected chalcogen precursors and organotriels known from literature in context of the herein introduced ionic approach towards the new class of compounds **3-6** presented here.

When H_2S or elemental chalcogens are reacted with trialkyltrieles, the heterocubane compounds $[(\mu_3\text{-}E)_4(MR)_4]$ (M = Al, Ga, In; R = Me_2EtC, *t*Bu) emerge (Scheme 1, i).[9,10] By deprotonation of silylated thioles $HSSiR'_3$ (R' = alkyl), or desilylation of bistrialkylsilylchalcogenides with trialkyltrieles, the formation of four-membered dimer-like neutral compounds with bridging silylchalcogenolate moieties of the type $[R_2M(\mu_3\text{-}ESiR'_3)]_2$ can be observed (Scheme 1, ii).[11,12]

Scheme 1. i: formation of the group 13/16 heterocubane compounds $[RM(\mu_3\text{-}E)]$ (I).[9,10] ii: formation of the group 13/16 dimer-like $[R_2M(\mu_2\text{-}ESiR_3)]_2$ (II).[11,12] iii: formation of the group 13/16 four-membered chalcogenidoorganometalates 3-6 (Cat = organic cation, here: $DMPyr^+$).

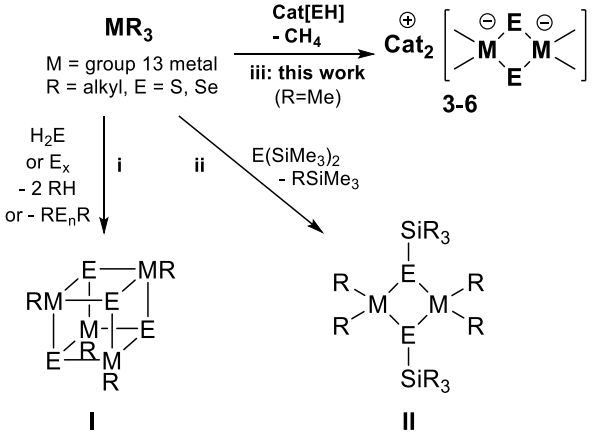

Organic onium salts with hydrochalcogenide anions have been made accessible in high purity without contamination of metals, halides and water by deprotonation of H_2E with the corresponding methylcarbonate salts $Cat[OCO_2Me]$.[13] This high purity qualifies these salts to be reacted with highly air- and moisture sensitive compounds such as the trialkyltriels. Herein we introduce a synthesis in which ionic-liquid-like hydrochal-

cogenide salts Cat[EH] (E = S, Se) are used as starting materials to incorporate chalcogen atoms into dinuclear chalcogenido diorganometalate compounds. Their protolytic reaction with group 13 alkyls Me_3M (M = Ga, In) is investigated here (Scheme 1, iii). Few literature-known examples of lower nuclearity chalcogenido gallates and indates are known. They are synthesized by reaction of alkali metal hydrochalcogenides with MCl_3 to yield the trianionic, trinuclear six-membered rings $[(Cl_2M)(\mu_2\text{-}E)]_3^{3-}$ (M = Ga, In; E = S, Se).[14]

Results and discussion

The syntheses of the hydrochalcogenide salts were performed according to literature known procedures (Scheme 2).[13] DMPyr[SH] (**1**) was prepared by deprotonation of H_2S with DMPyr[OCO_2Me] in methanol. DMPyr[SeH] (**2**) was prepared by adding $Se(SiMe_3)_2$ to a solution of DMPyr[OCO_2Me] in methanol.

Scheme 2. Preparation of the hydrochalcogenide salts DMPyr[SH] (1) and DMPyr[SeH] (2).

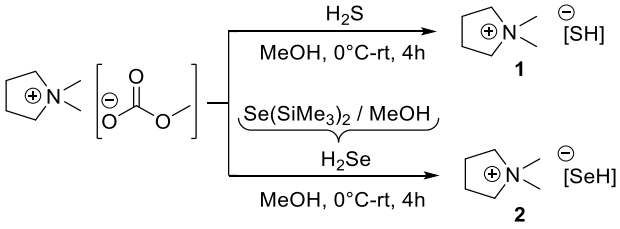

Single crystals of DMPyr[SH] (**1**) suitable for X-ray analysis could be obtained by slow diffusion of diethyl ether into a solution of **1** in acetonitrile at room temperature. **1** crystallizes in the space group $P2_1/n$ with four formula units per unit cell. One $DMPyr^+$ cation is non-covalently bonded to three hydrosulfide anions via H-bonds that range from 2.75 Å to 2.88 Å **(**Figure 1**).** The most similar structurally characterized compound known to literature is the *N,N*-butylmethylpyrrolidinium ($BMPyr^+$) homologue BMPyr[SH], in which also three sulfur atoms are non-covalently connected to one $BMPyr^+$ cation via H-bonds that range from 2.64 Å to 2.87 Å.[13]

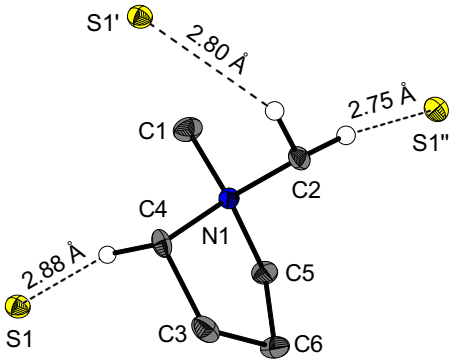

Figure 1. Molecular structure of DMPyr[SH] (**1**). Only protons involved in H-bonds are shown. Ellipsoids shown at the 50% level. Symmetry operations I: -1+x, y, z; II: -1/2+x, 1/2-y, 1/2+z. Selected bond lengths (in Å) and angles (in °): C1-N1 1.493(2), C2-N1 1.503(1), C4-N1 1.511(1), C5-N1 1.511(1), C4-C3 1.527(2), C3-C6 1.550(2), C5-C6 1.526(2), C1-N1-C2 109.95(8), C1-N1-C5 111.67(8), C1-N1-C5-C6 –161.66(9), C5-C6-C3 104.96(9), C5-C6-C3-C4 –2.2(1), C6-C3-C4 105.59(9), C6-C3-C4-N1 –23.7(1), C3-C4-N1-C2 –77.3(1), S1-C4 3.776(1), S1-C4-N1 94.00(6), S1-C4-N1-C5 –64.6(7).

X-ray suitable single-crystals for the selenium homologue DMPyr[SeH] (**2**) could be obtained by slow gas phase diffusion of diethyl ether into a saturated solution of **2** in a mixture of acetonitrile and diethyl ether at ambient temperature for several days. DMPyr[SeH] (**2**) crystallizes in the space group $P2_1/n$ with four ion pairs per unit cell. One $DMPyr^+$ cation is non-covalently bonded to two selenium atoms by two H-bonds to protons of the same *N*-bond methyl group that range from 2.85 Å to 2.92 Å (Figure 2).

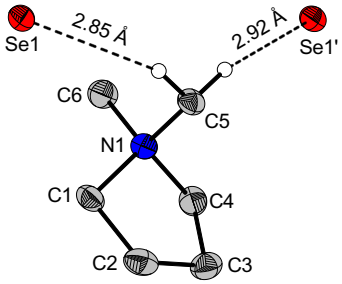

Figure 2. Molecular structure of DMPyr[SeH] (2). Only protons involved in H-bonds are shown. Ellipsoids shown at the 50% level. Symmetry operations I: 1/2+x, 1/2-y, 1/2+z. Selected bond lengths (in Å) and angles (in °): C6-N1 1.495(4), C5-N1 1.497(4), C1-N1 1.511(4), C4-N1 1.513(4), C1-C2 1.529(5), C2-C3 1.546(5), C4-C3 1.528(5), C6-N1-C5 109.9(2), C6-N1-C4 111.3(2), C6-N1-C4-C3 –159.4(3), C4-C3-C2 105.8(2), C4-C3-C2-C1 3.9(3), C3-C2-C1 104.9(3), C3-C2-C1-N1 –28.7(3), C2-C1-N1-C5 –75.0(3), Se1-C5 3.758(3), Se1-C5-N1 92.8(2), Se1-C5-N1-C4 –170.6(2).

The interionic contacts of the literature known homologues R_4N[SeH] (R = Me,[15] Bu[16]) and the 1-Ethyl-3-methylimidazolium (EMIm) salt EMIm[SeH][13] are not comparable with the herein discussed contacts. The closest interionic contact in Me_4N[SeH] and Bu_4N[SeH] are 3.12 Å[15] and 3.06 Å[16] respectively, while the H-bonds between the aromatic imidazolium attached protons and the selenium atom in EMIm[SeH] range from 2.81 Å to 2.95 Å.[13] In contrast to **1** and **2**, the comparable homologue organic hydrochalcogenide salts

MMIm[SH] and MMIm[SeH] show H-bonding modes that do not differe qualitatively.[17]

The ^{1}H NMR spectra of the salts **1** and **2** confirm the reported proton shifts of the anions: –4.04 ppm for $[SH]^-$ (**1**) and –6.62 ppm for $[SeH]^-$ (**2**).[13] The hydrochalcogenide anions are more and more pronounced high-field shifted with increasing atomic number of the involved chalcogenatom, which consistently fits the reported trend (Figure 3).[13,15]

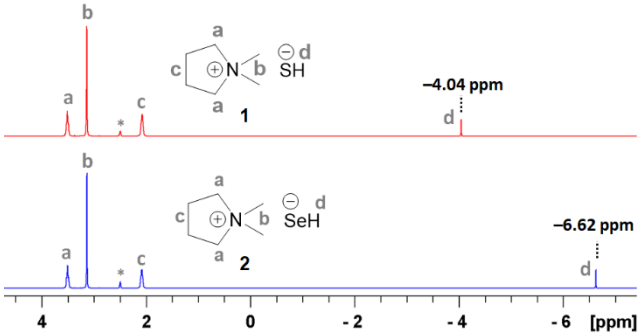

Figure 3. ^{1}H NMR (300.3 MHz, *dmso-d^6) of the hydrochalcogenide salts DMPyr[SH] (**1**, top row) and DMPyr[SeH] (**2**, bottom row).

When a solution of Me_3M (M = Ga, In) in tetrahydrofuran is added to a suspension of the hydrochalcogenide salt DMPyr[EH] (E = S, Se) at low temperature, a clear solution is obtained within a few minutes. This indicates an increase in liphophilicity that might be traced back on the formation of an intermediate hydrochalcogenido trimethylmetalate adduct between the hydrochalcogenide anion and the trimethyltriel compound (Scheme 3, I). After warming up this solution to room temperature and continuous stirring for a few hours, a colorless precipitate emerges. After removal of all volatiles in fine vacuum, a colorless powder is obtained. ^{1}H NMR spectra and elemental analyses confirm the presence of the title compounds $DMPyr_2[Me_2M(\mu_2\text{-}E)]_2$ **3-6** that arise by onefold methane elimination. Single-crystal X-ray analyses show the presence of four membered dimer-like dianions $[Me_2M(\mu_2\text{-}E)]_2^{2-}$ with four-membered ringstructures for all combination of E = S, Se and M = Ga, In (Scheme 3).

Scheme 3. Preparation of the title compounds 3-6 from trimethyltrieles and the hydrochalcogenides 1 and 2 via the intermediate adduct I.

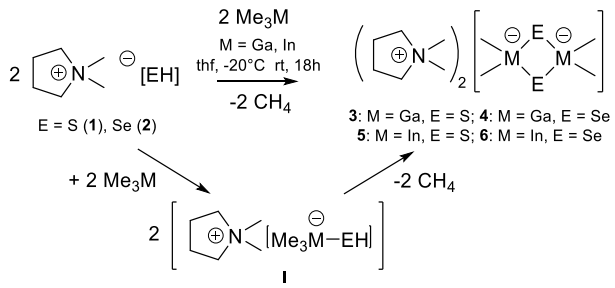

Single crystals of $DMPyr_2[Me_2Ga(\mu_2\text{-}S)]_2$ (**3**) suitable for X-ray analysis could be obtained by diffusion of pentane into a saturated solution of **3** in tetrahydrofuran at room temperature for few days. **3** crystallizes in the monoclinic space group $P2_1/n$ with two ion pairs per unit cell. Due to crystallographically disordered cations the interionic interactions could not be reliably identified (Figure 4).

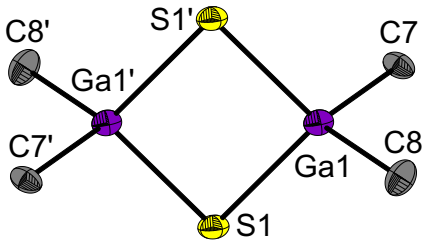

Figure 4. Molecular structure of the dianion present in $DMPyr_2[Me_2Ga(\mu_2\text{-}S)]_2$ (**3**). Cations and protons are not shown for clarity. Due to disordered cations, non-covalent interionic interactions cannot be discussed. Ellipsoids shown at the 50% level. Symmetry operations I: 1-x, -y, 1-z. Selected bond lengths (in Å) and angles (in °) of the anion: Ga1-S1 2.3225(5), Ga1-S1' 2.3293(4), S1-Ga1-S1' 97.27(1), Ga1-S1'-Ga1' 82.73(1), Ga1-C7 2.032(2), Ga1-C8 2.012(2), C7-Ga1-C8 108.62(7), Ga1'-S1'-Ga1-C7 117.38(5), Ga1'-S1-Ga1-C8 119.00(5).

Single crystals of $DMPyr_2[Me_2Ga(\mu_2\text{-}Se)]_2$ (**4**) suitable for X-ray analysis could be obtained by diffusion of pentane into a saturated solution of **4** in tetrahydrofuran at 0°C for few days. **4** crystallizes in the monoclinic space group $P2_1/n$ with two ion pairs per unit cell. One crystallographically unique interionic H-bond with 2.93 Å between the both selenium atoms in the anion and two $DMPyr^+$ cations could be identified (Figure 5).

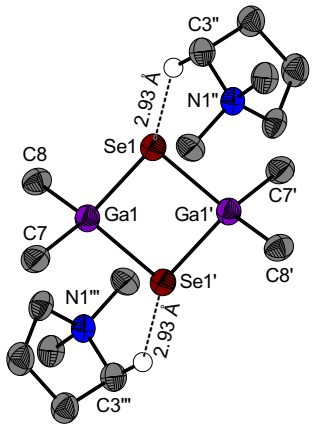

Figure 5. Molecular structure of $DMPyr_2[Me_2Ga(\mu_2\text{-}Se)]_2$ (**4**). Only protons active in H-bonds shown. Ellipsoids shown at the 50% level. Symmetry operations I: 1-x, 1-y, 1-z; II: -1/2+x, 1/2-y, ½+z; III: 3/2-x, 1/2+y, 1/2-z. Selected bond lengths (in Å) and angles (in °) of the anion: Ga1-Se1 2.453(1), Ga1-Se1' 2.461(1), Se1-Ga1-Se1' 82.41(4), Ga1-Se1-Ga1' 82.59(4), Ga1-C7 2.017(9), Ga1-C8 2.014(9), C7-Ga1-C8 109.0(4), Ga1'-Se1'-Ga1-C7 –118.4(3), Ga1'-Se1-Ga1-C8 –117.6(3).

Single crystals of $DMPyr_2[Me_2In(\mu_2\text{-}S)]_2$ (**5**) suitable for X-ray analysis could be obtained by diffusion of pentane into a saturated solution of **5** in tetrahydrofuran at room temperature for a few days. **5** crystallizes in the monoclinic space group $P2_1/n$ with two ion pairs per unit cell. One crystallographically unique interionic H-bond (2.83 Å) between one sulfur atom and a proton of the $DMPyr^+$ cation could be identified (Figure 6). The non-covalent interactions show remarkable similarity to those identified in the case of the selenium/gallium homologue **4**.

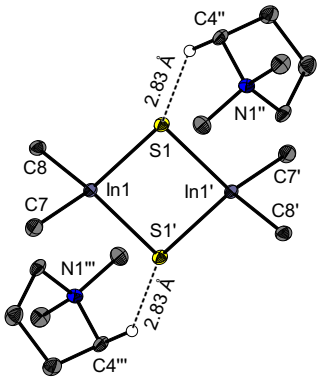

Figure 6. Molecular structure of DMPyr$_2$[Me$_2$In(μ_2-S)]$_2$ (**5**). Only protons active in H-bonds are shown. Ellipsoids shown at the 50% level. Symmetry operations I: -x, -y, -z; II: 1-x, -y, -z; III: -1+x, y, z. Selected bond lengths (in Å) and angles (in °) of the anion: In1-S1 2.5040(5), In1-S1' 2.5067(4), S1-In1-S1' 96.15(1), In1-S1-In1' 83.85(1), In1-C7 2.206(2), In1-C8 2.205(2), C7-In1-C8 108.45(6), In1'-S1'-In1-C7 –118.81(5), In1'-S1-In1-C8 116.64(4).

Single crystals of DMPyr$_2$[Me$_2$In(μ_2-Se)]$_2$ (**6**) suitable for X-ray analysis could be obtained from a sample containing an equimolar amount of DMPyr[SeSiMe$_3$][7] and InMe$_3$ for five days at room temperature in benzene. We suppose that the product emerges by partial hydrolysis or Me$_4$Si elimination. **6** crystallizes in the monoclinic space group $P2_1/n$ with two ion pairs per unit cell. Three crystallographically unique interionic H-bonds ranging from 2.98 Å to 2.90 Å between one selenium atom in the anion and different protons of three DMPyr$^+$ cations could be identified (Figure 7).

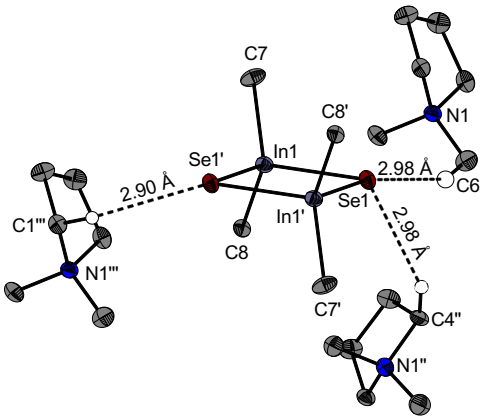

Figure 7. Molecular structure of DMPyr$_2$[Me$_2$In(μ_2-Se)]$_2$ (**6**). Only protons active in crystalographically unique H-bonds are shown. Ellipsoids shown at the 50% level. Symmetry operations I: 2-x, -y, 2-z; II: 1/2+x, ½-y, 1/2+z; III: 1+x, y, z. Selected bond lengths (in Å) and angles (in °) of the anion: In1-Se1 2.6208(4), In1-Se1' 2.6177(4), Se1-In1-Se1' 96.72(1), In1-Se1-In1' 83.28(1), In1-C7 2.209(3), In1-C8 2.212(3), C7-In1-C8 110.2(1), In1'-Se1'-In1-C7 –117.35(9), In1'-Se1-In1-C8 –116.58(8).

The ^{1}H NMR spectra of the title compounds show signals for two DMPyr$^+$ cations and one dianion, as indicated by the corresponding integrals (Figure 8). For the dianions a general trend towards more low field shift signals with increasing molecular weight can be observed. The influence on the anions' shift is stronger affected by the chalcogen atoms than by the metal atoms. The selenium compounds **4** and **6** are more low-field shifted than the corresponding signals of the sulfur homologues **3** and **5**, while the corresponding signal of the gallates **3** and **4** is slightly more high-field shifted compared to the indates **5** and **6**.

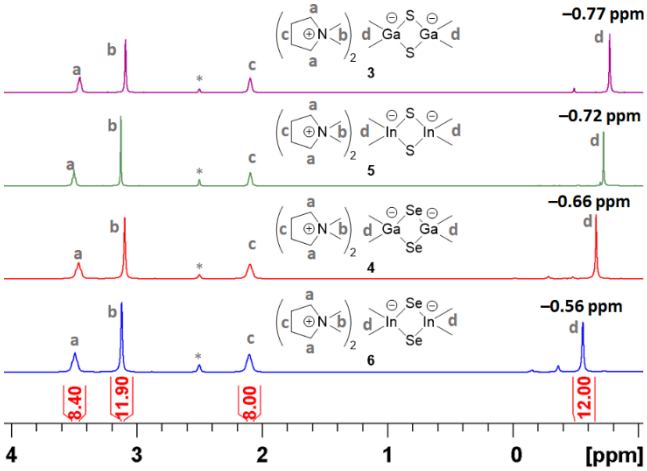

Figure 8: ^{1}H NMR spectra (**3**, 5: 500.2 MHz; 4, 5: 300.3 MHz, *dmso-d^6) of the chalcogenido dimethyltriellates DMPyr$_2$[Me$_2$M(μ_2-E)]$_2$ **3-6**.

This is contrary to the observations in the ^{77}Se NMR spectra of the selenium containing compounds, that show a more pronounced high-field shift with increasing molecular weight, with the free hydrochalcogenide anion in DMPyr[SeH] (**2**) having the most low field shift signal, and the anion in DMPyr$_2$[Me$_2$In(μ_2-Se)]$_2$ (**6**) showing the most high-field shift signal (Figure 9).

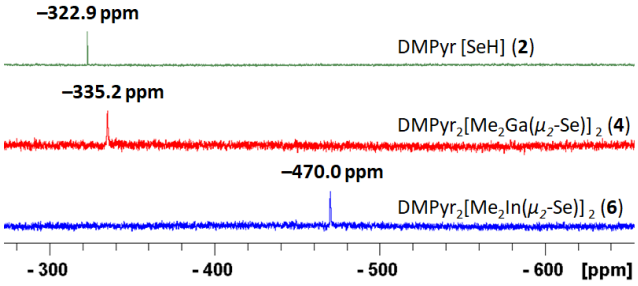

Figure 9. ^{77}Se NMR spectra (57.3 MHz, dmso-d^6) of the selenium containing title compounds DMPyr[SeH] (**2**, top row), DMPyr$_2$[Me$_2$Ga(μ_2-Se)]$_2$ (**4**, middle row), and DMPyr$_2$[Me$_2$In(μ_2-Se)]$_2$ (**6**, bottom row).

The indates DMPyr$_2$[Me$_2$In(μ_2-S)]$_2$ (**5**) and DMPyr$_2$[Me$_2$In(μ_2-Se)]$_2$ (**6**) can be further modified by formal addition of two equivalents of the correpsonding bistrimethylsilylchalcogenide to yield the *N,N'*-dimethylpyrrolidinium bis(trimethylsilylchalcogenolato)-dimethylindates DMPyr[Me$_2$In(SSiMe$_3$)$_2$] (**7**) and DMPyr[Me$_2$In(SeSiMe$_3$)$_2$] (**8**) (Scheme 4). A concerted addition mechanism can be considered, as the mixed substitution was possible for the reaction between DMPyr$_2$[Me$_2$In(μ_2-Se)]$_2$ (**6**) and an excess of S(SiMe$_3$)$_2$, that yields DMPyr [Me$_2$In(SSiMe$_3$)(SeSiMe$_3$)] (**8**), as indicated by a new signal for the indium attached methyl groups in the ^{1}H NMR spectra that differs from those of **7** and **8** (Figure 10).

Scheme 4. Assumend mechanism of addition of $E(SiMe_3)_2$ (E = S, Se) and the indates 5 and 6 towards heteroleptic silylchalcogenolato indates 7-9.

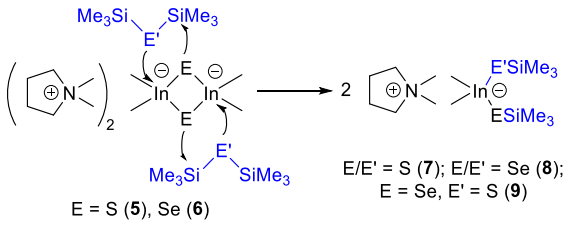

The reaction between $DMPyr_2[Me_2In(\mu_2\text{-}S)]_2$ (**5**) and an excess amount of $Se(SiMe_3)_2$ yields $DMPyr[Me_2In(SeSiMe_3)_2]$ (**8**), indicating that the In-Se bond is more stable compared to the In-S bond. Together with the elimination of $S(SiMe_3)_2$, the formation of In-Se bonds can be understood as the driving force that prevents a selective reaction to the mixed substituted species **9**. We assume there is an entropic driving force for the reaction between **6** and $S(SiMe_3)_2$ to yield the mixed substituted compound **9**. Alternatively $DMPyr[Me_2In(SSiMe_3)_2]$ (**7**) can be prepared via a mixed addition and salt elimination reaction by adding one equivalent of the organic trimethylsilylthiolate compound $DMPyr[SSiMe_3]$[7] with Me_2InCl and a subsequent substitution of the chloride with an additional equivalent of $DMPyr[SSiMe_3]$ (Scheme 5).

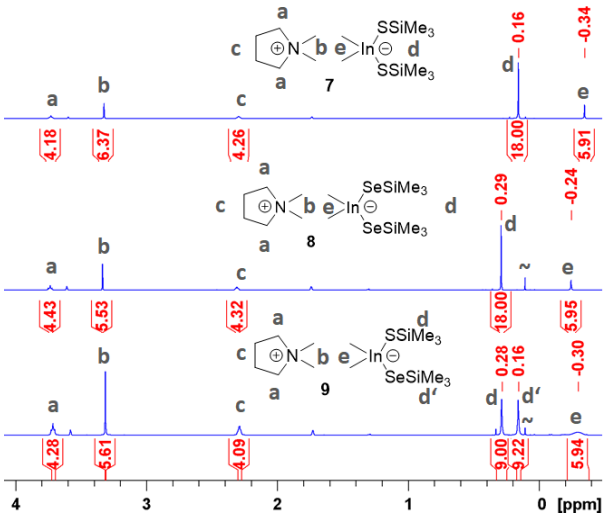

Figure 10. ^1H NMR spectra (250.1 MHz, *dmso-d^6) of the indates **7**, **8**, and **9**. The shift of the indium attached methyl groups of **9** implies the presence of a thio- and seleno-substituted metalate anion.

Compounds containing metal atoms attached to the silylchalcogenolate moiety $ESiMe_3$ are known as metastable and slightly modifyable chalcogenolate complexes $[L_nM(E\text{-}SiMe_3)_m]$ (L = neutral or anionic auxiliary ligand).[6,11,18–20] By choosing suitable precursors, like metal acetates M'OAc, chalcogen compounds of the kind M-E-M' can be obtained through selective desilylation by elimination of Me_3SiOAc.[6] Only two structural motives with organotrieles are known: the spirocyclic compounds $[(Me_2M)_6E(ESiMe_3)_4]$ (M = Ga, In; E = S, Se),[21] and $[iPr_3PCu(\mu_3\text{-}ESiMe_3)(InMe_3)]$ (E = S, Se),[22] the addition product of the of $InMe_3$ and $iPr_3PCuESiMe_3$, that unites all atoms necessary to act as $CuIn(S_xSe_{1-x})_2$ materials precursors.[20,22]

Scheme 5. The successful reactions between the chalcogenidoindates 5 and 6 to get the heteroleptic silylchalcogenolatodimethylindates 7 and 8, and the mixed substituted silylchalcogenolate 9.

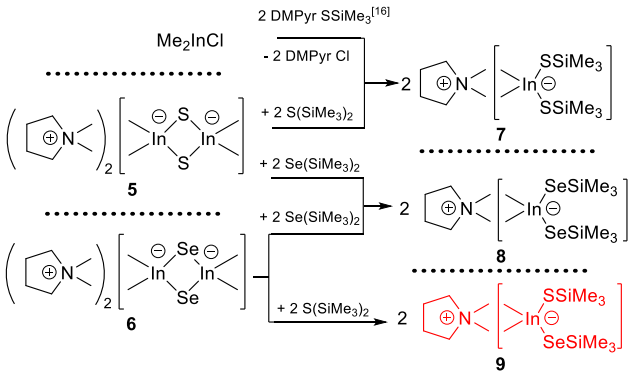

Subsequent indation of $DMPyr_2[Me_2In(\mu_2\text{-}S)]_2$ (**5**) with two equivalents of trimethylindium results in the formation of the adduct species $DMPyr_3[Me_2In(\mu_3\text{-}S\text{-}InMe_3)]$ (**10**) as confirmed by NMR spectra and elemental analysis. Single crystals of poor quality allow to assume this adduct species to build up a trimer-like six-membered ring structure with twist-boat conformation that enables the bulky terminal trimethylindate units to obtain an equatorial position to avoid ring strain (supporting information). The ring expansion can be attributed to charge delocalization. The conformative rigidity of the ring structure explains the split signal in the ^1H NMR for the cyclic dimethylindate units, and the broad singlet for the terminal trimethylindate moieties (Figure 11).

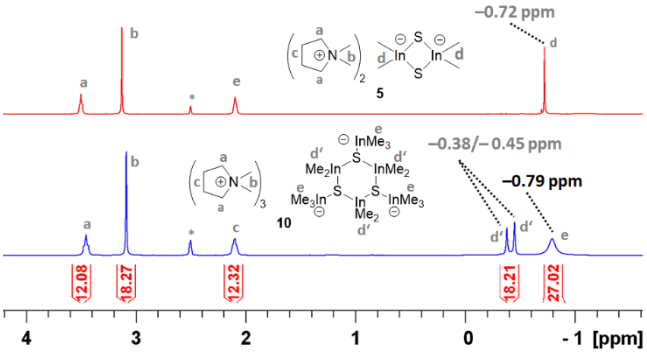

Figure 11: ^1H NMR spectra (500.1 MHz for **5**, 300.1 MHz for **10**, *dmso-d^6) of $DMPyr_2[Me_2In(\mu\text{-}S)]_2$ (**5**) before (top row), and after addition of two equivalents of $InMe_3$ and the formation of $DMPyr_3[Me_2In(\mu_3\text{-}S\text{-}InMe_3)]_3$ (**10**) (bottom row).

In order to obtain single crystals for a valid structure determination of $DMPyr_3[Me_2In(\mu_3\text{-}S\text{-}InMe_3)]_3$ (**10**) a saturated solution of **10** in a mixture of tetrahydrofuran and pentane was stored at room temperature for 14 days. Unexpectedly, the grown crystals were identified as the salt $DMPyr_2[(Me_2In)_6(\mu_3\text{-}S)_4]$ (**11**) that contains a hexanuclear inverse heteroadamantane cage dianion. **11** crystallises in the tetragonal space group $I4_1/acd$ with disordered cations and 16 ion pairs per unit cell and half a molecule of tetrahydrofurane per formula unit (Figure 12).

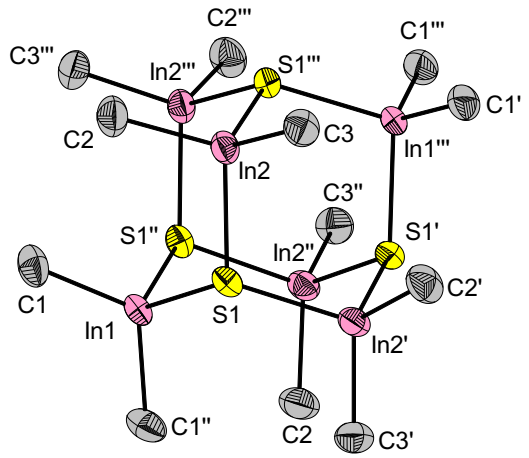

Figure 12. Molecular structure of the dianion in $DMPyr_2[(Me_2In)_6(\mu^3\text{-}S)_4]$ (**11**). Protons, cations, and solvent molecules are not shown for clarity. Ellipsoids shown at the 50% level. Symmetry operations I: 3/4–y, –1/4+x, 1/4–z; II: 1–x, 1/2–y, z; III: 1/4+y, 3/4–x, 1/4–z. Selected bond lengths (in Å) and angles (in °) of the anion: S1-In1 2.522(1), S1-In2 2.522(1), S1-In2' 2.522(1), S1''-In1-S1 106.96(4), S1-In2-S1''' 107.15(4), In1-S1-In2' 111.80(5), In1-S1-In2 109.60(5), In1-C1 2.174(5), In2-C2 2.177(6), In2-C3 2.181(5), C1-In1-C1'' 118.5(2), C2-In2-C3 118.0(2), S1-In1-C1 108.2(1), S1-In1-C1'' 107.3(1), In2-S1-In1-C1'' 177.9(2), C1-In1-S1-In2' –176.0(2), C2-In2-S1-In2' 174.4(2), C2-In2-S1-In1 178.8(2), In1-S1-In2'-S1' 59.65(6), In1-S1-In2-S1''' –63.5(6).

Comparable anion structures have been reported for the chalcogenidohydridoborates $Cs[(H_2B)_6(\mu_3\text{-}E)_4]$ (E = S, Se).[23] We assume a similar mechanism for the formation of **11**: as **11** arises out of **10** by long term storage at room temperature we claim that a thermally induced elimination of $DMPyr[InMe_4]$ under formation of the cage structure in **11** takes place (Figure 13, top row). We were not able to selectively synthesize **11**, but we could collect some hints that support this thermolysis assumption (supporting information). After stirring a solution of **10** in diglyme for 18 h at 100 °C and removing all volatiles in fine vacuum, a colorless solid is obtained. The number of signals and the corresponding integrals in the ^{1}H NMR of the residue fit the assumption concerning the mechanism (Figure 13, bottom row).

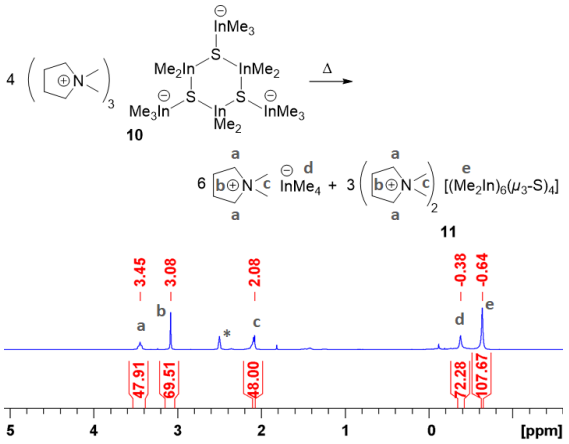

Figure 13. Assumed mechanism for the formation of **11** (top row). The corresponding signals in the ^{1}H NMR spectra (300.2 MHz, *dmso-d^6) (bottom row) of the residue obtained by controlled thermolysis fits stoichiometric assumptions.

We assume the formation of the cage anion can be understood in terms of the indation-supported ring expansion from the dianion **5** to **10** and subsequent cage formation by dismutation to **11** as shown in Scheme 6.

Scheme 6. Assumed mechanism for the formation of cage compound 11 *via* 10 starting from 5.

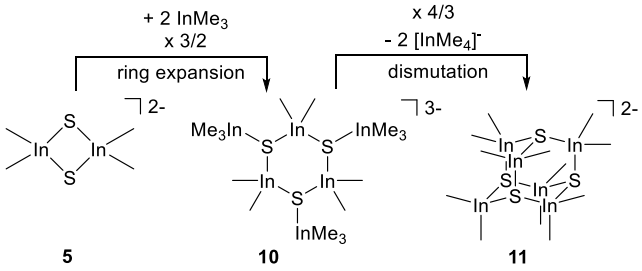

Summary

Herein the deprotonation of hydrochalcogenide anions of organic salts DMPyr[EH] (E = S (**1**), Se (**2**)) with trimethylgallium and indium MMe_3 (M = Ga, In) was investigated. Simple protolysis leads to a comprehensive set of dinuclear chalcogenidogallates $DMPyr_2[Me_2Ga(\mu_2\text{-}E)]_2$ (**3**: E = S (3); E = Se (4) and chalcogenido indates $DMPyr_2[Me_2In(\mu_2\text{-}E)]_2$ (E = S (**5**), Se (**6**)). Dinuclear and dianionic chalcogenido indates **5** and **6** were shown to be cleaved into mononuclear indates $DMPyr[Me_2In(ESiMe_3)_2]$ (E = S (**7**), Se (**8**)) by reaction with an excess of $E(SiMe_3)_2$. Treating $DMPyr_2[Me_2In(\mu\text{-}Se)]_2$ (**6**) with an excess of $S(SiMe_3)_2$ leads to the mixed substituted heterochalcogenido indate DMPyr $[Me_2In(SSiMe_3)(SeSiMe_3)]$ (**9**).

By addition of two equivalents of trimethylindium to $DMPyr_2[Me_2In(\mu_2\text{-}S)]_2$ (**5**) a terminal trimethylindate unit is added to each highly charged sulfur atom resulting in better charge delocalization and ring expansion into a hexanuclear trianionic cluster $DMPyr_3[Me_2In(\mu_3\text{-}S\text{-}InMe_3)]_3$ (**10**). Long term storage of **10** in solution leads to $DMPyr_2[(Me_2In)_6(\mu_3\text{-}S)_4]$ (**11**) displaying an interesting inverse heteroadamantane cage identified crystallographically. Based on model reactions it is likely, that **10** decomposes to **11** by thermolysis and under elimination of DMPyr $[InMe_4]$. All in all, new valuable triel chalcogenido metallate building blocks and a first set of their further transformation were presented.

EXPERIMENTAL SECTION

Methods and Devices

All preparative operations were conducted by using standard Schlenk techniques and freshly dried solvents. All solvents were dried according to common procedures[24] and passed through columns of aluminium oxide, R3-11G-catalyst (BASF) or stored over molecular sieves (3 Å or 4 Å). Other reagents were used as received unless stated otherwise. Literature known procedures were used as reported or slightly modified to synthesize $DMPyr[SSiMe_3]$,[7] Me_2InCl[25] and $E(SiMe_3)_2$ (E = S, Se).[26] Elemental analyses (C, H, N, S) were carried out by the service department for routine analysis with a vario MICRO cube (Elementar). Samples for the elemental analysis

were weighted into tin capsules inside a nitrogen filled glovebox. ^{1}H and proton decoupled ^{13}C NMR spectra were recorded in automation with a Bruker Avance II 300 spectrometer, ^{29}Si- and ^{77}Se NMR spectra were recorded by the service department for NMR analyses with a Bruker Avance II HD 300, DRX 400 or Avance III 500 spectrometer. All spectra were recorded at ambient temperature. ^{1}H- and ^{13}C NMR spectra were calibrated using residual proton signals of the solvent (dmso-d^{6}: δ_H 2.50 ppm, δ_C 39.52 ppm, thf-d^{8}: δ_H 3.58 & 1.72 ppm, δ_C 67.21 & 25.31 ppm). ^{29}Si NMR spectra were referenced externally ($SiMe_4$: δ_{Si} 0.00 ppm) just as ^{77}Se NMR spectra (Me_2Se δ_{Se} 0.00 ppm).

Representative Synthetic Procedures

Synthetic procedures for **1**, **3**, **4**, **6**, **8**, **9** and the attempts to synthesize **11** are provided in the supporting information.

Synthesis of *N,N*-dimethylpyrrolidinium hydroselenide DMPyr[SeH] (2): $Se(SiMe_3)_2$ (6.88 g, 30.5 mmol, 1.1 eq.) was added to a solution of *N,N*-dimethylpyrrolidinium methylcarbonat (4.86 g, 27.8 mmol, 1.0 eq) in 30 mL methanol at 0 °C. The reaction mixture was stirred for 30 min at 0 °C and for 1 hour at room temperature. All volatiles were removed in fine vacuum and the residue was diluted in acetonitrile until a saturated solution is obtained. Storing this saturated solution at –30 °C yields greenish crystals that are collected by filtration and washed two times with 10 mL diethyl ether. DMPyr[SeH] (**2**, 3.90 g, 21.6 mmol, 78%) was obtained as slightly greenish crystals. The yield can be enhanced by further saturation of the mother liquor and subsequent recrysalisation cycles. **^{1}H NMR** (300.3 MHz, dmso-*d*^{6}) δ_H = 3.51 (m, 4H, $(CH_3)_2N(CH_2CH_2)_2$), 3.14 (s, 6H, $(CH_3)_2N(CH_2CH_2)_2$), 2.09 (m, 4H, $(CH_3)_2N(CH_2CH_2)_2$), –6.62 (s, 1H, *H*Se) ppm. **^{13}C NMR** (75.5 MHz, dmso-*d*^{6}) δ_C = 64.6 (t, $^{1}J_{CN}$ = 3.2 Hz $(CH_3)_2N(CH_2CH_2)_2$), 50.9 (t, $^{1}J_{CN}$ = 3.9 Hz, $(CH_3)_2N(CH_2CH_2)_2$), 21.3 (s, $(CH_3)_2N(CH_2CH_2)_2$) ppm. **^{77}Se NMR** (57.3 MHz, dmso-*d*^{6}) δ_{Se} = –322.9 (s, *Se*H) ppm. **Anal. calcd.** for $C_6H_{15}N_1Se_1$: C, 40.0; H, 8.4; N, 7.8. Found: C, 40.0; H, 8.5; N, 8.0.

Synthesis of *N,N*-dimethylpyrrolidinium dimethylsulfidoindate DMPyr$_2$[Me$_2$In(μ_2-S)]$_2$ (5): To a suspension of DMPyr[SH] (0.096 g, 0.73 mmol, 2.0 eq.) in 10 mL thf a solution of Me_3In (0.121 g, 0.76 mmol, 2.1 eq.) in 10 mL thf was slowly added at –20 °C. The reaction mixture is allowed to obtain room temperature within 18 h under continuous stirring. The mixture becomes clear after approximately 15 min, and after approximately 2 hours a colorless solid precipitates. After the 18 h a colorless cloudy suspension is obtained. All volatiles were removed in fine vacuum and the residue was washed twice with 10 mL of pentane. DMPyr$_2$[Me$_2$MIn(μ_2-S)]$_2$ (0.170 g, 0.31 mmol, 87%) is obtained as colorless powder. **^{1}H NMR** (500.2 MHz, dmso-d^{6}) δ_H = 3.50 (m, 8H, $(CH_3)_2N(CH_2CH_2)_2$), 3.13 (s, 12H, $(CH_3)_2N(CH_2CH_2)_2$), 2.09 (m, 8H, $(CH_3)_2N(CH_2CH_2)_2$), –0.72 (s, 12H, $In(CH_2)_2$ x 2) ppm. **^{13}C NMR** (125.8 MHz, dmso-*d*^{6}) δ_C = 64.6 (t, $^{1}J_{CN}$ = 3.2 Hz, $(CH_3)_2N(CH_2CH_2)_2$), 50.9 (t, $^{1}J_{CN}$ = 3.9 Hz, $(CH_3)_2N(CH_2CH_2)_2$), 21.3 (s, $(CH_3)_2N(CH_2CH_2)_2$), –0.3 (s, $In(CH_2)_2$) ppm. **Anal. calcd.** for $C_{16}H_{40}In_2N_2S_2$: C, 34.7; H, 7.3; N, 5.1; S, 11.6. Found: C, 34.5; H, 7.6; N, 5.2; S, 11.3.

Synthesis of *N,N*-dimethylpyrrolidinium bis(trimethylsilylthiolato)dimethylindate DMPyr[Me$_2$In(SSiMe$_3$)$_2$] (7): $S(SiMe_3)_2$ (0.057 g, 0.32 mmol, 1.5 eq.) is slowly added to a suspension of DMPyr$_2$[Me$_2$In(μ_2-S)]$_2$ (**5**) (0.060 g, 0.11 mmol, 0.5 eq.) in 10 mL thf at –78 °C. The reaction mixture is slowly allowed to obtain room temperature within 18 h and stirred, until a clear solution is obtained. After removing all volatiles in fine vacuum, the oily residues are washed with 5 mL pentane and dried in fine vacuum. DMPyr[Me$_2$In(SSiMe$_3$)$_2$] (**7**, 0.087 g, 0.20 mmol, 88%) is obtained as colorless and oily wax. **^{1}H NMR** (500.2 MHz, THF-d^{8}) δ_H = 3.71 (m, 4H, $(CH_3)_2N(CH_2CH_2)_2$), 3.31 (s, 6H, $(CH_3)_2N(CH_2CH_2)_2$), 2.29 (m, 4H, $(CH_3)_2N(CH_2CH_2)_2$), 0.16 (s, 18H, $(H_3C)_2In(SSi(CH_3)_3)_2$), –0.34 (s, 6H, $(H_3C)_2In(SSi(CH_3)_3)_2$) ppm. **^{13}C NMR** (125.8 MHz, THF-d^{8}) δ_C = 66.5 (t, $^{1}J_{CN}$ = 3.2 Hz, $(CH_3)_2N(CH_2CH_2)_2$), 52.5 (t, $^{1}J_{CN}$ = 4.0 Hz, $(CH_3)_2N(CH_2CH_2)_2$), 22.6 (s, $(CH_3)_2N(CH_2CH_2)_2$), 6.5 (s, $(H_3C)_2In(SSi(CH_3)_3)_2$), –1.9 (s, $(H_3C)_2In(SSi(CH_3)_3)_2$) ppm. **^{29}Si NMR** (99.4 MHz, THF-d^{8}) δ_{Si} = 8.6 (s, $(H_3C)_2In(SSi(CH_3)_3)_2$) ppm. **Anal. calcd.** for $C_{14}H_{38}InNS_2Si_2$: C, 36.9; H, 8.4; N, 3.1; S, 14.1. Found: C, 36.9; H, 8.2; N, 3.6, S, 13.1. Note that crude product was investigated.

Synthesis of DMPyr$_3$[Me$_2$In(μ_3-SInMe$_3$)]$_3$ (10): To a suspension of DMPyr$_2$[Me$_2$In(μ_2-S)]$_2$ (**5**) (0.100 g, 0.180 mmol, 1.5 eq.) in 3 mL thf a solution of 0.058 g Me_3In (0.058 g, 0.361 mmol, 3.0 eq.) in 5 mL thf was added dropwise at –78 °C. The reaction mixture was allowed to obtain room temperature within 18 h. A clear solution is obtained, that is separated from all volatiles in fine vacuum. The colorless residue is washed with 5 mL pentane and dried in fine vacuum. DMPyr$_3$[Me$_2$In(μ_3-S-InMe$_3$]$_3$ (**10**) was obtained as colorless solid with a yield of 0.145 g (0.111 mmol, 92%). **^{1}H NMR** (300.1 MHz, dmso-d^{6}) δ_H = 3.45 (m, 12H, $(CH_3)_2N(CH_2CH_2)_2$), 3.08 (s, 18H, $(CH_3)_2N(CH_2CH_2)_2$), 2.10 (m, 12H, $(CH_3)_2N(CH_2CH_2)_2$), –0.38 & –0.45 (2 x s, 18H, $(H_3C)_2In$), –0.79 (bs, 27H, μ3-S-In(CH_3)$_3$) ppm. **^{13}C NMR** (75.5 MHz, dmso-d^{6}) δ_C = 64.8 (t, $^{1}J_{CN}$ = 3.1 Hz, $(CH_3)_2N(CH_2CH_2)_2$), 51.0 (t, $^{1}J_{CN}$ = 4.1 Hz, $(CH_3)_2N(CH_2CH_2)_2$), 21.3 (m, 12H, $(CH_3)_2N(CH_2CH_2)_2$), –0.79 & –0.88 (2 x s, $(H_3C)_2In$), –0.79 (bs, 27H, μ3-S-In(CH_3)$_3$) ppm.* **Anal. calcd.** for $C_{33}H_{87}In_6N_3S_3$: C, 30.2; H, 6.7; N, 3.2; S, 7.3. Found: C, 30.9; H, 6.7; N, 3.5, S, 6.6. Note that crude product was investigated. *The signals in the ^{13}C NMR spectrum are quite weak. The split signal for the indium attached methyl groups is hardly determinable. The signal for the μ$_3$-$InMe_3$ groups cannot be identified clearly.

ASSOCIATED CONTENT

Experimental procedures, NMR-spectra, crystallographic detail, supporting experiments for the formation of the inverse heteroadamantane compound DMPyr$_2$[(Me$_2$In)$_6$(μ$_3$-S)$_4$] by thermolysis of DMPyr$_3$[Me$_2$In(μ_3-S-InMe$_3$)] and several attempts to prepare **11**.

AUTHOR INFORMATION

Corresponding Author

* Fachbereich Chemie and Materials Science Center, Philipps-Universität, Hans-Meerwein-Str. 4, 35043 Marburg, Germany. E-mail: JSU@staff.uni-marburg.de.

Funding Sources

Financial support of the German Research Foundation DFG and its priority program SPP 1708: “Material Synthesis near Room Temperature” is gratefully acknowledged.

ACKNOWLEDGMENT

We thank Roman-Malte Richter and Hui Qu for synthetic contributions, Simon Werner for valuable suggestions, and the service facilities of the chemistry department of the Philipps Universität Marburg for NMR spectroscopy, elemental analysis and XRD for measurements and fruitful discussion.

REFERENCES

(1) Devillanova, F.; Du Mont, W.-W.; Gimeno, C.; Haiduc, I.; Arca, M.; Vito, L.; Verani, G.; Rawson, G. J.; Chivers, T.; Zhang, W.-J. Handbook of Chalcogen Chemistry: New Perspectives in Sulfur, Selenium and Tellurium, 2nd ed.; Royal Society of Chemistry, Cambridge, **2013**.

(2) Jacobs-Gedrim, R. B.; Shanmugam, M.; Jain, N.; Durcan, C. A.; Murphy, M. T.; Murray, T. M.; Matyi, R. J.; Moore, R. L.; Yu, B. Extraordinary photoresponse in two-dimensional In(2)Se(3) nanosheets. *ACS nano* **2014**, *8*, 514–521.

(3) Ramanujam, J.; Singh, U. P. Copper indium gallium selenide based solar cells – a review. *Energy Environ. Sci.* **2017**, *10*, 1306–1319.

(4) Taher, D.; Wallbank, A. I.; Turner, E. A.; Cuthbert, H. L.; Corrigan, J. F. Alk-2-ynyl Trimethylsilyl Chalcogenoethers by Nucleophilic Substitution of Propargyl Bromides. *Eur. J. Inorg. Chem.* **2006**, 4616–4620.

(5) Hartle, M. D.; Meininger, D. J.; Zakharov, L. N.; Tonzetich, Z. J.; Pluth, M. D. NBu_4SH provides a convenient source of HS(-) soluble in organic solution for H_2S and anion-binding research. *Dalton Trans.* **2015**, *44*, 19782–19785.

(6) DeGroot, M. W.; Corrigan, J. F. Metal-Chalcogenolate Complexes with Silyl Functionalities: Synthesis and Reaction Chemistry. *Z. Anorg. Allg. Chem.* **2006**, *632*, 19–29.

(7) Finger, L. H.; Scheibe, B.; Sundermeyer, J. Synthesis of organic (trimethylsilyl)chalcogenolate salts CatTMS-E (E = S, Se, Te): The methylcarbonate anion as a desilylating agent. *Inorg. Chem.* **2015**, *54*, 9568–9575.

(8) Gil, B.; Aulombard, R.-L., Eds. Semiconductor Heteroepitaxy: Growth Characterization and Device Applications. *World Scientific*, Singpaore, **1996**.

(9) Harlan, C. J.; Gillan, E. G.; Bott, S. G.; Barron, A. R. tert -Amyl Compounds of Aluminum and Gallium: Halides, Hydroxides, and Chalcogenides. *Organometallics* **1996**, *15*, 5479–5488.

(10) Stoll, S. L.; Bott, S. G.; Barron, A. R. Selenide and selenolate compounds of indium: A comparative study of In–Se bond-forming reactions. *J. Chem. Soc., Dalton Trans.* **1997**, 1315–1322.

(11) Medina-Ramírez, I.; Floyd, C.; Mague, J.; Fink, M. Silylated gallium and indium chalcogenide ring systems as potential precursors to ME (E = O, S) materials. *Open Chemistry* **2013**, *11*, 1225-1238.

(12) Rahbarnoohi, H.; Taghiof, M.; Heeg, M. J.; Dick, D. G.; Oliver, J. P. Synthesis and Structural Characterization of Dimeric and Trimeric Indium Thiolates. *Inorg. Chem.* **1994**, *33*, 6307–6314.

(13) Finger, L. H.; Sundermeyer, J. Halide-Free Synthesis of Hydrochalcogenide Ionic Liquids of the Type Cat HE (E=S, Se, Te). *Chem. Eur. J.* **2016**, *22*, 4218–4230.

(14) Krebs, B.; Bobb, W.; Wellmer, H.-J.; Wiesmann, K. Chalkogenohalogenogallate(III) und -indate(III): Eine neue Verbindungsklasse in der dritten Hauptgruppe. Synthese und Struktur von $[Ph_4P]_2[In_2SX_6]$, $[Et_4N]_3[In_3E_3Cl_6]$ MeCN und $[Et_4N]_3[Ga_3S_3Cl_6]$ THF (X = Cl, Br; E = S, Se). *Z. Anorg. Allg. Chem.* **1994**, *620*, 1234–1246.

(15) Batchelor, R. J.; Einstein, F. W. B.; Gay, I. D.; Jones, C. H. W.; Sharma, R. D. Syntheses and solid-state NMR of tetrabutylammonium hydrogen telluride, tetramethylammonium hydrogen selenide and bis(tetramethylammonium) ditelluride and x-ray crystal structures of Me_4NSeH and $(Me_4N)_2Te_2$. *Inorg. Chem.* **1993**, *32*, 4378–4383.

(16) Fargher, H. A.; Lau, N.; Zakharov, L. N.; Haley, M. M.; Johnson, D. W.; Pluth, M. D. Expanding reversible chalcogenide binding: supramolecular receptors for the hydroselenide (HSe^-) anion. *Chem. Sci.* **2019**, *10*, 67–72.

(17) Guschlbauer, J.; Vollgraff, T.; Sundermeyer, J. Systematic study on anion-cation interactions via doubly ionic H-bonds in 1,3-dimethylimidazolium salts comprising chalcogenolate anions MMIm ER (E = S, Se; R = H, *t*Bu, $SiMe_3$). *Dalton Trans.* **2019,** *48*, 10971-10978.

(18) Azizpoor Fard, M.; Levchenko, T. I.; Cadogan, C.; Humenny, W. J.; Corrigan, J. F. Stable -$ESiMe_3$ Complexes of Cu(I) and Ag(I) (E=S, Se) with NHCs: Synthons in Ternary Nanocluster Assembly. *Chem. Eur. J.* **2016**, *22*, 4543–4550.

(19) Rozic, K. N. W.; Azizpoor Fard, M.; Khalili Najafabadi, B.; Corrigan, J. F. Metal Trimethylsilylthiolates for the Synthesis of Trinuclear $MnPd_2$ Complexes. *Z. Anorg. Allg. Chem.* **2017**, *643*, 973–979.

(20) a) Kluge, O.; Biedermann, R.; Holldorf, J.; Krautscheid, H. Organo-gallium/indium chalcogenide complexes of copper(I): Molecular structures and thermal decomposition to ternary semiconductors. *Chem. Eur. J.* **2014**, *20*, 1318–1331. b) Guschlbauer J.; Vollgraff, T.; Sundermeyer, J. Homoleptic Group 13 Trimethylsilylchalcogenolato Metalates $[M(ESiMe_3)_4]^-$ (M = Ga, In; E = S, Se): Metastable Precursors for Low-Temperature Syntheses of Chalcogenide-Based Materials. *Inorg. Chem.* **2019**, DOI: /10.1021/acs.inorgchem.9b02453.

(21) Kluge, O.; Puidokait, M.; Biedermann, R.; Krautscheid, H. Synthese und Kristallstruktur der spirocyclischen Gallium- und Indium-Chalkogen-Heterocyclen $[(Me_2Ga)_6S(SSiMe_3)_4]$, $[(Me_2Ga)_6Se(SeSiMe_3)_4]$ und $[(Me_2In)_6S(SSiMe_3)_4]$. *Z. Anorg. Allg. Chem.* **2007**, *633*, 2138–2140.

(22) Biedermann, R.; Kluge, O.; Fuhrmann, D.; Krautscheid, H. Synthesis and Crystal Structures of $[(iPr_3P)_2Cu(\mu\text{-}ESiMe_3)(InMe_3)]$ (E = S, Se): Lewis Acid-Base Adducts with Chalcogen Atoms in Planar Coordination. *Eur. J. Inorg. Chem.* **2013**, *2013*, 4727–4731.

(23) Binder, H.; Loos, H.; Dermentzis, K.; Borrmann, H.; Simon, A. $[(BH_2)_6S_4]^{2-}$, $[(BH_2)_6Se_4]^{2-}$: Neue Chalcogenoborwasserstoff-Anionen mit Adamantanstruktur. *Chem. Ber.* **1991**, *124*, 427–432.

(24) Armarego, W. L. F.; Perrin, D. D. Purification of laboratory chemicals, 4. ed., reprint; Butterworth-Heinemann: Oxford, **2002**.

(25) Brauer, G. Handbook of Preparative Inorganic Chemistry V2, 2nd ed.; Elsevier Science: Burlington, **1965**.

(26) So, J.-H.; Boudjouk, P. Convenient Syntheses of Hexamethyldisilathiane and Tetramethyldisilathiane. *Synthesis* **1989**, 306–307.

SYNOPSIS TOC. The syntheses and structures of the chalcogenidoorgantrielate compounds $Cat_2[Me_2M(\mu_2\text{-}E)]_2$ (M = Ga, In; E = S, Se) from are described. Addition of bis(trimethylsilyl)chalcogenides yields silylated organotrielates, while addition of trimethyltriles yields the formation of metalate anions with higher aggregation.

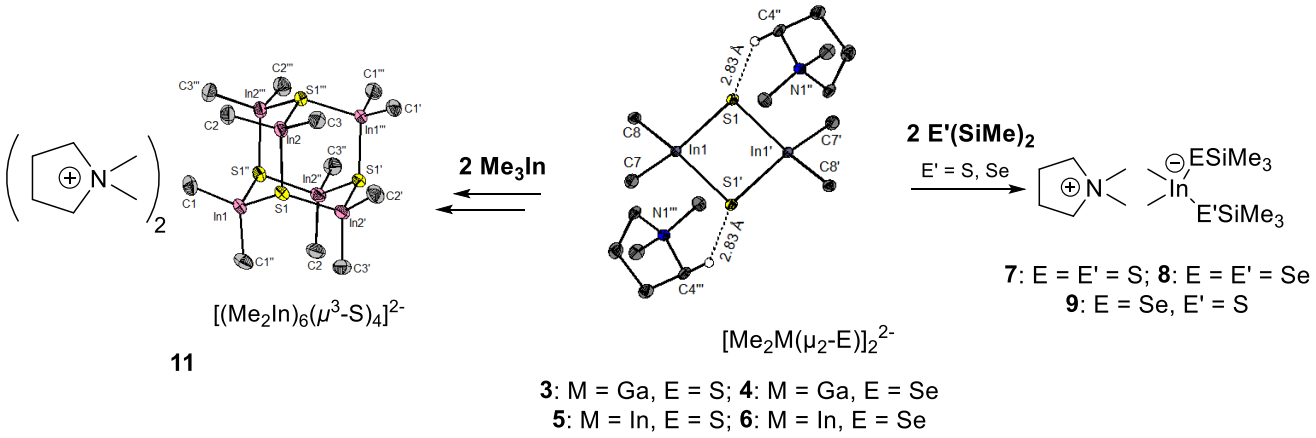

7: E = E' = S; **8**: E = E' = Se
9: E = Se, E' = S

3: M = Ga, E = S; **4**: M = Ga, E = Se
5: M = In, E = S; **6**: M = In, E = Se

Dimethylpyrrolidinium Chalcogenido-Dimethylgallates and -indates $DMPyr_2[Me_2M(\mu_2\text{-}E)]_2$ (M = Ga, In; E = S, Se): Their use in the Synthesis of Higher or Lower Order Chalcogenidoindates

Jannick Guschlbauer, Lars H. Finger, Tobias Vollgraff, Klaus Harms, Jörg Sundermeyer*

Philipps-Universität Marburg, Hans-Meerwein-Straße 4, 35032 Marburg, Germany,
*Email: JSU@staff.uni-marburg.de

Supporting Information

Contents

Experimental section

General considerations

All preparative operations were conducted by using standard Schlenk techniques and freshly dried solvents. All solvents were dried according to common procedures[1] and passed through columns of aluminium oxide, R3-11G-catalyst (BASF) or stored over molecular sieves (3 Å or 4 Å). Other reagents were used as received unless stated otherwise. Literature known procedures were used as reported or slightly modified to synthesize DMPyr [$SSiMe_3$],[2] Me_2InCl[3] and $E(SiMe_3)_2$ (E = S, Se).[4]

Elemental analyses (C, H, N, S) were carried out by the service department for routine analysis with a vario MICRO cube (Elementar). Samples for the elemental analysis were weighted into tin capsules inside a nitrogen filled glovebox. ^{1}H and proton decoupled ^{13}C-NMR spectra were recorded in automation with a Bruker Avance II 300 spectrometer, ^{29}Si- and ^{77}Se-NMR spectra were recorded by the service department for NMR analyses with a Bruker Avance II HD 300, DRX 400 or Avance III 500 spectrometer. All spectra were recorded at ambient temperature. ^{1}H- and ^{13}C-NMR spectra were calibrated using residual proton signals of the solvent (dmso-d^6: δ_H 2.50 ppm, δ_C 39.52 ppm, thf-d^8: δ_H 3.58 & 1.72 ppm, δ_C 67.21 & 25.31 ppm). ^{29}Si-NMR spectra were referenced externally ($SiMe_4$: δ_{Si} 0.00 ppm) just as ^{77}Se-NMR spectra (Me_2Se δ_{Se} 0.00 ppm).

*Synthesis of N,N-Dimethylpyrrolidinium hydrosulfide DMPyr[SH] (**1**)*

A constant flow of hydrogen sulfide was fed into a solution of *N,N*-dimethylpyrrolidinium methylcarbonat (7.00 g, 40.0 mmol, 1.0 eq.) in 30 mL methanol for 30 minutes at room temperature. After flushing the solution with a constant flow of argon for 5 minutes all volatiles were removed in fine vacuum. The residue was recrystallized from a acetonitrile/diethyl ether mixture at –30 °C. After filtration and washing the residue for two times with 10 mL diethyl ether the crystals were dried in fine vacuum. DMPyr[SH] (**1**, 3.68 g, 27.6 mmol, 69%) was obtained as colorless solid. The yield can be enhanced by further saturation of the mother liquor and subsequent recrysalisation cycles.

^{1}H-NMR (300.1 MHz, dmso-d^6) δ_H = 3.51 (m, 4H, $(CH_3)_2N(CH_2CH_2)_2$), 3.14 (s, 6H, $(CH_3)_2N(CH_2CH_2)_2$), 2.08 (m, 4H, $(CH_3)_2N(CH_2CH_2)_2$), –4.04 (s, 1H, *H*S) ppm. **^{13}C-NMR** (75.5 MHz, dmso-d^6) δ_C = 64.7(t, $^{1}J_{CN}$ = 3.0 Hz $(CH_3)_2N(CH_2CH_2)_2$), 50.8 (t, $^{1}J_{CN}$ = 3.8 Hz, $(CH_3)_2N(CH_2CH_2)_2$), 21.3 (s, $(CH_3)_2N(CH_2CH_2)_2$) ppm. **Anal. calcd.** for C6H15N1S1: C, 54.1; H, 11.4; N, 10.5; S, 24.1. Found: C, 53.9; H, 11.4; N, 10.6; S, 25.2.

*Synthesis of N,N-Dimethylpyrrolidinium hydroselenide DMPyr[SeH] (**2**)*

$Se(SiMe_3)_2$ (6.88 g, 30.5 mmol, 1.1 eq.) was added to a solution of *N,N*-dimethylpyrrolidinium methylcarbonat (4.86 g, 27.8 mmol, 1.0 eq) in 30 mL methanol at 0 °C. The reaction mixture was stirred for 30 min at 0 °C and for 1 hour at room temperature. All volatiles were removed in fine vacuum and the residue was diluted in acetonitrile until a saturated solution is obtained. Storing this saturated solution at –30 °C yields greenish crystals that are collected by filtration and washed two times with 10 mL diethyl ether. DMPyr[SeH] (**2**, 3.90 g, 21.6 mmol, 78%) was obtained as slightly greenish crystals. The yield can be enhanced by further saturation of the mother liquor and subsequent recrysalisation cycles.

^{1}H-NMR (300.3 MHz, dmso-d^6) δ_H = 3.51 (m, 4H, $(CH_3)_2N(CH_2CH_2)_2$), 3.14 (s, 6H, $(CH_3)_2N(CH_2CH_2)_2$), 2.09 (m, 4H, $(CH_3)_2N(CH_2CH_2)_2$), –6.62 (s, 1H, *H*Se) ppm. **^{13}C-NMR** (75.5 MHz, dmso-d^6) δ_C = 64.6 (t, $^1J_{CN}$ = 3.2 Hz $(CH_3)_2N(CH_2CH_2)_2$), 50.9 (t, $^1J_{CN}$ = 3.9 Hz, $(CH_3)_2N(CH_2CH_2)_2$), 21.3 (s, $(CH_3)_2N(CH_2CH_2)_2$) ppm. **^{77}Se-NMR** (57.3 MHz, dmso-d^6) δ_{Se} = –322.9 (s, *Se*H) ppm. **Anal. calcd.** for C6H15N1Se1: C, 40.0; H, 8.4; N, 7.8. Found: C, 40.0; H, 8.5; N, 8.0.

*Synthesis of the N,N-Dimethylpyrrolidinium dimethylchalcogenidotrielates $DMPyr_2[Me_2M(\mu_2\text{-}E)]_2$ (**3-6**)*

As the title compounds **3-6** can be prepared analogly, the general procedure is described.

To a suspension of **DMPyr[EH]** in 10 mL thf a solution of **Me_3M** in 10 mL thf was slowly added at –20 °C. The reaction mixture is allowed to obtain room temperature within 18 h under continuous stirring. The mixture becomes clear after approximately 15 min, and after approximately 2 hours a colorless solid precipitates. After the 18 h a colorless cloudy suspension is obtained. All volatiles were removed in fine vacuum and the residue was washed twice with 10 mL of pentane. The target compound **$DMPyr_2[Me_2M(\mu\text{-}E)]_2$** is obtained as colorless powder.

Used amounts of educts and yields of the syntheses of 3-6:

$DMPyr_2[Me_2M(\mu_2\text{-}E)]_2$	**DMPyr[EH]**	**Me_3M**	**Yield**
$DMPyr_2[Me_2Ga(\mu_2\text{-}S)]_2$ (3)	E = S 0.115 g, 0.86 mmol, 2.0 eq.	M = Ga 0.104 g, 0.90 mmol, 2.1 eq.	0.193 g, 0.41 mmol, 96%
$DMPyr_2[Me_2Ga(\mu_2\text{-}Se)]_2$ (4)	E = Se 0.129 g, 0.72 mmol, 2.0 eq.	M = Ga 0.129 g, 0.72 mmol, 2.1 eq.	0.191 g 0.34 mmol, 94%
$DMPyr_2[Me_2In(\mu_2\text{-}S)]_2$ (5)	E = S 0.096 g, 0.72 mmol, 2.0 eq.	M = In 0.121 g, 0.76 mmol, 2.1 eq.	0.170 g, 0.31 mmol, 87%
$DMPyr_2[Me_2In(\mu_2\text{-}Se)]_2$ (6)	E = Se 0.111 g, 0.62 mmol, 2.0 eq	M = In 0.104 g, 0.65 mmol, 2.1 eq.	0.183 g, 0.28 mmol, 92%

DMPyr$_2$[Me$_2$Ga(μ_2-S)]$_2$ (3)

^{1}H-NMR (500.1 MHz, dmso-d^6) δ_H = 3.45 (m, 8H, $(CH_3)_2N(CH_2CH_2)_2$), 3.09 (s, 12H, $(CH_3)_2N(CH_2CH_2)_2$), 2.09 (m, 8H, $(CH_3)_2N(CH_2CH_2)_2$), –0.77 (s, 12H, $Ga(CH_2)_2$ x 2) ppm. **^{13}C NMR** (125.8 MHz, dmso-*d*^{6}) δ_C = 64.7 (t, $^1J_{CN}$ = 3.0 Hz, $(CH_3)_2N(CH_2CH_2)_2$), 50.9 (t, $^1J_{CN}$ = 3.8 Hz, $(CH_3)_2N(CH_2CH_2)_2$), 21.3 (s, $(CH_3)_2N(CH_2CH_2)_2$,), –0.4 (s, $Ga(CH_2)_2$ x 2) ppm. **Anal. calcd.** for $C_{16}H_{40}Ga_2N_2S_2$: C, 41.4; H, 8.7; N, 6.0; S, 13.8. Found: C, 42.3; H, 9.5; N, 6.3; S, 12.9. Note that the crude product was investigated. Deviations could be traced back on the excess of Me_3Ga.

DMPyr$_2$[Me$_2$Ga(μ_2-Se)]$_2$ (4)

^{1}H-NMR (300.2 MHz, dmso-d^6) δ_H = 3.46 (m, 8H, $(CH_3)_2N(CH_2CH_2)_2$), 3.10 (s, 12H, $(CH_3)_2N(CH_2CH_2)_2$), 2.10 (m, 8H, $(CH_3)_2N(CH_2CH_2)_2$), –0.66 (s, 12H, $Ga(CH_2)_2$ x 2) ppm. **^{13}C-NMR** (125.8 MHz, dmso-*d*^{6}) δ_C = 64.7 (t, $^1J_{CN}$ = 2.9 Hz, $(CH_3)_2N(CH_2CH_2)_2$), 51.0 (t, $^1J_{CN}$ = 3.8 Hz, $(CH_3)_2N(CH_2CH_2)_2$), 21.3 (s, $(CH_3)_2N(CH_2CH_2)_2$), –1.1 (s, $Ga(CH_2)_2$) ppm. **^{77}Se-NMR** (57.3 MHz, dmso-d^6) δ_{Se} = -335.2 (s, $[Me_2Ga(\mu\text{-}Se)]_2^{2-}$) ppm. **Anal. calcd.** for $C_{16}H_{40}Ga_2N_2Se_2$: C, 34.5; H, 7.2; N, 5.0. Found: C, 35.9; H, 8.2; N, 5.0. Note that the crude product was investigated. Deviations could be traced back on the excess of Me_3Ga.

DMPyr$_2$[Me$_2$In(μ_2-S)]$_2$ (5)

^{1}H-NMR (500.2 MHz, dmso-d^6) δ_H = 3.50 (m, 8H, $(CH_3)_2N(CH_2CH_2)_2$), 3.13 (s, 12H, $(CH_3)_2N(CH_2CH_2)_2$), 2.09 (m, 8H, $(CH_3)_2N(CH_2CH_2)_2$), –0.72 (s, 12H, $In(CH_2)_2$ x 2) ppm. **^{13}C-NMR** (125.8 MHz, dmso-*d*^{6}) δ_C = 64.6 (t, $^1J_{CN}$ = 3.2 Hz, $(CH_3)_2N(CH_2CH_2)_2$), 50.9 (t, $^1J_{CN}$ = 3.9 Hz, $(CH_3)_2N(CH_2CH_2)_2$), 21.3 (s, $(CH_3)_2N(CH_2CH_2)_2$), –0.3 (s, $In(CH_2)_2$) ppm. **Anal. calcd.** for $C_{16}H_{40}In_2N_2S_2$: C, 34.7; H, 7.3; N, 5.1; S, 11.6. Found: C, 34.5; H, 7.6; N, 5.2; S, 11.3.

DMPyr$_2$[Me$_2$In(μ_2-Se)]$_2$ (6)

^{1}H-NMR (300.2 MHz, dmso-d^6) δ_H = 3.49 (m, 8H, $(CH_3)_2N(CH_2CH_2)_2$), 3.12 (s, 12H, $(CH_3)_2N(CH_2CH_2)_2$), 2.10 (m, 8H, $(CH_3)_2N(CH_2CH_2)_2$), –0.56 (s, 12H, $In(CH_2)_2$ x 2) ppm. **^{13}C-NMR** (125.8 MHz, dmso-*d*^{6}) δ_C = 64.7 (t, $^1J_{CN}$ = 3.0 Hz, $(CH_3)_2N(CH_2CH_2)_2$), 50.9 (t, $^1J_{CN}$ = 3.8 Hz, $(CH_3)_2N(CH_2CH_2)_2$), 21.3 (s, $(CH_3)_2N(CH_2CH_2)_2$), –0.0 (s, $In(CH_2)_2$) ppm. **^{77}Se-NMR** (57.3 MHz, dmso-d^6) δ_H = –470.0 (s, $[Me_2Ga(\mu\text{-}Se)]_2^{2-}$) ppm. **Anal. calcd.** for $C_{16}H_{40}In_2N_2Se_2$: C, 29.7; H, 6.2; N, 4.3. Found: C, 29.7; H, 6.0; N, 4.7.

*Synthesis of the N,N-Dimethylpyrrolidinium bis(trimethylsilylchalcogenolato)dimethylchalcogenidoindates DMPyr[$Me_2In(ESiMe_3)_2$] (**7-9**)*

As complexes with $ESiMe_3$-moiety show a pronounced instability towards some common solvents, the usage was restricted on inert ethers and aliphats. As chlorinated solvents and dmso-d^6 decompose the target anions, the usage of THF-d^8 was indicated for NMR-analysis. Our first method to prepare DMPyr [$Me_2In(SSiMe_3)_2$] (**7**) was the addition/substitution reaction between one equivalent of Me_2InCl and two equivalents of DMPyr [$SSiMe_3$]. After separation of one equivalent of the byproduct DMPyr [Cl] the target molecule is obtained. By silylation of the indate dianion $DMPyr_2[Me_2In(\mu\text{-}S)]_2$ (**5**) with $S(SiMe_3)_2$ no byproducts emerge, and the pure target compound is obtained quantitatively by simple removing all volatiles in fine vacuum. For both methods the target compounds could be obtained in purely and quantitatively, but the latter one is way more convenient, and also allows the preparation of the mixed substituted compound DMPyr [$Me_2In(SSiMe_3)(SeSiMe_3)$] (**7**).

Preparation of DMPyr[$Me_2In(SSiMe_3)_2$] (7) by addition/substitution of DMPyr[$SSiMe_3$] to Me_2InCl
To a suspension of DMPyr [$SSiMe_3$] (0.36 g, 1.76 mmol, 2.0 eq.) in 5 mL thf a solution of Me_2InCl (0.16 g, 0.88 mmol, 1.0 eq.) is added dropwise at –78 °C. The reaction mixture is slowly warmed to room temperature within 18 h. the suspension is filtered. All volatiles were removed from the filtrate in fine vacuum, and the colorless oily residue was washed with 5 mL pentane, and the residue dried in fine vacuum. The target compound is obtained as colorless wax. The identity of the product was proven via ^{1}H-NMR and ^{29}Si-NMR that were identical to those of **7** prepared by the other method.

*Preparation of DMPyr [$Me_2In(ESiMe_3)(E'SiMe_3)$] (**7-9**) by addition of $E'(SiMe_3)_2$ to **3-6***
$E'(SiMe_3)_2$ is slowly added to a suspension of $DMPyr_2[Me_2In(\mu_2\text{-}E)]_2$ in 10 mL thf at –78 °C. The reaction mixture is slowly allowed to obtain room temperature within 18 h and stirred, until a clear solution is obtained. After removing all volatiles in fine vacuum, the oily residues are washed with 5 mL pentane and dried in fine vacuum. The target compounds **7-9** are obtained as colorless waxes.

Used amounts of educts and yields of the syntheses of 7-9:

DMPyr [$Me_2In(ESiMe_3)(E'SiMe_3)$]	**$DMPyr_2[Me_2In(\mu_2\text{-}E)]_2$**	**$E'(SiMe_3)_2$**	**Yield**
E = E' = S (7)	E = S 0.060 g, 0.11 mmol, 0.5 eq.	E' = S 0.057 g, 0.32 mmol, 1.5 eq.	0.087 g, 0.20 mmol, 88%
E = E' = Se (8)	E = Se 0.060 g, 0.09 mmol, 0.5 eq.	E' = Se 0.063 g, 0.28 mmol, 1.5 eq.	0.092 g 0.17 mmol, 90%
E = Se, E' = S (9)	E = Se 0.060 g, 0.09 mmol, 0.5 eq.	E' = S 0.050 g, 0.28 mmol, 1.5 eq.	0.081 g, 0.16 mmol, 87%

DMPyr[Me$_2$In(SSiMe$_3$)$_2$] (7)

^{1}H-NMR (500.2 MHz, THF-d^8) δ_H = 3.71 (m, 4H, $(CH_3)_2N(CH_2CH_2)_2$), 3.31 (s, 6H, $(CH_3)_2N(CH_2CH_2)_2$), 2.29 (m, 4H, $(CH_3)_2N(CH_2CH_2)_2$), 0.16 (s, 18H, $(H_3C)_2In(SSi(CH_3)_3)_2$), –0.34 (s, 6H, $(H_3C)_2In(SSi(CH_3)_3)_2$) ppm. **^{13}C-NMR** (125.8 MHz, THF-d^8) δ_C = 66.5 (t, $^1J_{CN}$ = 3.2 Hz, $(CH_3)_2N(CH_2CH_2)_2$), 52.5 (t, $^1J_{CN}$ = 4.0 Hz, $(CH_3)_2N(CH_2CH_2)_2$), 22.6 (s, $(CH_3)_2N(CH_2CH_2)_2$), 6.5 (s, $(H_3C)_2In(SSi(CH_3)_3)_2$), –1.9 (s, $(H_3C)_2In(SSi(CH_3)_3)_2$) ppm. **^{29}Si-NMR** (99.4 MHz, THF-d^8) δ_{Si} = 8.6 (s, $(H_3C)_2In(SSi(CH_3)_3)_2$) ppm. **Anal. calcd.** for $C_{14}H_{38}InNS_2Si_2$: C, 36.9; H, 8.4; N, 3.1; S, 14.1. Found: C, 36.9; H, 8.2; N, 3.6, S, 13.1.

DMPyr[Me$_2$In(SeSiMe$_3$)$_2$] (8)

^{1}H-NMR (500.1 MHz, THF-d^8) δ_H = 3.71 (m, 4H, $(CH_3)_2N(CH_2CH_2)_2$), 3.31 (s, 6H, $(CH_3)_2N(CH_2CH_2)_2$), 2.29 (m, 4H, $(CH_3)_2N(CH_2CH_2)_2$), 0.29 (s, 18H, $(H_3C)_2In(SeSi(CH_3)_3)_2$), –0.24 (s, 6H, $(H_3C)_2In(SeSi(CH_3)_3)_2$) ppm. **^{13}C-NMR** (125.8 MHz, THF-d^8) δ_C = 66.7 (t, $^1J_{CN}$ = 3.1 Hz, $(CH_3)_2N(CH_2CH_2)_2$), 52.7 (t, $^1J_{CN}$ = 4.0 Hz, $(CH_3)_2N(CH_2CH_2)_2$), 22.6 (s, $(CH_3)_2N(CH_2CH_2)_2$), 6.9 (s, $(H_3C)_2In(SeSi(CH_3)_3)_2$ ppm.* **Anal. calcd.** for $C_{14}H_{38}InNSe_2Si_2$: C, 30.6; H, 7.0; N, 2.6. Found: C, 30.3; H, 6.6; N, 3.0.

*The signal for the indium attached methyl groups could not be identified in the ^{13}C-NMR spectrum, as the concentration of the saturated solution of **8** in THF-d^8 is not high enough. No ^{29}Si- and ^{77}Se-NMR spectra were obtained for this reason.

DMPyr[Me$_2$In(SeSiMe$_3$)(SSiMe$_3$)$_2$] (9)

^{1}H-NMR (500.1 MHz, THF-d^8) δ_H = 3.71 (m, 4H, $(CH_3)_2N(CH_2CH_2)_2$), 3.31 (s, 6H, $(CH_3)_2N(CH_2CH_2)_2$), 2.29 (m, 4H, $(CH_3)_2N(CH_2CH_2)_2$), 0.28 (s, 9H, $(H_3C)_2In(SeSi(CH_3)_3)(SSi(CH_3)_3)$), 0.16 (s, 9H, $(H_3C)_2In(SeSi(CH_3)_3)(SSi(CH_3)_3)$), –0.30 (s, 6H, $(H_3C)_2In(SeSi(CH_3)_3)(SSi(CH_3)_3)$) ppm. **^{13}C-NMR** (125.8 MHz, THF-d^8) δ_C = 66.6 (t, $^1J_{CN}$ = 3.1 Hz, $(CH_3)_2N(CH_2CH_2)_2$), 52.6 (t, $^1J_{CN}$ = 4.0 Hz, $(CH_3)_2N(CH_2CH_2)_2$), 22.6 (s, $(CH_3)_2N(CH_2CH_2)_2$), 6.9 (s, $(H_3C)_2In(SeSi(CH_3)_3)(SSi(CH_3)_3)$), 6.5 (s, $(H_3C)_2In(SeSi(CH_3)_3)(SSi(CH_3)_3)$) ppm.* **Anal. calcd.** for $C_{14}H_{38}InNSeSSi_2$: C, 33.5; H, 7.6; N, 2.6, S, 6.4. Found: C, 32.4; H, 6.8; N, 3.4; S, 4.9. Note that the crude product was investigated. The oily appearance of the product made washing processes and the exact preparation of the elemental analysis sample difficult. Deviations might be traced back on small amounts of unreacted ($DMPyr_2[Me_2In(\mu\text{-}Se)]_2$ (**6**)).

*The signal for the indium attached methyl groups could hardly be identified, due to the low concentration of the saturated solution of **9** in THF-d^8. Therefore also no ^{29}Si- and no ^{77}Se-NMR spectra could be obtained.

*Preparation of DMPyr$_3$[Me$_2$In(μ_3-S-InMe$_3$]$_3$ (**10**)*

To a suspension of DMPyr$_2$[Me$_2$In(μ_2-S)]$_2$ (**5**) (0.100 g, 0.180 mmol, 1.5 eq.) in 3 mL thf a solution of 0.058 g Me$_3$In (0.058 g, 0.361 mmol, 3.0 eq.) in 5 mL thf was added dropwise at –78 °C. The reaction mixture was allowed to obtain room temperature within 18 h. A clear solution is obtained, that is separated from all volatiles in fine vacuum. The colorless residue is washed with 5 mL pentane and dried in fine vacuum. DMPyr$_3$[Me$_2$In(μ$_3$-S-InMe$_3$]$_3$ (**10**) was obtained as colorless solid with a yield of 0.145 g (0.111 mmol, 92%).

^{1}H-NMR (300.1 MHz, dmso-d^6) δ_H = 3.45 (m, 12H, (CH$_3$)$_2$N(CH$_2$C*H*$_2$)$_2$), 3.08 (s, 18H, (C*H*$_3$)$_2$N(CH$_2$CH$_2$)$_2$), 2.10 (m, 12H, (CH$_3$)$_2$N(CH$_2$C*H*$_2$)$_2$), –0.38 & –0.45 (2 x s, 18H, (*H*$_3$C)$_2$In), –0.79 (bs, 27H, μ3-S-In(C*H*$_3$)$_3$) ppm. **^{13}C-NMR** (75.5 MHz, dmso-d^6) δ_C = 64.8 (t, $^1J_{CN}$ = 3.1 Hz, (CH$_3$)$_2$N(CH$_2$*C*H$_2$)$_2$), 51.0 (t, $^1J_{CN}$ = 4.1 Hz, (*C*H$_3$)$_2$N(CH$_2$CH$_2$)$_2$), 21.3 (m, 12H, (CH$_3$)$_2$N(CH$_2$*C*H$_2$)$_2$), –0.79 & –0.88 (2 x s, (H$_3$*C*)$_2$In), –0.79 (bs, 27H, μ3-S-In(*C*H$_3$)$_3$) ppm.* **Anal. calcd.** for C$_{33}$H$_{87}$In$_6$N$_3$S$_3$: C, 30.2; H, 6.7; N, 3.2; S, 7.3. Found: C, 30.9; H, 6.7; N, 3.5, S, 6.6. Note that crude product was investigated.

*The signals in the ^{13}C-NMR spectrum are quite weak. The multiplicity of th N-attached carbon atoms was determined manually. The split signal for the indium attached methyl groups is hardly determinable. The ^{13}C-NMR-signal for the μ$_3$-InMe$_3$ groups cannot be identified clearly.

NMR-Spectra

*DMPyr[SH] (**1**)*

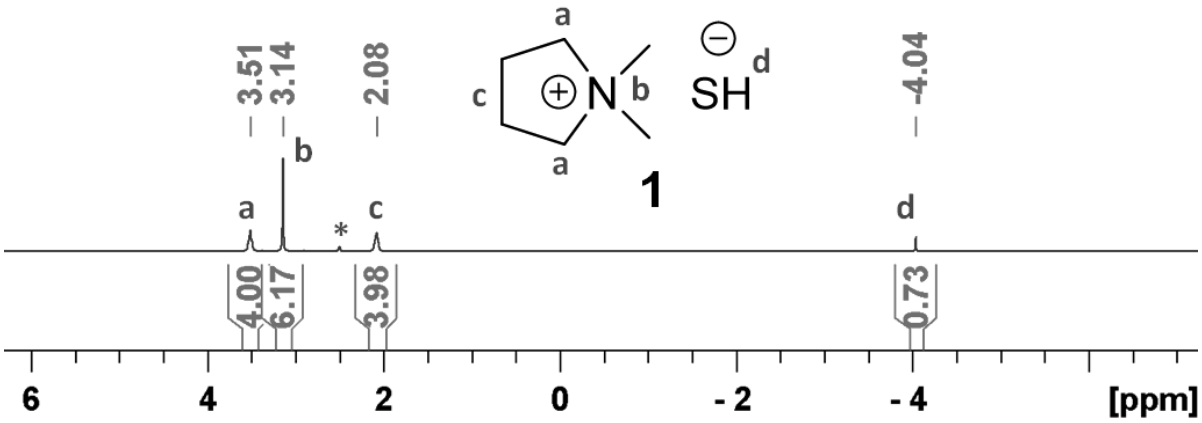

^{1}H-NMR (300.3 MHz, *dmso-d^{6}) of DMPyr [SH] (**1**)

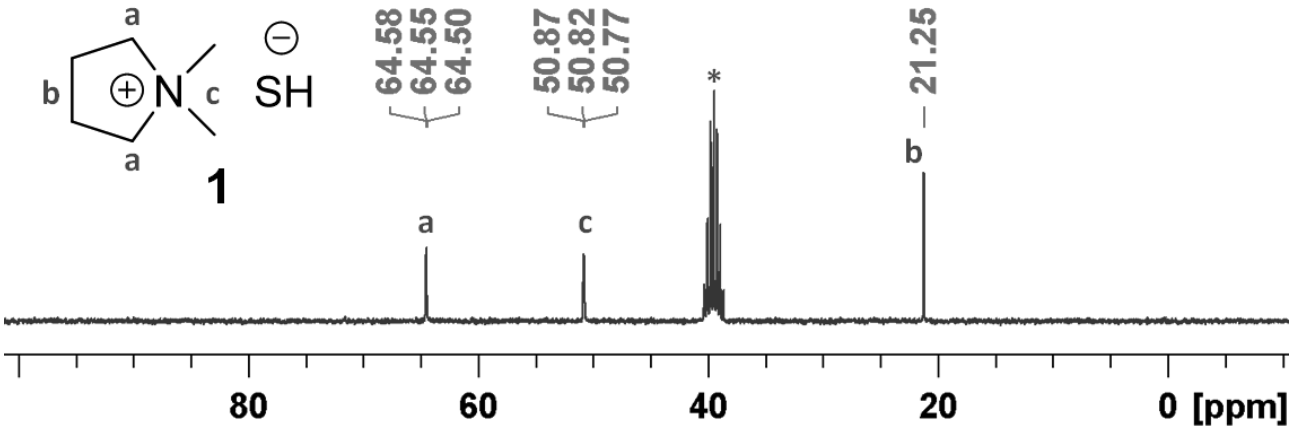

^{13}C-NMR (75.5 MHz, *dmso-d^{6}) of DMPyr [SH] (**1**)

*DMPyr[SeH] (**2**)*

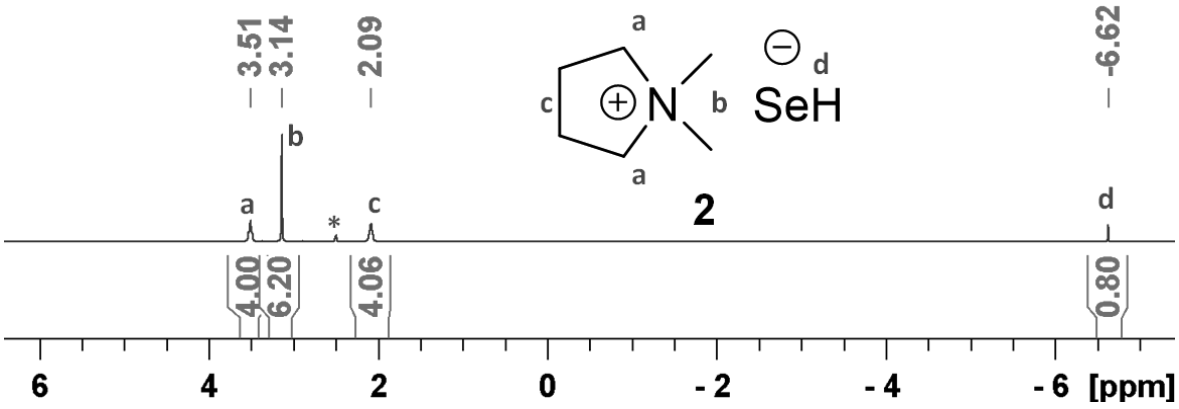

^{1}H-NMR (300.3 MHz, *dmso-d^{6}) of DMPyr [SeH] (**2**).

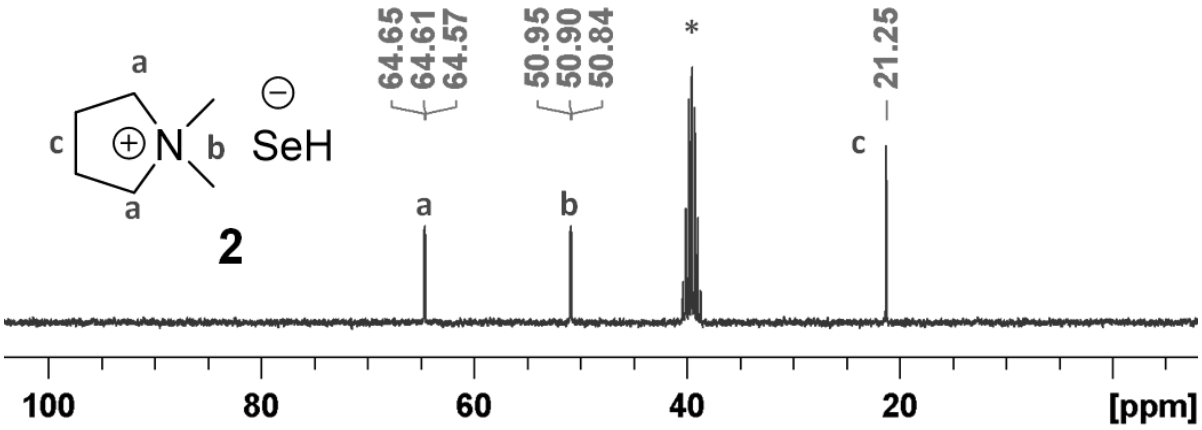

^{13}C-NMR (172.1 MHz, *dmso-d^{6}) of DMPyr [SeH] (**2**).

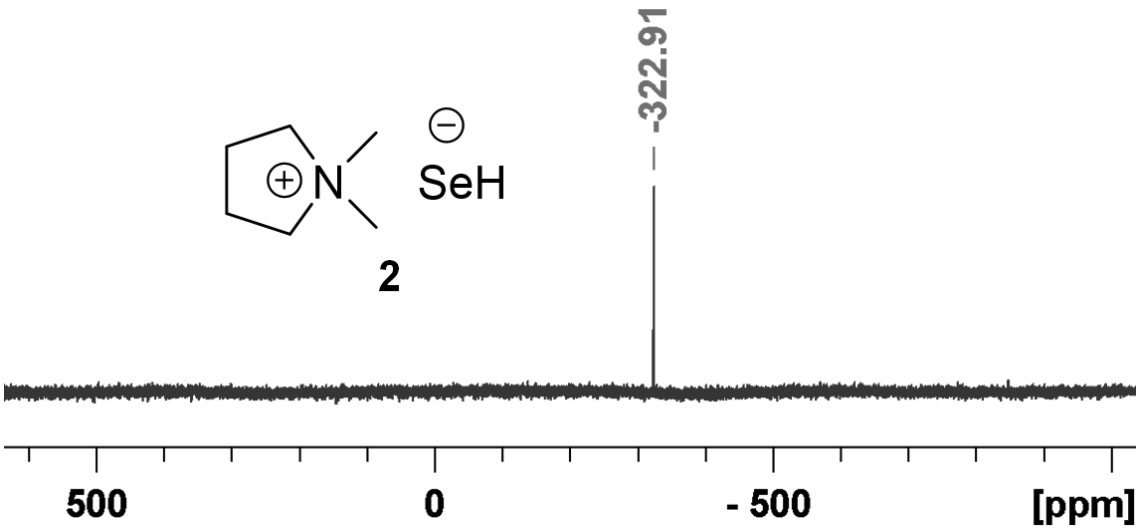

^{77}Se-NMR (57.3 MHz, dmso-d^{6}) of DMPyr [SeH] (**2**).

*DMPyr$_2$[Me$_2$Ga(μ_2-S)]$_2$ (**3**)*

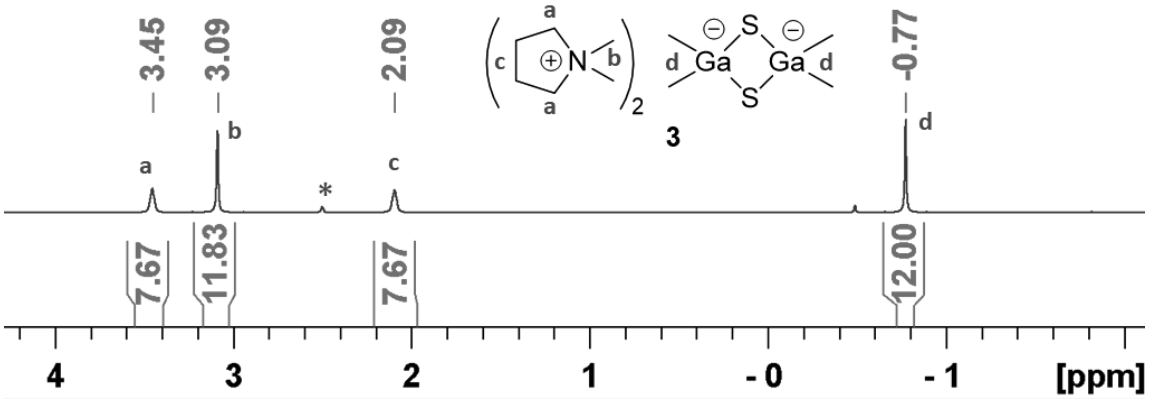

^{1}H-NMR (500.1 MHz, *dmso-d^6) of DMPyr$_2$[Me$_2$Ga(μ_2-S)]$_2$ (**3**).

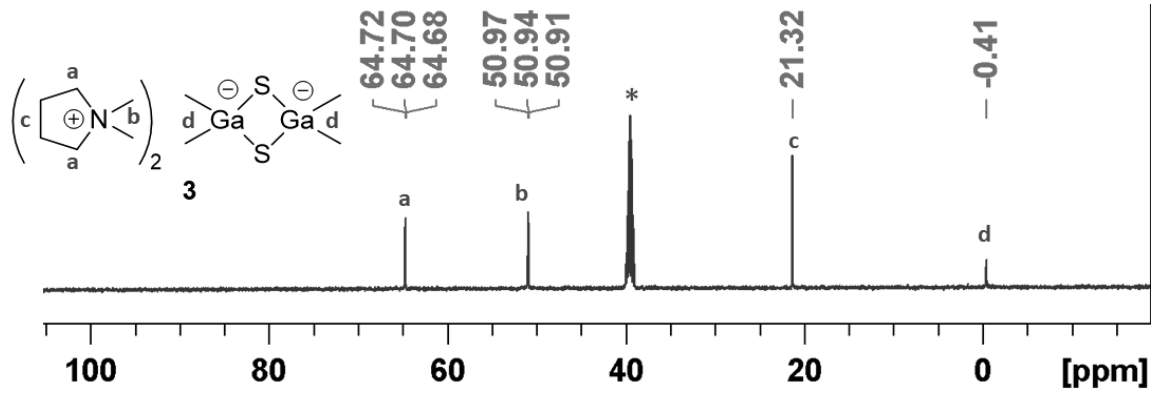

^{13}C-NMR (125.8 MHz, *dmso-d^6) of DMPyr$_2$[Me$_2$Ga(μ_2-S)]$_2$ (**3**).

*DMPyr$_2$[Me$_2$Ga(μ_2-Se)]$_2$ (**4**)*

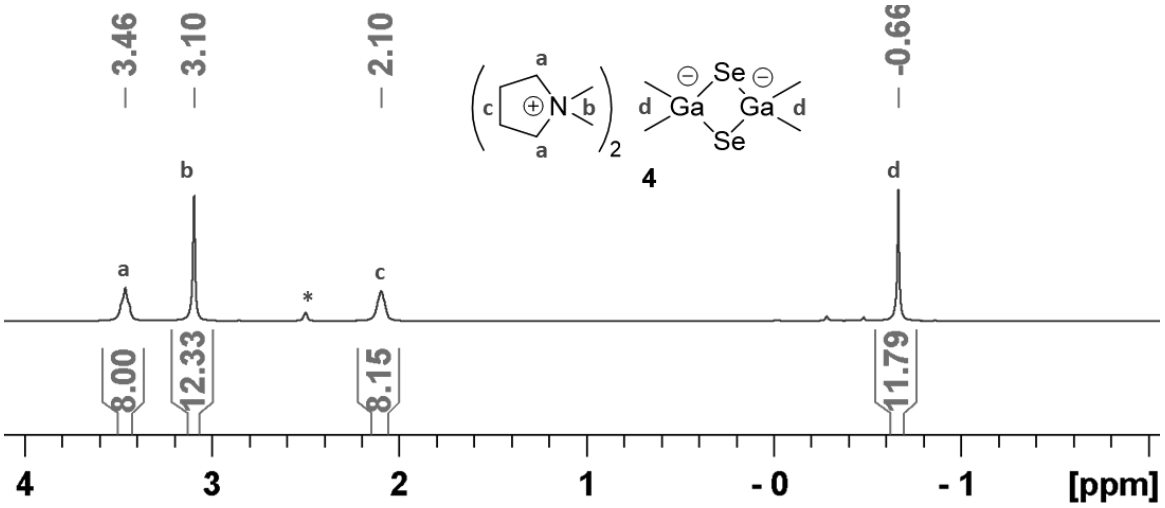

^{1}H-NMR (300.1MHz, *dmso-d^6) DMPyr$_2$[Me$_2$Ga(μ_2-Se)]$_2$ (**4**).

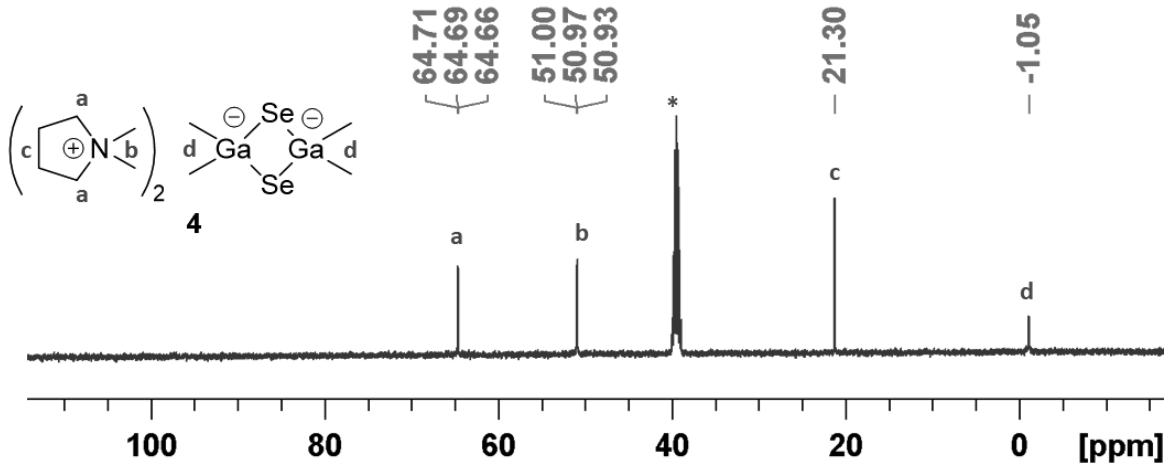

^{13}C-NMR (125.8 MHz, *dmso-d^6) of DMPyr$_2$[Me$_2$Ga(μ_2-Se)]$_2$ (**4**).

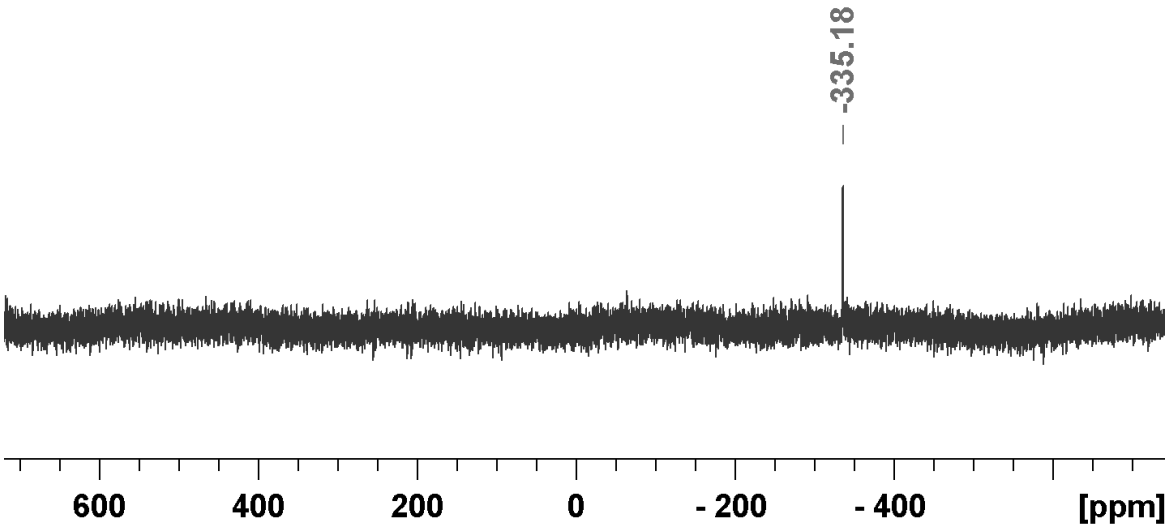

^{77}Se-NMR (57.3 MHz, *dmso-d^6) of DMPyr$_2$[Me$_2$Ga(μ_2-Se)]$_2$ (**4**).

*DMPyr$_2$[Me$_2$In(μ_2-S)]$_2$ (**5**)*

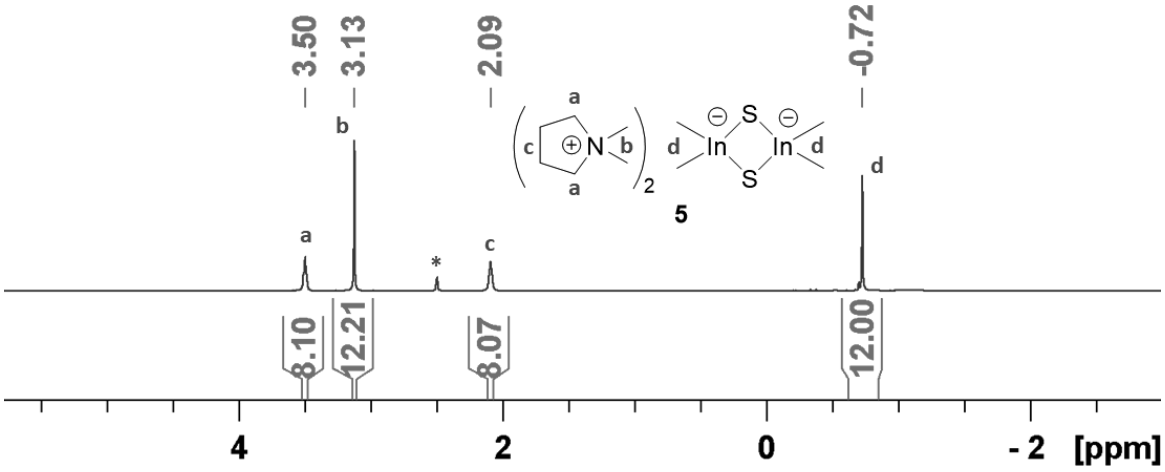

^{1}H-NMR (500.2 MHz, *dmso-d^6) DMPyr$_2$[Me$_2$In(μ_2-S)]$_2$ (**5**).

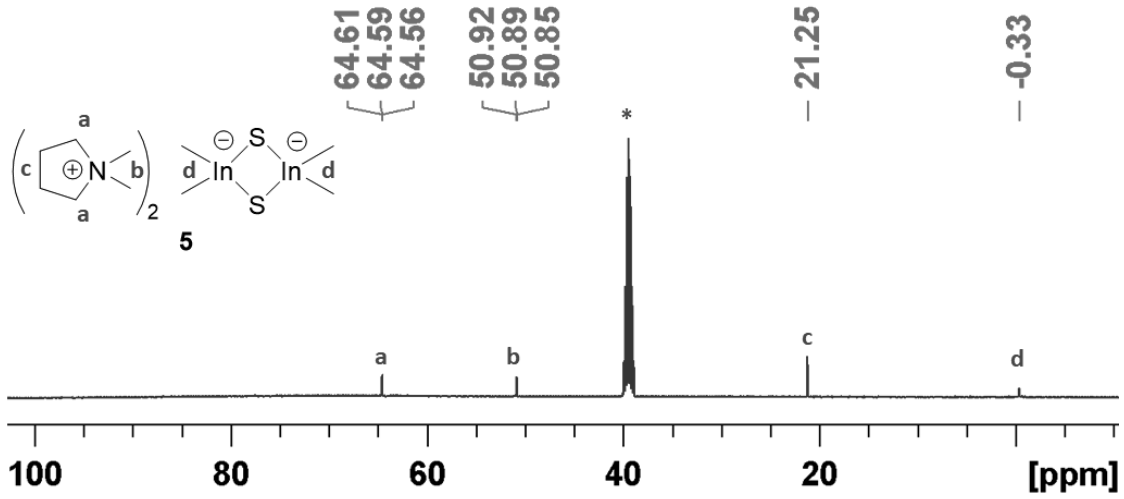

^{13}C-NMR (125.8 MHz, *dmso-d^6) of DMPyr$_2$[Me$_2$In(μ_2-S)]$_2$ (**5**).

*$DMPyr_2[Me_2In(\mu_2\text{-}Se)]_2$ (**6**)*

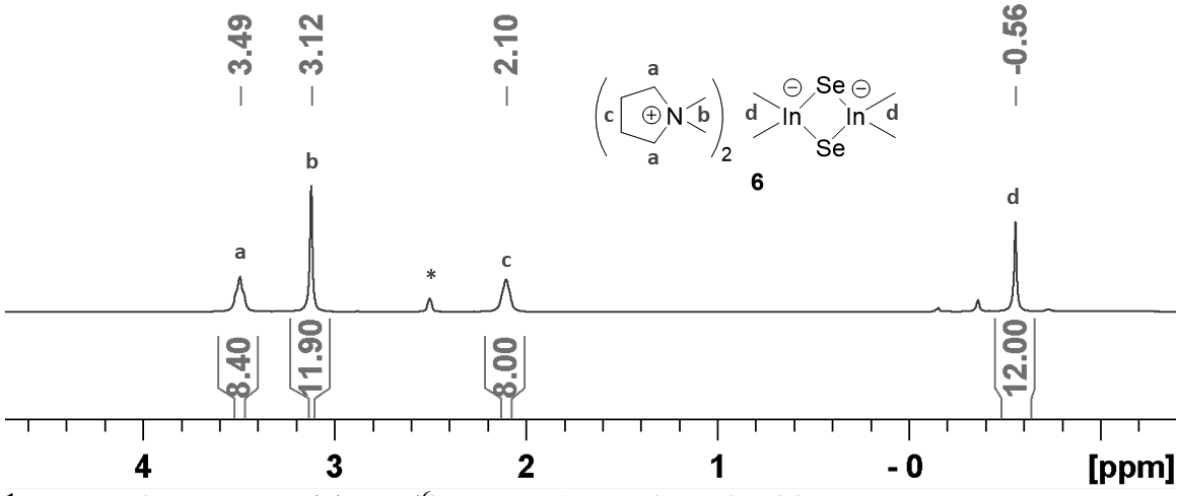

^{1}H-NMR (300.2 MHz, *dmso-d^6) $DMPyr_2[Me_2In(\mu_2\text{-}Se)]_2$ (**6**).

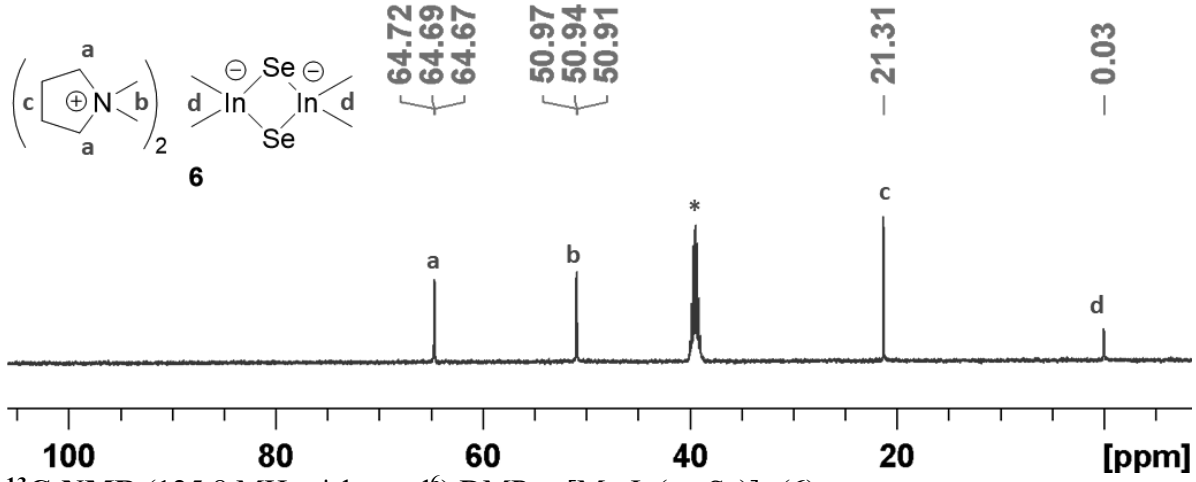

^{13}C-NMR (125.8 MHz, *dmso-d^6) $DMPyr_2[Me_2In(\mu_2\text{-}Se)]_2$ (**6**).

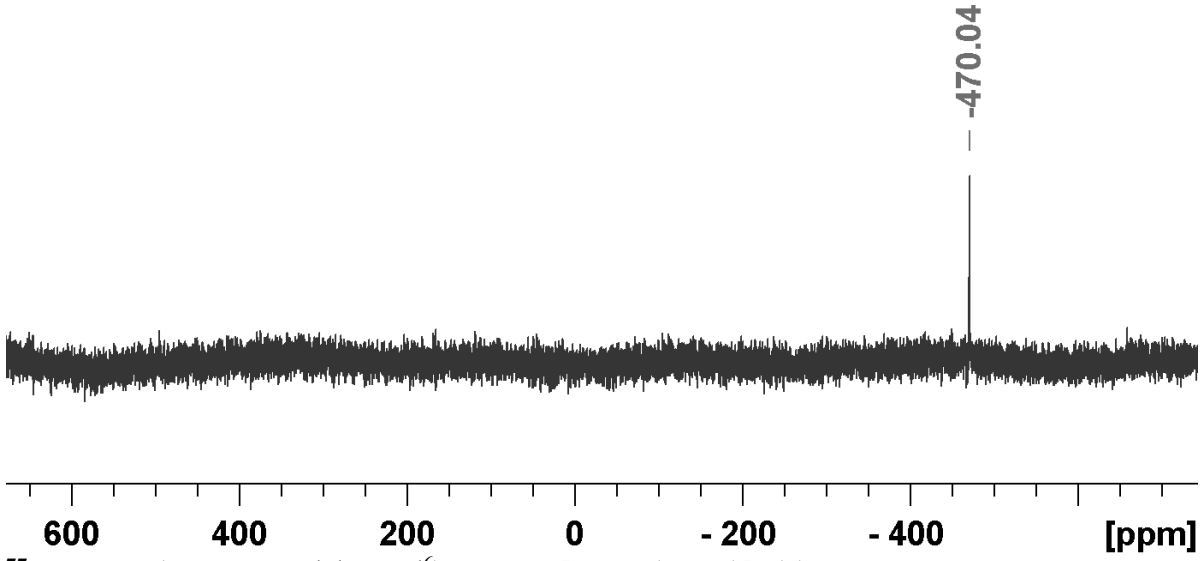

^{77}Se-NMR (57.3 MHz, *dmso-d^6) $DMPyr_2[Me_2In(\mu_2\text{-}Se)]_2$ (**6**).

DMPyr[Me₂In(SSiMe₃)₂] (7)

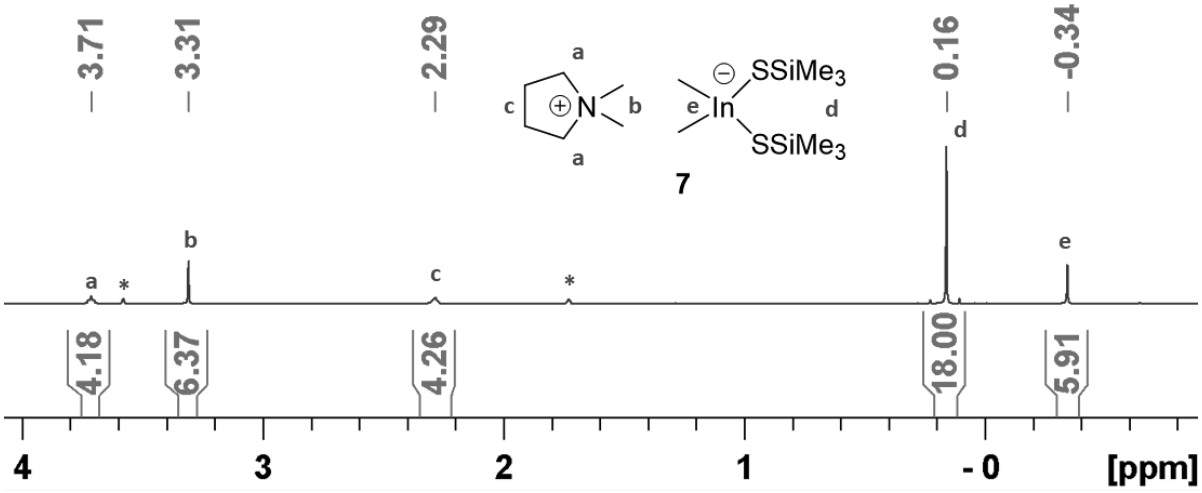

[1]H-NMR (500.2 MHz, *THF-d[8]) of DMPyr [Me₂In(SSiMe₃)₂] (**7**)

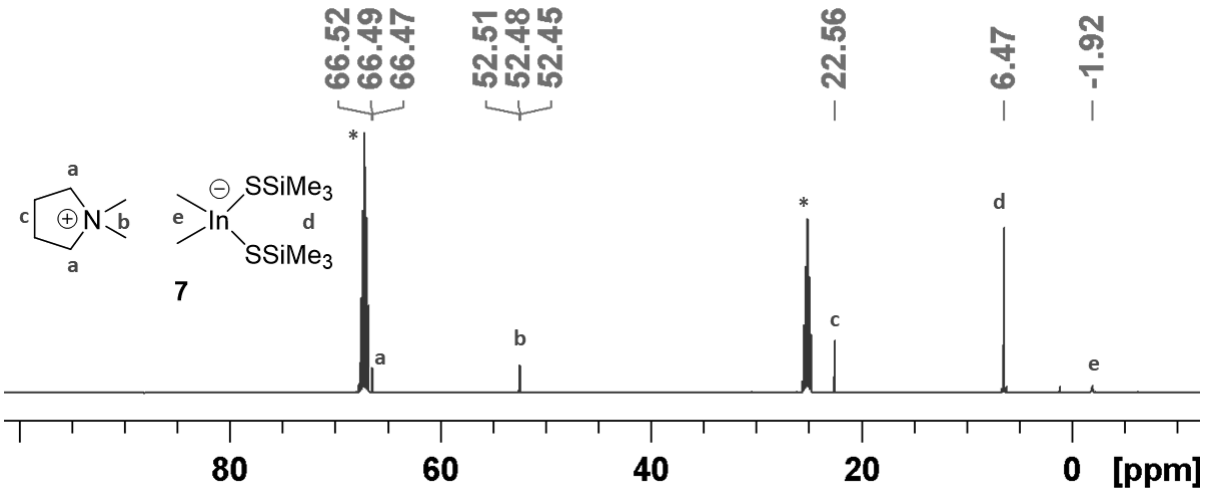

[13]C-NMR (125.8 MHz, *THF-d[8]) of DMPyr [Me₂In(SSiMe₃)₂] (**7**)

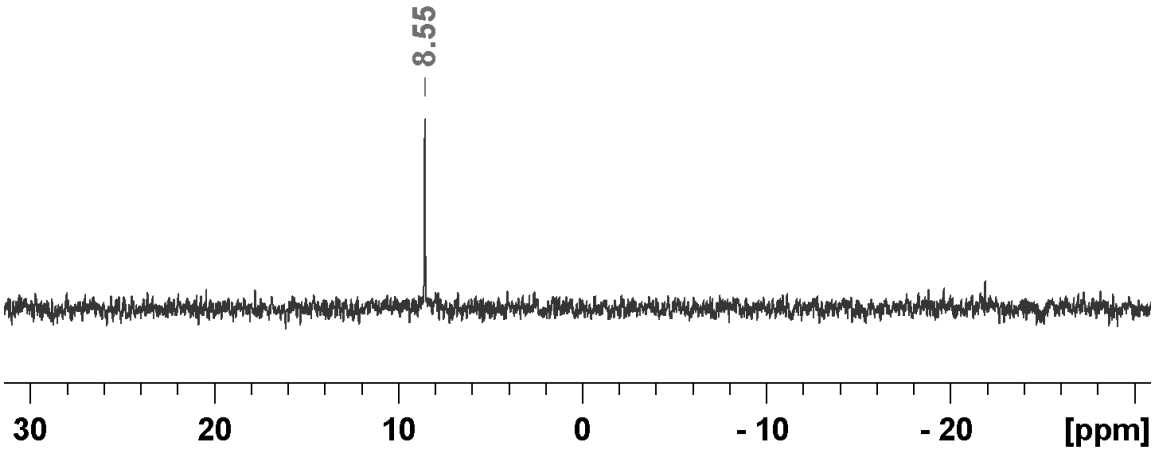

[29]Si-NMR (99.4 MHz, *THF-d[8]) of DMPyr [Me₂In(SSiMe₃)₂] (**7**)

*DMPyr[Me₂In(SeSiMe₃)₂] (**8**)*

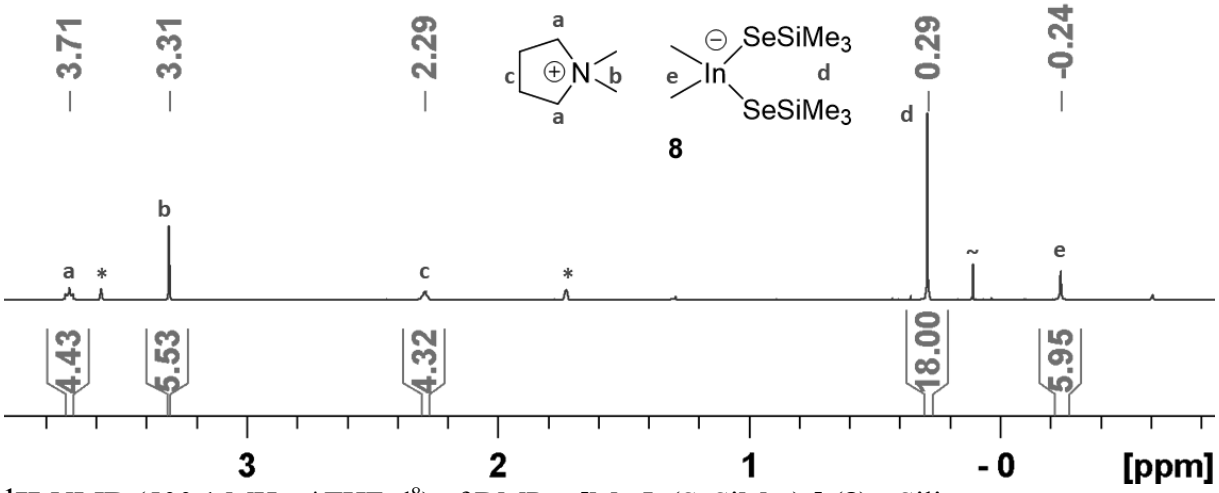

[1]H-NMR (500.1 MHz, *THF-d[8]) of DMPyr [Me₂In(SeSiMe₃)₂] (**8**), ~Silicon grease.

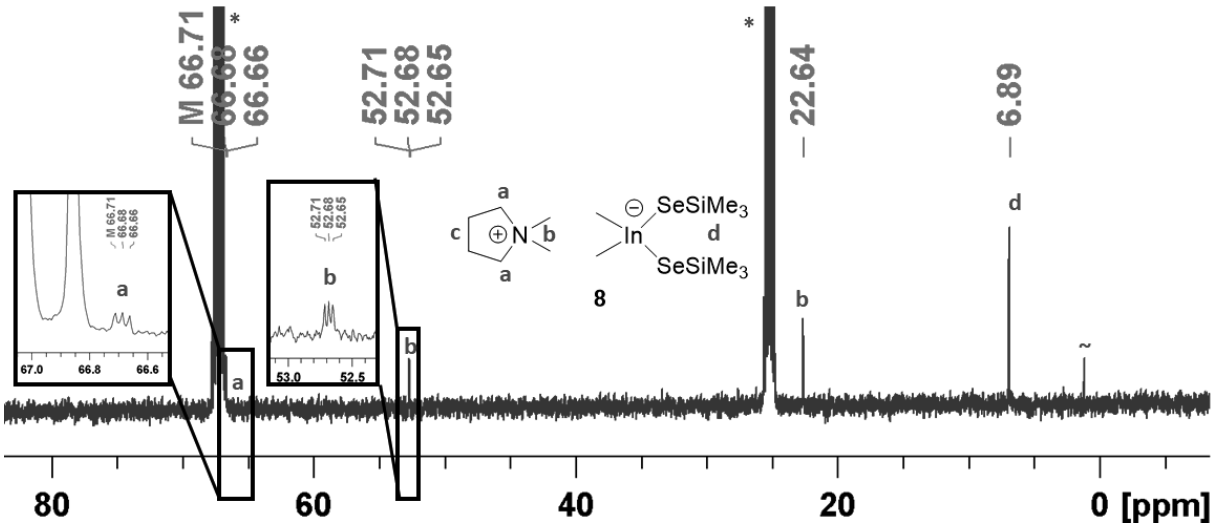

[13]C-NMR (125.8 MHz, *THF-d[8]) of DMPyr [Me₂In(SeSiMe₃)₂] (**8**), ~Silicon grease.

The signal for the indium attached methyl groups could not be identified, as the concentration of the saturated solution of **8** in THF-d[8] is not high enough. No [29]Si- and [77]Se-NMR spectra were obtained for this reason.

*DMPyr[Me₂In(SeSiMe₃)(SSiMe₃)] (**9**)*

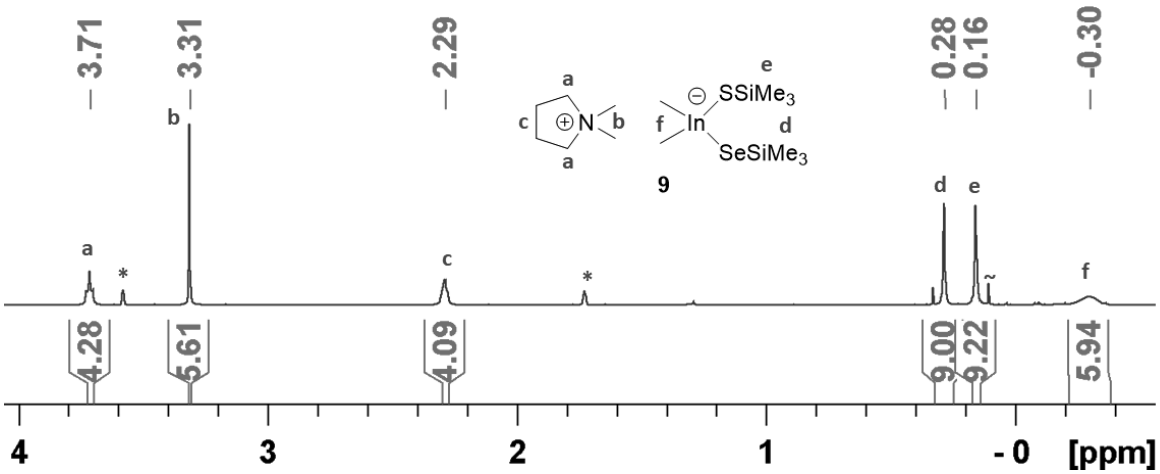

[1]H-NMR (500.1 MHz, *THF-d[8]) of DMPyr [Me₂In(SeSiMe₃)(SSiMe₃)] (**9**), ~Silicon grease.

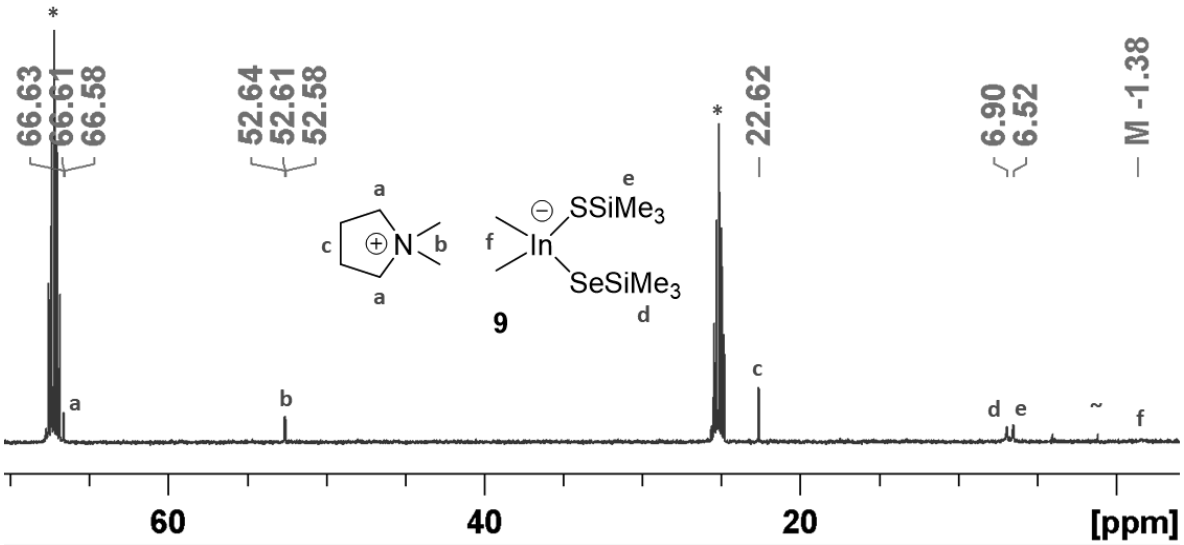

[13]C-NMR (125.8 MHz, *THF-d[8]) of DMPyr [Me₂In(SeSiMe₃)(SSiMe₃)] (**9**), ~Silicon grease.

The signal for the indium attached methyl groups could hardly be identified, due to the low concentration of the saturated solution of **9** in THF-d[8]. Therefore no [29]Si- and no [77]Se-NMR spectra could be obtained.

*DMPyr$_3$[Me$_2$In(μ$_3$-S-InMe$_3$]$_3$ (**10**)*

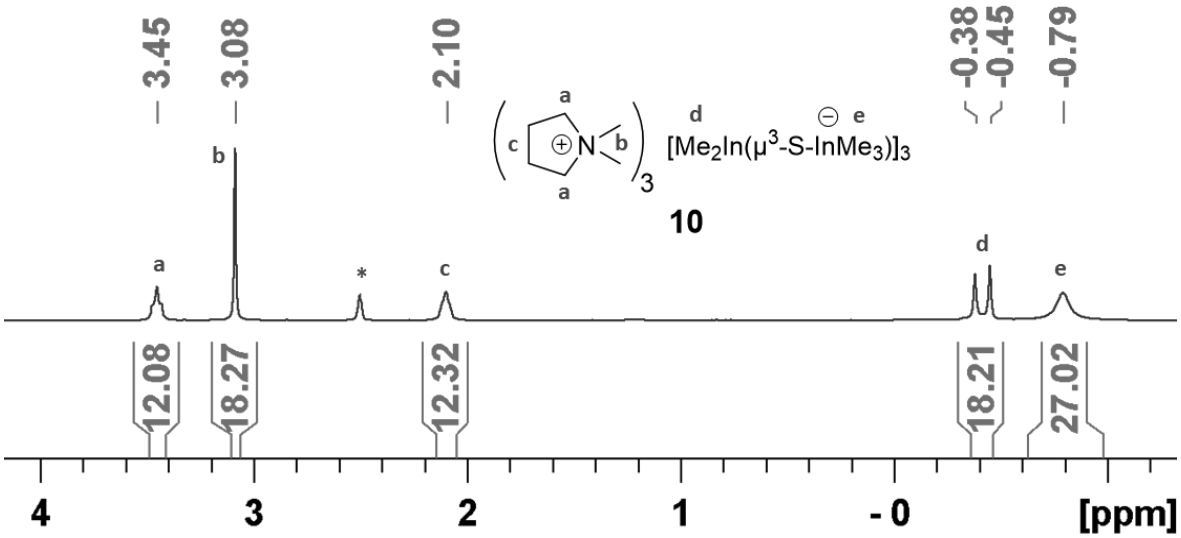

^{1}H-NMR (300.1 MHz, dmso-d^6) of DMPyr$_3$[Me$_2$In(μ$_3$-S-InMe$_3$]$_3$ (**10**).

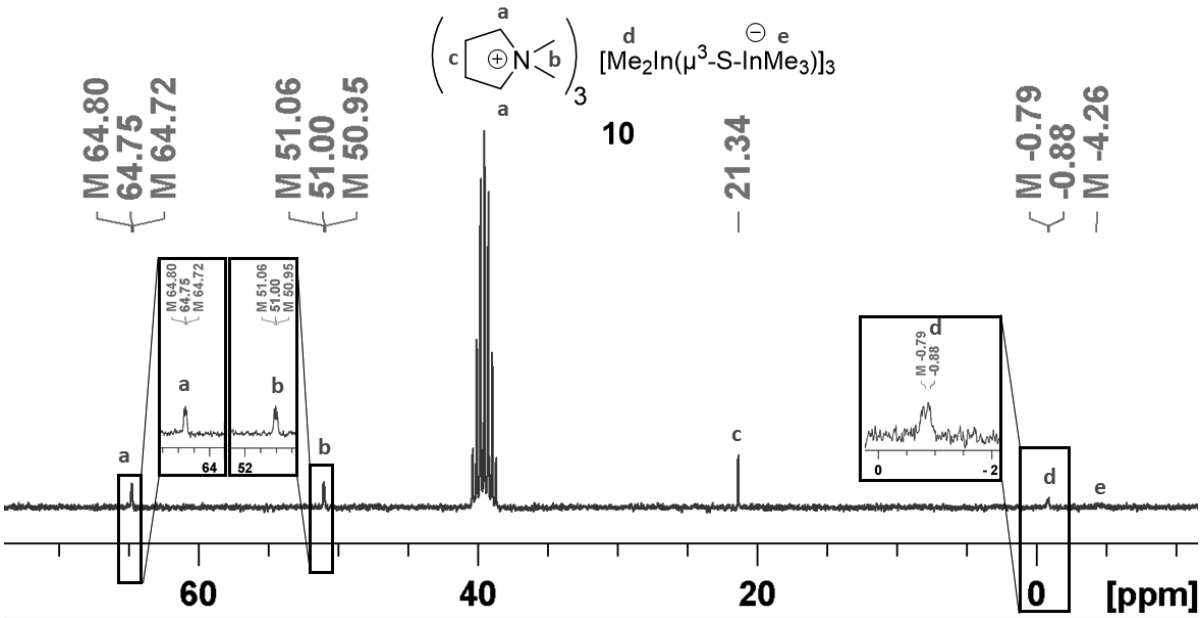

^{13}C-NMR (75.5 MHz, dmso-d^6) of DMPyr$_3$[Me$_2$In(μ$_3$-S-InMe$_3$]$_3$ (**10**).

Note that the split signal of the indium attached methyl groups of **10** could be caused by the conformative rigidity determined by the twist-boat conformation that could be identified in the crystallographically determined molecular structure of the anion.

Crystallographic information

The data collection for the single-crystal structure determination was performed on a Stoe Stadivari diffractometer or a Bruker D8 Quest diffractometer by the X-ray service department of the Fachbereich Chemie, University of Marburg. Information concerning the used hard-ware, and software used for Data collection, cell refinement and data reduction as well as structure solution and refinement can be reviewed in the attached CIF-files. After the solution (Shelxt)[5] and refinement process (Shelxl 2017/1)[6] the data was validated by using Platon.[7] All graphic representations were created with Diamond 4.[8]

*XRD data for the hydrochalcogenides DMPyr[SH] (**1**) and DMPyr[SeH] (**2**)*

Table S1: XRD crystal and refinement data of DMPyr[SH] (**1**) and DMPyr[SeH] (**2**).

	DMPyr[SH] (1)		**DMPyr[SeH] (2)**	
CCDC code	1910798		1910797	
Identification code	majg06		jgdmpsehloesen	
Empirical formula	C6 H15 N S		C6 H14 N Se	
Formula weight	133.25		179.14	
Temperature	100(2) K		100(2) K	
Wavelength	0.71073 Å		0.71073 Å	
Crystal system	Monoclinic		Monoclinic	
Space group	P 21/n		P 21/n	
Unit cell dimensions	a = 6.7084(4) Å	α= 90°.	a = 6.9056(3) Å	α= 90°.
	b = 11.7617(7) Å	β= 94.632(2)°.	b = 11.8466(6) Å	β= 94.578(4)°.
	c = 9.9595(5) Å	γ = 90°.	c = 10.1507(4) Å	γ = 90°.
Volume	783.26(8) $Å^3$		827.76(6) $Å^3$	
Z	4		4	
Density (calculated)	1.130 Mg/m^3		1.437 Mg/m^3	
Absorption coefficient	0.322 mm^{-1}		4.449 mm^{-1}	
F(000)	296		364	
Crystal size	0.250 x 0.190 x 0.130 mm^3		0.375 x 0.210 x 0.119 mm^3	
Theta range for data collection	2.685 to 27.127°.		2.647 to 34.584°.	
Index ranges	-8<=h<=7, -14<=k<=15, -12<=l<=12		-10<=h<=10, -18<=k<=14, -16<=l<=14	
Reflections collected	8889		14464	
Independent reflections	1733 [R(int) = 0.0254]		3345 [R(int) = 0.0670]	
Completeness to theta = 25.242°	100.0 %		99.7 %	
Absorption correction	Semi-empirical from equivalents		Semi-empirical from equivalents	
Max. and min. transmission	0.7455 and 0.7044		0.0926 and 0.0109	
Refinement method	Full-matrix least-squares on F2		Full-matrix least-squares on F2	
Data / restraints / parameters	1733 / 0 / 79		3345 / 0 / 75	
Goodness-of-fit on F2	1.081		1.059	
Final R indices [I>2sigma(I)]	R1 = 0.0266, wR2 = 0.0655		R1 = 0.0483, wR2 = 0.1065	
R indices (all data)	R1 = 0.0307, wR2 = 0.0674		R1 = 0.0855, wR2 = 0.1191	
Extinction coefficient	n/a		n/a	
Largest diff. peak and hole	0.252 and -0.196 $e.Å^{-3}$		0.880 and -1.476 $e.Å^{-3}$	

*XRD data for the gallates $DMPyr_2[Me_2Ga(\mu_2\text{-}S)]_2$ (**3**) and $DMPyr_2[Me_2Ga(\mu_2\text{-}Se)]_2$ (**4**)*

Table S2: XRD crystal and refinement data of $DMPyr_2[Me_2Ga(\mu_2\text{-}S)]_2$ (**3**) and $DMPyr_2[Me_2Ga(\mu_2\text{-}Se)]_2$ (**4**).

	$DMPyr_2[Me_2Ga(\mu_2\text{-}S)]_2$ (3)		**$DMPyr_2[Me_2Ga(\mu_2\text{-}Se)]_2$ (4)**	
CCDC code	1910795		1910796	
Identification code	majg12C4		jg370loesen	
Empirical formula	C16 H40 Ga2 N2 S2		C16 H40 Ga2 N2 Se2	
Formula weight	464.06		557.86	
Temperature	100(2) K		100(2) K	
Wavelength	0.71073 Å		1.54186 Å	
Crystal system	Monoclinic		Monoclinic	
Space group	P 21/n		P 21/n	
Unit cell dimensions	a = 9.5961(4) Å	α= 90°.	a = 9.8332(7) Å	α= 90°.
	b = 12.0450(5) Å	β= 102.3790(10)°.	b = 12.1082(11) Å	β= 102.272(6)°.
	c = 9.9485(4) Å	γ = 90°.	c = 9.9276(8) Å	γ = 90°.
Volume	1123.16(8) $Å^3$		1154.99(16) $Å^3$	
Z	2		2	
Density (calculated)	1.372 Mg/m^3		1.604 Mg/m^3	
Absorption coefficient	2.584 mm^{-1}		6.440 mm^{-1}	
F(000)	488		560	
Crystal size	0.450 x 0.230 x 0.180 mm^3		0.382 x 0.161 x 0.042 mm^3	
Theta range for data collection	2.676 to 27.151°.		5.751 to 66.594°.	
Index ranges	-12<=h<=12, -15<=k<=15, -12<=l<=12		-11<=h<=11, -14<=k<=13, -7<=l<=11	
Reflections collected	37739		11710	
Independent reflections	2483 [R(int) = 0.0382]		2042 [R(int) = 0.0997]	
Completeness to theta = 25.242°	99.9 %		99.8 %	
Absorption correction	Semi-empirical from equivalents		Semi-empirical from equivalents	
Max. and min. transmission	0.7455 and 0.5293		0.0600 and 0.0074	
Refinement method	Full-matrix least-squares on F2		Full-matrix least-squares on F2	
Data / restraints / parameters	2483 / 85 / 170		2042 / 0 / 104	
Goodness-of-fit on F2	1.055		0.996	
Final R indices [I>2sigma(I)]	R1 = 0.0192, wR2 = 0.0505		R1 = 0.0806, wR2 = 0.1973	
R indices (all data)	R1 = 0.0216, wR2 = 0.0513		R1 = 0.0933, wR2 = 0.2072	
Extinction coefficient	n/a		n/a	
Largest diff. peak and hole	0.591 and -0.257 $e.Å^{-3}$		2.409 and -1.596 $e.Å^{-3}$	

*XRD data for the indates $DMPyr_2[Me_2In(\mu\text{-}S)]_2$ (**5**) and $DMPyr_2[Me_2In(\mu\text{-}Se)]_2$ (**6**)*

Table S3: XRD crystal and refinement data of $DMPyr_2[Me_2In(\mu_2\text{-}S)]_2$ (**5**) and $DMPyr_2[Me_2In(\mu_2\text{-}Se)]_2$ (**6**).

	$DMPyr_2[Me_2In(\mu_2\text{-}S)]_2$ (5)		$DMPyr_2[Me_2In(\mu_2\text{-}Se)]_2$ (6)	
CCDC code	1910796		1910794	
Identification code	majg12c1		jg14	
Empirical formula	C16 H40 In2 N2 S2		C16 H40 In2 N2 Se2	
Formula weight	554.26		648.06	
Temperature	100(2) K		100(2) K	
Wavelength	0.71073 Å		0.71073 Å	
Crystal system	Monoclinic		Monoclinic	
Space group	P 21/n		P 21/n	
Unit cell dimensions	a = 9.7075(4) Å	α= 90°.	a = 9.9187(6) Å	α= 90°.
	b = 12.1404(5) Å	β= 100.208(2)°.	b = 12.2925(9) Å	β= 100.434(2)°.
	c = 9.9277(5) Å	γ = 90°.	c = 9.9398(8) Å	γ = 90°.
Volume	1151.49(9) $Å^3$		1191.88(15) $Å^3$	
Z	2		2	
Density (calculated)	1.599 Mg/m^3		1.806 Mg/m^3	
Absorption coefficient	2.184 mm^{-1}		4.988 mm^{-1}	
F(000)	560		632	
Crystal size	0.530 x 0.070 x 0.060 mm^3		0.250 x 0.106 x 0.083 mm^3	
Theta range for data collection	2.676 to 27.169°.		2.662 to 25.245°.	
Index ranges	-12<=h<=12, -15<=k<=15, -12<=l<=12		-11<=h<=11, -14<=k<=14, -11<=l<=11	
Reflections collected	34138		11756	
Independent reflections	2560 [R(int) = 0.0527]		2148 [R(int) = 0.0464]	
Completeness to theta = 25.242°	100.0 %		100.0 %	
Absorption correction	Semi-empirical from equivalents		Semi-empirical from equivalents	
Max. and min. transmission	0.7455 and 0.6218		0.7452 and 0.6075	
Refinement method	Full-matrix least-squares on F2		Full-matrix least-squares on F2	
Data / restraints / parameters	2560 / 0 / 104		2148 / 0 / 104	
Goodness-of-fit on F2	1.071		1.068	
Final R indices [I>2sigma(I)]	R1 = 0.0141, wR2 = 0.0296		R1 = 0.0209, wR2 = 0.0407	
R indices (all data)	R1 = 0.0184, wR2 = 0.0303		R1 = 0.0306, wR2 = 0.0431	
Extinction coefficient	n/a		n/a	
Largest diff. peak and hole	0.277 and -0.367 $e.Å^{-3}$		0.508 and -0.382 $e.Å^{-3}$	

*XRD data for the inverse heteroadamantane cage compound $DMPyr_2[(Me_2In)_6(\mu^3\text{-}S)_4]$ (**11**)*

Table S4: XRD crystal and refinement data of $DMPyr_2[(Me_2In)_6(\mu_3\text{-}S)_4]$ (**11**).

	$DMPyr_2[(Me_2In)_6(\mu_3\text{-}S)_4]$ (11)	
CCDC code	1910799	
Identification code	majgl2inb	
Empirical formula	C14 H36 In3 N O0.50 S2	
Formula weight	635.02	
Temperature	100(2) K	
Wavelength	0.71073 Å	
Crystal system	Tetragonal	
Space group	I 41/a c d	
Unit cell dimensions	a = 17.0977(11) Å	α= 90°.
	b = 17.0977 Å	β= 90°.
	c = 32.377(2) Å	γ = 90°.
Volume	9464.7(14) $Å^3$	
Z	16	
Density (calculated)	1.783 Mg/m^3	
Absorption coefficient	3.072 mm^{-1}	
F(000)	4960	
Crystal size	0.435 x 0.403 x 0.195 mm^3	
Theta range for data collection	2.382 to 27.143°.	
Index ranges	-21<=h<=17, -19<=k<=21, -41<=l<=41	
Reflections collected	40556	
Independent reflections	2619 [R(int) = 0.0961]	
Completeness to theta = 25.242°	99.9 %	
Absorption correction	Semi-empirical from equivalents	
Max. and min. transmission	0.7455 and 0.4882	
Refinement method	Full-matrix least-squares on F2	
Data / restraints / parameters	2619 / 132 / 131	
Goodness-of-fit on F2	1.046	
Final R indices [I>2sigma(I)]	R1 = 0.0379, wR2 = 0.0612	
R indices (all data)	R1 = 0.0678, wR2 = 0.0684	
Extinction coefficient	n/a	
Largest diff. peak and hole	0.894 and -0.692 $e.Å^{-3}$	

*Structural XRD consideration for $DMPyr_3[Me_2In(\mu_3\text{-}InMe_3)]_3$ (**10**)*

Data was collected with a Bruker D8 QUEST area detector diffractometer equipped with with MoK_α radiation, a graded multilayer mirror monochromator (λ = 0.71073 Å) and a PHOTON-100 CMOS detector using an oil-coated shock-cooled crystal at 100(2) K. Absorption effects were corrected semi-empirical using multiscanned reflexions (SAINT V8.37A (Bruker AXS Inc., 2015)). Cell constants were refined using 9785 of observed reflections of the data collection. The structure was solved by direct methods by using the program XT V2014/1 (Bruker AXS Inc., 2014) and refined by full matrix least squares procedures on F^2 using SHELXL-2017/1 (Sheldrick, 2017). The non-hydrogen atoms have been refined anisotropically, carbon bonded hydrogen atoms were included at calculated positions and refined using the 'riding model' with isotropic temperature factors at 1.2 times (for CH_3 groups 1.5 times) that of the preceding carbon atom. Data were of low quality. Only data up to Theta 23.3 was used during refinement. Split positions were refined for the In and S positions. Large anisotrop displacement factors for the cations indicate non-resolved disorder. High difference electron density indicates that the refinement is not complete.

10 crystallizes in the space group P_{-1} with eight formula units per unit cell. Despite the low quality of the crystallographic data, the shape and the conformation and the connectivity of the anion can be qualitatively identified. A discussion of bond lengths and angles is only possible on a coarse level. The anion has a trimer-like six-membered ring structure in the twist-boat conformation that allows the terminal trimethylindate moieties to obtain an equatorial orientation. As methyl groups attached to the cyclic bond indium atoms obtain an axial and an equatorial orientation, we assume these methyl groups' signals in the ^{1}H- and ^{13}C-NMR-spectra are split into two. In **figure S1** a qualitatively representative anion from the eight different formula units set of XRD data is shown without disordered atoms.

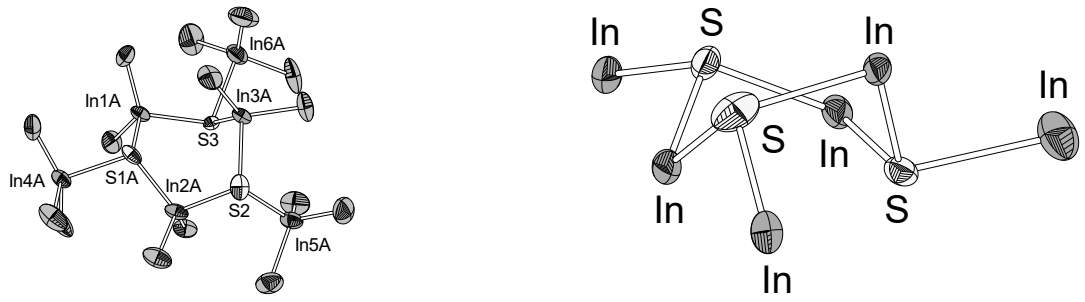

Figure S1: Crystallographically determined molecular structure of the anion present in $DMPyr_3[(Me_2In(\mu_3\text{-}S\text{-}InMe_3)]_3$ (**10**) (left hand side: trianion) with a twist-boat conformation (right hand side: binary framework of the anion). Protons, disordered atoms, and cations are not shown for clarity. Only one of eight crystallographically independend anions of the elemental cell is shown. Ellipsoids shown in 50% level. Selected bond lengths (in Å) and angles (°) of the shown representative anion: In1A-S1A 2.51(2); S1A-In2A 2.51(2); In2A-S2 2.57(3); S2-In3A 2.64(2); In3A-S3 2.49(2); S3-In1A 2.50(2); S1A-In4A 2.57(3); S1A-In4A 2.57(3); S2-In5A 2.44(2); S3-In6A 2.66(2), S1A-In2A-S2 102.6(7), In2A-S2-In3A 100.1(8), S2-In3A-S3 103.3(7), In3A-S3-In1A 105.2(7), S3-In1A-S1A 99.9(7), In1A-S1A-In2A 105.8(6), In1A-S1A-In2A-In4A –109.8(9), In2A-S2-In3A-In5A –108(1), In3A-S3-In1A-In6A 98.0(9), S1A-In1A-S3-In3A –44.6(8), S3-In3A-S2-In2A –32.8(9).

Table S5: XRD crystal and refinement data for $DMPyr_3[Me_2In(\mu^3\text{-}S\text{-}InMe_3)]_3$ (**10**).

	$DMPyr_3[(Me_2In(\mu^3\text{-}S\text{-}InMe_3)]_3$ (10)	
Identification code	JG085_0m	
Habitus, colour	colorless needle	
Crystal size	0.180 x 0.170 x 0.120 mm^3	
Crystal system	Triclinic	
Space group	P-1	Z = 8
Unit cell dimensions	a = 18.4827(7) Å	α= 61.516(2)°.
	b = 25.5703(11) Å	β= 87.572(2)°.
	c = 26.6454(12) Å	γ = 69.629(2)°.
Volume	10258.7(8) $Å^3$	
Cell determination	9785 peaks with Theta 2.3 to 20.8°.	
Empirical formula	C33 H87 In6 N3 S3	
Moiety formula	C15 H45 In6 S3, 3(C6 H14 N)	
Formula weight	1311.15	
Density (calculated)	1.698 Mg/m^3	
Absorption coefficient	2.797 mm^{-1}	
F(000)	5184	
Data collection:		
Diffractometer type	Bruker D8 QUEST area detector	
Wavelength	0.71073 Å	
Temperature	100(2) K	
Theta range for data collection	2.208 to 23.257°.	
Index ranges	-20<=h<=20, -28<=k<=28, -29<=l<=29	
Data collection software	APEX3 (Bruker AXS Inc., 2015)[9]	
Cell refinement software	SAINT V8.37A (Bruker AXS Inc., 2015)[10]	
Data reduction software	SAINT V8.37A (Bruker AXS Inc., 2015)	
Solution and refinement:		
Reflections collected	124803	
Independent reflections	29472 [R(int) = 0.0549]	
Completeness to theta = 23.257°	99.9 %	
Observed reflections	21271[I > 2σ(I)]	
Reflections used for refinement	29472	
Absorption correction	Semi-empirical from equivalents[11]	
Max. and min. transmission	0.2049 and 0.1669	
Largest diff. peak and hole	3.046 and -1.518 $e.Å^{-3}$	
Solution	dual/ difmap[12,13]	
Refinement	Full-matrix least-squares on F2[13]	
Treatment of hydrogen atoms	mixed, constr	
Programs used	XT V2014/1 (Bruker AXS Inc., 2014), SHELXL-2017/1 (Sheldrick, 2017), DIAMOND (Crystal Impact), ShelXle (Hübschle, Sheldrick, Dittrich, 2011)	
Data / restraints / parameters	29472 / 5054 / 1949	
Goodness-of-fit on F2	1.078	
R index (all data)	wR2 = 0.2350	
R index conventional [I>2sigma(I)]	R1 = 0.0911	

Attempts to synthesize DMPyr$_2$[(Me$_2$In)$_6$(μ^3-S)$_4$] (11)

As the investigated single crystal that could be crystallographically identified as DMPyr$_2$[(Me$_2$In)$_6$(μ^3-S)$_4$] (**11**) emerged from a sample that contained a saturated solution of DMPyr$_3$[(Me$_2$In)(μ^3-S-InMe$_3$)]$_3$ (**10**) in tetrahydrofurane and was stored at room temperature for several weeks, we assumed **11** to be a thermal decomposition product of **10**. To support this theory some experiments were conducted: the defined thermolysis of **10**, and several attempts to synthesize the inverse heteroadamantane cage anion.

*Thermolysis of **10***

One possible access to **11** is the thermal treatment of **10**, as it is possible to formulate a dismutation mechanism in which four equivalents of **10** decompose to six equivalents of DMPyr[InMe$_4$] and three equivalents of **11** (**Scheme S1**).

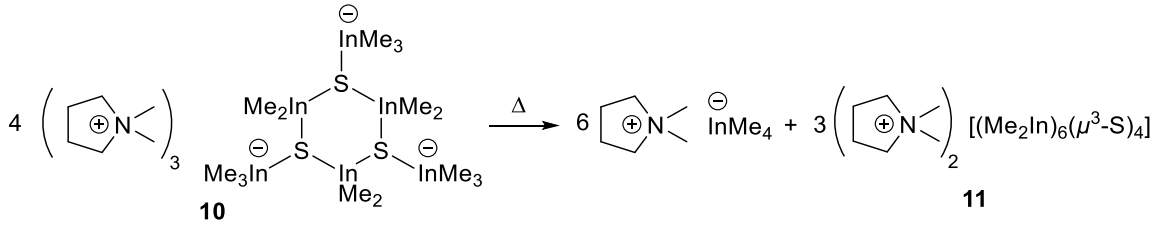

Scheme S1. Proposed dismutation mechanism for the formation of **11** by thermolysis of **10**.

To support this assumption a defined thermolysis experiment was conducted. As the solubility of DMPyr[InMe$_4$] and **11** are comparable, the emerging mixture is investigated.

A solution of 50 mg of **10** in diglyme (10 mL) was stirred at 100 °C for 18 h. All volatiles were removed in fine vacuum and the remaining colorless solid is dried in fine vacuum. The ^{1}H-NMR spectrum fits a mixture of six equivalents of DMPyr[InMe$_4$] and three equivalents of **11**.

^{1}H-NMR (300.1 MHz, dmso-d^6): δ_H = 3.45 (m, 48H, 9 x (H$_2$C)$_2$(*H*$_2$C)$_2$N(CH$_3$)$_2$), 3.08 (s, 63H, 9 x (H$_2$C)$_2$(H$_2$C)$_2$N(C*H*$_3$)$_2$), 2.08 (m, 48H, 9 x (H$_2$C)$_2$(H$_2$C)$_2$N(C*H*$_3$)$_2$), –0.38 (bs, 72H, 6 x In(CH$_3$)$_4$), –0.64 (bs, 108H, 3 x [(*H*$_3$C)$_2$In)$_6$(μ^3-S)$_4$]) ppm. We point out, that the reliability of integration is restricted, as the signals are quite broad (**figure S2**).

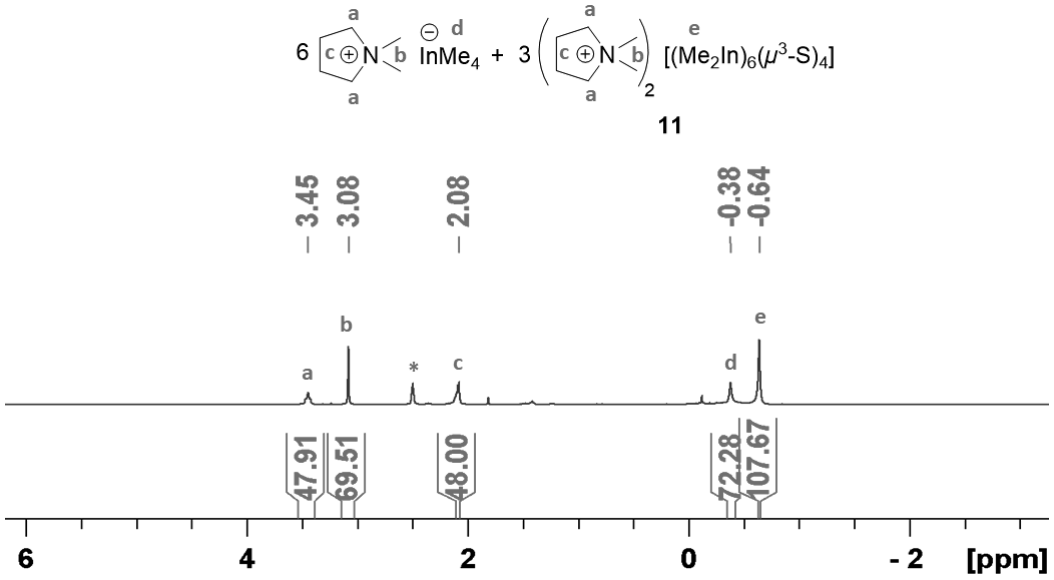

Figure S2: ^{1}H-NMR (300.1 MHz, *dmso-d^{6}) of the thermolysis product of **10**.

To realize the preparation of **11**, we tried to perform the formation of the inverse heteroadamantane cage by the reactions shown in **Scheme S3**: via elimination of $SiMe_4$ (**Scheme S2**, A), or $ClSiMe_3$ (**Scheme S2**, B/C). These reaction pathways were chosen to avoid nonvolatile byproducts. However, it was not possible to prepare **11** (or the representative with Ph_4P^+ cation **11-Ph$_4$P**) purely.

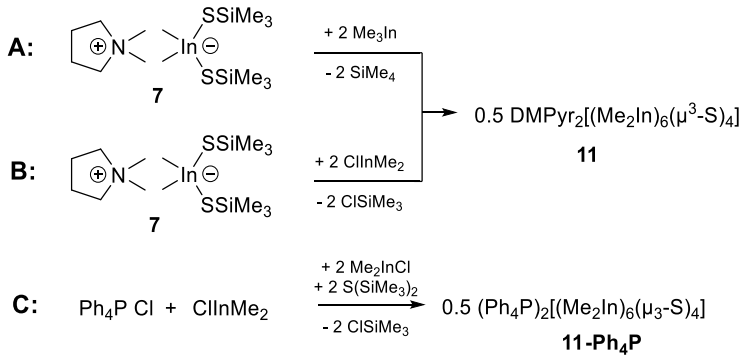

Scheme S2. Attempts to prepare **11** by elimination of $SiMe_4$ (**A**) or $ClSiMe_3$ (**B**/**C**).

*A: Attempt to prepare **11** starting from **7** by elimination of $SiMe_4$*

To a solution of DMPyr[$Me_2In(SSiMe_3)_2$] (**7**) (0.076 g, 0.16 mmol, 2.0 eq.) in 5 mL thf a solution of Me_3In (0.053 g, 0.32 mmol, 4.0 eq.) in 5 mL thf was added dropwise at –100 °C. The reaction mixture was allowed to obtain room temperature during a time period of 18 h. All volatiles of the slightly cloudy mixture were removed in fine vacuum. The colorless residue was dried in fine vacuum and investigated by ^{1}H-NMR spectroscopy.

^{1}H-NMR (300.1 MHz, dmso-d^6): δ_H = 3.44 (m, 8H, 2 x $(H_2C)_2(H_2C)_2N(CH_3)_2$), 3.08 (s, 12H, 12 x $(H_2C)_2(H_2C)_2N(CH_3)_2$), 2.08 (m, 8H, 2 x $(H_2C)_2(H_2C)_2N(CH_3)_2$), –0.63 (s, 36H, $[(H_3C)_2In)_6(\mu_3\text{-}S)_4]$) ppm. Impurities are indicated by signals at 0.06 ppm, –0.11 ppm, and –0.36 ppm with a total intensity of 41 proton equivalents per formula unit of the desired product. The impurities cannot be removed by washing with pentane or diethyl ether (**figure S3**). The signal at –0.63 ppm is assumed to be the signal for the $[(H_3C)_2In)_6(\mu_3\text{-}S)_4]^{2-}$ dianion (compare the signal at –0.64 ppm in **figure S2**).

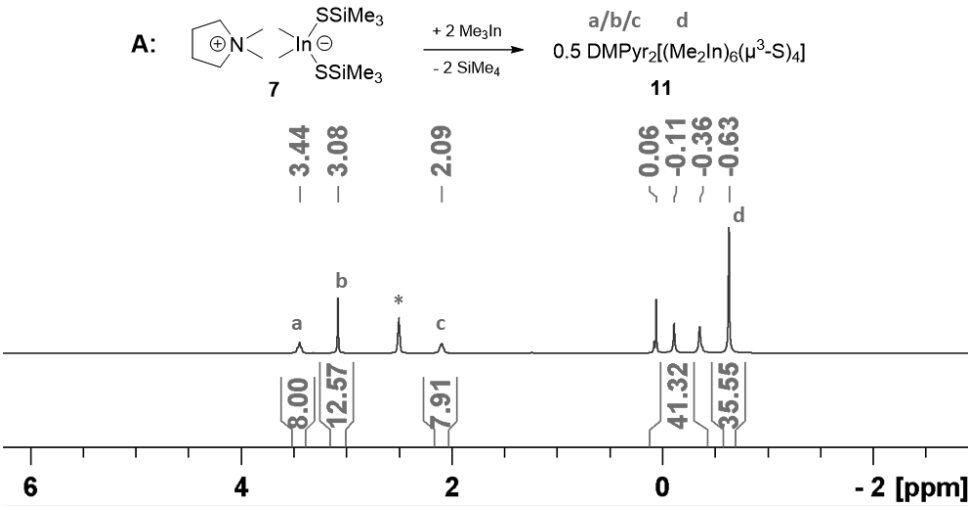

Figure S3: **^{1}H-NMR** (300.1 MHz, *dmso-d^6) of the attempt to synthesize compound **11** by elimination of $SiMe_4$. Impurities between 0.06 ppm and –0.36 ppm could not be avoided or removed.

***B**: Attempt to prepare **11** starting from **7** by elimination of $ClSiMe_3$*

$DMPyr[Me_2In(SSiMe_3)_2]$ (**7**) (0.050 g, 0.11 mmol, 2.0 eq.) and $ClInMe_2$ (0.043 g, 0.22 mmol, 4.0 eq.) are diluted in in 5 mL thf at –78 °C. The reaction mixture was allowed to obtain room temperature during a time period of 18 h. All volatiles of the slightly cloudy mixture were removed in fine vacuum. The colorless residue was dried in fine vacuum and investigated by ^{1}H-NMR spectroscopy.

^{1}H-NMR (300.1 MHz, dmso-d^6): δ_H = 3.45 (m, 8H, 2 x $(H_2C)_2(H_2C)_2N(CH_3)_2$), 3.08 (s, 12H, 12 x $(H_2C)_2(H_2C)_2N(CH_3)_2$), 2.10 (m, 8H, 2 x $(H_2C)_2(H_2C)_2N(CH_3)_2$), –0.63 (s, 6H,* $[(H_3C)_2In)_6(\mu^3\text{-}S)_4]$) ppm. *The intensity of the signal at –63 ppm is too low indicating a uncomplete conversion. Impurities are indicated by signals at 0.06 ppm, –0.11 ppm, and –0.36 ppm with a total intensity of 36 proton equivalents per formula unit of the desired product. The impurities cannot be removed by washing with pentane or diethyl ether (**Figure S4**).

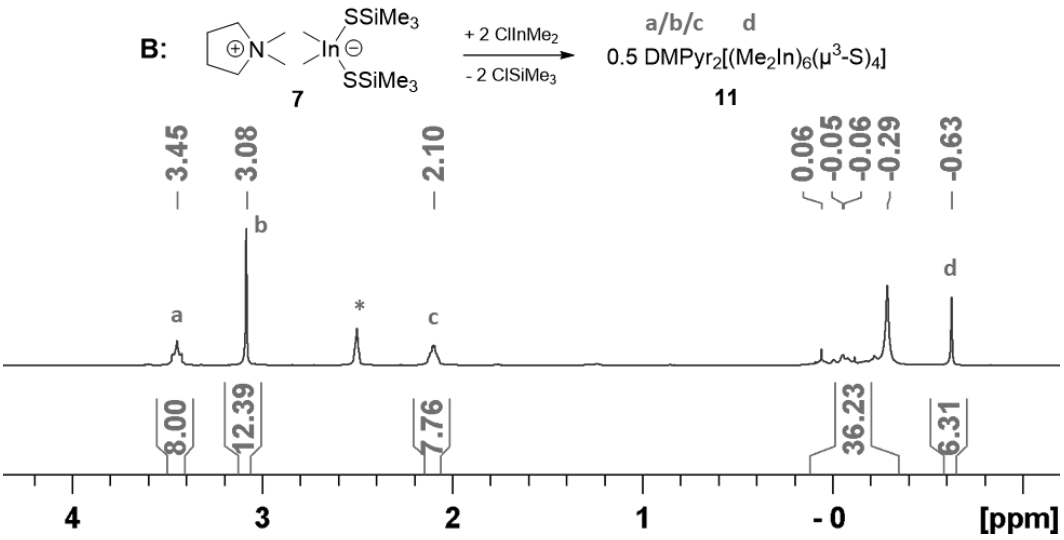

Figure S4: **^{1}H-NMR** (300.1 MHz, *dmso-d^6) of the attempt to synthesize compound **11** by elimination of $ClSiMe_3$. Impurities between 0.06 ppm and –0.29 ppm could not be avoided or removed.

***C**: Attempt to prepare **11-Ph$_4$P** starting from **7** by elimination of $ClSiMe_3$*

To a suspension of $Ph_4P[Cl]$ (0.067 g, 0.17 mmol, 2.0 eq.) in 5 mL thf a solution of $ClInMe_2$ (0.032 g, 0.17 mmol, 2.0 eq.) in 5 mL thf was stirred for 18 h at room temperature to obtain a clear solution of $Ph_4P[Me_2InCl_2]$. $S(SiMe_3)_2$ (0.064 g, 0.36 mmol, 4.0 eq.) was added dropwise to a solution of Me_2InCl (0.065 g, 0.36 mmol, 4.0 eq.) in 5 mL at –20 °C. The solution was allowed to obtain room temperature within a time period of 18 h to obtain a solution of $[Me_2In(\mu_2\text{-}SSiMe_3)]_2$. To the $Ph_4P[Me_2InCl_2]$ solution the solution of $[Me_2In(\mu_2\text{-}SSiMe_3)]_2$ was slowly added at –78 °C. The reaction mixture was allowed to warm to room temperature within a time period of 18 h. All volatiles of the solution were removed in fine vacuum. The colorless residue was dried in fine vacuum and investigated by ^{1}H-NMR spectroscopy.

^{1}H-NMR (300.1 MHz, dmso-d^6): δ_H = 7.97-7.78 (m, 40 H, $(C_6H_5)_4P$), –0.63 (s, 6H*, $[(H_3C)_2In)_6(\mu^3\text{-}S)_4]$) ppm. *The intensity of the signal at –63 ppm is too low, indicating a uncomplete conversion. Impurities are indicated by signals between 0.06 ppm and –0.29 ppm with a total intensity of 36 proton equivalents per two cations. The impurities cannot be removed by washing with pentane or diethyl ether (**Figure S5**).

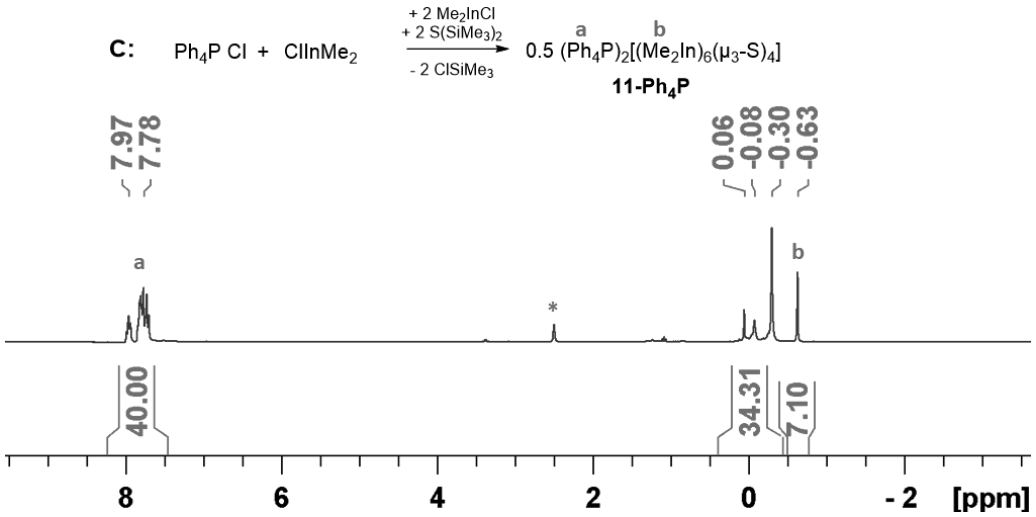

Figure S5: **^{1}H-NMR** (300.1 MHz, *dmso-d^6) of the attempt to synthesize compound **11-Ph$_4$P** by elimination of $ClSiMe_3$. Impurities between 0.06 ppm and –0.30 ppm could not be avoided or removed.

In **Figure S6** the ^{1}H-NMR spectra of the attempts to prepare 11 from **Scheme S2**, and the ^{1}H-NMR spectra obtained by the thermolysis of **10** (**Scheme S1**) are layered together. The signal assigned to the inverse heteroadamantane cage anion $[(H_3C)_2In)_6(\mu_3\text{-}S)_4]^{2-}$ at the ^{1}H-NMR spectrum (– 0.64 ppm) of the thermolysis experiment can be found in the attempts to synthesise the anion (–0.63 ppm, the minor deviation could be a concentration effect). We think this is a good reason to assume this signal to be assignable to the $[(H_3C)_2In)_6(\mu_3\text{-}S)_4]^{2-}$ anion. Though we want to point out, that we were not able to perform a complete and selective synthesis of **11**.

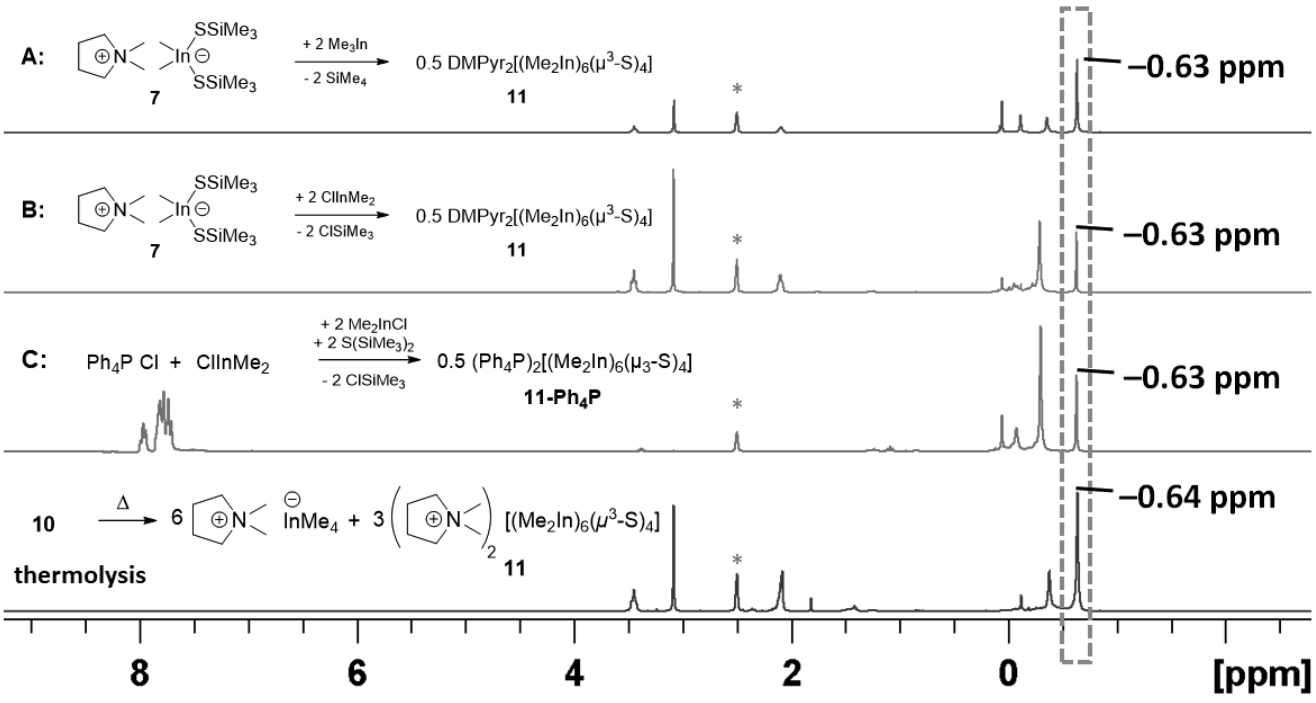

Figure S6: ^{1}H-NMR (300.1 MHz, *dmso-d^6) spectra of the thermolysis product of **10** (bottom row) and the attempts to synthesize compounds **11** (**A**/**B**) and **11-Ph$_4$P** (**C**) that contain the $[(H_3C)_2In)_6(\mu_3\text{-}S)_4]^{2-}$ anion.

References

(1) Armarego, W. L. F.; Perrin, D. D. *Purification of laboratory chemicals*, 4. ed., reprint; Butterworth-Heinemann: Oxford, 2002.

(2) Finger, L. H.; Scheibe, B.; Sundermeyer, J. Synthesis of organic (trimethylsilyl)chalcogenolate salts CatTMS-E (E = S, Se, Te): The methylcarbonate anion as a desilylating agent. *Inorg. chem.* **2015**, *54*, 9568–9575, DOI: 10.1021/acs.inorgchem.5b01665.

(3) Brauer, G. *Handbook of Preparative Inorganic Chemistry V2*, 2nd ed.; Elsevier Science: Burlington, 1965.

(4) So, J.-H.; Boudjouk, P. Convenient Syntheses of Hexamethyldisilathiane and Tetramethyldisilathiane. *Synthesis* **1989**, *1989*, 306–307, DOI: 10.1055/s-1989-27235.

(5) Sheldrick, G. M. Crystal structure refinement with SHELXL. *Acta crystallographica. Section C, Structural chemistry* **2015**, *71*, 3–8, DOI: 10.1107/S2053229614024218.

(6) Hübschle, C. B.; Sheldrick, G. M.; Dittrich, B. ShelXle: A Qt graphical user interface for SHELXL. *Journal of applied crystallography* **2011**, *44*, 1281–1284, DOI: 10.1107/S0021889811043202.

(7) Spek, A. L. Structure validation in chemical crystallography. *Acta crystallographica. Section D, Biological crystallography* **2009**, *65*, 148–155, DOI: 10.1107/S090744490804362X.

(8) K. Brandenburg, H. P. *Diamond*; Crystal Impact GbR: Bonn, **2012**.

In preparation

Organic Methylcarbonate Salts Comprising Non-methylated Onium Cations Cat[OCO_2Me] (Cat = Ph_4P^+, PPN^+, TBA^+) via Fluoride-Induced Demethylation of Dimethylcarbonate

Jannick Guschlbauer, Tobis Vollgraff, Ahmed Fetoh, Jörg Sundermeyer

ARTICLE

Organic Methylcarbonate Salts Comprising Non-methylated Onium Cations Cat[OCO_2Me] (Cat = Ph_4P^+, PPN^+, TBA^+) via Fluoride-Induced Demethylation of Dimethylcarbonate

Jannick Guschlbauer,[a] Tobias Vollgraff,[a] Ahmed Fetoh,[a] Jörg Sundermeyer*[a]

Abstract: Herein the preparation of organic methylcarbonate salts with symmetrically substituted phosphonium and ammonium cations Cat[OCO_2Me] (Cat = Ph_4P^+, PPN^+, TBA^+). They are obtained by demethylation of dimethylcarbonate with organic fluoride salts Cat[F] or fluoridophosphoranes. The title compounds can be used for common desilylation reactions to obtain ionic compounds that show a higher crystallisation tendency than classical methyl-onium salts obtained via state of the art methylcarbonate ionic liquid synthesis. This is illustrated by presenting a complete set of crystallographically characterized homologues of $Ph_4P[ESiMe_3]$ (E = S, Se, Te).

Introduction

Organic salts and ionic liquids with a methylcarbonate anion are commercially established as versatile precursors for an atom efficient green synthesis of other ionic liquids and organic cation salts in high purity.[1,2] Methylcarbonate induced deprotonation[1,3] of even weak acids or desilylation[4] of suitable silanes are two established paths, taking advantage of the formation of only volatile by-products CO_2, MeOH and Me_3SiOMe and isolation of highly pure organic cation salts without any traces of water or metal cation and halide impurities.

However, the established green synthesis of the methylcarbonate salts via quaternization of *N*-alkylimidazole, amine, guanidine or phosphine nucleophiles by methylation with dimethylcarbonate under solvothermal conditions leads to some restrictions concerning the cation: While *N*-alkyl-*N'*-methylimidazolium methylcarbonates are only stable in diluted methanolic solution,[5,6] the ammonium and phosphonium cations are – due to the type of synthesis strategy – at least mono-methylated. An alternative to prepare 1,3-dialkylimidazolium salts without the danger of carboxylation of C-H acidic positions in the imidazolium cation is using the highly nucleophilic, naked [S*t*Bu]$^-$ anion (instead of methylcarbonate) as desilylating agent.[7] For the preparation of non-methylated ammonium methylcarbonate salts, only few examples are known: By addition of CO_2 to $R_4N[OMe]$,[8] or by demethylation of Me_2CO_3 by $R_4N[OH]$ in MeOH.[9] As phosphonium cations tend to decompose in the presence of these highly basic and nucleophilic *O*-donor anions, these reactions cannot simply be transferred towards the P-homologues. Alternative strategies like salt eliminations using $Ph_4P[Cl]$ and the metal salts Ag- or $Na[O_2COMe]$ tend to fail, as these inorganic methylcarbonate precursors are highly instable and insoluble in common solvents, respectively.

Results and Discussion

With the aim to investigate organic cation salts with highly nucleophilic anions we prepared a set of fluorides Cat[F] by anion exchange using the well-established route of ion metathesis of equimolar amounts of Cat[BF_4] and KF in methanol.[10a] Here we report the synthesis and XRD molecular structure of $Ph_4P[F]$ (**1**) obtained by this method. The latter is not a phosphonium fluoride salt but a neutral fluoridophosphorane with coordination number 5 at the phosphorus atom. **1** crystallizes from toluene in the monoclinic space group in *P*21/*n* with four formula units per unit cell. The phosphorous atom shows a distorted trigonal bipyramidal coordination sphere. Fluoride occupies an axial position (Figure 1). The terminal P-F bond length of 1.7582(8) Å is longer than in the gas phase of PF_5 (or similar)[10b] but shorter than the two P-F bonds (2.646 Å and 1.820 Å) in the PPN[F], displaying an intramolecular P-F-P bride.[10a]

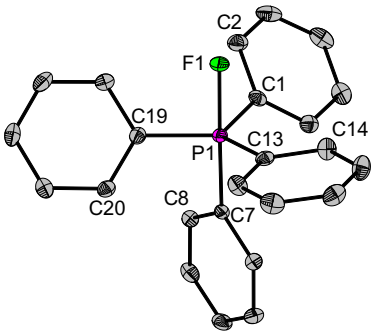

Figure 1. Crystallographically determined molecular structure of $Ph_4P[F]$ (**1**). Protons are omitted for clarity. Ellipsoids are shown in 50% level. Selected bond lengths in Å and angles in °: P1-F1 1.7582(8), P1-C1 1.842(1), P1-C7 1.902(1), P1-C13 1.826(1), P1-C19 1.836(1), C2-C1 1.398(2), C7-C8 1.403(2), C13-C14 1.391(2), C19-C20 1.400(2), F1-P1-C1 85.77(5), F1-P1-C7 178.24(5), F1-P1-C13 85.05(5), F1-P2-C19 87.25(5) C1-P1-C7 92,49(6), C1-P1-C13 118.82(6), C1-P1-C19 122.23(6), C7-P1-C13 95.57(6), C7-P1-C19 93.91(6), C2-C1-P1-F1 -44.6(1), C8-C7-P1-F1 -71(2), C14-C13-P1-F1 -84.2(1), C20-C19-P1-F1 -144.77(1).

[a] J. Guschlbauer, T. Vollgraff, Dr. A. Fetoh, Prof. Dr. J. Sundermeyer
Departement of Chemistry
Philipps-Universität Marburg
Hans Meerwein Straße 4, 35034 Marburg
E-mail: JSU@staff.uni-marburg.de

Although, fluoride is quasi covalently attached to a highly distorted latent tetraphenylphosphonium moiety, the P-F bond can easily be cleaved by suitable electrophiles such as DMC. Thermodynamic driver for such reaction is the formation of a more stable C-F instead of P-F bond. Additional driving force is provided by the release of strain during the formation of the remaining cation. The high nucleophilicity of the fluoride anion can be utilized in the onefold demethylation of dimethylcarbonate Me_2CO_3 in solvothermal conditions at 140 °C for 72 h in the presence of methanol (Scheme 1). The complete conversion of **1** into **2-Ph$_4$P** can be verified by elemental analyses and the signals' relative intensities in the ^{1}H NMR spectra (Figure 2). The product is free of H-bonded methanol. **2-Ph$_4$P** is most likely an ionic compound, which is proven by the signals for the methylcarbonate anion in the ^{1}H/^{13}C NMR spectra that is identical to the corresponding shifts of literature known naked methylcarbonate salts.[4]

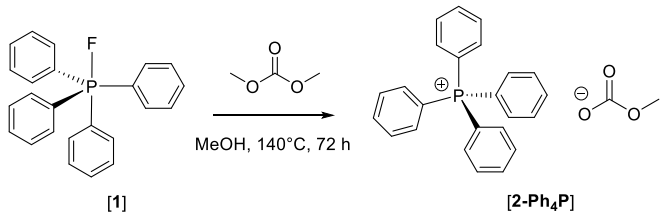

Scheme 1. Preparation of $Ph_4P[OCO_2Me]$ (**2-Ph$_4$P**) by onefold methylation of Me_2CO_3 with $Ph_4P[F]$ (**1**) under solvothermal conditions.

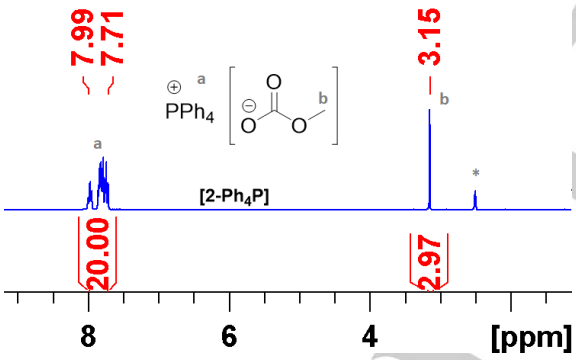

Figure 2. ^{1}H NMR (300.1 MHz, [d$_6$]DMSO) of $Ph_4P[OCO_2Me]$. This spectrum confirms the complete reaction of the fluoridophosphorane to the methylcarbonate salt.

As no suitable single crystals of **2-Ph$_4$P** could be grown for XRD structure determination, we transferred the reaction route on other organic fluoride salts, like the PPN[F], and TBA[F] · 3 H_2O. Within PPN[F] the fluoride is known to be attached the two phosphorous atoms.[10] However, the demethylation of Me_2CO_3 can be performed according to the procedure shown in Scheme 1 to yield **2-PPN**. Single crystals suited for XRD structure determination could be grown from a solution in a mixture of acetonitrile and diethyl ether. **2-PPN** crystallizes in the monoclinic space group *P*21/*c* with eight ion pairs and four molecules of acetonitrile per unit cell (Figure 3). There are no P···O interactions between methylcarbonate anion and cation. Each oxygen atom of the methylcarbonate anions is bonded either to C-H acidic positions of the cation or of the solvent acetonitrile via H-bonds. The C-H···O bond distances are ranging from 2.34 Å to 2.50 Å. The distance C77-H77A···O1 of the interacting solvent acetonitrile is observed at 2.41 Å. CH-activation with methylcarbonate salts is commonly observed for imidazolium-cations.[5]

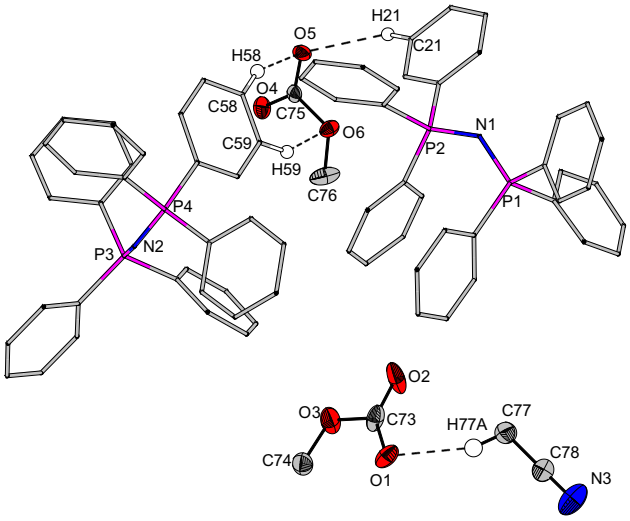

Figure 3. Molecular structure of PPN[OCO_2Me] (**2-PPN**). Ellipsoids of the anions are shown at the 50% level. Only protons involved in some H-Bonds shown for clarity. Selected bond lengths (in Å) and angles (in °): O1-C73 1.244(3), O2-C73 1.238(3), O3-C73 1.415(3), O3-C74 1.410(3), O1-C73-O2 130.8(2), O1-C73-O3 115.4(2), O2-C73-O3 113.8(2), C73-O3-C74 117.0(2), C74-O3-C73-O1 4.0(3), C74-O3-C73-O2 -175.4(2), N3-C78 1.132(3), C78-C77 1.441(4), N3-C78-C77 179.1(3), C77-H77A 0.98, C78-C77-H77A 160.9(2), H77A-O1 2.406(2), C77-H77A-O1 160.9(2), C73-O1-H77A 94.6(2), C73-O1-H77A-C77 32.2(6), O4-C75 1.231(3), O5-C75 1.231(3), O6-C75 1.406(3), O6-C76 1.421(3), O4-C75-O5 130.6(2), O4-C75-O6 116.9(2), O5-C75-O6 112.5(2), C75-O6-C76 116.1(2), C21-H21 0.95, O5-H21 2.50, O5-H21-C21 143.9(1), C75-O5-H21-C21 -81.1(3), C58-H58 0.95, O5-H58 2.34, O5-H58-C58 150.7(1), C75-O5-H58-C58 16.2(3), C59-H59 0.95, O6-H59 2.499(2), C59-H59-O6 140.7(1), C59-H59-O6-C75 -6.6(3).

Despite our concerns of the methylcarbonate anion's stability towards water, we also successfully converted the most common organic fluoride salt as trihydrate TBA[F] · 3 H_2O into TBA[OCO_2Me] (**2-TBA**) by this method. This implies that minor amounts of water do not decompose the methylcarbonate anion. Single crystals suitable for XRD structure determination could be grown from a mixture of tetrahydrofuran and pentanes. **2-TBA** crystallizes in the monoclinic space group *P*21/*n* with four ion pairs per unit cell. Each cation is attached to three methylcarbonate anions by H-bonds reaching from 2.40 Å to 2.44 Å to protons attached to the alpha-carbon atoms. Thereby each terminal oxygen atom acts as H-bond acceptor (Figure 4). For further reactions we preferred to use **2-Ph$_4$P** as starting material. Though **2-Ph$_4$P** did not yield good single crystals itself, the products prepared by this compound show a high tendency to crystallize well. Therefore, we were able to prepare a set of homologues trimethylsilylchalcogenolate anions with the Ph_4P^+ cation by single desilylation of $E(SiMe_3)_2$ (E = S, Se, Te) with $Ph_4P[OCO_2Me]$ at room temperature in tetrahydrofuran (Scheme 2). In accord with previous studies we did not observe any double desilylation towards $[E]^{2-}$ salts.[4]

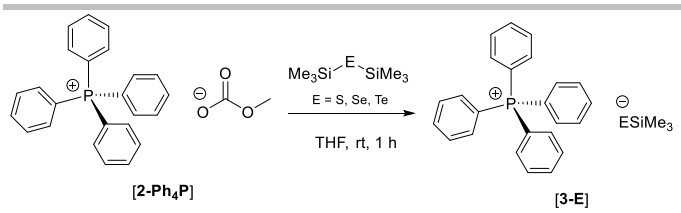

Scheme 2. Preparation of $Ph_4P[ESiMe_3]$ (**3-E**, E = S, Se, Te) by single desilylation of $E(SiMe_3)_2$ with $Ph_4P[OCO_2Me]$ (**2-Ph$_4$P**).

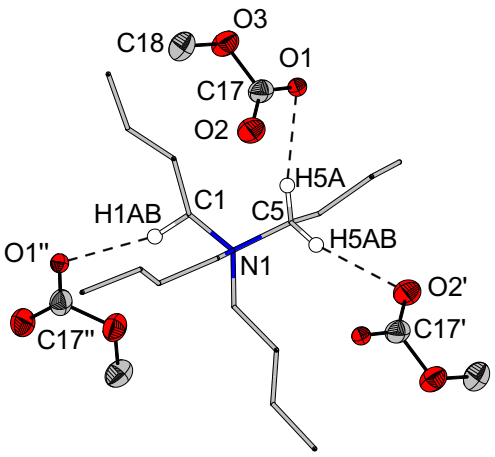

Figure 4. Molecular structure of TBA[OCO_2Me] (**2-TBA**). Ellipsoids of the anions are shown at the 50% level. Only protons involved in H-Bonds shown for clarity. Selected bond lengths (in Å) and angles (in °): O1-C17 1.247(2), O2-C17 1.240(2), O3-C17 1.404(2), O1-C17-O2 130.4(2), O2-C17-O3 116.8(2), O1-C17-O3 112.8(2), O3-C18 1.424(3), C18-O3-C17 115.5(2), C5-H5A 0.97, O1-H5A 2.44, O1-H5A-C5 166.1(1), C17-O1-H5A-C5 -173.3(4), C5-H5AB 0.97, H5A-C5-H5AB 107.4, H5AB-O2' 2.439(1), C5-H5AB-O2' 149.3(1), C5-H5AB-O2'-C17' -153.4(2), C1-H1AB 0.97, O1''-H1AB 2.40, O1''-H1AB-C1 161.6(1), C17''-O1''-H1AB-C1 118.5(3). Symmetry operations: I: 1-x, 1-y, 1-z; II: 1/2-x, 1/2+y, 1/2-z.

Single crystals for the structural characterization of all homologues $Ph_4P[ESiMe_3]$ (E = S, Se, Te) could be grown by diffusion of pentanes into a thf-solution of the product at –30 °C during several days $Ph_4P[SSiMe_3]$ (**3-S**) crystallizes in the orthorhombic space group *Pbca* with eight formula units per unit cell. One $[SSiMe_3]^-$ anion is noncovalently bond to two tetraphenylphosphonium cations by H-bonds to the protons in *ortho*- and *meta*-position to the phosphorous centre (2.82 Å and 2.85 Å respectively) (Figure 5).

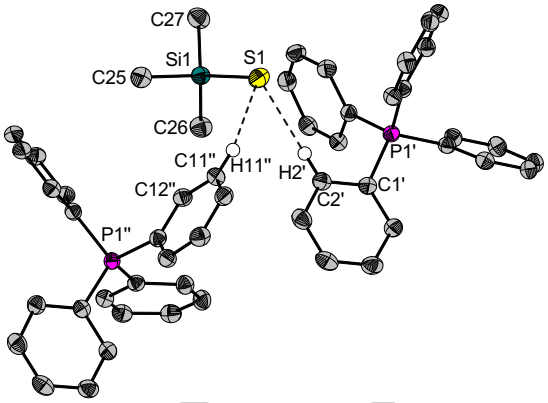

Figure 5. Molecular structure of $Ph_4P[SSiMe_3]$ (**3-S**). Ellipsoids are shown at the 50% level. Only protons involved in H-Bonds shown for clarity. Selected bond lengths (in Å) and angles (in °): S1-Si1 2.0647(8), Si1-C25 1.885(2), Si1-C26 1.885(2), Si1-C27 1.884(2), S1-Si1-C25 115.37(7), S1-Si1-C26 111.30(7), S1-Si1-C27 111.43(7), C25-Si1-C26 106.14(9), C26-Si1-C27 108.7(1), C27-Si1-C25 103.4(1), S1-H2' 2.82, C2'-H2' 0.93, S1-H2'-C2' 143(1), Si1-S1-H2'-C2' -138.9(2), C1'-C2' 1.393(3), C1'-C2'-H2' 120.3(2), C1'-C2'-H2'-S1' -120.2(2), S1-H11'' 2.85, C11''-H11'' 0.93, Si1-S1-H11''-C11'' 22.8(3), C12''-C11'' 1.385(3), C12''-C11''-H11'' 120.2(2), C12''-C11''-H11''-S1 -1.7(4). Symmetry operations: I: 1/2+x, y, 1/2-z; II: 1-x, -1/2+y, 1/2-z.

$Ph_4P[SeSiMe_3]$ (**3-Se**) crystallizes in the monoclinic space group *P*21/*c* with four formula units per unit cell. Each $[SeSiMe_3]^-$ anion is non-covalently bonded to two tetraphenylphosphonium cations with protons in *meta* and *para* position to the *ipso* C-P atom (2.92 Å and 2.93 Å respectively) (Figure 6). The different H-bonding modes observed for **3-S** and **3-Se** are probably an effect of the larger atomic radius of Se, and the longer E-Si bond, as described elsewhere for analogue salts with e. g. *N,N'*-dimethylimidazolium.[7,4]

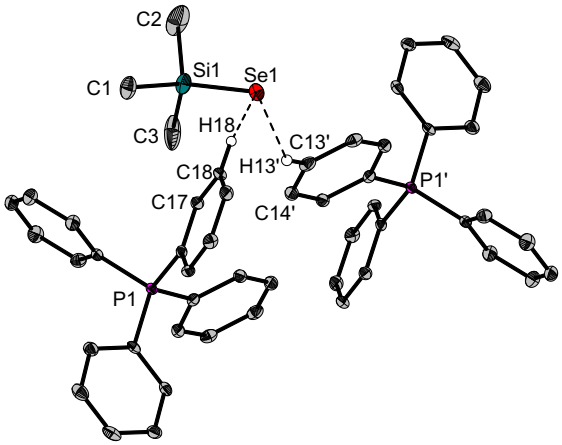

Figure 5. Crystallographically determined molecular structure of $Ph_4P[SeSiMe_3]$ (**3-Se**). Ellipsoids of are shown at the 50% level. Only protons involved in H-Bonds shown for clarity. Selected bond lengths (in Å) and angles (in °): Se1-Si1 2.2102(9), Si1-C1 1.882(2), Si1-C2 1.880(3), Si1-C3 1.880(3), Se1-Si1-C1 113.75(7), Se1-Si1-C2 111.0(1), Se1-Si1-C3 112.9(8), C1-Si1-C2 111.01(1), C2-Si1-C3 108.0(2), C3-Si1-C1 106.0(1), Se1-H13' 2.93, C13'-H13' 0.95, Se1-H13'-C13', 144.9(1), Si1-Se1-H13'-C13' 108.6(2), C14'-C13' 1.389(3), C14'-C13'-H13' 119.9, C14'-C13'-H13'-Se1 -147,5(1), Se1-H18 2.92, Se1-H18-C18 132,4(1), Si1-Se1-H18-C18 70.1(1), C17-C18 1.385(2), C17-C18-H18 120.0, C17-C18-H18-Se1 -21.6(2). Symmetry operations: I: 2-x, 1-y, 1-z.

$Ph_4P[TeSiMe_3]$ (**3-Te**) crystallizes in the monoclinic space group *P*21 with two formula units per unit cell (Figure 7). The ion pair does not show any bonding interaction. This is the first structurally characterized example of a compound with uncoordinated $[TeSiMe_3]^-$ anion.

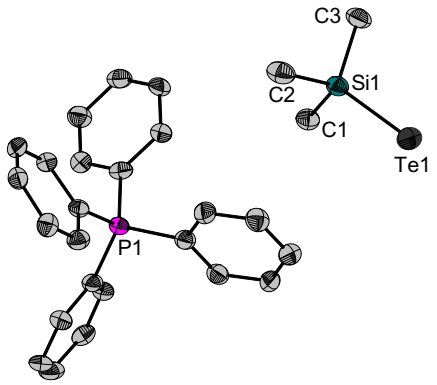

Figure 7. Crystallographically determined molecular structure of Ph_4P [$TeSiMe_3$] (**3-Te**). Ellipsoids are shown at the 50% level. Protons are omitted for clarity. Selected bond lengths (in Å) and angles (in °): Te1-Si1 2.447(2), Si1-C1 1.884(9), Si1-C2 1.89(1), Si1-C3 1.89(1), Te1-Si1-C1 111.7(3), Te1-Si1-C2 113.8(3), Te1-Si1-C3 113.8(3), C1-Si1-C2 106.9(4), C2-Si1-C3 104.5(4), C3-Si1-C1 105.5(4).

Conclusions

Herein we demonstrated an alternative approach, fluoride-induced demethylation of DMC, to prepare nicely crystallizing organic salts with the highly reactive and nucleophilic methylcarbonate anion. It turned out, that the starting material $Ph_4P[F]$ (**1**) is in fact a highly reactive fluoridophosphorane, which can be stored as a masked fluoride donor at room temperature without decomposition. Its nucleophilicity was used to demethylate Me_2CO_3. Thereby, we expanded the scope of available cations for the established organic methylcarbonate salts that had not been well characterized so far, TBA[OCO_2Me] (**2-TBA**), or even to inaccessible ones up to now, $Ph_4P[OCO_2Me]$ (**2-Ph_4P**) and PPN[OCO_2Me] (**2-PPN**). These highly basic salts are valuable synthons to introduce TBA^+, Ph_4P^+ and PPN^+ cations into highly crystalline secondary products. This was demonstrated by the isolation and characterization of so far not accessible single crystals of organic cation salts with naked $[TeSiMe_3]^-$ anions.

Experimental Section

General considerations

All preparative operations were conducted by using standard Schlenk techniques and freshly dried solvents. All solvents were dried according to common procedures[11] and passed through columns of aluminium oxide, R3-11G-catalyst (BASF) or stored over molecular sieves (3 Å or 4 Å). Other reagents were used as received unless stated otherwise. Literature known procedures were used as reported or slightly modified to synthesize $E(SiMe_3)_2$ (E = S, Se, Te).[12] Elemental analyses (C, H, N, S) were carried out by the service department for routine analysis with a vario MICRO cube (Elementar). Samples for the elemental analysis were weighted into tin capsules inside a nitrogen filled glovebox. ^{1}H and proton decoupled ^{13}C NMR spectra were recorded in automation with a Bruker Avance II 300 spectrometer, ^{29}Si-, 77Se and ^{125}Te NMR spectra were recorded by the service department for NMR analyses with a Bruker Avance II HD 300, DRX 400 or Avance III 500 spectrometer. All spectra were recorded at ambient temperature. ^{1}H- and ^{13}C NMR spectra were calibrated using residual proton signals of the solvent (dmso-d^6: δ_H 2.50 ppm, δ_C 39.52 ppm, thf-d^8: δ_H 3.58 & 1.72 ppm, δ_C 67.21 & 25.31 ppm). ^{29}Si NMR spectra were referenced externally ($SiMe_4$: δ_{Si} 0.00 ppm) just as the ^{77}Se NMR spectra (Me_2Se δ_{Se} 0.00 ppm) and the ^{125}Te NMR spectra (Me_2Te δ_{Se} 0.00 ppm). TBAF · 3 H_2O was used as obtained by commercial supplier. PPN[F] was prepared according to literature.[10a] $Ph_4P[F]$ was prepared analogously starting from $Ph_4P[Cl]$ instead of PPN[Cl].

Synthesis of $Ph_4P[F]$ (1): The preparation of **1** is similar to the literature-known method that was used to prepare PPN[F].[10] Instead of PPN [Cl] the corresponding salt $Ph_4P[Cl]$ was used as starting point. Ph_4P-F (**1**) is obtained as a colorless powder. The target compound was usually directly diluted in MeOH to proceed with the demethylation procedure. X-ray suited crystals were obtained from a solution in toluene at room temperature. ^{1}H-NMR (300.19 MHz, d^8-THF): δ = 7.28 (broad s) ppm. ^{13}C-NMR (75.48 MHz, d^8-THF): δ = 134.0-127.9 (several signals with different multiplicities) ppm. No ^{13}P and no ^{19}F NMR spectra could be obtained and the ^{13}C-NMR spectrum is of questionable quality as the solubility in d^8-THF is quite low, though better than in dmso-d^6 and C_6D_6.

Synthesis of $Ph_4P[OCO_2Me]$ (2-Ph_4P): Into an autoclave $Ph_4P[F]$ (**1**) (7.60 g, 0.021 mol, 1.00 eq.) was diluted in a mixture of Me_2CO_3 (20 mL, 0.24 mol, 11.4 eq.) and MeOH (5 mL). The reaction mixture was stirred for 3 days at 140 °C. All volatiles were removed in fine vacuum until a colorless residue is obtained. MeCN is added to this residue until a clear solution is obtained. To this solution diethyl ether is added slowly until the solution is saturated. The solution is stored at –30 °C for crystallization. The huge colorless blocks can be isolated by filtration, and the mother liquor can be collected for further crystallization steps. **2-Ph_4P** is obtained with a yield of 5.62 g (0.014 mol, 65%). ^{1}H-NMR (300.13 MHz, d^6-DMSO): δ = 7.99-7.71 (m, 20H, $[PPh_4]^+$), 3.15 (s, 3H, $[OCO_2CH_3]^-$) ppm. ^{13}C-NMR (75.48 MHz, *d^6-DMSO): δ = 155.4 (s, $[OCO_2CH_3]^-$), 135.3 (d, $^4J_{PC}$ = 3.2 Hz) & 134.5 (d, $^3J_{PC}$ = 10.3 Hz) & 130.4 (d, $^2J_{PC}$ = 13.0 Hz) & 117.7 (d, $^1J_{CP}$ = 88.7 Hz) (signals for the Ph_4P^+ cation), 50.7 (s, $[OCO_2CH_3]^-$) ppm. Elemental analysis found (calcd.) (%) for $C_{26}H_{23}O_3P$ (414.4 g mol^{-1}): C 74.9 (75.3), H 5.8 (5.6).

Synthesis of PPN[OCO_2Me] · 0.5 MeCN (2-PPN · 0.5 MeCN): The synthesis was performed analogously to the preparation of **2-Ph_4P**, using PPN[F] (9.36 g, 16.8 mmol, 1.0 eq.), Me_2CO_3 (20 mL, 0.24 mol, 14.3 eq.), and MeOH (5 mL) and stirring the reaction mixture for 5 days at 140°C. **2-PPN · 0.5 MeCN** is obtained with a yield of 7.19 g (11.3 mmol, 67%). ^{1}H-NMR (300.13 MHz, d^6-DMSO): δ = 7.71-7.51 (m, 30H, $[N(PPh_3)_2]^+$), 3.15 (s, 3H, $[OCO_2CH_3]^-$), 2.07 (s, 1.5H, 0.5 x H_3CCN) ppm. ^{13}C-NMR (75.48 MHz, d^6-DMSO): δ = 155.4 (s, $[OCO_2CH_3]^-$), 133.6 (s*) & 131.9 (m*) & 129.5 (m*) & 126.8 (dd, $^1J_{CP}$ = 107.6 Hz, $^2J_{CN}$ = 2.5 Hz) (signals for the PPN^+ cation), 118.0 (s*, H_3CCN), 50.7 (s, $[OCO_2CH_3]^-$), 1.1 (s, H_3CCN) ppm. *The expected multiplet could not be resolved as the intensity of the corresponding signals is too low. Elemental analysis found (calcd.) (%) for $C_{39}H_{34.5}N_{1.5}O_3P_2$ (634.2 g mol^{-1}): C 73.3* (73.9), H 5.5 (5.5), N 3.6 (3.3). *The deviation in the C-value might be an artefact of the measurement as the C-content is outside the standard-range.

Synthesis of TBA[OCO_2Me] (2-TBA): The synthesis of **2-TBA** was performed analogously to the preparation of **2-Ph_4P**, using TBAF · 3 H_2O (3.10 g, 9.83 mmol, 1.0 eq.), Me_2CO_3 (9 mL, 0.11 mol, 11.2 eq.), and MeOH (5 mL) and stirring the reaction mixture for 3 days at 140°C. **2-TBA** is obtained with a yield of 2.30 g (7.24 mmol, 74%). ^{1}H-NMR (300.13 MHz, d^6-DMSO): δ = 3.18 (t, $^3J_{HH}$ = 3.8 Hz, 8H*, $[N(CH_2CH_2CH_2CH_3)_4]^+$), 3.15 (s, 3H*, $[OCO_2CH_3]^-$), 1.57 (pent., $^3J_{HH}$ = 7.7 Hz, 8H $[N(CH_2CH_2CH_2CH_3)_4]^+$), 1.31 (sext., $^3J_{HH}$ = 7.5 Hz, 8H $[N(CH_2CH_2CH_2CH_3)_4]^+$), 0.93 (t, $^3J_{HH}$ =

7.4 Hz 12H) ppm. *As the signals for the methylcarbonate anion and the *N*-attached methylene-groups coincide, only the sum of the integrals of these signals is accessible that equals 11. ^{13}C-NMR (75.48 MHz, d^6-DMSO): δ = 155.4 (s, [O*C*O$_2$CH$_3$]$^-$), 57.5 (t, $^1J_{CN}$ = 3.2 Hz, [N(*C*H$_2$CH$_2$CH$_2$CH$_3$)$_4$]$^+$), 50.7 (s, [OCO$_2$*C*H$_3$]$^-$), 23.0 (s, [N(CH$_2$*C*H$_2$CH$_2$CH$_3$)$_4$]$^+$), 19.2 (s, [N(CH$_2$CH$_2$*C*H$_2$CH$_3$)$_4$]$^+$), 13.4 (s, [N(CH$_2$CH$_2$CH$_2$*C*H$_3$)$_4$]$^+$) ppm. Elemental analysis found (calcd.) (%) for $C_{18}H_{39}NO_3$ (317.51 g mol^{-1}): C 68.2 (68.1), H 12.3 (12.4), N 4.6 (4.4).

Synthesis of Ph$_4$P[SSiMe$_3$] (3-S): S(SiMe$_3$)$_2$ (0.52 g, 2.92 mmol, 1.3 eq) was added dropwise to a solution of Ph$_4$P [OCO$_2$Me] (**2-Ph$_4$P**) (0.93 g, 2.25 mmol, 1.0 eq.) in thf (10 mL) at 0 °C and stirred for five minutes at 0 °C. The solution was warmed to room temperature and stirred for a further 30 min. After removing all volatiles in fine vacuum an yellowish solid is obtained. The residue is diluted in 10 mL thf and pentane is added until saturation of this solution, and this mixturre is stored at –30 °C for some days. After filtration colorless crystals of Ph$_4$P[SSiMe$_3$] (**3-S**) were obtained with a yield of 0.83 g (1.87 mmol, 83%). ^{1}H-NMR (300.19 MHz, *d^6-DMSO): δ = 8.00-7.71 (m, 20H, [P*Ph*$_4$]$^+$), –0.07 (s, 9H, [SSi*Me*$_3$]$^-$) ppm. ^{13}C-NMR (75.48 MHz, *d^6-DMSO): δ = 135.3 (d, $^4J_{PC}$ = 3.0, [P(C(CH)$_2$(CH)$_2$*C*H)$_4$]$^+$), 134.5 (d, $^3J_{PC}$ = 10.4 Hz, [P(C(CH)$_2$(*C*H)$_2$CH)$_4$]$^+$), 130.4 (d, $^2J_{PC}$ = 12.8 Hz, [P(C(*C*H)$_2$(CH)$_2$CH)$_4$]$^+$), 117.6 (d, $^2J_{PC}$ = 88.7 Hz, [P(*C*(CH)$_2$(CH)$_2$CH)$_4$]$^+$), 8.9 (s, [SSi*Me*$_3$]$^-$) ppm. ^{29}Si-NMR (59.65 MHz, d^6-DMSO): δ = –0.76 (s, [SSi*Me*$_3$]$^-$) ppm. Elemental analysis found (calcd.) (%) for $C_{27}H_{29}PSSi$ (444.65 g mol^{-1}): C 72.9 (72.9), H 6.3 (6.6), S 6.3 (7.2).

Synthesis of Ph$_4$P[SeSiMe$_3$] (3-Se): The synthesis was performed analogously to the preparation of **3-S**, using **2-Ph$_4$P** (0.17 g, 0.41 mmol, 1.0 eq.) and Se(SiMe$_3$)$_2$ (0.14 g, 0.44 mol, 1.1 eq.). **3-Se** is obtained with a yield of 0.15 g (0.31 mmol, 75%). ^{1}H-NMR (300.25 MHz, d^6-DMSO): δ = 8.00-7.71 (m, 20H, [Ph$_4$P]$^+$), 0.08 (s, 9H, [SeSiMe$_3$]$^-$) ppm. ^{13}C-NMR (75.50 MHz, d^6-DMSO): δ = 135.3 (d, $^4J_{PC}$ = 2.8 Hz, [P(C(CH)$_2$(CH)$_2$*C*H)$_4$]$^+$), 134.5 (d, $^3J_{PC}$ = 10.5 Hz, [P(C(CH)$_2$(*C*H)$_2$CH)$_4$]$^+$), 130.4 (d, $^2J_{PC}$ = 12.3 Hz, [P(C(*C*H)$_2$(CH)$_2$CH)$_4$]$^+$), 117.8 (d, $^2J_{PC}$ = 8.9, [P(*C*(CH)$_2$(CH)$_2$CH)$_4$]$^+$), 9.2 (s, [SeSi*Me*$_3$]$^-$) ppm. ^{29}Si-NMR (59.65 MHz, d^6-DMSO): δ = –5.33 (t, $^1J_{SiSe}$ = 90.8 Hz, [Se*Si*Me$_3$]$^-$) ppm. ^{77}Se-NMR (57.26 MHz, d^6-DMSO): δ = –423.7 (s*, [*Se*SiMe$_3$]$^-$) ppm. *the expected multiplicity by coupling with the silicon-nuclei is not resolved. Elemental analysis found (calcd.) (%) for $C_{27}H_{29}PSeSi$ (491.55 g mol^{-1}): C 66.0 (66.0), H 6.0 (6.0).

Synthesis of Ph$_4$P[TeSiMe$_3$] (3-Te)*: Te(SiMe$_3$)$_2$ (0.084 g, 0.31 mmol, 1.1 eq) was added dropwise to a degassed solution of Ph$_4$P [OCO$_2$Me] (**2-Ph$_4$P**) (0.115 g, 0.28 mmol, 1.0 eq.) in thf (10 mL) at 0 °C and stirred for five minutes at 0 °C. The solution was warmed to room temperature and stirred for a further 30 min. After removing all volatiles in fine vacuum an orange solid is obtained. The residue is diluted in 10 mL thf. Pentane is added until saturation of this solution, and this mixturre is stored at –30 °C for some days. After filtration orange crystals of Ph$_4$P [TeSiMe$_3$] (**3-Te**) were obtained with a yield of 0.094 g (0.17 mmol, 63%). ^{1}H-NMR (300.25 MHz, *d-DMSO): d = 8.00-7.71 (m, 20H, [Ph$_4$P]$^+$), 0.32~ (s, < 9H, [TeSiMe$_3$]$^-$) ppm. ^{13}C-NMR (75.50 MHz, d^6-DMSO): d = 135.3 (d, $^4J_{PC}$ = 2.8 Hz, [P(C(CH)$_2$(CH)$_2$*C*H)$_4$]$^+$), 134.5 (d, $^3J_{PC}$ = 10.5 Hz, [P(C(CH)$_2$(*C*H)$_2$CH)$_4$]$^+$), 130.4 (d, $^2J_{PC}$ = 12.3 Hz, [P(C(*C*H)$_2$(CH)$_2$CH)$_4$]$^+$), 117.6 (d, $^2J_{PC}$ = 89.2Hz, [P(*C*(CH)$_2$(CH)$_2$CH)$_4$]$^+$), 10.2~ (s, [TeSi*Me*$_3$]$^-$) ppm. ^{29}Si-NMR (59.65 MHz, *d^6-DMSO): d = –28.0~ (s, [Te*Si*Me$_3$]$^-$) ppm. ^{125}Te-NMR (94.73 MHz, *d^6-DMSO): d = –1138.7 (s, [*Te*SiMe$_3$]$^-$) ppm. Elemental analysis found (calcd.) (%) for $C_{27}H_{29}PTeSi$ (540.19 g mol^{-1}): C 59.6 (60.0), H 5.0 (5.4). ~Note that the anion signal is always accompanied with a signal for O(SiMe$_3$)$_2$, the hydrolysis product at 0.06 ppm (^{1}H NMR), 2.0 ppm (^{13}C NMR), and 7.6 ppm (^{29}Si NMR) which arises due to diffusion of H$_2$O into the NMR-sample and the extreme sensitivity of the compound. The sum over the signal for the anion and O(SiMe$_3$)$_2$ yields the correct amount of anion related protons. *As the tellurium containing compounds in this reaction tend to decompose unter exposure to light, aluminum foil was wrapped around all devices. For the lighter homologues this is not necessary.

Acknoledgements

Financial support of the German Research Foundation DFG and its priority program SPP 1708: "Material Synthesis near Room Temperature" is gratefully acknowledged. We thank Haowen Wang and Hui Qu for their synthetic contributions.

References

[1] Roland Kalb, WO 2005021484 A2, **2004**.

[2] a) B. Oelkers, J. Sundermeyer, *Green Chem.* **2011**, *13*, 608-618. b) J. D. Holbrey, R. D. Rogers, S. S. Shukla, C. D. Wilfred, *Green Chem.*, **2010**,*12*, 407-413. c) J. D. Holbrey, W. M. Reichert, I. Tkatchenko, E. Bouajila, O. Walter, I. Tommasi, R. D. Rogers, *Chem. Commun.* **2003**, 28-29.

[3] L. H. Finger, J. Sundermeyer, *Chem. Eur. J.* **2016**, *22*, 4218-4230.

[4] L. H. Finger, B. Scheibe, J. Sundermeyer, *Inorg. Chem.* **2015**, *54*, 9568-9575.

[5] J. D. Holbrey, W. M. Reichert, I. Tkatchenko, E. Bouajila, O. Walter, I. Tommasi, R. D. Rogers, *Chem. Commun.* **2003**, 28-29.

[6] L. H. Finger, J. Guschlbauer, K. Harms, J. Sundermeyer, *Chem. Eur. J.* **2016**, *22*, 16292-16303.

[7] J. Guschlbauer, T. Vollgraff, J. Sundermeyer, *Dalton Trans.* **2019**, 48, 10971-10978.

[8] V. Trieu, R. Weber, S. R. Waldvogel, J. Heijl, T. Gieshoff, WO 2018091370 A1, **2016**.

[9] M. Hatano, Y. Tabata, Y. Yoshida, K. Toh, K. Yamashita, Y. Ogura, K. Ishihara, *Green Chem.* **2018**, *20*, 1193-1198.

[10] a) C. Bolli, J. Gellhaar, C. Jenne, M. Keßler, H. Scherer, H. Seeger, R. Uzun, *Dalton Trans.* **2014**, *43*, 4326-4334. b) D. Mootz, M. Wiebcke, *Z. anorg. allg. Chem.* **1987**, *545*, 39-42.

[11] W. L. F. Armarego, D. D. Perrin *Purification of laboratory chemicals*, 4th ed., paperback ed.; Butterworth-Heinemann: Oxford, 1997.

[12] J.-H. So, P. Boudjouk, *Synthesis* **1989**, 4, 306-307.

FULL PAPER

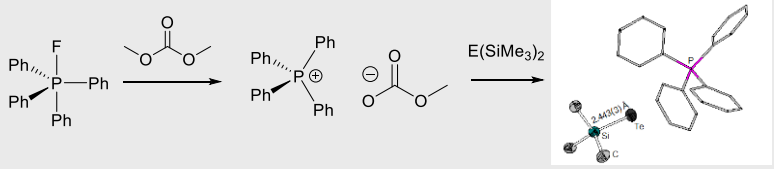

*Author(s), Corresponding Author(s)**

Page No. – Page No.

Title

Organic Methylcarbonate Salts Comprising Non-methylated Onium Cations Cat[OCO_2Me] (Cat = Ph_4P^+, PPN^+, TBA^+) via Fluoride-Induced Demethylation of Dimethylcarbonate

Jannick Guschlbauer,[a] Tobias Vollgraff,[a] Ahmed Fetoh,[a] Jörg Sundermeyer*[a]

Supporting Information

Content

1. NMR-Spectra

*1.1 $Ph_4P[F]$ (**1**)*

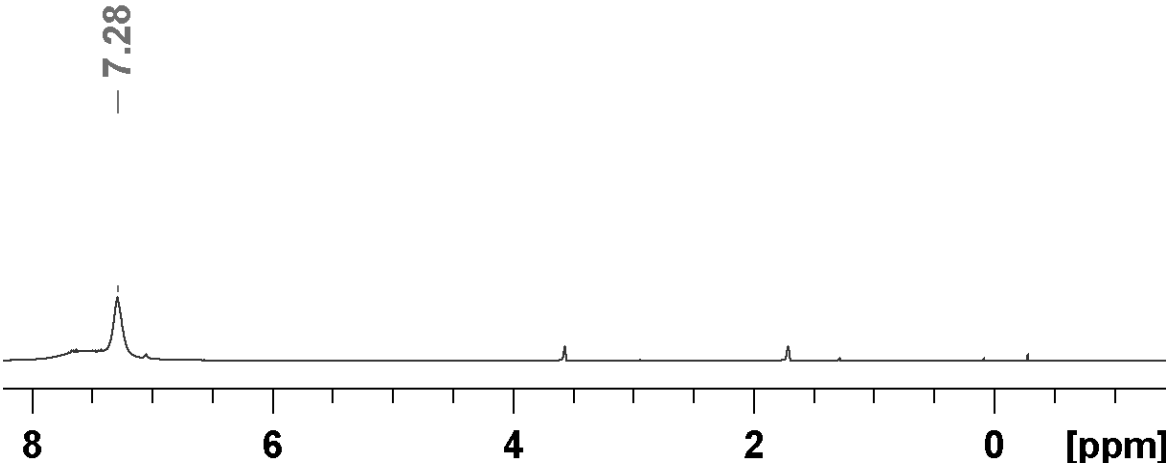

^{1}H-NMR (300.19 MHz, d^{8}-THF): Very broad signal at 7.28 ppm.

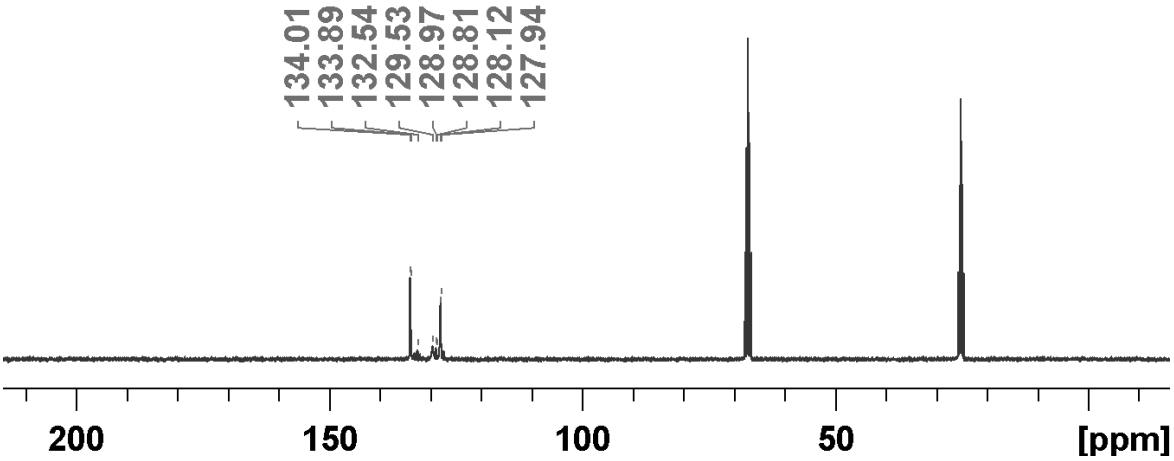

^{13}C-NMR (75.48 MHz, d^{8}-THF): Multiple signals between 134-128 ppm.

No ^{19}F- and ^{31}P-NMR spectra could be obtained. This is probably caused by the low solubility of **1** in d^{8}-THF (which is also low in d^{6}-DMSO and in C_6D_6).

*1.2 $Ph_4P[OCO_2Me]$ (**2-Ph_4P**)*

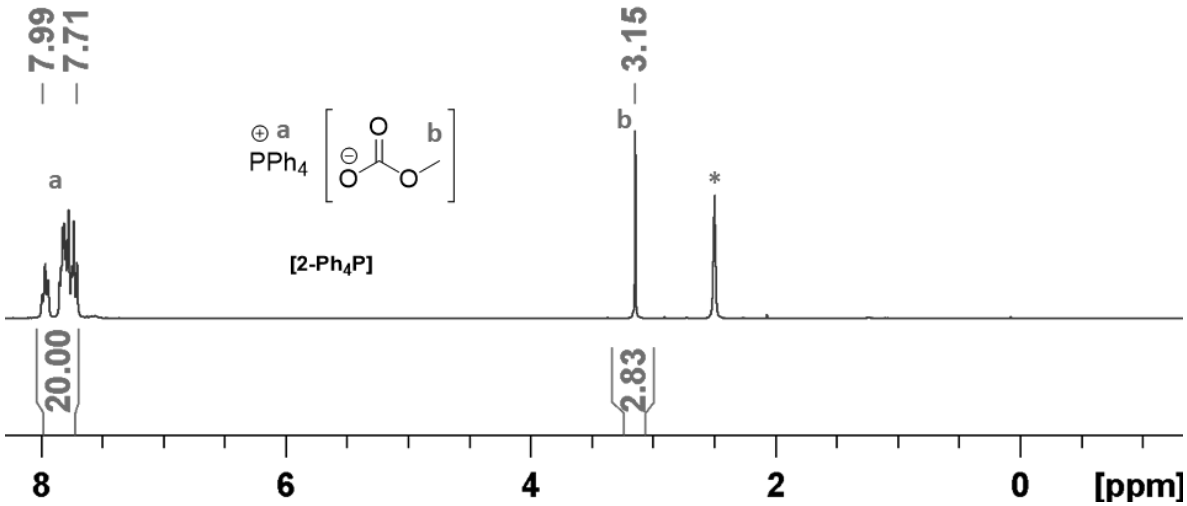

^{1}H-NMR (300.13 MHz, *d^6-DMSO)

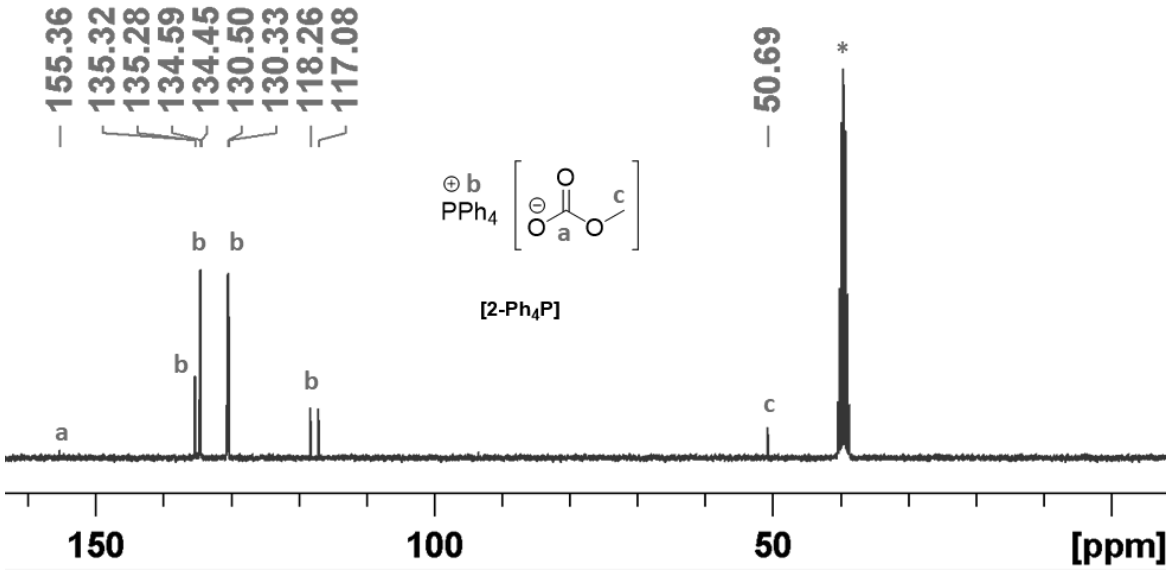

^{13}C-NMR (75.48 MHz, *d^6-DMSO).

*1.3 PPN[OCO₂Me] · 0.5 MeCN (**2-PPN**)*

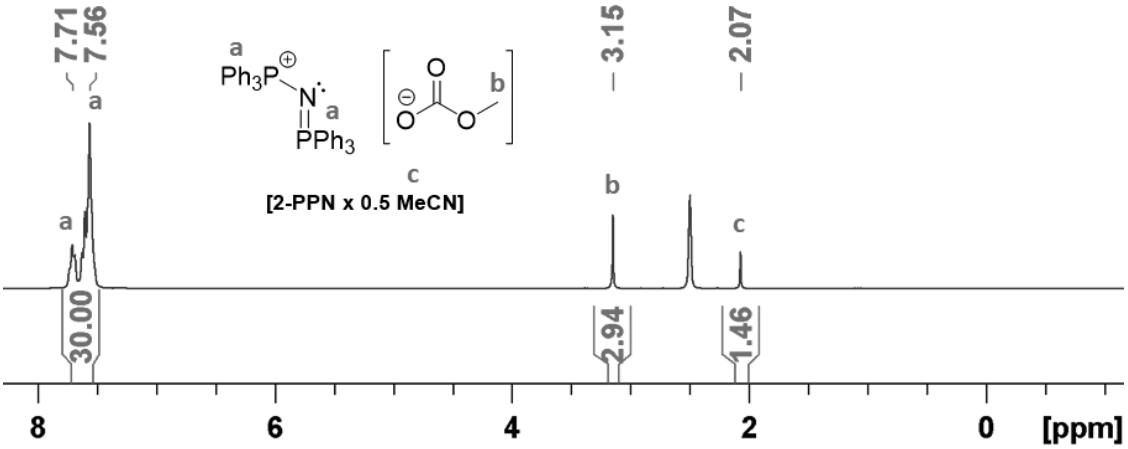

[1]H-NMR (300.13 MHz, *d[6]-DMSO).

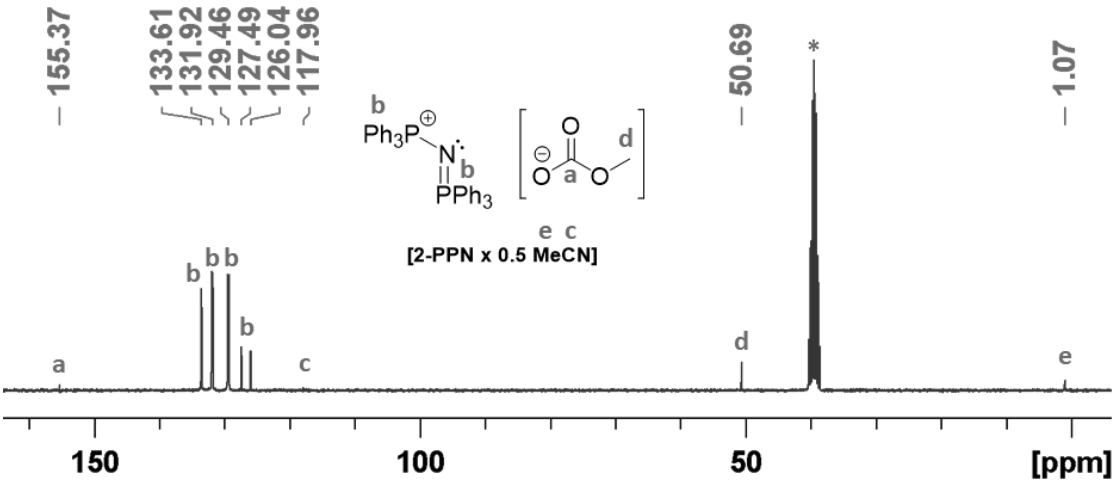

[13]C-NMR (75.48 MHz, *d[6]-DMSO) expected multiplets for PPN-cation and MeCN could not be resolved as the intensity oft he corresponding signals is too low.

*1.4 TBA[OCO₂Me] (**2-TBA**)*

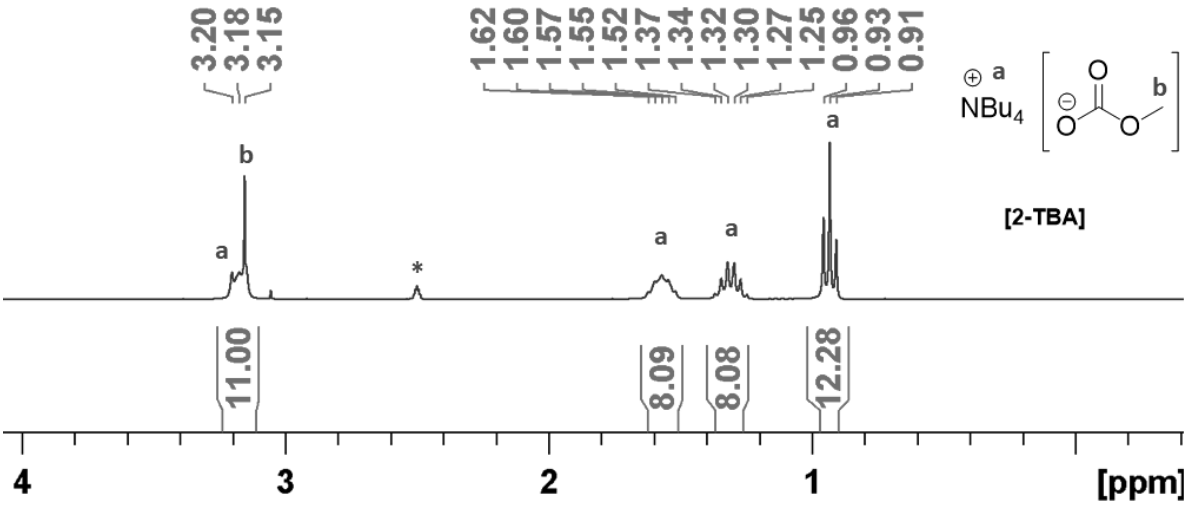

[1]H-NMR (300.13 MHz, *d[6]-DMSO). The signals for the methylcarbonate anion and the N-attached methylene-groups coincide. The sum of the integrals of these signals equals the expected amount of 11.

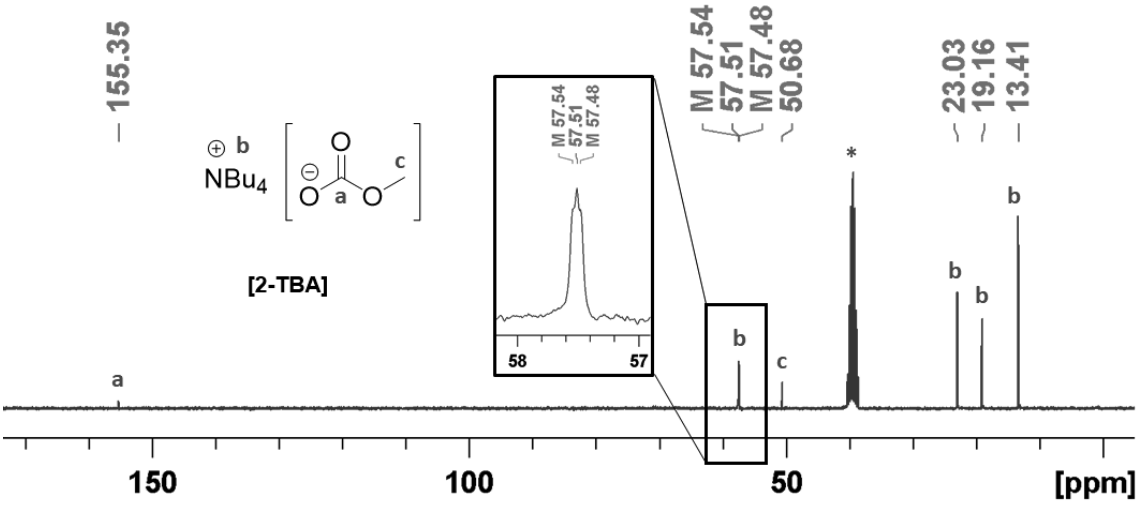

[13]C-NMR (75.48 MHz, *d[6]-DMSO).

*1.5 $Ph_4P[SSiMe_3]$ (**3-S**)*

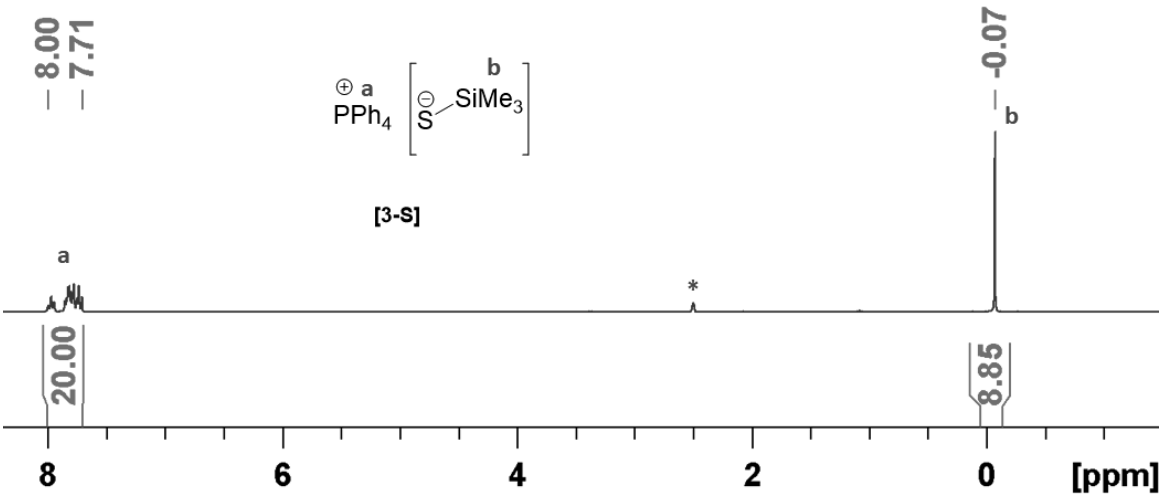

^{1}H-NMR (300.19 MHz, *d^{6}-DMSO).

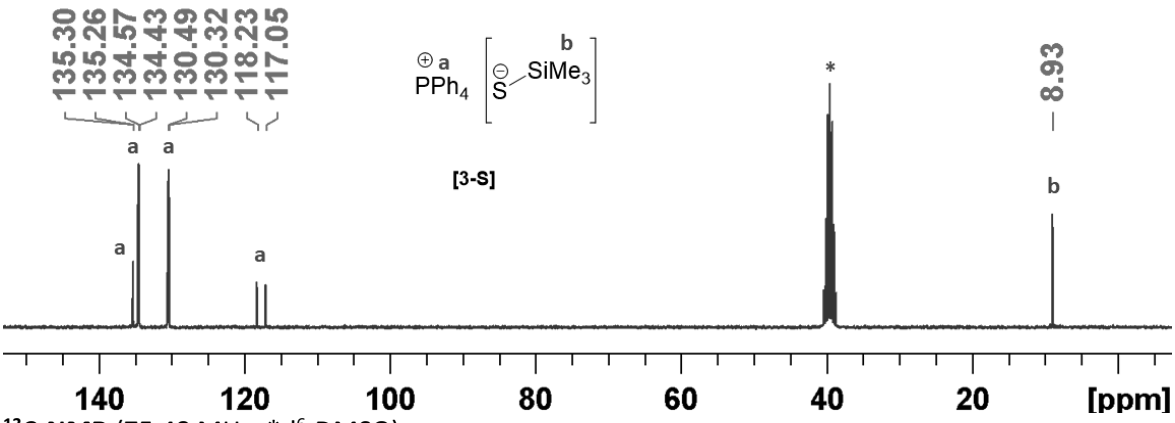

^{13}C-NMR (75.48 MHz, *d^{6}-DMSO).

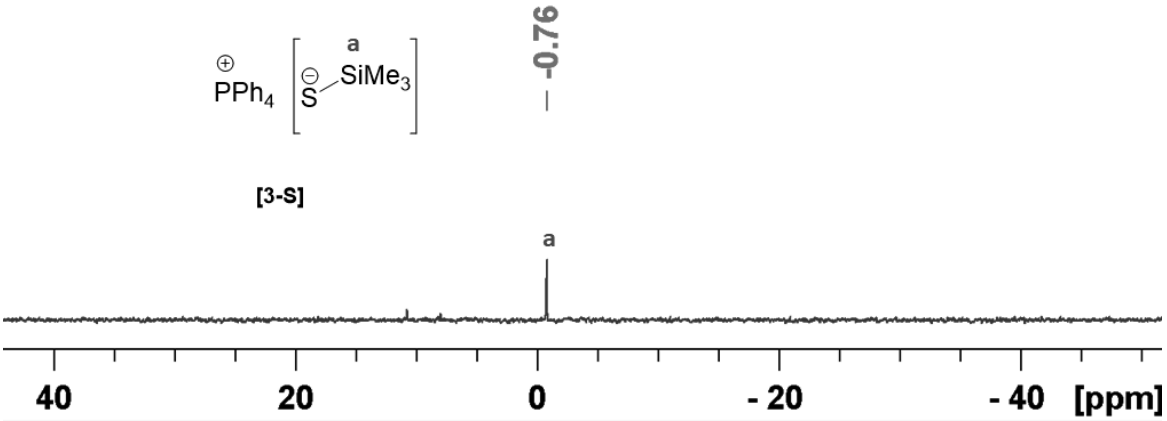

^{29}Si-NMR (59.65 MHz, d^{6}-DMSO).

*1.6 $Ph_4P[SeSiMe_3]$ (**3-Se**)*

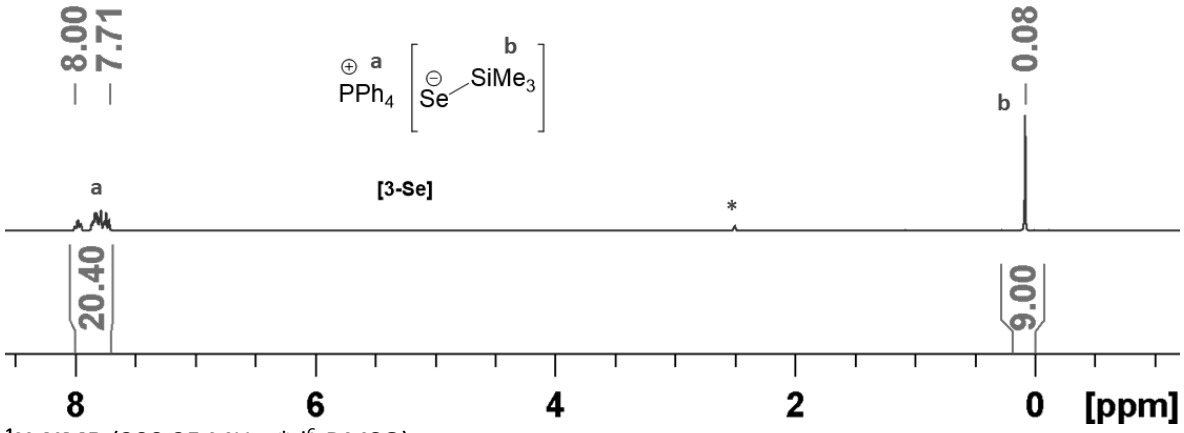

^{1}H-NMR (300.25 MHz, *d^6-DMSO).

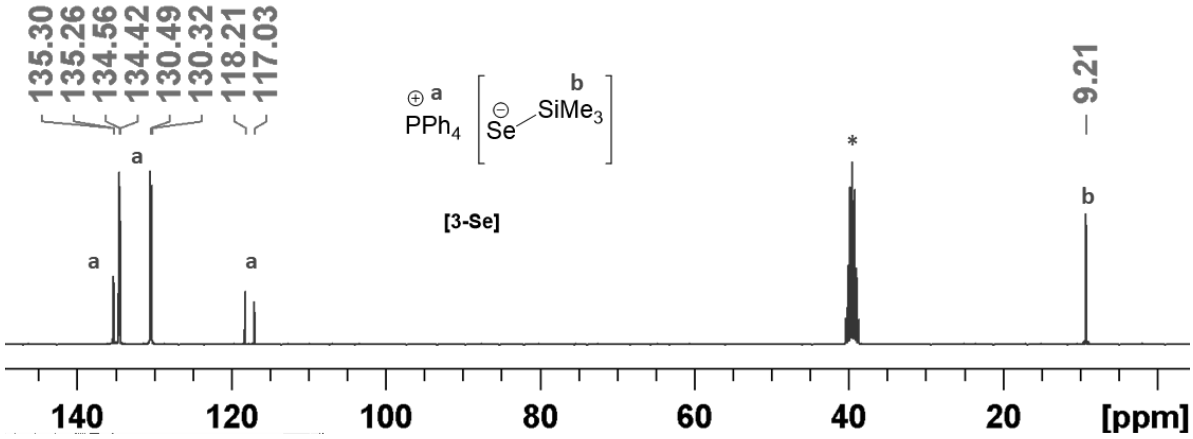

^{13}C-NMR (75.50 MHz, *d^6-DMSO).

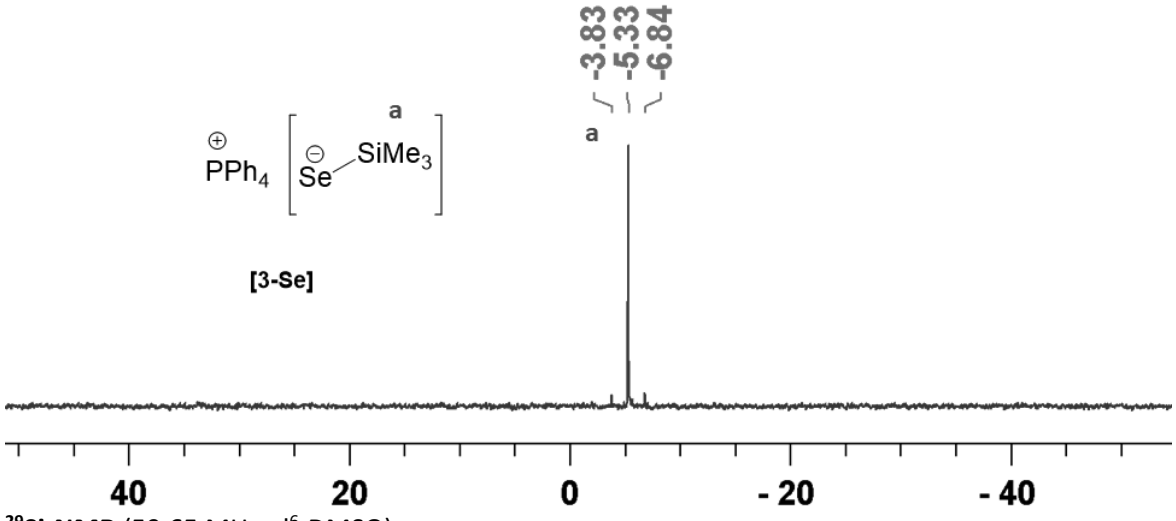

^{29}Si-NMR (59.65 MHz, d^6-DMSO).

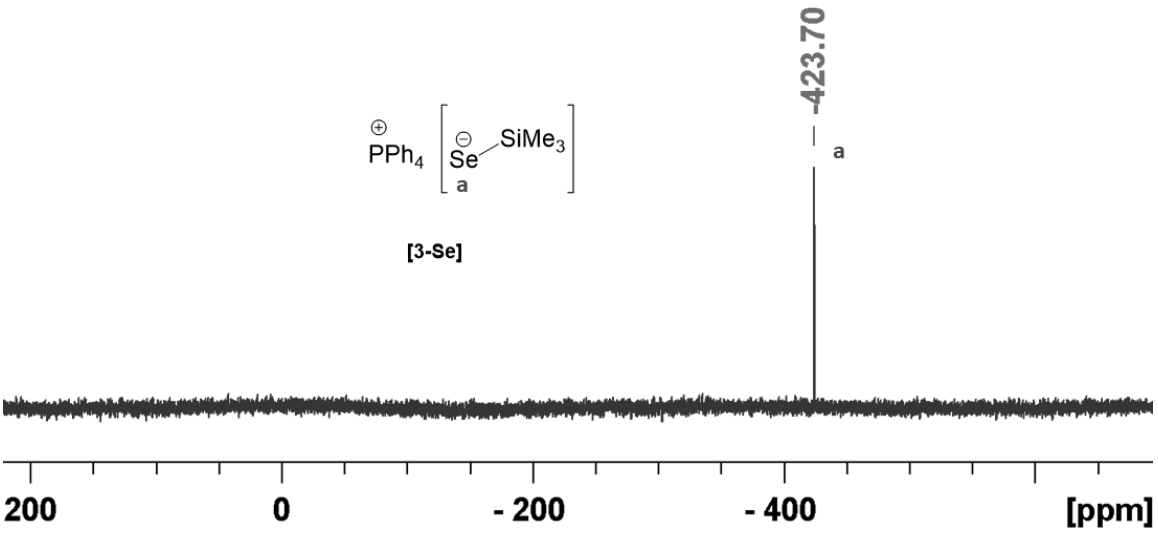

^{77}Se-NMR (57.26 MHz, d^6-DMSO).

*1.7 $Ph_4P[TeSiMe_3]$ (**3-Te**)*

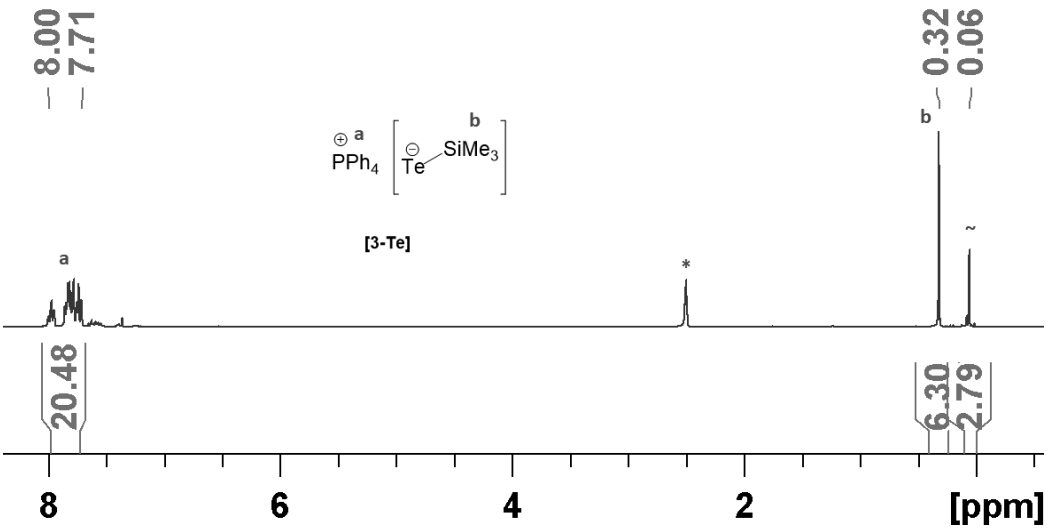

^{1}H-NMR (300.25 MHz, *d^6-DMSO). The signal at 0.06 ppm can be assigned to $O(SiMe_3)_2$ which arises due to diffusion of H_2O into the NMR-sample.

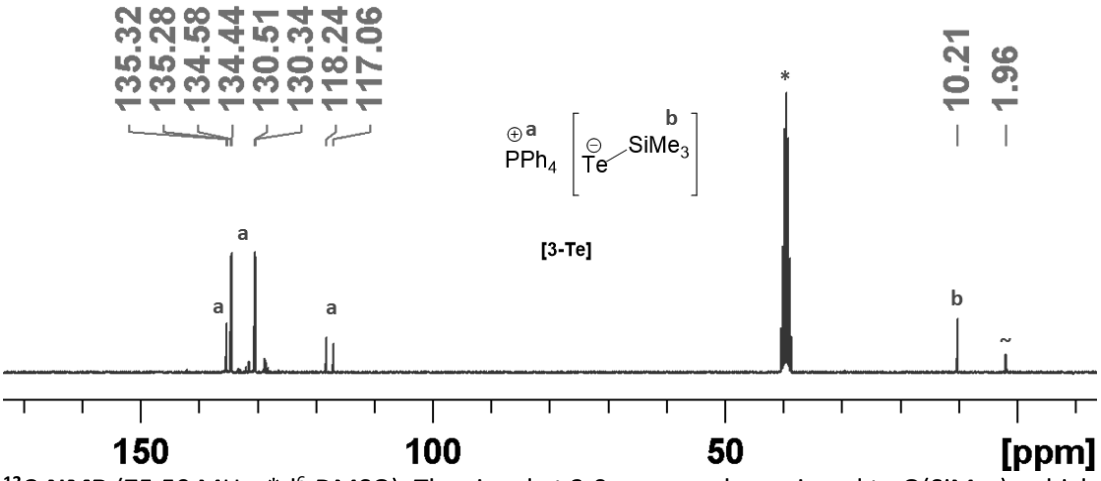

^{13}C-NMR (75.50 MHz, *d^6-DMSO). The signal at 2.0 ppm can be assigned to $O(SiMe_3)_2$ which arises due to diffusion of H_2O into the NMR-sample.

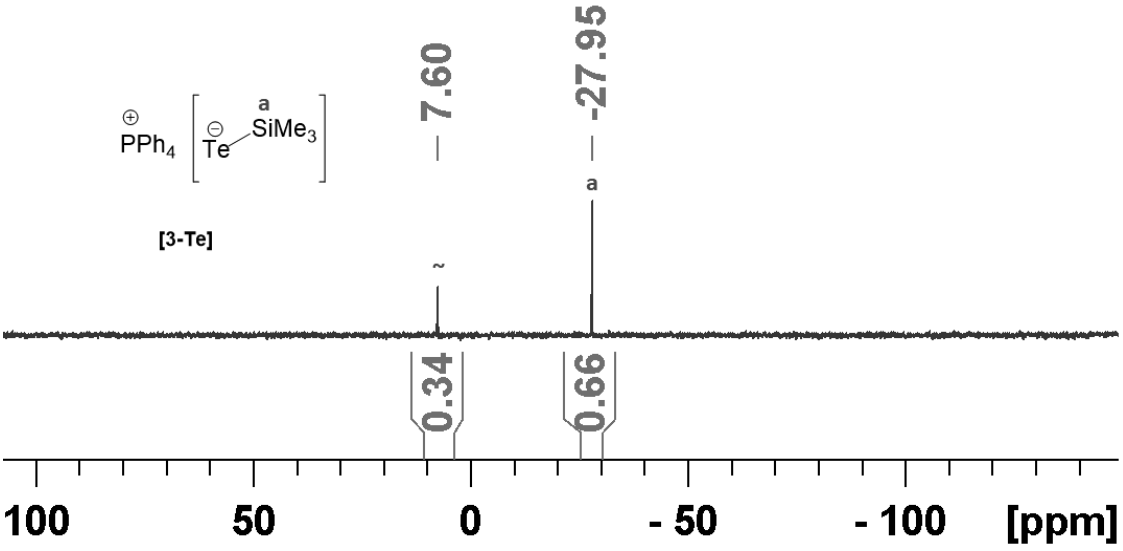

^{29}Si-NMR (59.65 MHz, *d^6-DMSO). The signal at 7.6 ppm can be assigned to $O(SiMe_3)_2$ which arises due to diffusion of H_2O into the NMR-sample.

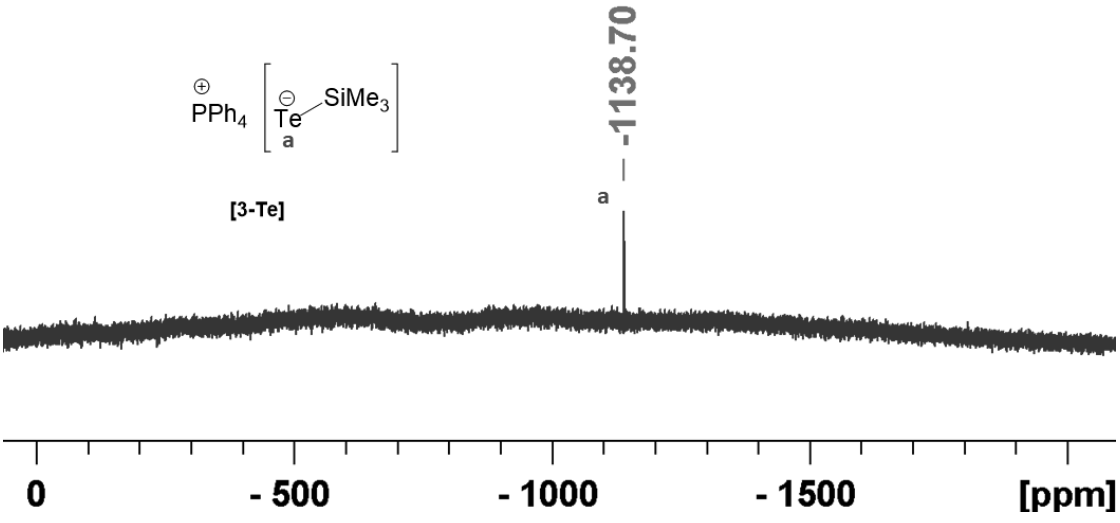

^{125}Te-NMR (94.73 MHz, *d^6-DMSO).

2. Crystallographic data

Table S1: XRD-data of $Ph_4P[F]$ (**1**)

	$Ph_4P[F]$ (1)
Identification code	tvdpph4floesen
Empirical formula	$C_{24}H_{20}FP$
Formula weight	358.37
Temperature/K	100(2)
Crystal system	monoclinic
Space group	$P2_1/n$
a/Å	9.7884(4)
b/Å	18.6328(6)
c/Å	10.2715(4)
α/°	90
β/°	90.900(3)
γ/°	90
Volume/Å^3	1873.14(12)
Z	4
ρ_{calc}g/cm^3	1.271
μ/mm^{-1}	1.398
F(000)	752.0
Crystal size/mm^3	0.226 × 0.186 × 0.155
Radiation	CuKα (λ = 1.54178)
2Θ range for data collection/°	9.492 to 132.998
Index ranges	$-11 \le h \le 10$, $-11 \le k \le 22$, $-10 \le l \le 12$
Reflections collected	13605
Independent reflections	3299 [R_{int} = 0.0234, R_{sigma} = 0.0170]
Data/restraints/parameters	3299/0/235
Goodness-of-fit on F^2	1.037
Final R indexes [I>=2σ (I)]	R_1 = 0.0312, wR_2 = 0.0851
Final R indexes [all data]	R_1 = 0.0339, wR_2 = 0.0866
Largest diff. peak/hole / e Å^{-3}	0.31/-0.35

Table S2: XRD-data of **2-PPN** and **2-TBA**.

	PPN[$MeCO_3$] · 0.5 MeCN (2-PPN)	**TBA[$MeCO_3$] (2-TBA)**
Identification code	hq07_0m_a_PPNMeCO3	jg207loesen_TBAMeCO3
Empirical formula	$C_{78}H_{69}N_3O_6P_4$	$C_{18}H_{39}NO_3$
Formula weight	1268.24	317.50
Temperature/K	100(2)	100(2)
Crystal system	monoclinic	monoclinic
Space group	$P2_1/c$	$P2_1/n$
a/Å	10.620(2)	10.7894(3)
b/Å	35.750(7)	13.2294(3)
c/Å	17.320(3)	14.1702(4)
α/°	90.00(3)	90
β/°	97.36(3)	104.247(2)
γ/°	90.00(3)	90
Volume/Å^3	6521(2)	1960.41(9)
Z	4	4
ρ_{calc}g/cm^3	1.292	1.076
μ/mm^{-1}	0.174	0.557
F(000)	2664.0	712.0
Crystal size/mm^3	0.633 × 0.310 × 0.232	0.235 × 0.182 × 0.115
Radiation	MoKα (λ = 0.71073)	CuKα (λ = 1.54178)
2Θ range for data collection/°	4.42 to 49.998	34.372 to 132.962
Index ranges	$-12 \le h \le 12$, $-42 \le k \le 42$, $-20 \le l \le 20$	$-12 \le h \le 12$, $-15 \le k \le 7$, $-16 \le l \le 16$
Reflections collected	175688	22909
Independent reflections	11494 [R_{int} = 0.0607, R_{sigma} = 0.0261]	3339 [R_{int} = 0.0408, R_{sigma} = 0.0256]
Data/restraints/parameters	11494/6/823	3339/0/204
Goodness-of-fit on F^2	1.092	1.067
Final R indexes [I>=2σ (I)]	R_1 = 0.0411, wR_2 = 0.0905	R_1 = 0.0473, wR_2 = 0.1327
Final R indexes [all data]	R_1 = 0.0542, wR_2 = 0.0960	R_1 = 0.0570, wR_2 = 0.1372
Largest diff. peak/hole / e Å^{-3}	0.60/-0.33	0.64/-0.22

Table S3: XRD-data of **3-S** and **3-Se**.

	$Ph_4P[SSiMe_3]$ (3-S)	**$Ph_4P[SeSiMe_3]$ (3-Se)**
Identification code	jg224loesen_Ph4PSSiMe3	af01_0m_a_Ph4PSeSiMe3
Empirical formula	$C_{27}H_{29}PSSi$	$C_{27}H_{29}PSeSi$
Formula weight	444.62	491.52
Temperature/K	100(2)	100(2)
Crystal system	orthorhombic	monoclinic
Space group	Pbca	$P2_1/c$
a/Å	17.6627(3)	10.511(2)
b/Å	15.3022(3)	9.071(2)
c/Å	18.0163(4)	26.773(5)
α/°	90	90.00(3)
β/°	90	99.08(3)
γ/°	90	90.00(3)
Volume/$Å^3$	4869.41(17)	2520.8(9)
Z	8	4
ρ_{calc}g/cm^3	1.213	1.295
μ/mm^{-1}	2.344	1.612
F(000)	1888.0	1016.0
Crystal size/mm^3	0.231 × 0.187 × 0.151	0.624 × 0.286 × 0.197
Radiation	CuKα (λ = 1.54178)	MoKα (λ = 0.71073)
2Θ range for data collection/°	9.818 to 132.992	4.592 to 54.248
Index ranges	$-20 \le h \le 9$, $-18 \le k \le 18$, $-21 \le l \le 21$	$-13 \le h \le 13$, $-11 \le k \le 11$, $-32 \le l \le 34$
Reflections collected	42306	57425
Independent reflections	4276 [R_{int} = 0.0326, R_{sigma} = 0.0146]	5577 [R_{int} = 0.0480, R_{sigma} = 0.0241]
Data/restraints/parameters	4276/0/274	5577/0/274
Goodness-of-fit on F^2	1.140	1.032
Final R indexes [I>=2σ (I)]	R_1 = 0.0357, wR_2 = 0.1045	R_1 = 0.0273, wR_2 = 0.0588
Final R indexes [all data]	R_1 = 0.0395, wR_2 = 0.1064	R_1 = 0.0345, wR_2 = 0.0615
Largest diff. peak/hole / e $Å^{-3}$	0.22/-0.41	0.41/-0.32

Table S4: XRD-data of **3-Te**.

	$Ph_4P[TeSiMe_3]$ (3-Te)
Identification code	jg354loesen_Ph4PTeSiMe3
Empirical formula	$C_{27}H_{29}PSiTe$
Formula weight	540.16
Temperature/K	100(2)
Crystal system	monoclinic
Space group	$P2_1$
a/Å	9.5283(2)
b/Å	10.6121(2)
c/Å	12.3821(3)
α/°	90
β/°	90.136(2)
γ/°	90
Volume/Å^3	1252.02(5)
Z	2
ρ_{calc}g/cm^3	1.433
μ/mm^{-1}	10.510
F(000)	544.0
Crystal size/mm^3	0.371 × 0.176 × 0.077
Radiation	CuKα (λ = 1.54186)
2Θ range for data collection/°	7.14 to 132.974
Index ranges	$-11 \leq h \leq 11$, $-12 \leq k \leq 11$, $-13 \leq l \leq 14$
Reflections collected	19271
Independent reflections	3978 [R_{int} = 0.0501, R_{sigma} = 0.0338]
Data/restraints/parameters	3978/1/276
Goodness-of-fit on F^2	1.062
Final R indexes [I>=2σ (I)]	R_1 = 0.0415, wR_2 = 0.1103
Final R indexes [all data]	R_1 = 0.0438, wR_2 = 0.1119
Largest diff. peak/hole / e Å^{-3}	1.04/-1.18
Flack parameter	0.051(10)